Canadian
Journal of Chemistry

Symposium on Some Fundamental Aspects of Atomic Reactions

The papers that follow were presented at a symposium held at McGill University, Montreal, on September 6 and 7, 1960, under the auspices of the Physical Chemistry Subject Division of the Chemical Institute of Canada and organized by the chairman of the symposium, Dr. J. C. Polanyi of the University of Toronto. A few of the papers presented are not published here because of prior commitments.

The executive committee of the subject division wishes to express its gratitude to the symposium chairman, to McGill University for its generous co-operation in the use of its facilities, and to the Editor-in-Chief and staff of the Canadian Journal of Chemistry for their valuable assistance.

THE TRANSFER REACTIONS OF HALOGEN ATOMS[1]

G. C. FETTIS, J. H. KNOX, AND A. F. TROTMAN-DICKENSON

ABSTRACT

Extensive results on the reactions of fluorine, chlorine, and bromine atoms with alkanes and with some other molecules have been obtained from the study of competitive halogenations. The comparison of the A factors of the reactions provides an excellent test of the transition state theory. The activation energies of the bromine atom reactions can be combined with measurements of the activation energies for the reactions of alkyl radicals with hydrogen bromide to yield unusually reliable values of bond strengths. Information on the influence of polar effects on the activation energies of atomic reactions can be obtained from results on the reactions of fluorine and chlorine atoms with methyl halides.

The reaction of a halogen with a pair of hydrocarbons can be represented by the following steps:

$$\begin{align} X + R^1H &= XH + R^1 \\ R^1 + X_2 &= R^1X + X \end{align} \quad [1]$$

$$\begin{align} X + R^2H &= XH + R^2 \\ R^2 + X_2 &= R^2X + X \end{align} \quad [2]$$

In this paper we shall be concerned with the rate constants and Arrhenius factors for reactions [1] and [2] and for those of the reverse processes [−1] and [−2]. The relative values of k_1 and k_2 can be found by competitive methods in two ways. The first is the consumption method in which the amounts of R^1H and R^2H removed from a mixture during reaction with a halogen are determined. Then

$$\frac{k_1}{k_2} = \frac{-d[R^1H]/dt. \ [R^2H]}{-d[R^2H]/dt. \ [R^1H]} .$$

In practice this relation is used in its integrated form and the conversions are kept below about 20–30%. This method was particularly attractive before the development of gas chromatography for it was much simpler to analyze for small quantities of R^1H and R^2H than of the corresponding halides. It was employed by Pritchard, Pyke, and Trotman-Dickenson (1) to study chlorine atom reactions and later by Mercer and Pritchard (2) to study fluorine atoms.

The second method depends upon the measurement of the rate of formation of the halides formed. The rate constants are then obtained from

$$\frac{k_1}{k_2} = \frac{d[R^1X]/dt. \,[R^2H]}{d[R^2X]/dt. \,[R^1H]}.$$

The integrated form of the equation need not be used as the percentage conversions should be kept very low to avoid secondary reactions of the halides. Fortunately halides are not more than 10 times as reactive as their parent alkanes. This approach was first used by Hass, McBee, and Weber (3) in their studies of chlorinations. Their work was done on a large scale in flow systems, so that sufficient chlorides were formed for analysis by distillation. They worked at high temperatures. Some isomerization of the chlorides probably occurred so that the results do not agree well with those of later workers. Knox (4) applied gas chromatography to the problem and was able to reduce the scale of reaction by about 10^4 and at the same time improve the accuracy. The method has the great advantage that isomeric products can be distinguished and reactivities directly assigned to specific types of hydrogen atom. The attack on hydrogen is not simply followed because hydrogen halides are not easily determined by gas chromatography and are produced in reactions of all hydrogen-containing compounds.

Relative rate constants obtained by competitive methods can be placed on an absolute scale if the constant for one member of the series can be absolutely determined. Fortunately the rate constant for the attack of a chlorine atom on molecular hydrogen has been determined by three groups of workers whose results are in good agreement. Kistiakowsky and Van Artsdalen have carefully measured the rate of reaction of bromine atoms with methyl bromide and methane (5). No rate constant for a fluorine atom reaction has been measured. In this work it has been assumed that the value of the A factor calculated for the reaction of fluorine atoms with ethane is correct and that the activation energies for attack on hydrocarbons heavier than ethane are zero. The justification for these assumptions will be apparent in what follows.

Table I summarizes the results that have been obtained at Edinburgh, together with

TABLE I

Rate constants, A factors, and activation energies for reactions of the type $X + RH = HX + R$

RH	Fluorine atoms (8)			Chlorine atoms (9)			Bromine atoms (10)		
	$\log k$ (25°)	$\log A$	E	$\log k$ (25°)	$\log A$	E	$\log k$ (100°)	$\log A$	E
H_2	12.8	14.0	1.71^2	9.8	13.9	5.50^7	3.3^5	13.7	17.5
CH_4	13.1	14.0	1.21	10.6	13.4	3.85^1	3.3	14.0	18.3
Primary									
C_2H_6	13.5	13.7	0.28	13.2	14.0	1.04^1	6.1	13.9	13.4
C_3H_8	13.4	13.4	0	13.3	14.0	1.00	—	—	—
n-C_4H_{10}	13.3	13.3	0	13.2	13.9	0.79	—	—	—
iso-C_4H_{10}	13.6	13.6	0	13.5	14.1	0.82	—	—	—
neo-C_5H_{12}	13.7	13.7	0	13.6	14.3	0.92	5.9	14.2	14.3
Secondary									
C_3H_8	13.0	13.0	0	13.3	13.9	0.68	7.7	13.7	10.1
n-C_4H_{10}	13.3	13.3	0	13.8	13.9	0.27	7.2	13.2	10.2
cyclo-C_3H_6	13.4	13.4	0	10.7	13.7	4.1	—	—	—
cyclo-C_4H_8	—	—	—	13.8	14.4	0.83	—	—	—
Tertiary									
iso-C_4H_{10}	12.8	12.8	0	13.2	13.2	0.02	8.9	13.3	7.5

NOTE: A and k are in cm^3 $mole^{-1}$ sec^{-1}; E is in kilocalories $mole^{-1}$.

a few other results of our own and of other workers. The experimental details and a full comparison of the results with the rather small number available from other sources are fully discussed in the original papers to which reference is made. With the notable exception of the bromination results of Van Artsdalen's group the present work is in excellent agreement with the small amount of recent work by other authors. Benson and Buss (6) have discussed at length the probable reasons for the unreliability of the results of Van Artsdalen's very careful work. These results were always suspect because they appeared to be out of line with those for all other atomic reactions.

The A Factors

According to transition state theory the A factor for a bimolecular reaction is given by

$$A = e^2.(kT/h) \exp [(\Delta S_{tr}^{\pm} + \Delta S_{rot}^{\pm} + \Delta S_{vib}^{\pm})/R].$$

The translational entropies of activation can be calculated exactly from the molecular weights of the reactants and complexes. The accuracy of the calculated value of the rotational entropy of activation is limited by the uncertainty of the exact configuration of the complex and, to a lesser degree, of the reactant. The C—H and C—C bond lengths have throughout been assumed to be 1.10 and 1.54 Å except that the half-order bonds

$\geq$C—H—X have been taken as 0.18 Å longer than the corresponding single bonds. The

two extreme forms of the n-butane – halogen complexes in which the molecule is fully extended or completely curled up yield rotational entropies of activation that differ by less than 10%. Since intermediate configurations are much more profitable, it is unlikely that the error arising from assumptions about the configurations are large as this.

The calculation of the vibrational entropies of activation is less certain and has a greater effect upon the result obtained. It has been assumed that many of the vibrations in RH will be little changed by the addition of the halogen atom and that their contributions to $\Delta S_{vib}^{\pm}$ will largely cancel. Only a few vibrations intimately connected with the part of the molecule to which the halogen atom is attached will give rise to important contributions. These vibrations are the C—H stretching and C—H wagging in the hydrocarbon which are replaced by five new vibrations in the activated complex. The C—H stretching becomes the reaction co-ordinate and the C—H wagging becomes the wagging of H—X against the rest of the hydrocarbon. The three additional vibrations are the symmetrical stretching of the C—H—X bonds and the doubly degenerate bending of the C—H—X bonds. Pitzer (11) deduced $\Delta S_{vib}^{\pm}$ for the reaction

$$Cl + H_2 = HCl + H$$

from the observed A factor and found that the bending and stretching frequencies were 560 cm^{-1} and 1460 cm^{-1} respectively. It has here been assumed that the force constants for these modes of vibration are the same for all the complexes and that the corresponding frequencies can therefore be calculated by classical mechanics for the different groups, R, and atoms, X.

The calculated and experimental A factors are compared for each type of halogen in Table II. In only one instance does A_{exp} differ from A_{calc} by more than a factor of 4. The transition state theory, therefore, accounts very well for the magnitude of the A factors. Even the deviations from the calculated values show a fairly regular pattern as can be seen by comparing the columns of ratios. This encourages us to think that the experimental results are adequate to sustain the test of a more precise theory if

TABLE II
A factors for halogen atom reactions

RH	log A_{exp}/A_{calc}		
	F	Cl	Br
H_2	+0.29	+0.01	+0.24
CH_4	+0.24	−0.68	−0.36
Primary C—H bonds			
C_2H_6	0.00*	−0.10	−0.41
C_3H_8	−0.05	+0.25	—
n-C_4H_{10}	−0.03	+0.20	—
iso-C_4H_{10}	+0.04	+0.24	—
neo-C_5H_{12}	+0.06	+0.31	+0.03
Secondary C—H bonds			
C_3H_8	−0.03	+0.52	+0.18
n-C_4H_{10}	+0.08	+0.50	+0.08
cyclo-C_3H_6	−0.17	−0.16	—
cyclo-C_4H_8	—	+0.56	—
Tertiary C—H bonds			
iso-C_4H_{10}	+0.15	+0.41	+0.12

*This value is assumed and the others for fluorine based on it.

one could be found. Since the deviations are more extreme for the heavier halogens, it is likely that the wagging of the H—X bond or the bending of the C—H—X bonds have not been correctly accounted for.

The Activation Energies

The activation energies of the reactions of the higher hydrocarbons with chlorine closely approach zero. It is not surprising that no differences between the activation energies for attack on the higher hydrocarbons by fluorine could be detected. There is probably no energy barrier to attack on these compounds.

The activation energies of the bromine atom reactions vary widely and are of greater interest because of the relation that they bear to the strengths of the bonds broken. The heat of reaction is related to the activation energies for the forward and reverse reactions by the equation

$$\Delta H_1 = E_1 - E_{-1}.$$

Since $D(H—Br)$ is known, $D(R^1—H)$ can be found if E_1 and E_{-1} are measured. At the moment, the values of E_{-1} are not accurately known and consequently the measurements do not yield the bond strengths directly. Until the E_{-1}'s have been determined it is convenient to use the Polanyi relation as a method of interpolation. This leads to the results shown below, which is based on the currently accepted values of $D(Me—H)$ and $D(Bu^t—H)$.

R	E_1	E_{-1}	$D(R—H)$
Me	18.3	1.8	102.5
Et	13.4	(2.5)	96.9
Pr^i	10.2	(3.1)	93.1
Bu^t	7.5	(3.6)	90.0

Information about E_{-1} can be obtained by photolysing a source of R^1 in a mixture of hydrogen bromide and iodine. The products are then analyzed for RH and RI. Hence

$$\frac{k_{-1}}{k_2} = \frac{R_{R^1H}}{R_{R^1I}} \frac{[I_2]}{[HBr]}$$

where k_3 refers to

$$R^1 + I_2 = R^1I + I. \hspace{3cm} [3]$$

So far preliminary experiments have been carried out with methyl ethyl ketone as the source of ethyl radicals. Hence we find that

$$E_{-1} - E_3 = 2.3 \text{ kcal mole}^{-1}.$$

It seems likely that the activation energies for the attack of radicals on iodine are very small and may well be zero. The value for ethyl agrees well with that listed above. Further investigations along these lines are clearly required.

Polar Effects

Although bond strengths largely determine the activation energies of the reactions of halogen atoms, polar effects are also important. This has been realized for some years. Recent experiments by Fredricks and Tedder (12) have extended our knowledge. We have attempted to study polar effects in the fluorination, chlorination, and less systematically, in the bromination of halogenated methanes. Fluorination is the most satisfactory because the reactions are so exothermic that the bond strengths are unlikely to be important, and all variations can be ascribed to the polar nature of the activated complexes. The available results are shown in Table III. The first conclusion to be drawn from the table is that more results are needed. The second is that there is little parallelism between the reactivities of the halogenated methanes and the α-hydrogen atoms in the halogenated n-butanes.

TABLE III

Relative rate constants for the reactions of halogen atoms with halogenated methanes

	F	Cl	Br
CH_4	1	1	1
CH_3Cl	0.33*	4.9, 0.7†	90, 34†
CH_2Cl_2	0.07*	7.5	—
$CHCl_3$	0.6*	3.9	—
CH_3Br	0.23*	0.3†	14
CH_3F	0.3†	0.9†	10†
Temp., °C	25	100, 146†	100, 146†

*Values obtained at Edinburgh by Dr. R. Foon.
†Reactivities of α-hydrogen atoms in halogenated butanes.

REFERENCES

1. H. O. PRITCHARD, J. B. PYKE, and A. F. TROTMAN-DICKENSON. J. Am. Chem. Soc. 77, 2629 (1955).
2. P. D. MERCER and H. O. PRITCHARD. J. Phys. Chem. 63, 1468 (1959).
3. H. B. HASS, E. T. McBEE, and P. WEBER. Ind. Eng. Chem. 27, 1190 (1935); 28, 333 (1936).
4. J. H. KNOX. Chem. & Ind. 1631 (1955).
5. G. B. KISTIAKOWSKY and E. R. VAN ARTSDALEN. J. Chem. Phys. 12, 479 (1944).
6. S. W. BENSON and J. H. BUSS. J. Chem. Phys. 28, 301 (1958).
7. P. G. ASHMORE and J. CHANMUGAM. Trans. Faraday Soc. 49, 254 (1953).
8. G. C. FETTIS, J. H. KNOX, and A. F. TROTMAN-DICKENSON. J. Chem. Soc. 1064 (1960).
9. J. H. KNOX and R. L. NELSON. Trans. Faraday Soc. 55, 937 (1959).
10. G. C. FETTIS, J. H. KNOX, and A. F. TROTMAN-DICKENSON. Submitted for publication.
11. K. S. PITZER. J. Am. Chem. Soc. 79, 1804 (1957).
12. P. S. FREDRICKS and J. M. TEDDER. J. Chem. Soc. 144 (1960).

SURFACE-CATALYZED ATOM RECOMBINATIONS THAT PRODUCE EXCITED MOLECULES[1]

Paul Harteck, Robert R. Reeves, and Gene Mannella

ABSTRACT

Various metal surfaces such as nickel, cobalt, copper, and silver give rise to a reddish uminosity in a stream of N- and O-atoms. Spectroscopic and photographic analysis of these glows indicate the formation of electronically excited molecules on the metal surface which diffuse into the gas phase and radiate. Two parallel processes are involved: the formation of an NO($B\ ^2\Pi$), which results in NO β radiation, and the formation of an $N_2(A\ ^3\Sigma_u^+)$, which, in collision, crosses into the $N_2(B\ ^3\Pi_g)$ state and then radiates back to the $A\ ^3\Sigma_u^+$, giving the N_2 first positive system. The N_2 first positive system observed here shows the strongest bands from $v' = 8$ and 6; these vibrational levels straddle the $A\ ^3\Sigma_u^+ - B\ ^3\Pi_g$ potential energy curve crossing point. This crossing-over of N_2 molecules into the ($B\ ^3\Pi_g$) at this point may explain the observed strong $v' = 6$ transition in normal N-atom recombination if it is assumed that some of the N-atoms recombine into the $A\ ^3\Sigma_u^+$ in addition to the $^5\Sigma_g^+$ state.

The N_2 second positive system ($C\ ^3\Pi_u \rightarrow B\ ^3\Pi_g$) has also been observed over copper in an N- and O-atom stream. This is most surprising since the $N_2(C\ ^3\Pi_u)$ has about 1.4 ev more than D_{N_2}.

INTRODUCTION

A program of research in upper atmosphere chemistry has been underway in this laboratory for the past several years. This investigation has centered about the reactions of N-atoms and O-atoms. The results of this study to date have included determinations of the rate coefficients of the following reactions (1, 2, 3).

$$NO + O + M \rightarrow NO_2 + M \qquad [1]$$

$$N + N + M \rightarrow N_2 + M \qquad [2]$$

$$O + O + M \rightarrow O_2 + M \qquad [3]$$

In order to determine the absolute atom concentrations necessary to obtain the rate constant in the second-order reactions [2] and [3], gas-phase titration procedures were developed for each of the atom species. A modified procedure was then developed which permitted the titration of mixed N- and O-atom streams in a single step. During some of the work with mixed N- and O-atom streams, silver foil was used to catalytically recombine the O-atoms, leaving the N-atoms unchanged. It was noticed in this work that a reddish glow appeared adjacent to the silver surface, particularly if the silver had contacted the orthophosphoric acid used to condition the walls of the decay tube. Further investigation showed that the glow was definitely in the gas phase and was not a corona, since it slowly faded out with the afterglows if the discharges were turned off. Further study of this glow showed it to be due to the surface-catalyzed recombination of N- and O-atoms to form electronically excited molecules.

DISCUSSION

It was subsequently discovered that cobalt and nickel also produced the luminosity, but much brighter than over the silver. The glow grew in size with decreasing pressure

and was unaffected by magnetic fields. Spectroscopic analysis showed the first positive system of N_2 and the NO β bands. The mixing of N- and O-atom streams had been observed to produce the same band systems by the gas-phase reactions

$$N(^4S) + N(^4S) + M \rightarrow N_2(^1\Sigma_g^+) + M \qquad [2a]$$

$$N_2(^1\Sigma_g^+) \rightarrow N_2(B\ ^3\Pi_g)_{v=12} \qquad [2b]$$

$$N_2(B\ ^3\Pi_g) \rightarrow N_2(A\ ^3\Sigma_u^+) + h\nu\ \text{(1st positive)} \qquad [2c]$$

and

$$N(^4S) + O(^3P) + M \rightarrow NO(B\ ^2\Pi) + M \qquad [4]$$

$$NO(B\ ^2\Pi) \rightarrow NO(X\ ^2\Pi) + h\nu\ (\beta\ \text{bands}) \qquad [4a]$$
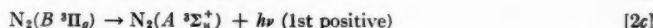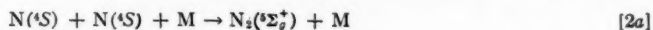
However, several important differences were apparent in the spectral analysis of the glows produced over the metals. The radiation from [2c] showed the strongest transitions to be from $v' = 12, 11, 10 \ldots$ The spectrum of the glow showed the most intense bands to be from $v' = 8$ and 6. Also, the mixing of N- and O-atom streams is observed to produce NO γ bands in addition to the β bands. No γ bands were observable on our plates.

Thus, it was apparent that the metal surface was catalytically recombining atoms into an electronically excited state. This molecule, instea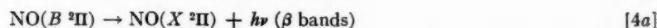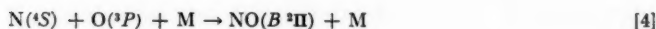d of giving its energy of excitation and coming off the surface in the ground state, was actually diffusing into the gas phase and radiating. Since both N- and O-atoms appeared necessary to produce the glow, it was postulated that the primary molecule being formed was the $NO(B\ ^2\Pi)$. This species could be formed on the metal surface, diffuse into the gas phase, and then radiate or react with an N-atom to form $N_2(B\ ^3\Pi_g)$, which then radiated. The early work done on nickel produced glows which were several millimeters thick and the lifetime estimated from the diffusion distance was not inconsistent with the available estimates of the lifetime of the $NO(B\ ^2\Pi)$. However, cobalt produced a very enhanced glow at 1 mm pressure, which was 10–15 mm thick and which required only a very small amount of O-atoms. Photographic analysis of this glow using red and blue filters showed two parallel radiations: an intense blue extending only a few millimeters into the gas phase, and a red which extended very far out into the gas phase and which showed an unsymmetry due to the flowing stream which was not visible to the unaided eye. When nickel was used, a strong blue was evident and only a medium red; when cobalt was used, practically no blue appeared but the red was very large.

From these results it was concluded that two parallel processes were occurring on the surface. One involved the formation of $NO(B\ ^2\Pi)$ via [4]. This molecule leaves the surface and goes into the gas phase where it radiates. The thickness of the blue radiation is in excellent agreement with the diffusion distance calculated using the lifetime of 10^{-6} sec recently reported in the literature (4).

The second process occurring must involve the formation of an excited N_2 as the primary product. It is possible to explain the strong radiation from $v' = 8$ and 6 and the long lifetime of the species responsible for the glow by assuming that an $N_2(A\ ^3\Sigma_u^+)$ is formed on the surface. (In the case of cobalt, the small amount of O-atoms necessary to enhance the glow are probably required to condition the metal surface and permit the absorbed N-atoms which eventually form the excited molecule to be attached with an electron volt or less.) The $N_2(A\ ^3\Sigma_u^+)$ and $(B\ ^3\Pi_g)$ potential energy curves cross at

about 8.5–9.0 ev or $v' = 8$–6. The metastable $N_2(A\ ^3\Sigma_u^+)$, which is the upper level of the well-known Vegard–Kaplan system, forms on the metal surface, diffuses into the gas phase and, by collision, crosses into the $(B\ ^3\Pi_g)$ state. This crossing-over would be at $v' = 8$–6 and the $N_2(B\ ^3\Pi_g)$ would immediately radiate back to the $(A\ ^3\Sigma_u^+)$. The lifetime of the species responsible for the red glow as calculated both from the diffusion distances and the linear velocity of the gas stream and the unsymmetry of the glow is about 10^{-3} sec. This would represent the time required by the $N_2(A\ ^3\Sigma_u^+)$ to relax vibrationally to the crossing point and by collision cross into the $(B\ ^3\Pi_g)$ state. Since the radiative lifetime of the $(A\ ^3\Sigma_u^+)$ is reported to be at least 10^{-2} sec (5), the time interval of 10^{-3} sec is sufficient for any necessary relaxation and the crossing-over to occur.

The $N_2(A\ ^3\Sigma_u^+)$–$(B\ ^3\Pi_g)$ crossing may have another interesting ramification in the presently accepted theory on N-atom recombination as outlined in [2a], [2b], and [2c] (6, 7). This theory postulates the $N_2(^5\Sigma_g^+)$–$(B\ ^3\Pi_g)$ crossing to be at $v' = 12$ and is supported by observations that bands from $v' = 12$, 11, and 10 are the most intense and the transition from $v' = 13$ is never observed in the nitrogen afterglow. However, an unusually intense band from $v' = 6$ has been discussed by several authors (8, 9). No really conclusive explanation has ever been offered for this observation. It is suggested that the lower levels of the $(B\ ^3\Pi_g)$ are populated by an analogous mechanism via the formation of a certain percentage of $(A\ ^3\Sigma_u^+)$ molecules in normal N-atom recombination.

From the observations and comparison of glows over cobalt and nickel, it appears that cobalt favors the formation of $N_2(A\ ^3\Sigma_u^+)$, while nickel favors the $NO(B\ ^2\Pi)$. The glows over nickel always appear a little bluish to the eye. In the case of $N_2(A\ ^3\Sigma_u^+)$ formation on the surface of cobalt, the reaction

$$N_2(A\ ^3\Sigma_u^+) + O\ ^3P \rightarrow NO(B\ ^2\Pi) + N(^4S) \qquad [5]$$
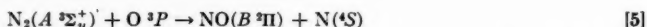
could account for some of the small amount of blue observed over cobalt. The $NO(B\ ^2\Pi)$ over nickel could similarly react,

$$NO(B\ ^2\Pi) + N(^4S) \rightarrow N_2(B\ ^3\Pi_g) + O(^3P), \qquad [6]$$
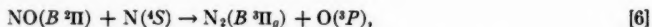
accounting for some of the first positive bands there. To what extent these exchange reactions occur is not known at the present.

A red glow with N- and O-atoms similar to those produced over silver, nickel, and cobalt has also been produced over copper, although it has been reported in the literature that electrolytically deposited copper can be used to extinguish the nitrogen afterglow (10, 11). The copper surface is slightly attacked. However, if the copper is maintained at approximately 15–20° C in a stream of N-atoms alone, the blue glow of the second positive system of nitrogen appears $(C\ ^3\Pi_u \rightarrow B\ ^3\Pi_g)$. This blue glow is less intense than the red glows observed earlier and extends about 2 mm into the gas phase. Transitions from the $(C\ ^3\Pi_u)$ state are indeed very striking, since the excitation of this level is about 11.2 ev, compared with D_{N_2}, which is only 9.76 ev. The mechanism for such a reaction must then necessarily involve three atoms or two excited species.

CONCLUSIONS

Surface-catalyzed excitation of N- and O-atoms can give rise to a number of excited species. What we originally believed to be a rather singular effect must now include the formation of $NO(B\ ^2\Pi)$, $N_2(A\ ^3\Sigma_u^+)$, and even $N_2(C\ ^3\Pi_u)$. We believe that this is the first recognition of this effect.

REFERENCES

1. P. HARTECK, R. R. REEVES, and G. MANNELLA. J. Chem. Phys. **29,** 1333 (1958).
2. P. HARTECK, R. R. REEVES, and G. MANNELLA. J. Chem. Phys. **29,** 608 (1958).
3. R. R. REEVES, G. MANNELLA, and P. HARTECK. J. Chem. Phys. **32,** 946 (1960).
4. J. C. KECK *et al.* Ann. Phys. (N.Y.), **7,** 1 (1959).
5. W. LICHTEN. J. Chem. Phys. **26,** 306 (1957).
6. J. BERKOWITZ, W. A. CHUPKA, and G. B. KISTIAKOWSKY. J. Chem. Phys. **25,** 457 (1956).
7. A. G. GAYDON. Dissociation energies. Dover, New York. 1950.
8. O. OLDENBERG. Phys. Rev. **90,** 727 (1953).
9. G. CARIO and J. KAPLAN. Z. Physik, **58,** 769 (1920).
10. RAYLEIGH. Proc. Roy. Soc. A, **85,** 219 (1911).
11. E. J. B. WILLEY. J. Chem. Soc. 2188 (1927).

ON THE EXCITATION OF THE EMISSION SPECTRUM OF NCO IN SOLID MATRICES CONDENSED AT 4° K[1]

R. W. NICHOLLS[2] AND S. L. N. G. KRISHNAMACHARI[3]

ABSTRACT

Seventeen broad (∼50 Å wide) spectral features have been excited in emission between 3000 Å and 4600 Å in the products of a microwave discharge through N_2 deposited on a cold (4° K) surface on which the discharge products of $CO + N_2$ had been previously condensed. The features which lie between 3650 Å and 4470 Å show close agreement with those observed in absorption by Dixon during the flash photolysis of NCO and assigned to the $A\ ^2\Sigma - X\ ^2\Pi_i$ transition. It therefore seems likely that the emission features arise from NCO also as a result of the reaction

$$N(^2P) + CO(X\ ^1\Sigma^+) \rightarrow NCO \begin{cases} A\ ^2\Sigma^+ \\ B\ ^2\Pi_i \end{cases}$$
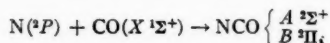
at the solid surface.

1. INTRODUCTION

During the past few years, extensive spectroscopic studies have been made upon the luminosities arising from solids condensed between 1° K and 80° K from the products of microwave discharges maintained in a variety of gases, but mostly in N_2, A, O_2, and mixtures of them (1, 2, 3, 4, 5). Much of the work has been carried out with N_2–A mixtures (sometimes including a small oxygen impurity) (3, 5) and the spectra in these cases consisted almost entirely of atomic features of NI and OI and specific band systems of N_2, O_2, NO, and NO_2. Nearly all of the spectral features so far identified arise from transitions which, in the gas phase at least, are relatively forbidden (e.g. the "α" (^2D–^4S), and "μ" (^2P–^4S) features of NI; the "β" (^1S–^1D) feature of OI; the Vegard–Kaplan ($A\ ^3\Sigma_u^+$–$X\ ^1\Sigma_g^+$) system of N_2; the Herzberg ($A\ ^3\Sigma^+$–$X\ ^3\Sigma_g^-$) system of O_2; and the "M" ($^4\Pi$–$^2\Pi$) system of NO). Some allowed transitions (e.g. NO β ($B\ ^2\Pi$–$X\ ^2\Pi$); NO γ ($A\ ^2E$–$X\ ^2\Pi$) systems) have been reported (3). In general, however, the forbidden transitions predominate in the spectra of the solids because short-lived excited species decay radiatively during transit between the discharge and the cooled surface, while the longer lived metastable excited species are deposited and isolated from radiationless de-excitation influences before they can loose their energy.

It has therefore been thought worth while to attempt to excite forbidden transitions of other molecules, particularly those containing carbon, and also to attempt to excite in emission the spectra of polyatomic species. Most of the work on polyatomic spectra of low temperature solid matrices has so far been in absorption (6) although the "B" bands of NO_2 have been recognized in emission for some time.

This paper therefore describes some experiments with discharged $N_2 + CO$ and the conditions under which NCO may be excited in the condensed solid. A subsequent paper (7) will discuss conditions under which CO_2^+ spectra can be excited.

The electronic spectrum of NCO was first observed in emission at low dispersion both in fluorescence from, and in discharges through, C_2H_5NCO, and later in absorption at much higher dispersion by flash photolysis of the same compound (8). Subsequent high dispersion studies by Dixon (9), of the absorption spectrum arising from flash photolysis of HNCO, lead to definitive identifications and rotational analysis of bands of the

---

$A\ ^2\Sigma^+-X\ ^2\Pi_i$ transition between 3603 Å and 4484 Å. Dixon (10) has recently analyzed bands of the $B\ ^2\Pi_r-X\ ^2\Pi_i$ transition between 2650 Å and 3200 Å using the same technique. Robinson and McCarty (11) have also reported identification of one strong absorption feature (at 4400 Å) of NCO in a low temperature solid condensed at 4.2° K from a discharge through N_2, O_2, and CH_4.

2. EXPERIMENTAL PROCEDURE AND RESULTS

Our experiments were carried out in a pyrex dewar flask, which has been described by Schoen *et al.* (12), in which the bottom of the central liquid helium container was a wedge-shaped "finger" on which the deposits were formed. All of the helium container except the terminal finger was protected against thermal radiation by a concentric cylindrical pyrex shield which contained liquid nitrogen. N_2 and CO gas flows were individually controlled by needle valves and were measured by floating ball flowmeters. The gas mixture was passed through a 2450 Mc/sec microwave discharge maintained at a few millimeters of pressure, and the discharge products flowed upwards through a "Wood" type light trap onto the liquid helium cooled finger. Prior to starting the discharge, the space around the finger was maintained at a vacuum of better than 10^{-6} mm Hg. During deposition it is believed that the pressure does not rise above 1 micron Hg.

The solid deposit formed on the pyrex finger exhibited a feeble blue luminescence over à wide range of N_2:CO mixtures. Its spectrum appears to be CO_2^+ and will be described elsewhere (7). After the solid condensed from the mixed gas stream had been built up for a few minutes, the CO flow was stopped and the deposition of discharged N_2 was continued. A marked surface color change from blue to bright yellow occurred in the luminescence from the deposit and the spectrum was easily recorded in a few minutes exposure of Kodak 103-F emulsion in a Hilger F/4 quartz spectrograph.

A typical spectrum is shown in Fig. 1 together with a mercury arc calibration. The spectrum consists of the atomic features "μ" ($^2P-^4S$) of NI at 3478 Å, "α" ($^2D-^4S$) of NI at 5228 Å, "β" ($^1S-^1D$) of OI at 5549 Å together with 18 broad (50 Å) features between 3000 Å and 4600 Å. Fifteen of these features (3206 Å–4600 Å) are relatively strong and three (3000 Å–3206 Å) are extremely weak. The wavelengths of the bands including their widths and estimates of intensity on a scale of 0 to 5 are given in Table I, and,

TABLE I

Wavelengths and identification

Wavelength range (Å) and eye estimate intensities on a scale of 0–5	NCO band-head wavelengths (Å) and eye estimate intensities on a scale of 0–100 (9, 10)	Transition (9, 10)	Comments
3000–3015 (0)			CO_2^+
3075–3090 (0)			
3140–3165 (0)	⎧3150 (strong) ⎨3148	$B\ ^2\Pi_i-X\ ^2\Pi_i$ (0,0,0–0,0,0)	See (10)
3206–3230 (1)			
3240–3250 (2)			CO_2^+
3270–3305 (2)		All following transitions are $A\ ^2\Sigma-X\ ^2\Pi_i$	
3335–3380 (3)			
3410–3460 (3)			
3480–3500 (4)			CO_2^+; NI (μ)
3500–3545 (4)			
3570–3630 (5)			Weak (<5) $A\ ^2\Sigma-X\ ^2\Pi_i$ feature 3603–3630 Å

TABLE I (*concluded*)

Wavelength range (Å) and eye estimate intensities on a scale of 0–5	NCO band-head wavelengths (Å) and eye estimate intensities on a scale of 0–100 (9, 10)	Transition (9, 10)	Comments
3650–3710 (5)	3642 (20)	$0,0^0,2$ $^2\Sigma^+$–$0,0^1,0$ $^2\Pi_i$	
	3655 (10)	$0,0^0,2$ $^2\Sigma^+$–$0,0^1,0$ $^2\Pi_i$	
	3733 (15)	$0,2^0,1$ $^2\Sigma^+$–$0,0^1,0$ $^2\Pi_i$	
3750–3800 (4)	3786 (15)	$1,0^0,1$ $^2\Sigma^+$–$0,0^1,0$ $^2\Pi_i$	
	3787 (10)	$0,2^0,1$ $^2\Sigma^+$–$0,0^1,0$ $^2\Pi_i$	
	3800 (10)	$1,0^0,1$ $^2\Sigma^+$–$0,0^1,0$ $^2\Pi_i$	
3800–3830 (5)			CO_2^+
3860–3920 (5)	3927 (5)	$1,2^0,0$ $^2\Sigma^+$–$0,0^1,0$ $^2\Pi_i$	Weak (<5) A $^2\Sigma$–X $^2\Pi_i$ bands 3874–3907 Å
	3949 (5)	$0,1^1,1$ $^2\Pi$–$0,1^0,0$ $^2\Sigma^+$	
	3956 (20)	$0,1^1,1$ $^2\Pi$–$0,1^2,0$ $^2\Delta_i$	
3940–4025 (4)	3971 (15)		
	3977 (40)	$0,1^1,1$ $^2\Pi$–$0,1^2,0$ $^2\Delta_i$	
	3981 (10)	$0,0^0,1$ $^2\Sigma$–$0,0^1,0$ $^2\Pi_i$	
	3993 (40)	$0,0^0,1$ $^2\Sigma$–$0,0^1,0$ $^2\Pi_i$	
	4099 (5)	$0,3^1,0$ $^2\Pi$–$0,1^0,0$ $^2\Sigma^+$	
4080–4120 (3)	4106 (10)	$0,3^1,0$ $^2\Pi$–$0,1^2,0$ $^2\Delta_i$	
	4122.6 (10)	$1,1^1,0$ $^2\Pi$–$0,1^0,0$ $^2\Sigma^+$	
	4122.7 (10)	$0,3^1,0$ $^2\Pi$–$0,1^2,0$ $^2\Delta_i$	
	4128 (5)	$1,1^1,0$ $^2\Pi$–$0,1^2,0$ $^2\Delta_i$	No comparable features observed in solid spectrum
	4134.6 (30)	$0,2^0,0$ $^2\Sigma^+$–$0,0^1,0$ $^2\Pi_i$	
	4137 (10)	$0,2^0,0$ $^2\Sigma^+$–$0,0^1,0$ $^2\Pi_i$	
4145–4180 (1)	4144 (5)	$1,1^1,0$ $^2\Pi$–$0,1^2,0$ $^2\Delta_i$	
	4150.1 (30)	$1,0^0,0$ $^2\Sigma^+$–$0,0^1,0$ $^2\Pi_i$	
	4150.25 (30)	$0,2^0,0$ $^2\Sigma^+$–$0,0^1,0$ $^2\Pi_i$	
	4154 (10)	$1,0^0,0$ $^2\Sigma^+$–$0,0^1,0$ $^2\Pi_i$	
	4167 (30)	$1,0^0,0$ $^2\Sigma^+$–$0,0^1,0$ $^2\Pi_i$	
4180–4220 (1)			CO_2^+
	4257 (10)	$0,1^1,0$ $^2\Pi$–$0,0^1,0$ $^2\Pi_i$	
	4275 (10)	$0,1^1,0$ $^2\Pi$–$0,0^1,0$ $^2\Pi_i$	
	4328 (5)	$0,2^2,0$ $^2\Delta$–$0,2^3,0$ $^2\phi_i$	
4275–4370 (2)	4348 (30)	$0,1^1,0$ $^2\Pi$–$0,1^0,0$ $^2\Sigma^+$	
	4350 (20)	$0,1^1,0$ $^2\Pi$–$0,1^0,0$ $^2\Sigma^+$	
	4351 (10)	$0,1^1,0$ $^2\Pi$–$0,1^0,0$ $^2\Sigma^+$	
	4357 (30)	$0,1^1,0$ $^2\Pi$–$0,1^2,0$ $^2\Delta_i$	
	4361 (5)	$0,1^1,0$ $^2\Pi$–$0,1^2,0$ $^2\Delta_i$	
	4375 (30)	$0,1^1,0$ $^2\Pi$–$0,1^2,0$ $^2\Delta_i$	
	4385 (100)	$0,0^0,0$ $^2\Sigma^+$–$0,0^1,0$ $^2\Pi_i$	
	4389 (30)	$0,0^0,0$ $^2\Sigma^+$–$0,0^1,0$ $^2\Pi_i$	
4400–4470 (1)	4404 (100)	$0,0^0,0$ $^2\Sigma^+$–$0,0^1,0$ $^2\Pi_i$	
	4409 (10)	$0,0^0,0$ $^2\Sigma^+$–$0,0^1,0$ $^2\Pi_i$	
4560–4600 (1)			

as is discussed below, there are good reasons for thinking that 17 of the bands are due to NCO. Owing to the diffuseness of the features there is perhaps a 10 Å uncertainty in the wavelengths.

DISCUSSION

Dixon's band-head wavelengths, transition assignments, and rough intensity estimates for the NCO A $^2\Sigma^+$–X $^2\Pi_i$ system are also given in Table I grouped for ease of comparison with our features. He used an intensity scale of 0 to 100 and we have only included bands with intensities greater than 5. Not only is a very strong correlation seen
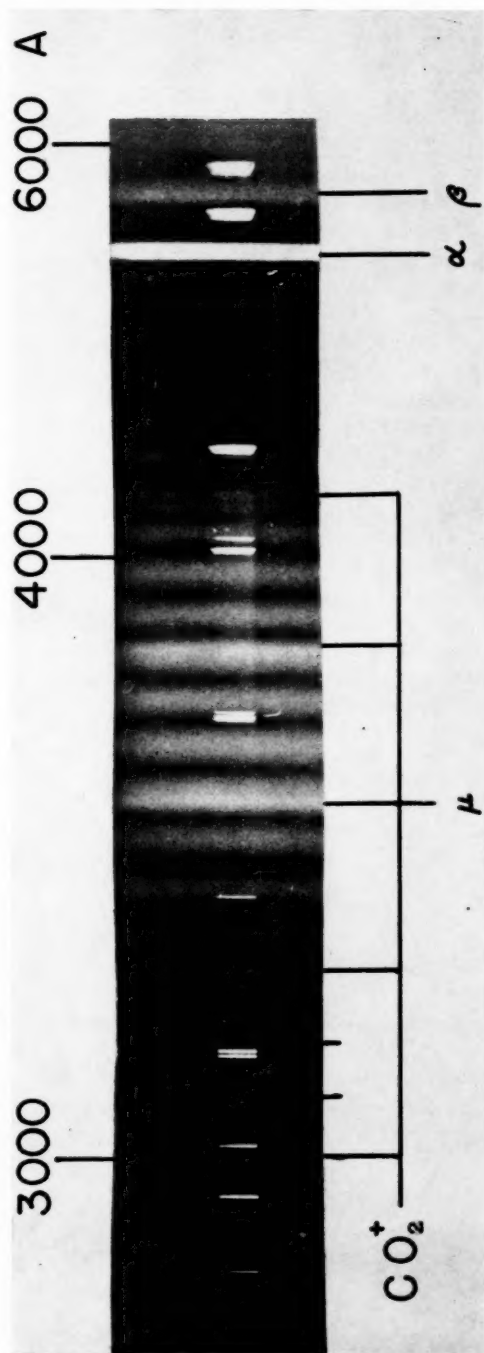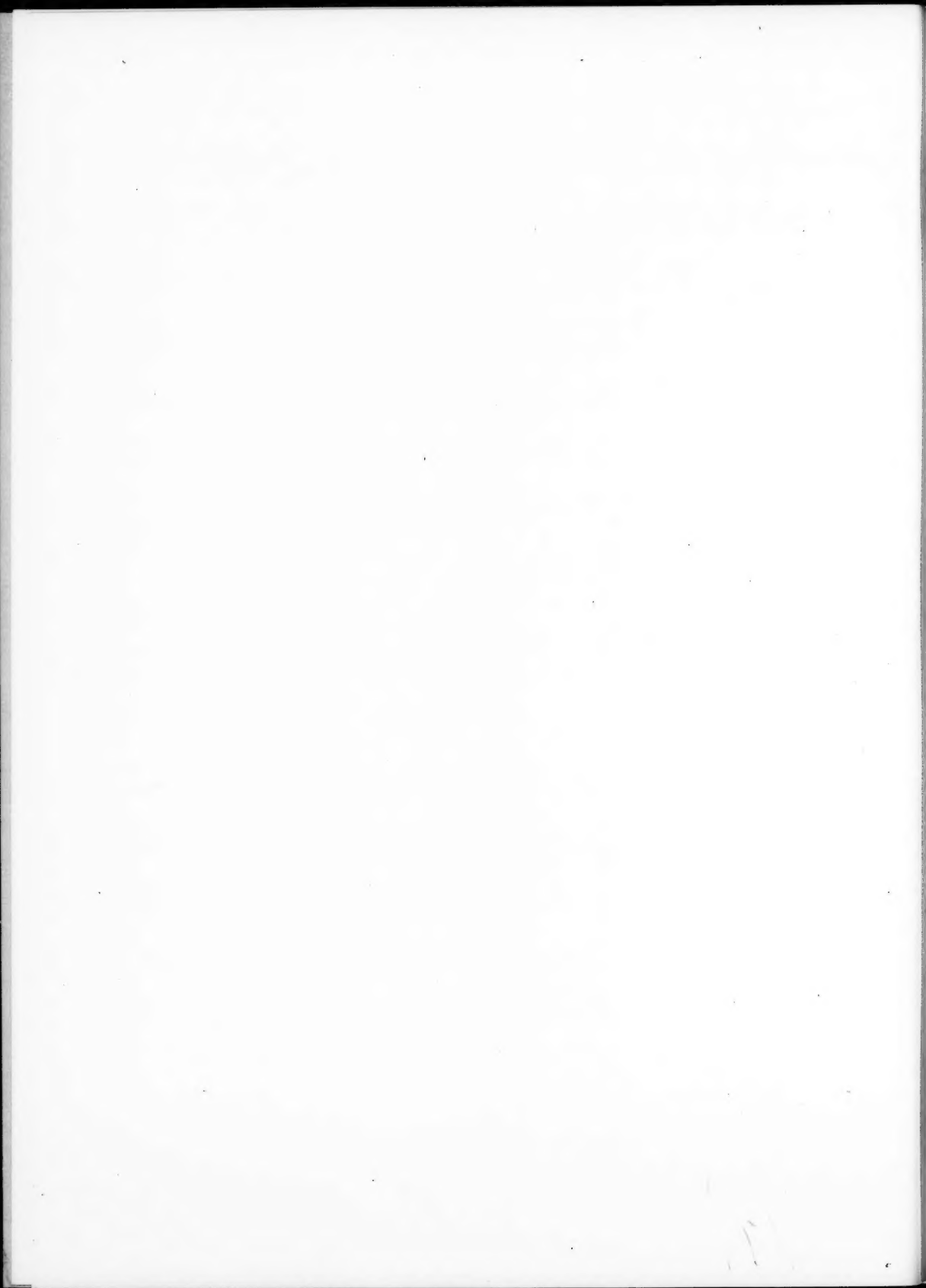
Plate I

Fig. 1. Spectrum of luminosity arising from the action of discharged nitrogen on CO at 4° K.
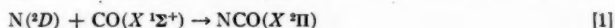
in Table I between groups of Dixon's band heads and each of our features between 3650 Å and 4470 Å, but there is also good correlation between the spaces between our features and the regions where Dixon records absence of bands or very weak bands.
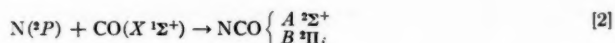
On this basis it seems very plausible to assign not only those of our features with which there is a strong correlation with those of Dixon to overlaps of strong NCO bands but also to assign those which lie between 3000 Å and 3630 Å and between 4560 Å and 4600 Å (which lie outside the range reported in absorption) to the same emitter.

Each of our features undoubtedly arises from the overlap of a number of adjacent bands whose rotational structure is not very extensive at the low temperature of the source. It will be observed in Fig. 1 that all or part of each of five features has been assigned to bands of CO_2^+. These assignments derive from experiments referred to above (7) on the spectra of condensed discharged $CO + N_2$. One CO_2^+ feature in Fig. 1 is also assigned in part to "μ" of NI. The three features between 3000 Å and 3165 Å are extremely weak and there is a possibility that there is a contribution to them from bands of the $B\,{}^2\Pi_i\text{–}X\,{}^2\Pi_i$ system of NCO reported by Dixon (10) to lie between 2677 Å and 3167 Å. In particular the 3140–3165 feature may be the strong 000–000 transition of this system. Alternatively these bands may be a continuation of the $A\,{}^2\Sigma\text{–}X\,{}^2\Pi_i$ system.

While the flash photolysis experiments involve the decomposition of HNCO into fragments, the mechanism operative in our experiments is almost certainly one of synthesis of NCO [either in the gas phase near the cold finger (no NCO spectrum is seen from the discharge itself), or as is more likely, on the surface of the cold finger itself]. This surface was prepared by deposition of discharged $CO + N_2$ and will therefore have a high concentration of ground state $(X\,{}^1\Sigma^+)$ CO molecules on it. The surface was then treated with the discharge products of N_2, a significant number of which are N atoms in ${}^2P$, ${}^2D$, and ${}^4S$ (ground) states as is shown by the presence of "α" and "μ" in the spectra. Thus $N + CO$ collisions occur at the surface. Dixon has pointed out (9) that

$$N({}^2D) + CO(X\,{}^1\Sigma^+) \rightarrow NCO(X\,{}^2\Pi) \tag{1}$$

and

$$N({}^2P) + CO(X\,{}^1\Sigma^+) \rightarrow NCO \begin{cases} A\,{}^2\Sigma^+ \\ B\,{}^2\Pi_i \end{cases} \tag{2}$$

are energetically possible and plausible processes. Before collision, the CO molecules were most probably in the $v = 0$ level, but the N atoms will collide with the kinetic energy of the discharge $(T \sim 300\text{–}400° \text{K})$. NCO can therefore be formed in excited vibrational levels such as is required by the identifications of Table I. It may be remarked in passing that the possibility of forming NCO $(B\,{}^2\Pi_i)$ by equation [2] makes reasonably plausible the possible assignment of our 3140–3165 feature to the strong (000–000) transition of the $B\,{}^2\Pi\text{–}X\,{}^2\Sigma$ transition.

It should not be overlooked that it may also be possible to form CON and CNO in the collision mechanism (equation [2]) and with our experimental arrangement. Further work on these possibilities is in progress.

ACKNOWLEDGMENTS

REFERENCES

1. A. Bass and H. P. Broida.   The trapping of free radicals at low temperatures. Academic Press, Inc., New York. 1960.
2. A. Bass and H. P. Broida.   Phys. Rev. **101**, 1740 (1956).
3. M. Peyron and H. P. Broida.   J. Chem. Phys. **30**, 139 (1959).
4. M. Peyron, I. Hörl, H. Brown, and H. P. Broida.   J. Chem. Phys. **30**, 1304 (1959).
5. H. P. Broida and M. Peyron.   J. Chem. Phys. **32**, 1068 (1960).
6. D. A. Ramsay.   Optical spectroscopy of free radicals. 1960. p. 169. Ref. 1.
7. S. L. N. G. Krisnamachari and R. W. Nicholls.   To be published. 1960.
8. R. Holland, D. W. G. Style, R. N. Dixon, and D. A. Ramsay.   Nature, **182**, 336 (1958).
9. R. N. Dixon. Phil. Trans. Roy. Soc. A, **252**, 165 (1960).
10. R. N. Dixon.   Can. J. Phys. **38**, 10 (1960).
11. M. McCarty, Jr. and G. W. Robinson.   J. chim. phys. **56**, 721 (1959).
12. L. J. Schoen, L. E. Kuentzel, and H. P. Broida.   Rev. Sci. Instr. **29**, 633 (1958).

ABSOLUTE RATE MEASUREMENTS OF O-ATOM REACTIONS WITH ETHYLENE AND WITH BUTANE[1]

L. Elias and H. I. Schiff

ABSTRACT

The absolute rate constants for the primary reactions of O-atoms with ethylene and with butane have been determined in a fast-flow system. The O-atoms were produced by electrodeless discharge of O_2 and allowed to react with the hydrocarbon introduced downstream. Addition of a small amount of NO to the gas stream enabled a photometric monitoring of the O-atoms in the reaction zone. The initial atom concentration was determined by NO_2 titration. The reaction could be stopped at any point in the reaction zone by means of a movable surface of cobalt oxide. The hydrocarbon concentration at any point could then be determined by condensation downstream and analysis of the products.

Rate measurements were carried out over the temperature range $-50°$ to $200°$ C. The rates were found to be consistent with a two-body mechanism. For O-atoms with ethylene,

$$k = 1.8(\pm0.6)\times10^{-11}\ e^{-1600/RT} \text{ cm}^3 \text{ molecule}^{-1} \text{ sec}^{-1}$$

and for O-atoms with butane,

$$k = 5.0(\pm1.6)\times10^{-11}\ e^{-4200/RT} \text{ cm}^3 \text{ molecule}^{-1} \text{ sec}^{-1}.$$

INTRODUCTION

Cvetanović has recently measured relative rate constants for the reactions of oxygen atoms with a series of olefins (1). This study enabled him to make interesting deductions about the effect of structure on the rates and mechanisms of these reactions. Absolute rate constants were estimated by comparison with the value for the reaction $O + NO_2$ reported by Ford and Endow (2), which was, in turn, based on the rate constant for the reaction $O + O_2 + M$, obtained by Benson and Axworthy (3) from their mechanism for the thermal decomposition of ozone.

Notwithstanding the high caliber of the work of these authors, it seemed desirable to measure the absolute value of the rate constant directly for one of these olefin reactions. It also seemed important to determine its activation energy and steric factor, since such data are virtually non-existent.

The present paper reports the measurement of the absolute rate constant and its temperature dependence for the reaction of O-atoms with ethylene. For comparison purposes, similar measurements were also obtained for the reaction of O-atoms with n-butane.

Principle of the Method

The rate constant of interest is that of the initial attack of an O-atom on an olefin molecule. The subsequent reactions are complicated and lead to a variety of products which depend on the ratio of atomic to molecular oxygen. Cvetanović has found, however, that the presence of molecular oxygen does not affect the rate of consumption of the olefin (4), which indicates that the initial O-atom attack is rate-determining. Consequently, no attempt was made in this work at a detailed product analysis.

The rate of disappearance of hydrocarbon can then be represented by a simple bimolecular equation,

[1]
$$-\frac{d[RH]}{dt} = k[O][RH].$$

Integration of this equation between reaction time limits t_1 and t_2 gives

[2]
$$\ln \frac{[RH]_1}{[RH]_2} = k \int_{t_1}^{t_2} [O]dt.$$

As a result of secondary reactions, [O] will be a complex function of time. However, in a well-defined flow system, time can be related to distance. [O] can then be measured along the length of the reaction vessel and the integral evaluated graphically. The rate constant is then obtained from the measurement of [RH] at times t_1 and t_2 and the value of the integral in that time interval.

The only assumptions involved in this method for determining k are that RH is neither reformed nor consumed in the secondary reactions. It is extremely unlikely that RH will be the product of any reaction of radicals resulting from the attack of O-atoms on the hydrocarbon. The radicals are also much more likely to react with O_2, which is present in large excess, than with the parent hydrocarbon. The validity of these assumptions, as well as the independence of the rates on $[O_2]$, is attested to by the good agreement of the relative rate constants for butane and ethylene obtained in this work with that obtained by Cvetanović (4) using a completely different technique, and in the absence of O_2.

EXPERIMENTAL

Apparatus

A conventional fast-flow system was used which incorporated the usual arrangement of fine-control needle valves and calibrated flowmeters. Molecular oxygen was dissociated to the extent of a few per cent by a microwave discharge in the manner described previously (5). Precautions were taken to exclude mercury vapor from the apparatus. The discharge tube was connected to the reaction vessel represented in Fig. 1. The latter consisted of a pyrex tube 16 mm i.d. and 30 cm long, surrounded by an outer jacket through which tap water could .be flowed. The reaction vessel was thermostatted at higher temperatures by the vapors of appropriate liquids boiling in a flask attached to the apparatus at F and refluxing in a condenser attached at C. To achieve temperatures below $20°$ C, the outer jacket was replaced by a double-walled vacuum jacket, open at the top, into which could be placed suitable mixtures of ethanol and powdered dry ice.

A movable coil of platinum wire D_1, coated with cobalt oxide, served to remove all the atoms from the gas stream (5). It was mounted on a glass rod which could be moved axially along the reaction tube by rotation of the tygon-covered rod T, which pressed against it. This device was used to stop the reaction at selected positions, and thereby permitted an accurate control of the reaction time.

D_2 was a similar movable coil of copper wire (a less efficient catalyst for O-atom recombination) which was used to decrease the oxygen atom concentration by lowering it into the gas stream.

The hydrocarbon was introduced through the multiple jet J_1, which consisted of a small bulb in which five equally spaced small holes were blown in a plane transverse to the direction of the oxygen stream.
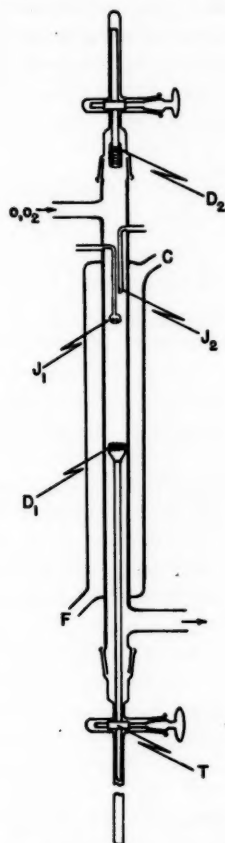
FIG. 1.   Reaction vessel.

Materials

Linde tank oxygen rated to contain less than 0.1% N_2 was used without further purification. Matheson reagent grade ethylene and butane were 'trap-to-trap' distilled before use. Nitric oxide, also a Matheson product, was freed of NO_2 by passage through Caroxite, a commercial CO_2 absorbent. NO_2 was prepared by addition of O_2 to NO and stored with a small excess of O_2.

O-Atom Measurement

In previous studies in this laboratory (5, 6), O-atom concentrations were measured with an isothermal calorimeter. This technique could not be used in the present study, since preliminary experiments indicated that species produced in the secondary reactions liberated heat to the calorimeter. Consequently, a small amount of NO was added to the gas stream through J_2, and the resulting light emission used to monitor the O-atom concentration along the reaction tube. The change in [O] with time was measured photometrically in the manner suggested by Kaufman (7). The feasibility of this method depends on the following facts:

(1) The consumption of O-atoms by NO is relatively slow at these pressures, since it can be represented as occurring by the three-body process

$$O + NO + M \rightarrow NO_2 + M.$$
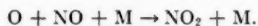
(2) The subsequent reaction

$$O + NO_2 \rightarrow NO + O_2$$

is fast and regenerates the NO so that the NO concentration remains essentially constant.

(3) The light emission is independent of the amount and nature of any third body and can be represented by

$$O + NO \rightarrow NO_2 + h\nu.$$

Thus for a given amount of NO the intensity depends only on the partial pressure of O-atoms.

The relative light intensity was measured by means of a IP21 photomultiplier tube. The phototube housing was mounted on rails and could be moved parallel to the reaction vessel. Collimating slits were used to limit detection of light from a 2-mm section of the reaction tube.

To convert the photometer readings to atom concentrations, it was only necessary to know the absolute value of [O] at one point in the reaction vessel. The value of $[O]_0$, the atom concentration at the inlet J_1, was determined by NO_2 titration. The NO flow was stopped, and an excess amount of NO_2 was added through J_1. The NO produced, which equals $[O]_0$, was trapped downstream with the excess NO_2. The trapped NO was determined by the amount of oxygen consumed in converting the mixture of the oxides to NO_2. It was found that NO could be trapped quantitatively at liquid nitrogen temperature only if the ratio of NO_2 to NO in the oxygen stream was greater than 2. Use of lower ratios resulted in some loss of NO by pumping and by oxidation in the trap. Blank experiments, in which synthetic mixtures of NO_2 and NO were introduced through J_1 with a molecular oxygen stream, showed that the uncertainty in the analysis was less than 2%.

The use of a Wratten 23A filter in front of the collimating slits of the phototube ensured that signal from the weak 'blue' flame resulting from the O-hydrocarbon reaction was negligible relative to that from the O–NO emission.

The presence of the small amount of NO did not affect the rate of the reaction under study, as evidenced from the constancy of the rate constant and the [O] decay curves when the NO flow was changed by a factor of 10 or more. In some experiments with butane the reaction flame was so feeble that the trace of NO formed in the discharge from the N_2 impurity in the oxygen was sufficient for accurate phototube readings. Rate constants determined using this 'afterglow' to monitor [O] were identical with those obtained when the glow was greatly enhanced by addition of NO.

This technique also provided a very sensitive visual test for the efficiency of coil D_1 in removing the atoms and stopping the reaction. A sharp discontinuity of the glow at the top of the coil indicated complete atom consumption. This discontinuity became more diffuse and extended further down the coil at higher atom flows.

Experimental Procedure

In a typical experiment the oxygen was passed through the discharge and the reaction tube for at least an hour to ensure that steady conditions had been achieved; $[O]_0$ was then determined by NO_2 titration. NO was then added through J_2, hydrocarbon

through J_1, and the O-atom profile determined photometrically. The NO flow was stopped, and the coil D_1 was introduced to stop the reaction at some position in the reaction tube. The products were then trapped downstream at liquid nitrogen temperature and removed for analysis when a sufficiently large sample had been collected. During this removal the gas leaving the reaction vessel was made to bypass the trap in order to leave the gas flow undisturbed.

The products were then distilled at $-90°$ C through a column of Caroxite. Mass spectrometric and gas chromatographic analyses showed that the effluent gas consisted only of unreacted hydrocarbon. This indicated that the Caroxite absorbed the oxygen-containing products which were volatile at $-90°$ C. The measurement of unconsumed hydrocarbon could thus be effected in a matter of minutes.

The procedure was then repeated with the coil D_1 at some new position. The determination of [RH] at several positions down the reaction tube permitted the evaluation of k by equation [2] for a variety of time intervals.

The presence of the coil D_1 in the reaction zone should not affect the rate measurements if it recombines atoms much faster than it catalyzes the reaction of O-atoms with the hydrocarbon on its surface. That this condition was fulfilled was shown by the following experiment. A reactant flow could be chosen which resulted in the complete consumption of O-atoms within the length of the reaction tube. For such experiments the coil D_1 was not needed to define the reaction zone. Since [O] decays to zero, no explicit knowledge of t_2 is required to evaluate the integral in equation [2]. The values of $[RH]_1$ and $[RH]_2$ are the concentrations at the inlet and that remaining after all the atoms are consumed. The rate constants obtained in these experiments were indistinguishable from those obtained when the coil was present. Although the presence of the coil evidently does not affect the initial reaction, it might well influence the course of the secondary reactions.

Since the reactions under study were quite exothermic, it was necessary to limit the reactant flow rates to prevent temperature rises which would increase the measured rate constant. Temperature measurements were effected by replacing the D_1 coil asesmbly by a thermocouple well. For the butane reaction, the flow rates used were such that the temperature increase in the reaction zone did not exceed 3 C°. Due to the lower activation energy of the ethylene reaction, a temperature rise of 10 C° could be tolerated without noticing an increase in the measured rate.

RESULTS AND DISCUSSION

Table I shows the results of an experiment in which the ethylene flow rate was sufficiently large to consume all the atoms within the reaction vessel. Columns 2 and 3 show the decrease in [O] and $[C_2H_4]$ with time. The coil D_1 was used to stop the reaction at positions 1, 2, and 5 cm from the jet J_1. The last number in column 3 is the value of $[C_2H_4]$ recovered in the absence of the coil. The rate constants shown in column 6 were calculated from equation [2] for the distance intervals shown in column 5. These results show that the presence of the coil does not affect the rate measurement and that there is no trend in the value of k with a 13-fold change in reaction time. These results also afford a very stringent test on the method, since the ratio of reactant concentrations differ by several orders of magnitude over the time intervals used. It will be noted that the ratio of O-atoms consumed to ethylene consumed (column 4) is never less than one. This is consistent with the basic assumption of the method, viz., that the ethylene is attacked only in the initial reaction. The fact that this ratio decreases and approaches unity at

TABLE I

Rate constant k as a function of reaction time for the reaction $O + C_2H_4$

Distance from J_1 (cm)	10^{-14} [O] (molecule cm^{-3})	10^{-14} [C$_2$H$_4$] (molecule cm^{-3})	$\frac{\Delta[O]}{\Delta[C_2H_4]}$	Distance interval used to calculate k (cm)	$10^{12}\, k$ (cm^3 molecule^{-1} sec^{-1})
0	4.5$_6$	4.62			
			2.3	0–1	0.9
1	0.8$_9$	3.05			
			1.2	1–2	1.2
2	0.4$_2$	2.65			
3	0.2$_1$		1.0	2–5	1.2
5	0.0$_7$	2.30			
7	0.0$_4$				
9	0.0$_2$		1	5–13	1.1
11	0.00				
13	0.00	2.19		0–13	1.0

NOTE: Temperature, 20° C; pressure, 1.0 mm Hg; linear flow, 515 cm/sec.

TABLE II

Effect of pressure on $k(O + C_2H_4)$

Pressure (mm)	0.25	0.49	1.0	2.0	3.4	4.9	7.5
$10^{12}\, k$ (cm^3 molecule^{-1} sec^{-1}	1.2	1.0	1.0	1.2	1.1	1.4	1.3

NOTE: Temperature, 20° C.

TABLE III

Effect of pressure on $k(O + C_4H_{10})$

Pressure (mm)	0.22	0.45	1.0	2.0	3.5	4.2
$10^{14}\, k$ (cm^3 molecule^{-1} sec^{-1})	2.4	2.4	2.4	2.3	2.2	2.4

NOTE: Temperature, 7° C.

TABLE IV

Effect of variation of initial reactant concentrations on $k(O + C_2H_4)$

Expt. No.	10^{-14} [O]$_0$ (molecule cm^{-3})	10^{-14} [C$_2$H$_4$]$_0$ (molecule cm^{-3})	$10^{12}\, k$ (cm^3 molecule^{-1} sec^{-1})
A$_1$	6.1	1.8	1.0
A$_2$	3.0	1.8	1.0
A$_3$	2.0	1.8	1.2
A$_4$	1.0	1.8	1.1
B$_1$	3.0	1.7	1.1
B$_2$	1.5	1.7	1.2
C$_1$	1.6	3.6	1.1
C$_2$	1.6	1.8	1.0
C$_3$	1.6	.9	1.1
D$_1$	3.2	3.9	.9$_3$
D$_2$	3.2	1.6	1.1

NOTE: A and C series: temperature, 20° C; pressure, 3.4 mm.
B and D series: temperature, 20° C; pressure, 1.0 mm.

the end of the reaction suggests (*a*) that O-atom consumption by free radicals becomes less efficient at low values of [O] and (*b*) that free radicals react with O_2 in preference to ethylene.

The independence of the rate constant on total pressure is shown in Table II for the C_2H_4 reaction, and in Table III for the C_4H_{10} reaction. The pressure was mainly due to
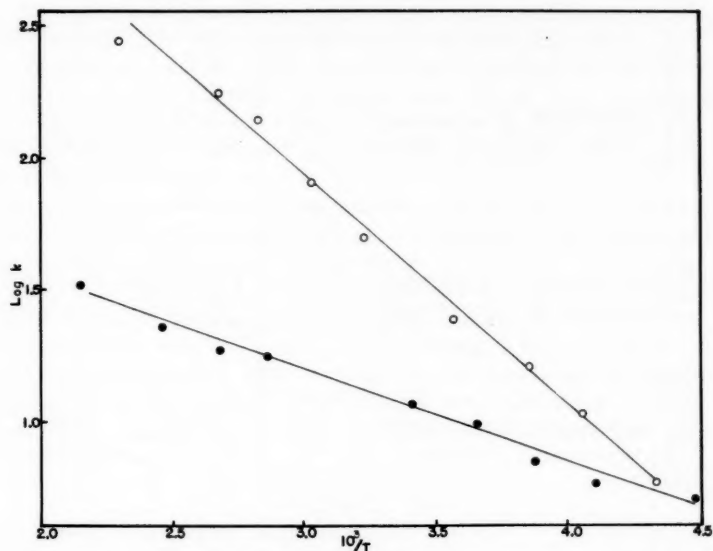
FIG. 2.   Arrhenius plots. $\bigcirc$ 10^{14} k for O + C_4H_{10}; $\bullet$ 10^{13} k for O + C_2H_4.

TABLE V

Effect of variation of initial reactant concentrations on $k(O + C_4H_{10})$

Expt. No.	$10^{-14} [O]_0$ (molecule cm^{-3})	$10^{-14} [C_4H_{10}]_0$ (molecule cm^{-3})	$10^{14} k$ (cm^3 molecule^{-1} sec^{-1})
E_1	4.0	1.6	8.0
E_2	2.0	1.6	8.0
E_3	1.0	1.6	7.7
E_4	.7	1.6	8.0
F_1	1.5	10.0	2.5
F_2	1.5	4.2	2.5
F_3	1.5	1.8	2.1

NOTE: E series: temperature, 57° C; pressure, 0.47 mm.
F series: temperature, 7° C; pressure, 0.22 mm.

O_2. Similar constancy for the value of k was obtained when the pressure was increased by addition of large amounts of inert gas to the oxygen. This result is significant since it has been shown that discharged oxygen contains a proportion of excited oxygen O_2^*, which decreases with addition of helium (8). If ethylene were attacked by O_2^* differences in k might be expected when helium is added. Constant values of k were, however, obtained with O_2–He mixtures from 3.5 to 100 mole% O_2.

Tables IV and V show the independence of k on the reactant concentrations for the C_2H_4 and C_4H_{10} reactions respectively.

These results clearly indicate that the rate-controlling steps in these reactions are second order, first order in each of the reactants.

Rate constants were determined for the C_2H_4 reaction over the temperature range −50° C to 192° C and for the n-C_4H_{10} reaction from −42° C to 160° C. Account was taken in the calculations of the effect of temperature on the concentrations and linear velocities of the reactants. The results are shown in Tables VI and VII and the Arrhenius plots in Fig. 2. These curves yield activation energies of 1.6±0.2 and 4.2±0.2 kcal/mole

TABLE VI

Variation of k with temperature (O + C_2H_4)

Temp. (°C)	Pressure (mm)	Total flow (μmolecules sec⁻¹)	10^{-14} [O]$_0$ (molecule cm⁻³)	10^{-12} [Od]t (molecule cm⁻³ sec⁻¹)	10^{-14} [C_2H_4]$_0$ (molecule cm⁻³)	$\dfrac{[C_2H_4]_1}{[C_2H_4]_2}$	$10^{12}\,k$ (cm³ molecule⁻¹ sec⁻¹)
−50	0.97	53	3.32	1.91	2.76	2.85	0.55
−50	0.97	53	4.15	1.88	4.03	2.52	0.50
−30	0.97	53	4.12	1.24	5.50	2.05	0.58
−15	0.97	51	5.25	2.12	3.77	4.16	0.67
−15	0.93	48	2.38	0.95$_0$	3.42	1.93	0.69
0	1.00	52	2.20	0.80$_5$	2.75	2.15	0.95
20					(cf. Tables I, II, and IV)		1.1$_6$
77	1.02	51	1.80	0.49$_2$	2.64	2.37	1.7$_6$
100	1.03	51	2.39	0.69$_6$	2.56	3.33	1.7$_2$
100	1.03	51	2.64	0.53$_2$	3.53	2.61	1.8$_0$
134	1.04	51	1.61	0.37$_8$	2.32	2.32	2.2$_4$
192	1.05	51	1.87	0.32$_2$	2.80	2.58	2.9$_4$
192	1.05	51	1.87	0.36$_7$	2.22	3.44	3.3$_6$

TABLE VII

Variation of k with temperature (O + C_4H_{10})

Temp. (°C)	Pressure (mm)	Total flow (μmolecules sec⁻¹)	10^{-14} [O]$_0$ (molecule cm⁻³)	10^{-12} [Od]t (molecule cm⁻³ sec⁻¹)	10^{-14} [C_4H_{10}]$_0$ (molecule cm⁻³)	$\dfrac{[C_4H_{10}]_1}{[C_4H_{10}]_2}$	$10^{14}\,k$ (cm³ molecule⁻¹ sec⁻¹)
−42	0.43	18.5	4.2	13.9	1.86	1.08$_5$	0.58
−27	0.45	18.5	4.4	12.0	1.95	1.13$_5$	1.0$_5$
−14	0.43	18.5	3.8	9.7$_6$	1.69	1.16$_7$	1.5$_3$
7				(cf. Tables III and V)			2.4
36	0.45	17.0	4.3	4.07	1.80	1.22$_6$	4.9
57				(cf. Table V)			8.0
80	0.47$_5$	18.0	2.9	1.71	1.63	1.26$_5$	13.7
100	0.47$_5$	18.0	2.8	1.32	1.60	1.26$_6$	17.$_5$
100	0.48	18.5	2.3	1.02	1.90	1.20$_0$	17.8
160	0.49	17.0	3.0	1.21	1.34	1.46$_0$	27.7

for the C_2H_4 and $n\text{-}C_4H_{10}$ reactions respectively, with corresponding pre-exponential factors of $1.8(\pm 0.6) \times 10^{-11}$ and $5.0(\pm 1.6) \times 10^{-11}$ cm³ molecule⁻¹ sec⁻¹.

The rate constant of 1.2×10^{-12} cm³ molecule⁻¹ sec⁻¹ obtained for the C_2H_4 reaction at 25° C can be compared with Cvetanović's figure of 0.29×10^{-12} (1) and that of Ford and Endow of 0.76×10^{-12} (9). Since the last two values are derived indirectly from relative measurements using quite different experimental techniques, the agreement can be considered to be satisfactory.

The ratio of the rate constants for the ethylene and butane reactions was found to be 28 ± 3 at 25° C. Cvetanović (4) found this ratio to be 22 ± 5 from relative rate measurements. Again, the agreement is quite satisfactory.

Cvetanović (1) has suggested that the trend in rate constants for O-atom reactions with olefins is due to a trend in activation energy alone. On this basis his data would imply that the ethylene reaction has an activation energy 2.8 kcal greater than that of the 2,3-dimethylbutene-2 reaction. This is clearly inconsistent with the absolute value of 1.6 ± 0.2 kcal/mole for the value of E for the ethylene reaction found in the present work. It would therefore appear that the trend in k's for the olefin series must also involve a trend in steric factors.

REFERENCES

1. R. J. Cvetanović. J. Chem. Phys. **30**, 19 (1959).
2. H. W. Ford and N. Endow. J. Chem. Phys. **27**, 1156 (1957).
3. S. W. Benson and A. E. Axworthy, Jr. J. Chem. Phys. **26**, 1718 (1957).
4. R. J. Cvetanović. J. Chem. Phys. **23**, 1375 (1955).
5. L. Elias, E. A. Ogryzlo, and H. I. Schiff. Can. J. Chem. **37**, 1680 (1959).
6. E. A. Ogryzlo and H. I. Schiff. Can. J. Chem. **37**, 1690 (1959).
7. F. Kaufman. Proc. Roy. Soc. (London), A, **247**, 123 (1958).
8. E. A. Ogryzlo. Ph.D. Thesis, McGill University, Montreal, Que. 1958.
9. H. W. Ford and N. Endow. J. Chem. Phys. **27**, 1277 (1957).

PRESSURE DEPENDENCE OF ROTATIONALLY PERTURBED LINES IN THE ULTRAVIOLET BAND SPECTRUM OF CN[1]

H. P. BROIDA AND SIDNEY GOLDEN[2]

ABSTRACT

Intensity measurements of the components of rotationally perturbed lines ($K' = 4, 7, 11$, and 15) in the 0,0 transition of the violet system ($B\,{}^2\Sigma^+$–$X\,{}^2\Sigma^+$) of the CN formed in an "active" nitrogen flame have been made at pressures from 0.1 to 100 mm Hg. A simple kinetic model considering competition between formation, radiation, and collisional interchange of states gives a reasonable fit to the data over the entire range of measured pressures. At high pressures the intensity ratios of the components of rotationally perturbed lines depend only upon the radiative transition probabilities and at low pressures, only upon the relative rates at which they are populated. At intermediate pressures, the intensity ratios depend upon the collision frequency for the interchange of the rotationally perturbed states. The collision frequency determined in this manner is of the same order of magnitude as the gas kinetic collision frequency.

INTRODUCTION

The violet bands of CN ($B\,{}^2\Sigma^+$–$X\,{}^2\Sigma^+$) show intensity anomalies originating in the $v' = 0$ level of the $B\,{}^2\Sigma^+$ state caused by perturbations of rotational levels with the $v' = 10$ level of the $A\,{}^2\Pi_i$ state. Herzberg (1) first noticed that lines $K' = 4, 7$, and 15 of the 0,0 band of the violet system were greatly enhanced at low pressures in discharges and in "active" nitrogen flames. Beutler and Fred (2) found that the enhanced lines consisted of doublets and suggested that the anomalously high intensities of these lines are caused by interaction of these rotational levels with corresponding rotational levels of the $v' = 10$ (3)* level of the $A\,{}^2\Pi_i$ state. This suggestion was confirmed by Wager's measurements (4, 5) of the perturbations in both the 10,4 band of the red system and the 0,0 band of the violet system. In addition he found another rotationally perturbed level, $K' = 11$, also consisting of a doublet. Recently, Kiess and Broida (6, 7) found that the enhancement of the perturbed lines was increased greatly at pressures below 1 mm Hg and that under conditions in which transitions from the $K' = 4, 7$, and 15 levels are enhanced in the violet system, lines from corresponding rotational levels in the $v' = 10$ state of the red system ($A\,{}^2\Pi_i$–$X\,{}^2\Sigma^+$) are weakened.

This paper reports the intensity measurements of the so-called *main* and *extra* lines of the rotationally perturbed pairs in the 0,0 transition of the violet system over a pressure range from 0.1 to 100 mm Hg. The *main* lines correspond to normally allowed transitions; the *extra* lines correspond to normally forbidden transitions. A mathematical model developed on the basis of kinetic considerations has been devised to fit the data. The ratio of the intensity of the extra line to that of the main line is expressed as a function of three parameters and the pressure. One parameter, $2k_M/k_E$, is the ratio of the radiative transition probability of the main line to that of the extra line. The factor of two appears as a result of the fact that the main line itself is an unresolved doublet. The k_M/k_E ratios found from measurements of the pressure variation of the intensity ratios for the lines $K' = 7$, 11, and 15 are in good agreement with the determinations of Wager (5) found from measure-

ments of perturbed line displacements. Another parameter, α, is interpreted to mean that CN is formed in the upper state of the extra line at approximately three times the rate that CN is formed in the upper state of the main line. The third parameter, k_c/k_M, gives a rate of collisional depopulation compared with the rate of radiative transition.

EXPERIMENTAL PROCEDURE

CN emission was obtained by mixing "active" nitrogen with gases of compounds containing carbon in a simple reaction chamber similar to that of Wager (5) and of Kiess and Broida (6). Bright flames were observed at the point of mixing, and at lower pressures the flame filled the entire reaction tube (300 mm long and 45 mm diameter). Prepurified nitrogen (stated by the manufacturer to be of 99.997% purity) was taken from cylinders through float-ball flowmeters by means of Tygon tubing and was admitted by a stopcock into the discharge region. Pyrex glass (washed with soap, rinsed with a 12% solution of HF, and then rinsed with distilled water) was used in the remainder of the apparatus. Because CH_2Cl_2 gave the brightest flames in this burner (particularly at pressures below 1 mm Hg), it was used for most experiments. CH_2Cl_2 vapor was admitted to the reaction chamber through a stopcock from a graduated tube containing liquid CH_2Cl_2 (C.P.).

In most experiments, a 2450-megacycle electrodeless discharge (125 watts) was used to dissociate the nitrogen. A small percentage of nitrogen atoms (8) found in such discharges at pressures near 1 mm Hg. For pressures above 20 to 30 mm Hg, it was necessary to use a 800-watt generator.* In addition for some work below 0.2 mm, a spark discharge using $7\mu f$ and 3000 volts at 1 kilowatt with aluminum electrodes about 1 meter apart was found to give brighter reactions.

Pressure was measured with a Bourdon gauge which could be read to 0.05 mm Hg. A McLeod gauge was used for calibration and for measuring nitrogen pressures below 1 mm.

Spectra were recorded with a high resolution grating monochromator with photo-multiplier detection.† This instrument, used with 7 micron slits, is able to resolve lines of 0.03 Å separation. Since peak heights were used for intensity measurements, relative intensities of lines closer than about 0.1 Å were not reliable.

Under the best conditions, for pressures between 0.2 and 20 mm Hg and for values greater than 0.1, intensity ratios were reproducible to about ±2%. However, for weak flames at very low and very high pressures the reliability was not as good. For pressures lower than 0.1 mm Hg, errors of 50% in the intensity ratio were possible. These errors are associated with the very weak signals obtained.

EXPERIMENTAL DATA

Figures 1 and 2 illustrate the effect of pressure on the perturbed lines. With decreasing pressure the main lines, M, become increasingly enhanced so that at very low pressures they are more than 10 times the intensity of their neighbors. The extra lines, E, increase relative to the main lines. The extra lines occur on the short wavelength side of the main lines for $K' = 7$, 11, and 15 and on the long wavelength side of $K' = 4$. At the very lowest pressures, below 0.1 mm Hg, the extra lines at $K' = 7$, 11, and 15 were more than twice the intensity of the main lines.

Wager (5) has measured the separations of the extra lines from the perturbed main
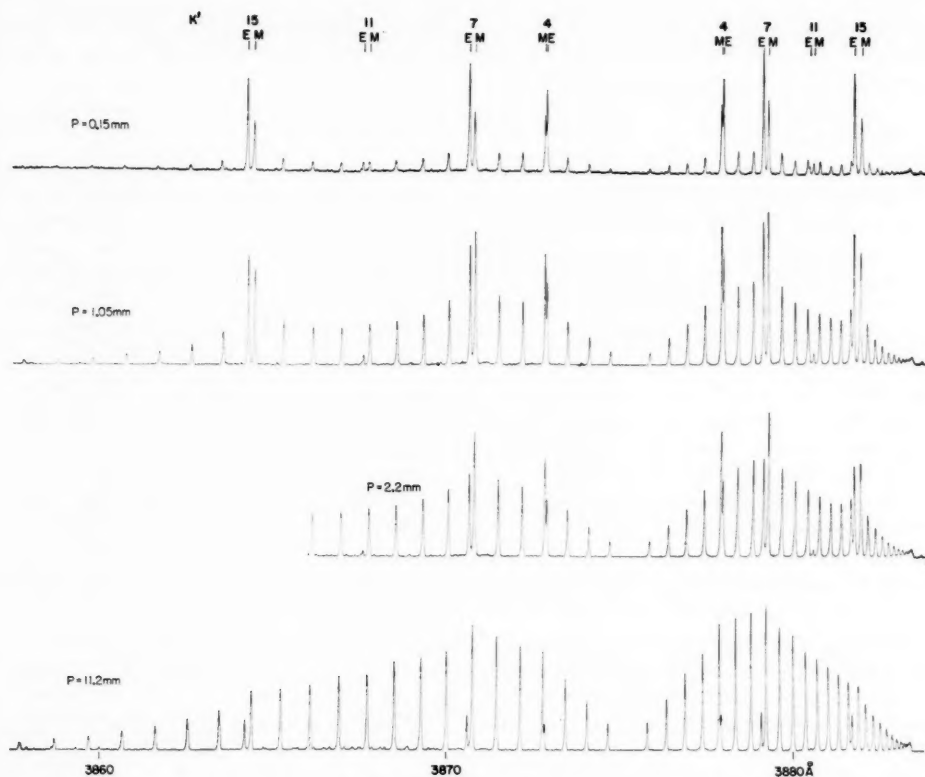
FIG. 1. Spectra of the violet CN emission from "active" nitrogen flames at several pressures.

lines to be -0.352, $+0.938$, $+1.177$, and $+1.212$ cm^{-1} respectively for $K' = 4, 7, 11$, and 15. Since the separation of lines from $K' = 4$ levels were not sufficiently resolved for reliable intensity measurements, intensity measurements on these lines have been excluded from detailed analysis.

Measured ratios of the intensity of the extra line, I_E, to the intensity of the main line, I_M, as obtained from peak height measurements at pressure from 0.08 to 100 mm Hg are shown in Figs. 3, 4, and 5. Pressure is the variable having the largest influence on I_E/I_M. The data have been obtained over a period of 18 months. Small effects on I_E/I_M caused by different relative amounts of CH_2Cl_2 and N_2 were noticeable but were too small for systematic measurement. No effects on the ratio were found to be caused by the type of discharge, the power in the discharge, the size or type of reaction chamber, flow rate, or the reactant.

The addition of appreciable amounts of argon or helium had a small but measureable effect on the ratio between 2 and 20 mm Hg. This is illustrated in Table I where I_E/I_M is given for various proportions of added helium. The effect of rare gas is the same whether it is added before or after the discharge. Other gases—N_2, O_2, CO, or CO_2—had little effect (much less than the rare gases) on I_E/I_M.
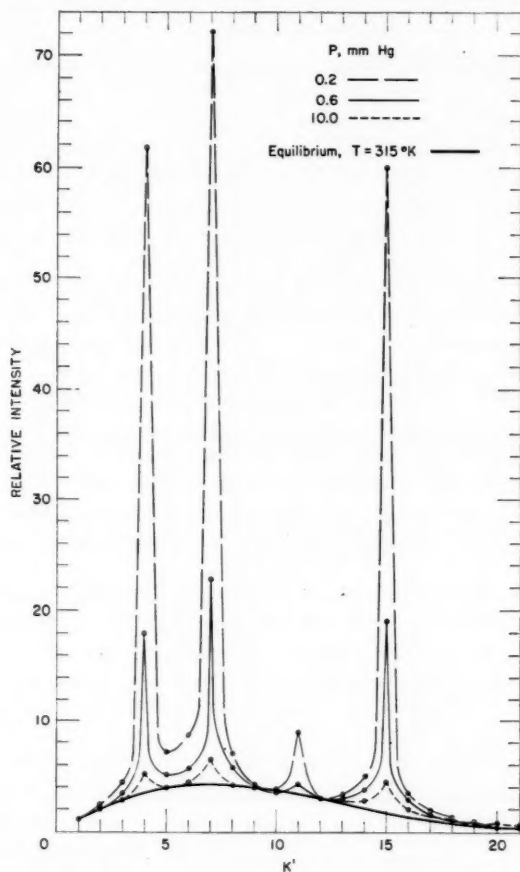
FIG. 2. Effect of pressure on the enhancement of the perturbed lines; the sum of the extra and the main lines is used. For comparison with the measured intensities, there also is shown a Boltzmann distribution calculated for the measured (6) gas temperature of 300° K.

TABLE I

Measured values of I_E/I_M for $K' = 15$ as affected by added helium

Total pressure, mm Hg	Ratio of helium to nitrogen			
	0	1	10	100
0.8	1.39		1.35	
1.4	1.14	1.16	1.13	
2.2	.93	.93	.97	
3.4	.76	.82	.84	
5.0	.62	.71	.72	.75
7.5	.51	.61	.61	.63
10	.45	.52	.57	.57
15	.38	.44	.47	.47
20	.34	.39	.42	.40
25	.32	.33	.39	.38
30	.29	.29		.33
40	.285			.31
45	.28			.30
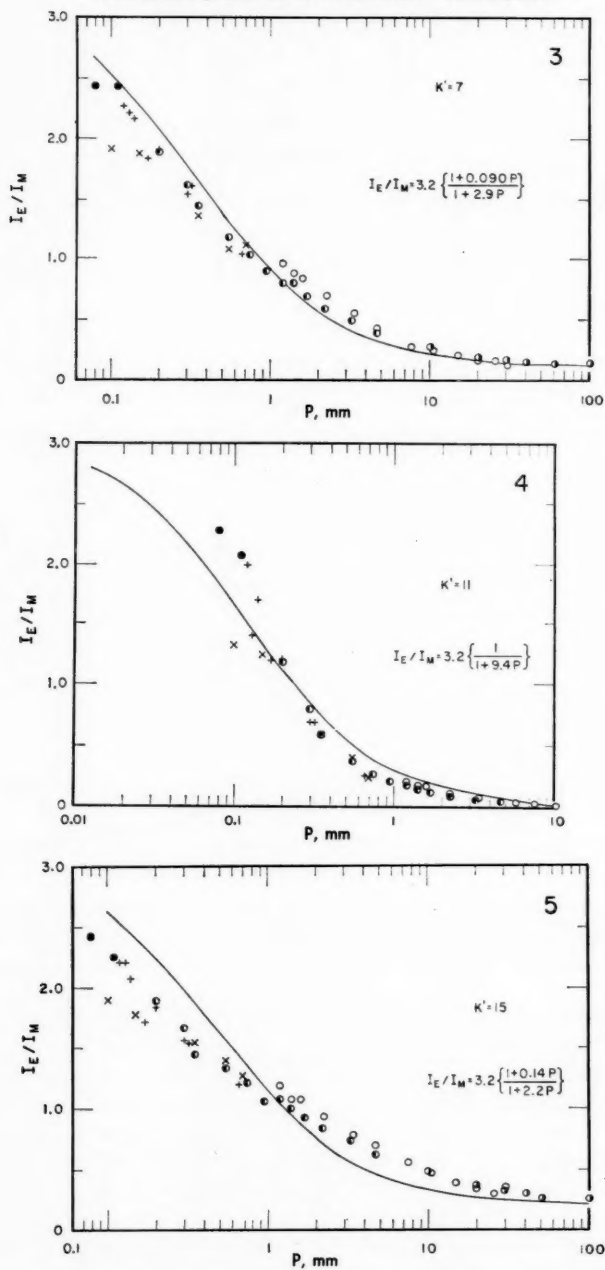
FIG. 3. Measured intensity ratios, I_E/I_M, for $K' = 7$ at various pressures and the curve calculated from equation [13] and the parameters listed in Table II.

FIG. 4. Measured intensity ratios, I_E/I_M, for $K' = 11$ at various pressures and the curve calculated from equation [13] and the parameters listed in Table II.

FIG. 5. Measured intensity ratios, I_E/I_M, for $K' = 15$ at various pressures and the curve calculated from equation [13] and the parameters listed in Table II.

THEORETICAL MODEL

The model to be elaborated here is concerned mainly with the formation of CN molecules in those states which are affected by rotational perturbations. The energy relations of those states has been discussed in some detail by Wager (5). The upper states involved are degenerate doublets (or nearly so). However, only one of the spin components in the $B\ ^2\Sigma$ state and only one of the Λ components in the $A\ ^2\Pi$ state interact via a rotational perturbation (9). Thereby, the component derived from the $A\ ^2\Pi$ state acquires an enormously increased probability of transition to the ground state: this transition corresponds to the extra line. The other component of the $A\ ^2\Pi$ state is unaffected and has negligible intensity. By contrast, both components of the $B\ ^2\Sigma$ state have large transition probabilities, so that the main line that they produce is an unresolved doublet. However, the relative intensity of these doublets depends upon the relative rates at which they are being populated.

Figure 6 is a simplified energy level diagram indicating that the transitions associated with the doublets observed in the violet CN bands may be presumed to involve not only the radiative transitions, M and E, but also those ascribable to the formation of the CN molecule in the various states and those ascribable to non-radiative transitions. For simplicity, only non-radiative transitions between the members of each group of upper states are taken into account explicitly. The remaining possible non-radiative transitions are considered collectively in terms of the otherwise net rate of production into each of the pair of rotationally perturbed excited states. A diagram like Fig. 6 is applicable to each rotationally perturbed pair of states and the associated unperturbed state.

It is assumed that the various processes indicated schematically by the diagram occur with rates which are simply proportional to the appropriate concentration of relevant species. Thus, for example, the emission from the normally allowed member of the perturbed pair $(V' \rightarrow V)$ would have an intensity equal to $k'_M[V']$, where $[V']$ is the concentration of CN molecules occupying the indicated state. Similarly, the rate at which CN molecules experience collisions which take them from one of the pair of perturbed states to the other, say $(V' \rightarrow R')$, is given by $k_{-c}\ [V']\ [N_T]$, where $[N_T]$ is the total concentration of species which are effective in inducing these non-radiative transitions.*
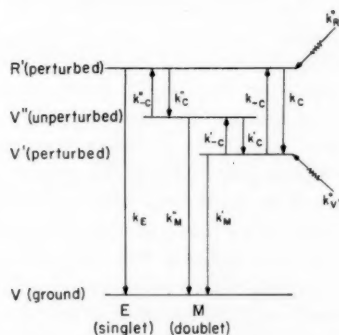
FIG. 6. Simplified energy level diagram, illustrating the transitions explicitly considered in the theoretical model involving the rotationally perturbed states of CN. The various k's refer to rate constants employed in the text.

*It may be noted that a more satisfactory expression which would take into account the different effectiveness of the individual species comprising the system would be exhibited in the form of a linear combination of their respective concentrations. Alternatively, the present simple form ascribes a composition dependence to the collisional rate constants.

Because of the complexity of the production processes, the rates associated with them will not be given explicitly. Instead, $k^0_{R'}$ and $k^0_{V'}$ will be taken as the net rate of production into states R' and V' (apart from processes of collisional exchange) and will be assumed to depend upon the concentration and composition of the system. All rates are to be understood in terms of changes in concentration per unit time.

The intensity of radiation (neglecting self-absorption) emitted from the perturbed component of the main line ($V' \rightarrow V$) is given by

[1] $$I'_M = k'_M [V'],$$

while for the unperturbed component ($V'' \rightarrow V$)

[2] $$I''_M = k''_M [V''].$$

Clearly, the intensity of the observed unresolved main line corresponds to

[3] $$I_M = I'_M + I''_M.$$

The intensity of the extra line ($R' \rightarrow V$) is given by

[4] $$I_E = k_E [R'].$$

At any instant, the rates of change of molecules in the excited states are

[5] $$\frac{d[V']}{dt} = k^0_{V'} + k_c[R'][N_T] + k'_c[V''][N_T] - k_{-c}[V'][N_T] - k'_{-c}[V'][N_T] - k'_M[V'],$$

[6] $$\frac{d[V'']}{dt} = k''_c[R'][N_T] + k'_{-c}[V'][N_T] - k'_c[V''][N_T] - k''_{-c}[V''][N_T] - k''_M[V''],$$

[7] $$\frac{d[R']}{dt} = k^0_{R'} + k_{-c}[V'][N_T] + k''_{-c}[V''][N_T] - k_c[R'][N_T] - k''_c[R''][N_T] - k_E[R'].$$

The solution of these equations will give the dependence of the line intensities upon the total concentration and, hence, the pressure of the system.

However, it is not possible to solve the preceding equations without some explicit statement regarding the rates of production. In addition the complete solution of the equations is of interest only for transient circumstances, whereas the experimental conditions dealt with here are practically stationary. As a consequence, attention will be devoted only to the stationary solutions of the equations. To solve the equations, several assumptions will be introduced:

stationary hypothesis:

[8] $$\frac{d[V']}{dt} = \frac{d[V'']}{dt} = \frac{d[R']}{dt} = 0;$$

collision hypothesis:

[9] $$\begin{cases} k_c = k_{-c} \\ k'_c = k'_{-c} \\ k''_c = k''_{-c} \end{cases}$$

and

[10] $$k_c = k'_c = k''_c;$$

production hypothesis:

[11] $$k^0_{R'} = \alpha k^0_{V'}, \qquad\qquad \alpha \text{ constant.}$$

The first assumption is justified on the basis of the experimental conditions. The second assumption partly conforms to microscopic reversibility which, however, is strictly applicable for conditions close to equilibrium. Equation [10] is introduced for simplicity. The third assumption also is introduced for simplicity. However, it is to be expected that the relative rates of production of CN molecules into the pair of perturbed states will vary with the mode of their production, especially when the latter is altered markedly (i.e., discharge vs. flame production). Since the radiative transition probabilities of the two components of the main line are the same,

[12] $$k'_M = k''_M = k_M.$$

Equations [5]–[7] are greatly simplified by substituting equations [8]–[12] and can be solved for the measured intensity ratio,

[13] $$I_E/I_M = \frac{\alpha + (1+\alpha)(k_c/k_M)[N_T]}{1 + 2(1+\alpha)(k_c/k_E)[N_T]}.$$

For indefinitely great pressures

[14] $$(I_E/I_M) \rightarrow 1/2(k_E/k_M), \qquad [N_T] \rightarrow \infty,$$

a result that is in accord with the notion that an equilibrium distribution among the various states should be achieved by the CN molecules at sufficiently high pressures. For extremely low pressures, on the other hand,

[15] $$I_E/I_M \rightarrow \alpha, \qquad [N_T] \rightarrow 0,$$

which is consistent with the hypothesis of production expressed in equation [11]. For sufficiently low pressures, one may expect that the rate of collisions in altering the populations in the various states becomes negligibly small, in which case the steady production must be equated to the rate of radiative transitions.

Equation [13] can be rearranged in a variety of ways and one form which is convenient for the subsequent analysis is the following:

[16] $$\frac{\alpha - (I_E/I_M)}{(I_E/I_M) - 1/2(k_E/k_M)} = 2(1+\alpha)(k_c/k_E)[N_T].$$

ANALYSIS OF EXPERIMENTAL DATA

The measured values of the intensity ratios have been subjected to an analysis in the light of the foregoing section and a reasonable fit is found. However, any fit of the data involving the empirical evaluation of three parameters cannot be weighted too heavily in judging the soundness of the theory. To achieve more confidence in the model described previously, the parameters must be compared with estimates of their values obtained from entirely different considerations of the phenomena. Such comparisons will be made in the course of the present section and give increased confidence in the general model.

Preliminary efforts at a least-squares analysis for the parameters were made but this approach was discarded because erratic values for the parameters resulted, one group of experimental data giving values of parameters seemingly unrelated to another group of data. Such discrepancies were caused by small effects due to changes in mixtures and flow rates of the reactants and to an inability to make sufficiently precise pressure measurements at low pressures.

The procedure employed to evaluate the parameters was an iterative one. It is evident

that the asymptotic behavior at high and low pressures of the ratio of intensity I_E/I_M will give two parameters in equation [13]. Thus a preliminary value of α could be estimated from an extrapolated value of I_E/I_M at low pressures. The resulting value was employed in equation [16] to yield an expression which gave a linear extrapolation to high pressures, permitting an estimate to be made of k_E/k_M. The value resulting was then employed to obtain an expression which gave a linear extrapolation to low pressures, permitting a redetermination of the value of α. The iteration needed repetition only once to yield parameters which remained unchanged (to within 10%). With the final values of α and k_E/k_M obtained, the remaining parameter could be determined as an average value for all of the data. This procedure was carried through for the lines with $K' = 7$ and 15. The final plots for $K' = 7$ are given in Figs. 7 and 8 to illustrate the procedure for obtaining the asymptotic limits.
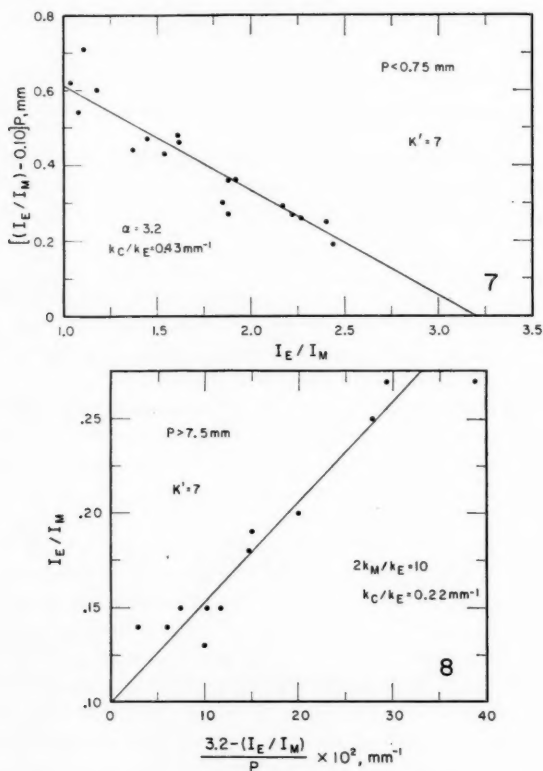
FIG. 7. The use of equation [13] to determine α.
FIG. 8. The use of equation [13] to determine $2k_M/k_E$.

The values of α which were obtained, as already indicated by the original data, suggested that the various lines exhibited a more-or-less uniform value of this parameter. To establish this, and eliminate the experimental uncertainties in the values of the pressure (at low pressures), the data were treated as in Fig. 9. The ratios of intensities of the lines
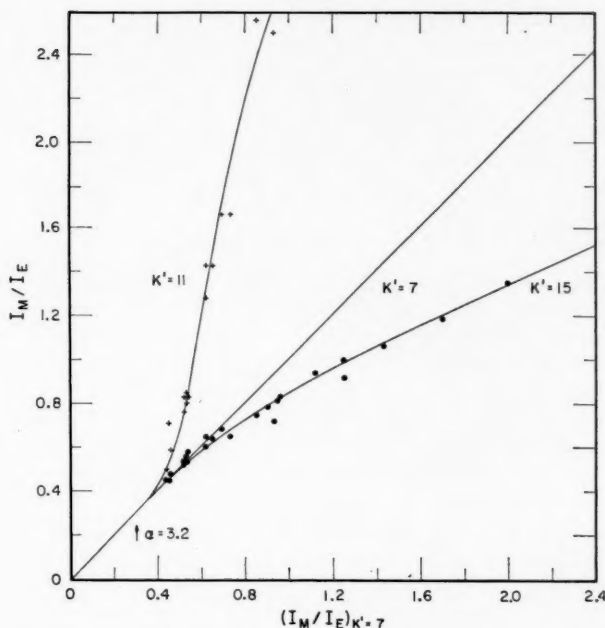
FIG. 9.   Relations between intensity ratios at the same pressure for $K' = 7$, 11, and 15.

corresponding to $K' = 11$ and 15 have been plotted against the value for $K' = 7$, each point corresponding to the *same* value of the pressure, but differing, for any pair of lines, from point to point. It seems reasonable to suppose that for $K' = 7$, 11, and 15, α is approximately 3.2 since the curves for $K' = 11$ and 15 extrapolate smoothly to the value found for $K' = 7$.

With a more-or-less uniform value of α taken as 3.2 the analysis can be carried out to estimate k_E/k_M for the lines $K' = 7$, 11, 15 by extrapolation to high pressures. However, it is immediately apparent that the data for $K' = 11$ have a very small value of k_E/k_M from the low values of I_E/I_M at high pressures. The accuracy of the data do not permit a reliable estimate of k_E/k_M to be made for this line. As can be seen from equation [16], small values of k_E/k_M yield a pressure dependence (i.e. $[N_T]$) which is more reliably given by

[17] $\alpha - (I_E/I_M) \sim 2(1+\alpha)\ (k_e/k_E)[N_T](I_E/I_M),$

providing $k_E/k_M \ll 1$, which is apparently valid in the range of data where reliable estimates of I_E/I_M can be made. As a result k_e/k_E can be estimated from the data, but not k_e/k_M. The results obtained are summarized in Table II where $[N_T]$ has been measured in millimeters of mercury, for the lines with $K' = 7$, 11, 15.

The values of k_M/k_E obtained here from intensity measurements are uniformly one-half the values previously obtained by Wager (5) from wavelength measurements. However, Wager failed to consider that the main lines actually consist of doublets, only one component of which is affected by the rotational perturbation. It is evident that the frequency

TABLE II

Summary of the parameters

K'	α	$2k_M/k_E$	k_M/k_E (Wager)	$k_c/k_M,$ mm^{-1}	$k_c/k_E,$ mm^{-1}
7	3.2	10	10.6	0.068	0.34
11	3.2	>100 (est.)	130	—	1.13
15	3.2	5	5.6	0.104	0.26

displacements will be greater than those observed for the unresolved main line. Consequently the mixing of the two perturbed states will be greater than the values obtained by Wager, resulting in a smaller value of k_M/k_E. Better measurements of the perturbed line displacements should be possible from spectra obtained from flames at pressures near 0.1 mm Hg, so that the displacement of the main line will be less influenced by the unperturbed component.

The parameters have been incorporated into equation [13] for the ratio of intensities and the calculated curves are compared with the data in Figs. 3, 4, and 5 for pressures less than 100 mm, beyond which value the change in intensity ratio with pressure is very small. The fit to the data is relatively good.

One additional piece of information may be obtained from the data. The quantity k_c can be determined if the value of k_M is known (or that of k_E) or estimated. Since the ratio gives, when multiplied by the pressure, a measure of the ratio of collision frequency to the reciprocal of the radiative lifetime, these quantities may be evaluated independently. It is estimated from kinetic theory that a molecule of CN has approximately 10^6 collisions per second at 1 mm pressure and 300° K. Thus, for a radiative lifetime of 10^{-7} to 10^{-8} sec, it is estimated that $(k_c/k_M) \sim 0.1 - 0.01$ substantially in agreement with the observed values. Therefore, k_c is in fact a collision frequency corresponding essentially to the kinetic theory value. It seems unlikely that any more precise comparison can be made with the values obtained from our present analysis and those obtained otherwise. Rare gases (Table I) decrease k_c as compared with nitrogen.

DISCUSSION

The analysis of the experimental data provides support for the simple model which has been assumed; a competition between formation rates, radiative transitions, and collisional interchanges between the components of rotationally perturbed states seems adequate to account in a general way for the effect of pressure upon the relative intensities of the perturbed and extra lines in the emission spectrum of CN ($B\ ^2\Sigma^+ - X\ ^2\Sigma^+$).

Nevertheless, the mathematical model, which has been presented, represents a great simplification of the actual state of affairs. This can be seen in part from the trends in the disparity between the data and the fitted curves. A more detailed examination would reveal that the parameters which have been used are better to be regarded as depending somewhat upon other parameters such as pressure. For example, k_c/k_E for the low-pressure extrapolation (Fig. 7) differs by about a factor of two from that for the high-pressure extrapolation (Fig. 8); fitting the whole range of pressures (Fig. 3 and Table II) gives intermediate values. Thus the results reported here represent some sort of average value. However, we should emphasize that the parameter α has been weighted in terms of low-pressure behavior. There seems to be no simple way of determining this quantity reliably under the opposite extreme of pressure.

Because the model, which has been considered, has not dealt with the relative intensities of lines of different K's, the analysis is far from complete. In fact, since the anomalous intensities of the rotationally perturbed lines would seem to depend upon the actual rates of forming the CN in the several excited states, the present analysis, dealing with the *relative* rates of formation of specific pairs of these states, can only have a minor influence on that problem. Indeed the tacit use of a more-or-less constant value of α itself raises questions to which we have no ready answer.

REFERENCES

1. G. HERZBERG.   Z. Physik, **52**, 815 (1928).
2. H. BEUTLER and M. FRED.   Phys. Rev. **61**, 107 (1942).
3. G. HERZBERG and J. G. PHILLIPS.   Astrophys. J. **108**, 163 (1948).
4. A. T. WAGER.   Phys. Rev. **61**, 107 (1942).
5. A. T. WAGER.   Phys. Rev. **64**, 18 (1943).
6. N. H. KIESS and H. P. BROIDA.   Seventh Symposium on Combustion. Butterworth Scientific Publications, London. 1959. p. 207.
7. N. H. KIESS and H. P. BROIDA.   To be published.
8. J. T. HERRON, J. L. FRANKLIN, P. BRADT, and V. H. DIBELER.   J. Chem. Phys. **30**, 879 (1959).
9. G. HERZBERG.   Molecular spectra and molecular structure. I. Spectra of diatomic molecules. D. Van Nostrand Co., Inc., New York. 1950. p. 286.

ELECTROPHILIC CHARACTER OF OXYGEN ATOMS[1]

R. J. CVETANOVIĆ

ABSTRACT

The relative rates of reactions of oxygen atoms with a number of olefins in the vapor phase determined in previous work are summarized and supplemented by some additional results. The uncertainty in the values of the relative rate constants is now believed to be reduced to only a few per cent. A number of simple correlations observed previously have been re-examined on the basis of the more complete and more accurate list of values available at present. These correlations show a distinct electrophilic character of oxygen atoms in their reactions with olefins and their potential significance for the understanding of the finer details of these addition processes is discussed.

INTRODUCTION

Possibilities of finding simple correlations between reaction rates and physical properties of the reactants have been extensively explored at various times in the past with the object of establishing the factors which contribute to chemical reactivity. Thus, for example, considerations of the likely potential energy changes when two molecules interact have suggested linear dependence of activation energies on such quantities as heats of reaction or singlet–triplet excitation energies (1–6). In the case of metathetical reactions such views have found little experimental support. Some addition reactions, on the other hand, at least those involving a number of aromatic hydrocarbons (5, 6) and a somewhat restricted group of olefins (7), appear to show simple relations of this kind.

Reactions of atoms with series of structurally related compounds are particularly attractive for this type of investigation, especially if they can be studied under conditions where complications from solvent effects of variable magnitude can be eliminated. Solvent effects are of course absent in vapor phase reactions, but until very recently there were essentially no rate data for series of addition reactions in the vapor phase. An exception to this represented the reactions of H-atom additions to olefins, investigated by Robb and Melville (8). However, the work now in progress in this laboratory on these reactions at higher pressures and with the use of a different technique (9) reveals some differences in the values of the rate constants from those obtained by these authors. A discussion of the trends in reactivity in this reaction series has, therefore, to be delayed until the current work is completed.

Although free atoms as a rule possess unpaired electrons and thus have free radical character, they may be expected to react in particular reactions as either electrophilic, nucleophilic, or radical reagents. The type of the reactant character exhibited will be largely determined by the relative values of the electron affinities and ionization potentials of the atoms and their reaction partners.

In the past several years extensive information on the vapor phase reactions of oxygen atoms with olefins has been accumulated in this laboratory. Both the mechanism (10, 11) and the relative rates (12) have been investigated in considerable detail. The results of these studies show that ground-state oxygen atoms, which are diradicals, behave as distinctly electrophilic reagents in their reactions with olefins. The relative rates were found to exhibit approximate simple correlations with some physical properties of olefins

and also to give linear "free energy" plots with the corresponding rates of some other electrophilic reagents studied in solutions. All such correlations show as a rule smaller or greater individual deviations from the basic trends. These deviations are only partly ascribable to experimental errors. In the present paper the earlier findings are summarized and supplemented by some additional experimental results with the particular object of obtaining further information on the extent and the nature of deviations from some of the observed correlations.

EXPERIMENTAL

Oxygen atoms were generated by mercury-photosensitized decomposition of nitrous oxide and the nitrogen produced served as an internal actinometer. A detailed study of this reaction (13) had shown that in this decomposition only nitrogen and oxygen atoms were initially formed. The oxygen atoms are in all probability in their ground, triplet $O(^3P)$ state. This is required by the spin conservation rule and is confirmed by comparisons with the analogous reactions with oxygen atoms generated by photolysis of nitrogen dioxide (14).

A circulating reaction system of total volume of 415 ml was used. The gases were circulated by means of an all-glass vertical plunger pump. The reaction cell was cylindrical, 5 cm in diameter and 10 cm long, and was illuminated by two low-pressure mercury lamps, one at each end of the cell. The reactant olefins were measured manometrically on a constant volume burette. By using mercury cutoffs instead of stopcocks the reactant olefins were kept from coming in contact with stopcock grease during the transfer into the reaction system and the run. Nitrous oxide was measured manometrically on a volume of 1000 ml before its introduction into the reaction vessel.

The rate constants of oxygen atom additions to olefins were measured relative to that of cyclopentene. In the cyclopentene reaction, ethylene is an important product while with the other olefins studied it is not formed or is produced at best only in very small amounts. At various olefin-to-cyclopentene ratios various amounts of ethylene are produced and the ratio of the rate constants can be calculated from the expression*

$$[1] \qquad k_1/k_2 = \log\{1 - [\Delta N_2/(a_1)_1] + [\Delta C_2H_4/\alpha_2(a_1)_1]\}/\log\{1 - [\Delta C_2H_4/\alpha_2(a_2)_1]\},$$

where subscript 2 refers to cyclopentene; $(a_1)_1$ and $(a_2)_1$ are the initial amounts of the competing olefin and cyclopentene, respectively; ΔN_2 and ΔC_2H_4 are the respective amounts of N_2 and C_2H_4 produced; and α_2 is C_2H_4/N_2 in the reaction of oxygen atoms with cyclopentene alone. In separate experiments α_2 has been found to be 0.270 at 26° C. The values of ΔC_2H_4 used in equation [1] have to be corrected for any ethylene produced from the competing olefin in the absence of cyclopentene. This is done by using the expression†

$$[2] \qquad (\Delta C_2H_4)_{corrected} = [(\Delta C_2H_4)_{total} - \beta\Delta N_2]/(1 - \beta/\alpha_2),$$

where β is C_2H_4/N_2 in the absence of cyclopentene. In view of the relative magnitudes of α_2 and β these corrections are very small.

Of the reaction products only N_2 and C_2H_4 were of interest in the present work. Analyses were made therefore only for the non-condensible gases and the C_2 fraction. Both fractions were measured manometrically on a constant volume burette. The former was further analyzed by the use of a Cu–CuO furnace at about 250° (to remove CO and any H_2)

*Equation (5) of reference 12.
†Rearranged equation (2) of reference 12.

followed by mass spectrometric analysis to determine the small amount of CH_4 in the recovered N_2. The C_2 fraction was analyzed by mass spectrometer. A Le Roy still (15) followed by a "pump-out" trap was used to separate the two fractions from the rest of the products and the excess reactants present.

The reactants were of the best available grade and were degassed and bulb-to-bulb distilled *in vacuo* before use. Peroxides were removed from cyclopentene by filtering through an activated alumina column and rapid introduction into the vacuum apparatus. Large excess of nitrous oxide and high total pressures ensured no interference from chemical quenching reactions by the olefins.

RESULTS AND DISCUSSION

In the earlier work (12) it was found that *trans*-2-butene reacted somewhat more rapidly with oxygen atoms than *cis*-2-butene. However, the difference was almost comparable to the cumulative uncertainty in these determinations at that time and the reality of this observation was therefore in doubt. For this reason the relative rates of these two olefins have been redetermined with the use of the cyclopentene technique. This technique and the additional improvements in the handling of the reactants and the products have permitted appreciably more accurate determination of the relative rates than was originally possible. The results are given in Table I, in which the rate constants are determined relative to that of cyclopentene. It is seen that the rate of

TABLE I

Determination of relative rate constants for *cis*-2-butene, *trans*-2-butene, and *n*-1-hexene

(The amounts of the reactants and of the nitrogen produced are given in millimeters in 415 ml at 25° C; the amounts of the other products are given relative to the nitrogen produced; a_2 = cyclopentene)

Run	Temp., °C	$\dfrac{(a_1)_i}{(a_2)_i}$	$(a_1)_i$ (mm)	$(a_2)_i$ (mm)	N_2O (mm)	Irradiation (min-utes)	ΔN_2 (mm)	$\dfrac{CO}{N_2}$	$\dfrac{CH_4}{N_2}$	$\dfrac{C_3H_6}{N_2}$	$\dfrac{C_2H_4}{N_2}$	$\dfrac{k_1}{k_2}$
					(I) a_1 = *cis*-2-Butene							
169	(27.4)		4.17	—	495.2	60	1.529	.017	.007	.094	.012	—
170	27.3	3.09	21.06	6.81	497.9	60	1.463	.019	.008	.060	.085	.801
171	26.0	1.69	12.44	7.38	496.9	90	2.251	.019	.010	.047	.122	.774
172	25.9	.97	8.26	8.50	495.0	90	2.297	.019	.006	.032	.154	.808
173	26.7	.74	8.08	10.89	490.8	90	2.281	.021	.007	.027	.170	.822
Mean 26.5												0.801±.014
					(II) a_1 = *trans*-2-Butene							
177	(24.5)		8.20	—	496.2	90	2.388	.020	.006	.069	.016	—
180	(26.8)		8.58	—	499.1	90	2.314	.021	.004	.070	.016	—
176	26.8	2.01	16.87	8.38	489.1	90	2.232	.019	.005	.039	.101	.954
175	25.5	1.19	9.68	8.14	495.2	90	2.309	.019	.005	.031	.130	1.010
174	26.4	1.18	9.26	7.82	493.7	90	2.298	.018	.005	.032	.131	.995
178	26.0	1.02	8.23	8.08	508.0	90	2.322	.018	.005	.025	.148	.878
179	26.8	.61	7.85	12.80	493.7	90	2.262	.020	.005	.016	.176	.919
Mean 26.3												0.951±.042
					(III) a_1 = *n*-1-Hexene							
182	(27.5)		9.12	—	497.7	90	2.272	.022	—	—	—	—
185	25.6	4.82	22.63	4.69	496.9	90	2.092	.017	—	—	.130	.215
183	26.8	4.52	20.27	4.48	494.5	90	2.086	.018	—	—	.128	.222
186	24.1	3.90	20.27	5.19	494.5	90	2.075	.019	—	—	.139	.222
184	25.2	2.73	20.65	7.55	504.3	90	2.060	.017	—	—	.165	.215
181	26.6	.69	9.00	13.07	494.5	90	2.168	.021	—	—	.234	.214
Mean 25.7												0.218±.004

addition of oxygen atoms to *trans*-2-butene is about 15% greater than it is for *cis*-2-butene. This is in approximate agreement with the previous finding although the difference between the two olefins is now found to be slightly smaller than in the earlier work.

Table I also includes the results of the determinations of the relative rate of reaction of oxygen atoms with *n*-hexene-1, which was not measured before. The particular interest in this compound in connection with the present work will be evident from the discussion which follows.

The temperature dependence of the relative rates of addition of oxygen atoms to several representative olefins has been recently determined. A full report on this work is being published elsewhere (16) and only a summary of the Arrhenius parameters obtained is given in Table II. In all cases the ratio of the pre-exponential factors (relative

TABLE II

Ratios of the Arrhenius pre-exponential factors and the differences
in activation energies

(The subscript CP refers to cyclopentene, and TME to
tetramethyl ethylene)

Olefin	A/A_{CP}	$E - E_{CP}$ (cal/mole)	$E - E_{TME}$ (kcal/mole)
Ethylene	1.01	2008	2.60
1-Butene	.74	.803	1.40
1,3-Butadiene	1.14	205	.80
Cyclopentene	1	0	.60
Cyclohexene	.89	−13	.58
Isobutene	.67	−130	.47
Trimethyl ethylene	1.18	−485	.11
Tetramethyl ethylene	1.25	−596	0

to cyclopentene) is very close to unity. Within the experimental error the differences in reactivities in this reaction series appear then to be essentially entirely due to differences in the activation energies. In view of this any correlation of the logarithms of the rate constants for these reactions is to a good approximation equivalent to a correlation of the activation energies.

A list of the values available at present of the relative rate constants of the reactions of oxygen atoms with olefins at 25° C is given in Table III. As indicated in the table, besides several new determinations, most of these values are recent redeterminations and they agree very well with the previous values (12) which were in most cases obtained by

TABLE III

Relative rates of addition of oxygen atoms to olefins at 25° C

(The value for isobutene is taken as unity)

Olefin	Relative rate constant	Olefin	Relative rate constant
Ethylene	0.040[a]	*cis*-2-Pentene	0.90[b]
Propylene	0.23[b]	Cyclopentene	1.19[a]
1-Butene	0.23[a]	Cyclohexene	1.08[a]
1-Hexene	0.26[c]	Trimethyl ethylene	3.17[a]
Isobutene	1.00	Tetramethyl ethylene	4.07[a]
cis-2-Butene	0.95[c]	1,3-Butadiene	0.97[a]
trans-2-Butene	1.13[c]		

[a]Reference 16. [b]Reference 12. [c]Present work.

quite different techniques. The only exception to this is provided by *cis*-2-butene for which the rate constant determined in the present work is about 12% greater than previously found (12). It is believed that the present figures are accurate to within a few per cent in contrast to the previously estimated uncertainty of 10 to 15%.

The electrophilic character of oxygen atoms in their reactions with olefins is evident from the continuous increase in reactivity with increasing number of alkyl substituents on the doubly bonded carbon atoms, which primarily determine the electron-donating power, i.e. the basicity of olefins. Furthermore, in agreement with the electrophilic character of oxygen atoms their rate of addition to butadiene is comparable to that of two-substituted ethylenes while for radical reagents it would be expected to be much larger.

The logarithms of the relative rate constants of the reactions of oxygen atoms with olefins were previously found to be approximately linearly correlated with the following physical properties of the olefins (12): ionization potentials, heats of hydrogenation, and spectroscopic excitation energies. Also approximate linear free energy plots were obtained with some other series of electrophilic reactions (12), as well as approximate linear correlations with the theoretically derived excitation energies and bond orders (17). In view of the more complete and more accurate list of the relative rate constants for this reaction series now available (Table III), and additional literature information for some of the other reaction series considered, it is necessary to examine these correlations in somewhat greater detail.

In Fig. 1 are plotted logarithms of the relative rate constants for several series of electrophilic reactions against the ionization potentials of olefins. Of these series the oxygen atom additions to olefins are the only series of vapor phase reactions. The CCl_2 and CBr_2 series will be disregarded for the moment. It is seen that the bromination reactions give a good linear correlation. However, information is lacking for a greater variety of compounds that would permit finding out whether deviations shown by the oxygen atom and the peracetic acid series would appear in this case as well. In the latter two series it is found that the values of the rate constants for all the singly substituted ethylenes remain essentially constant and thus do not follow the trend in the ionization potentials. The same holds also for the two-substituted ethylenes.

In Fig. 2 relative rate constants are plotted against the excitation energies obtained by molecular orbital calculations (17). Excellent linear correlation is shown by the peracetic acid series. The same is also largely true for the oxygen atom and the bromination series, although in the former the value for tetramethyl ethylene is somewhat low and in the latter there is perhaps suggestion of a slight curvature. The value for the reaction of oxygen atoms with butadiene does not fit into this plot, although it does fit quite well into the ionization potential plot in Fig. 1 and the plot of the log k values against the bond orders in Fig. 3 (in these plots butadiene is indicated by squares instead of circles). The bond orders have been obtained by molecular orbital calculations (17) and they correlate well with the logarithms of the rate constants for the peracetic acid, oxygen atom, and bromination series, although the plots are slightly curved.

The deviations from the straight line plots in Fig. 1 for the oxygen atom and the peracetic acid series are as a rule larger for bigger substituents. Thus, for example, in the oxygen atom series the deviations for the monosubstituted ethylenes are in the order propylene < 1-butene < *n*-1-hexene, and similarly for the peracetic acid series the order is propylene < *n*-1-pentene < *n*-1-hexene < *n*-1-octene < *n*-1-decene. In view of this, the deviations could perhaps be ascribed to steric hindrance. However, it is significant that these deviations disappear in the plots against the theoretically derived excitation
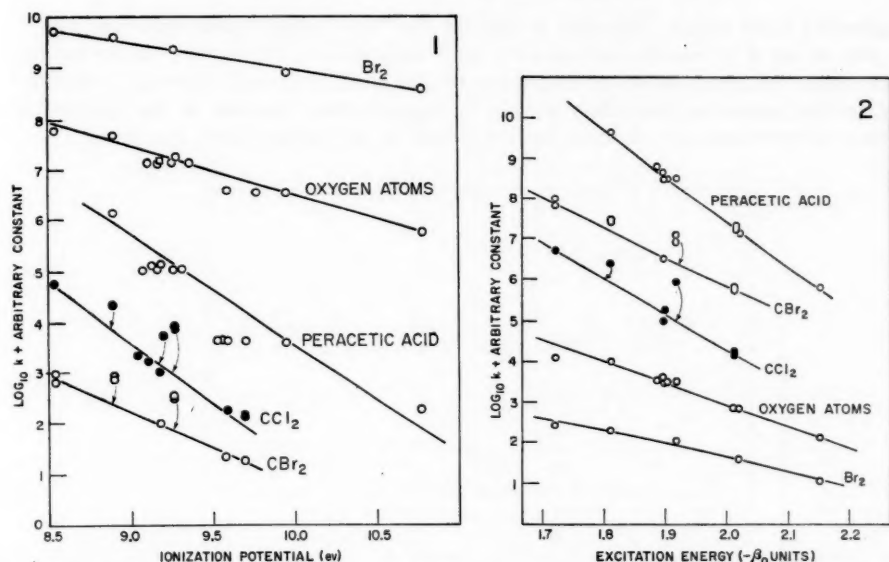
FIG. 1. Plot of log *k* values against the ionization potentials. (Source of data: Ionization potentials—J. Collin and F. P. Lossing. J. Am. Chem. Soc. **81**, 2064 (1959); R. E. Honig. J. Chem. Phys. **16**, 105 (1948). *Bromination reactions*—S. V. Anantakrishnan and C. K. Ingold. J. Chem. Soc. 984, 1396 (1935). *Peracetic acid reactions*—J. Boeseken and J. Stuurman. Rec. trav. chim. **56**, 1034 (1937); J. Boeseken and C. J. A. Hanegraaff. Rec. trav. chim. **61**, 69 (1942); D. Swern. J. Am. Chem. Soc. **69**, 1692 (1947). CBr₂ and CCl₂ reactions—W. von E. Doering and Wm. A. Henderson, Jr. J. Am. Chem. Soc. **80**, 5274 (1958) with some results for CBr₂ reactions from P. S. Skell and A. Y. Garner. J. Am. Chem. Soc. **78**, 5430 (1956). *Oxygen atom reactions*—taken from Table III of the present work.)

FIG. 2. Plot of log *k* values against the excitation energies. (Source of data: excitation energies. reference 17; rate constants, as given in caption of Fig. 1.)
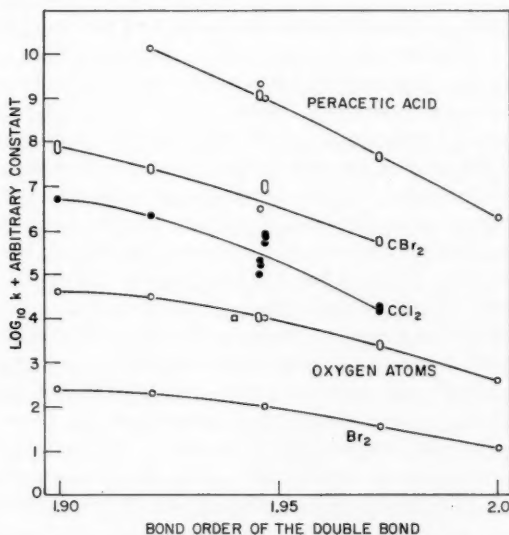

FIG. 3. Plot of log *k* values against the bond orders of the olefinic double bonds. (Source of data: bond orders, reference 17; rate constants, as given in caption of Fig. 1.)

energies and bond orders. The same is true for the "free energy" plots shown in Fig. 4. The plot of log k values for the peracetic acid reactions vs. log k_O (the values for the oxygen atom reactions) shows no deviations of this kind. It appears, therefore, that the trend in the ionization potentials is only an approximate measure of the basicity of olefins as determined, for example, by the trends in the oxygen atom reactions.
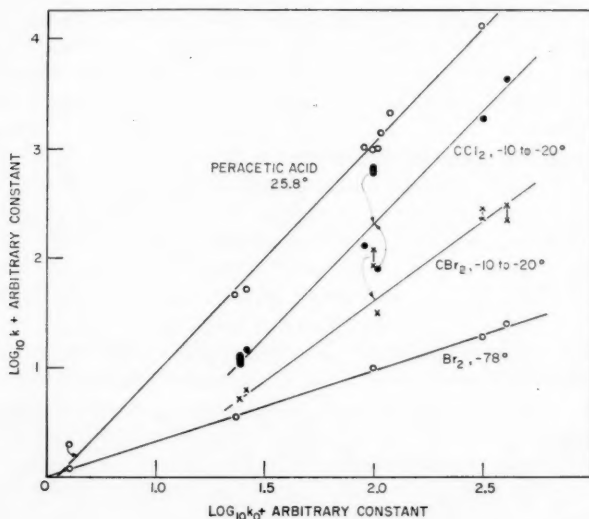

FIG. 4. Free energy plots for bromination, peracetic acid, CBr_2, CCl_2, and oxygen atom reactions with olefins. (Source of data: as given in caption of Fig. 1.)

There is little quantitative information on the basicity of olefins. The basicity towards silver ion was found by Winstein and Lucas (18) to decrease rather than increase with increasing alkyl substitution, presumably because of steric hindrance to the approach of the large ion to the π-electrons of the olefin. Brown and Brady (19) have measured Henry's law constants for olefin–HCl mixtures at $-78°$ and the order of basicity found by these authors is qualitatively the same as the order of reactivity for the considered electrophilic reactions. Unfortunately the data cannot be used for a quantitative correlation. West (20) has recently obtained some quantitative information for the basicity of a number of olefins towards phenols from the shifts in the frequency of the O—H infrared band due to hydrogen bond formation. Plots of log k values against the frequency shifts due to hydrogen bonding of olefins with p-fluorophenol are given in Fig. 5. For the bromination series the available information is very incomplete. For the oxygen atom and the peracetic acid series there is a good correlation except that the shifts are exceptionally large for the α,α-disubstituted olefins* and therefore these compounds show large deviations. In addition to this irregularity, the experimental uncertainty in these values of about ± 6 cm^{-1} is relatively large for the purpose of quantitative correlations of this kind.

The mechanisms of reactions of electrophils with aromatic compounds have been extensively investigated. The mechanism of electrophilic aromatic substitution has been

*Possible reasons for this are discussed in reference 20. In Fig. 5 the frequency shift for 2-methyl-1-butene has been used for isobutene, for which the frequency shift was not determined.
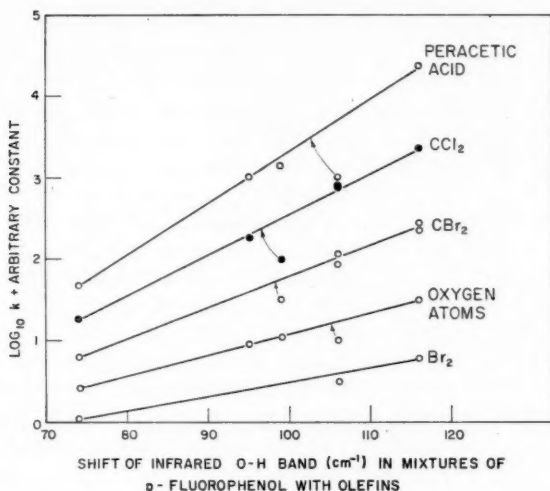
FIG. 5. Plot of log k values against the frequency shift of infrared O—H band in mixtures of p-fluorophenol with olefins. (Source of data: frequency shifts, reference 20; rate constants, as given in caption of Fig. 1.)

recently discussed by Brown (21) with the conclusion that it involves unsymmetrical inner charge-transfer complexes (or σ complexes) as stable intermediates, rather than outer complexes (or π complexes), in which only slight charge transfer to the electrophil occurs. He derived certain theoretical quantities (Z values) as indices of chemical reactivities of positions in aromatic compounds for a given electrophil. These are largely determined by the difference of the electron affinity of the electrophil and the ionization potentials of the aromatic compounds. An extension of this treatment to some electrophilic addition reactions appears to be contemplated.

In the case of oxygen atom addition to olefins there is indication that the rate of addition and the orientation are not governed by the same factors. This conclusion is based on the observation (11, 12) that in 2-pentene the addition takes place exclusively at the doubly bonded C-atom to which methyl group is attached (and not to the one to which ethyl group is attached) although the rates of addition to propylene and to 1-butene are the same and in both cases terminal addition occurs. Similarly the rates of addition to 2-butene and 2-pentene are again about the same. If the same factors governed the over-all reactivity and the orientation, about equal addition to the two doubly bonded C-atoms in 2-pentene would be expected. For these reasons it appears that the transition state responsible for the observed activation energies must occur quite early in the reaction process, perhaps as shown qualitatively in Fig. 6.

In their approach to an olefinic double bond, oxygen atoms experience at first a repulsion, but already at relatively large distances the electrostatic interaction leads to a lowering of the potential energy of the system. It seems necessary to assume that at this stage the atoms are not localized on one of the two doubly bonded C-atoms and the minimum at A in Fig. 6 is visualized as perhaps corresponding to a charge-transfer complex (using this term somewhat loosely). In this particular process the very exothermic transformation to the intermediate B is believed to occur rapidly and does not influence
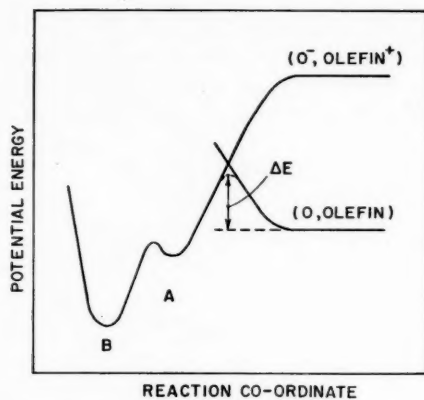
FIG. 6. Potential energy – reaction co-ordinate schematic diagram for the reaction of oxygen atoms with olefins.

the over-all rate of addition. In B the oxygen atom is localized on one of the two double-bond C-atoms and this intermediate is believed to be a triplet biradical (probably with some Zwitterion character) when the oxygen atoms reacting with the olefin are in their ground state (^3P). In agreement with this, both *cis*- and *trans*-epoxides are formed from internal olefins, and also intramolecular rearrangements to carbonyl compounds take place (11).

It is also possible that in some cases the transformation from A to B in Fig. 6 may be rather slow, in which case the observed rate is a composite quantity, as discussed in connection with a study of the rates of ozone addition to olefins in the vapor phase (22).

The diagram in Fig. 6 is of the type discussed in the Introduction and one could, therefore, adopt the usual assumptions (1–6) and from simple geometrical considerations arrive at the prediction of approximate linear dependence of the activation energies on such a property of the olefins as, for example, the ionization potentials. At the same time, some of these assumptions are very arbitrary and can only be justified by extensive agreement of experimental observations with the predictions. Moreover, the exact significance of the experimentally observed approximate linear correlations is uncertain since several physical properties of the olefins show approximately parallel trends.

The significance of the free energy plots in Fig. 4 has been discussed in some detail previously (12). In as much as in a plot of log k_1 vs. log k_2 the linear correlation persists over a temperature range, then in each one of the two reaction series either (*a*) the entropies of activation are to a good approximation equal for all the members of the series (isoentropic series), (*b*) the enthalpies of activation are equal (isoenthalpic series), or (*c*) there is linear correlation between the enthalpies and entropies of activation (compensating or additive enthalpy–entropy effect). In view of this, the slope of the free energy plot for peracetic acid and oxygen atoms represents the constant ratio of the activation energy differences for equal structural changes in the olefins multiplied by the inverse ratio of the absolute temperatures at which rate determinations have been made in the two series (cf. equation (14*a*) of reference 12) since both these series of reactions are approximately isoentropic. Any contributions of the solvent effects to the activation energies of the peracetic acid reactions must be small or to a good approximation constant

for the considered cases. These conclusions perhaps also approximately apply to the other series of reactions considered here, although their temperature coefficients at sufficiently large temperature intervals are not known.

The good correlations in the free energy plots in Fig. 4 for the peracetic acid and bromination reactions, when plotted against the logarithms of the rate constants of the oxygen atom reactions, show that these values can serve as an empirical measure of the basicity of olefins as it manifests itself in such addition reactions. This is equivalent to defining Hammett σ and ρ functions for these processes (12).

The series of CBr_2 and CCl_2 reactions with olefins have been considered here for the sake of completeness. They show general electrophilic trends but at the same time there are some large systematic deviations in the plots in Figs. 1–5. Thus, for example, in Fig. 4 the rate constants for cyclohexene are too low and for isobutene they are too high. In the plot in Fig. 5, the discrepancy for cyclohexene remains while it disappears for the α,α-disubstituted olefins. This is due to the exceptionally high values obtained for infrared O—H band frequency shifts in mixtures of phenols with these latter compounds and it may perhaps be fortuitous. There is need for more extensive experimental information on these reaction series in order to ascertain in greater detail the extent and the nature of the deviations.

ACKNOWLEDGMENTS

REFERENCES

1. R. A. Ogg, Jr. and M. Polanyi. Trans. Faraday Soc. 31, 604 (1935).
2. M. G. Evans and M. Polanyi. Trans. Faraday Soc. 34, 11 (1938).
3. M. G. Evans. Discussions Faraday Soc. 2, 271 (1947).
4. M. G. Evans, J. Gergely, and E. C. Seaman. J. Polymer Sci. 3, 866 (1948).
5. M. Levy and M. Szwarc. J. Am. Chem. Soc. 77, 1949 (1955).
6. M. Szwarc. J. Phys. Chem. 61, 40 (1957); J. H. Binks and M. Szwarc. J. Chem. Phys. 30, 1494 (1959).
7. C. Walling. J. Phys. Chem. 64, 166 (1960).
8. H. W. Melville and J. C. Robb. Proc. Roy. Soc. (London), A, 196, 445, 466, 479, 494 (1949).
9. K. R. Jennings and R. J. Cvetanović. To be published.
10. R. J. Cvetanović. J. Chem. Phys. 25, 376 (1956).
11. R. J. Cvetanović. Can. J. Chem. 36, 623 (1958).
12. R. J. Cvetanović. J. Chem. Phys. 30, 19 (1959).
13. R. J. Cvetanović. J. Chem. Phys. 23, 1203 (1955).
14. S. Sato and R. J. Cvetanović. Can. J. Chem. 36, 279, 970, 1668 (1958); 37, 953 (1959).
15. D. J. Le Roy. Can. J. Research, B, 28, 492 (1950).
16. R. J. Cvetanović. J. Chem. Phys. In press.
17. S. Sato and R. J. Cvetanović. J. Am. Chem. Soc. 81, 3223 (1959).
18. S. Winstein and H. J. Lucas. J. Am. Chem. Soc. 60, 836 (1938).
19. H. C. Brown and J. D. Brady. J. Am. Chem. Soc. 74, 3570 (1952).
20. R. West. J. Am. Chem. Soc. 81, 1614 (1959).
21. R. D. Brown. J. Chem. Soc. 2224 (1959).
22. T. Vrbaski and R. J. Cvetanović. Can. J. Chem. 38, 1053 (1960).

ATOMIC REACTIONS IN THE UPPER ATMOSPHERE[1]

JOSEPH KAPLAN, WILLIAM J. SCHADE, CHARLES A. BARTH, AND ALVIN F. HILDEBRANDT

ABSTRACT

The reaction rates of nine upper atmosphere chemical reactions have been analyzed with a digital computer. The dependence of the loss rates of atomic nitrogen and atomic oxygen as well as the relative concentrations of nitric oxide and nitrogen dioxide in the upper atmosphere are given. Using a flow system, nitrogen atoms were produced and then titrated by the addition of NO. The resulting nitrogen and oxygen atom densities were measured with an e.p.r. spectrometer. The dependence of the intensities of the nitrogen afterglow and the NO afterglow were related to the atom densities. An excitation mechanism for OI 5577 has been determined from the relation of the intensity of λ 5577 to the atom densities.

ATOMIC REACTIONS IN THE CHEMOSPHERE

In the upper half of the earth's chemosphere between 65 and 120 km, reactions involving atomic species constitute the predominant chemical activity. The atoms involved are those produced by the solar photodissociation of the molecular atmospheric gases, nitrogen, oxygen, and hydrogen. The atoms react with one another and with the remaining molecules that are present. The dominant upper atmosphere reactions between atomic nitrogen and atomic oxygen and their various molecular forms are described by the following nine equations:

$$N + N + M \rightarrow N_2 + M \tag{1}$$

$$N + O + M \rightarrow NO + M \tag{2}$$

$$O + O + M \rightarrow O_2 + M \tag{3}$$

$$N + NO \rightarrow N_2 + O \tag{4}$$

$$N + O_2 \rightarrow NO + O \tag{5}$$

$$O + O_2 + M \rightarrow O_3 + M \tag{6}$$

$$O + O_3 \rightarrow O_2 + O_2 \tag{7}$$

$$NO + O + M \rightarrow NO_2 + M \tag{8}$$

$$NO_2 + O \rightarrow NO + O_2 \tag{9}$$

In the first three reactions atomic nitrogen and atomic oxygen recombine in three-body reactions. Atomic nitrogen also reacts rapidly with nitric oxide and more slowly with molecular oxygen in reactions 4 and 5. The formation and destruction of ozone are governed by reactions 6 and 7 and the formation and destruction of nitrogen dioxide, by reactions 8 and 9. The rate coefficients for reaction 1 and reactions 4 through 9 are available in the recent literature (1, 2). Recently, in an experiment at the Jet Propulsion Laboratory, the rate coefficients of reactions 2 and 3 have been measured (3).

The differential equations describing the rates of change of density of the various species are the following:

$$-[\dot{N}] = 2k_1[N]^2[M] + k_2[N][O][M] + k_4[N][NO] + k_5[N][O_2] \tag{10}$$

$$-[\dot{O}] = k_2[N][O][M] + 2k_3[O]^2[M] - k_4[N][NO] - k_5[N][O_2] + k_6[O][O_2][M] + k_7[O][O_3] + k_8[NO][O][M] + k_9[NO_2][O] \tag{11}$$

$$-[\dot{N}O] = -k_3[N][O][M] + k_4[N][NO] - k_5[N][O_2] + k_8[NO][O][M] - k_9[NO_2][O] \qquad [12]$$

$$-[\dot{O}_2] = -k_3[O]^2[M] + k_5[N][O_2] + k_6[O][O_2][M] - 2k_7[O][O_3] - k_9[NO_2][O] \qquad [13]$$

$$-[\dot{O}_3] = -k_6[O][O_2][M] + k_7[O][O_3] \qquad [14]$$

$$-[\dot{N}O_2] = -k_8[NO][O][M] + k_9[NO_2][O] \qquad [15]$$

This set of simultaneous, non-linear differential equations has been numerically integrated for several different initial conditions on the Jet Propulsion Laboratory's IBM 704 digital computer (3). The results of one of these numerical calculations may be seen in Fig. 1. Although the atom densities used in this calculation pertain to a laboratory
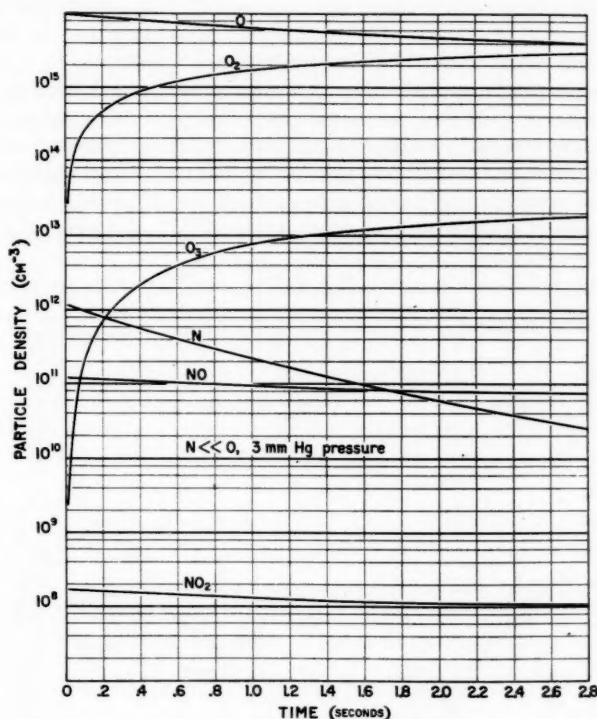
FIG. 1.   Change of particle densities with time.

experiment, the conditions are analogous to those of the upper atmosphere in that the density of oxygen atoms is much greater than the density of nitrogen atoms. An analysis of the results of this numerical integration when applied to the chemosphere between 80 and 120 km gives the following results:

1. The rate of loss of atomic nitrogen is governed by its reaction with molecular oxygen, reaction 5.

2. The concentration of nitric oxide is determined by reaction 5 and the reaction of atomic nitrogen with nitric oxide, reaction 4. The density of nitric oxide is much less than, and proportional to, the density of the molecular oxygen present.

$$[NO] = k_5/k_4[O_2] \qquad [16]$$

3. The concentration of nitrogen dioxide in the upper atmosphere is governed by the reactions of atomic oxygen with nitric oxide and nitrogen dioxide, reactions 8 and 9. The density of nitrogen dioxide is less than, and proportional to, the density of nitric oxide.

$$[NO_2] = (k_8/k_9)[M][NO] \qquad [17]$$

4. The rate of loss of atomic oxygen is determined by its three-body recombination, reaction 3.

ATOM DENSITY MEASUREMENTS

In some recent work at the Jet Propulsion Laboratory, atom densities of mixtures of nitrogen atoms and oxygen atoms have been measured with an electron paramagnetic resonance spectrometer (4). With this technique, atom densities as low as 5×10^{12} atoms/cm³ have been determined. The nitrogen atoms are produced in a flow system by a 2450-mc microwave discharge operating at a total pressure of 3 mm Hg. The oxygen atoms were produced by titrating the atomic nitrogen with nitric oxide. The resulting mixture of atoms was pumped through the e.p.r. resonant cavity, which is located between the pole faces of an electromagnet. It is in this cavity that the atom densities are measured. The ground state of atomic nitrogen is ^4S with $J = 3/2$ and a Lande g factor of 2. Atomic oxygen has a ^3P ground state with a Lande g factor of $3/2$. Both the $J = 2$ and $J = 1$ states of oxygen are measured.

The results of this study are shown in Fig. 2. The atom densities are plotted along the
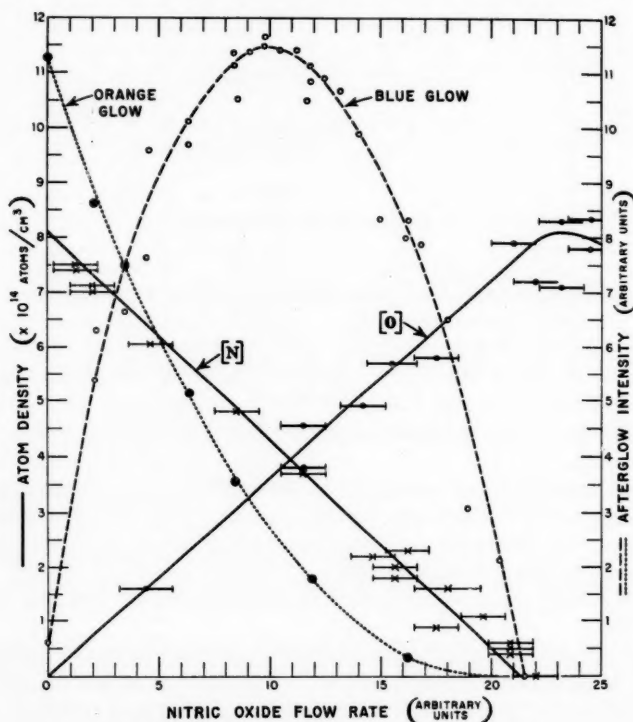

FIG. 2. Dependence of afterglow intensities on atom densities.

ordinate and the amount of NO added is plotted along the abscissa. Since the atomic nitrogen – nitric oxide reaction is very fast (1), for every nitric oxide molecule added, a nitrogen atom is converted into an oxygen atom before the gas enters the resonant cavity. Hence, the straight lines with slopes of 45° and −45° for the oxygen and nitrogen atom densities, respectively. Nitric oxide was continued to be added after all the nitrogen atoms were consumed. The loss of oxygen atoms on the right-hand side of the figure is governed by the nitric oxide – atomic oxygen reaction which is still taking place as the gas is pumped through the resonant cavity. Figure 1 is a decay study of the experimental conditions occurring near the minimum of nitrogen atom density and the maximum of oxygen atom density.

AFTERGLOW INTENSITY MEASUREMENTS

The intensity of the molecular nitrogen first positive bands that are emitted by the nitrogen afterglow is proportional to the square of the nitrogen atom density (5). In some work at the University of California, Los Angeles, it has been shown that the intensity of the nitric oxide beta bands is proportional to the product of the nitrogen atom density and the oxygen atom density (6). Using the preceding technique of addition of NO to atomic nitrogen, the atomic nitrogen density was decreased and the atomic oxygen density was increased. A simultaneous photometric recording of the intensities of the N_2 first positive bands and the NO beta bands provides data for interpreting the dependence of the intensity of the NO beta bands on the relative atomic densities of oxygen and nitrogen. A plot of I_b (intensity of NO beta bands) against the square root of the intensity of the N_2 first positive bands then yields a parabolic curve. This curve is consistent with the interpretation that the fast reaction 4 produces an increase in the atomic oxygen density which is equal in magnitude to the decrease in atomic nitrogen density, i.e.,

$$d[O] = -d[N].$$ [18]

Integration of 18 gives

$$[O] = [N_0] - [N],$$ [19]

in which $[N_0]$ is the initial atomic nitrogen density before addition of NO and the initial atomic oxygen density is zero. Assuming that the emission of the beta bands follows a recombination of type 2, the intensity of the beta bands can be written

$$I_b = k_b[N][O][M].$$ [20]

Substitution of [19] into [20] gives

$$I_b = k_b[M][N]([N_0] - [N])$$ [21]

so that a plot of [21] against [N] produces the same parabolic curve obtained experimentally. The afterglow recombination mechanism 2 was also concluded in previous work (7). The dependence of the intensity of the N_2 first positive bands and the nitric oxide beta bands is plotted in Fig. 2 against flow rate of added nitric oxide. The parabolic shape of these curves illustrates their relationship to the nitrogen and oxygen atom densities.

Excitation of the atomic oxygen green line, OI 5577, which is a prominent spectral feature emanating from the upper atmosphere, has been studied recently by the addition of NO to active nitrogen (6). When atomic oxygen is added to atomic nitrogen by reaction 4, OI 5577 is found to be excited. As more NO is added to the system, the intensity of λ 5577 goes through a maximum value and decreases rapidly as the atomic nitrogen

density approaches zero. An excitation mechanism which is consistent with the relation between the intensity of λ 5577 and the variation of the atomic species is found to be

$$N + N + O \rightarrow N_2 + O(^1S) \tag{22}$$

$$O(^1S) \rightarrow O(^1D) + \lambda\ 5577 \tag{23}$$
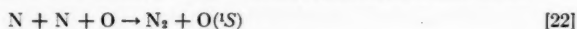
in which ^1S is the upper state and ^1D the lower state of atomic oxygen for the emission of λ 5577. When sufficient NO is added to the system so that all atomic nitrogen has been removed, a condition is obtained in which the only remaining atomic species is that of oxygen so that $[O] = [N_0]$ (see Fig. 2). Under this condition the excitation of OI 5577 should take place by the reaction

$$O + O + O \rightarrow O_2 + O(^1S) \tag{24}$$

$$O(^1S) \rightarrow O(^1D) + \lambda\ 5577 \tag{25}$$

which was proposed for the excitation occurring in the upper atmosphere (8). It has been found in the laboratory that reaction 22 is much more efficient than reaction 24 in the excitation of the ^1S state of atomic oxygen.

<div align="center">REFERENCES</div>

1. G. B. KISTIAKOWSKY and G. G. VOLPI. J. Chem. Phys. 27, 1141 (1957); 28, 665 (1958).
2. F. KAUFMAN. J. Chem. Phys. 28, 352 (1958).
   P. HARTECK, R. R. REEVES, and G. MANELLA. J. Chem. Phys. 29, 608 (1958).
   J. F. HERRON, J. L. FRANKLIN, P. BRADT, and V. H. DIBELER. J. Chem. Phys. 30, 879 (1959).
   R. R. REEVES, G. MANELLA, and P. HARTECK. J. Chem. Phys. 32, 632 (1960).
   S. KRONGELB and M. W. P. STRANDBERG. J. Chem. Phys. 31, 1196 (1959).
   S. W. BENSON and A. E. AXWORTHY. J. Chem. Phys. 26, 1718 (1957).
   H. W. FORD and N. ENDOW. J. Chem. Phys. 27, 1156 (1957).
3. C. A. BARTH. J. Chem. Phys. Submitted for publication.
4. A. F. HILDEBRANDT and C. A. BARTH. J. Chem. Phys. Submitted for publication.
5. J. BERKOWITZ, W. A. CHUPKA, and G. B. KISTIAKOWSKY. J. Chem. Phys. 25, 457 (1956).
6. W. J. SCHADE and J. KAPLAN. To be published.
7. F. KAUFMAN and J. R. KELSO. J. Chem. Phys. 27, 1209 (1957).
   F. KAUFMAN. J. Chem. Phys. 28, 992 (1958).
   C. A. BARTH, W. J. SCHADE, and J. KAPLAN. J. Chem. Phys. 30, 347 (1959).
8. S. CHAPMAN. Phil. Mag. 23, 657 (1937).

THREE-BODY RECOMBINATION OF GASEOUS IONS[1]

Takayuki Fueno, Henry Eyring, and Taikyue Ree

ABSTRACT

The recombination of gaseous ions in the presence of third bodies is assumed to follow a sequence of two bimolecular steps: $M + X^+ \rightleftharpoons MX^+$ and $MX^+ + Y^- \rightarrow XY + M$. The termolecular rate constants of the over-all processes are calculated for several ionized gases at various temperatures. For the calculation, the equilibrium internuclear separation and the corresponding binding energy of a complex ion, MX^+, are obtained by minimizing the inter-action energy between M and X^+, which is approximated to the sum of the Lennard-Jones potential for the M–X interaction and the polarization energy between M and X^+. The re-combination coefficients of some ionized gases at 288° K and various pressures are calculated and compared with the observed data. The agreement is found to be satisfactory. The limita-tions of this theoretical approach are discussed.

INTRODUCTION

The surplus energy evolved by the neutralization (or recombination) between positive and negative ions in a gaseous phase can be removed as radiation or taken up as the energy of excitation or homolytic dissociation of the recombination product (1, 2). Thomson (3) developed a gas-kinetic theory of the ion recombination occurring by the three-body process. The theory was based on the concept that two ions of opposite signs are only capable of recombination if either of the two ions collides with an uncharged molecule within a certain maximum distance from the other. The theory has proved very successful in the pressure range from 100 to 1000 mm Hg.

Recently, Bunker and Davidson (4) have proposed a kinetic theory to account for the rates of halogen atom recombinations in the presence of various third bodies. The theory assumes that an equilibrium concentration of intermediate complex is formed between halogen atoms and third bodies and that the collisions of the complexes with halogen atoms result in the halogen atom recombinations, releasing the third-body molecules. The dependence of the termolecular reaction rate constants upon temperature and third body has thus been interpreted quantitatively.

The present paper outlines a theoretical method of predicting the rates of the three-body recombinations of gaseous ions. The treatment pursues essentially the Bunker–Davidson theory for atom recombinations (4), except that, in our approach, the electrostatic nature of the recombining species is also taken into account. The theory is successfully applied to the calculation of the recombination coefficients for some ionized gases.

CALCULATION METHOD

An over-all three-body process of ion recombination, $X^+ + Y^- + M \rightarrow XY + M$, is assumed to be divided into a sequence of two bimolecular steps:

$$M + X^+ \underset{k_{-1}}{\overset{k_1}{\rightleftharpoons}} MX^+ \qquad [i]$$

$$MX^+ + Y^- \overset{k_2}{\rightarrow} XY + M \qquad [ii]$$

where M denotes a third body. If MX^+ is a loose complex and M is in a large excess

compared with X^+ and Y^-, then MX^+ will be in equilibrium with X^+ and M, undisturbed by step [ii]. Then the rate constant, k_t, for the over-all termolecular process can be approximated as (4, 5)

$$[1] \qquad\qquad\qquad\qquad k_t = K_1 k_2,$$

K_1 being the equilibrium constant for step [i].

Assuming that the complex MX^+ is an ion cluster, we now calculate the equilibrium constant, K_1. The complex may be loose enough so that M and X^+ are free to rotate and vibrate within the complex (6). Then, all the internal parts of the partition functions of the separated reactants will also appear in the partition function of the complex and will cancel out in the expression of the equilibrium constant, K_1, in terms of partition functions. Thus,

$$[2] \qquad\qquad\qquad K_1 = \frac{F_{t,MX^+} F_{v,MX^+} F_{r,MX^+}}{F_{t,M} F_{t,X^+}} \, e^{\epsilon_m/kT}$$

where ϵ_m is the binding energy of MX^+, and the subscripts t, v, and r indicate that the F's are respectively the translational, vibrational, and rotational partition functions of the substances indicated.

If we assume that the complex is a rigid rotor as well as a harmonic oscillator and that neither of the rotational and vibrational energies of the complex can exceed the binding energy ϵ_m, then (7)

$$[3] \qquad\qquad\qquad F_{r,MX^+} = \frac{8\pi^2 \mu_+ r_m^2 kT}{h^2} (1 - e^{-\epsilon_m/kT})$$

and

$$[4] \qquad\qquad\qquad F_{v,MX^+} = \frac{1 - e^{-\epsilon_m/kT}}{1 - e^{-\epsilon_v/kT}}$$

where μ_+ is the reduced mass of the complex, r_m the equilibrium internuclear distance between M and X^+ in the complex, and ϵ_v the vibrational quantum of the $M-X^+$ bond. Substituting all the partition functions into eq. 2, we obtain

$$[5] \qquad\qquad K_1 = \frac{h^3}{(2\pi\mu_+ kT)^{3/2}} \cdot \frac{8\pi^2 \mu_+ r_m^2 kT}{h^2} \cdot \frac{(1 - e^{-\epsilon_m/kT})^2 e^{\epsilon_m/kT}}{1 - e^{-\epsilon_v/kT}} .$$

For step [ii] of the recombination we assume that every collision between MX^+ and Y^- leads to the neutralization with the liberated energy which is carried away by the third body, M. Then, assuming that the steric factor for the collision is unity, we can write

$$[6] \qquad\qquad\qquad k_2 = Q \left\{ \frac{8kT(m + m_+ + m_-)}{\pi(m + m_+)m_-} \right\}^{\frac{1}{2}},$$

where Q is the effective collision cross section, and m, m_+, and m_- are the masses of M, X^+, and Y^-, respectively.

The feature of the collision cross section for ion recombinations is largely different from that of the usual gas-kinetic collisions, because of a considerable extent of coulombic attraction between the two recombining ionic partners. One charged particle can be captured by the other when the attraction exceeds the relative kinetic energy of the ion pair. If the gaseous ions are in thermal agitation, the largest permissible distance of approach, δ, for ions to recombine is (3)

$$[7] \qquad\qquad\qquad\qquad \delta = \frac{2e^2}{3kT},$$

where e is the electronic charge and δ is of the order of 10^{-6} cm at ordinary temperatures. The effective cross section, Q, for the ion recombination is given by

$$[8] \qquad Q = \pi\delta^2 = \frac{4\pi e^4}{9k^2T^2}.$$

From eqs. 1, 5, 6, and 8 we finally obtain the termolecular rate constant, after the proper cancellation,

$$[9] \qquad k_t = \frac{32\pi h e^4 r_m^2 (m+m_+ +m_-)^{\frac{3}{2}}}{9\mu_+^{\frac{1}{4}} m_-^{\frac{1}{4}} (m+m_+)^{\frac{1}{4}} k^2 T^2} \cdot \frac{(1-e^{-\epsilon_m/kT})^2 e^{\epsilon_m/kT}}{1-e^{-\epsilon_v/kT}}.$$

In order to obtain the values of k_t for recombining systems from eq. 9 it is necessary to evaluate the three parameters, r_m, ϵ_m, and ϵ_v. For evaluating the r_m and ϵ_m, both the X$^+$ and M are idealized as rigid spheres. If X and M are molecules with little or no permanent dipole, then the potential of interaction between X$^+$ and M will be reasonably approximated to the sum of the Lennard-Jones potential of interaction between the two neutral molecules and the polarization energy, i.e., the attraction between the static charge on X$^+$ and the dipole moment induced on M

$$[10] \qquad \epsilon_L(r) = 4\epsilon_0\left\{\left(\frac{\sigma}{r}\right)^{12} - \left(\frac{\sigma}{r}\right)^6\right\} - \frac{\alpha e^2}{2r^4}.$$

Here ϵ_0 and σ respectively denote the maximum depth of the potential well and the closest approach for the interaction between X and M, r is the internuclear separation of the MX$^+$ complex, and α is the angle-average polarizability of M. The equilibrium distance, r_m, and the corresponding binding energy, ϵ_m, of the complex can be obtained by minimizing the $\epsilon_L(r)$ with respect to r, provided that the values of ϵ_0, σ, and α are known.

The vibrational quantum, ϵ_v, can be calculated from [8]

$$[11] \qquad \epsilon_v = 2a\,(\epsilon_r\epsilon_m)^{\frac{1}{2}}$$

where $\epsilon_r = h^2/8\pi^2\,\mu_+ r_m^2$ and a is a parameter appearing in the Morse potential function for the complex in the form

$$[12] \qquad \epsilon_M(r) = \epsilon_m[\{1-e^{-a[(r/r_m)-1]}\}^2 - 1].$$

The value of a is obtainable, in principle, by making the Morse potential curve (eq. 12) fit the Lennard-Jones-type potential curve (eq.10). A practical method employed here for this purpose is setting the bond-stretching force constant, f_M, derived from the Morse function

$$[13] \qquad f_M = \left[\frac{d^2\epsilon_M(r)}{dr^2}\right]_{r=r_m} = \frac{2a^2\epsilon_m}{r_m^2}$$

equal to the force constant, f_L, from the Lennard-Jones-type function

$$[14] \qquad f_L = \left[\frac{d^2\epsilon_L(r)}{dr^2}\right]_{r=r_m} = \frac{24\epsilon_0}{r_m^2}\left\{26\left(\frac{\sigma}{r_m}\right)^{12} - 7\left(\frac{\sigma}{r_m}\right)^6\right\} - \frac{10\alpha e^2}{r_m^6}.$$

Thus, the three parameters, r_m, ϵ_m, and ϵ_v, involved in eq. 9 can straightforwardly be evaluated for the interacting systems for which the data of the relevant parameters, ϵ_0, σ, and α are available.

COMPARISON WITH EXPERIMENTS

It is experimentally established that the rates of recombination of gaseous ions are of a first order with respect to each concentration of positive and negative ions. The bimolecular rate constants, ρ, defined as

$$[15] \qquad \frac{d(X^+)}{dt} = \frac{d(Y^-)}{dt} = -\rho(X^+)(Y^-),$$

are usually called the recombination coefficients (1, 2). If the recombination takes place by the two-step mechanism assumed in this paper, the recombination coefficient should be equal to the product of the termolecular rate constant and the third-body concentration, i.e.

$$[16] \qquad \rho = k_t(M).$$

Over the pressure range from 100 to 760 mm Hg, the values of ρ for the recombinations in familiar gases such as CO, CO_2, SO_2, N_2O, and air have been observed to be proportional to the gas pressure (9). This observation indicates that over this pressure range the three-body process is the most important for the recombinations of ions at least in the cases of the above-mentioned molecular gases.

In order to obtain the value of ρ for recombining ions in a given gas, molecular configurations of X^+ and Y^- need to be specified. According to the mass spectroscopic experiments, most of the positive ions formed by electron impact with molecules are, in general, of the simple molecular type, i.e., the lowest appearance potential of a positive ion from a molecule corresponds to the simple removal of an electron without dissociation (10). Probably, a similar generalization applies to the ionizations of molecular gases resulting from the action of X-rays, a method which was often employed in earlier years (9, 11). Thus, it is assumed throughout the present paper that X^+ is the molecular ion formed by the removal of an electron from M.

Negative ions can be formed by the collisions of electrons with neutral molecules. However, it is not, as a rule, obvious what products result from the collisions. The best information has been given by mass spectroscopic studies. For instance, the most prominent negative ion observed in air and oxygen under pressures of 0.1 to 10 mm Hg has been identified to be O^-, instead of O_2^- (12). The atomic ion O^- is found to be the most abundant (or the only) negative ion also in the cases of CO (13), CO_2 (14), N_2O (15), NO (13, 15), NO_2 (16), and SO_2 (17). Thus, it appears very likely that the gaseous oxide molecules as well as oxygen molecules produce negative ions most effectively by the "resonance electron-capture dissociation (18)." In our calculation, therefore, Y^- is assumed to be the atomic ion O^- for all of the oxygen-containing molecules investigated.

According to the procedure described in the preceding section, all the potential parameters associated with the $M—X^+$ interactions were calculated for various gases. The data of the Lennard-Jones potential parameters, σ and ϵ_0, and the polarizability, α, for these gases were taken from the literature (19). All of the parametric values obtained are summarized in Table I.

Figure 1 shows the potential curves of interaction between CO_2^+ and CO_2 as a typical example of the $M—X^+$ interaction curves. The potential parameters used for drawing these curves are those listed in Table I. It is seen in Fig. 1 that the Morse curve somewhat deviates from the Lennard-Jones-type curve when the internuclear separation is fairly large compared with the equilibrium separation. However, any further modification of

TABLE I

Potential parameters for the ion–molecule interaction

Gas	σ^* (Å)	ϵ_0/k^* (°K)	$\alpha \times 10^{24}$† (cm³)	r_m (Å)	$\epsilon_m \times 10^{13}$ (erg)	$f_L \times 10^3$ (dyne cm^{-1})	a	$\epsilon_v \times 10^{14}$ (erg)
H$_2$	2.928	37.0	0.79	2.591	1.561	11.90	5.058	8.894
O$_2$	3.433	113	1.60	3.342	1.350	6.627	5.236	1.659
N$_2$	3.681	91.5	1.76	3.576	1.146	4.801	5.176	1.509
Air	3.617	97.0	1.73‡	3.516	1.189	5.216	5.207	1.551
CO	3.706	88.0	1.95	3.567	1.231	5.230	5.198	1.665
CO$_2$	3.897	213	2.65	3.972	1.341	4.899	5.369	1.217
SO$_2$	4.290	252	3.72	4.431	1.312	3.919	5.415	0.9016
N$_2$O	3.879	220	3.00	3.827	1.502	8.976	6.788	1.690

*Reference 19, p. 1111.
†Reference 19, p. 950.
‡Obtained by taking the weighted average of the data for O$_2$ and N$_2$.

the a-value in this respect will not be made here because it does not yield any serious change in the results obtained from the present approximation.

Using the parametric values given in Table I, the values of the equilibrium constant, K_1, and the reaction rate constants, k_2 and k_t, were calculated for several gases at 288, 600, and 1000° K. The results are given in Table II.

TABLE II

Calculated values of K_1, k_2, and k_t

Gas	Temp. (°K)	$K_1 \times 10^{21}$ (cm³ molecule^{-1})	$k_2 \times 10^6$ (cm³ ion^{-1} sec^{-1})	$k_t \times 10^{26}$ (cm³ ion^{-1} molecule^{-1} sec^{-1})
H$_2$	288	4.697	9.970	4.683
	600	0.4291	3.315	0.1422
	1000	0.1382	1.541	0.02130
O$_2$	288	4.152	3.231	1.342
	600	0.6404	1.074	0.06878
	1000	0.2493	0.4993	0.01245
Air	288	3.296	3.266	1.076
	600	0.5868	1.086	0.06373
	1000	0.2361	0.5048	0.01192
CO	288	2.578	3.277	0.8448
	600	0.4409	1.090	0.04806
	1000	0.1756	0.5064	0.008892
CO$_2$	288	5.850	3.142	1.838
	600	0.9339	1.045	0.09759
	1000	0.3681	0.4855	0.01787
SO$_2$	288	5.536	3.064	1.696
	600	0.9241	1.019	0.09417
	1000	0.3693	0.4735	0.01749
N$_2$O	288	4.845	3.142	1.522
	600	0.6479	1.045	0.06771
	1000	0.2444	0.4855	0.01187

Inspection of the data in Table II indicates that the negative temperature-dependence of k_t is not only a consequence of the decreasing nature of K_1 with increasing temperature but it is also due to the same tendency of k_2. In fact, at relatively high temperatures, the latter constant appears to depend upon the temperature to the same extent as the former does.
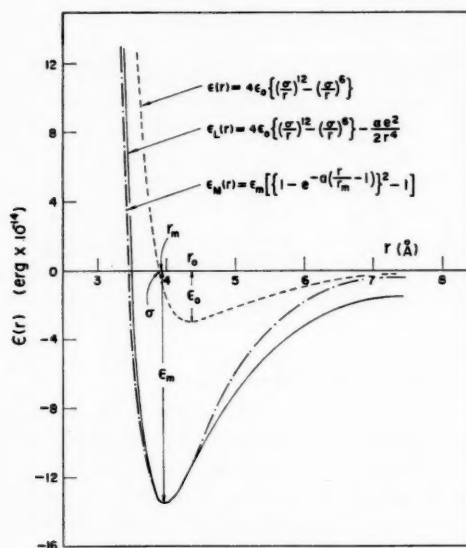
FIG. 1.   The potential curves of interaction between CO_2 and $CO_2{}^+$.

TABLE III

Calculated and observed ion-recombination coefficients at 288° K

Gas	Pressure (mm Hg)	$\rho_{calc} \times 10^6$ (cm³ ion⁻¹ sec⁻¹)	$\rho_{obs} \times 10^{6*}$ (cm³ ion⁻¹ sec⁻¹)	$\dfrac{\rho_{obs}}{\rho_{calc}}$
H_2	760	1.19	1.44†	1.2
O_2	760	0.342	1.61†	4.7
Air	743	0.268	1.68	6.3
	662	0.239	1.48	6.2
	462	0.167	1.03	6.2
	363	0.131	0.83	6.3
	307	0.111	0.73	6.6
	197	0.0711	0.44	6.2
CO	757	0.215	0.87	4.1
	690	0.196	0.77	3.9
	556	0.158	0.63	4.0
	409	0.116	0.45	3.9
	247	0.0700	0.22	3.1
CO_2	729	0.449	1.65	3.7
	614	0.379	1.45	3.8
	498	0.307	1.20	3.9
	373	0.230	0.93	4.0
	265	0.163	0.67	4.1
	175	0.108	0.49	4.5
SO_2	680	0.387	1.32	3.4
	504	0.287	1.08	3.8
	444	0.253	0.91	3.6
	338	0.192	0.73	3.8
	200	0.114	0.42	3.7
	83.5	0.0475	0.26	5.5
N_2O	749	0.382	1.36	3.6
	596	0.304	1.15	3.8
	430	0.220	0.81	3.7
	294	0.150	0.53	3.5
	200	0.102	0.33	3.2

*Reference 9, unless otherwise noted.
†Reference 20.

For the gases listed in Table II, the values of ion-recombination coefficients, ρ, were calculated under varying pressures at 288° K. In Table III, the calculated values are compared with the observed data (9). Except for H_2 and air, the calculated values of ρ are too small by a roughly constant factor of 4. In the case of air the factor is about 6. Yet, the disagreement is not as bad as it sounds, in view of the crudeness of the approximations involved in the present theory. Generally the calculated values agree with experiment at least in order of magnitude. In this sense, therefore, the coincidence found for H_2 is considered as accidental.

DISCUSSION

(A) Termolecular Reaction and the Steady-State Treatment

Under the assumption of the stationary concentration of MX^+, the over-all rate of ion recombinations is expressed by

[17]
$$v = \frac{k_1 k_2 (M)(X^+)(Y^-)}{k_{-1} + k_2(Y^-)},$$

which can be kinetically third order if $k_{-1} \gg k_2 (Y^-)$. The last condition is fulfilled in the recombining systems investigated, in the following way:

Since k_{-1} is the rate constant for the unimolecular decomposition of MX^+, one may expect that $k_{-1} \simeq 10^{13} e^{-\epsilon_m/kT} \sec^{-1}$. If we choose $\epsilon_m = 1.4 \times 10^{-13}$ erg for a complex ion, then k_{-1} comes out to be ca. $3 \times 10^{11} \sec^{-1}$ at ordinary temperatures. On the other hand, the bimolecular rate constant, k_2, at 288° K is approximately 3×10^{-6} cm^3 ion^{-1} sec^{-1} for most gases investigated, as seen in Table II. Therefore, k_{-1} will be larger than $k_2 (Y^-)$ until (Y^-) exceeds 10^{17} ions cm^{-3} (or 3.7×10^{-3} in mole fraction in a gas at the normal temperature and pressure). In many ionization phenomena the ion concentrations are much smaller than this limiting concentration, and so it is very probable that $k_2 (Y^-)$ is sufficiently small compared with k_{-1}. In addition, the condition $k_{-1} \gg k_2 (Y^-)$ is favored by high temperatures and low pressures, because k_2 has a negative temperature coefficient and (Y^-) will become smaller with decreasing pressure.

Obviously the theory is subjected to a serious restriction concerned with the steady-state hypothesis. In order that the time lag between the formation and destruction of MX^+ is negligible, the concentration of MX^+ as an intermediate should be at all times much less than that of X^+ as a reactant. To check this point, the concentration ratios, $(MX^+)/(X^+)$, were calculated from

[18]
$$\frac{(MX^+)}{(X^+)} = K_1(M)$$

for the gases in question, using the values of K_1 given in Table II. The calculated ratios at 288° K and 1 atmosphere pressure are: H_2, 0.119; O_2, 0.106; air, 0.084; CO, 0.066; CO_2, 0.149; SO_2, 0.141; N_2O, 0.124. Although these ratios are not actually small compared with unity, they do appear to be small enough to neglect for the present purpose. This situation becomes more serious under higher pressures, because the concentration ratio increases proportionally with the increasing pressure. Therefore, under pressures much higher than 1 atmosphere, the over-all recombination cannot be approximated by $K_1 k_2 (M)(X^+)(Y^-)$ even if the condition $k_1 \gg k_2(Y^-)$ is satisfied.

Moreover, it has been shown experimentally that, although the recombination coefficients increase linearly with the increasing pressure up to approximately 1000 mm Hg, they attain the maximum values around this limiting pressure and then decrease

gradually as the pressure increases further (1, 2). Apparently, the latter phenomenon is not attributable to the three-body process. It is thus concluded that the present theory does not apply to the ion recombinations occurring under gas pressures higher than 1000 mm Hg.

(B) The Potential Parameters

As has already been described, all the potential parameters necessary for the calculation of K_1 are obtainable from the interrelations among these parameters provided that the values for ϵ_0, σ, and α are known. Thus the calculated data for the ion-recombination coefficients are essentially dependent upon these three parameters. Of the three, ϵ_0 is the least important, because the equilibrium separation, r_m, of an M—X$^+$ binding is usually close to σ where the Lennard-Jones potential is zero as seen in Table I. In other words, the maximum binding energy of the complex is mainly due to the polarization force at the separation, r_m, and it can even be approximated with a reasonable accuracy to the polarization force at the internuclear separation of σ (see Fig. 1 as an example). Thus, it should be noticed that the calculated values of the recombination coefficients are particularly sensitive to the empirical values of σ chosen.

The close agreement between theory and experiment found for the ρ's for hydrogen will break down with a more reasonable choice of the σ-value. In the calculation, σ ($= 2.928$ Å) was the closest approach for elastic collisions between hydrogen molecules, and the ion cluster H$_2$—H$_2$$^+$ was assumed to be stable at an internuclear separation, 2.591 Å, which was obtained by using the above value of σ. According to Eyring, Hirschfelder, and Taylor (6), however, an irreversible process

$$H_2 + H_2^+ \rightarrow H_3^+ + H \qquad\qquad \text{[iii]}$$

can take place very rapidly. Actually, it has been deduced from experiments that reaction [iii] occurs in nearly every collision between H$_2$ and H$_2$$^+$ (21). If we consider that the pre-neutralization equilibrium in the case of hydrogen is

$$H_2 + H_3^+ \rightleftharpoons H_2\text{—}H_3^+ \qquad\qquad \text{[iv]}$$

rather than

$$H_2 + H_2^+ \rightleftharpoons H_2\text{—}H_2^+, \qquad\qquad \text{[v]}$$

then the equilibrium internuclear separation in the intermediate complex will be larger on account of more bulkiness of H$_3$$^+$ than that of H$_2$$^+$. As a result, the binding energy of the complex and consequently the calculated values of K_1 and ρ will become correspondingly smaller.

(C) An Alternative Mechanism

So far the discussion has been confined to the recombination mechanism in which positive ions, X$^+$, are assumed to be equilibrated with their ion clusters prior to the neutralization with negative ions, Y$^-$. However, there is no definite reason why an alternative mechanism

$$M + Y^- \rightleftharpoons MY^- \qquad\qquad \text{[vi]}$$
$$MY^- + X^+ \rightarrow XY + M \qquad\qquad \text{[vii]}$$

can be eliminated from the consideration. Nevertheless, the mechanism does not seem very likely, because there would be a large possibility that the detachment of electrons (or ionization of MY$^-$) occurs on the collisions of MY$^-$ with M. The possibility of this ionizaton is much larger than that of the second step [vii], because of the presence of a

large excess of M and the small electron affinities of the negative ions in general. The electrons thus liberated could collide with M to reproduce the negative ions Y^-, the concentration of which would therefore be maintained until they are neutralized with the partners, MX^+. There is then no participation of step [vii] in the ion recombinations. This point is, of course, still open to question and needs further consideration in the future.

ACKNOWLEDGMENTS

REFERENCES

1. H. S. W. Massey and E. H. S. Burhop. Electronic and ionic impact phenomena. Oxford at the Clarendon Press. 1952. Chap. 10.
2. A. von Engel. Ionized gases. Oxford at the Clarendon Press. 1955. Chap. 6.
3. J. J. Thomson. Phil. Mag. **47**, 337 (1924).
4. D. L. Bunker and N. Davidson. J. Am. Chem. Soc. **80**, 5090 (1958).
5. S. W. Benson. The foundations of chemical kinetics. McGraw-Hill Book Co., Inc., New York. 1960. p. 306.
6. H. Eyring, J. O. Hirschfelder, and H. S. Taylor. J. Chem. Phys. **4**, 479 (1936).
7. D. Britton. J. Phys. Chem. **63**, 1464 (1959).
8. A. G. Gaydon. Dissociation energies. Dover Publishers, Inc., New York. 1950. p. 29.
9. H. Thirkill. Proc. Roy. Soc. A, **88**, 477 (1913).
10. J. J. Thomson and G. P. Thomson. Conduction of electricity through gases. Vol. 1. 3rd ed. Cambridge. 1933. Chap. 3.
11. J. J. Thomson and G. P. Thomson. Conduction of electricity through gases. Vol. 2. 3rd ed. Cambridge. 1928. Chap. 2.
12. H. S. W. Massey. Negative ions. 2nd ed. Cambridge. 1950. p. 2.
13. H. S. W. Massey. Negative ions. 2nd ed. Cambridge. 1950. p. 58.
14. J. D. Craggs and B. A. Tozer. Proc. Roy. Soc. A, **254**, 229 (1960).
15. B. E. Knox and B. P. Burtt. J. Chem. Phys. **28**, 1256 (1958).
16. R. E. Fox. J. Chem. Phys. **32**, 285 (1960).
17. H. Neuert and O. Rosenbaum. Naturwissenschaften, **41**, 85 (1954).
18. F. H. Field and J. L. Franklin. Electron impact phenomena. Academic Press, Inc., New York. 1957. p. 25.
19. J. O. Hirschfelder, C. F. Curtiss, and R. B. Bird. Molecular theory of gases and liquids. John Wiley & Sons, Inc., New York. 1954.
20. K. T. Compton and I. Langmuir. Revs. Mod. Phys. **2**, 123 (1930).
21. J. O. Hirschfelder, C. F. Curtiss, and R. B. Bird. Molecular theory of gases and liquids. John Wiley & Sons, Inc., New York. 1954. p. 1095.

A COMBINED FLASH PHOTOLYSIS AND SHOCK WAVE METHOD FOR THE STUDY OF BROMINE ATOM RECOMBINATION OVER A WIDE TEMPERATURE RANGE[1]

GEORGE BURNS AND D. F. HORNIG

ABSTRACT

A combined flash photolysis shock wave experiment is described in which bromine is first flash photolyzed, then compressed and heated by a shock wave, and finally allowed to recombine at the high temperature. Some of the problems connected with working in a shock tube used as a photolysis vessel are analyzed. The apparatus was used to measure recombination rates with argon as a third body at room temperature, to estimate the efficiency of bromine as a third body at room temperature, and to obtain a preliminary measurement of the recombination rate of bromine in the presence of argon at 950° K.

INTRODUCTION

The rate of the three-body recombination of both iodine and bromine atoms has been measured as a function of temperature between 300° K to 550° K by the flash photolysis method (1–4). Recombination rates have also been calculated from rates of dissociation and equilibrium constants in iodine, bromine, and oxygen (5–12). In every case the rate of recombination decreases with increasing temperature.

The source of this temperature effect has been the subject of considerable theoretical discussion and it may arise from several sources.

(a) An approximately $1/T$ temperature dependence appears in the statistical theories of Wigner (13) and of Keck (14).

(b) The fact that for attracting molecules the collision cross section decreases with increasing molecular velocity will produce a decrease in the rate as the mean velocity increases, similar to the effect on gaseous viscosities (15).

(c) If the reaction proceeds through the sequence

$$A + M \rightleftharpoons AM$$

$$AM + A \rightarrow A_2 + M,$$
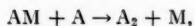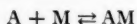
the fall-off may be attributed to the decreasing equilibrium concentration of the complex AM. This latter suggestion has been particularly in vogue recently (16–19). However, the existing experimental data do not cover a wide enough temperature range to make any unambiguous choices so it seemed important to extend the temperature range of direct recombination rate measurements.

It seemed possible to do this by using flash photolysis to dissociate the halogen molecule and a shock wave to heat the gas. Several variations of such an experiment might be considered.

1. If the gas is initially photolyzed and then heated, the photolysis is carried out at the initial gas density and the recombination is carried out at a gas density two to four times higher. This results in faster recombination, an important feature since it is only possible to maintain the high temperature for a limited time in the shock tube. An intrinsic limitation of this approach is that in order to observe recombination, the photolytic dissociation must exceed the equilibrium thermal dissociation behind the shock wave. In

most experimental arrangements this would make it possible to reach temperatures in the vicinity of 2000° C.

2. If the gas is initially heated and then photolyzed the upper temperature limitation of the first approach is removed since the photolytic dissociation is added to the thermal dissociation. However, in this case the rates are from 2^3 to 4^3 lower for comparable initial conditions because of the density effect.

3. Either of the first two methods can be applied to a reflected shock wave. Reflected shocks have the advantage that higher temperatures and gas densities may be reached while at the same time the gas behind the reflected wave is not in motion. However, a variety of problems involving shock wave dynamics have complicated previous experiments with reflected waves (20, 21).

In designing an experiment, then, one must arrive at a suitable compromise among a variety of factors.

APPARATUS

A diagram of the apparatus utilized is shown schematically in Fig. 1. The low-pressure section, a 3-in. diameter pyrex glass shock tube, was filled with the bromine–argon mixture to be studied. When a cellulose acetate diaphragm (X), separating the low-pressure section from the helium-filled high-pressure section was punctured, a shock wave was sent through the low-pressure gas, compressing it and heating it to the desired temperature.
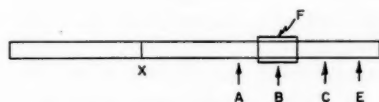

FIG. 1.   Diagram of the apparatus.

By the time the disturbance reached station A a shock wave had been formed. Station A activated the time delay circuits which triggered the flash lamps (F), started the oscilloscope sweeps, etc. When the shock was about to enter the illuminated region the high-voltage condensers were discharged through the flash lamp, dissociating about 20% of the Br$_2$. The partially dissociated gas was subsequently compressed and heated by the shock wave. Since the gas behind the shock front was in motion the dissociated gas was carried down the tube and the optical absorption, from which the concentration of Br$_2$ could be measured, was studied at successive times by stations C and E.

The distance between the electrodes of the flash lamps was 25 cm; they were made of 1.9-cm diameter quartz tubes filled with xenon at a pressure of 100 mm Hg. The electrodes were made of 1/4-in. tungsten rods. In order to minimize the inductance the return lead from each lamp was made of copper foil covering the outer half of each tube. These lamps had an inductance of 1.8 microhenries and a resistive impedance of 1 ohm. The light pulse had a width at half peak intensity of 7 microseconds when a 3.75-μf condenser was discharged through a single lamp. The resistance and inductance of the rest of the circuit was negligible compared with those of the lamp.

Up to eight of these lamps were arranged in a ring, each parallel to the shock tube and separated from it by 1/8 inch, inside a reflecting box. They were operated in parallel and were capable of dissipating up to 4000 joules/flash in less than 10 microseconds. In order to make absorption measurements the eight lamps were separated into two groups of

four and the measuring beam (B) was directed through the gap, at right angles to lamps and shock tube.

The flash lamps were each connected to separate capacitors. They were fired simultaneously by triggered spark gaps connected in series with the lamps. The spark gap electrodes consisted of a 1/4-in. diameter nickel hemisphere and a plane nickel electrode. The 2-mm diameter trigger electrode was inserted in a 4-mm diameter hole in the plane electrode. The trigger electrodes were pulsed by transformers which delivered approximately 6 kv with a rise time of 10 ± 1 microseconds. Using separate thyratrons to pulse the primaries it was possible to fire the eight flash lamps with a simultaneity of less than one microsecond.

Each measuring station (A, B, C, and E) consisted of a photomultiplier, an optical system, and an incandescent lamp source. Stations C and E were used to follow the changes in bromine concentration and to measure the shock velocity; A was used to trigger the flash lamps and to measure shock velocity. B was used only to study flash photolysis at room temperature. The rise time of the photomultiplier circuits was less than one microsecond and a square wave decayed 0.5% in 1 millisecond. Over the range of light intensities used the intensity measurements were accurate to within 1%.

At station B the intensity of the flash was roughly 10^5 times that of the incandescent source in the measuring circuit. Therefore care had to be taken to minimize the effect of scattered light which could damage the photomultiplier tube or at least affect its sensitivity. Aside from the strong peak there was a "tail" continuing for another 150 microseconds or so, which interfered with subsequent measurements. It was not established whether this was caused by continuing light output from the gas or by luminescence of the quartz walls of the flash lamps.

The main source of scattering was the glass wall of the shock tube. The effect of scattering was minimized by using a well-collimated optical system, relatively low photomultiplier voltage (190 v), and a relatively intense light source for the measuring circuit (8 v, 18-amp tungsten ribbon lamp). Measurements were all made at 4420 Å through an interference filter. The signal-to-noise ratio at station B was over 1000. Stations C and E were well removed from the flash lamps so that the problem of scattered light was less severe. The signal-to-noise ratio at these stations was about 300.

The low-pressure section of the shock tube was an 11-ft section of 3-in. I.D. pyrex pipe. The high-pressure section was a 6-ft section of 3-in. I.D. brass fitted with a knife-type plunger used to break the diaphragm, made of 10 or 15 mil cellulose acetate. The density in the flows in the shock wave was constant to within $\pm3\%$. This was probably the largest single experimental uncertainty leading to scatter in the experimental results.

The pressure of inert gas in the low-pressure section was measured with a mercury manometer and that of bromine, by a butyl phthalate manometer buffered with argon. The gases were thoroughly mixed in a 3-liter flask.

Although the system was originally vacuum tight, the strong shocks used caused leaks between sections of the shock tube which were very hard to eliminate. It is not believed that the air which was admixed with the argon could have produced an error over 1%.

STATIC EXPERIMENTS

In order to test the apparatus, measurements were first carried out at room temperature in a closed cell 3 inches in diameter and 27 cm long. Recombination constants in the rate equation $d[Br_2]/dt = k_{app}[Ar][Br]^2$ were measured over a 15-fold range in the [Br]/[Ar] ratio. All of the measurements were made at station B (Fig. 1). At each concentration

ratio at least five traces of the scattered light and of scattered light plus deflection due to the changing Br_2 concentration were taken.

Further room temperature experiments were carried out using the shock tube itself as a reaction vessel (but with no shock wave). The results obtained in all of the static experiments are given in Table I. Both the absolute value of the experimental rate constant and the scatter in our data compare well with previously published work.

TABLE I

Rate of recombination of bromine atoms at room temperature

	$[Br_2] \times 10^4$ moles/liter	Diluent gas $\times 10^2$ moles/liter	Diluent	No. of runs	$k_{app}(\times 10^{-9}$ l^2 mole^{-2} sec$^{-1})$
This work[a]	0.96	0.66	Ar	11	3.47±0.2
"	"	1.50	"	6	3.24±0.3
"	"	2.50	"	8	2.9±0.3
"	"	3.67	"	5	2.9±0.3
"	1.92	0.639	"	5	2.9±0.3
"	"	1.48	"	9	3.5±0.3
"	"	2.57	"	7	3.0±0.2
"	"	3.68	"	5	3.5±0.1
"	1.55	0.639	"	6	3.4±0.4
"	"	1.51	"	5	2.95±0.2
"	"	2.50	"	5	3.04±0.2
"	"	3.68	"	11	3.2±0.2
This work[b]	2.05	3.76	"	10	$(3.1^d-3.7^e)$±0.3
"	0.78	3.88	"	6	$(3.4^d-3.6^e)$±0.3
Givens and	1.57	3.72	"		2.9
Willard (4)	2.4	2.08	"		4.6
"	2.2	1.05	"		5.6
"	2.7	0.675	"		12.7^c
"	3.36	0.55	"		19
Rabinowich and Wood (mean value)(22)			"		2.4±0.5
This work[b]	1.10	3.92	He	5	1.3^e±0.1
Rabinowich and Wood (mean value) (22)			"		1.35±0.15

[a]Closed vessel.
[b]Open cell (shock tube).
[c]At 37° C.
[d]Assuming no expansion.
[e]Assuming equilibrium expansion.

On the other hand, our data are in rather serious disagreement with those of Givens and Willard (4) as regards the dependence of the experimental rate constant on the $[Br_2]/[Ar]$ ratio. When this ratio was high our records showed a definite effect of heating by the flash and wave systems were set up in the closed reaction vessel (Fig. 2). We have
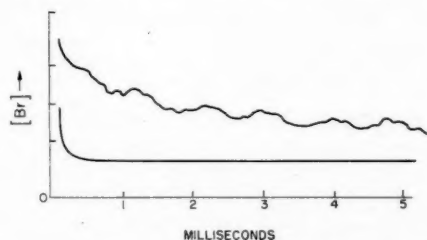

MILLISECONDS

FIG. 2. Oscilloscope traces showing scattered light and recombination of bromine atoms in a closed vessel containing 1.92×10^{-4} moles/liter of Br_2 and 6.39×10^{-3} moles/liter of Ar. Vertical scale 4.5×10^{-6} moles/liter Br per small division.

used the midpoint of the waves for measurement and it is hard to see how this can account for the disagreement. On the other hand, as regards this dependence, our results agree reasonably well with those of Strong and Basila (23) and Christie, Roy, and Thrush (24).

If both Br_2 and Ar act as third bodies for the recombination, the apparent rate constant is given by

[1] $$k_{app} = k_{Ar} + \frac{[Br_2]}{[Ar]} k_{Br_2}$$

so that the rate constant for Br_2 acting as a third body is obtained from the slope of Fig. 3. We have not taken enough data at high $[Br_2]/[Ar]$ ratios to obtain a reliable value of k_{Br_2}. It is plain, though, that the ratio of k_{Br_2}/k_{Ar} from our results (ca. 20) is much smaller than that of Givens and Willard (4). The values of k_{Br_2} reported recently are summarized in Table II.
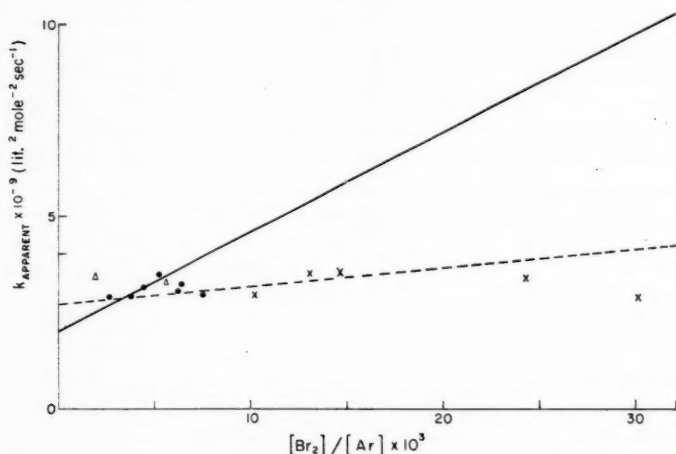

FIG. 3. Dependence of the recombination rate constant upon $[Br_2]/[Ar]$. Closed circles, oscilloscope trace shows no detectable waves; crosses, waves can be observed; triangles, experiments in shock tube used as a reaction vessel; solid line, dependence predicted from reference 4; dashed line, dependence predicted from reference 23 and reference 24.

TABLE II

Rate constant for bromine atom recombination with Br_2 as third body

Investigators	k_{Br_2}, l^2 mole^{-2} sec^{-1}
Strong and Basila (1958) (23)	49×10^9
Givens and Willard (1959) (4)	260×10^9
Christie, Roy, and Thrush (1959) (24)	48×10^9
This work	$<50 \times 10^9$

In order to determine this rate constant accurately more data must be taken at higher values of the $[Br_2]/[Ar]$ ratio. It would be particularly advantageous to use He instead of Ar as the diluent in such studies since He is about three times less efficient than Ar as a third body. In this case the slope of a plot similar to Fig. 3 could be determined with about three times more precision.

THERMAL EFFECTS

Heating by the Flash

When the flash dissociates the Br_2 the bromine atoms are released with a kinetic energy equal to the difference between the photon energy and the energy necessary to produce two $^2P_{3/2}$ atoms (45.6 kcal) or most often a $^2P_{1/2}$ and a $^2P_{3/2}$ atom (56.05 kcal). This excess kinetic energy is degraded to heat in a very few collisions. As a consequence the gas is heated from a few degrees to as much as 100° C, depending on the dilution and flash intensity, within the duration of the flash.

In a closed cell experiment in which the illumination is absolutely uniform, the only result is that the recombination is measured at a higher temperature. If the illumination is non-uniform there are further effects. The temperature, and hence the pressure, are increased more in the region of most intense illumination so that compression waves are propagated into the regions of less intense illumination, giving rise to oscillations in the record as sound waves are reflected back and forth through the cell. This phenomenon is illustrated in Fig. 2. Even if the wave motion is averaged there is an effect since the more intensely illuminated regions gradually expand while the less intensely illuminated regions are compressed, giving rise to a local gas density different from that to which the cell was filled. In particular, if the illumination is symmetrical about the midpoint of a cylindrical cell, the density, ρ_t, is given by the expression

$$[2] \qquad \frac{\rho_t}{\rho_0} = \left(\frac{\bar{P}_t}{P_1}\right)^{1/\gamma}$$

where $\bar{P}_t$ is the average final pressure in the tube, P_1 is that immediately after the flash, and ρ_0 the gas density before the flash.

$$[3] \qquad P_1 = \rho_0 R T_1 \quad \text{and} \quad \bar{P}_t = \rho_t R \bar{T}_t.$$

Finally,

$$[4] \qquad \begin{aligned} T_1 - T_0 &= Q/C_v \\ \bar{T}_t - T_0 &= \bar{Q}/C_v \end{aligned}$$

where Q is the excess kinetic energy produced in the Br atoms and C_v is the heat capacity. In a typical case in the experiments described in the last section, the illumination at the ends of the closed 27-cm cell was about 75% of that in the center. At the highest Br_2/Ar ratio $T_1 - T_0$ was about 10° C while the corresponding $\bar{T}_t - T_0$ was about 9.1° C. In that case $\bar{P}_t/P_1 = 0.993$ and $\rho_t/\rho_0 = (0.993)^{0.6} = 0.996$. The resultant errors are therefore not serious. We have not pursued this matter in the present experiments.

When the cell is open ended, as in a shock tube, the effects are much larger. In that case the initially heated gas expands until its pressure is back to the initial pressure so that equation [2] becomes

$$[5] \qquad \rho_t = \rho_0 (P_1/P_0)^{1/\gamma}$$

and for 10° C heating, $\rho_t = 0.98\rho_0$. Since a 2% density change by expansion would produce a change in the bromine absorption comparable to that produced by dissociation, it was considered necessary to study this initial heating experimentally in the shock tube.

The initial heating was studied under conditions where it would be maximized and the rate of recombination would be made negligible during the experiment, namely in pure bromine at low concentration (0.44–0.77×10^{-5} moles/liter). When pure Br_2 was photolyzed in the shock tube, a bromine absorption record similar to that in Fig. 4 was obtained

at station B. There was an abrupt decrease in the Br_2 concentration immediately following the flash because of the photolytic dissociation. This was followed by a slow further decrease which became much more rapid during the first millisecond. After about two milliseconds the gas was completely expanded and a new, relatively constant, value of $[Br_2]$ was reached.

It was clear that the second process was the anticipated expansion since the time at which it occurred was almost exactly equal to the expected time of arrival (1.3 milliseconds) of a sound wave from the edge of the illuminated region (where the expansion would be initiated). This conclusion was checked further by adding helium to the bromine to increase the velocity of sound and in that case the final plateau of Fig. 4 was reached in less than one millisecond.
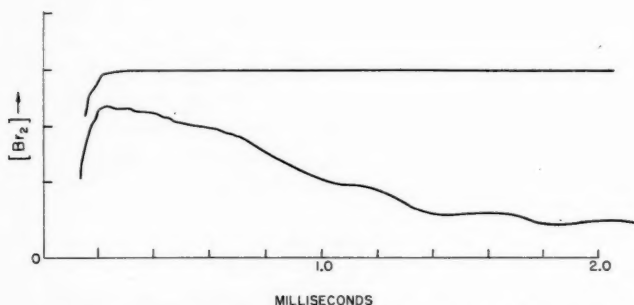

FIG. 4. Oscilloscope trace showing scattered light and expansion of bromine due to initial heating. Shock tube filled with 0.7×10^{-4} moles/liter Br_2. Vertical scale: 7.7×10^{-6} moles/liter Br_2 per division.

A final check that the phenomenon observed was indeed the expansion was obtained by observing the compression wave which the expanding gas in the illuminated region sent through the unilluminated part of the tube. The disturbance was observed at stations C and E; it was found that it propagated at a velocity almost exactly equal to that of sound in bromine and had its origin in the illuminated region at the time of the flash.

It was possible, therefore, to estimate the initial heating quantitatively from these experiments. The initial concentration, $[Br_2]_0$, was known from the initial pressure as well as from the optical absorption. The concentration, $[Br_2]_1$, immediately after the flash could be determined by extrapolating the record back to $t = 0$. Consequently

$$[6] \qquad\qquad\qquad [Br]_1 = 2([Br_2]_0 - [Br_2]_1)$$

and the degree of dissociation was

$$[7] \qquad\qquad\qquad \alpha = ([Br_2]_0 - [Br_2]_1)/[Br_2]_0$$

If Q calories were released for each molecule dissociated, the temperature after the flash was

$$[8] \qquad\qquad\qquad T_1 = T_0 + \frac{Q\alpha[Br_2]_0}{(1-\alpha)[Br_2]_0 C_{Br_2} + 2\alpha C_{Br}} .$$

Hence Q could be determined if T_1 was known. T_1 could be determined from the temperature after the adiabatic expansion since

[9]
$$\frac{T_1}{T_t} = \left(\frac{[Br_2]_1}{[Br_2]_t}\right)^{\gamma-1},$$

and T_t was known from the equation of state (if the final pressure equals the initial pressure),

[10]
$$\frac{T_t}{T_0} = \frac{[Br_2]_0}{[1+2\alpha][Br_2]_t}.$$

Hence Q could be determined from a single record similar to Fig. 4 since $[Br_2]_t$ could be measured from the final plateau.

Five experiments in pure Br_2 at a concentration of 0.75×10^{-4} moles/liter with four lamps firing yielded $Q = 9.6$ kcal/mole. Another set of four experiments at a concentration 0.48×10^{-4} moles/liter gave $Q = 5.7$ kcal/mole although the scatter among the determinations, using from one to four lamps, was only about 10%. The reason for the discrepancy is not known. However, the presence of as much as 1 mm Hg of air in the tube would account for it.

Because of the uncertainty in α caused by the difficulty in extrapolating to $t = 0$, another set of experiments was carried out in which argon was added to almost atmospheric pressure (3.88×10^{-2} moles/liter). The rate constant was determined in the usual way by plotting $1/Br$ vs. time. Extrapolating this straight line to $t = 0$ gave the initial concentration of Br atoms (8.6×10^{-7} moles/liter per flash lamp). Using the value of α determined in this way to fix the $t = 0$ point on another set of 35 runs in pure Br_2 at a concentration of 0.7×10^{-4} moles/liter gave $Q = 8.5$ kcal/mole.

These experiments were not carried further because our main interest was in high-dilution experiments where the heating and expansion effects were very small. Their importance lies in the fact that they show that the expansion is a smooth process and that it is possible to work quantitatively under conditions where the heating and expansion are large.

Recombination Heating

When recombination takes place the heat evolved warms the gas and in an open tube the consequent expansion may produce large effects. If the expansion is rapid enough so that inertial forces are significant the hydrodynamic conservation equations must be applied (8). When that is not the case there will be a free expansion of the heated gas at a constant pressure. We then have

[11]
$$[\dot{Br}_2] = \left(\frac{\partial Br_2}{\partial \alpha}\right)_{T,P} \dot{\alpha} + \left(\frac{\partial Br_2}{\partial T}\right)_{P,\alpha} \dot{T}.$$

For a three-body recombination

[12]
$$\left(\frac{\partial Br_2}{\partial \alpha}\right)_{T,P} \dot{\alpha} = k[Br]^2[M].$$

From the equation of state

[13]
$$\left(\frac{\partial Br_2}{\partial T}\right)_{P,\alpha} = -\frac{[Br_2]}{T}.$$

For a constant pressure process

$$\dot{H} = \dot{q},$$

so that

[15] $([Br_2]C_{pBr_2}+[Br]C_{pBr}+[M]C_{pM})\,\dot{T} = Dk[Br]^2[M].$

Therefore equation [11] becomes simply

[16] $[\dot{Br_2}] = k[Br]^2[M]\left(1-\dfrac{D[Br_2]}{([Br_2]C_{pBr_2}+[Br]C_{pBr}+[M]C_{pM})T}\right).$

Under conditions of high dilution this simplifies to

[17] $[\dot{Br_2}] = k[Br]^2[M]\left(1-\dfrac{D[Br_2]}{[M]C_{pM}T}\right).$

It should be noted, therefore, that as recombination proceeds the Br_2 concentration may either decrease or increase. A similar situation exists for dissociation reactions and there both cases have been observed experimentally (8). In general, though, the bromine molecule concentration will increase during recombination when the gas is sufficiently dilute and decrease for pure Br_2 at any practicable temperature.

Cooling by the Walls

Norrish *et al.* (16) have called attention to the problem created by cooling at the walls. In a conventional photolysis cell the observations are made longitudinally. Cooling at the walls results in increased gas density near the walls and decreased density in the center of the tube where observations are made. In our apparatus observations were made transversely so that in first approximation the effect of cooling at the walls is averaged out, providing the cell is long enough so that the end walls are far removed. Consequently, we have for the present neglected this effect.

HIGH-TEMPERATURE MEASUREMENTS

Recombination measurements were made at $950°$ K in mixtures of 0.6% Br_2 in Ar. The low-pressure section of the shock tube was filled with bromine at a concentration of $(3.7\pm.05)\times10^{-5}$ moles/liter and argon at a concentration of $(6.05\pm.05)\times10^{-3}$ moles/liter. The total pressure was 11.4 cm Hg. The high-pressure section was filled with He at a pressure of three atmospheres. The strength of the shock wave produced when the diaphragm was ruptured was determined by measuring the time of passage between stations A, B, C, and E. All three shocks had an average velocity of 0.90 mm/microsecond over the 964-mm path from A to C. The third shock showed an average velocity of 0.92 mm/microsecond over the total path of 1297 mm so that its apparent velocity over the last 333 millimeters was 0.98 mm/microsecond. It is not yet known whether this represents experimental error or whether there was a genuine acceleration of the shock. Using the velocity 0.90 mm/microsecond (Mach number = 2.80), the compression ratio across the shock was 2.89 and the temperature behind the shock was $950°$ K. If the velocity was as high as 0.97 mm/microsecond (Mach number = 3.00) the corresponding numbers would be 2.99 and $1060°$ K.

The photolysis was carried out with eight lamps discharging a total of 32.25 mf at 10.4 kv. Since station B was not used, the initial Br atom concentration was determined in a separate photolysis on pure bromine at room temperature (no shock). Bromine

molecules (22%) were dissociated in the photolysis. The initial heating amounted to 5.3° C. The subsequent expansion would amount to 1% at 300° K and 0.34% at 950° K. Since the expansion should have been complete after about 750 microseconds it took place partially before and partially after the arrival of the shock wave at about 200 microseconds. Because of the high degree of dissociation the expansion had only a very minor effect on these measurements.

The rate constants were obtained from the initial bromine concentration, determined separately, and corrected for the expansion and the recombination which occurred before arrival of the shock (6%), plus the bromine atom concentration at the center of the pulse when it arrived at stations C (0.76 millisecond later) and E (1.30 milliseconds). The rate constants were corrected for the recombination heating, a correction of 7.7%.

The rate constants obtained on three high-temperature experiments were:

Expt.	Time range, milliseconds	k, l^2 mole^{-2} sec^{-1}
I	0–0.76	6.4×10^8
	0.76–1.3	7.9×10^8
II	0–0.76	9.0×10^8
III	0.76–1.3	9.7×10^8
		Average $8.2 \pm 1.1 \times 10^8$

DISCUSSION

The most striking feature of previous work on bromine and iodine is that it was difficult to fit the low-temperature flash photolysis data and the high-temperature shock wave data to a single k vs. T curve. It was hoped that an intermediate temperature point might indicate where the difficulty lay. Furthermore, the various theoretical approaches suggest different forms of the k vs. T curve. The complex mechanism yields a function $k = Ae^{E/RT}$ whereas most other considerations yield functions of the form $k = B/T^n$.

The various measurements are therefore plotted as a function of temperature in Fig. 5; a straight line on the three representations shown would correspond to the functions: (A) $k = B/T^n$, (B) $k = Ae^{E/RT}$, and (C) $k = Ae^{-BT}$. The present work agrees reasonably well with the results of Willard and co-workers at room temperature but the rate constant at 950° K is substantially higher than would be predicted by extrapolation of their data.

A point of some interest is the fate of the $^2P_{1/2}$ atoms, which comprise roughly 50% of those produced in the initial photolysis, since they cannot lead directly to the formation of ground state molecules. If they were collisionally degraded to the $^2P_{3/2}$ state the 10.4 kcal released ought to appear in our experiments as heat and this does not seem to have been the case. They might, however, undergo a radiative transition and lose the energy as a photon. If their lifetime exceeds the recombination time (ca. 1 millisecond), though, all flash photolysis results would be in error unless the lifetime of the excited molecules produced from these atoms is short compared with the recombination time. This problem has been considered previously (16) but the evidence for neglecting this possibility does not seem conclusive to us.

If the $^2P_{1/2}$ atoms do not enter the observed recombination, the rate constants would be about four times greater and it should be noted that since the corresponding problem does not arise in thermal dissociation (e.g. in shock waves) this would help bring the flash photolysis and shock wave results into better agreement.
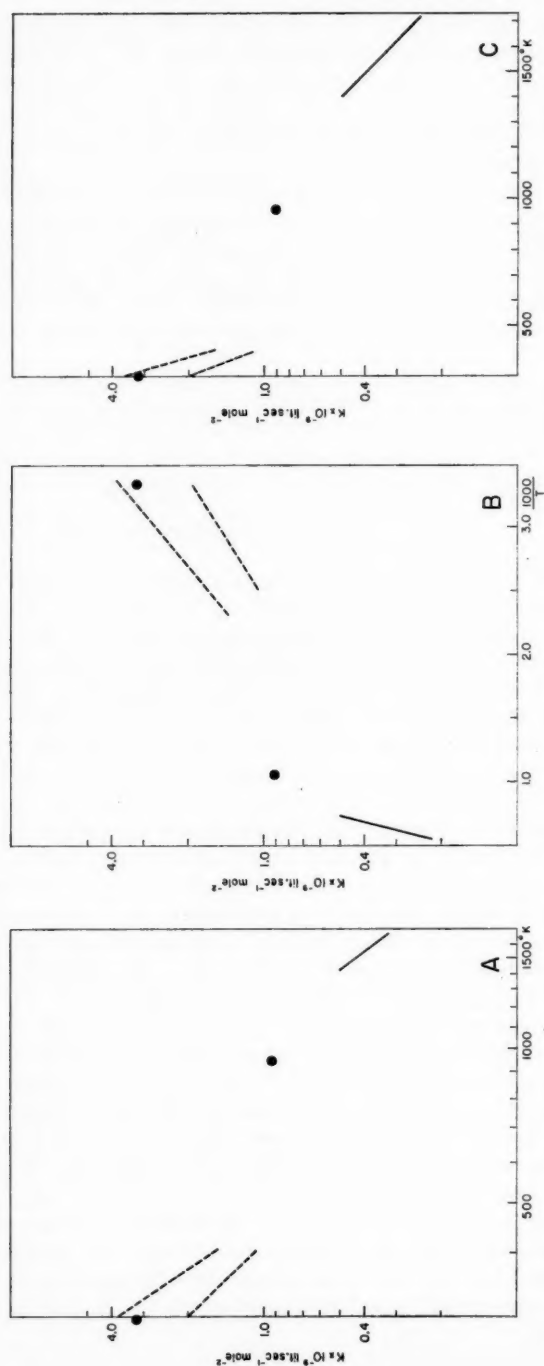
FIG. 5. Temperature dependence of recombination rate constant. (A) Log–log representation; (B) Arrhenius representation; (C) log k vs. T representation. Closed circles, present experiment; solid line, estimated from reference 12; upper dashed line, estimated from reference 2; lower dashed line, estimated from reference 4.

CONCLUSIONS

The combination of flash photolyses with the shock tube to obtain recombination rates at high temperatures appears quite feasible. All of the major problems, such as the various thermal effects, appear soluble and it has been possible to obtain preliminary results of reasonable accuracy for bromine recombination at 950° K. It now seems possible to reach higher temperatures, to improve the accuracy, and to work at lower dilutions.

ACKNOWLEDGMENTS

REFERENCES

1. K. E. RUSSEL and J. SIMONS.   Proc. Roy. Soc. A, **217**, 271 (1953).
2. R. L. STRONG, J. C. W. CHIEN, P. E. GRAF, and J. E. WILLARD.   J. Chem. Phys. **26**, 1287 (1957).
3. D. L. BUNKER and N. DAVIDSON.   J. Am. Chem. Soc. **68**, 5085 (1958).
4. W. G. GIVENS, JR. and J. E. WILLARD.   J. Am. Chem. Soc. **81**, 4773 (1959).
5. D. BRITTON, N. DAVIDSON, W. GEHMAN, and G. SCHOTT.   J. Chem. Phys. **25**, 804 (1956).
6. D. BRITTON and N. DAVIDSON.   J. Chem. Phys. **25**, 810 (1956).
7. D. F. HORNIG.   Ann. N. Y. Acad. Sci. **67**, 463 (1957).
8. H. B. PALMER and D. F. HORNIG.   J. Chem. Phys. **26**, 98 (1957).
9. D. L. MATTHEWS.   Phys. Fluids, **2**, 170 (1959).
10. S. R. BYRON.   J. Chem. Phys. **30**, 1380 (1959).
11. R. ENGLEMAN and N. DAVIDSON.   J. Am. Chem. Soc. In press. (1960).
12. D. BRITTON.   J. Phys. Chem. In press. (1960).
13. E. P. WIGNER.   J. Chem. Phys. **5**, 720 (1937).
14. J. C. KECK.   J. Chem. Phys. **32**, 1035 (1960).
15. J. O. HIRSHFELDER.   Molecular theory of gases and liquids. Wiley, New York. 1954. pp. 552–559.
16. M. T. CHRISTIE, A. J. HARRISON, R. G. W. NORRISH, and G. PORTER.   Proc. Roy. Soc. A, **231**, 446 (1955).
17. D. L. BUNKER and N. DAVIDSON.   J. Am. Chem. Soc. **80**, 5090 (1958).
18. O. K. RICE.   Monatsh. Chem. **90**, 330 (1959).
19. D. L. BUNKER.   J. Chem. Phys. **32**, 1001 (1960).
20. J. P. TOENNIES and P. F. GREENE.   J. Chem. Phys. **26**, 665 (1957).
21. R. A. STREHLOW and A. COHEN.   J. Chem. Phys. **28**, 983 (1958).
22. E. RABINOWITCH and W. C. WOOD.   Trans. Faraday Soc. **32**, 907 (1936).
23. M. R. BASILA.   The flash photolysis and recombination of bromine. Ph.D. Thesis, Rensselaer Polytechnic Institute. August 1958.
24. M. T. CHRISTIE, R. S. ROY, and B. A. THRUSH.   Trans. Faraday Soc. **55**, 1139 (1959).

THE ROLE OF Hg 6^3P_0 ATOMS IN MERCURY PHOTOSENSITIZATION

I. REACTIONS IN THE PRESENCE OF NITROGEN[1]

G. H. KIMBELL AND D. J. LE ROY

ABSTRACT

A quantitative investigation has been made of the factors affecting the concentration of mercury 6^3P_0 atoms formed by collisions of the second kind between mercury 6^3P_1 atoms and nitrogen. The absorption of 4047 Å (6^3P_0–7^3S_1) and the emission of 2656 Å (6^3P_0–6^1S_0) were studied in the pressure range 0.06 mm to 140 mm. Both types of measurement indicate that the forbidden line arises from spontaneous as well as collision-induced emission. The lifetime for spontaneous emission is estimated to be 4.2×10^{-4} sec.

The production of mercury 6^3P_0 atoms by collisions of the second kind between 6^3P_1 atoms and nitrogen is well known. The methods used to study their relative concentration and reactivity are of five main types.

The absorption of the line 4047 Å, corresponding to the transition 6^3P_0–7^3S_1, was first observed by Wood and Gaviola (1), and has been applied quantitatively by a number of others (2, 3, 4, 5). Correlation of the apparent concentration of 6^3P_0 atoms with cell geometry suggested that these atoms have a relatively long lifetime and are deactivated on the wall (2). With increasing nitrogen pressure the concentration reaches a maximum (3) and shows some indication of a fall-off at pressures above 20 mm (4).

As a result of the absorption of 4047 Å there is an increase in the population of the 7^3S_1 level. The intensity of the resulting emission of 4358 Å (7^3S_1–6^3P_1) and 5461 Å (7^3S_1–6^3P_2) has been used as a measure of the 6^3P_0 concentration (6).

Elevation of 6^3P_0 atoms to the 6^3P_1 level requires only 5 kcal per mole and can be brought about by collisions with nitrogen molecules. Because of the long lifetime of the former compared with that of the latter (1.1×10^{-7} sec), the emission of 2537 Å will continue for some time after the exciting radiation of that wavelength is cut off; its intensity can then be correlated with the concentration of 6^3P_0 atoms (5, 7, 8).

The liberation of electrons when 6^3P_0 atoms collide with metal plates has been used as a quantitative measure of their concentration (9, 10, 11), but the method may be complicated by the fact that Hg_2^+ ions appear to be produced homogeneously (4).

Although the transition 6^3P_0–6^1S_0 is forbidden by the usual selection rules, it has been observed by Wood (12) and others. Its wavelength *in vacuo* (2656.39 Å) lies close to the pseudotriplet, 2655.92, 2654.47, 2652.83, arising from transitions between the levels 7^1D_2, 7^3D_1, 7^3D_2, and the 6^3P_1 level, and can be separated from these only with a spectrograph of high dispersion. Laroze and Cojan (13) have tried to get around this difficulty by passing the light from the primary lamp through a filter designed to reduce the intensity of the pseudotriplet, relative to that of 2537 Å, by a large factor. Unfortunately, while this would reduce the rate of formation of $7D$ atoms from 6^3P_1 atoms, it would not affect their rate of formation by such processes as the absorption of 2535.5 Å by 6^3P_0 atoms to give 7^3D_1 atoms. Indeed, it was found in the present work that the intensity of the line 2654.47 Å increased very markedly in the presence of small amounts

of nitrogen and was reduced below that of the forbidden line only at relatively high pressures.

EXPERIMENTAL

The apparatus in its present form was designed to permit measurements of the absorption of 4047 Å as well as of the emission of the forbidden line; its main features may be seen in Fig. 1. Two primary lamps of the low-pressure mercury-rare gas type were used.
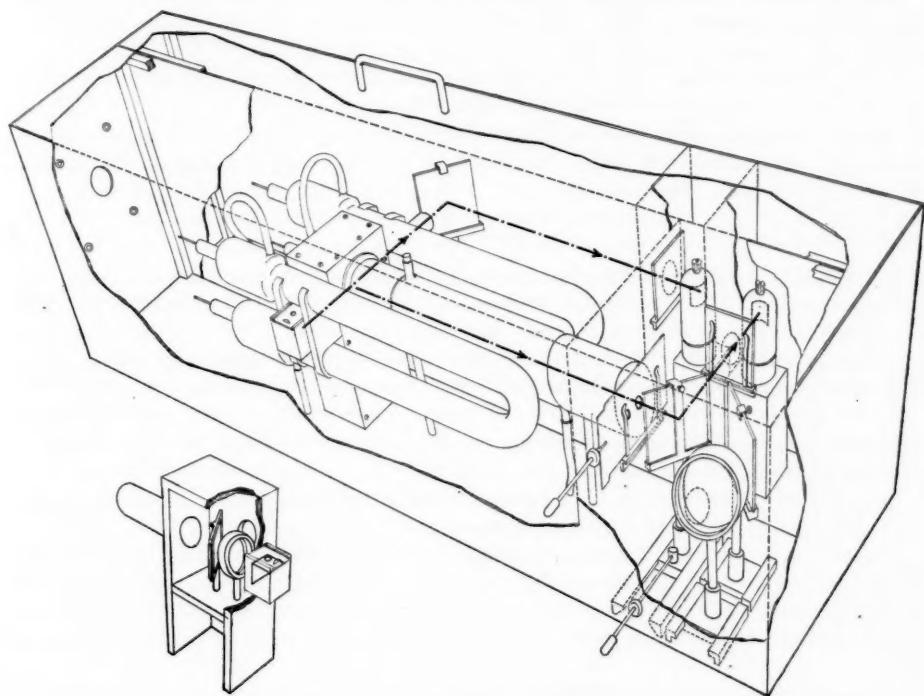

FIG. 1. Apparatus for studying absorption of 4047 Å and emission of 2656 Å by mercury 6^3P_0 atoms.

These were made entirely of fused quartz, including the jacketed electrode chambers, which were maintained at 29° C. The lamps were U-shaped and were mounted with their long axes parallel to that of the cell. The latter was also of fused quartz, and consisted of an outer tube 28 cm long and 5.5 cm O.D. and an inner tube 20 cm long and 3.1 cm I.D. The annular space between the tubes was filled with a filter solution of aqueous nickel sulphate, which removed essentially all of the 4047 Å radiation coming from the primary lamps (14). Close-fitting metal cylinders covered each end of the cell, leaving a central portion 18 cm long exposed to the light from the two lamps. Nitrogen and mercury vapor entered and left the cell through blackened side arms at each end of the cell, adjacent to the plane quartz windows.

To study the absorption of 4047 Å a beam of light from the end of one of the lamps was rendered parallel and then split into two roughly equal beams by a partially transmitting first surface mirror. One served as a reference beam, the other was passed longitudinally through the cell. The analysis beam was circular in cross section and 0.6 cm in diameter. By means of Corning filters each beam was made monochromatic before falling on separate GL-935 photocells. The photocell circuit used to measure the absorption of 4047 Å was similar to that described previously (15) except that the electrometer was a General Radio Type 1230-A.

The cell, lamps, photocells, etc. were mounted inside a metal box which was separated into lighttight shielded compartments by metal partitions. The cell compartment was flushed continuously with nitrogen to eliminate ozone formation.

Our procedure differed from that of previous workers in that we allowed the nitrogen and mercury vapor to flow through the cell continuously in order to avoid the build-up of impurities which might come off the walls of the cell. Nitrogen of the highest purity obtainable was passed over copper oxide at 250° C, over copper filings at 900° C, and then through a trap cooled with liquid air. After the gas had passed through a capillary flowmeter incorporating a mercury U-tube manometer, its pressure was lowered to the desired value by passing it through an Edwards LB-1 needle valve. An excess of mercury vapor was then added to the gas by passing it through a trap maintained at 40° C and containing a pool of mercury in the bottom and adherent drops of mercury on the sides. The mercury concentration in the gas was then adjusted to a value corresponding to saturation at 15.0° C by passing it through two long narrow traps kept at this temperature. After the gas had passed through the cell its pressure was lowered to the operating value for the diffusion pump by means of a second valve. The pressure in the cell was measured by a variable range mercury manometer connected to the cell through a stopcock connected to the exit tube.

Apparent concentrations of 6^3P_0 atoms (hereafter referred to as Hg⁰ for simplicity) were obtained in terms of the optical density, $K^0L(\text{Hg}^0) = \log_{10}(I_0/I_t)$, in which K^0 is the extinction coefficient for the absorption of 4047 Å by Hg⁰ atoms and L is the length of that part of the cell illuminated by the lamps. The measurements corresponding to I_0 (100%) were made by closing the needle valve on the upstream side of the cell and pumping continuously. Tests showed that no correction needed to be made for scattered light.

In making measurements on the emission of the forbidden line the diameter of the exit diaphragm of the cell was increased from 0.6 to 1.0 cm, the mirror which reflected the analysis beam of 4047 Å onto its photocell was slid out of place and the emitted light was allowed to fall on a quartz lens mounted over a hole in the side of the metal box. The conjugate foci of this lens were at the center of the cell and the slit of the spectrograph.

The spectrograph was of the Littrow type and had one 60° and one 30° prism. In the wavelength region of the forbidden line the dispersion was approximately two angstroms per millimeter. Plates were monitored by a recording microphotometer. Individual values of γ were obtained for each plate, using as standards the intensity of the forbidden line at a fixed pressure of nitrogen and various exposure times. Correction for the failure of the reciprocity law was made by using calibrated screens placed at the exit diaphragm of the cell. The screens were calibrated *in situ* using the optical arrangement for 4047 Å transmission measurements. The intensities of the forbidden line at various pressures of nitrogen were computed relative to the intensity for the standard pressure.

RESULTS AND DISCUSSION

The results on the absorption of 4047 Å for a wide range of nitrogen pressures are shown in Fig. 2. Assuming that K^0 is independent of nitrogen pressure, a dangerous
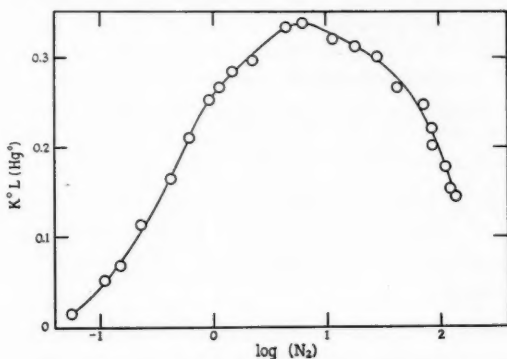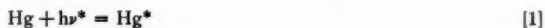

FIG. 2. Optical density, $K^0L(\mathrm{Hg}^0)$, for the absorption of 4047 Å by mercury 6^3P_0 atoms as a function of nitrogen pressure.

assumption, it would appear that (Hg^0) reaches a maximum at about 5–10 mm and then falls off. On the other hand, the intensity of the forbidden line, shown in Fig. 5, is constant in the region 10–150 mm.

In order to make a kinetic analysis of the steady-state processes occurring in the cell under constant illumination the following reactions are considered; for simplicity 6^3P_1 atoms are referred to as Hg*, 6^1S_0 atoms as Hg.

$$\mathrm{Hg} + h\nu^* = \mathrm{Hg}^* \tag{1}$$

$$\mathrm{Hg}^* = \mathrm{Hg} + h\nu^* \tag{2}$$

$$\mathrm{Hg}^* + \mathrm{N}_2 = \mathrm{Hg} + \mathrm{N}_2 \tag{3}$$

$$\mathrm{Hg}^* + \mathrm{N}_2 = \mathrm{Hg}^0 + \mathrm{N}_2 \tag{4}$$

$$\mathrm{Hg}^0 = \mathrm{Hg} \ (\text{on wall}) \tag{5}$$

$$\mathrm{Hg}^0 = \mathrm{Hg} + h\nu^0 \tag{6}$$

$$\mathrm{Hg}^0 + \mathrm{N}_2 = \mathrm{Hg} + \mathrm{N}_2 \tag{7}$$

$$\mathrm{Hg}^0 + \mathrm{N}_2 = \mathrm{Hg}^* + \mathrm{N}_2 \tag{8}$$

$$\mathrm{Hg}^0 + \mathrm{N}_2 = \mathrm{Hg} + h\nu^0 + \mathrm{N}_2 \tag{9}$$

Since the rate of [5] will be inversely proportional to the pressure of nitrogen it will be written as $k_5(\mathrm{Hg}^0)/(\mathrm{N}_2)$. The reactivation of Hg^0 atoms to the Hg* level by collisions with nitrogen has been observed by Samson (8) and others. The energy requirement would be 5.0 kcal per mole, close to the excess energy of the N_2 molecule formed in reaction [4]. However, the probability of such a molecule being deactivated by collisions with normal nitrogen molecules is far greater than its probability of undergoing reaction [8], except at very low pressures. Similar considerations apply to the excited nitrogen molecules formed in reactions [3] and [7]. It will therefore be assumed that the energy distribution in the nitrogen is essentially Boltzmann, and that the rate of reaction [8]

will be given by $k_8(Hg^0)(N_2)$, with an activation energy of at least 5.0 kcal per mole.

For the steady state the above mechanism yields the following relation between (Hg^0) and (N_2):

(i) $$1/K^0L(Hg^0) = A/(N_2)^2 + B/(N_2) + C + D(N_2),$$

in which
$$A = k_2k_5/k_4I_a^*K^0L,$$
$$B = [(k_3+k_4)k_5+k_2k_6]/k_4I_a^*K^0L,$$
$$C = [(k_3+k_4)k_6+k_2(k_7+k_8+k_9)]/k_4I_a^*K^0L,$$
$$D = [(k_3+k_4)(k_7+k_8+k_9)-k_4k_8]/k_4I_a^*K^0L,$$

and I_a^* is the rate of formation of Hg* atoms by reaction [1]. It is convenient to use an expression for $1/K^0L(Hg^0)$ rather than for $1/(Hg^0)$ since the former is obtained directly from the transmission measurements; consideration will be given later to the possible variation of K^0 with pressure.

(a) Absorption Measurements

While the general shape of the curve in Fig. 2 is in agreement with a function of the form given in (i), more detailed information can be obtained by examining the low-, medium-, and high-pressure regions. In Fig. 3 the quantity $(N_2)^2/K^0L(Hg^0)$ is plotted
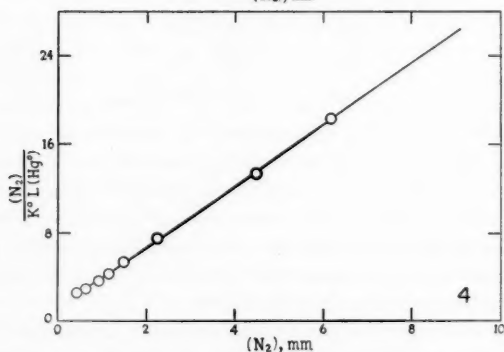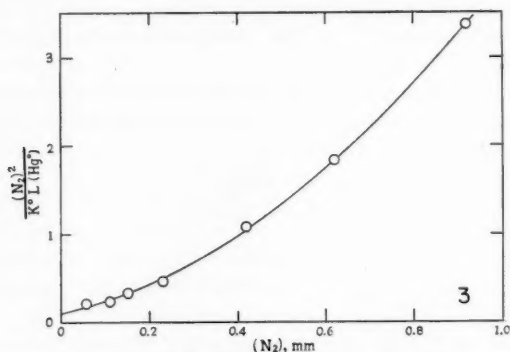

FIG. 3. $(N_2)^2/K^0L(Hg^0)$ as a function of nitrogen pressure in the low-pressure range.
FIG. 4. $(N_2)/K^0L(Hg^0)$ as a function of nitrogen pressure in the medium-pressure range.

against (N_2) for pressures below 1 mm. The smooth curve is plotted from the function $A + B(N_2) + C(N_2)^2$ in which the constants $A = 0.0974$ mm², $B = 1.171$ mm, $C = 2.597$ were obtained by the method of least squares.

In Fig. 4 the function $(N_2)/K^0L(Hg^0)$ is plotted against (N_2) for the pressure region 0.62 to 6.17 mm. The smooth curve is a plot of $A/(N_2) + B + C(N_2)$, in which $A = 0.0974$ as derived previously, $B = 1.116$, and $C = 2.780$. In this case the values of B and C were obtained by applying the method of least squares to the function $(N_2)/K^0L(Hg^0) - 0.0974/(N_2)$. To avoid crowding together of experimental points the lower part of the curve of Fig. 4, including the turnup is not shown. Although there is relatively little difference between the two sets of values of B and C, we prefer to use those corresponding to Fig. 4, since it is in this region that they play their most important role.

The value of D was obtained by taking the simple average of the quantity $[1/K^0L(Hg^0) - 0.094/(N_2)^2 - 1.116/(N_2) - 2.780]/(N_2)$ in the pressure region 9.26 to 137.0 mm; this was equal to 0.023 mm⁻¹ with a mean deviation of 0.004.

Matland (16) obtained a value of approximately 0.4×10^{-16} cm² for σ^2 for the quenching of 2537 Å by nitrogen, corresponding to a value of 2.1×10^5 mm⁻¹ sec⁻¹ for $(k_3 + k_4)$. From the work of Alpert, McCoubrey, and Holstein (17) it would appear that with the mercury concentration and cell dimensions used in the present work there should be a negligible amount of imprisonment, and hence k_2 will be approximately 10⁷ sec⁻¹. The quantity $(k_3 + k_4)/k_2$ will then be 2.1×10^{-2} mm⁻¹. Since $B/A = (k_3 + k_4)/k_2 + k_6/k_5 = 11.4$, it follows that the first term can be neglected and that k_6/k_5 is equal to 11.4 mm⁻¹.

In order to evaluate k_6 it is necessary to obtain a relation between k_5 and the diffusion coefficient of Hg⁰ atoms in nitrogen. Under steady illumination the relation between (Hg^0) and r, the radial distance from the axis of the cylindrical reaction cell is given by

(ii) $$\partial^2(Hg^0)/\partial r^2 + (1/r)\partial(Hg^0)/\partial r - a(Hg^0) + b = 0,$$

in which $a = [k_6 + (k_7 + k_8 + k_9)(N_2)]/D^0$; $b = k_4(Hg^*)(N_2)/D^0$; and D^0 is the diffusion coefficient of Hg⁰ atoms in nitrogen.

Since the cell is more or less uniformly irradiated by the four arms of the two U-shaped lamps, the radius of the cell is only 1.55 cm, and the partial pressure of mercury corresponded to saturation at 15° C, we feel justified in assuming that I_a^*, and hence (Hg^*), is uniform throughout the cell. This is supported by the work of Pinder and Le Roy (18) on the extinction coefficient for the absorption of 2537 Å by mercury, in which they used a lamp similar to those used in the present work. Actually, any decrease in (Hg^*) as r approaches zero will be partially compensated by an increase in the rate of reaction [8], since (Hg^0) will increase as r approaches zero.

The solution of (ii) is

(iii) $$(Hg^0) = \frac{b}{a}\left[1 - \frac{\Sigma(\alpha\rho^2/4)^n/(n!)^2}{\Sigma(\alpha/4)^n/(n!)^2}\right],$$

in which $\alpha = aR^2$, $\rho = r/R$, R is the radius of the cell, and the summations are for all integral values of n from zero to infinity. Since D^0 is inversely proportional to (N_2) it follows that a and α will approach zero as (N_2) approaches zero. Hence, at low pressures,

(iv) $$(Hg^0) \to bR^2(1 - \rho^2)/4 \to \frac{k_4 I_a^*(N_2)}{4k_2 D^0}(1 - \rho^2)$$

or, at the axis of the cell,

(v) $$(Hg^0) \to \frac{k_4 I_a^*(N_2)}{4k_2 D^0}.$$

Since the radius of the analysis beam is approximately one-fifth that of the cell, the average value of (Hg^0) in the beam will differ from that at the axis by a negligible amount. Comparison of (v) with the limiting low-pressure value of (Hg^0) given by (i) shows that

(vi) $$k_5 = 4D^0(N_2)/R^2.$$

Since there are no certain values of D^0 in the literature, we have used the data of Spier (19) on the diffusion coefficient of Hg in nitrogen. These were obtained under conditions similar to those of the present experiments: 1.12 to 1.75 mm pressure and 292.2° to 298.7° K. Assuming a square law dependence of D^0 on the temperature, and an inverse first-power dependence on the pressure, the average value of D^0 at 1 mm pressure and 25° C is 124 cm² sec⁻¹, from which k_5 is calculated to be 206 mm sec⁻¹.

From this value of k_5 and the empirical values of A, B, and C, the following kinetic parameters were obtained: $k_6 = 2.35 \times 10^3$ sec⁻¹ (i.e. natural lifetime is 4.25×10^{-4} sec); $(k_7+k_8+k_9) = 5.84 \times 10^3$ mm⁻¹ sec⁻¹ $= 1.09 \times 10^{11}$ cm³ mole⁻¹ sec⁻¹. Assuming that $k_4 \gg k_3$ and that the coefficient D is not invalidated by pressure broadening, values of (k_7+k_9) and k_8 are found to be 2.32×10^3 mm⁻¹ sec⁻¹ and 3.52×10^3 mm⁻¹ sec⁻¹, respectively. Assuming that reactions [7] and [9] have no activation energy, their mean value of σ^2 is 4.5×10^{-19} cm². The value of σ^2 for reaction [8] is 31.5×10^{-16} cm², assuming an activation energy of 5.0 kcal per mole in the expression, $k_8 = \sigma^2 (8\pi RT/\mu)^{1/2} e^{-E/RT}$; this appears to be high; whether or not this is the result of incomplete deactivation of excited N_2 molecules formed in reactions such as [3], [4], or [7] cannot be established until the possible influence of pressure broadening is ascertained.

The absorption measurements clearly indicate the occurrence of [6]; the lifetime of the 6^3P_0 state, with respect to emission was found to be 4.25×10^{-4} sec. This value was derived from experiments at pressures less than 1 mm, where errors from pressure broadening should be negligible, but involved the assumption that Hg^0 and Hg have the same diffusion coefficient. Whether or not we can conclude that there is also a collision-induced emission by reaction [9] is open to some question. Even if we neglect pressure-broadening effects in the high-pressure region it is possible to evaluate (k_7+k_9), but not k_9 alone. The constant intensity of the forbidden line in the high-pressure region, as shown in Fig. 5, would obtain if both k_7 and k_9 were equal to zero, but this would imply a very strong dependence of K^0 on nitrogen pressure in the region 10 to 137 mm.

(b) Emission Measurements

The effect of nitrogen pressure on the intensity of the forbidden line is shown in Fig. 5. According to the present mechanism the intensity should be proportional to $[k_6+k_9(N_2)](Hg^0)$. Qualitatively the results are in agreement with a relation of this form in which (Hg^0) is related to the nitrogen pressure by equation (i). However, it was necessary to assume a much larger value of D than that derived from the absorption measurements. The best agreement was obtained by using $A = 0.0974$, $B = 1.116$, $C = 2.78$, and $D = 2.0$, together with a value of 0.4 for k_6/k_9. The value of the latter is not in serious disagreement with that derived from the absorption measurements, which gave a value of 1.0 for $k_6/(k_7+k_9)$.

In comparing the results of the two series of experiments it must be borne in mind that although there is unequivocal evidence for pressure-dependent emission of the forbidden line, any conclusions about the particular form of the emission process will be influenced by the interpretation of the data given in Figs. 2 and 5. If the fall-off in
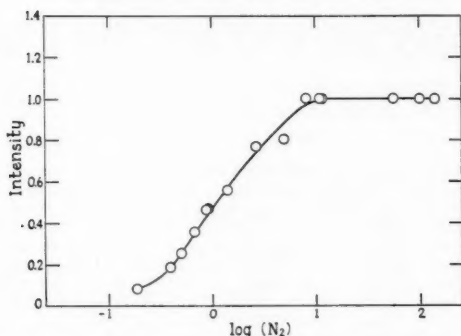
Fig. 5. Intensity of the forbidden line, 2656 Å, in arbitrary units as a function of nitrogen pressure.

$K^0L(\mathrm{Hg}^0)$ at high pressures is due only to pressure broadening effects, then the coefficient D in equation (i) is actually zero; in which case all of the emission would have to be by reaction [6]. However, this would predict a considerably higher emission intensity below 10 mm than was actually found. On the other hand, if all emission is assumed to occur by reaction [9] it would not be possible to interpret the results of the absorption measurements in the low-pressure regions where pressure broadening effects are not likely to be serious. One factor that has not been taken into consideration is that the lamps were operated on 60-cycle alternating current, which might invalidate the use of the steady-state assumption.

Although it is evident that further work will have to be done in order to resolve the quantitative discrepancies between the two sets of measurements, the present work has shown that in any future attempt to interpret the behavior of mercury 6^3P_0 atoms cognizance must be taken of the spontaneous and collision-induced emission of the forbidden line.

REFERENCES

1. R. W. Wood and E. Gaviola.   Phil. Mag. **6**, 271 (1928).
2. E. Gaviola.   Phil. Mag. **6**, 1154, 1167 (1928).
3. H. Klumb and P. Pringsheim.   Z. Physik, **52**, 610 (1928).
4. J. A. Berberet and K. C. Clark.   Phys. Rev. **100**, 506 (1955).
5. M. L. Pool.   Phys. Rev. **33**, 22 (1929); **38**, 955 (1931).
6. T. Asada, R. Ladenburg, and W. Tietze.   Z. Physik, **29**, 549 (1928).
7. H. W. Webb and H. A. Messenger.   Phys. Rev. **40**, 466 (1932).
8. E. W. Samson.   Phys. Rev. **40**, 940 (1932).
9. S. Sonkin.   Phys. Rev. **43**, 788 (1933).
10. J. H. Coulliette.   Phys. Rev. **32**, 636 (1928).
11. B. de B. Darwent and F. G. Hurtubise.   J. Chem. Phys. **20**, 1684 (1952).
12. R. W. Wood.   Proc. Roy. Soc. **106**, 679 (1924).
13. G. Laroze and J. L. Cojan.   Compt. rend. **995** (1958).
14. M. Kasha.   J. Opt. Soc. Am. **38**, 929 (1948).
15. M. J. Dignam, W. G. Forbes, and D. J. Le Roy.   Can. J. Chem. **35**, 1341 (1957).
16. C. G. Matland.   Phys. Rev. **92**, 637 (1953).
17. D. Alpert, A. O. McCoubrey, and T. Holstein.   Phys. Rev. **76**, 1257 (1949).
18. J. A. Pinder and D. J. Le Roy.   Can. J. Chem. **35**, 588 (1957).
19. J. L. Spier.   Physica, **7**, 381 (1940).

HIGH ENERGY REACTIONS OF ATOMIC HYDROGEN[1]

Michael Henchman,[2] David Urch,[3] and Richard Wolfgang

ABSTRACT

The chemistry of hot hydrogen atoms has been studied using tritium of high kinetic energy as produced by nuclear recoil. The possibilities and limitations of this technique are discussed using a collision theory for reactions of atoms having a very high initial energy. Using this theory and certain experimental data, it is concluded that hot hydrogen atoms react to combine with organic molecules at very high collision efficiency (of the order of approximately 0.2 to 0.4) in the energy range 3–10 ev. There is no indication that collisions at much higher energies lead to combination. With most systems, e.g. alkanes, a wide variety of reactions is observed. The systematics of these hot reactions is discussed and evidence on their detailed mechanism is presented. It appears that most products are formed by a fast displacement of an atom or group by the hot hydrogen. There is no evidence for the formation of a common, internally equilibrated, collision complex which decays on a statistically determined basis to the various products. Instead, the course of the reactions seems largely governed by the direction and point of impact of the hot atom. Thus, stereochemical evidence indicates that axial approach of the hot hydrogen atom along the C—H bond axis leads to abstraction while approach at large angles to this axis results in displacement without Walden inversion. In some cases sufficient excitation energy is introduced in the hot displacement process to cause further decomposition of the primary product. This model of high-energy reactions is compared with that of thermal reactions and its general implications are briefly discussed.

Perhaps the severest limitation on the study of chemical kinetics has been the scarcity of data on high-energy interactions. Little information on such interactions is obtainable from results on thermally excited species. Thermal reactions generally have very low collision efficiencies which are sensitively dependent on the activation energy. As a consequence only those reaction modes with minimum activation energies are observed. In a sense these modes are only limiting cases of the high-energy situation. Here activation energies are no longer large compared with the energies available; consequently collision efficiencies should be higher and a much wider variety of reactions may be expected.
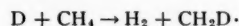
Thus up to a few years ago, the only known reaction between atomic hydrogen and methane was simple abstraction, as it proceeds with thermal hydrogen (1, 2)

$$D + CH_4 \rightarrow HD + CH_3 \cdot$$
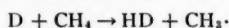
But other reactions of hydrogen atoms are quite conceivable; for instance, exchange

$$D + CH_4 \rightarrow CH_3D + H$$

or perhaps

$$D + CH_4 \rightarrow H_2 + CH_2D \cdot$$
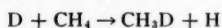
and so on. These reactions are interesting and a priori one might expect them to occur at higher energies, where the system may follow paths on the reaction surface other than those going through the lowest saddle point.

There has been no shortage of interest in possible high-energy reactions. Rather, what has been lacking is the means of producing high energy or "hot" species under controlled conditions, where their elementary reactions might be studied. Some work has been done, generating hot atoms and radicals by photochemical dissociation; but, in general, these have still not been of sufficient energy to react in a qualitatively different manner from their low-temperature thermal counterparts (3). In principle, the ideal system for the

study of high kinetic energy atoms and other species would be monoenergetic molecular beams of controllable energy. However, for work in what is chemically perhaps the most interesting energy range—of the order of 1 to 20 ev—it does not appear that present beam techniques are likely to give useful results for some time.

In the meantime it appears that high-energy recoils from certain nuclear reactions may provide systems in which high-energy atomic reactions may be studied under controlled conditions. In our laboratory we have used recoil tritium from the nuclear reaction $He^3(n,p)T$ as a source of hot atoms. This paper briefly surveys our recent and largely unpublished results and uses them as a basis for discussion of a model of hot atom reactions.

METHOD

The principle of the recoil method as used for hot hydrogen atoms is very simple (4). He^3 is mixed in a quartz ampoule with the gas whose reactions with hot hydrogen are to be studied. (A lithium salt may be substituted for He^3 in condensed systems.) Hot hydrogen in the form of recoil tritium is generated by exposure to neutrons. This will react to form trace quantities of various products which are labeled due to the radioactivity of the contained tritium. These products are then separated, generally by gas chromatography, and assayed using an internal flow proportional counter attached to the chromatography unit (5, 6). Any of the products may then be degraded to determine the intramolecular position of the tritium.

While this method is basically simple there are a number of pitfalls to be avoided. In the first place unless the nuclear reaction gives rise to a well-defined species, it becomes a difficult problem in itself simply to determine the nature of the reactant. Thus radiative neutron capture (n,γ reaction) usually yields a recoil species with an energy between 1 and 1000 ev, which may or may not be charged, and which may or may not be neutralized before undergoing "chemical" reaction. Fortunately the $He^3(n,p)T$ reaction yields ions of very high energy, 2×10^5 ev; neutralization of these ions occurs at 10^4 ev in non-ionic media; in an energy range well above that in which they may react to become chemically bound (4). This nuclear reaction is thus a well-defined source of atoms of essentially infinite energy, which lose energy by collision until they react or are reduced to thermal energies.

Secondly, the high-energy release associated with the nuclear reactions will cause gross radiation damage to the system and may build up a significant level of reactive impurities. This effect is controlled by using only a trace amount of recoil tritium—of the order of 10^{14} atoms—a device made possible, of course, by its radioactivity. The tracer level experiment has the further advantage of eliminating the confusing type of secondary process where more than one hydrogen atom is involved.

A final important point of technique is being able to distinguish between hot reactions and the thermal reactions of those atoms which have been collisionally deactivated (7). These thermal reactions are effectively eliminated by the addition of a small concentration of a scavenger, such as I_2, with which the thermalized species will react preferentially. On the other hand the hot reactions are unaffected since hot atoms have an effective lifetime of only a few collisions and are therefore unlikely to encounter the scavenger.

COLLISION KINETICS AND ENERGY DEPENDENCE

The main disadvantage of using nuclear recoil as a source of hot atoms is that the reactions occur over a range of energies, from the highest possible energy where combination may take place down to (but not including) the thermal region. It is for this reason that molecular beams are, in principle, preferable; they would make possible a direct and

explicit measurement of reaction probability as a function of energy. However, even if recoil atoms cannot be used to study reactions at a single energy, their distribution of energies is well defined and their collision kinetics can thus be treated analytically (7). In a sense the collision theory of hot atoms, briefly outlined below, is quite analogous to collision theories of thermal species whose Boltzmann energy distribution yields expressions such as the Arrhenius equation.

Kinetic Theory

Consider a system (7) of hot atoms which lose energy in successive collisions but may react to combine between energies E_2 and E_1. Above E_2 the collisions are too energetic to result in stable combination and E_1 is the minimum energy required for reaction. Let $n(E)dE$ be the differential probability of collision at energy E, f the probability that a collision will be with a reactive species, and $p(E)$ the probability that such a collision at energy E will result in combination. Then the total probability P that the hot atom will react during its lifetime is given by

[1]
$$P = \int_{E_2}^{E_1} fp(E)n(E)dE.$$

$n(E)$ is evaluated assuming that the initial energy is much greater than E_2, that the reaction threshold E_1 is above thermal energies, and that the energy loss is as by elastic collisions. P can then be evaluated (7)

[2]
$$P = 1 - \exp\left[-\frac{f}{\alpha} I \right]$$

[3]
$$I = \int_{E_1}^{E_2} \frac{p(E)}{E} dE$$

where α is the average logarithmic energy loss per collision. P, the total probability of hot reaction, is experimentally measurable and f and α may be calculated from the composition of the system. Similar considerations (7) lead to expressions for the total probability of hot reaction P_i to give a specific product i.

This detailed theory has been tested (7) using the reactions

$$CH_4 + T \rightarrow CH_3T + H, \qquad\qquad [4]$$
$$CH_4 + T \rightarrow CH_2T\cdot + H_2. \qquad\qquad [5]$$

f and α were varied by adding rare gas moderators. The effect of these is to reduce the total probability of hot reactions by reducing the number of collisions of the hot atom with methane. Figure 1 shows the probability of formation of CH_3T in the presence of
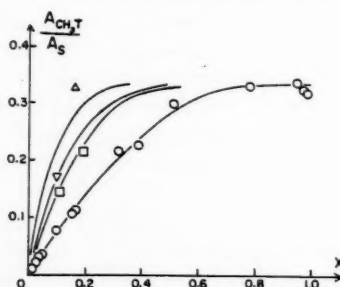

FIG. 1. Plot of the relative yield of labeled methane as function of the mole fraction of methane. Moderators: helium O, neon □, argon ▽, xenon △.

various amounts of He, Ne, A, and Xe. The points are experimental and the lines through them calculated from the kinetic theory. The fit is good within experimental error and the treatment is evidently a valid representation of the system.[4]

Energy Dependence

This model of hot reactions makes it clear that high-energy recoil atoms cannot supply explicit and absolute information on the energy dependence of the collision efficiency $p(E)$. As obtained from this treatment $p(E)$ is wrapped up in the definite integral I. The only energy information that can be directly obtained from the detailed theory is on the relative average energies at which various products are formed in a given system (7). Thus it appears that the two hot atom reactions of methane ([4] and [5]) proceed at about the same average energy.

Information on the energy range in which hot reactions can occur must come from calculations on the dynamics of the collision (which are quite difficult) and from the character of the reactions which are observed. Data on the lower energy limit (E_1) comes from experiments in which Hamill et al. (3) have observed that the hydrogen displacement reaction does not occur with photochemically generated hydrogen atoms of 1 to 2 ev. At the other limit, the only conceivable way in which a very high-energy hydrogen atom (>10–20 ev) can undergo displacement reaction [4] is by transferring most of its kinetic energy to the ejected hydrogen in a quasi-elastic or billiard-ball (8) collision. This would leave the incoming atom with sufficiently little energy so that it could be captured by the methyl group. (Such a process can be considered as essentially an atom–atom collision, where one of the atoms is held in a relatively shallow potential well to the rest of the molecule, with which it is then only weakly coupled.)

It has been calculated by Cross (9) that if displacement reaction [4] with CH_4 and CD_4 occurs by such a pure billiard-ball mechanism, there should be an isotope effect of about 3. No such large effect is experimentally observed, indicating that this type of mechanism is not important (9). Apparently reaction occurs in an energy range where valence bond coupling is strong, i.e. as far as transfer of momentum is concerned the incoming atom collides with the molecule, or a large part of it, instead of a single atom within it. This finding was not unexpected in view of the earlier observation that alkyl groups and halogen atoms as well as hydrogen atoms could be displaced. The tritium must therefore have a kinetic energy of the order of magnitude of valence bond energies. This conclusion is consistent with the products observed from other systems, for the energy deposited in a hot displacement reaction appears to be insufficient to cause extensive decomposition or rearrangement. This topic will be discussed later in this paper.

Collision Efficiencies

If, therefore, the conclusion is that the hot hydrogen reacts to combine while between 2 and 20 ev or, more likely still, while between 3 and 10 ev, the kinetic theory can be used to calculate collision efficiencies. From equation [3] the collision efficiency $p(E)$ averaged over the entire energy interval E_2 to E_1 is

$$[6] \qquad \overline{p(E)} = \frac{I}{\ln(E_2/E_1)}$$

For the methane system I has been measured to be 0.4 (7). Fortunately $\overline{p(E)}$ is quite insensitive to the energy range E_2/E_1. Using the values just quoted we find that for hot

[4]Conversely, these considerations provide a further proof that the reactions studied are indeed hot. A fit cannot be obtained even if there is only a small contribution by thermal processes (7).
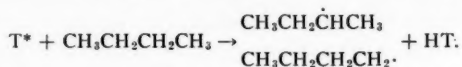
atom reactions collision efficiencies are of the order of 0.2 to 0.4. These values are several orders of magnitudes higher than those for thermal reactions of a similar nature and are one of the distinguishing characteristics of hot atom reactions.

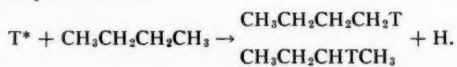### SYSTEMATICS OF HOT HYDROGEN ATOM REACTIONS

The reaction of hot tritium with hydrocarbons (4, 10, 11, 12, 13), alcohol (14), acetone (14), carboxylic acids (15), and various solid compounds (16) has been investigated. The types of reactions found are quite similar in all those systems. We can therefore use the results of a recent study (13) we have made of the alkane system as a representative example of the systematics of hot hydrogen displacement reactions. (Hot hydrogen addition reaction, as studied in alkenes (10), is a separate class of mechanism and will not be discussed here.)

As in most systems about two-thirds to three-quarters of hot hydrogen atoms in pure alkanes will undergo reaction before reaching thermal energies. The types of reactions found are as follows, in decreasing order of relative importance (butane is used as example):
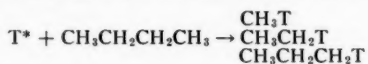
(I) Hydrogen atom abstraction. This reaction, the only one observed at thermal energies, also occurs with hot hydrogen (although with a much higher collision yield).

$$T^* + CH_3CH_2CH_2CH_3 \rightarrow \begin{matrix} CH_3CH_2\overset{\cdot}{C}HCH_3 \\ CH_3CH_2CH_2CH_2\cdot \end{matrix} + HT.$$

(II) Hydrogen atom displacement:

$$T^* + CH_3CH_2CH_2CH_3 \rightarrow \begin{matrix} CH_3CH_2CH_2CH_2T \\ CH_3CH_2CHTCH_3 \end{matrix} + H.$$

(III) Replacement of alkyl group to form a degraded alkane:

$$T^* + CH_3CH_2CH_2CH_3 \rightarrow \begin{matrix} CH_3T \\ CH_3CH_2T \\ CH_3CH_2CH_2T \end{matrix}$$

(IV) Replacement of two groups to form a radical. Either two hydrogen atoms or a hydrogen atom and an alkyl group may be displaced by the hot tritium atom, e.g.,

$$T^* + CH_3CH_2CH_2CH_3 \rightarrow CH_3CH_2CH_2CHT\cdot.$$
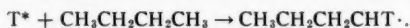
The resulting radical may combine with iodine scavenger to form alkyl iodide. Alternatively it may decompose into a smaller radical and an alkene by breaking a C—C bond without rearrangement, e.g.,

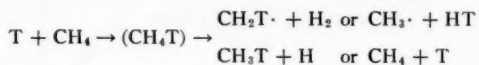$$CH_3CH_2CH_2CHT\cdot \rightarrow CH_3CH_2\cdot + CH_2CHT.$$
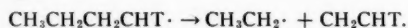
(This type of decomposition has also been observed with similar radicals made by hot atom addition to alkenes (10).)

These reactions account for essentially the entire yield. No built-up or rearranged products are formed. The relative importance of these various types of reactions with the alkanes are given in Table I. However, their relative probabilities vary sharply and in a specific manner from system to system. It is in this variation that we must look for clues to the mechanism.

MECHANISM

We have mentioned earlier that in high-energy processes the activation energies should become less important in determining the path of a reaction. This is reflected in the

result that $90\pm2\%$ of the hot reactions are hydrogen abstraction or displacement and less than 10% involve displacement of an alkyl group. In other words the probability of C—H bond rupture is about four times greater than with the weaker C—C bond. This finding also implies that hot displacement reactions do not pass through a common intermediate or collision complex of sufficient lifetime to permit internal equilibration of energy, as has been suggested (17, 18). Such an intermediate would certainly be expected to decompose at least as often by breaking a weaker rather than a stronger bond. There appears to be no data supporting the supposition that hot displacement reactions do go through such quasi-equilibrated intermediates. For instance, if HT and $CH_2T\cdot$ were produced from methane by decomposition of a common activated complex, in which the incident and the CH_4 hydrogen atoms have become indistinguishable

$$T + CH_4 \rightarrow (CH_4T) \rightarrow \begin{array}{l} CH_2T\cdot + H_2 \text{ or } CH_3\cdot + HT \\ CH_3T + H \quad \text{ or } CH_4 + T \end{array}$$

their ratio $HT/CH_2T\cdot$ would be expected, on a purely statistical basis, to be $2:3$. Even allowing for possible isotope effects the observed ratio of 9:1 hardly supports such a mechanism (4). Instead, all results are consistent with the hypothesis that the displacement reaction is a fast, direct, localized event occurring on a time scale comparable to a bond vibration ($\sim10^{-14}$ sec).[5]

Stereochemistry of Hot Atom Displacement

If hot reactions are thus not controlled by energetics, or the statistically determined decay of a common collision complex, we must turn to stereochemical factors affecting displacement and abstraction processes, as the major determinant of hot atom reactions. For example, it appears to be a reasonable hypothesis that the C—H bond is attacked more readily than the C—C bond because of its greater exposure. Two related questions then arise: (*a*) Does hydrogen displacement proceed by a Walden inversion mechanism? and (*b*) What determines whether the hydrogen atom is displaced or abstracted? The answers to these questions have been sought in experiments on the retention of spatial configuration during hydrogen displacement.

The first experiment performed using hot tritium indicated that configuration was retained during hydrogen displacement. The system was glucose (19, 20) and it yielded a substantial amount of glucose labeled at hydrogen atoms attached to asymmetric carbon atoms. Had inversion occurred, other labeled hexoses would have been obtained instead. Retention of configuration has also been demonstrated in displacement at the hydrogen attached to the asymmetric center in alanine (21). However, since these experiments were carried out in the solid phase, they left open the possibility that the molecule was constrained to keep its configuration only by the crystal structure.

Experiments were therefore carried out on the retention of configuration in the vapor phase. The displacement reaction for gaseous optically active *sec*-butyl alcohol was studied. There is no change in configuration about the asymmetric carbon atom during the displacement of both the hydrogen bonded directly to it and those in the methyl and ethyl groups. These results actually show $90\pm10\%$ retention of configuration.

With this information we can now discuss a more detailed model for the hydrogen abstraction and displacement, which together account for 90% of the hot reactions in

[5]*It is interesting to compare the fast displacement reactions with the addition reactions of hot hydrogen to double bonds in alkenes. In the latter case it can be clearly shown that a long-lived radical intermediate is formed (10). These well-defined intermediates may each decompose into two or three sets of alternative products.*

alkanes. If Walden inversion is unimportant, it can be postulated that to react with a bound hydrogen, the incoming hot hydrogen must approach within a wide cone about the C—H bond axis (see Fig. 2). However, if the approach is directly along the C—H bond

(a) H Atom Abstraction

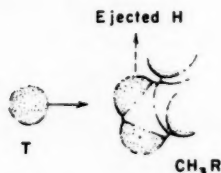(b) Displacement of H Atom

Ejected H

FIG. 2. Stereochemistry of the abstraction and displacement of hydrogen from an alkane.

axis, displacement could not occur as it would be difficult to juxtapose the positions of the H and T atoms. But abstraction of the H atom should be entirely possible for this approach. This is in accord with calculations of Gorin et al. (22), showing that axial attack along the C—H bond is the most favorable route for hydrogen abstraction. This mechanism is also consistent with the finding that abstraction from CH_2D_2 yields equal amounts of HT and DT (23). Thus we arrive at the tentative conclusion that hot hydrogen attack at small angles to the C—H bond, within a small inner cone about the bond axis, normally leads to abstraction, whereas approach at large angles, within a larger co-axial cone, usually results in displacement (see Fig. 2).

This model is crude and obviously oversimplified. But it can be tested. Consider a particular C—H in an alkane. Methyl or methylene groups attached to the carbon will obstruct those approaches of the hot atom at large angles to the C—H bond axis and will reduce the amount of displacement. Approaches at small angles will not be affected and hence there will be no steric obstruction of the abstraction reaction. We consider that the displacement reaction in methane is unobstructed and that replacement of one of these hydrogens by a methyl or methylene group reduces the amount of displacement at one of the remaining hydrogens, relative to that of abstraction, by a factor $(1-\Omega)$. Experimentally the ratio abstraction/displacement is found to be unity for methane. On this simple picture, for an alkane containing n hydrogens, of which n_1 are primary, n_2 secondary, and n_3 tertiary,

$$\frac{\text{abstraction}}{\text{displacement}} = \frac{n}{n_1(1-\Omega)+n_2(1-\Omega)^2+n_3(1-\Omega)^3}.$$

The experimental and calculated values of this ratio are plotted in Fig. 3 for all the alkanes listed in Table I and for cyclopentane. The value $\Omega = 0.45$ for the obstruction
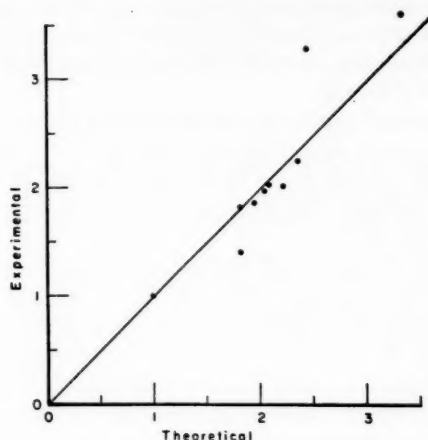
FIG. 3. Comparison of the theoretical and experimental values of the ratio of hydrogen abstraction to hydrogen displacement for cyclopentane and the alkanes listed in Table I. The obstruction parameter $\Omega = 0.45$.

TABLE I

Summary of product distribution from non-cyclic alkanes (relative to yield of labeled parent molecule)

	T-Labeled product	Corresponding replacement	Molecule reacting with hot hydrogen								
			CH_4	C_2H_6	⋀	⋀⋁	⋗‒	⋀⋁	⋗⋖	✛	⋀⋁⋀
I	HT	Abstraction	1.0	1.82	1.97	1.99	1.92	2.37	2.03	1.40	3.28
II	Parent molecule	H atom	1.0	1.0	1.0	1.0	1.0	1.0	1.0	1.0	1.0
III	Degraded alkane	Alkyl group	—	0.12	0.15	0.15	0.17	0.19	0.21	0.23	0.31
IV	Methyl iodide[a] (initially $CH_2T\cdot$)	Alkyl group[b] + H atom or two H atoms	0.12[b]	0.14	0.06	0.09	0.05	0.08	0.09	0.09	0.07
IV	Alkene (initially radical)	Alkyl group + H atom	—	0.11	0.08	0.08	0.09	0.10	0.09	~0.05	0.12
	Rearranged and built-up products	Unaccounted for[c]	—	~0.03	0.00	0.01	0.01	0.00	0.00	0.01	0.02

[a]In presence of I_2 scavenger only.
[b]2H displacement in case of CH_4.
[c]Not compatible with formation as direct consequence of a hot displacement reaction.

parameter gives the best fit. This is a simple-minded calculation with obvious shortcomings. The principal one is that it attributes the same amount of obstruction to any attached group, regardless of whether it is, say, methyl or isopropyl. Nevertheless, we suggest that the excellent correlation between calculation and experiment provides evidence for the detailed model used for hydrogen abstraction and displacement as well as the more general postulate that the course of the reaction depends primarily on the angle of approach and the point of impact of the hot atom.

Alkyl Group Displacement

It is tempting to try and generalize the hydrogen displacement mechanism for the displacement of larger atoms and groups. Such replacement has been shown to occur. Odum (24) finds that fluorine, chlorine, bromine, and iodine in alkyl halides have a high probability of being displaced by a hot hydrogen atom.

$$T^* + CH_3X \rightarrow CH_3T + X$$

Rowland and co-workers have demonstrated the occurrence of hot hydrogen displacements of halogens and also of nitro groups in aromatic systems (25).

This would seem to indicate that degraded alkanes are formed by direct alkyl group displacement (reaction type III), e.g.,

$$CH_3CH_2CH_2CH_3 \rightarrow CH_3T \text{ or } CH_3CH_2T \text{ or } CH_3CH_2CH_2T.$$
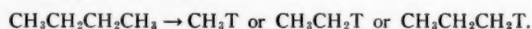
In this single-step mechanism it is postulated that the hot hydrogen attacks the C—C bond in a direction nearly perpendicular to the bond axis. It would displace one group and combine with the other. This mechanism is consistent with the following results for the alkane system (13).

1. Displacement of an alkyl group is less probable than that of an H atom. This may be correlated with the greater steric obstruction of the C—C bond.

2. The amount of an alkane RT formed depends on the number of R groups in the reacting molecule. Thus the amount of methane formed from the pentanes increases in the order cyclopentane $<$ n-pentane $<$ isopentane $<$ neopentane.

3. In attacking a C—C bond the tritium preferentially combines with the smaller of the groups joined by the bond. This bias is more pronounced if the two groups are very dissimilar in size. Thus neopentane yields eight times as much methane-T as isobutane-T.

Although direct alkyl group displacement is not the only possible mechanism for the formation of the degraded alkanes (see footnote 6) it appears to be the most likely. Its validity would be established by showing that configuration is retained in the formation of the degraded alkanes.

The direct displacement mechanism can also account for the production of radicals (reaction type IV). Two atoms or groups would have to be displaced, e.g.,

$$T^* + CH_3CH_2CH_2CH_3 \rightarrow H_2 + CH_3CH_2CH_2CHT.$$
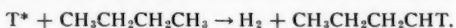
This mechanism is plausible but there is as yet insufficient evidence to regard it as more than a tentative hypothesis.

EXCITATION ENERGY IN PRIMARY PRODUCT OF HYDROGEN DISPLACEMENT

It is likely that some of the energy of the incident hot atom will remain as excitation in the product of the displacement process. Although we have presented evidence that the point and direction of impact is the primary determinant of the reaction path, this excitation energy may also be a factor in determining the final product. That this energy is very unlikely to be large (of the order of 10 ev) is indicated by the very small yields of products requiring multiple bond rupture for their formation. Thus only traces of acetylene are formed by hot hydrogen reaction with alkanes; similarly, the yield of methylacetylene and allene by reaction with alkenes is less than 1% (10, 11, 13).

The excitation energy is sufficient to cause some decomposition of the product of the primary displacement especially in sensitive systems. Thus carboxylic acids tend to decarboxylate following hot hydrogen displacement (15), e.g.,

$$CH_3COOH + T^* \rightarrow CH_2TCOOH^* \rightarrow CH_3T.$$
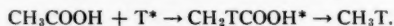
The resulting decarboxylated hydrocarbon can presumably also be produced by direct displacement of —COOH. But the yield of this product decreases very rapidly with increasing chain length. This indicates that most of it must have been formed by decomposition of excited acid molecules. As the size of such molecules increases so does their lifetime (26) and it becomes more likely that they lose their energy by collision rather than decomposition.

Other systems also provide evidence for deposition of moderate amounts of excitation

energy on displacement. When a hydrogen atom bound to the sp^2 carbon atom in cis and trans dichloroethylenes is replaced, configuration is lost in 30% of the events (13). This loss is probably due to rotation about the double bond requiring an activation energy of about 2 ev.

Reaction of hot hydrogen with cyclopropane yields at least 15% as much propylene as substituted cyclopropane (13, 17). The isomerization of cyclopropane to propylene has an activation energy of 3 ev. At the pressures at which the experiment was carried out, this would mean that about 4 ev of excitation had been introduced during hydrogen atom displacement.

The examples quoted are particularly sensitive systems, and even in them the fraction of the total products formed by rearrangement or decomposition of a species excited in the initial displacement is not large. In the more stable alkane systems, the only significant products, which could plausibly be formed by such decomposition, are the alkyl radicals (Systematics, reaction type IV), e.g.,

$$T^* + CH_3CH_2CH_3 \rightarrow CH_2TCH_2CH_3{}^* \rightarrow CH_2TCH_2 \cdot + CH_3 \cdot.$$
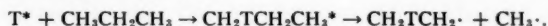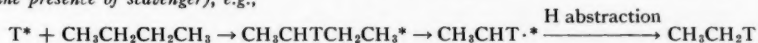
Radicals account for only about 5% of the total yield from alkanes and they could also have been produced by the two group displacement mechanism mentioned earlier.[6]

CONCLUSION

While the studies briefly outlined here represent only a small start towards understanding the chemical properties of hot hydrogen atoms, it does appear that the broad outlines of a mechanism are emerging. The significance of our findings may be summarized by comparing the model for hot reactions with that for thermal processes.

In thermal reactions only a small fraction $e^{-\Delta E/kT}$ (where ΔE is the activation energy) of species have sufficient energy for reaction. Even these species have barely sufficient energy and their only possible path over the energy surface must pass through a saddle point. This is evidenced by the fact that only a small fraction of collisions between species of sufficient energy result in reaction. This fraction p is, of course, the so-called steric factor and $pe^{-\Delta E/kT}$, the collision efficiency, is thus usually a very small number. By contrast we have shown that when a hydrogen atom with a kinetic energy of the order of 3 to 10 ev strikes a molecule, there is a high probability, approaching one-half, that it will react. This must in part simply result from the fact that all systems have energy in excess of the minimum activation energy, so that the factor $e^{-\Delta E/kT}$ approaches unity. What is more significant, however, is that many of the hot atoms have considerably more than the minimum energy for reaction. As a result, their possible paths over the reaction energy surface are not restricted to passage through the lowest saddle point, and a much wider

---

[6]*It may be proposed that degraded alkanes (Systematics, reaction type III) can be produced as a result of excitation energy left in hydrogen displacement and not by direct alkyl displacement. If decomposition of the primary product could yield hot radicals, these could form degraded alkane molecules by hydrogen abstraction (even in the presence of scavenger), e.g.,*

$$T^* + CH_3CH_2CH_2CH_3 \rightarrow CH_3CHTCH_2CH_3{}^* \rightarrow CH_3CHT \cdot {}^* \xrightarrow{\text{H abstraction}} CH_3CH_2T$$

This mechanism has difficulties however. An excited radical normally decomposes to a smaller radical and an alkene (10). To abstract hydrogen, the radical would therefore have to have kenetic rather than internal energy. The production of such species is rather improbable. Furthermore, to account for the distribution of products, e.g. the 8:1 ratio of methane-T: isobutane-T from neopentane, it would have to be postulated that the C—C bond broken was nearly always that closest to the site of the original displacement; in other words that there was little intramolecular energy transfer. Even so it is very difficult to account for the relative constancy, or even increase, in the ratio of total degraded alkanes to hydrogen substitution, that is observed with increasing chain length of the reacting alkane (Table I). However, a final decision on this mechanism must await data on the retention of configuration of the degraded alkanes. This and other alternative mechanisms can be finally excluded if it is shown that configuration is retained in alkyl displacement.

range of impact parameters can lead to reaction. Many different kinds of reactive collisions become possible. A variety of products may result, as illustrated by the alkane data, and their relative yields are not primarily governed by energy considerations. As a consequence, differences in chemical reactivity as conventionally understood become unimportant: for example, hydrogen atoms are about equally well displaced whether they are aromatic or aliphatic (23). Furthermore, the availability of excess energy may result in the products of the initial displacement being left with a range of excitation energies. There is, however, considerable evidence to suggest that these excitation energies are quite moderate. This is not unexpected for, in collisions, where the hot hydrogen has too much energy, it cannot lose enough momentum to combine.

This model is not consistent with the view that the course of hot reactions is governed by the statistically determined decay of a common intermediate or collision complex. Such a mechanism is essentially an extension of transition state theory of unimolecular decompositions. It has recently been proposed by Magee and Hamill (18) as possibly accounting for the reactions of low-energy hot atoms of photochemical origin. It seems unlikely that such a theory could be a valid representation of the reactions of atoms having more than about 2 ev of energy. Because of this excess kinetic energy, passage along the reaction co-ordinate is so rapid that there is insufficient time for internal equilibration of energy in the collision complex. The fate of this complex thus cannot be predicted by calculating the relative probabilities of decomposition, through various channels, of an equivalent internally equilibrated complex. Instead, the manner in which the collision complex disintegrates is determined by the particular manner in which it was put together.[7]

We thus postulate that the initial hot displacement reaction occurs by a fast ($\sim 10^{-14}$ sec) localized "direct" displacement. The course of this process is governed primarily by the direction and point of impact. These stereochemical considerations are of a different nature than that encountered in the "steric factor" of thermal reactions. In the thermal case it was simply a matter that with the minimal energy available only a certain approach could lead to reaction. With hot hydrogen, reaction appears likely for many types of approaches. What is governed by the stereochemistry is not so much whether reaction will take place but what kind of reaction will take place. An example is provided by the situation with alkanes, where approach co-axial to a C—H bond leads to abstraction, whereas approach at a larger angle results in displacement.

ACKNOWLEDGMENTS

REFERENCES

1. M. R. Berlie and D. J. Le Roy. Can. J. Chem. **32**, 650 (1954).
2. R. Klein, J. R. McNesby, M. D. Scheer, and L. J. Schoen. J. Chem. Phys. **30**, 58 (1959).
3. R. J. Carter, W. H. Hamill, and R. R. Williams. J. Am. Chem. Soc. **77**, 6457 (1955).
4. M. Amr El-Sayed, P. J. Estrup, and R. Wolfgang. J. Phys. Chem. **62**, 1356 (1958).
5. R. Wolfgang and F. S. Rowland. Anal. Chem. **30**, 903 (1958).
6. R. Wolfgang and C. F. MacKay. Nucleonics, **16**, 69 (1958).
7. P. J. Estrup and R. Wolfgang. J. Am. Chem. Soc. **82**, 2661, 2665 (1960).
8. W. F. Libby. J. Am. Chem. Soc. **69**, 2523 (1947).

[7]*However, hot* addition *reactions of hydrogen to double bonds yield excited radicals of relatively long life. The subsequent decomposition of these radicals can presumably be treated by absolute rate theory of unimolecular reactions.*

9. J. CROSS and R. WOLFGANG. Unpublished work.
10. D. URCH and R. WOLFGANG. J. Am. Chem. Soc. **81**, 2025 (1959).
11. J. K. LEE, B. MUSGRAVE, and F. S. ROWLAND. *From* preprint of article submitted to J. Am. Chem. Soc.
12. M. C. SAUER, JR. and J. E. WILLARD. J. Phys. Chem. **64**, 359 (1960).
13. D. URCH and R. WOLFGANG. Unpublished work.
14. W. F. HOFF, JR. and F. S. ROWLAND. J. Am. Chem. Soc. **79**, 4867 (1957).
15. A. M. ELATRASH, R. H. JOHNSEN, and R. WOLFGANG. J. Phys. Chem. **64**, 785 (1960).
16. F. S. ROWLAND and R. WOLFGANG. Nucleonics, **14**, 58 (1956).
17. J. K. LEE, B. MUSGRAVE, and F. S. ROWLAND. J. Am. Chem. Soc. **81**, 3803 (1959).
18. J. L. MAGEE and W. H. HAMILL. J. Chem. Phys. **31**, 1380 (1959).
19. F. S. ROWLAND, C. N. TURTON, and R. WOLFGANG. J. Am. Chem. Soc. **78**, 2354 (1956).
20. H. KELLER and F. S. ROWLAND. J. Phys. Chem. **62**, 1373 (1958).
21. J. G. KAY, R. P. MALSAN, and F. S. ROWLAND. J. Am. Chem. Soc. **81**, 5050 (1959).
22. E. GORIN, W. KAUZMANN, J. WALTER, and H. EYRING. J. Chem. Phys. **7**, 633 (1939).
23. W. G. BROWN and J. L. GARNETT. Int. J. Appl. Rad. and Isotopes, **5**, 114 (1959).
24. R. ODUM and R. WOLFGANG. Unpublished results.
25. R. M. WHITE and F. S. ROWLAND. Unpublished results.
26. L. S. KASSEL. J. Phys. Chem. **32**, 225 (1928).

THE REACTIONS OF HYDROGEN ATOMS WITH SOME
ORGANIC LIQUIDS[1]

R. B. Ingalls and J. R. Hardy

ABSTRACT

Measurements have been made of isotopic exchange and deuterium pressure change during deuterium atom bombardment of o-terphenyl, toluene, and eicosane just above their melting points. The number of molecules of HD formed was larger than the number of molecules lost or gained by the gas phase. A mechanism of reaction of deuterium atoms with aromatic liquids is proposed.

INTRODUCTION

During studies of the radiation chemistry of some aromatic liquids (1), a need for a better understanding of the reactions of hydrogen atoms with aromatic molecules became apparent. There have been a number of studies of the action of hydrogen or deuterium atoms with aromatic or double-bond systems in the gas and solid phases reported (2), but reactions of hydrogen atoms in organic liquids have been largely neglected. Experimental difficulties encountered in such studies may be in part responsible for this state of affairs.

Hydrogen atoms are important intermediates in the radiation-induced formation of both high molecular weight products and hydrogen gas in aromatic and vinyl hydrocarbon systems (3). Therefore, a knowledge of their reactions is necessary for an understanding of the radiation chemistry of these materials. A knowledge of hydrogen atom reactions would also contribute indirectly to our knowledge of energy transfer and other important processes in radiation chemistry by allowing the separation of these reactions from other effects (4).

The work reported here is part of an effort to gain better understanding of the reactions of hydrogen atoms with aromatic materials by direct experimentation. Purified deuterium gas was dissociated into atoms on a hot tungsten filament. The gas, containing a small fraction of atoms, was cooled by indirect momentum transfer with thermostatted walls of the reaction vessel before impinging on the surface of the liquid under investigation. The gas consumed or formed during the reaction was measured, and the formation of HD was determined by mass spectroscopy.

EXPERIMENTAL

Deuterium gas, obtained from Stuart Oxygen Company, was further purified by storage as uranium deuteride. Its isotopic purity was determined by mass spectroscopy to be 99.5%.

Reagent grade toluene, obtained from Mallinckrodt, was distilled through a $2\frac{1}{4}$-ft glass-helix packed column and dried over calcium hydride. No impurities were detectable by gas–liquid partition chromatography.

Eastman Kodak white label eicosane and o-terphenyl were used without further purification. High-temperature gas–liquid partition chromatography indicated no impurities in the o-terphenyl and 2.4% of lower boiling impurities in the eicosane.

An appropriate quantity of deuterium gas was measured into the system and pumped into a 2-liter measuring volume and micromanometer head. The 2-liter volume and the micromanometer head were maintained constant within 0.2° C at about 36° C. After a period of about 15 minutes was allowed for temperature equilibration, the micromanometer head was isolated and the main portion of the gas was pumped into a 5-liter storage bulb. During the run, the deuterium gas was circulated from this bulb through the reaction cell (see drawing of reaction cell, Fig. 1). The storage bulb was designed so that mixing of the gas occurred during circulation.
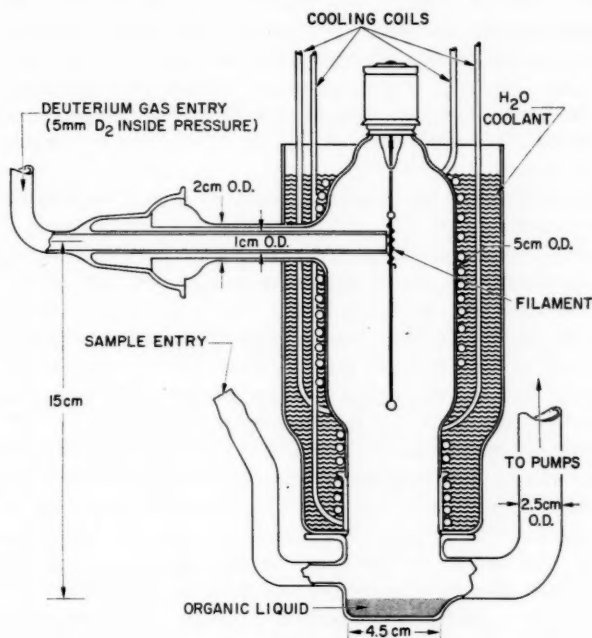

FIG. 1.   Reaction cell.

It is important to understand that the pressure in the reaction cell during the run was about 5 mm of Hg* and that at this pressure, the mean free path of deuterium is nearly three orders of magnitude smaller than the dimensions of the reaction cell. Therefore, many of the deuterium atoms are prevented from getting to the wall to recombine while traveling the 15 centimeters from the filament to the surface of the liquid reactant. Indirect thermal contact with the thermostatted walls of the reaction cell does cool the gas, however, to within a degree or so of the temperature of the wall.

In order to prevent back diffusion of the organic vapors to the filament, a degassed sample was introduced into the reaction cell while the deuterium gas was being circulated. The reaction cell was brought to a constant temperature somewhat above the melting

*In order to pump deuterium rapidly at 5 mm, two mercury diffusion pumps were used in series. One was an 80-liter per second, three-stage pump and the other was a single-stage pump designed to pump into pressures up to 20 mm of Hg. The gas was pumped through the reaction cell at about 2 liters per minute when the inlet pressure to the big pump was maintained at about 0.2 mm of Hg by a controlled leak. Three traps were maintained at liquid nitrogen temperatures throughout the experiments.

point of the sample which was stirred magnetically to increase the heat transfer with the bath. The filament was then brought up to temperature for an appropriate length of time. The gas was then pumped into the 2-liter bulb, permitted to come to temperature, and allowed to equilibrate with only one side of the micromanometer head. In this way, the pressure change which occurred during the reaction could be measured directly with the micromanometer to a precision greater than one part in a thousand. A sample of the gas was analyzed by mass spectroscopy for isotopic composition.

RESULTS

The experimental results are given in Table I. The values reported in the column headed % pressure per minute are equal to $(\Delta P \times 100)/(P \times T)$, where ΔP is the observed pressure change during the run, P is the pressure in the 2-liter measuring volume, and T is the length of the run in minutes. The corrected* increase in percentage of HD in the D_2 during the run divided by the time of the run in minutes is reported in the column headed % HD per minute.

A change in the geometry of the apparatus occurred between o-terphenyl runs 5 and 6. This did not significantly affect the ratio of HD formation to pressure change, although the rates of conversion dropped by approximately a factor of 4. Total conversion of the deuterium gas was about 10% in the runs with o-terphenyl and toluene, but was considerably less in the runs with eicosane. Blank runs with helium and o-terphenyl prove that cracking of the organic on the filament does not contribute to the results. This is not surprising in view of the low vapor pressure (less than 10 microns) of the materials at their melting point.† For the same reason, a gas phase reaction of organic vapors and deuterium atoms does not contribute significantly to the results.

The organic materials were examined by gas chromatography after reaction. A comparison of the sensitivity of the starting o-terphenyl and a 4.8-g sample from which 2.2×10^{-4} moles of HD had been produced indicated that exchange of deuterium for hydrogen had occurred in the o-terphenyl during the reaction. Using internal standards for comparison (5), the area under the curve for the starting material was $0.5\% \pm .05\%$ less than the area under the curve of the reacted material. This can be explained in terms of an increase in heat capacity and resulting increase in thermal conductivity of the o-terphenyl upon substitution of deuterium for some of the hydrogen (6).

No internal standard was used in the examination of the eicosane since impurities of the order of 2.4% were found in the unreacted material. The area under the curve for the impurity peaks was significantly reduced relative to the eicosane peaks in the reacted material. This effect may be due in part to substitution of deuterium and in part due to the selective reaction of the impurities.

Gas chromatographic examination of the reacted toluene revealed low yields of higher-boiling products. Bibenzyl was the major product, but its yield corresponded to only 1 mole per 10^4 moles HD formed. This indicates that abstraction of hydrogen from toluene is not important at these low temperatures ($-80°$ C).

The values reported for the runs made with eicosane and toluene are preliminary and are intended only to support in a general way the results obtained with o-terphenyl. The eicosane results are open to question on two counts:

1. The conversions were low, decreasing our accuracy.

*A small correction for exchange on the walls was made based on results from blank runs.
†This type of experiment is limited in applicability to materials of extremely low vapor pressures at the temperature of the reaction.
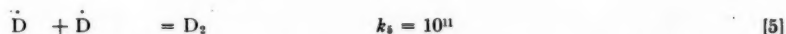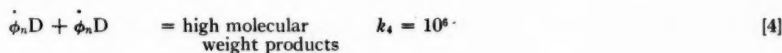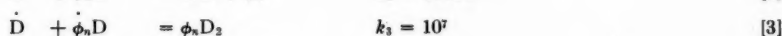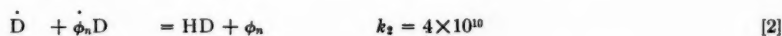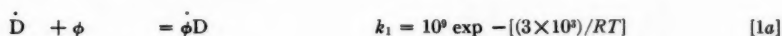
2. The 2.4% impurities in the eicosane may have been consumed disproportionately during the reaction.

The toluene runs were made at an earlier date and are more difficult experimentally so that the accuracy is probably not as high as in the runs with o-terphenyl.

A more detailed study of these materials as well as several other classes of organic compounds is being planned.

DISCUSSION

The reaction of thermal deuterium atoms with liquid o-terphenyl at 60° to 75° C produces more molecules of HD than there are molecules lost from the gas phase. Similar results were obtained with toluene at −88° to −79° C (see Table I). We propose the following mechanism for these systems:

$$\dot{D} + \phi = \dot{\phi}D \qquad k_1 = 10^9 \exp -[(3 \times 10^3)/RT] \qquad [1a]$$

$$\dot{\phi}D + (n-1)\phi = \dot{\phi}_nD \qquad [1b]$$
$$n = 1, 2, 3, \ldots$$

$$\dot{D} + \dot{\phi}_nD = HD + \phi_n \qquad k_2 = 4 \times 10^{10} \qquad [2]$$

$$\dot{D} + \dot{\phi}_nD = \phi_nD_2 \qquad k_3 = 10^7 \qquad [3]$$

$$\dot{\phi}_nD + \dot{\phi}_nD = \text{high molecular} \qquad k_4 = 10^6 \qquad [4]$$
$$\qquad\qquad\qquad\qquad \text{weight products}$$

$$\dot{D} + \dot{D} = D_2 \qquad k_5 = 10^{11} \qquad [5]$$

In this set of equations, ϕ represents a molecule of the substrate, $\dot{\phi}D$ and $\dot{\phi}_nD$ represent free radicals containing the structure

and respectively.
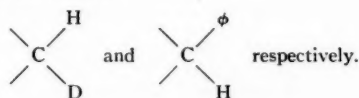
The formation of D_2 by a reaction analogous to reaction [2] does occur, but it is slower than the production of HD for two reasons:

1. an isotope effect is expected for the reaction with $\dot{\phi}D$, which will favor the formation of HD (7); and
2. in reactions with $\dot{\phi}_nD$, $n = 2, 3, \ldots$, the deuterium is not likely to be in an activated position.

The production of D_2 by a reaction analogous to reaction [2] is not equivalent to reaction [5] since its rate depends on $(\dot{D})(\dot{\phi}_nD)$ instead of $(\dot{D})^2$. However, we chose to neglect it in this treatment since its effects are small.

The values of the specific reaction rate constants chosen for reactions [4] and [5] are in agreement with the theory of bimolecular combination of two radicals (8). However, the rate constants for reactions [1a], [1b], [2], and [3] require some comment. Reaction [1b] is not specified since its value is not needed for the calculations we have made. It has been assumed that the rate constants for the reactions of $\dot{\phi}_nD$ are independent of n in order to simplify the treatment. The activation energy for reaction [1a] was chosen to be consistent with the values observed for the addition of hydrogen to double bonds (2), assuming reaction [3], which is a radical combination reaction, to have zero activation

energy. k_3 and the pre-exponential term in k_1 were chosen slightly lower than would be predicted theoretically in order to keep the value of k_2 (which as calculated depends on k_3 and k_1) well below the rate of collision between two particles.

TABLE I

Filament temperature, °K	Temperature of liquid reactant, °C	% Pressure per minute	% HD per minute	$\dfrac{\% \text{ HD}}{\% \text{ Pressure}}$
(A) Terphenyl				
1705	59.5	−0.27	0.38	−1.78
*1744	62.0	−0.22	0.66	−3.00
1800	75.0	−0.23	0.78	−3.36
*1755	75.0	−0.25	0.74	−2.56
1805	75.0	−0.29	0.63	−2.24
1855	59.0	−0.07	0.35	−4.32
1890	60.0	−0.04	0.29	−7.15
*1895	60.0	−0.04	0.15	−3.45
				Average 3.48±1.12
(B) Eicosane				
1733	37.5	+0.03	0.05	+1.67
*1827	37.0	+0.03	0.10	+3.33
*1816	37.0	+0.04	0.09	+2.25
				Average 2.42±0.61
(C) Toluene				
2095	−79	−.04	.45	−11.8
*2137	−79	−.086	.14	− 1.57
2060	−79	−.05	.18	− 3.21
*2067	−79	−.02	.07	− 3.61
2070	−88	−.03	.32	−11.4
*2087	−88	−.07	.15	− 2.09
				Average 5.61±3.99

*These rows refer to runs made using the same sample of organic liquid as used in the preceding run without purification.

The value of k_2 can be calculated from the experimental data in the following manner: HD is produced about three times as fast as molecules are lost from the gas phase in the experiments with o-terphenyl (see Table I). Therefore one can write the following relationship:

$$[6] \qquad k_2(\dot{D})(\phi_n D) = 2 \times 3\,[(k_1(\overset{..}{D})(\phi) + k_3(\dot{D})(\phi_n D) - k_2(\dot{D})(\phi_n D)].$$

Solving for k_2, we obtain

$$[7] \qquad k_2 = \frac{k_1(\phi) + k_3(\dot{\phi}_n D)}{7/6(\phi_n D)}.$$

This expression for k_2 may then be substituted in the following steady-state equations:

$$[8] \qquad \frac{d(\dot{D})}{dt} = I - k_1(\dot{D})(\phi) - (k_2 + k_3)(\dot{D})(\phi_n D) - k_5(\dot{D})^2 = 0$$

and

$$[9] \qquad \frac{d(\dot{\phi}_n D)}{dt} = k_1(\dot{D})(\phi) - (k_2 + k_3)(\dot{D})(\phi_n D) - k_4(\phi_n D)^2 = 0,$$

where I = rate of initiation of deuterium atoms in the liquid, to obtain the following set of equations:

[10] $$I = (\dot{D})\,[(13/7k_1\,(\phi)+13/7k_3\,(\dot{\phi}_nD)+k_5\,(\dot{D})],$$

[11] $$k_4\,(\dot{\phi}_nD)^2+13/7k_3\,(\dot{D})\,(\dot{\phi}_nD)-1/7k_1\,(\phi)\,(\dot{D}) = 0.$$

A numerical value of I which is necessary for the solution of equations [10] and [11] may be obtained by the following series of approximations.

The half life of the deuterium atoms is less than 10^{-7} seconds* in the reaction with o-terphenyl. Therefore the steady-state concentration of deuterium atoms is a strong function of the distance from the surface where the atoms are introduced into the liquid. An exact mathematical description of this reaction including the spatial distribution of radical concentrations is not available at this writing. We will therefore assume the reaction to be homogeneous in a small volume near the surface of the liquid.

The reaction volume, V, has been estimated to be about 10^{-4} cc.† The rate of initiation of deuterium atoms, I, is taken to be the number of moles of deuterium atoms that react per second divided by the reaction volume V. Therefore,

$$I = (10^{-7}\text{ mole sec}^{-1})/10^{-4}\text{ cc} = 10^{-3}\text{ mole sec}^{-1}\text{ cc}^{-1} = 1\text{ mole sec}^{-1}\text{ liter}^{-1}.$$

Using this value of I, equations [10] and [11] can be solved simultaneously by numerical methods yielding the values of 1.4×10^{-7} moles liter^{-1} and 8.8×10^{-4} moles liter^{-1} for the steady-state concentrations of deuterium atoms and $(\dot{\phi}_nD)$ radicals. $k_2 = 3.9\times10^{10}$ mole liter^{-1} sec^{-1} can now be obtained from equation [7]. This value of k_2 corresponds to a steric factor of about 0.1 if the reaction is considered to have a zero activation energy. There is some question as to whether this value is reasonable since there have been no values reported in the literature for analogous reactions. Even the steric factors for abstraction reactions from saturated hydrocarbons are not known unequivocally since various results have been reported (10).

Using this mechanism, results, qualitatively similar to those observed with o-terphenyl, are expected for toluene, if it is assumed that abstraction from the methyl group is not important at $-80°$ C. This assumption can be justified as follows: It has been shown by several workers that, in a series of related elementary reactions, the energy of activation,

*Most of the deuterium atoms that enter the liquid react by reaction [1a] at the initiation rates used in the experiment. (This can easily be ascertained, assuming the proposed mechanism to be correct, by multiplying together the rate constants and appropriate steady-state concentrations to obtain actual reaction rates.) Therefore, the half life of the deuterium atoms in o-terphenyl is determined mainly by reaction [1a]. $k_1(\phi)$ is a pseudo first-order rate constant with a value of 4×10^7. Thus, the half life of a deuterium atom in o-terphenyl is approximately $\ln 2/k_1(\phi) \sim 10^{-7}$ sec.

†A value for the volume V in which the reaction is considered to proceed is equal to the product of the surface area of the liquid (5 cm²) and the distance, Δx, the atoms diffuse in a time equal to their half life in the substrate (about 10^{-7} sec). To find Δx, we substitute approximate values for each of the terms in Ficks first law of diffusion

$$D\frac{d(\dot{D})}{dx} = F.$$

The numerical value of D, the Ficks law diffusion coefficient for the diffusion of deuterium atoms in liquid o-terphenyl, was found to have the approximate value of $D = 2\times10^{-3}$ by the absolute reaction rate theory (9). An approximation for the gradient of the deuterium atom concentration $d(\dot{D})/dx$ is the steady-state concentration of deuterium atoms in the reaction volume divided by Δx. An approximation of the steady-state concentration is the flux of deuterium atoms into the reaction volume (10^{-7} moles/sec) times the half life of the deuterium atoms (10^{-7} sec) divided by the reaction volume (5 cm² Δx). The flux F diffusing into the reaction volume from the surface is 10^{-7} moles/5 cm² sec.

Substituting these values into the diffusion equation, we obtain

$$2\times10^{-3}\frac{(10^{-7}\times10^{-7}-0)/5\Delta x}{\Delta x} = 10^{-7}/5.$$

Thus $\Delta x = 1.4\times10^{-5}$ and the reaction volume $V = 7\times10^{-5}$ cc $\sim 10^{-4}$ cc.

E, of the reaction can be related empirically to the heat of reaction in a simple manner (11). For abstraction reactions, there is some evidence (12) for the relationship

$$E = 11.5 - 0.25Q$$

where Q is the exothermic heat of reaction in kilocalories per mole.

Taking the value 77.5 kcal for the heat of dissociation of the C—H bonds of the methyl group of toluene, the heat of reaction Q for

$$C_6H_5CH_3 + H = C_6H_5CH_2 + H_2 \qquad + Q_1 \qquad\qquad [12]$$

is $Q_1 = 24.9$ kcal.* Thus, the activation energy for the abstraction of hydrogen from the methyl group of toluene is about 5.3 kcal, which is about 2.3 kcal higher than the activation energy required for reaction [1a] (see pp. 7 and 8). Therefore at $-80°$ C reaction [1a] should be almost 400 times as fast as abstraction from the methyl group if the pre-exponential terms are equal. Low yields of bibenzyl (see p. 6) also indicate that abstraction from the methyl group is unimportant. The assumption that abstraction from the methyl group of toluene does not compete effectively with reaction [1a] therefore seems reasonable.

In calculating the products to be expected from the reaction with toluene, the only parameter which is not already specified is the initiation rate. The value of I for the work with toluene is probably quite similar to that for the experiments with o-terphenyl since $\ln 2/k_1$ (ϕ) and the net rate of deuterium conversion is similar. Thus, the initiation rate is probably similar and the ratio of the products is expected to be only slightly different due to the difference in k_1 at the lower temperature. Experimental results for toluene reported in Table I are similar to those of o-terphenyl within experimental error.

In the reaction with eicosane the ratio of the percentage of HD produced to the percentage of pressure increase is not very different from 2, the value to be expected if abstraction of hydrogen from the substrate were the only reaction involving deuterium atoms. This is not surprising since the abstraction of hydrogen by a deuterium atom from a saturated hydrocarbon proceeds with an activation energy of about 9 kcal (13), so that the lifetime of a deuterium atom in eicosane at $37°$ C should be about 10^{-4} seconds. Thus the reaction volume is some three orders of magnitude larger than in the case of o-terphenyl, and the initiation rate is therefore correspondingly lower. It can be shown that smaller amounts of products formed by the reaction of deuterium atoms with other radicals are to be expected at these lower initiation rates (14). Thus, the results obtained with eicosane are consistent with the concepts upon which the proposed mechanism is based.

The proposed mechanism has the additional advantage that it is in general accord with a number of seemingly unrelated results reported in the literature.

1. Very low values of the pre-exponential terms in the rate constants for addition reactions of atoms (and radicals) to double bonds have often been reported (12). These values correspond to steric factors of 10^{-3} to 10^{-5}.
This addition reaction

$$2\dot{D} + \phi = \phi D_2$$
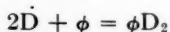
is probably a two-step process composed of reactions [1a] and [3]. Since the second step is in strong competition with equations [2] and [4], the steric factor for the over-all hydrogenation reaction would be expected to be low. Thus, the low steric factors previously reported can be accounted for.

*If 89.9 kcal/mole is taken to be the value for the heat of dissociation of the methyl C—H bonds, Q_1 is 13.5 kcal.

2. Deuterium-hydrogen exchange during the hydrogenation of olefins by atomic hydrogen at $-195°$ C has been recently reported (15), indicating that HD can be formed by a low activation energy process. Since reaction [2] is strongly exothermic, it is likely to have a low activation energy.

3. In the radiation chemistry of benzene, it has been found that the formation of hydrogen gas increases more rapidly than does polymer formation with increasing L.E.T. (16). This increased hydrogen formation relative to polymer formation with increasing L.E.T. corresponds to an increase of products formed by reaction [2] relative to products formed by reactions [1b] and [4] as the initiation rate is increased. Thus, these results may be accounted for by the mechanism proposed in this paper.

4. During radiolysis experiments at low hydrogen atom initiation rates, exchange with perdeutero aromatic additives occurs to a very limited extent (17).

This mechanism predicts a value of the steady-state concentration of $\phi_n D$ which is subject to experimental verification. An attempt to test the mechanism by studying the steady-state concentration of the $\phi_n D$ radicals in this system by electron spin resonance spectroscopy will be made.

ACKNOWLEDGMENTS

REFERENCES

1. R. B. INGALLS.   Hydrogen formation in the radiolysis of liquid toluene. To be published.
   J. G. BURR and J. M. SCARBOROUGH. J. Phys. Chem. In press.
2. B. DE B. DARWENT and R. ROBERTS.   Discussions Faraday Soc. **14**, 55 (1953).
   H. W. MELVILLE and J. C. ROBB.   Proc. Roy. Soc. A, **202**, 181 (1950).
   P. E. ALLEN, H. W. MELVILLE, and J. C. ROBB.   Proc. Roy. Soc. A, **218**, 311 (1953).
   R. KLEIN and M. D. SCHEER.   J. Phys. Chem. **62**, 1011 (1958).
3. E. COLLINSON and A. J. SWALLOW.   Chem. Revs. **56**, 471 (1956).
4. M. BURTON and W. N. PATRICK.   J. Phys. Chem. **58**, 421 (1954).
   W. N. PATRICK and M. BURTON.   J. Phys. Chem. **58**, 424 (1954).
5. R. A. BAXTER and R. T. KEEN.   Anal. Chem. **31** (1959).
   R. T. KEEN, R. A. BAXTER, M. A. ROTHERAM, J. L. MILLER, and R. C. SHEPARD. Naa-SR-4356.
       Methods of analysis of polyphenyl reactor coolants.
6. R. B. INGALLS, R. H. SHUDDE, and R. SHEPARD.   Analysis of isotopic composition of organic materials
       by thermal conductivity using gas chromatography. To be published.
7. K. B. WIBURG.   Chem. Revs. **55**, 713 (1955).
8. A. F. TROTMAN-DICKENSON.   Free radicals: an introduction. Methuen & Co., Ltd., London. 1959.
       p. 35.
9. A. GLASSTONE, K. J. LAIDLER, and H. EYRING.   The theory of rate processes. McGraw-Hill Book Co.,
       Inc., New York. 1941.
10. M. R. BERLIE and D. J. LE ROY.   J. Chem. Phys. **20**, 200 (1952).
    D. J. LE ROY.   Discussions Faraday Soc. **14**, 120 (1953).
    B. DE B. DARWENT and R. ROBERTS.   Discussions Faraday Soc. **14**, 55 (1953).
11. M. G. EVANS and M. POLANYI.   Trans. Faraday Soc. **32**, 1933 (1936); **34**, 11 (1938).
    E. T. BUTLER and M. POLANYI.   Trans. Faraday Soc. **39**, 19 (1943).
    H. STEINER and A. R. WATSON.   Discussions Faraday Soc. **2**, 88 (1947).
    N. N. TIKHOMIROVA and V. V. VOEVODSKII.   Doklady Akad. Nauk S.S.S.R. **79**, 993 (1951). English
       translation, Natl. Research Council Can. TT-260 (1951).
12. A. N. N. SEMINOV.   Some problems of chemical kinetics and reactivity. Pergamon Press, London. 1958.
13. B. DE B. DARWENT and R. ROBERTS.   Discussions Faraday Soc. **14**, 55 (1953).
14. R. B. INGALLS and R. H. SHUDDE.   Hydrogen atom reactions in organic radiation chemistry. To be
       published.
15. F. G. PONOMAREV and V. L. TALROSE.   Doklady Akad. Nauk S.S.S.R. **130**, 1 (120–121) (1960).
16. W. G. BURNS.   The irradiation of polyphenyls with different types of radiation. Presented at Congress
       Scientifico, Seziane Nucleare, Rome (1959).
17. P. V. PHUNG and M. BURTON.   Radiation Research, **7**, 199 (1957).
    M. BURTON and W. N. PATRICK.   J. Phys. Chem. **58**, 421 (1954).
    W. N. PATRICK and M. BURTON.   J. Phys. Chem. **58**, 424 (1954).

AN IMPROVED TECHNIQUE FOR THE OBSERVATION OF INFRARED CHEMILUMINESCENCE: RESOLVED INFRARED EMISSION OF OH ARISING FROM THE SYSTEM H + O₂[1]

P. E. CHARTERS AND J. C. POLANYI

ABSTRACT

A multiple reflection apparatus for the observation of infrared chemiluminescence is described. By means of this apparatus infrared emission from the system $H + O_2$ has been identified as being due to vibrationally excited OH radicals in levels $v = 1, 2$, and 3 of the ground electronic state. The resolved infrared spectrum of the OH fundamental has been observed for the first time without interference from other emission. The most likely source of excited OH is the reaction $H + HO_2 \rightarrow OH\dagger + OH$. The vibrational 'temperature' of OH† (vibrationally excited OH in its ground electronic state) in our system is in the region of $T_V = 2240°$ K. These findings are discussed in relation to Krassovsky's suggestion that reaction between H and O_2 could account for the Meinel hydroxyl bands in the night sky.

INTRODUCTION

Infrared emission arising from the gaseous system $H + O_2$, at room temperature, has been reported by Cashion and Polanyi (1). The emission consisted principally of three broad unresolved bands extending from 3400 to 4000 cm⁻¹, with maxima at 3600, 3730, and 3830 cm⁻¹ (2.78, 2.68, and 2.61 μ). The intensity of the first peak could be varied, by varying reagent flows, independently of the other two, indicating that it was due to a separate emitting species. It was thought that this might be the hydroxyl radical, OH, with ν_0 for $v = 1 \rightarrow v = 0$ at 3570 cm⁻¹ (2). The other two maxima were of constant relative intensity and it was suggested that these might be either the Q and R branches of the ν_3 O—H stretching fundamental of water (ν_0 at 3755.8 (3)) or alternatively the O—H stretching fundamental of the HO₂ radical. In either case the P branch would presumably be masked by the other emission, attributed to the hydroxyl radical.

Prior to the work described above, McKinley, Garvin, and Boudart (4) had observed visible and photographic-infrared regions of the spectrum from OH formed in the reaction $H + O_3$. They failed, however, to observe any emission whatever from the system $H + O_2$. They concluded, in agreement with suggestions made by Bates and Nicolet (5), and by Herzberg (6), that the reaction $H + O_3$ was responsible for the Meinel hydroxyl bands in the airglow (7). This result later received further support from a careful re-examination of the visible and photographic-infrared emission (8) and recently an examination of the infrared emission (9).

Krassovsky (10), however, has put forward the view (criticized by Bates and Moisei-witsch (11)) that the evidence concerning the Meinel hydroxyl bands is more consistent with the formation of excited OH in a reaction $H + O_2$. He considered that this reaction, to be sufficiently exothermic, would have to involve vibrationally excited O₂. At first sight the results of Cashion and Polanyi (1) might appear to lend support to Krassovsky's view. The present investigation was undertaken in the hope of clarifying this point. In order to do this it was necessary in the first place to establish that the system $H + O_2$ does in fact give rise to vibrationally excited hydroxyl, and that the excited hydroxyl is present as a result of chemical reaction, not as a result of diffusion of reagents or products into the discharge or spreading of the discharge into the reaction zone. Once this has been

done a comparison of the distribution of excited OH among vibrational levels with that observed in the upper atmosphere might help to decide whether the reaction could account for the Meinel hydroxyl bands.

At the same time it was hoped that the identity of the 3730 and 3830 cm^{-1} emission, due it was thought to H_2O or HO_2, could be established.

The apparatus used in this investigation represents a major departure from that used by Cashion and Polanyi; it will therefore be described in some detail. The system $H + O_2$ was used for the first trial of this apparatus since the reagents are relatively non-corrosive. In work presently being undertaken in this laboratory the same apparatus is being used for a re-investigation of the infrared emission from $H + Cl_2$ at pressures several orders of magnitude less than those at which detectable emission was obtained in the experiments of Cashion and Polanyi (12).

<div align="center">EXPERIMENTAL</div>

Reaction Cell

A diagram of the reaction cell is given in Fig. 1. Partially dissociated hydrogen entered the cell from four Wood discharge tubes through 6 mm I.D. nozzles that protruded into
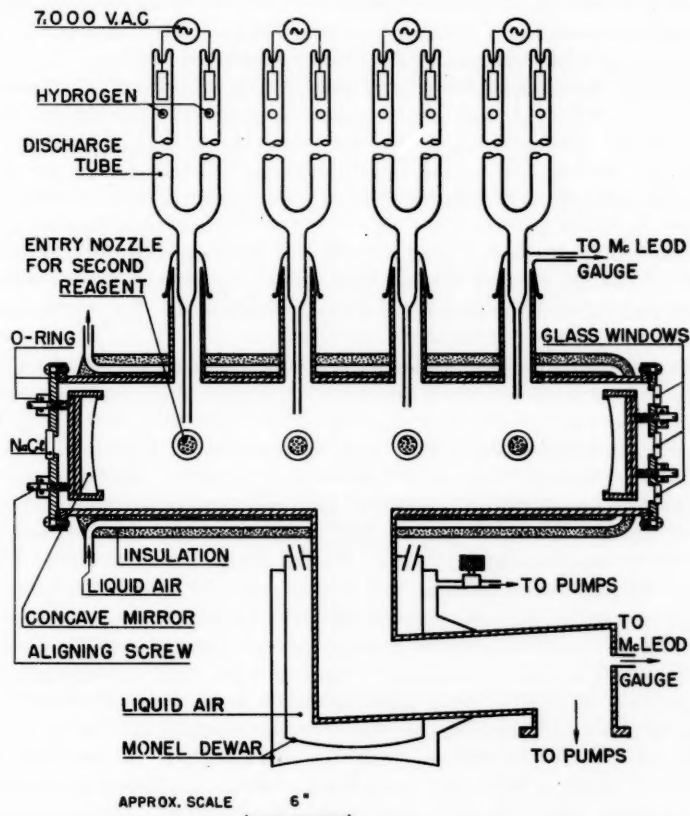

FIG. 1. Cross section of the reaction cell.

the cell to a point just above the cone of radiation visible to the spectrometer. Before use the discharge tubes (made from pyrex) were washed with dilute hydrofluoric acid and coated with an approximately 60% solution of phosphoric acid. The other reactant (in this case oxygen) diffused into the cell through sintered glass plugs placed in four side arms. These side arms ended flush with the walls of the reaction cell, since the cone of light with multiple reflection extended laterally across the entire diameter of the mirrors (see below). In each of the eight side arms linking the glass part of the apparatus to the reaction vessel, the connection was made through a 40/50 standard-taper metal cone and glass socket.

The cell itself consisted of a monel tube $6\frac{1}{4}$ in. I.D. $\times 23\frac{1}{2}$ in. long. The ends were sealed by $8\frac{1}{2}$ in. diameter monel plates held against "O" rings. The emission was viewed by the spectrometer through a sodium chloride window in the center of the front plate, the plate nearest the spectrometer. A vertical row of three glass windows in the back plate facilitated the alignment of the mirrors, mounted internally at either end of the reaction cell.

The reaction products passed out of the cell through a centrally located 4 in. I.D. monel pipe welded to the cell. A fixed metal dewar surrounded this pipe almost to the point where it entered an N.R.C. O.B.-4 booster pump (4 in. I.D.; 240 l./sec at 10^{-2} mm, falling to 50 l./sec at 10^{-1} mm). An Edwards "Speedivac" ISC450B pump (450 l./min) provided the backing pressure, and was connected to the diffusion pump through a Veeco valve ($1\frac{1}{2}$ in. port opening) and a length of $1\frac{1}{2}$ in. I.D. flexible steel tubing.

Monel was used throughout the cell and exit pipe to reduce corrosion when studying reactions involving halogens, and also to permit coating with phosphoric acid without deterioration of the metal surface. In practice it was found that phosphoric acid slowly reacted with the surface, and in the experiments described in this paper the cell was coated first with a thin layer of polystyrene and then with phosphoric acid over this base layer.

By switching leads on the four high-voltage transformers the reaction cell could be made earth for the high-voltage alternating current. The discharge then struck directly down into the reaction cell, filling the cell with the pink atomic hydrogen glow that was normally restricted to the U of the discharge tube.

Provision was made for cooling the entire cell by blowing liquid air through copper coils which followed a path back and forth along the length of the cell. The coils were clamped against the cell and were insulated by $1\frac{1}{2}$ inches of glass wool.

The mirror system consisted of four concave mirrors, all four having very closely matched radii of curvature; the system was identical with that suggested by Welsh and co-workers (13, 14) for use in high-resolution Raman spectroscopy. The radius of curvature of the mirrors in our system was 50.094 cm, diameter 14 cm, and average thickness 1.5 cm. The mirrors were made for us by the Perkin–Elmer Company of Norwalk, Conn., U.S.A. The dimensions were chosen so that the 15° cone of radiation accepted by the $f/4$ optical system of our spectrometer very nearly filled the back mirrors (furthest from the spectrometer). Each "pair" of mirrors (one pair at either end of the cell) was made from a single mirror which had been cut along a vertical axis so that the two halves could be adjusted separately and light could pass through a 0.5–2.0 mm (adjustable) slit-like gap between them. Under operating conditions the source optics of the spectrometer had its focal plane at a point centrally placed in the gap between the front pair of mirrors, on a level with the silvered surface of these mirrors. If the mirrors had not been present, only emitters within the 15° cone of light centered on the focal plane, emitting in the direction defined by the cone, would have contributed to the observed emission. With the

mirrors present, a succession of such cones displaced laterally from one another fell within the line-of-sight of the spectrometer. This was the origin of the gain in intensity.

The mirror mounts, made entirely from monel, were based on a design due to Welsh and Shepherd (15). Each of the four mirrors, backed by springs, was held by clips to a plate. This plate was held by screws to a backing plate, the two plates being free to slide over each other for coarse horizontal and vertical alignment of the mirrors. The backing plate in turn was held down by springs on to three metal columns, two of adjustable height and a fixed one surmounted by a ball bearing. The adjustable columns extended into rods which passed through "O" rings and fine threads in the external end plates. By adjusting the two rods appropriate to any one of the four mirrors, that mirror could be aligned while the apparatus was under vacuum, and while chemiluminescent emission was being observed.

We wish to acknowledge here the skilled machining of Mr. Hans Hellenkamp, who constructed the reaction cell.

The efficiency of the multiple reflection system is markedly dependent on the reflectivity of the mirrors, approaching $1/1-r$ (r is the reflectivity) when the number of reflections is large. The mirrors in this apparatus were in contact with the reacting gases. To minimize deterioration they were first front-surface coated with silver (reflectivity 98.8% at $3\,\mu$ (16)) and then coated with ca. 1700 Å layer of cryolite or magnesium chloride. Coating was either carried out on an apparatus kindly made available by Professor H. L. Welsh and Professor J. C. Stryland of the Department of Physics, or was carried out professionally by Canadian Arsenals Ltd., Toronto.

Spectrometer

The spectrometer was a model 112G Perkin–Elmer double-pass grating instrument employing a Bausch and Lomb 300 groove/mm plane grating blazed at $3\,\mu$ in the first order. Several modifications were made in the instrument. A liquid-air-cooled lead sulphide detector was installed in the position provided by the makers for "external detectors". The housing for the cooled lead sulphide cell was identical with that described in a recent communication (17) .The detector itself has a sensitive surface 2.5 mm × 0.25 mm, sandwiched between two layers of sapphire. It was mounted *in vacuo* behind a sapphire window. The detector, made by Infrared Industries Inc., Waltham, Mass., U.S.A., had one half of peak sensitivity at $3.3\,\mu$ (ref. 17).

The source optics supplied by the makers was replaced by optics of slightly different design; the sequence of mirrors was reversed so that incoming radiation encountered first a spherical concave mirror (80 mm diameter, 294 mm radius) and then a plane mirror (55 mm square) placed close to the concave mirror. The source optics housing could then be reduced in size to 22 cm × 17 cm, eliminating the space between source optics and foreprism monochromater, normally occupied by an absorption cell. The source optics focus remote from the foreprism monochromater slit then fell at a point 14 cm from the front of the source optics housing, instead of being 2–3 cm from the housing as in the normal instrument. This alteration was necessary since the focal plane of the source optics must be brought to a point on a level with the front surface of the mirrors inside the reaction cell, 5.6 cm from the front (sodium chloride) window of the cell.

The gap between the front window of the cell and the front window of the source optics housing was bridged by a tube which was continuously flushed with dry air, as was the whole of the remainder of the path traversed by the radiation from the reaction cell through the spectrometer to the lead sulphide cell. This was of importance since

emission was to be observed in regions of the spectrum where water vapor absorbs strongly.

To permit calibration without interference with the closed optical path linking the spectrometer to the reaction cell, the source optics was provided with a sodium chloride window at one side. A diagonal mirror within the source optics housing, mounted on an externally actuated swivel, could be swung into the optical path so that either a mercury lamp (for wavelength calibration) or a globar (for sensitivity calibration) could be viewed by the spectrometer.

The spectrometer was mounted on a table with provision for hydraulic lifting, and also for lateral and to-and-fro movement of the table top by means of adjusting screws. This degree of adjustment was required since the reaction vessel was rigidly attached to a separate rack carrying the reagent flow system and pumps. To facilitate the alignment of the spectrometer to the reaction cell, and the alignment of the multiple reflection system within the reaction cell, a light bulb was mounted permanently inside the spectrometer on a solenoid arm so that it could be moved into a position behind the foreprism monochrometer slit by closing a switch. This made possible rapid checks of alignment during the course of an experiment; at the same time a check could be made for deterioration of the mirrors, by counting the number of images formed at the front mirrors by the multiple cones of light within the cell (13, 14).

In the 112G spectrometer the grating table can swing through an angle of no more than 12°; to cover one order of the grating it is therefore necessary to insert "pins" into the grating table and thus obtain a coarse change in the range of angles being scanned. Changing pins necessitates removal of the entire grating monochromater housing, exposing the optics to the atmosphere. To avoid this we duplicated the pin mechanism at the lower end of the grating table shaft, beneath the instrument. Pins could then be rapidly inserted and removed without interfering with the flow of dry air through the apparatus.

Reagents

The hydrogen and oxygen flows were metered by measuring the pressure drops across two calibrated capillaries. Absolute pressure could be measured on a McLeod gauge just ahead of the cell and on one just beyond it (see Fig. 1); both of these pressure points were linked by wide tubing to the cell. The two pressures differed only slightly, but the former was taken as the true value since this measuring point was linked directly to the reaction cell through tubing in which no flow took place.

In most experiments the hydrogen was Dominion Oxygen Co. Electrolytic grade, 99.8% minimum purity. This was passed through a Deoxo unit guaranteed to reduce oxygen concentration to less than one part per million. In some experiments water was frozen out in a liquid air trap. The oxygen in most experiments was Linde Air Products Co., U.S.P. grade. However, to check for possible effects of slight impurities a portion of spectrum was retraced replacing both reagents simultaneously with Matheson research grade reagents. This grade of hydrogen contains less than the following mol.% impurities; oxygen 0.001%, nitrogen 0.03%, carbon dioxide 0.005%, water 0.001%. The oxygen contains less than the following percentage impurities; carbon dioxide 0.1%, carbon monoxide 0.01%, argon 0.01%, nitrogen 0.05%, hydrogen 0.01%, water 0.0002%.

RESULTS AND DISCUSSION

Figures 2 and 3 are reproductions of actual traces of the emission obtained in the 2950–3800 cm^{-1} (3.39–2.63 μ) and the 6600–7150 cm^{-1} (1.52–1.40 μ) regions of the spectrum. Four different grating slit widths were used in making these traces, varying from 0.400 mm for the strongest emission (section A of the trace) to 2.000 mm for the
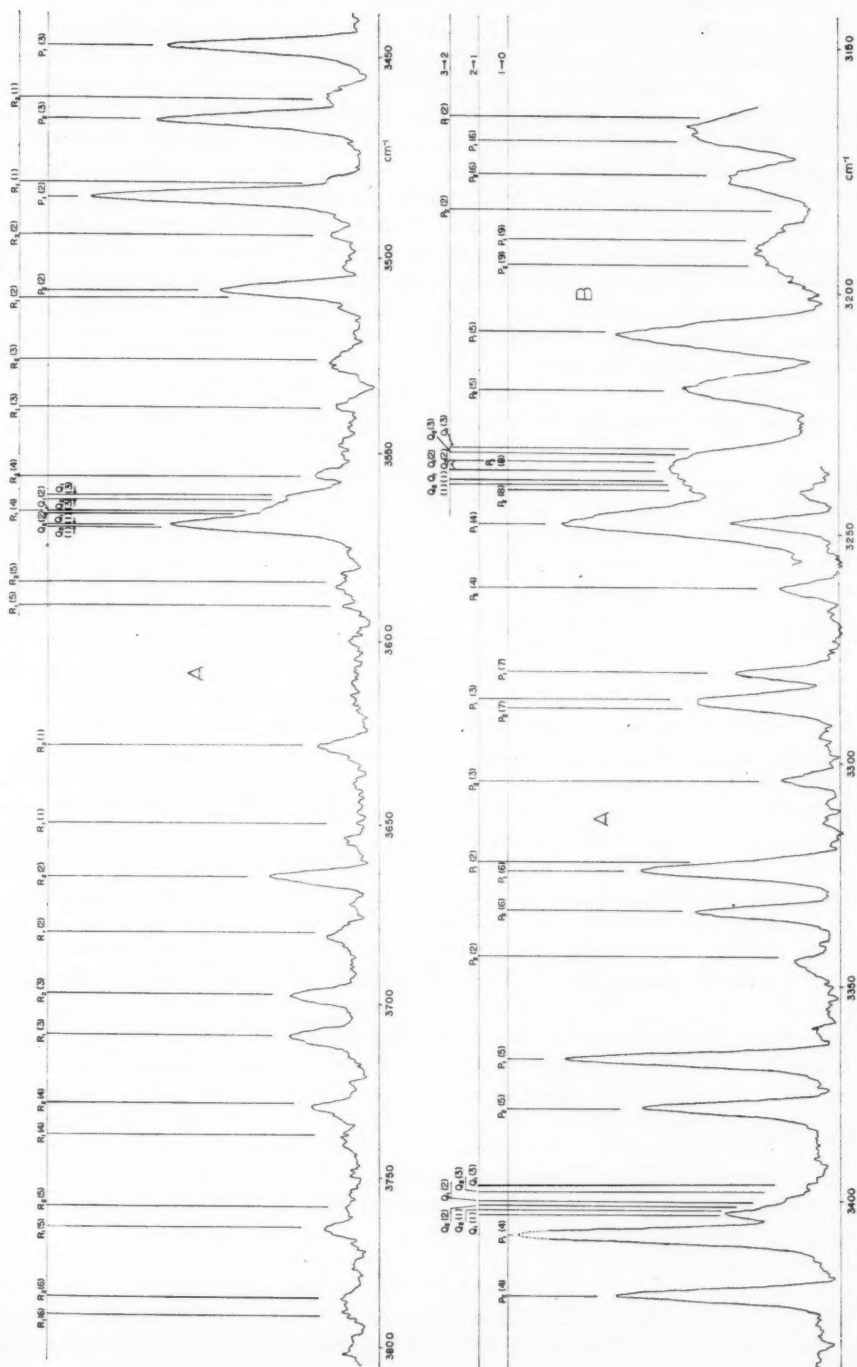
FIG. 2. The fundamental (Δv = 1) OH emission spectrum from the system H + O₂. A, slit width 0.400 mm. B, slit width 1.000 mm.
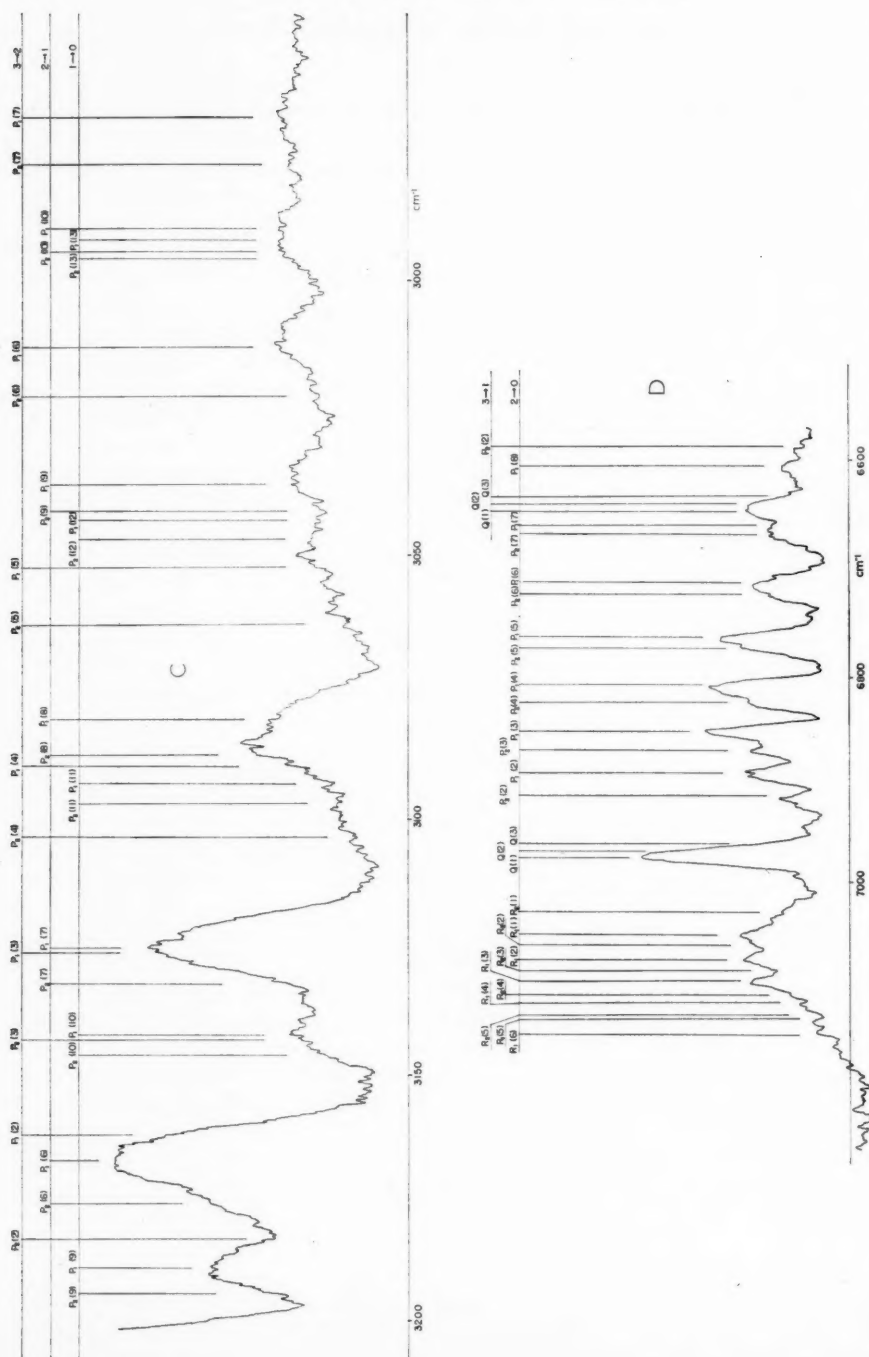
FIG. 3. The fundamental ($\Delta v = 1$) and first overtone ($\Delta v = 2$) OH emission spectrum from the system H + O$_2$. C, slit width 2.000 mm D (overtone), slit width 1.100 mm.

weakest (section C of the trace). These data are recorded beneath the figures. No other emission was observed, though attempts were made to detect emission in the 3700–4000 cm^{-1} region, where Cashion and Polanyi observed emission (due to water vapor or HO_2) and at 5333 cm^{-1} where these workers observed emission due to atomic hydrogen. The experimental conditions applicable to these traces were hydrogen flow 2500 μmoles/sec, oxygen flow 1200 μmoles/sec, pressure in the reaction vessel 4.0 mm Hg, pumping by mechanical pump only, transit time through cone-of-sight 0.15 second. Reagents were standard grade hydrogen and oxygen used without drying of either reagent. The reaction cell was at room temperature and the mirrors were freshly coated.

Standard grade reagents were used since in a separate experiment it was shown that use of Matheson research grade reagents made no difference to the emission. Passing both reagents through liquid air traps also had no effect on the emission. Deliberately saturating both hydrogen and oxygen streams with water vapor, so that the partial pressure of water vapor in the discharge tube and reaction vessel became ca. 0.13 mm Hg, caused a 30% drop in emission intensity (in the region from 3400–3500 cm^{-1} that was scanned) but otherwise had no effect.

The region of spectrum from 3400–3500 cm^{-1} was traced at five total pressures ranging from 4.0 mm to 0.51 mm, while the molar inflow ratio of reagents was kept constant. The intensity of the emission was found to vary approximately linearly with total pressure.

An attempt was made to estimate the H atom concentration by measuring the heat liberated by atoms recombining at a hot tungsten filament placed in the reaction cell. The method used (Tollefson and Le Roy (18)) was first to clean the wire by prolonged heating in a stream of hydrogen passing through the cell, and then, by means of an a-c. bridge, to measure the rise in temperature of the wire as atoms recombined on it. Next, in the absence of H atoms, an external current was passed through the wire, and the current required to heat the wire to the same temperature as before was accurately measured. Knowing the resistance of the wire, the power liberated by the passage of the current could be calculated; this was identical with the power liberated by the recombining atoms. Knowing the surface area of the wire and assuming recombination at every collision the pressure of H in the gas could be calculated. The pressure measured was only ca. 5.10^{-3} mm of H at 4.0 mm total H_2 pressure with two discharge tubes running. We would expect 1.10^{-2} mm with all four tubes running. This constitutes a lower limit, but if correct it would mean that our H atom pressure may be only in the region of one third to one tenth of that obtained by Cashion and Polanyi (12, 17).

The spectrometer was calibrated using the lines of a low-pressure mercury lamp. The calibration was made under different conditions of slit width and chart speed to the actual trace. As a result the observed spectrum was found to be shifted bodily by 3 cm^{-1} to higher frequencies than the published values for OH. Accepting the published value (see below) for one line in the fundamental region ($P_1(2)$ of $1 \rightarrow 0$) and one in the overtone region (P_1 (3) of $2 \rightarrow 0$) and applying a correction for this apparent small shift, the remaining ca. 35 sharpest peaks fell within ±0.5 cm^{-1} of the published values. The OH line frequencies were taken from an extensive compilation of OH frequencies made by Dr. H. P. Gush and Dr. E. H. Richardson on the University of Toronto digital computer. The calculation was based on spectroscopic constants obtained by Dieke and Crosswhite (19) and by Herman and Hornbeck (20). We are most grateful to Dr. Gush and Dr. Richardson for providing us with a copy of these tables.

The correspondence of the calculated frequencies with our observed lines leaves no doubt that we are observing emission due to three bands within the fundamental of OH

in its ground electronic state $(^2\Pi, v(1 \rightarrow 0), v(2 \rightarrow 1), v(3 \rightarrow 2))$ and two bands in the first overtone region $(^2\Pi, v(2 \rightarrow 0), v(3 \rightarrow 1))$. At the narrower slit widths used in this work the lines of each band are well resolved into spin (but not lambda) doublets. All the lines in the spectrum can be accounted for as OH lines.

A striking feature of the spectrum is the complete absence of emission due to water vapor. The only previous observation of the fundamental infrared spectrum of OH has been in emission from flames, particularly in the work of Plyler and co-workers (21, 22, 23). The hydroxyl emission is accompanied by a strong water emission that tends to overlap many OH lines, and makes observation of the R branch of $1 \rightarrow 0$ impossible. Since water will be present in most systems in which OH is being formed, including the reaction system $H + O_2$ which we have studied, any non-specific method of excitation (thermal excitation, or excitation by electrical discharge) will give rise at the same time to H_2O and OH emission. In our system we are bound to postulate a highly specific method of excitation; this, of course, is most likely to be a chemical reaction. The specific nature of chemical reaction may well make infrared emission from chemical systems a valuable spectroscopic source of "clean" infrared spectra (cf. 24).

In some experiments the discharge was made to strike down into the reaction cell. Emission due to vibrationally excited water vapor was then observed. The appearance of water vapor emission could be due to physical excitation of the water molecules in the discharge.

We are able positively to identify this discharged-induced emission as being due to excited water molecules. If the unidentified emission observed by Cashion and Polanyi was also due to water, the question arises as to why water emission was not observed in the present investigation, under normal operating conditions. The answer may possibly lie in the fact that our reaction cell and discharge in normal operation are separated by 15–20 cm of narrow (6 mm I.D.) tubing and 15 cm of 28 mm I.D. tubing, whereas in Cashion and Polanyi's apparatus the discharge was separated by only 0.5 cm of 28 mm I.D. tubing from the cell. Back diffusion of water vapor into the discharge could perhaps have given rise to the emission observed by the earlier workers. However, this is far from certain. Our system also differs from theirs in other notable respects; the pressure in the present work was 10 times as high (but attempts to observe H_2O emission at lower pressure failed), the transit time was 0.25–0.10 times as great in our experiments, and the H atom pressure may have been as little as 0.1 times Cashion and Polanyi's.

The proximity of the discharge to the reaction cell in the work of Cashion and Polanyi probably accounts for the fact that they observed emission due to atomic hydrogen. They believed that this emission arose from electronically excited atomic hydrogen in their reaction cell, and not to reflected light from the discharge. This is in accord with the finding that in our system, where the discharge is removed to a distance from the reaction cell, emission from atomic hydrogen is absent. Moreover in our system the atomic hydrogen emission can be made to appear if the discharge is struck down into the reaction cell.

In our experiments we found no trace of any emission, either under normal operating conditions or with the discharge striking into the reaction cell, that could have been ascribed to the hydroperoxy radical, HO_2.

For reasons outlined above we consider that the vibrationally excited OH in our system is present as a result of some chemical reaction. The reaction between atomic hydrogen and ozone is a well-established source of vibrationally excited hydroxyl. However, it can be excluded in our system on several counts. The reagents entering the reaction cell

certainly contained no ozone. It might be argued that after entering the reaction cell a very small amount of oxygen might have diffused up into the discharge and been converted to ozone. The argument would rest upon the fact that in a system such as ours traces of ozone might produce enough OH† (vibrationally excited hydroxyl in its ground electronic state) to account for the observed emission. But Herron and Schiff (25) have shown that the passage of pure oxygen at 2 mm pressure through a Wood discharge tube produces an amount of ozone which is below the limit of detection of a mass spectrometer. Furthermore, back diffusion into the discharge must be slight, and a very large gain in intensity would be expected if the discharge were brought down into the reaction cell. However, if there was an increase in the intensity of the OH† emission on striking the discharge down into the cell, it was a small increase (2 times or less, masked by water emission). Finally it should be noted that the vibrational "temperature" of OH† in our system (see below) is one-quarter that observed by Garvin, Broida, and Kostkowski in a recent examination of the H + O₃ emission in the infrared (their analysis was based on overtone transitions since they did not observe the OH fundamental bands) (9). Since their experiments were made in the same region of total pressures as ours, with considerable amounts of H₂, H₂O, and O₂ present in the system (ozone amounted to a few per cent), it seems most probable that the difference in vibrational temperature of the OH† in the two systems is due to a difference in the chemical processes by which it is produced.

The possibility exists that traces of NO₂ in the system might give rise to the observed weak emission since Cashion and Polanyi (26) found that this is a rapid reaction producing strong OH and H₂O emission. NO₂ would have to be formed in the discharge from air leaking into the apparatus. (An upper limit for the pressure of NO₂ that could conceivably be formed in this way is ~10⁻⁵ mm.) However, in this case the emission should persist even if the O₂ flow is cut off, whereas the emission disappeared when this was done.

It would appear that the emission arises in some way from reaction between atomic hydrogen and molecular oxygen.

Reference has already been made to Krassovsky's (10) suggestion that reaction between atomic hydrogen and vibrationally excited oxygen might lead to the formation of vibrationally excited hydroxyl,

$$H + O_2\dagger \rightarrow OH\dagger + O \qquad Q = -16.7 \text{ kcal/mole.} \qquad [1]$$
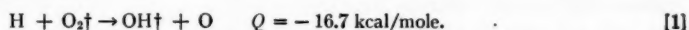
Q is the heat of reaction assuming reagent and product molecules to be in their ground vibrational levels ($D(O—O) = 118.0$ (27), $D(O—H) = 101.3$ kcal/mole (28)). To account for the formation of OH† in $v = 3$ ($E(v = 3) = 29.2$ kcal/mole) the oxygen molecule would have to have 45.9 kcal of vibrational energy. Recombination of atomic oxygen could lead to the formation of such highly vibrating molecules. (Fairly direct evidence for the formation of highly vibrating molecules as product of atomic association is to be found in reference 17.) Formation and recombination of O atoms should become far more important if the discharge strikes down into the reaction cell where O₂ is in plentiful supply. However, as already observed, no more than a small increase in intensity was obtained when this was tried.

It appears more probable that the primary reaction is

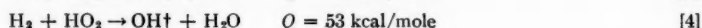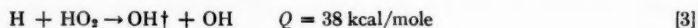$$H + O_2 + M \rightarrow HO_2 + M \qquad Q = 47 \text{ kcal/mole,} \qquad [2]$$
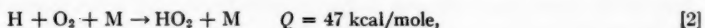
for which strong evidence has been found by a number of authors. The work of Foner and Hudson (29) comes closest to our experimental conditions. They brought together
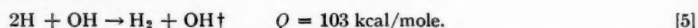
atomic H from a Wood discharge tube and oxygen at room temperature and examined the reaction mixture mass spectrometrically. At 30–40 mm pressure they obtained HO_2, OH, and H_2O as products, in the ratio 1.4:30:92. At 1 mm pressure (30) they detected no HO_2 but substantial amounts of OH and H_2O. It seems likely that HO_2 was also being formed in their low-pressure experiments, but was rapidly consumed. Foner and Hudson (30) have in fact suggested that at low pressure (∼1 mm) HO_2 is formed, not, however, in the gas phase but at the wall. The HO_2, they believe, will then react with H at the wall, forming OH if the wall is at room temperature, or H_2O_2 if the wall is at liquid air temperature. We have tried cooling our reaction cell to liquid air temperature but have failed to obtain reproducible results, perhaps due to changes in mirror alignment or reflectivity. Nonetheless on three occasions out of four we have observed stronger OH emission from the cold cell (temperature −185° C, measured on a thermocouple attached to the cell wall—the mirrors were probably only at −10° to −20° C). This increase in intensity is surprising in view of the fact that Foner and Hudson found that no OH is formed in a cold cell.

The volume-to-surface ratio in our cell is much greater than that in Foner and Hudson's small reaction tube. Taking our value for H (which is a minimum) we calculate that each HO_2 suffers at least 23 collisions with H for each wall collision. Burgess and Robb (31) have found the collision efficiency of this reaction at room temperature to be unity. If this is correct to within an order of magnitude, most HO_2 radicals in the room temperature system will react in the gas phase before reaching the wall. Foner and Hudson's suggestion that in the room temperature system OH is formed at the wall would require in the present case either that OH emits while adsorbed on the mirror surface (the only part of the "wall" in the line-of-sight) or that hydroxyl is desorbed at high vibrational temperature, i.e. as OH†. Neither of these processes seems likely, but neither can definitely be excluded.

Subsequent gas phase reactions, following the formation of HO_2, which could result in the production of vibrationally excited hydroxyl are

$$H + HO_2 \rightarrow OH\dagger + OH \qquad Q = 38 \text{ kcal/mole} \qquad [3]$$

$$H_2 + HO_2 \rightarrow OH\dagger + H_2O \qquad Q = 53 \text{ kcal/mole} \qquad [4]$$

with a very minor contribution from

$$2H + OH \rightarrow H_2 + OH\dagger \qquad Q = 103 \text{ kcal/mole.} \qquad [5]$$

($D(H–O_2) = 47\pm2$ kcal/mole is from Foner and Hudson (32), $D(HO–O) = 63$ kcal/mole from thermodynamic data (33).) Reaction [5] must be of relatively little importance in view of the fact that it involves a ternary reaction between three species present only in low concentration. The relative importance of [3] and [4] cannot easily be assessed. Using the data of Burgess and Robb (31), [3] is favored by having a collision efficiency 60 times that of [4]; however, this advantage may be offset in our system by a concentration ratio (upper limit) of $H_2:H = 400:1$. Leaving aside the uncertain question of the relative over-all rates of [3] and [4], reaction [3] seems a much more likely source of vibrationally excited hydroxyl since it conforms to the pattern followed by all known exothermic exchange reactions which produce vibrationally excited products: vibrational excitation appears in the new bond being formed and little if any appears in the residue of the molecule under attack.

Reaction [3] is of special interest since it is one in which an activated complex splits into two fragments of identical composition. It would be interesting to know whether

these fragments are identical also in internal energy. If [3] is the origin of the OH† that we observe in $v = 3$ (and $v = 2$) we can confidently say that the internal energy is unequally distributed since even distribution would necessitate an endothermic reaction which would be slow at room temperature. This is shown in Table I. In the table Q_{TRV}

TABLE I

Heats of reactions forming OH† ($v = 2$, $v = 3$) from H + HO₂

Products of the reaction	Q_{TR} ($= Q_{TRV} - E(v)$) kcal/mole
Even distribution of vibration	
[3] a 2OH† ($v = 3$)	-20
[3] b 2OH† ($v = 2$)	-2
Uneven distribution of vibration	
[3] c OH† ($v = 3$)+OH† ($v = 2$)	-11
[3] d OH† ($v = 3$)+OH† ($v = 1$)	-1
[3] e OH† ($v = 3$)+OH	9
[3] f OH† ($v = 2$)+OH† ($v = 1$)	8
[3] g OH† ($v = 2$)+OH	18

is the total heat of reaction (called Q above). Q_{TR} is the heat of reaction available for translation and rotation after the stated amount of energy has gone into vibration. It is clear from the table that the fastest reactions producing OH† in $v = 2$ and $v = 3$ involve uneven distribution of energy among the otherwise identical products. If then H + HO₂ is the principal source of OH† in $v = 2$ and $v = 3$ it would follow that the activated complex HOOH dissociates preferentially to OH† + OH. This would be in accord with the suggestion (Polanyi (34)) that in the activated complex of the exothermic exchange reaction the new bond being formed is extended relative to normal internuclear separation for the isolated product molecule, and that this extension persists in a large measure as the complex disintegrates forming highly vibrating product. For reaction [3] this might be written as, H + O—OH → H- - -O—OH → H—O† + OH.

Evidence has been adduced above which contradicts Krassovsky's suggestion that the reaction between atomic hydrogen and vibrationally excited oxygen could constitute an important source of vibrationally excited hydroxyl. In our view the most likely source of OH† is the reaction between atomic hydrogen and HO₂. This would rule out the possibility that reactions involving H and O₂ could account for the Meinel hydroxyl bands, since these bands involve OH† in vibrational levels $v \leqslant 9$, whereas the room-temperature reaction H + HO₂ could only produce OH† in levels $v \leqslant 4$.

There remains the possibility that the Meinel hydroxyl bands originating in vibrational levels $v \leqslant 4$ may arise, to a greater or lesser extent, from reaction between H and O₂. To investigate this possibility we have calculated the approximate relative population distribution among vibrational levels of OH in our system. The calculation has been made by comparing the intensities of corresponding rotational lines within different bands of the $\Delta v = 1$ sequence. The lines in question, their measured areas, their areas corrected to a common scale (corrected for change in slit width, transmissivity of the instrument, and sensitivity of the detector), the ratios of intensities (taken from these corrected areas), the ratios of transition probabilities, the ratios of populations, and the derived vibrational 'temperatures', T_V, are shown in Table II. The areas were corrected for change in transmissivity of the instrument and changing sensitivity of the detector, from one wavelength to another, by comparing an experimental trace of the globar taken with

TABLE II

Relative populations in levels $v = 1$, $v = 2$, and $v = 3$ of OH†

Line	Area (arbitrary units)	Corrected area	Intensity ratio	Transition probability ratio	Population ratio	T_V (°K)
				$A_{2,1}/A_{1,0}$	N_2/N_1	
P_1 (5) [2 → 1]	38.7	134				
P_1 (5) [1 → 0]	32.1	673	5.02	1.83	9.19	2215
P_2 (5) [2 → 1]	23.9	82.9				
P_2 (5) [1 → 0]	21.4	435	5.25	1.83	9.61	2170
P_2 (4) [2 → 1]	28.8	99.8				
P_2 (4) [1 → 0]	24.1	468	4.69	1.83	8.58	2288
				$A_{3,1}/A_{1,0}$	N_3/N_1	
P (6)*[3 → 2]	19.5	46.8				
P (6)*[1 → 0]	45.7	948	20.3	2.75	55.8	2379
						Mean T_V = 2240

*$P_1(6) + P_2(6)$.

the lead sulphide detector (at the same slit width as the chart being calibrated), with the theoretical trace to be expected from a detector of uniform sensitivity and a spectrometer of uniform transmissivity. The theoretical trace was calculated from the black-body formula using the temperature of the globar as measured on a calibrated optical pyrometer, and taking the emissivity of the globar at various wavelengths from the data of Silverman (35). Relative populations ($N_{v'}$) were then obtained from the relative intensities ($I^K_{v',v''}$) by means of the relation

$$\frac{(N_{v'})_2}{(N_{v'})_1} = \frac{(I^K_{v',v''})_2 \cdot (\nu^K_{v',v''} \cdot A_{v',v''})_1}{(I^K_{v',v''})_1 \cdot (\nu^K_{v',v''} \cdot A_{v',v''})_2}$$

where $(\nu^K_{v',v''})_1$ and $(\nu^K_{v',v''})_2$ are the frequencies of the lines being compared, and $(A_{v',v''})_1$ and $(A_{v',v''})_2$ are the Einstein transition probabilities appropriate to the bands. Ratios of Einstein transition probabilities were calculated from data given by Garvin and coworkers (8, 9). Our calculation involves the assumption that the rotational temperature is the same in all three bands, $v(1 \to 0)$, $v(2 \to 1)$, $v(3 \to 2)$. We neglect the effect of vibration–rotation interaction on the rotational line strength.

The distribution of vibrators among vibrational levels clearly corresponds to a lower temperature, $T_V \approx 2240 \pm 60°$ K at 4 mm pressure, than that derived by Chamberlain and Smith (36) for $v = 1, 2, 3$ of OH in the night sky, $T_V \approx 8000°$ K at a pressure of about 10^{-2} mm, or that obtained from the reaction $H + O_3$ in the laboratory, $T_V \approx 9250°$ K at pressures in the range 2–5 mm (9). Of the two laboratory systems, $H + O_3$ corresponds much more closely in vibrational temperature of the OH† product to the Meinel bands. However, the significance of this correspondence will remain uncertain until the $H + O_3$ system has been examined at a pressure in the region of 10^{-2} mm. We plan an investigation on these lines, making use of the apparatus described here.

REFERENCES

1. J. K. CASHION and J. C. POLANYI.   J. Chem. Phys. **30**, 316 (1959).
2. G. HERZBERG.   Spectra of diatomic molecules. D. Van Nostrand Co., Inc., New York. 1950.
3. G. HERZBERG.   Infrared and Raman spectra. D. Van Nostrand Co., Inc., New York. 1945.
4. J. D. McKINLEY, D. GARVIN, and M. J. BOUDART.   J. Chem. Phys. **23**, 784 (1955).
5. D. R. BATES and M. NICOLET.   J. Geophys. Research, **55**, 301 (1950).
6. G. HERZBERG.   J. Roy. Astron. Soc. Can. **45**, 100 (1951).
7. A. B. MEINEL.   Astrophys. J. **111**, 555 (1950); **112**, 120 (1950).
8. D. GARVIN.   J. Am. Chem. Soc. **81**, 3173 (1959).
9. D. GARVIN, H. P. BROIDA, and H. J. KOSTKOWSKI.   J. Chem. Phys. **32**, 880 (1960).
10. V. I. KRASSOVSKY.   The airglow and aurora. Pergamon Press, London. 1956. p. 197.
11. D. R. BATES and B. L. MOISEIWITSCH.   J. Atmospheric and Terrest. Phys. **8**, 305 (1956).
12. J. K. CASHION and J. C. POLANYI.   J. Chem. Phys. **29**, 455 (1958); **30**, 1097 (1959).
13. H. L. WELSH, C. CUMMING, and E. J. STANSBURY.   J. Opt. Soc. Am. **41**, 712 (1951).
14. H. L. WELSH, E. J. STANSBURY, J. ROMANKO, and T. FELDMAN.   J. Opt. Soc. Am. **45**, 338 (1955).
15. G. G. SHEPHERD.   Ph.D. Thesis, Department of Physics, University of Toronto, Toronto, Ont. 1956.
16. D. M. GATES, C. C. SHAW, and D. BEAUMONT.   J. Opt. Soc. Am **48**, 88 (1958).
17. J. K. CASHION and J. C. POLANYI.   Proc. Roy. Soc. (London). In press.
18. E. L. TOLLEFSON and D. J. LE ROY.   J. Chem. Phys. **16**, 1057 (1948).
19. G. H. DIEKE and H. M. CROSSWHITE.   Bumble bee report No. 87. Johns Hopkins University. 1948.
20. R. C. HERMAN and G. A. HORNBECK.   Astrophys. J. **118**, 214 (1953).
21. E. K. PLYLER and J. J. BALL.   J. Chem. Phys. **20**, 1178 (1952).
22. H. C. ALLEN, JR., L. R. BLAINE, and E. K. PLYLER.   Spectrochim. Acta, **9**, 126 (1957).
23. E. K. PLYLER and E. D. TIDWELL.   J. Research Natl. Bur. Standards, **61**, 263 (1958).
24. J. K. CASHION and J. C. POLANYI.   J. Chem. Phys. **30**, 317 (1959).
25. J. T. HERRON and H. I. SCHIFF.   Can. J. Chem. **36**, 1159 (1958).
26. J. K. CASHION and J. C. POLANYI.   Unpublished work.
27. T. L. COTTRELL.   The strengths of chemical bonds. Butterworth Scientific Publications, London. 1958.
28. R. F. BARROW and A. R. DOWNIE.   Proc. Phys. Soc. (London), A, .**69**, 178 (1956).
29. S. N. FONER and R. L. HUDSON.   J. Chem. Phys. **21**, 1374, 1608 (1953).
30. S. N. FONER and R. L. HUDSON.   J. Chem. Phys. **23**, 1974 (1955).
31. R H. BURGESS and J. C. ROBB.   Chem. Soc. (London), Spec. Publ. No. 9, 167 (1958).
32. S. N. FONER and R. L. HUDSON.   J. Chem. Phys. **23**, 1364 (1955).
33. NATL. BUR. STANDARDS (U.S.), Circ. 500, February (1952).
34. J. C. POLANYI.   J. Chem. Phys. **31**, 1338 (1959).
35. S. SILVERMAN.   J. Opt. Soc. Am. **38**, 989 (1948).
36. J. W. CHAMBERLAIN and C. A. SMITH.   J. Geophys. Research, **64**, 611 (1959).

HOT ATOM REACTIONS AND RADIATION-INDUCED EFFECTS IN THE REACTIONS OF RECOIL TRITIUM WITH CYCLOPROPANE[1]

J. K. Lee, Burdon Musgrave, and F. S. Rowland

ABSTRACT

Recoil He^3 (n, p) tritium atoms have been reacted with cyclopropane in the gas phase under a variety of experimental conditions. The labeled hydrocarbon and molecular hydrogen products have been separated by gas chromatography and assayed by gas proportional counting.

The observed products show a strong dependence upon irradiation dose—cyclopropane is very inert toward reactions with hydrogen atoms and organic radicals, and the labeled olefinic products react preferentially, in effect as scavengers, with the reactive species from radiolysis of the parent molecule.
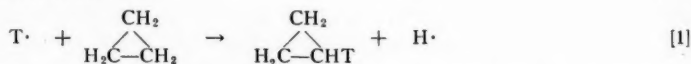
Energetic tritium atoms are able to react with cyclopropane to give labeled cyclopropane as a product without causing isomerization or decomposition of the molecule. The relative yields of cyclopropane and propylene are dependent upon the average collisional de-excitation times, indicating that a fraction of the labeled cyclopropane molecules are decomposing in times of approximately 10^{-9} seconds. Cyclopropane, propylene, ethylene, hydrogen, and small amounts of allene and methylacetylene are observed as "hot" products in the presence of gaseous free radical scavengers. Many additional compounds are found as the result of free radical and/or radiolysis reactions in the absence of scavengers.

The "hot" reactions are explained in terms of the single-step interactions of high kinetic energy tritium atoms with the cyclopropane molecules—the energy for endothermic and high activation energy processes is obtained from the recoil energy. The kinetic energy of the recoil atom at reaction is estimated to be of the order of 130 kcal/mole for some of the observed labeled compounds.

INTRODUCTION

The reactions of recoil tritium atoms from the nuclear reaction $He^3(n,p)T$ with saturated and unsaturated aliphatic hydrocarbons have been studied in detail in several laboratories, and the general outline of behavior is now well known (1–9). It will be assumed from these experiments, and from similar experiments with recoil tritium atoms from the $Li^6(n,\alpha)T$ reaction in condensed phases (10), that the recoiling atoms react predominantly while still "hot" in the sense of possessing excess kinetic energy from the nuclear recoil. As a result of this excess kinetic energy, the tritium atom is able to react at many positions in the molecule which are inaccessible to thermal hydrogen atoms (25° C) because of the high activation energies involved.

The cyclopropane molecule offers an interesting opportunity for further elucidation of the nature of these "hot" reactions because of its relatively high activation energy for substitution reaction—no deuterated cyclopropane was observed in mixtures of thermal deuterium atoms and cyclopropane (11)—and its ready thermal isomerization to propylene at temperatures in the range of 400–500° C (12). Preliminary experiments have already been reported which demonstrated that tritium-labeled cyclopropane can readily be obtained in good yield from the reactions of recoil tritium atoms with cyclopropane, as in reaction [1] (13).

$$T\cdot \;+\; \begin{array}{c} CH_2 \\ \triangle \\ H_2C{-}CH_2 \end{array} \;\rightarrow\; \begin{array}{c} CH_2 \\ \triangle \\ H_2C{-}CHT \end{array} \;+\; H\cdot \qquad [1]$$

More detailed experiments have now been carried out on the mechanism of reaction of energetic tritium atoms with cyclopropane. The most pertinent variables in these

experiments have been the length of the irradiation, the pressure of cyclopropane, and the absence or presence of other gases, especially nitric oxide and/or helium, during the irradiation.

EXPERIMENTAL

The experimental conditions of these experiments are quite similar to those established previously in our studies of olefinic hydrocarbons (9). Mixtures of He^3, cyclopropane, and any other gases to be added were prepared in a vacuum system, and sealed into irradiation tubes made of 20-mm I.D. Pyrex 1720 glass, in lengths of about 5–8 cm. He^3 was obtained from Oak Ridge and freed from tritium-labeled impurities by combustion over CuO at 600° C, and passage through a liquid nitrogen trap (14). The level of radioactive impurity gases in the He^3 after this purification was less than 50 d.p.m./cc S.T.P. of $(T_2 + HT)$, and less than 50 d.p.m./cc S.T.P. of CH_3T or other aliphatic hydrocarbons. These activity levels are negligible in comparison to the neutron-induced radioactivity in each of the irradiated samples. The other gases were all obtained from the Matheson Company and have quoted purities of $>99\%$ for He and NO, and $>99.5\%$ for cyclopropane. Our measurements on the cyclopropane showed no detectable hydrocarbon impurities as large as 0.01%.

The irradiation tubes were exposed to neutrons in the instrument tunnel facility of the Brookhaven National Laboratory, which has a nominal flux of 2.8×10^9 n/cm² sec and an ambient temperature of about 30° C. Irradiations were carried out for periods of time varying from 2 hours to 6 days in this facility. The actual neutron flux during irradiation was somewhat reduced by neutron absorption in the Pyrex 1720 glass, and by self-shielding during simultaneous irradiation of many samples. Neutron flux calculations based on the observed tritium radioactivity fall in the range $0.5–1.0 \times 10^9$ n/cm² sec, as shown in Table I.

The distribution of radioactivity among molecular hydrogen and the various hydrocarbon molecules was obtained for each irradiated sample by gas chromatographic separation and flow proportional counting of the chromatographic effluent gas. Two or more aliquots were run on each sample, usually a large aliquot on a 50-ft dimethylsulpholane (DMS) column at 25° C, and a smaller aliquot on 10 ft silica gel at 85° C. The counting gas consisted of the helium carrier gas and methane in about a 50–50 mixture, the methane being added after the carrier gas had passed through a thermal conductivity detector for determination of macroscopic radiation damage. Further details have been given previously (15, 16).

Aliquots of some samples were run through a 50-ft safrole column in order to determine the relative contributions of n-butane – neopentane and cyclopropane–acetylene. In the usual dimethylsulpholane runs, the former pair are unseparated and acetylene is obscured by the large cyclopropane peak immediately preceding it. Acetylene contributions are also measured on the silica gel column, although they are partially obscured when propane is present in large amounts. The parent peaks usually overload the DMS column and emerge somewhat early; other components are practically unaffected by the overload of the parent compound.

RESULTS

Variation in Length of Irradiation

The yields of tritium radioactivity found in various molecules, measured relative to cyclopropane as 100, are shown in Table I for a series of irradiations carried out under

TABLE I

Distribution of tritium radioactivity from $He^3(n,p)T$ in cyclopropane: effect of length of irradiation
(Yields relative to cyclopropane = 100)

Gas, Δ	70.4	72.4	72.1	78.1	76.7	80.4	74.5	73.2
Pressure He³	2.0	2.0	2.0	1.3	2.0	1.3	2.0	1.3
Irradiation time, hours	138	48	48	48	24	8	4	2
Neutron flux (from T product on) counts observed			8×10⁸	7×10⁸	6×10⁸	9×10⁸	7×10⁸	7×10⁸
In Δ peak	29,000	6,000	25,500	16,800	8,650	2,530	1,900	660
Product, Δ	100	100	100	100	100	100	100	100
HT	141	138	138	159	147±2	140±5	153±6	150±10
CH₂T	11	11	9					
C—C	28	26	22	25	22±1	16±1	11±2	33±5
C=C	7	9	10	11	10±1	10±1	12±2	—
C≡C	2	2	2	2	2	—	—	—
C—C—C	54	52	48	51	44±2	37±2	20±2	23±5
C—C=C	9	15	15	19	22±1	31±2	49±3	54±5
C=C=C	1	1	1	1	2±1	2±2	2±2	—
C\C/ C—C	13	15	14	13	16±1	21±2	7±2	29±5
C—C—C—C	39	35	30	29	25±1	15±1	7±2	9±3
C\ C/ C/ \C (C—C—C=C)	1	2	2	2	3±0.5	3±1	5±1	—
C\C/ C—C—C	24	28	23	21	22±1	17±2	7±1	—
C—C—C—C—C	6	9	5	5	4±0.5	5±2	—	—
Δ—C	3	3	4	5	4±0.5	3±1	2±1	—
"170"*	—	12	10	10	10±1	12±2	9±2	—

*C₆ peak at 170 minutes or DMS; not conclusively identified.

nearly constant conditions except for the length of the irradiation. As can readily be seen, the relative yields of several labeled unsaturated molecules fall, and the yields of the corresponding saturated aliphatic products increase, with increasing radiation time. The total number of counts actually measured in the cyclopropane peak and the flux estimate from the total observed tritium activity are also given in Table I for the irradiations. The shortest irradiations did not create much tritium radioactivity, and the quoted errors are calculated from the statistical uncertainty of the observed counts. For runs of 48 hours or longer, the statistical uncertainty is probably less than other possible errors. The irradiation times were varied from 2 to 138 hours; duplicate samples at 48 hours were separately irradiated several months apart and analyzed on both the dimethylsulpholane and safrole columns.

Nitric Oxide Experiments

The observed tritium distributions are given in Table II for a series of experiments carried out in the presence of nitric oxide. The usual role of nitric oxide in these experiments is to react with free radicals and thermal hydrogen atoms, and to remove them from the reacting system, thus protecting other recoil reaction products, e.g. propylene and ethylene, from secondary reactions with radiation-induced species. At the same time, all labeled compounds are eliminated which involve thermal atoms or radicals in
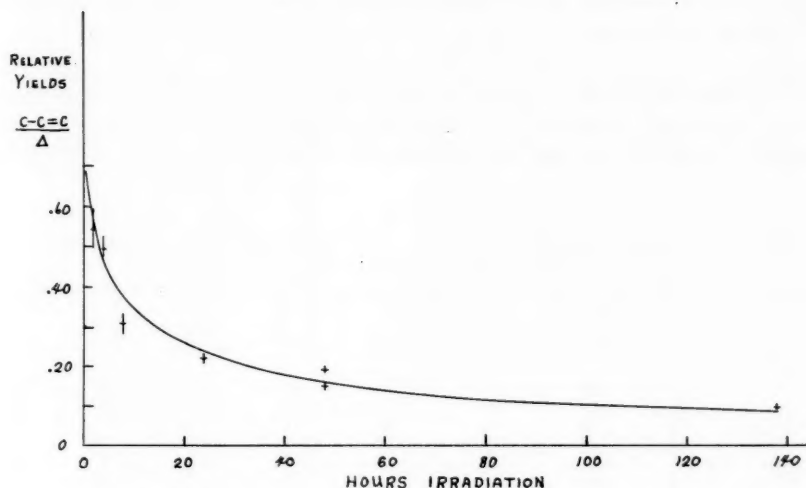
FIG. 1. Propylene yield vs. irradiation time. $G(\text{H}) = 5$, $G(\text{olefin}) = 4$. $k_4/k_7 = 8 \times 10^{-5}$.

TABLE II

Distribution of tritium radioactivity from $\text{He}^3(n,p)\text{T}$ in cyclopropane – nitric oxide mixtures

Gas, Δ	72.7	66.4	40.6	33.2	19.9	21.4
Pressures He³	1.9	1.9	1.8	1.8	1.6	1.6
NO	5.0	7.7	4.3	5.0	2.1	1.8
Neutron flux $\sim 10^9$ n/cm² sec						
Counts observed in Δ peak*	19,000	66,000	56,000	12,000	22,000	17,000
Irradiation time, hours	48	138	138	48	48	138
HT	131	131	131	133	133	131
CH₃T	2	2	2			2
C=C	6	6	7	6	7	7
C—C=C	7	16	35	7	30	38
Δ	100	99	97	92	93	90
C≡C	1	1	1	1	1	1
C=C=C	1	1	2	1	1	—
Δ—C	1	1	1	1	0	—
"125"†	2	5	6	7	2	—
"140"†	1	1	1	1	1	—

NOTE: C–C–C=C $\sim$ 0.3, "168" $\sim$ 0.3, others <0.1.
*Since the sample aliquots were not all of the same size, the listed observed counts show only the statistical counting accuracy of the analysis, and not the total or relative specific activities.
†Peaks at 125 minutes and 140 minutes on DMS not yet conclusively identified. C=C–C=C and C–C≡C or C–C–C=C–C have the correct retention times.

their production. Those labeled compounds which are unaffected by the presence of a radical scavenger are then assumed to be obtained from direct recoil reaction. A possible exception could occur if the direct reaction created a "hot" radical (e.g. ·CHT·), which was able to react very efficiently with the hydrocarbon molecule.

The nitric oxide experiments confirm hydrogen, ethylene, propylene, and cyclopropane

as products of recoil reaction, although the amounts observed are not always found in consistent ratios.

Pressure Effects

The tritium distributions have also been measured with a series of samples irradiated at various cyclopropane pressures from 7.9 to 80 cm Hg (plus 1–2 cm Hg of He³) and are recorded in Table III. The practice of expressing all products in terms of the parent

TABLE III
Distribution of tritium radioactivity from He³(n, p)T in cyclopropane: pressure effects
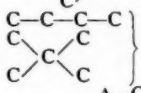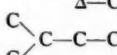(Neutron flux $\sim 10^9$ n/cm² sec)

Gas, Δ	72.4	70.4	50.9	48.7	17.3	18.1	7.9	9.2
He³, cm	2.0	2.0	1.7	1.7	1.7	1.7	2.1	2.1
Counts in Δ peak	6,000	28,000	27,000	80,000	28,000	27,000	14,000	11,000
Irradiation time, hours	48	138	48	138	48	138	48	138
Product, Δ	100	100	100	100	100	100	100	100
C—C—C	52	54	54	58	71	72	77	88
C—C≡C	15	9	16	7	13	9	14	7
HT	138	141	142	(143)	156	154	159	180
CH₃T	11	11	11		12	13	14	12
C—C	26	28	27	28	33	32	34	39
C=C	9	7	8	6	10	10	13	10
(C)(C)C—C [methylcyclopropane]	15	13	16	16	22	22	25	21
C—C—C—C								70
cyclobutane / methylcyclopropane group	35	39	36	46	50	52	53	—
C≡C	2	2	—	—	2	—	—	2
Δ—C	3	3	4	3	3	3	2	—
(C)(C)C—C—C [dimethylcyclopropane]	28	24	27	30	37	38	41	44
C—C—C—C—C	9	6	7	9	9	9	15	11
Estimated relative parent activity	100	100	98	98	92	91	87	80

yield is not very satisfactory for Tables II and III, for a comparison of the actual amounts of radioactivity observed in various compounds indicates that the percentage of labeled parent compound falls off with decreasing pressure. This parent fall-off is accompanied by an increase in the percentage of radioactivity observed as propane. There is no compound whose activity is necessarily constant through the pressure changes, although hydrogen is experimentally observed to be nearly so. We have chosen to hold the cyclopropane activity as 100 for comparison purposes. The column labeled estimated relative parent activity represents an estimate of the absolute change in the activity as cyclopropane.

Helium Moderator

The results of a series of runs carried out in the presence of moderator He⁴, with and without nitric oxide as a scavenger, are shown in Table IV. The actual yield of labeled hydrogen is not very much affected by changes in He⁴/cyclopropane ratio, but the yield of labeled cyclopropane falls markedly. Both propane and n-butane increase as the He⁴/parent ratio is increased.

TABLE IV

Distribution of tritium radioactivity from $He^3(n,p)T$ in cyclopropane–He^4 mixtures
(Neutron flux $\sim 10^9$ n/cm² sec)

Gas, Δ	52.5	23.8	22.6	7.8	10.1
He³, cm	2.0	1.6	1.6	1.5	1.5
He⁴	20.0	45.0	44.5	66.0	66.7
Counts in Δ peak	51,000	11,000	27,000	11,000	14,000
Irradiation time, hours	138	48	138	48	138
Product, Δ	100	100	100	100	100
HT	141	182	186	275	270
CH₃T	11	16	13	15	17
C—C	27	35	42	70	70
C=C	8	14	9	29	20
C≡C	9	6	8	14	13
C—C—C	49	74	81	110	115
C—C=C	15	19	10	26	16
cyclo C—C (C\C/C—C)	12	23	21	32	27
C—C—C—C / cyclobutane etc.	43	60	92	115	{124 —}
Δ—C	5	5	3	4	—
cyclo C—C—C	30	46	49	76	73
C—C—C—C—C	7	10	13	17	20

DISCUSSION

The distribution of tritium activity among the various possible molecular forms in a given system depends upon three separate steps:

(a) The primary reaction of the recoil tritium with a molecule of the medium. If, as is frequently true, this reaction occurs while the tritium atom possesses excess kinetic energy, this attack can be expected to be rather indiscriminate upon all species in the system. In lightly irradiated systems such as these, the "hot" reaction would then be with cyclopropane almost exclusively, for the total concentration of degradation products, free radicals, ions, etc. is always very small in comparison to the cyclopropane concentration. These "hot" reactions produce the initial recoil tritium yields.

(b) The "hot" product may itself be quite reactive, and be able to participate in further reactions in the system. This can happen if the "hot" product is either a labeled free radical, such as the $CH_2T\cdot$ or sec-$C_4H_8T\cdot$ suggested for other hydrocarbons (1, 3, 9), or if it is a molecule sufficiently vibrationally excited to undergo decomposition or isomerization. The identified stable labeled molecule will depend in each case on the further reactions of the radical or excited molecule involved. These reactions, unlike the "hot" reactions, can be strongly influenced by the presence or absence of reactive ions, atoms, and molecules from radiation degradation.

It is also possible to form a stable molecule in temperature equilibrium with the system which is able to undergo thermal chemical reactions with other molecules present. There have been no experimental indications of any such molecules in any of the hydrocarbon systems investigated in our laboratory. Furthermore, the known hydrocarbons do not react or undergo isotopic exchange over a period of several months at room

temperature, as confirmed by samples irradiated in duplicate and analyzed several months apart.

(c) The final distribution that is observed may also reflect subsequent alteration of the products of (a) and (b) by continued exposure to a radiation field. The perturbing effect of such radiation-induced reactions can readily be minimized, if the parent molecule is reasonably reactive toward radiation-produced species. If the parent molecule is rather inert, however, the brunt of the radiation damage may be borne by reactive product molecules present in low concentration, e.g. olefins, and will result in appreciable alteration in the observed amounts of these products.

The nitric oxide – scavenger experiments of Table II demonstrate that labeled hydrogen, cyclopropane, propylene, ethylene, and other molecules are all formed in the initial reaction of the "hot" tritium atom with cyclopropane. The experiments in the absence of nitric oxide show an appreciably different spectrum of labeled hydrocarbons, including substantial yields of a number of saturated aliphatic molecules that arise from the reactions of excited species, as in (b), or radiation alteration, as in (c).

Since reactions in both categories (b) and (c) are quite sensitive to the presence of radiation-produced reactive species in the rather unreactive cyclopropane, we must consider the radiation chemistry of the recoil system as well as the initial "hot" reactions with cyclopropane itself.
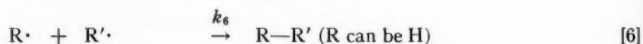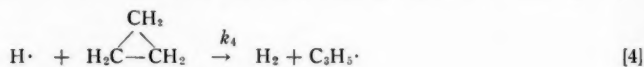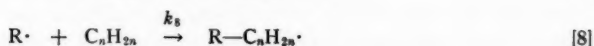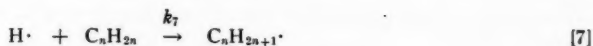
Radiation Effects

I. Ionization Processes

The recoil triton and proton from the $He^3(n,p)T$ reaction dissipate a total of 0.78 Mev for each tritium atom produced, and almost all of this energy is released as ionization and excitation in the gas phase. The identity of the ions, radicals, and atoms created by radiation effects can be estimated from the 70-volt mass spectra, as in the calculations of Futrell on n-hexane (17). Such a calculation, with the additional assumption that the ion–molecule reactions of $C_3H_5^+$ and $C_3H_6^+$ with cyclopropane go approximately as well as the corresponding reactions with propylene (18–20), clearly indicates the formation of substantial quantities of radiation produced ethylene and hydrogen atoms, as well as smaller yields of methyl and other radicals. Additional hydrogen atoms and or radicals will arise from the ion–electron or ion–ion recombination reactions.

II. Reactions of Hydrogen Atoms and Radicals

In pure cyclopropane, abstraction reactions such as [4] and [5] are the only important reactions that can occur for H atoms or radicals, except recombination as in [6].

$$H\cdot \ + \ H_2\overset{\displaystyle CH_2}{\underset{}{C}}\diagup\diagdown CH_2 \ \overset{k_4}{\rightarrow} \ H_2 + C_3H_5\cdot \qquad [4]$$

$$R\cdot \ + \ H_2\overset{\displaystyle CH_2}{\underset{}{C}}\diagup\diagdown CH_2 \ \overset{k_5}{\rightarrow} \ RH + C_3H_5\cdot \qquad [5]$$

$$R\cdot \ + \ R'\cdot \ \overset{k_6}{\rightarrow} \ R\!-\!R' \ (R \ can \ be \ H) \qquad [6]$$

As irradiation proceeds and olefinic products begin to accumulate, the atoms and radicals may react with them, too, as in [7] and [8], and the actual course of reaction will depend upon the relative rates of the individual reactions [4] to [9] for the various radicals involved.

$$\text{H·} \quad + \quad \text{C}_n\text{H}_{2n} \quad \overset{k_7}{\rightarrow} \quad \text{C}_n\text{H}_{2n+1}· \tag{7}$$

$$\text{R·} \quad + \quad \text{C}_n\text{H}_{2n} \quad \overset{k_8}{\rightarrow} \quad \text{R}—\text{C}_n\text{H}_{2n}· \tag{8}$$

Experimentally, it is observed that the sum of the relative yields of propylene and propane in Table I is reasonably constant over a factor of 70 in irradiation times, although the individual yields are changing. This observation strongly suggests that the most probable reaction for the removal of propylene from the system, and its lowered relative yield, is reaction [7] followed by the further addition of another hydrogen atom, probably by reaction [5] for the $\text{C}_n\text{H}_{2n+1}$ radical. The sum of the yields for ethane plus ethylene is also nearly constant for different irradiation times—the ethylene concentration does not fall as smoothly as the propylene yield, but there are difficulties in separating the ethane and ethylene radioactivity at these low count rates.

A crude calculation of the kinetic behavior of atoms and radicals in the cyclopropane system can be made by assuming that

(a) H atoms and olefin are produced continuously by radiation effects on cyclopropane;

(b) olefin is removed only by reaction with H atoms, as in reaction [7], followed by reaction [5];

(c) H atoms are removed only by reactions [4] and [7], and rapidly reach a steady-state equilibrium.

Such assumptions lead to a predicted curve of olefin concentration versus time of irradiation which depends on the parameters: (1) radiation G values of hydrogen and olefin, and (2) the ratio k_4/k_7. The olefin reaches a steady-state concentration eventually, and since the total radioactivity produced rises linearly with time, the fraction of radioactivity found as olefin falls steadily (21).* The propylene yields of Table I agree quite well with the crude estimate obtained using the parameters: $k_4/k_7 = 8 \times 10^{-5}$, $G(\text{H}) = 5$, and $G(\text{olefin}) = 4$. These G values are reasonable ones, and the value of k_4/k_7 used is in good agreement with measured values for this ratio (11, 22, 23). The intercept for the propylene yield at zero irradiation time corresponds to zero initial production of labeled propane, and allows the additional conclusion that the sum of propylene plus propane yields is a satisfactorily accurate measure of the *total* production of propylene in the system by "hot" reactions. In the subsequent discussion of the "hot" reactions themselves, we shall use this sum of yields as a measure of the labeled propylene production in comparison to the labeled cyclopropane yield.

Tritium Reactions at High Kinetic Energy

Previous gas-phase experiments have led to a hypothesis for the reactions of high-energy recoil atoms with hydrocarbons that is able to explain the observed effects quite satisfactorily (1–9). The most important characteristics of this hypothesis are that the tritium atoms react

(a) as neutral atoms—the predominant charge state for a moving hydrogen nucleus at energies from 10^4 ev down;

(b) while possessing kinetic energy greatly in excess of average thermal energies, and hence are able to both react in a very few collisions and to undergo reactions that are highly endothermic and/or have high activation energies. Essentially, all positions in

*K. Yang and P. Gant (J. Chem. Phys. (in press)) have reported steady-state concentrations of ethylene in cyclopropane of about $10^{-3} x(\text{cyclo-}\text{C}_3\text{H}_6)$ for cyclopropane irradiated with beta particles from tritium decay.

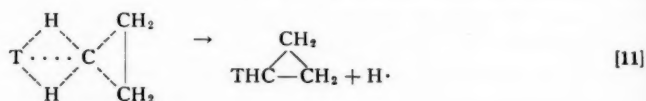a molecule are approximately equally subject to attack by, and reaction with, the recoil tritium atom.

(c) the reaction usually takes place so rapidly that only one parent molecule is involved—the reaction is completed before energy can be removed from the system by collisions.

(d) the reaction takes place through a transition complex and does not require "cages" or combination with other radicals in order to produce most of the observed radioactive molecules.

The recoil tritium reactions with both saturated and unsaturated positions of aliphatic molecules have been interpreted as involving momentarily a transition complex including the tritium recoil atom and all of the previously bonded substituents. This complex then decomposes by breaking one (or more) of these bonds, often leading to a stable molecule as a result. With cyclopropane, such a complex might be pictorially written as in [9] (without intending to indicate any specific details about the geometry and bonding involved).

$$T \ + \ \overset{CH_2}{\underset{H_2C-CH_2}{\triangle}} \quad \rightarrow \quad T\cdots C \overset{H \quad CH_2}{\underset{H \quad CH_2}{<}} \qquad [9]$$
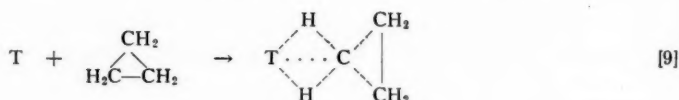
The lifetime of this complex is very short—it may only exist for one vibration or so, and equilibration of energy among the vibrational co-ordinates of the complex does not occur. The C_3H_6T complex above can break one of the bonds to the attacked carbon atom, with four possible reactions.

$$\rightarrow \ HT + C_3H_5 \cdot \qquad [10]$$

$$T\cdots C \overset{H \quad CH_2}{\underset{H \quad CH_2}{<}} \quad \rightarrow \quad TH\overset{CH_2}{\underset{}{\triangle}}CH_2 + H \cdot \qquad [11]$$

$$\rightarrow \ CH_2T-CH_2-CH_2 \cdot \qquad [12]$$

$$\rightarrow \ H_2C\overset{CH_2}{\underset{}{\triangle}}CH_2 + T \cdot \qquad [13]$$

The tritium atom emerging from reaction [13] will usually be degraded in energy and will react again as a "hot" atom or a thermal atom depending upon the energy remaining. Undoubtedly a relatively high activation energy is required for the tritium atom to penetrate into the molecule far enough to bond even briefly to one of the carbon atoms. The relative yields of equations [10]–[13] may very well be strongly energy dependent.

The tritium-labeled cyclopropane from reaction [11] will usually be produced in an excited vibrational state, and, if this energy is sufficient, can undergo the isomerization reaction [14] for which the activation energy is 65 kcal/mole (24). Some tritium would be

$$TH\overset{CH_2}{\underset{}{\triangle}}CH_2 \quad \rightarrow \quad CH_3-CH=CHT \qquad [14]$$
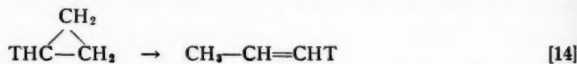
expected in all hydrogen positions of the propylene. The labeled n-propyl radical from reaction [12] must be excited since the reaction is highly exothermic as shown in Table V.
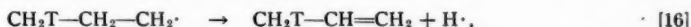
TABLE V

Energetics of formation of "hot" products in recoil tritium
reactions with cyclopropane

Reaction	ΔH (kcal/mole)

CH₂
△
T + H₂C—CH₂   →
CH₂

H₂C—CHT + H	~0
CH₃—CH=CHT + H	−8
CH₂=CHT + CH₃·	−20
CH₂=CHT + ·CH₂ + H·	+83
CH₂T—C≡CH + H₂ + H·	+31
CH₂T—C≡CH + 3H·	+135
CH₂=C=CHT + H₂ + H·	+32
CH₂=C=CHT + 3H·	+136

ΔH_f^0 used (isotopic differences ignored) (25–27)

CH₂ △ H₂C—CH₂	+12.7
CH₃—CH=CH₂	+4.9
CH₂=CH₂	+12.5
CH₃—C≡CH	+44.3
CH₂=C=CH₂·	+45.3
H	+52.1
CH₃·	32.0
·CH₂	83

This energy is sufficient to permit decomposition to labeled methyl and ethylene to occur readily,

$$CH_2T—CH_2—CH_2· \quad \rightarrow \quad CH_3T· + C_2H_4; \qquad [15]$$
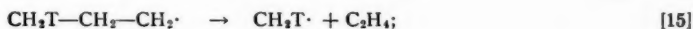
to hydrogen and propylene to occur less readily,

$$CH_2T—CH_2—CH_2· \quad \rightarrow \quad CH_2T—CH=CH_2 + H·, \qquad [16]$$

and perhaps to decompose as in reaction [17] to a hydrogen atom and the trimethylene radical,

$$CH_2T—CH_2—CH_2· \quad \rightarrow \quad ·CHT—CH_2—CH_2· + H·. \qquad [17]$$
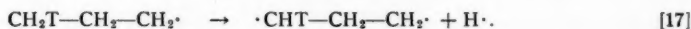
"Hot" Products

Cyclopropane

The identification of labeled cyclopropane among the radioactive products immediately indicates that reaction [1]—presumably by steps [9] plus [11]—is able to take place without further isomerization as in [14]. This failure to isomerize can be expected if the tritiated molecule is left with less vibrational energy than the 65 kcal/mole activation energy, or if the excess energy is not too great and can be removed by collision before isomerization.

The data of Table III show that the fraction of tritium activity found as labeled cyclopropane is greater at high pressures. (The results of Table IV show that the changes in He/Δ ratio of Table III are insufficient to explain the observed decreases in cyclopropane yield with decreased pressure during irradiation.) The increased cyclopropane

yield at higher pressures is readily explained as a competition between the isomerization reaction [14] and the removal of excitation by collision:

$$\left[\overset{CH_2}{\underset{THC-CH_2}{\triangle}} \right]^* + \overset{CH_2}{\underset{H_2C-CH_2}{\triangle}} \rightarrow \overset{CH_2}{\underset{THC-CH_2}{\triangle}} + \overset{CH_2}{\underset{H_2C-CH_2}{\triangle}} \qquad [18]$$

De-excitation of the excited n-propyl radical is not a satisfactory mechanism, for this de-excitation will not lead to labeled cyclopropane, but rather to an aliphatic hydrocarbon.

An estimate of the excitation energy required for reactions [14] and [15] to be competitive depends on the efficiency of collisions in removing excess vibrational energy. Since the excess energy is quite large, the collision efficiency is probably very high, approaching unity. The rate of isomerization must then be of the order of $10^9 \sec^{-1}$ in order to be competitive with gas collisions at 0.1 to 1.0 atmosphere pressure. Such a rate requires an excitation energy roughly double the activation energy for a molecule with 13 active degrees of freedom, and hence approximately 130 kilocalories/mole of internal energy. Almost all of this energy must be supplied from the original kinetic energy of the tritium, which must then have been at least 6–7 ev at the time of reaction. The possible alternate path to propylene by reactions [9] and [16] prevents additional conclusions about higher vibrational energies from being drawn from the experimental observation that substantial yields of propylene (plus propane) are found at the highest pressures used. Some information on the relative importance of the two paths to propylene formation could be obtained in principle by degradation of the propylene molecules in order to determine the intramolecular tritium distribution.

Ethylene, Allene, Methylacetylene, and Hydrogen

The unsaturated molecules ethylene, allene, and methylacetylene are all obtained in low yield from the recoil reactions in the presence of nitric oxide, as well as in its absence. Each of these molecules could arise from the decomposition of the excited intermediate by reactions other than [9] to [13], or by further decomposition of the propylene of [14] or [16], of the trimethylene radical from [17], or of the n-propyl radical from reaction [12].

Both allene and methylacetylene must be formed by a highly endothermic reaction, as shown in Table V. If the three hydrogen atoms that must be lost from the transition complex are all lost as separate atoms, a kinetic energy of more than 135 kcal/mole must be supplied by the recoiling tritium atom. The second possibility exists that two of these hydrogens are given off as H_2, as in reactions [19], from the unimolecular elimination of molecular hydrogen from an excited propylene molecule.

$$CH_2T-CH=CH_2 \Big\langle \begin{matrix} CH_2T-C\equiv CH + H_2 \\ CHT=C=CH_2 + H_2 \end{matrix} \qquad [19]$$
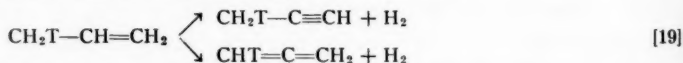
The over-all path by this sequence of reactions is only 31 and 32 kcal/mole endothermic, respectively. However, reactions such as [19] can be expected to have activation energies of the order of 40–60 kcal/mole, and again roughly double this energy would be required for decomposition before collisional deactivation. Hence, for either possible path to labeled methylacetylene or allene, an energy of about 120+ kcal/mole must be supplied from the kinetic energy of the recoil tritium. The unscavenged HT found in the nitric oxide systems may arise from an energetic hydrogen abstraction reaction. An alternate path that may be very important would be the intramolecular elimination of HT instead of H_2 from the excited propylene molecule, as in [19].

The excited n-propyl radical decomposition is exothermic over all in going to methyl plus ethylene, but the sequence of reaction [9] followed by [15] leads only to labeled methyl radical in the absence of some hydrogen transfer reactions in the excited radical. The decomposition of trimethylene diradical as in [20] is quite endothermic, but the energy requirements are no more severe than those for the formation of the other

$$\cdot CH_2-CH_2-CHT\cdot \quad \rightarrow \quad \cdot CH_2 + CH_2=CHT \tag{20}$$
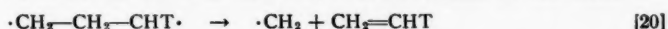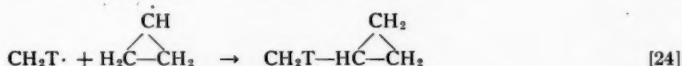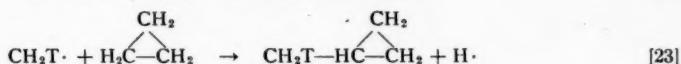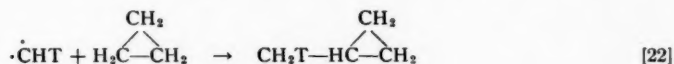
"hot" products. Since this reaction does not involve hydrogen transfer, it may be able to compete successfully. Furthermore, in the presence of so much excess vibrational energy, an excited trimethylene diradical for reaction [20] can probably be obtained readily by direct opening of the cyclopropane ring, as in [21]:

$$\begin{array}{c} CH_2 \\ \diagup \diagdown \\ H_2C-CHT \end{array} \quad \rightarrow \quad \cdot CH_2-CH_2-CHT\cdot \tag{21}$$
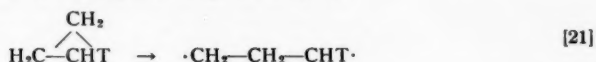
Methylcyclopropane and Butene-1

Methylcyclopropane could presumably arise in this system by any of these three reactions:

$$\cdot\dot{C}HT + H_2\overset{CH_2}{\overset{\diagup\diagdown}{C-CH_2}} \quad \rightarrow \quad CH_2T-H\overset{CH_2}{\overset{\diagup\diagdown}{C-CH_2}} \tag{22}$$

$$CH_2T\cdot + H_2\overset{CH_2}{\overset{\diagup\diagdown}{C-CH_2}} \quad \rightarrow \quad CH_2T-H\overset{\cdot\;\;CH_2}{\overset{\diagup\diagdown}{C-CH_2}} + H\cdot \tag{23}$$

$$CH_2T\cdot + H_2\overset{\dot{C}H}{\overset{\diagup\diagdown}{C-CH_2}} \quad \rightarrow \quad CH_2T-H\overset{CH_2}{\overset{\diagup\diagdown}{C-CH_2}} \tag{24}$$

The recent experiments of Butler and Kistiakowsky demonstrate that a mixture of butenes would also be expected from reaction [22] under these experimental conditions (28). Since the yields of isobutylene and *cis-* and *trans-*butene-2 are negligible, the methylene insertion reaction is probably negligible, too. Reaction [23] is endothermic and would require a "hot" $CH_2T\cdot$ group. The observation of some labeled butene-1 in the presence of radical scavenger (Table II) is consistent with this reaction.

The radical recombination reaction seems quite likely since C_3H_5: radicals (of unspecified structure) will be expected in good yield from the abstraction reactions [4] and [5] by hydrogen atoms and radicals, respectively. Similarly, the recombination of methyl with allyl radical [26] is probably the source of the labeled butene-1 found in this system.

$$CH_2T\cdot \quad + \quad CH_2=CH-CH_2\cdot \quad \rightarrow \quad CH_2T-CH_2-CH=CH_2 \tag{26}$$

Moderator Effect

Qualitatively, the changes in yields of cyclopropane and other molecules in the presence of He^4 (Table IV) are consistent with the removal of the excess kinetic energy of the recoil tritium in elastic collisions with the helium moderator. The energy loss reduces the probability of a large excess of vibrational energy, and hence of isomerization; it also reduces the probability of a successful reaction while still possessing the necessary activation energy for reaction with the cyclopropane molecule to form HT or labeled parent molecule. The more rapid decrease in the yield of labeled cyclopropane than of HT implies that the activation energy for the former is larger, as is also indicated by the thermal deuterium experiments of Schiff and Steacie.

Wolfgang and Estrup have presented a theory of high-energy kinetics and have applied it quite successfully to the recoil reactions of tritium with methane (4). The reactions in the cyclopropane system are sufficiently complicated, however, that additional experiments are required on radiation effects and on collisional de-excitation in He⁴–Δ mixtures before a suitable test of the applicability of the theory to this system can be made.

REFERENCES

1. M. El-Sayed and R. Wolfgang. J. Am. Chem. Soc. 79, 3286 (1957).
2. M. El-Sayed, P. J. Estrup, and R. Wolfgang. J. Phys. Chem. 11, 1356 (1958).
3. D. Urch and R. Wolfgang. J. Am. Chem. Soc. 81, 2025 (1959).
4. P. Estrup and R. Wolfgang. J. Am. Chem. Soc. In press.
5. D. Urch and R. Wolfgang. Am. Chem. Soc. 136th Meeting, Atlantic City, 1959.
6. A. A. Gordus, M. C. Sauer, Jr., and J. Willard. J. Am. Chem. Soc. 79, 3284 (1957).
7. J. B. Evans, J. Quinlan, M. C. Sauer, Jr., and J. Willard. J. Phys. Chem. 11, 1351 (1958).
8. M. C. Sauer, Jr. and J. Willard. J. Phys. Chem. 64, 359 (1960).
9. J. K. Lee, B. Musgrave, and F. S. Rowland. Am. Chem. Soc., 134th Meeting, Chicago, 1958; J. Am. Chem. Soc. In press.
10. W. J. Hoff, Jr. and F. S. Rowland. J. Am. Chem. Soc. 79, 4867 (1957).
11. H. I. Schiff and E. W. R. Steacie. Can. J. Chem. 29, 1 (1951).
12. H. O. Pritchard, R. G. Sowden, and A. F. Trotman-Dickenson. Proc. Roy. Soc. (London), A, 217, 563 (1953).
13. J. K. Lee, B. Musgrave, and F. S. Rowland. J. Am. Chem. Soc. 81, 3803 (1959).
14. J. K. Lee and F. S. Rowland. J. Inorg. & Nuclear Chem. 10, 336 (1959).
15. R. Wolfgang and F. S. Rowland. Anal. Chem. 30, 903 (1958).
16. J. K. Lee, B. Musgrave, and F. S. Rowland. Am. Chem. Soc. 137th Meeting, Cleveland, 1960.
17. J. H. Futrell. J. Am. Chem. Soc. 81, 5921 (1959).
18. D. P. Stevenson. J. Phys. Chem. 61, 1453 (1957).
19. D. O. Schissler and D. P. Stevenson. J. Chem. Phys. 24, 926 (1956).
20. F. W. Lampe and F. H. Field. Tetrahedron, 7, 189 (1959).
21. K. Yang and P. Gant. J. Chem. Phys. In press.
22. P. E. Allen, H. Melville, and J. C. Robb. Proc. Roy. Soc. A, 218, 311 (1953).
23. B. Darwent and R. Roberts. Discussions Faraday Soc. 14, 55 (1953).
24. H. O. Pritchard, R. G. Sowden, and A. F. Trotman-Dickenson. Proc. Roy. Soc. A, 217, 563 (1953).
25. A. F. Trotman-Dickenson. Free radicals: an introduction. Methuen. 1959.
26. S. W. Benson. The foundations of chemical kinetics. McGraw-Hill. 1960.
27. A. F. Trotman-Dickenson. Gas kinetics. Butterworth. 1955.
28. J. Butler and G. Kistiakowsky. J. Am. Chem. Soc. 82, 759 (1960).

# VIBRATIONAL DISEQUILIBRIUM IN REACTIONS BETWEEN ATOMS AND MOLECULES[1]

N. Basco and R. G. W. Norrish

ABSTRACT

Observations on the production of vibrationally excited oxygen molecules in the flash photolysis of nitrogen peroxide and of ozone have extended previous work on these systems. In the case of nitrogen peroxide it has been shown that oxygen molecules possessing the entire exothermicity of the reaction in the form of vibrational energy are produced. A new class of reactions is reported in which vibrationally excited hydroxyl radicals are produced under isothermal conditions by the reaction $O(^1D) + RH \rightarrow OH^* + R$, in which the energy for excitation is contributed by the electronic energy of the oxygen atom.

These and other cases of non-equilibrated energy distributions in reaction products and theories accounting for this phenomenon are reviewed.

The first clear indication that the energy distribution in a chemical reaction between an atom and a polyatomic molecule can differ appreciably both from equipartition and from the Maxwell–Boltzmann law was obtained by McKinley, Garvin, and Boudart (8), who showed that in the reaction

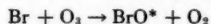$$H + O_3 \rightarrow OH + O_2 \qquad + 80 \text{ kcal}$$
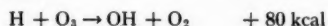
the hydroxyl radical was produced with up to nine quanta of vibrational energy (75 kcal). Soon after, Lipscomb, Norrish, and Thrush (4) detected oxygen molecules with up to eight quanta of vibrational energy (34 kcal) in the isothermal flash photolysis of nitrogen dioxide and chlorine dioxide and showed that these were produced in the reactions

$$O + NO_2 \rightarrow O_2 + NO \qquad + 46 \text{ kcal,}$$

and

$$O + ClO_2 \rightarrow O_2 + ClO_2 \qquad + 61 \text{ kcal.}$$
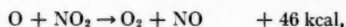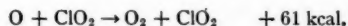
Other examples of this process viz.

$$O + O_3 \rightarrow O_2^* + O_2$$
$$Cl + O_3 \rightarrow ClO^* + O_2$$
$$Br + O_3 \rightarrow BrO^* + O_2$$
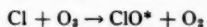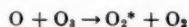
were found by McGrath and Norrish (1, 6, 7) in the flash photolysis of ozone and of chlorine and bromine in the presence of ozone. From these results they arrived at the general conclusion (1) that the exothermic reaction between an atom and a triatomic molecule

$$A + BCD = AB + CD \qquad + Q \text{ kcal}$$
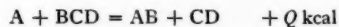
could lead to the accumulation of most of the energy Q in the newly formed bond AB.

More recently, several other examples have been reported by Cashion and Polanyi (2, 13, 14, 15), by Kaufman and Kelso (16), by Dressler (17), and by Thrush (18). These and other examples of this type of reaction are listed in Table I, which shows the exothermicity of the reactions (Q kcal/mole) together with the highest vibrational level observed.

The subject has been reviewed by McGrath and Norrish (1) and discussed from theoretical points of view by Polanyi (2) and by Smith (3). It is the purpose of this paper

TABLE I

| Reaction	Q (kcal)		Highest level observed and energy in kcal/mole	Reference
$O + ClO_2 \rightarrow O_2^* + ClO$	61		$8 = 34$	4
$O + NO_2 \rightarrow O_2^* + NO$	46	(48)?	$\begin{cases} 8 = 34 \\ 11 = 45\frac{1}{2}\ (12 = 49)? \end{cases}$	4 / 5
$O + O_3 \rightarrow O_2^* + O_2$	$\begin{cases} 138 \\ 93 \end{cases}$	$\begin{matrix} O(^1D) \\ O(^3P) \end{matrix}$	$17 = 66\frac{1}{2}$ / $19(?20) = 73$	6,7 / 5
$Br + O_3 \rightarrow BrO^* + O_2$	$\begin{cases} 19 \\ 29\frac{1}{2} \end{cases}$	$\begin{matrix} Br(P^{3/2}) \\ Br(P^{1/2}) \end{matrix}$	$4 = 8$	1, 6
$Cl + O_3 \rightarrow ClO^* + O_2$	$\begin{cases} 40 \\ 42\frac{1}{2} \end{cases}$	$\begin{matrix} Cl(P^{3/2}) \\ Cl(P^{1/2}) \end{matrix}$	$5? = 11$	1, 6
$O + H_2 \rightarrow OH^* + H$	43			
$O + HCl \rightarrow OH^* + Cl$	44			
$O + H_2O \rightarrow OH^* + OH$	29	$O(^1D)$	$2 = 19.8$	5
$O + NH_3 \rightarrow OH^* + NH_2$	45			
$O + CH_4 \rightarrow OH^* + CH_3$	45			
$H + O_3 \rightarrow OH^* + O_2$	80		$9 = 75$	8–12
$H + Cl_2 \rightarrow HCl^* + Cl$	45		$6 = 45$	13, 14
$H + Br_2 \rightarrow HBr^* + Br$	41		$5 = 34$	2
$H + HO_2 \rightarrow OH^* + OH$	38		$1 = 9.9$	15
$N + NO \rightarrow N_2^* + O$	70		$1 = 6.6$	16, 17
$H + F_2 \rightarrow HF^* + F$	98		$9 = 86$	18
$X + Na_2 \rightarrow NaX^* + Na$	$\begin{cases} 81 \\ 71 \\ 54 \end{cases}$	$\begin{matrix} (X = Cl) \\ (X = Br) \\ (X = I) \end{matrix}$		
$Na + ClX \rightarrow NaX^* + Cl$	$\begin{cases} 52? \\ 39? \\ 53? \end{cases}$	$\begin{matrix} (X = Cl) \\ (X = Br) \\ (X = I) \end{matrix}$	At least $48\frac{1}{2}$	20
$Na + HgX \rightarrow NaX^* + Hg$	$\begin{cases} 75 \\ 71? \end{cases}$	$\begin{matrix} (X = Cl) \\ (X = Br) \end{matrix}$		

to discuss various aspects of the production of vibrationally excited molecules in the reaction between an atom and a molecule in the light of our more recent results, which will now be briefly reported.

In the flash photolysis of ozone in the presence of ammonia, hydrogen, hydrogen chloride, methane, and water under isothermal conditions, we have observed in each case vibrationally excited hydroxyl radicals. So far, only the first and second excited levels have been detected, but further work is in progress. We suggest that the reaction in which they are produced is of the type

$$O(^1D) + RH \rightarrow OH^* + R.$$
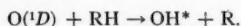
These reactions are of particular interest for two reasons. Firstly, methane and ammonia provide the first examples of this type of reaction involving molecules more complex than triatomic and, secondly, because it is the first time that the electronic energy of the approaching atom has been shown to appear as vibrational energy of the product in otherwise thermoneutral or endothermic reactions. It should be noted that, though in the photolysis of ozone the reaction

$$O(^1D) + O_3 \rightarrow O_2^* + O_2$$
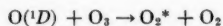
has been shown to be responsible for the production of O_2^*, the degree of vibrational excitation so far observed can be accounted for without involving the electronic energy. The observation of OH^* in the systems described confirms the place ascribed to the $O(^1D)$ atom in the photolysis of ozone by McGrath and Norrish (7).

The question of the extent to which the heat of reaction in the general case

$$A + BCD \rightarrow AB + CD$$
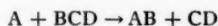
can appear as vibrational energy in the products has interested us for some time. We considered it likely that the species AB could be formed with any allowed vibrational energy up to the maximum. Where the highest permitted vibrational level has not so far been observed, we suspected that this might be a consequence of experimental difficulties. Accordingly, we have started reinvestigating some of the systems previously studied by flash photolysis. In the photolysis of NO_2 and ClO_2 (4) it seemed rather a coincidence that the highest vibrational level of O_2^* observed was 8 in each case though the exothermicities for the reactions

$$O + NO_2 \rightarrow O_2^* + NO$$

and

$$O + ClO_2 \rightarrow O_2^* + ClO$$

differed by 15 kcal.

In preliminary experiments with NO_2, we have now observed the 9th, 10th, and 11th (and 12th?) vibrational levels, the energy of the 11th level being equal to the exothermicity of the reaction. We have also observed very faintly the first and possibly the second vibrationally excited levels of NO, though this has yet to be confirmed.

In further studies on the flash photolysis of ozone, we have been able to observe the 18th and, very faintly, the 19th (and 20th?) vibrational level of O_2^*. Further work on this system is expected to provide evidence in connection with the reaction,

$$O_2^*{}_{(v-7)} + O_3 \rightarrow O(^1D) + 2O_2,$$

which McGrath and Norrish (7) have proposed, to explain the high quantum yield in the photolysis of ozone with ultraviolet radiation. We have also extended observation to shorter wavelengths and have observed the 11th and 10th (9th?) vibrationally excited levels of O_2.

In reactions of the type

$$A + BCD \rightarrow AB + CD \qquad + Q \qquad\qquad\qquad [1]$$
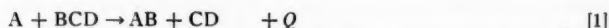
the evidence for the accumulation of most of the energy Q in the bond is thus quite convincing. We believe that the evidence now permits the generalization that, in all exothermic abstraction reactions, the heat of reaction will appear largely as vibrational energy of the products. However, the need for more experimental evidence is apparent and perhaps best illustrated by the fact that no reaction conforming strictly to equation [1] is yet known, B and D being either both hydrogen or oxygen atoms.

There is equally a need for theoretical treatments of the problem and here Polanyi (2) and Smith (3) have made significant contributions. Polanyi's valence bond resonance description of the activated complex ABC in the reaction

$$A + BC \rightarrow AB + C$$
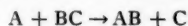
leads to the prediction that almost the entire heat of reaction will appear as vibrational energy of the bond AB. The transition complex is presumed to be most stable when the two resonance forms

$$AB—C$$

and

$$A—BC$$

have equal energy. Since in an exothermic reaction the bond AB is stronger than BC, the internuclear separation AB in the complex will be larger than in the isolated molecule, while the internuclear distance in B—C will be that of the isolated molecule. Since the energy of the complex is generally accepted to be only 5 ± 5kcal greater than of the two resonance forms and assuming that the probability of the transfer of an appreciable amount of energy to C is very small, even when there is a chemical affinity between them, the molecule AB will be formed with very nearly the entire heat of reaction in vibration.

As well as the detection of molecules AB possessing nearly all the heat of reaction as vibrational energy, the most important experimental test of this model is to demonstrate that initially all the molecules are formed in the highest observed vibrational state. So far, in all cases, a distribution of energies has been observed and though, in the case of the reaction studied by Polanyi (14),

$$H + Cl_2 \rightarrow HCl^* + Cl$$
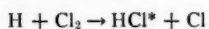
the energy distribution is reported (2) as corresponding qualitatively with a system relaxing from a high vibrational level, there is no certainty that all the HCl is initially formed with $v = 6$. Further, evidence has been furnished by Garvin, Broida, and Kostkowski (12) that in the reaction

$$H + O_3 \rightarrow OH^* + O_2$$
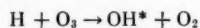
there is an appreciable production in all levels $v < 9$.

Restricted to the case A+BC, this model is a very plausible one and the experimental evidence strongly supports the idea that it is possible for at least some molecules to possess the entire heat of reaction.

It is not immediately apparent to what extent the model applies to the more general case

$$A + BCD \rightarrow AB + CD.$$
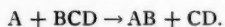
The probability of energy transfer between AB and CD in the transition complex may well be higher in this case, and this could result in the production of some molecules AB with appreciably less than the maximum possible vibrational excitation.

In a molecule of type BCB, the strength of the CB bond is not necessarily the same as in the isolated molecule CB. Where they differ appreciably, as, for example, in ozone, and nitrogen peroxide, a considerable reorganization of the CB bonds must take place when an atom is abstracted. We consider it reasonable to suppose that the ease with which this reorganization takes place could depend on the nature of the molecule BCB and of the atom A and, perhaps more important, on the relative spacial configuration of the atoms at the moment of impact. The effect of this reorganization would be to reduce on the average the amount of energy available for vibrational excitation of the AB molecule, though, in any particular collision, there would always be a definite probability of producing the molecule AB vibrationally excited to the fullest extent. Thus, on this model the observed population of all possible vibrational levels is a consequence of the nature of the reaction itself rather than of deactivation of molecules initially produced entirely in the highest vibrational level. A quantitative estimate of the relative initial population of the various vibrational levels will have to take into account the variation in reaction probability with the direction of approach of the atom relative to the configuration of the molecule BCD and it seems likely that the reaction is most probable when there is the most favorable configuration for maximum vibrational excitation of AB.

For a non-linear molecule BCD, it is reasonable to expect a fraction (not necessarily constant) of the heat of reaction to appear as rotational energy as well as translational energy of AB and CD and this should also be true for an oblique collision of an atom with a linear triatomic molecule. It also seems possible on this model for the molecule CD to be vibrationally excited to some extent.

Smith (3) postulates a definite maximum value for the fraction of the heat of reaction which can appear as vibration. This is limited by a kinematic factor $\sin^2 \beta$, where β is the angle of rotation required to take a co-ordinate system describing the reactants into one suitable for describing the products. The kinematic factor depends only on the masses M_A, M_B, M_C, and M_D of the atoms involved and can be calculated for the reaction

$$A + BC \rightarrow AB + C \left[\tan^2 \beta = \frac{M_B}{M_A} + \frac{M_B}{M_C} + \frac{M_B^2}{M_A M_C} \right]$$

and

$$A + BCD \rightarrow AB + CD \left[\tan^2 \beta' = \frac{M_B}{M_A} + \frac{M_B}{M_C + M_D} + \frac{M_B^2}{M_A(M_A + M_C)} \right].$$
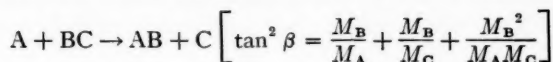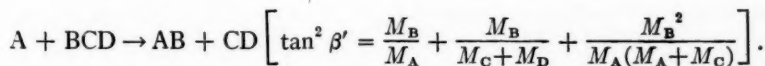
The theoretical maximum value of the fraction of energy appearing as vibration in the second case then lies in the range $\sin^2 \beta' - \sin^2 \beta$, the latter value applying if the influence of D is neglected.

The model is a remarkably simple one and predicts accurately in several cases where good experimental data is available, e.g., 0.96–0.97 for

$$H + O_3 \rightarrow OH^* + O_2$$

and 0.986 for

$$H + Cl_2 \rightarrow HCl^* + Cl$$
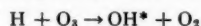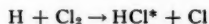
compared with experimental values of 0.94 and 1.0.

He points out that it fails in the case of

$$I + Na_2 \rightarrow NaI^* + Na$$
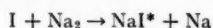
where the predicted value of 0.576 gives the NaI^* molecule insufficient energy for the reactions

$$NaI^* + Na \rightarrow NaI + Na^*$$
$$Na^* \rightarrow Na + h\nu$$
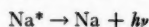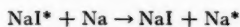
and suggests that there is either some peculiarity in the potential energy surface or the mechanism is in fact

$$Na + I_2 \rightarrow NaI^* + I$$

where $\sin^2 \beta = 0.9$, but this is in disaccord with Evans' and Polanyi's original conclusion (20).

We consider that it again appears inadequate in the reaction

$$O + NO_2 \rightarrow O_2^* + NO$$

where it predicts a maximum value of the vibrational energy of 31–35.2 kcal, agreeing very well with the value of 34 kcal ($v = 8$) previously reported (4). Now that we have observed the 9th, 10th, and 11th vibrational levels, it seems that the agreement was fortuitous in this case. The agreement of theory with experiment in the case of ozone

is again not conclusive, since the evidence is strong in favor of the O atom being in the (^1D) state (7), whereas the exothermicity was calculated for the reaction of the $O(^3P)$ atom. Further, since molecules with more than 17 quanta may react rapidly with O_3 (7) in the reaction

$$O_2{}^* + O_3 \rightarrow O(^1D) + 2O_2$$
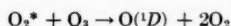
the failure in previous work to detect them spectroscopically was evidence for their taking part in this reaction rather than for their not being produced. As we have shown, the threshold is not sharp and molecules with 18 and more quanta have now been observed.

Finally, the values of $\sin^2 \beta$ for the reactions of the type

$$O(^1D) + RH \rightarrow OH^* + R$$
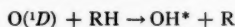
described earlier are insufficient, except in the case of H_2, for the observed production of the vibrationally excited hydroxyl radical.

A third model accounting for the production of vibrationally excited molecules in the reaction

$$A + BCD \rightarrow AB^* + CD$$

has recently been proposed by Simons (21). He visualizes the atom A approaching B with such a velocity that, when A is finally brought to rest relative to B, the internuclear distance of A—B is very short compared with the equilibrium distance, so that on separation the molecule AB is vibrationally hot. The conditions necessary to achieve this are that the B—C bond is weak relative to AB so that dissociation of the complex (ABCD) occurs easily and little of the impact of A on B is transmitted to the C—D bond. There must be also an attractive force between A and B to overcome the normal repulsion of non-interacting particles. This model accounts for the ready production of $O_2{}^*$ in the reactions

$$O(^3P) + NO_2 \rightarrow O_2{}^* + NO$$
$$O(^3P) + ClO_2 \rightarrow O_2{}^* + ClO$$
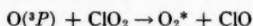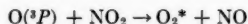
on the basis of electrons pin coupling between the paramagnetic species $O(^3P)$ and NO_2 or ClO_2 resulting in attraction. In the case of ozone, the diamagnetic ozone molecule is considered as a weakly bound complex of $O_2(^3\Sigma)$ and $O(^3P)$. Since the O_2—O bond is weak, the large internuclear distance favors the electron spin coupling. On this model the reaction

$$I + Na_2 \rightarrow NaI^* + Na$$
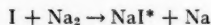
is particularly favored both on account of the low bond energy of the Na_2 molecule and the strong coulombic attraction between Na and I. Only qualitative tests of this model are possible and the author cites the reactions

$$O + SO_2 \rightarrow SO + O_2$$

and

$$O + Cl_2O \rightarrow O_2 + Cl_2$$
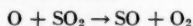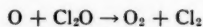
as being cases where the necessary conditions do not obtain, and therefore where vibrationally excited molecules should not be produced. He considers the failure of Oldershaw and Norrish (22) and of Edgecombe, Norrish, and Thrush (23) to observe $O_2{}^*$ in these systems as evidence for the model. In our opinion, a more detailed consideration of the

experimental conditions under which both these reactions could have occurred shows that in neither case could an appreciable concentration of O_2^* have been produced for reasons quite unconnected with the proposed model. Firstly, in the photolysis of SO_2 itself, the oxygen atom produced is necessarily $O(^3P)$ and O_2^* could obviously not be produced in the reaction

$$O(^3P) + SO_2 \rightarrow SO + O_2 \qquad -12 \text{ kcal.}$$
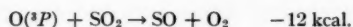
In the photolysis of SO_3, the sequence

$$SO_3 \rightarrow SO_2 + O(^1D)$$

$$O(^1D) + SO_2 \rightarrow O_2 + SO \qquad +33 \text{ kcal}$$
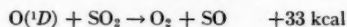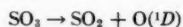
would, we believe, result in the production of O_2^* ($v < 7$) if it occurred. Considering the low absorption coefficient of SO_3 and the possible alternative primary photolysis step

$$SO_3 + h\nu \rightarrow SO + O_2$$
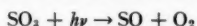
only low concentrations of SO_2 and $O(^1D)$ would be present. It is therefore unlikely that a detectable concentration of O_2^* would be produced in this system even if the reaction itself were efficient. In any case, the oxygen atoms would probably react preferentially with the much larger amount of SO_3 present than with SO_2. One should also take into account that observation below about 2270 Å was particularly difficult in view of the continuous absorption and, at longer wavelengths, transitions from $v'' < 4$ are weak. It would therefore have been difficult to detect a low concentration of O_2^*.

A somewhat stronger case might have been made for failure of the reaction

$$O + SO_3 \rightarrow O_2^* + SO_2$$

to produce a detectable concentration of O_2^*, but even here some of the above arguments still apply and provide a satisfactory explanation which does not involve the inherent unlikelihood of the reaction itself.

In the other example quoted by Simons, the photolysis of Cl_2O, it should be noted that the reaction

$$O + Cl\!-\!O\!-\!Cl \rightarrow O_2 + Cl_2 \qquad +76 \text{ kcal}$$
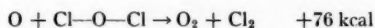
is not of the type $A + BCD$. Requiring the breaking of two bonds, it is easy to visualize that the entire exothermicity of the reaction is not, in any case, available for vibrational excitation of the oxygen molecule.

There are other good reasons accounting for the failure to observe excited species in this system. The primary reaction might well be

$$Cl_2O \overset{h\nu}{\rightarrow} Cl + ClO$$

as well as

$$Cl_2O \rightarrow 2Cl + O$$
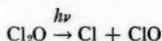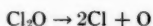
and the oxygen atom concentration may be low and would be further reduced by the reaction

$$O + Cl_2O \rightarrow 2ClO,$$
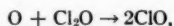
the concentration of ClO^* being below detectable limits.

In our opinion, therefore, the negative evidence from the two systems considered does not test the model proposed by Simons. Objections to it are firstly that the argument he applies to the reaction

$$O + O_3 \rightarrow O_2^* + O_2$$
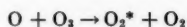
does not seem plausible when the atom involved is the $O(^1D)$ and, secondly, that it appears impossible to reconcile it with the occurrence of the reactions

$$O(^1D) + RH \rightarrow OH^* + R$$
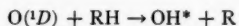
It is profitable to consider further to what extent the available experimental evidence provides tests for theoretical models. The information required is:

1. Conclusive evidence of the reaction in which the vibrationally excited species is produced.

2. Certainty that all the vibrational levels produced have been observed or, failing that, a convincing explanation of the absence of certain levels.

3. The relative populations of the various vibrational levels and this as a function of experimental conditions; in particular, the distribution of vibrational energies in the molecules at the instant of formation and the subsequent variation with time.

4. The presence or absence of vibrational energy in the other species produced in the case of an atom and a polyatomic molecule.

5. Whether the electronic and kinetic energy of the abstracting atom can contribute to the vibrational energy of the bond formed.

The evidence for the proposed mechanism of formation of the excited species in the reactions considered is on the whole quite strong but, in some cases, far from conclusive. Even where the mechanism is well established, it is worth while to re-examine the arguments in favor of the proposed mechanism and to consider alternatives.

The production of O_2^* in the flash photolysis of NO_2 and of ClO_2 provides particularly well-established examples of the reaction

$$O + OXO \rightarrow O_2^* + XO.$$

An alternative mechanism, considered at the time, was that the O_2 molecule was initially formed in the $^1\Delta_g$ or $^1\Sigma_g^+$ electronic states and that the higher vibrational levels of the $^3\Sigma_g^-$ ground state were populated by collision-induced radiationless transitions, or by magnetic dipole radiation. This was rejected on the ground that such transitions, involving the breaking of two selection rules, would be unlikely to occur sufficiently rapidly to account for the results. Whether these rules are relaxed sufficiently in the presence of low pressures of ClO_2 and ClO or of NO_2 and NO is again doubtful, except, possibly, while the configuration approximates closely to the transition complex $(O—O—X—O)$. In the extreme this reduces to the accepted mechanism and could only be distinguished from it if the calculated distribution of vibrational energies differed in the two cases.

In the case of ozone, the evidence (7) strongly supports the proposed mechanism

$$O(^1D) + O_3 \rightarrow O_2^* + O_2 \qquad +138 \text{ kcal.}$$
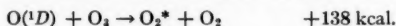
The possibility of the reaction,

$$O(^1D) + O_3 \rightarrow O_2(^3\Sigma_g^-) + O_2(^3\Sigma_u^-) \qquad -3 \text{ kcal,}$$
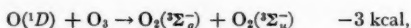
postulated by Benson (24) in connection with a photon-propagated chain decomposition of ozone, is, however, worth considering.

Population of high values of v'' by the process

$$O_2(^3\Sigma_u^-)(v' = 0) \rightarrow O_2(^3\Sigma_g^-)$$
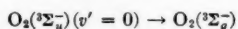
is expected on the Franck–Condon principle and the observed apparent maximum in the

vibrational energy distribution at $v'' = 13$ or 14 may be consistent with this mechanism. The endothermicity of the reaction is not a strong contrary argument in view of a probable low or zero value for the activation energy.

In most cases, vibrational levels corresponding in energy to the full exothermicity of the reaction have not been observed. It seems that the reason for this is more likely to be found in the limitations of present experimental techniques rather than in any fundamental restriction on the proportion of energy which can appear as vibration.

We hope to test this both by further work on systems previously studied by flash photolysis and by investigating new systems. As we have seen, preliminary results in the NO_2 system show that all energetically possible vibrational levels are produced and that the ClO_2 system should be capable of providing a definite test. The ozone system is much more difficult and the evidence available strongly suggests that direct observation of vibrational levels appreciably higher than those already reported is unlikely. On account of the diffuseness of the threshold, it should be possible to follow the decay of molecules with vibrational energy $\geqslant 70$ kcal which seem to participate in the reaction,

$$O_2^*(v'' > 17) + O_3 \rightarrow 2O_2 + O(^1D),$$
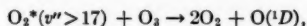
and so provide a direct test of this reaction. So far, only the 18th level has been observed with sufficient intensity for quantitative measurements; but it may be possible to achieve this with the 19th and 20th levels. It is again doubtful whether possible failure to observe vibrational levels higher than the second in the reaction

$$O(^1D) + RH \rightarrow OH^* + R$$
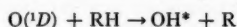
will be theoretically significant because of rapid physical deactivation and chemical reaction. The concentration of molecules in these levels is likely to be small and the low transition probabilities for absorption from those levels makes the systems experimentally difficult.

There is little definite information on the initial distribution of vibrational energy and on its variation with time. In spite of the theoretical advantage of better time resolution in flash photolysis, the only indication that the distribution changes with time is to be found in the observation of Lipscomb, Norrish, and Thrush (4) that the half-lives for the levels with $v'' > 6$, which are slightly shorter than those with $v'' = 6$, which are likewise shorter than those with $v'' < 6$. The same authors concluded from the slow rate of vibrational energy transfer that the energy distribution observed at the shortest time was that actually produced in the reaction. The closely similar distribution for the ClO_2 and the NO_2 systems at the shortest times is equally significant. No marked changes of intensity distribution with time in the case of O_2^* formed from ozone have been reported, though it is evident that in all cases much more detailed information is needed. The experimental difficulties are, however, considerable. It may well be possible to extrapolate the results obtained in flow systems to infinite flow rate and zero pressures and an attempt to do this had been planned (14). Provided that this can be unambiguously correlated with zero time, important information may be expected.

In flash photolysis, completely reliable information could only be expected when the half-life of the excited species is very long compared with the flash times and, except in the case of O_2^* produced in the ClO_2 system, it is not clear that this condition has not so far been met. As well as the errors involved in long extrapolations and the averaging effect if the flashes are comparatively long, the possibility that the initial distribution may be changed by absorption of radiation may have to be considered. The present evidence,

from flash photolysis, incomplete as it is, supports the hypothesis of an initial distribution rather than population of all levels from the highest observed level.

On any model which predicts that, in some collisions, only part of the energy can appear as vibration in AB, the question of whether any part of the excess can appear as vibration in the bond C—D can be considered. The suggestion cannot be directly tested in the case of ozone itself and the presence of ClO^* and NO^* has not been reported in the ClO_2 and NO_2 systems, nor of O_2^*, in the reactions of chlorine and bromine atoms with ozone. In the last-mentioned case, this could be a consequence of the experimental conditions and might also be explained in the case of ClO_2 by the approximate equality of the ClO bond strengths in ClO and ClO_2. In the case of NO_2, the probable rapid deactivation of NO^* by NO_2 and the experimental difficulty of observing a weak NO^* spectrum in the presence of a strong O_2^* spectrum makes the negative evidence of its not having been reported previously inconclusive on this point. The observation of the first and possibly also the second excited vibrational levels of NO in our reinvestigation of this system is also inconclusive, as it has not been possible yet to show definitely how they are produced. The other case where there is evidence of vibrational energy in the bond CD is equally uncertain. Oldershaw and Norrish (22) in the flash photolysis of SO_3 observed bands arising from the levels $v'' = 0, 1, 2$, and 3 of SO, though the system was at near room temperature, and they suggested that this might arise from the reaction

$$O(^1D) + SO_2 \rightarrow SO^* + O_2 \qquad +33 \text{ kcal}$$
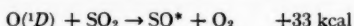
As we have pointed out, this reaction is an unlikely source of a detectable concentration of O_2^*, but it is conceivable that, under their experimental conditions, a probably smaller concentration of SO^* could be observed. It is also possible that SO^* may be produced in the initial photochemical split

$$SO_3 \xrightarrow{h\nu} SO + O_2.$$
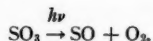
The participation of the electronic energy of the approaching atom in the vibrational energy of the bond formed is an interesting possibility. It can easily be imagined in the case of ozone if the oxygen molecule formed in the excited $^3\Sigma_u^-$ electronic state, but, unfortunately, it cannot be directly proved in this case unless the vibrational energy of the oxygen can be shown to exceed 93 kcal. In the absence of a convenient electronic state, the evidence is limited to the reactions

$$O(^1D) + RH \rightarrow OH^* + R$$

where the energy of vibration must come from the $O(^1D)$ atom if this mechanism is accepted. There seems to be, at present, no evidence for the participation of the kinetic energy of the approaching atom in vibrational excitation, except possibly the observation of the 12th vibrational level of oxygen in the flash photolysis of nitrogen peroxide (5). Recent work (19) has established the first N—O bond strength in NO_2 to be not greater than 71.2 kcal/mole and this makes the exothermicity of the reaction

$$O + NO_2 \rightarrow NO + O_2$$
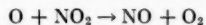
a maximum of 48 kcal, which is insufficient in itself to excite the 12th vibrational level in oxygen (49 kcal/mole).

The production of vibrationally excited species under isothermal conditions both by flash photolysis and the atomic flame technique provides a potentially powerful method for studying vibrational energy transfer and the chemical reactions of these species.

There is reason to believe that endothermic reaction is facilitated if one of the molecules possesses vibrational energy, e.g., in the reactions

$$H + O_2 \rightarrow OH + O \qquad\qquad\qquad [25]$$

$$O_2 + O_2 \rightarrow O + O_3 \qquad\qquad\qquad [26]$$

$$O_2 + O_3 \rightarrow 2O_2 + O(^1D) \qquad -69\,kcal \qquad [27]$$
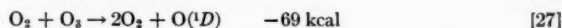
though there is no evidence from the flash photolysis of ozone for the reaction

$$O_2 + O_3 \rightarrow 2O_2 + O(^3P) \qquad -24\,kcal$$
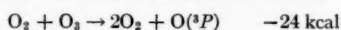
and the effect of this reaction, if it occurs, on the observed population of the various vibrational levels of O_2^* has not been considered in the preceding discussion.

The reaction

$$OH(v'' > 2) + H_2 \rightarrow H_2O + H \qquad +16\,kcal$$

has been proposed by Garvin, Broida, and Kostowsky (12) in the H atom / ozone flame to account for the large increase in line intensities of the upper levels as the mole fraction of hydrogen increases. According to their views, the lower levels, being present in higher concentrations, are preferentially removed, and the upper levels are repopulated by further reaction of the hydrogen atoms with ozone. However, it is not clear if this explanation is satisfactory if, as was reported, the hydrogen atoms were initially present in excess. It is hoped that more evidence will be obtained from a further study of the O_3/RH systems by flash photolysis.

Finally, the field covered by this review is an exciting one and much remains to be done. We are confident that the work now being planned in various laboratories will lead in the near future to a greatly increased understanding of the important fundamental principles involved.

ACKNOWLEDGMENT

REFERENCES

1. W. D. McGrath and R. G. W. Norrish. Z. physik. Chem. 15, 245 (1958).
2. J. C. Polanyi. J. Chem. Phys. 31, 1338 (1959).
3. F. T. Smith. J. Chem. Phys. 31, 1352 (1959).
4. F. J. Lipscomb, R. G. W. Norrish, and B. A. Thrush. Proc. Roy. Soc. A, 233, 455 (1956).
5. N. Basco and R. G. W. Norrish. To be published.
6. W. C. McGrath and R. G. W. Norrish. Proc. Roy. Soc. A, 242, 265 (1957).
7. W. D. McGrath and R. G. W. Norrish. Proc. Roy. Soc. A, 254, 317 (1960).
8. J. D. McKinley, D. Garvin, and M. J. Boudart. J. Chem. Phys. 23, 784 (1955).
9. T. M. Cawthorn and J. D. McKinley. J. Chem. Phys. 25, 583 (1956).
10. F. Kraus. Z. Naturforsch. 12a, 479 (1957).
11. D. Garvin. J. Am. Chem. Soc. 81, 3173 (1959).
12. D. Garvin, H. P. Broida, and H. J. Kostkowski. J. Chem. Phys. 32, 880 (1960).
13. J. K. Cashion and J. C. Polanyi. J. Chem. Phys. 29, 455 (1958).
14. J. K. Cashion and J. C. Polanyi. J. Chem. Phys. 30, 1097 (1959).
15. J. K. Cashion and J. C. Polanyi. J. Chem. Phys. 30, 316 (1959).
16. F. Kaufman and J. R. Kelso. J. Chem. Phys. 28, 510 (1958).
17. K. Dressler. J. Chem. Phys. 30, 1621 (1959).
18. B. A. Thrush. 7th International Symposium on Combustion. 1959. p. 243.
19. H. P. Broida, H. I. Schiff, and T. M. Sugden. To be published.
20. M. G. Evans and M. Polanyi. Trans. Faraday Soc. 35, 178 (1939).
21. J. P. Simons. Nature, 186, 551 (1960).
22. G. A. Oldershaw and R. G. W. Norrish. Proc. Roy. Soc. A, 249, 498 (1958).
23. F. H. C. Edgecombe, R. G. W. Norrish, and B. A. Thrush. Proc. Roy. Soc. A, 243, 24 (1957).
24. S. W. Benson. J. Chem. Phys. 26, 1351 (1957).
25. F. L. Schott and J. L. Kinsey. J. Chem. Phys. 29, 1177 (1958).
26. W. Jost. 7th International Symposium on Combustion. 1959. p. 190.

SEVEN MECHANISMS IN THE PHOTOLYSIS OF NO_2 BETWEEN 3100 AND 3700 Å[1]

HADLEY FORD

ABSTRACT

Nitrogen dioxide has been photolyzed by various investigators under seven different limiting conditions, all at wavelengths between 3100 and 3700 Å. The results are reviewed and discussed in terms of two general mechanisms, both of which quantitatively relate the experimental data. The mechanisms differ in that one postulates that atomic oxygen attacks NO_2 in two ways, yielding NO and O_2 in one case and excited NO_3 in the other. The excited NO_3 can decompose to form atomic oxygen and NO_2; it can be deactivated, or it can react with NO_2. The second mechanism postulates a single mode of attack on NO_2 by atomic oxygen, again yielding excited NO_3. The NO_3 can decompose to form NO and O_2; it can be deactivated, or it can react with NO_2. Of the two mechanisms the first seems more consistent with the thermal reactions of NO_2 and NO_3. It is believed that both the linear and the triangular NO_3 play important roles in the photolysis.

INTRODUCTION

The photolysis of nitrogen dioxide has been investigated (1–7) at various wavelengths of light and with varying pressures of NO_2 and inert gases. Quantum yield measurements are reasonably complete and consistent. It now appears that below 3700 Å atomic oxygen is an important product of the primary photochemical process. This report discusses the photolysis in terms of the following reactions:[2,3]

$$h\nu + NO_2 \rightarrow NO + O \tag{1}$$

$$O + O_2 + M \rightarrow O_3 + M \tag{2}$$

$$O + NO_2 + M \rightarrow NO_3 + M \tag{3}$$

$$O + NO_2 \rightarrow NO_3^* \tag{3a}$$

$$NO_3^* + M \rightarrow NO_3 + M \tag{3b}$$

$$O + NO_3 \rightarrow O_2 + NO \tag{4}$$

$$NO_3^* \rightarrow O_2 + NO \tag{4a}$$

$$NO_3^* \rightarrow NO_2 + O \tag{4b}$$

$$O + NO + M \rightarrow NO_2 + M \tag{5}$$

$$NO_3 + NO \rightarrow 2NO_2 \tag{6}$$

$$O_3 + NO \rightarrow NO_2 + O_2 \tag{7}$$

$$NO_3 + NO_2 \rightarrow N_2O_5 \tag{8}$$

$$N_2O_5 \rightarrow NO_3 + NO_2 \tag{9}$$

$$O + NO_2 + NO_2 \rightarrow O_2 + NO + NO_2 \tag{11}$$

$$NO_3^* + NO_2 \rightarrow O_2 + NO + NO_2 \tag{11a}$$

$$O_3 + NO_2 \rightarrow NO_3 + O_2 \tag{12}$$
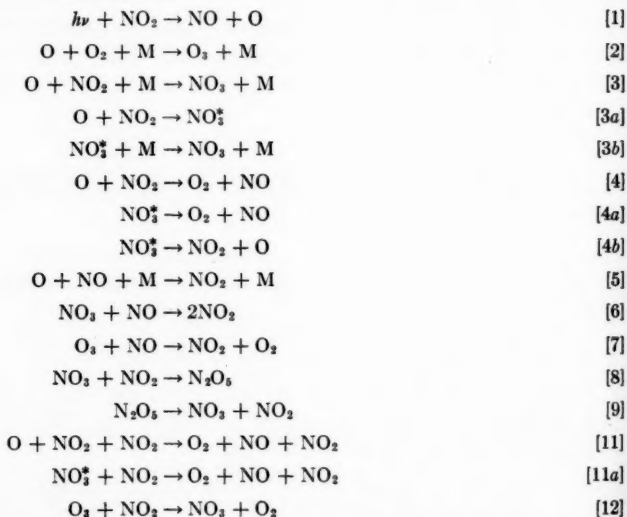
Some of these reactions have been studied by Ford and Endow (6), who obtained the relative rates of reactions [2], [3], [4], and [5]. Using Benson and Axworthy's (9) rate

constant for reaction [2], a quantitative mechanism was proposed. Since then, the rate constants have been measured and reported by others (9–12), and agreement is quantitative within the limits of precision for each rate constant.

Later (7), it was shown that the relative concentration of atomic oxygen calculated from k_1, k_2, k_3, k_4, and k_5 was actually observed over a wide range of concentrations of NO₂, NO, and O₂. This meant that k_3+k_4 was correct, relative to k_2 and k_5. Other work has isolated k_4 from k_3, and the value of k_4 has been independently determined and found to agree with the value previously reported.

As has been emphasized by Leighton and Perkins (13), however, it is possible that none of the assumed reaction mechanisms is precisely correct. It is the purpose of this report to discuss the interrelationships of the various reactions and to show how they relate experimental results in the photolysis of NO₂ below 3700 Å.

Seven mechanisms are discussed which have many steps in common; and, in general, as experimental variables are gradually changed, the shift from one mechanism to another is also gradual. Each mechanism is a special case of a generally satisfactory mechanism. It is assumed in the discussion that in the wavelength region of from 3100 to 3700 Å the mechanisms are not wavelength dependent. Even so, small changes in the primary quantum yield with wavelength would produce small changes in the rate constants.

Because of the great complexity of the many interrelated mechanisms and reactions, the mechanisms are discussed in the order of increasing complexity, rather than decreasing generality. It is believed that this should make for easier reading.

THE PRIMARY PROCESS

The appearance of fluorescence at wavelengths above 3700 Å, but not at shorter wavelengths, led Norrish (14) to the hypothesis that dissociation occurred only on the short-wavelength side of 3700 Å.

$$h\nu + NO_2 \rightarrow NO + O \tag{1}$$

To test this hypothesis Norrish photolyzed NO₂ in the presence of hydrogen, and since water was not produced, he concluded that reaction [1a] was the primary process at all wavelengths.

$$h\nu + NO_2 \rightarrow NO_2^* \tag{1a}$$

Norrish then assumed oxygen was produced by

$$NO^* + NO_2 \rightarrow NO + NO + O_2. \tag{14}$$

This is analogous to a similar reaction in the thermal decomposition of NO₂:

$$NO_2 + NO_2 \rightarrow NO + O_2 + NO. \tag{14a}$$

Light in reactions [1a] and [14] provides the energy for activation which is provided by thermal collisions in reaction [14a]. A rate constant for reaction [14] can be estimated by assuming it is the same as, or greater than, the pre-exponential factor of reaction [14a]. Thus from the data of Rosser and Wise (15)

$$k_{14} \geqslant 3 \times 10^9 \text{ liter mole}^{-1} \text{ sec}^{-1}.$$

The absence of water as noted by Norrish is explained by the extremely small collision yield for the reaction of atomic oxygen with hydrogen when compared with the collision

yield with NO_2. No water would be expected even if reaction [1] proceeded with a quantum yield of unity.

Hall (4), on the other hand, found that when mixtures of isotopically enriched oxygen and normal NO_2 were irradiated at 3130 Å, isotopic scrambling occurred to about the extent expected from the data of Ogg (16). Essentially no scrambling was present at 4047 Å. Hall concluded that reaction [1] was the primary process at 3130 Å and that reaction [1a] was the process at 4047 Å.

Later, Ford and Endow photolyzed NO_2 at 3660 Å, using trace amounts of NO_2 in nitrogen at 1 atm pressure, and found a quantum yield of 0.69 for NO_2 disappearance. Under these conditions

$$NO_2^* + M \rightarrow NO_2 + M \qquad [15]$$

should remove reaction [14] as a possibility. The authors assumed that reaction [1] had a quantum yield of one, and that reaction [3] followed by reaction [6] led to a decreased efficiency, which, by reaction [4], would otherwise have led to $\Phi = 2$ for nitrogen dioxide disappearance.[4] The agreement between the rate constant the authors reported for reaction [3] and that reported by Kaufman (10) for

$$O + SO_2 + M \rightarrow SO_3 + M \qquad [16]$$

$$k_3 = 1.0 \times 10^{11} \text{ liter}^2 \text{ mole}^{-2} \text{ sec}^{-1}$$

$$k_{16} = 3.0 \times 10^{10} \text{ liter}^2 \text{ mole}^{-2} \text{ sec}^{-1}$$

gives credence to the belief that the inefficiency is caused by reaction [3] and not by a decrease in the rate of reaction [1] with increasing pressure.

DISCUSSION OF MECHANISMS

Mechanism I

This is the limiting mechanism for the condition $(NO)/(NO_2) \rightarrow \infty$ in the presence of a third body. The mechanism is given by reactions [1] and [5],[5] which predict a quantum yield of zero. Experimentally, the conditions of mechanism I have been approached by Ford and Endow (6), who found the following relationship when trace amounts of NO_2 were photolyzed in nitrogen at 1 atm pressure:

(A) $$\frac{1}{\Phi_{NO_2}} = 1.45 + 0.178 \frac{NO}{NO_2}.$$

Thus for high values of $(NO)/(NO_2)$, $\Phi_{NO_2} \rightarrow 0$. Since the rate of reaction [5] is now well known (7–12), mechanism I becomes an important source of atomic oxygen at known, low concentrations.

In the limiting case of $(NO)/(NO_2) \rightarrow \infty$ the concentration of atomic oxygen is given by

(B) $$(O) = \frac{KI\Phi(NO_2)}{k_5(NO)(M)}.$$

The absorption coefficient has been measured by Hall and Blacet (17); the light intensity can be measured by any one of several methods, and k_5 has been reported by several investigators.

[4]Φ *is the over-all quantum yield of* NO_2 *disappearance;* Φ_{O_2} *is the over-all quantum yield of oxygen production.*
[5]*Although this is the simplest mechanism discussed, at least one alternative is possible. A discussion of the alternative mechanism is given in ref. 11.*

Author	Reference	k_5
Kaufman	10	2.0×10^{10}
Ford and Endow[6]	7	1.8×10^{10}
Ogryzlo and Schiff	11	1.8×10^{10}
Harteck, Reeves, and Manella	12	2.7×10^{10}

A value of k_5 of 6×10^9 was measured at 900 to 1000° K by Kaufman, Gerri, and Bowman (8), indicating a small, negative temperature coefficient. A value of 4.6×10^{13} calculated from the results of Kistiakowski and Volpi (18) is apparently in error, probably because the equations of a stirred flow reactor were not applicable as had been assumed. Since the values of k_5 of ref. 7, 9, and 10 cover a pressure interval of a few millimeters to 1 atm, the third-body dependence of reaction [5] is well established. Since the rate of reaction [17] is also known (7), reactions [1], [5], and [17] can be used to measure third-body efficiencies in reaction [5].

$$O + cis\text{-}2\text{-pentene} \rightarrow products \qquad [17]$$

Mechanism II

This mechanism represents the low-pressure limit in the photolysis of NO_2. Following photolysis, NO and NO_2 would compete for atomic oxygen in bimolecular reactions. If Kaufman (19) is correct and reaction [5a] occurs only once in 10^7 collisions, restrictions on (NO/NO_2) should not be severe.

$$O + NO \rightarrow NO_2 + h\nu \qquad [5a]$$

The mechanism is given by reaction [1] followed by reaction [4], or alternatively, reaction [1] followed by reactions [3a] and [4a]. Kistiakowski and Volpi (18) reported a lower limit for the rate of reaction [4], which can be compared with that from ref. 7:

$$\text{Kistiakowski and Volpi: } k_4 > 9.5 \times 10^8 \text{ liter mole}^{-1} \text{ sec}^{-1},$$

$$\text{Ford and Endow: } k_4 = 2.1 \times 10^9 \text{ liter mole}^{-1} \text{ sec}^{-1}.$$

Because of the obviously large error in the value of reaction [5] calculated from the work of Kistiakowski and Volpi, the agreement may well be fortuitous. In the absence of presently unknown radiative processes, the conditions of mechanism II should lead to a quantum yield of two.

Mechanism III

Experimental conditions: trace concentrations of nitrogen dioxide, swamping concentrations of oxygen

$$[(NO_2)/(O_2) < 2 \times 10^{-6}]$$

at high third-body pressures (e.g., 1 atm). This condition is frequently found in the lower atmosphere and can be described by reactions [1], [2], and [7]. Since the rates of reactions [2] and [7] are both known (5, 9, 11, and 20) and the rate of reaction [1] can presumably be determined from the light intensity, the concentrations of atomic oxygen, ozone, nitric oxide, and nitrogen dioxide can be calculated for steady state and for approach to steady state. Since the rate of reaction [2] is known with much more accuracy than that

[6]The value of k_2 reported in ref. 7 depends on the method of extrapolation of k_2 from the temperatures used by Benson and Axworthy to room temperature. From Benson and Axworthy $k_2 = 6.00 \pm 0.33 \times 10^7$ exp $(600/RT)$ liter² mole⁻² sec⁻¹; k_2 was obtained by direct substitution of the temperature (300° K) and with no assumption of a temperature dependence in the pre-exponential portion of k_2.

of reaction [7], calculated values of the steady-state concentrations of atomic oxygen should be considerably more accurate than those for ozone. Using Johnston and Crosby's (20) value for k_7 and assuming a primary quantum yield of unity, the ozone concentrations calculated were equal to those observed within a rather large combined experimental error (5).

Mechanism IV

Experimental conditions are the same as for mechanism III except that $(NO_2)/(O_2) > 10^{-6}$. Under these conditions when nitrogen dioxide is photolyzed below 3700 Å, the ozone concentration does not reach a constant steady-state value, but rather rapidly approaches a maximum concentration, and then this quasi-steady-state level gradually decreases. This decay is caused by atomic oxygen attacking nitrogen dioxide and converting the latter into nitric oxide. This, in turn, increases the rate of disappearance of ozone, by reaction [7], and causes the ozone level to decrease gradually. The mechanism, given in the terms of Ford and Endow, is [1], [2], [4], and [7]. In the same terms, reaction [3] followed by reaction [6] can be neglected. The reason for neglecting reactions [3] and [6] is that they have the effect of slightly decreasing the light intensity and not otherwise appreciably affecting the kinetics. Reactions [4] and [7], on the other hand, while proceeding even more slowly than reactions [3] and [6], have a profound effect on the steady-state ozone concentrations. The conditions of mechanism IV are the only known high-pressure conditions under which reaction [4] can be studied independently of reaction [3].

The observed rate of decay of the ozone concentration (17) and mechanism IV confirm that the rate of reaction [4] in nitrogen at 1 atm pressure was that reported by Ford and Endow (6). However, the relative concentrations of atomic oxygen observed in ref. 7 cannot be accounted for by reaction [4] alone. This is confirming evidence for the existence of reaction [3]. In polluted urban atmospheres generally $(NO_2)/(O_2) < 10^{-6}$, so that the conditions of mechanism IV are not met under average conditions.

Since steady-state conditions are not rapidly attained, (O) and (O_3) are functions of time over long time intervals. Atomic oxygen concentrations are given by

$$(C) \qquad (O) = \frac{KI(NO_2)}{k_2(O_2)(M)}$$

provided reaction [2] is fast compared with reactions [3] and [4]. Thus the concentration of atomic oxygen can be calculated if I, (NO_2), and (O_2) are known. The ozone concentration is approximated at any time by

$$(D) \qquad (O_3)_t \cong \frac{KI(NO_2)_t}{k_7(NO)_t}$$

and the rate of change of the steady-state ozone concentration by

$$(E) \qquad \frac{d(O_3)_{ss}}{dt} \cong \frac{KIk_4(O)(NO_2)(NO_2)_1}{k_7(NO)^2} .$$

The decay is slow because reaction [2] leads to a very low concentration of atomic oxygen. Reference 21, which will be published, discloses a more elegant approximation to the rate of ozone decay by this mechanism.

Mechanism V

Experimental conditions are the same as for mechanism III but with ozone added in trace amounts. The effect of added ozone on ozone formed during photolysis can be

explained only if reactions [1], [6], [7], [8], [9], and [12] are considered. Reaction [2] can be assumed to be fast (22). In this case the rate at which ozone is formed is given by reaction [1], which is known, and its rate of disappearance by reactions [7] and [12]. The over-all effect of photolysis is to suppress the ozone – nitrogen dioxide reaction. This is shown by the cancellation of all species in the following reactions:

$$h\nu + O_2 + NO_2 \rightarrow O_3 + NO \qquad\qquad [1a]$$

$$O_3 + NO_2 \rightarrow O_2 + NO_3 \qquad\qquad [12]$$

$$NO_3 + NO \rightarrow 2NO_2 \qquad\qquad [6]$$

The extent of this suppression was used to measure $k_6 k_8/k_9$. Since k_8/k_9 is the equilibrium constant for the dissociation of nitrogen pentoxide, k_6 can be calculated using the value of K_{eq} reported by Schott and Davidson (25). Thus $k_6 K_{eq} = 0.44$ sec^{-1} is in reasonable agreement with the value of 1.0 sec^{-1} reported by Hisatsune, Ogg, and Crawford (23). This agreement gives quantitative confirmation of the validity of mechanism V. The resulting derived value of k_6 is 3.4×10^9 liter mole^{-1} sec^{-1}.

Mechanism VI

This is the mechanism for the photolysis of nitrogen dioxide for conditions most frequently used and not involving trace reactant concentrations (1–4). The mechanism covers the millimeter pressure range for nitrogen dioxide with and without added inert gases. The following experimental facts must be explained:

1. In the millimeter pressure range the quantum yield of nitrogen dioxide disappearance[7] is constant and nearly equal to 2 (1–4).

2. In the photolysis of NO₂ in the millimeter pressure range the reciprocal of the quantum yields (either oxygen formation or nitrogen dioxide disappearance) is proportional to the pressure of added inert gas. Hall (4) has shown that

$$1/\Phi_{O_2} = 1 + k(M).$$

3. At atmospheric pressure of inert gas, the quantum yield decreases with decreasing concentrations of NO₂, extrapolating to a finite value as (NO₂) → 0, as shown by the data of refs. 4 and 6.

4. In the photolysis of NO₂ in the millimeter pressure range, the concentration of atomic oxygen is independent of the pressure of added inert gas. Proof of this seems definite if indirect. This conclusion is drawn from the data of Cvetanović (24), who photolyzed mixtures of *cis*-2-pentene, nitrogen dioxide, and nitrogen. Such directly found products as *cis*- and *trans*-β-pentene oxide formed at a rate which was independent of the pressure of added nitrogen over the internal of 0–400 mm. It is probable that the *cis*-2-pentene formed the oxides as a result of attack by atomic oxygen.

The facts can be explained by a variety of mechanisms, some of which can be ruled out on other grounds. The mechanism proposed by Ford and Endow for their conditions should be considered since their mechanism, consisting of [1], [3], [4], and [6], appears to yield quantitatively valid results.

Thus,

(F) $$1/\Phi_{O_2} = 1 + k_3(M)/k_4.$$

This is in the form reported by Hall. If it is assumed that NO₂, CO₂, and N₂ all have about the same efficiency as a third body, then from ref. 6,

(G) $$1/\Phi_{O_2} = 1 + 2.6 \times 10^{-3} P_{NO_2,CO_2,N_2}$$

[7]*This assumes the previously mentioned stoichiometry:* $2NO_2 \rightarrow 2NO + O_2$.

where the pressure is given in millimeters of mercury. Assuming quantum yield measurements are precise to within 10%, the effect of NO_2 pressure on the quantum yield would not be noticeable below 20 mm of NO_2. For CO_2 and propane being used as inert gases, the data from the work of Hall is shown in Fig. 1. The line calculated, using Ford and
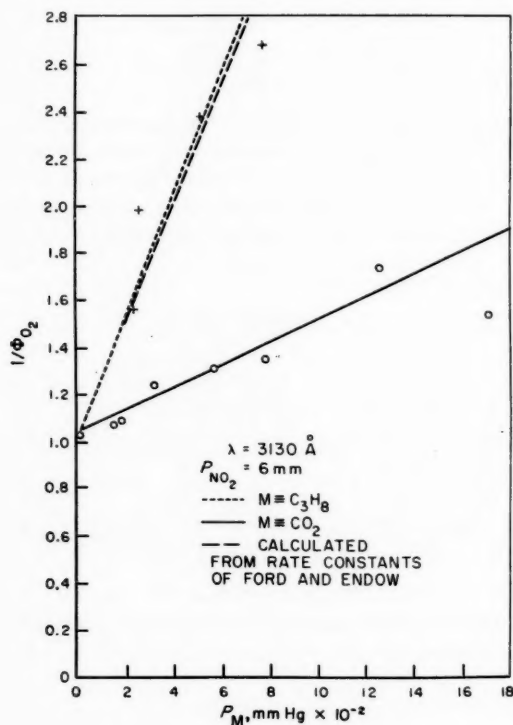
FIG. 1. Recpirocal quantum yield of oxygen appearance as a function of the pressure of added CO_2 and C_3H_8 from the data of hall.

Endow's values for k_3 and k_4 where nitrogen was used as a third body, is shown for comparison. It is obvious that CO_2 is not as efficient a third body as might reasonably have been expected from the rate constants of Ford and Endow and the mechanism given above. The mechanism predicts that the dependence of the quantum yield on added inert gas would be independent of the NO_2 concentration. This prediction is contrary to experimental results. Furthermore, according to this mechanism, the concentration of atomic oxygen is pressure dependent,

(H)
$$(O) = \frac{KI}{k_3(M)+k_4},$$

neglecting the case where large amounts of NO are present and reaction [5] is important. With the values of k_3 and k_4 reported by Ford and Endow, the concentration of atomic oxygen would decrease by a factor of two in going from 0 mm to 400 mm of N_2. This is contrary to the observations of Cvetanović (24).

The facts can be explained by at least two mechanisms which have several steps in common. The two mechanisms are given below for direct comparison:

Mechanism VIA

$$h\nu + NO_2 \rightarrow NO + O$$
$$O + NO_2 \rightarrow NO_3^*$$
$$NO_3^* + NO_2 \rightarrow NO + O_2 + NO_2$$
$$NO_3^* + M \rightarrow NO_3 + M$$
$$NO_3^* \rightarrow NO + O_2$$

Mechanism VIB

$$h\nu + NO_2 \rightarrow NO + O$$
$$O + NO_2 \rightarrow NO_3^*$$
$$NO_3^* + NO_2 \rightarrow NO + O_2 + NO_2$$
$$NO_3^* + M \rightarrow NO_3 + M$$
$$NO_3^* \rightarrow NO_2 + O$$
$$O + NO_2 \rightarrow O_2 + NO$$
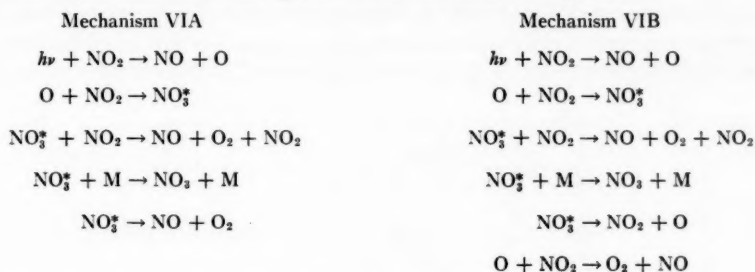
The remaining steps, consisting of reactions [2], [5], [6], [7], [8], [9], and [12], would be common to both mechanisms. If the usual steady state can be assumed for NO_3, mechanism VIA gives

(I)
$$1/\Phi_{NO_2} = 1/2 + \frac{\frac{1}{2}k_{3b}(M)}{k_{4a} + k_{11a}(NO_2)}$$

or

(J)
$$1/\Phi_{O_2} = 1 + \frac{k_{3b}(M)}{k_{4a} + k_{11a}(NO_2)}.$$

So far as is known, the quantum yields at high pressures (e.g., 1 atm) decrease with decreasing NO_2 concentration and approach a finite value as $(NO_2) \rightarrow 0$. Equations (I) and (J) give the correct pressure dependence and the correct quantum yield at low third-body pressure.

Quantatively the significance of mechanism VIA can be seen from the work of Hall (4). Besides obtaining the data represented in Fig. 1, Hall measured the quantum yields of O_2 appearance at 1 atm total pressure of propane and at various partial pressures of NO_2. A summary of his data is given below:

Condition	$2\Phi_{O_2} = \Phi_{NO_2}$
1 atm CO_2, 6 mm NO_2	1.4
1 atm propane, 6 mm NO_2	0.7
1 atm propane, $P_{NO_2} \rightarrow 0$	0.2

The value of 0.2 was extrapolated from Hall's data by the author. From this data and equation (J)

$$k_{3b}(C_3H_8)_{1\ atm} = 9.0k_{4a},$$
$$k_{11a}(NO_2)_{6\ mm} = 3.8k_{4a},$$
$$k_{3b}(CO_2)_{1\ atm} = 1.9k_{4a},$$
$$k_{3b}(N_2)_{1\ atm} = 1.9k_{4a} \text{ (see ref. 7)}.$$

If the mechanism is correct, CO_2 and N_2 are equally effective in deactivating excited NO_3. The pressure dependence of the quantum yield at constant NO_2 concentration and the dependence of the quantum yield on the concentration of NO_2 at 1 atm total pressure of propane give the same ratio for k_{11a} to k_{4a} within experimental error. At least formally,

the assumed mechanism and measured rate constants determine the quantum yield for all pressures of CO_2, N_2, and propane and for all concentrations of NO_2, provided the system is at room temperature and the concentrations are in the regions that have been most frequently studied. The dependence of the quantum yields on third-body pressure and on NO_2 concentration at 1 atm pressure of added gas are given in Figs. 2 and 3.
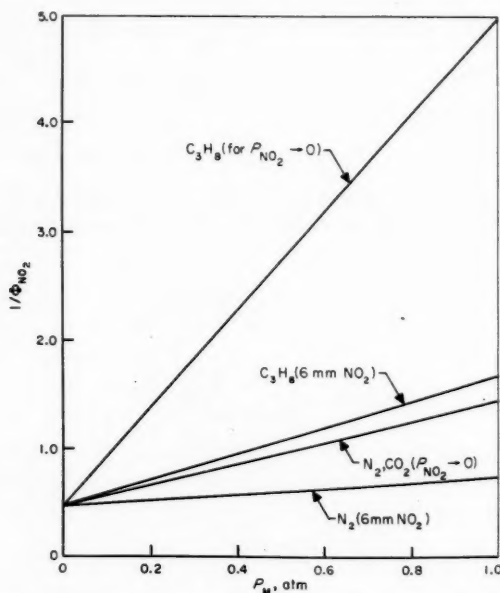
FIG. 2.   Reciprocal quantum yields of NO_2 disappearance as a function of pressure of added gas.
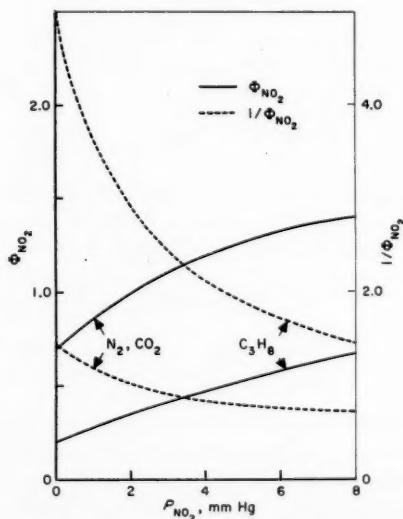
FIG. 3.   Quantum yields of NO_2 disappearance as a function of NO_2 partial pressure.

In the absence of appreciable amounts of NO or O_2 the concentration of atomic oxygen is simply KI/k_{3a}, and therefore independent of pressure, as required.

Mechanism VIB requires one more reaction than VIA, gives less clear-cut results, and requires more assumptions but nevertheless seems to be the more convincing of the two mechanisms. In the absence of appreciable NO and O_2, and making the reasonable assumption that $k_{3c} \gg k_{3b}(M)$

$$\text{(K)} \qquad \frac{1}{\Phi_{NO_2}} = 1/2 + \frac{\frac{1}{2}k_3(M)}{k_4 + [k_4 + k_{3a}][k_{11a}/k_{3c}](NO_2)} .$$

To fit the data of Hall to that of Ford and Endow

$$\text{(L)} \qquad [k_4 + k_{3a}]k_{11a}/k_{3c} = 2.6 \times 10^{13} \text{ liter}^2 \text{ mole}^{-2} \text{ sec}^{-1}.$$

At trace concentrations equation (K) reduces to the form given by the mechanism of Ford and Endow,

$$\text{(M)} \qquad \frac{1}{\Phi_{NO_2}} = 1/2 + \frac{k_3(M)}{2k_4} .$$

Thus, in fitting the two sets of data no changes are required in the values of k_3 and k_4 reported by the latter authors. This means that k_4 in equation (K) is known, leaving three unknowns in the one equation. The quantity, k_{3a}, is probably of the order of 5×10^{11} liter mole^{-1} sec^{-1} so that $k_4 \ll k_{3a}$. Or $k_{11a}/k_{3c} \cong 50$. A unimolecular decomposition of a diatomic molecule that might be of the order of 10^{13} sec^{-1}, whereas k_{3c} might be estimated at 10^9.

In this case $k_{11a} = 5 \times 10^{10}$ compared with a pre-exponential factor of 4×10^9 for the equivalent thermal reaction. It is, of course, easy to speculate about the relative values of the rate constants in equation (L), but the important point is that neither rate constants nor simple rate constant ratios can be calculated from available experimental data without additional assumptions. Quantum yields can be calculated and give the same dependence on pressure as shown by mechanism VIA (Fig. 2). Both mechanisms (VIA and VIB) can be used to calculate the dependence of the quantum yields on NO_2 concentration at 1 atm pressure of inert gas (Fig. 3).

For low concentrations of O_2 and NO, and for $k_{3b}(M) \ll k_{3c}$ the atomic oxygen concentration has the following dependence based on mechanism VIB:

$$\text{(N)} \qquad \text{(O)} = \frac{KI[k_{3c} + k_{11a}(NO_2)]}{k_4 k_{3c} + k_{11a}[k_{3a} + k_4]} .$$

Thus, the concentration of atomic oxygen is not pressure dependent. The two mechanisms will be considered in more detail following a discussion of mechanism VII.

Mechanism VII

This mechanism is based on a study of the photolysis of nitrogen dioxide at trace concentrations in nitrogen at atmospheric pressure and with varying amounts of added oxygen, nitric oxide, and *cis*-2-pentene. The latter was used as a tracer for atomic oxygen (6, 7). The mechanism incorporates reaction [5] into the general scheme and permits quantitative evaluation of the rate of reactions [3], [4], and [5], or, alternatively, [3a]

and [5] from Benson and Axworthy's rate constant for reaction [2]. Under the experimental conditions, all reactions except perhaps [11a] were playing a significant role. Quantum yield measurements were delayed so that reactions [6], [7], [8], [9], and [12] would have gone to completion. Therefore the significant steps in interpreting the experimental results are either reactions [1], [2], [3a], [3b], [4a], and [5], or [1], [2], [3], [4], and [5]. The latter mechanism was proposed by Ford and Endow and is consistent with mechanism VIA.

Experimentally, Ford and Endow found that $1/\Phi_{NO_2}$ was proportional to $(NO)/(NO_2)$ and to $(O_2)/(NO_2)$, and they measured the proportionality constants. Extrapolating $(NO)/(NO_2)$ and $(O_2)/(NO_2)$ to zero separately, they obtained a limiting quantum yield of 0.69 for NO_2 disappearance. The following relation was derived:

$$\text{(O)} \qquad 1/\Phi_{NO_2} = 1/2 + \frac{k_3(M)}{2k_4} + \frac{k_5(M)(NO)}{2k_4(NO_2)} + \frac{k_2(M)(O_2)}{2k_4(NO_2)},$$

based on reactions [1], [2], [3], [4], and [5]. An analogous expression, based on reactions [1], [2], [3a], [3b], [4a], and [5] is given by

$$\text{(P)} \qquad 1/\Phi_{NO_2} = 1/2 + \frac{k_{3b}(M)}{2k_{4a}} + \frac{(k_{4a}+k_{3b})k_5(NO)(M)}{2k_{4a}k_{3a}(NO_2)} + \frac{(k_{4a}+k_{3b})k_2(O_2)(M)}{2k_{4a}k_{3a}(NO_2)}.$$

At low values of $(NO)/(NO_2)$ and $(O_2)/(NO_2)$

$$\text{(Q)} \qquad 1/\Phi_{NO_2} = 1.45 = \frac{k_{4a}}{k_{3b}(M)}.$$

Also

$$\text{(R)} \qquad \frac{k_5(M)[k_{4a}+k_{3b}(M)]}{k_{4a}k_{3b}} = 1.33 \times 10^{-3}$$

and

$$\text{(S)} \qquad \frac{k_2(M)[k_{4a}+k_{3b}(M)]}{k_{4a}k_{3b}} = 0.36.$$

From these ratios and Benson and Axworthy's rate constant k_2, the value of k_{3a} can be calculated:

$$k_{3a} = 6.0 \times 10^9 \text{ liter mole}^{-1} \text{ sec}^{-1}.$$

Beyond that, the data only give the ratio of k_{4a} to k_{3b}.

From the mechanism (reactions [1], [2], [3a], [3b], [4a], and [5]):

$$\text{(T)} \qquad k_4 = \frac{k_{4a}k_{3a}}{k_{4a}+k_{3b}(M)},$$

$$\text{(W)} \qquad k_3 = \frac{k_{3a}k_{3b}}{k_{4a}+k_{3b}(M)},$$

$$\text{(X)} \qquad k_{11} = \frac{k_{3a}k_{11a}}{k_{4a}+k_{3b}(M)}.$$

Thus k_{3a} is the low-pressure limit of k_4. The variations of k_4, k_3, and k_{11} as functions of the third-body pressure and of the pressure of NO_2 are given in Figs. 4 through 7.
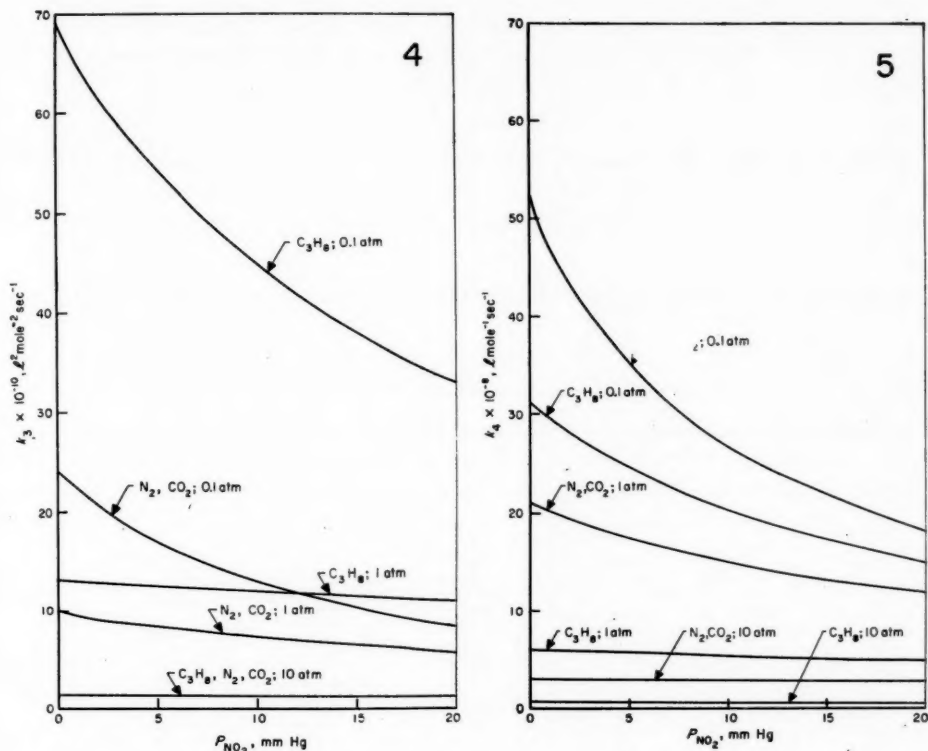
FIG. 4. Dependence of k_3 on NO_2 partial pressure at various partial pressures of matrix gas.
FIG. 5. Dependence of k_4 on NO_2 partial pressure at various partial pressures of matrix gas.

As it turns out, k_3, as given is constant with mechanism VIA. However, k_3 has a different definition consistent with VIB.

(Y)
$$k_3 = \frac{k_{3a}k_{3b}}{k_{4b}+k_{3b}(\mathrm{M})}.$$

For the usual case $k_{4b} \gg k_{3b}(\mathrm{M})$ the three-body recombination reaction would have the usual form, and k_3 would be independent of pressure in the region of interest.

In both equations (W) and (Y) the steady-state concentration of NO_3^* was calculated neglecting reaction [11a], and consequently k_3 is a limiting value as $(NO_2) \to 0$.
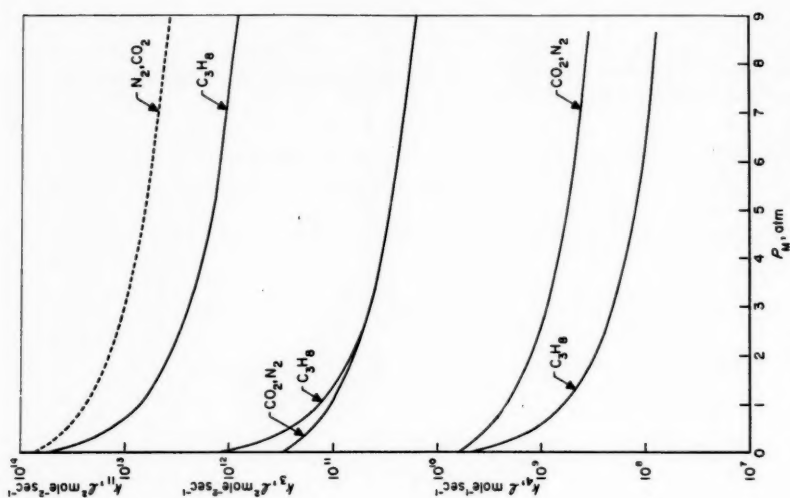
FIG. 7. Effective values of k_3, k_9, and k_{11}, based on the assumption that the excited-molecule mechanism is correct, for the case of $NO_2 \rightarrow 0$.
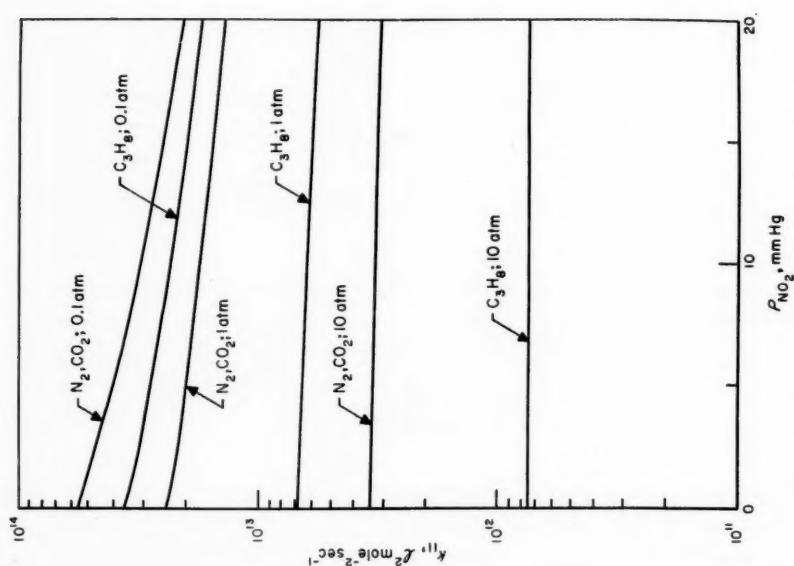
FIG. 6. Dependence of k_{11} on NO_2 partial pressure at various partial pressures of added gas.

DISCUSSION

The difficulties and ambiguities in the mechanism can be summarized with the question: What happens when atomic oxygen attacks NO_2? The photolysis of NO_2 provides no definite answer. The situation can be somewhat clarified by considering other reactions of NO_2. Thus Schott and Davidson (25) agree with Ashmore and Levitt (26) that both of the following reactions occur in the thermal decomposition of NO_2:

$$NO_2 + NO_2 \rightarrow 2NO + O_2 \qquad [10]$$

$$NO_2 + NO_2 \rightarrow NO_3 + NO \qquad [13]$$

Similarly Huffman and Davidson (27) agree with Johnston (28) that the following reactions are important in the thermal decomposition of N_2O_5:

$$NO_3 + NO_2 \rightarrow NO + O_2 + NO_2 \qquad [14]$$

$$NO_3 + NO_2 \rightarrow N_2O_5 \qquad [8]$$
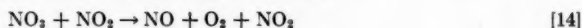
It is therefore of interest that Ford and Endow also postulated two reactions of atomic oxygen with NO_2:

$$O + NO_2 \rightarrow O_2 + NO \qquad [4]$$

$$O + NO_2 + M \rightarrow NO_3 + M \qquad [3]$$

The following appears to be a reasonable explanation of these reactions. When O, NO_2, or NO_3 attack NO_2, the approach to the NO_2 can follow either of two paths. The activated complex for each of the above cases would then be of the forms given below:

Reaction No.	Activated complex	Subsequent intermediate
[10]	ONOONO	OONO
[13]	ONON$_O^O$	
[14]	$_O^O$NOONO	OONO
[8]	$_O^O$NON$_O^O$	
[4]	OONO	OONO
[3]	ON$_O^O$	

When the activated complex is of the peroxy form, decomposition either occurs to give OONO or O_2 and NO. Evidence for the peroxy form of NO_3 has been found by Benson (29), who has shown that the activation energy of [14] is less than the endothermicity by about 2 kilocalories. Benson explains this by a two-step process:

$$_O^O NO + ONO \rightarrow ONO + OONO \qquad [15]$$

$$OONO + M \rightarrow O_2 + NO + M. \qquad [16]$$
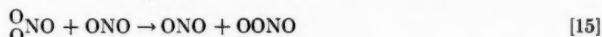
Reaction [14] would be unusual as an elementary reaction because NO_2 is both a reactant and a product. According to this explanation, reaction [14] is composite, the first step consisting of an abstraction reaction which results in the peroxy form of NO_3. A similar explanation applies to the attack of atomic oxygen and NO_2 on NO_2.

In distinguishing between mechanisms, it would seem that [4b] is much more probable than [4a]. An attack on NO_2 by atomic oxygen by two paths rather than one has a geometrical and structural basis, and is analogous to the other reactions mentioned above. In the opinion of the author mechanism VII and the equivalent mechanism VIB best conform to our present understanding of the chemistry of NO_2.

REFERENCES

1. H. H. HOLMES and F. DANIELS. J. Am. Chem. Soc. 56, 630 (1934).
2. R. G. DICKINSON and W. P. BAXTER. J. Am. Chem. Soc. 50, 774 (1928).
3. R. G. W. NORRISH. J. Chem. Soc. 51, 1158 (1929).
4. T. C. HALL, JR. Ozone catalysis of isotope exchange between molecular oxygen species. Ph.D. dissertation, University of California, Los Angeles. October, 1953.
5. H. W. FORD, G. J. DOYLE, and N. ENDOW. J. Chem. Phys. 26, 1337 (1957).
6. H. W. FORD and N. ENDOW. J. Chem. Phys. 27, 1156 (1957).
7. H. W. FORD and N. ENDOW. J. Chem. Phys. 27, 1277 (1957).
8. F. KAUFMAN, N. J. GERRI, and R. F. BOWMAN. J. Chem. Phys. 25, 106 (1956).
9. S. W. BENSON and A. E. AXWORTHY. J. Chem. Phys. 26, 1718 (1957).
10. F. KAUFMAN. J. Chem. Phys. 28, 352 (1958).
11. E. A. OGRYZLO and H. I. SCHIFF. Can. J. Chem. 37, 1690 (1959).
12. P. HARTECK, R. R. REEVES, and G. MANNELA. J. Chem. Phys. 26, 1333 (1957).
13. P. A. LEIGHTON and W. A. PERKINS. Photochemical secondary reactions in urban air. Rept. No. 24. Air Pollution Foundation, San Marino, California. August, 1958.
14. R. G. W. NORRISH. J. Chem. Soc. 51, 1604 (1929).
15. W. A. ROSSER, JR. and H. WISE. J. Chem. Phys. 24, 493 (1956).
16. R A. OGG and W. T. SUTPHEN. J. Chem. Phys. 21, 2078 (1953).
17. T. C. HALL and F. E. BLACET. J. Chem. Phys. 21, 1745 (1952).
18. G. B. KISTIAKOWSKY and G. G. VOLPI. J. Chem. Phys. 27, 1141 (1957).
19. P. KAUFMAN. Proc. Roy. Soc. A, 247, 123 (1958).
20. H. S. JOHNSTON and H. J. CROSBY. J. Chem. Phys. 22, 689 (1954).
21. H. W. FORD, G. J. DOYLE, and N. ENDOW. The reaction of atomic oxygen with nitrogen dioxide. To be published.
22. H. W. FORD, G. J. DOYLE, and N. ENDOW. J. Chem. Phys. 32, 1256 (1960).
23. I. C. HISATSUNE, R. A. OGG, JR., and B. CRAWFORD, JR. J. Am. Chem. Soc. 79, 4648 (1957).
24. S. SATO and R. J. CVETANOVIĆ. Can. J. Chem. 37, 953 (1959).
25. G. SCHOTT and N. DAVIDSON. J. Am. Chem. Soc. 80, 1841 (1958).
26. P. G. ASHMORE and B. P. LEVITT. Research (London), 9, S25 (1956).
27. R. E. HUFFMAN and N. DAVIDSON. J. Am. Chem. Soc. 81, 2311 (1959).
28. H. S. JOHNSTON. J. Am. Chem. Soc. 73, 4542 (1951).
29. S. W. BENSON. The foundations of chemical kinetics. McGraw-Hill, New York. 1960; and private communication.

THE PRODUCT EMITTER DIFFUSION FLAME:
THE REACTION OF NITRIC OXIDE WITH OXYGEN ATOMS[1]

DAVID GARVIN, PAUL P. GWYN, and JULES W. MOSKOWITZ

ABSTRACT

The use of the Polanyi diffusion flame technique as a diagnostic test for the identification of reactions that lead to light emission is presented. There is developed the mathematical model needed for the interpretation of such flames in which a product is responsible for the emission that is studied. The method is applied to the systems in which oxygen atoms and nitrogen atoms react with nitric oxide. The rate constant of the reaction $O + NO + M \rightarrow NO_2 + M$ at $293°$ K was determined as $k = 1.4 \times 10^{17}$ $(cc/mole)^2$ sec^{-1}.

INTRODUCTION

The Polanyi diffusion flame technique has been used numerous times for the measurement of rates of very fast reactions (1–5). It is applied here to a system in which several reactions of nitric oxide occur, both to determine rates and as a diagnostic tool to determine the probable reaction, which is studied directly. In part, this paper presents an experimental confirmation for the mechanism of the 'airglow' or 'oxygen afterglow' that has been identified and studied intensively in the past few years (6–10), and, in addition, there is presented the model needed for the interpretation of diffusion flames in which a product is the emitting species. This model is applied to a determination of the rate of the O+NO reaction as it may be studied in two systems. Finally, there are reported several qualitative observations on related reactions.

DIAGNOSTIC STUDIES

It is usually essential that the elementary reactions that are studied by the diffusion flame technique be established by some independent means. In some cases an a priori knowledge of the possible reactions is sufficient, and in others product analysis is helpful. In any case, such information is needed for the interpretation of the experiments because the lifetime or spatial distribution of a very reactive species is used as the basis for the quantitative measurements.

The special geometry of the diffusion flame system imposes severe conditions on the reactions that can be studied: they must be very fast, i.e., occur at least once in 10^5 collisions, and must be homogeneous. In this method one reagent (y) is fed in small amounts through an orifice into a low pressure atmosphere containing its reaction partner (z) in considerable excess. At the low pressures employed y penetrates the atmosphere principally by diffusion and reacts with z before reaching any wall surface.

If, in a given system, one reaction leads to immediate emission of light, and the spatial distribution of this emission is to be studied, the particular reaction that is responsible for it can be identified by employing as y and z the possible reactant pairs in the system. The light-emitting reaction will give a small, well-defined zone of emission near the orifice while the other reactions will give, at best, a diffuse emission throughout the reactor. Where several sets of reagent pairs lead to emission, other criteria (such as rate and spectral studies) must also be used.

A favorable case for the application of this type of test is the system in which nitric oxide may react either with oxygen or nitrogen atoms. The following reactions have been shown to be important.

$$O + NO \rightarrow NO_2^* \tag{1}$$

$$NO_2^* \rightarrow NO_2 + h\nu \tag{2}$$

$$O + NO_2 \rightarrow O_2 + NO \tag{3}$$

$$N + NO \rightarrow N_2 + O \tag{4}$$

$$N + NO_2 \rightarrow NO + NO \tag{5}$$

$$\rightarrow N_2 + O_2 \tag{6}$$

The rate of [1] has been determined independently by Kaufman (8) and by Harteck, Reeves, and Mannella (10). NO_2 is the probable emitter, but has not been positively identified. Reaction [3] has been studied by the flash photolysis technique and an excited oxygen molecule shown to be a primary product (11). Dressler (12) found evidence for [4] in the nitrogen 'afterglow', the nitrogen molecule being in an excited state. Also, limited emission of the oxygen 'afterglow' (1) in systems containing nitrogen atoms and nitrogen dioxide require consideration of reactions [5] and [6]. The sequence [1], [2], [3] is generally considered to explain the long-lived 'afterglow' in impure oxygen in which traces of NO are produced along with much larger quantities of oxygen atoms by an electric discharge.

TABLE I

Observations of reaction zones in systems related to the NO–O reaction

	Nozzle reagent	Atmosphere	Appearance of reaction zone
(a)	$O + O_2$	Air	Diffuse glow throughout reactor
(b)	NO	$O + O_2$	Diffuse glow throughout reactor
(c)	$O + O_2$	NO (excess)	Stable flame, small zone near nozzle
		NO + N_2	
(d)	$O + O_2$	NO_2 (excess)	No glow
(e)	$O + O_2$	NO_2 (limited)	Glowing zone with dark center
(f)	N + N_2 (active nitrogen)	N_2	Active nitrogen color, difficult to restrict
(g)	N + N_2	NO (excess)	Stable flame, spectrum same as that of (c)
(h)	N + N_2	NO_2	No zone, active nitrogen color diminished

Table I summarizes a number of observations made on these reactions using the usual diffusion flame arrangement. The behavior of (c) and (b) are consistent with the oxygen 'afterglow' mechanism. Reactions (d) and (e) agree with results found in oxygen atom titration experiments (8,10,13), and the behavior of (e) is to be interpreted as a sequence of [3] and [1]–[2]. Reaction (g) could be interpreted in terms of emission in [4], but the fact that the spectrum of (g) in the visible region is the same continuum as that produced by (c) is an argument in favor of the sequence [4]–[3]–[1]–[2]. This is in agreement with the other studies mentioned above.

These observations offer direct evidence that the reaction leading to emission in systems containing O and N atoms and an excess of NO is [1]–[2]. (When the supply of NO is limited and there is an abundant supply of N atoms the bands of NO are produced by atom recombination (14). These were not observed here.)

SPECTRA

Since our conclusions depend upon observation of the spectrum of the radiation produced in (c) and (g), the results of such studies are summarized here. Comparative spectra of the reaction zones in (c) and (g) were taken with a medium quartz Hilger Cornu type spectograph using Eastman Kodak type F plates to emphasize the red end of the spectrum. A continuum with faint banded structure extended from about 4400 Å to the plate limit (about 6600 Å). The intensity was not uniform, but the variations with wavelength were characteristic of the sensitivity of the emulsion, not of the flame. Similar spectra have been reported many times (7,8). A more extensive study of the airglow spectrum was made using a large aperture spectograph designed at the National Bureau of Standards (15).* With this instrument and films sensitive to the visible and the near infrared region the airglow spectrum was surveyed to beyond 11,000 Å. The continuum is strong out to the limit of the I-N emulsion (about 8900 Å) and continues to about 10,900 Å. No intensity measurements were made, but it was apparent that the continuum intensity was decreasing more rapidly than was the emulsion sensitivity as the long wavelength limit was approached. This spectrum should be studied in detail in any reinvestigation of the nitrogen dioxide spectrum.

System (h) was studied because reaction (5) is sufficiently exothermic to permit the production of NO in excited vibrational states that could lead to emission in the 1–2 micron region. An exposure of 144 minutes on I-Z film did not reveal any bands attributable to NO.

REACTION RATES: THE PRODUCT EMITTER DIFFUSION FLAME MODEL

There is presented in this section the mathematical model needed for the interpretation of diffusion flames in which a product molecule emits the radiation that is monitored. It has been used previously for the analysis of the $H+O_3$ system (16), and a similar treatment has been used recently by Rapp and Johnston (17) in connection with the nitric oxide – fluorine flame. The equations for the spatial distribution of reagents and intermediates are developed for the cases that may be applied to $O+NO$ and $N+NO$. The modifications that must be introduced when the flame is photometered or photographed are then presented. In a following section the application to these systems is discussed.

The reaction scheme that is applicable to the $O+NO$ system is

$$y+z \rightarrow w^* \qquad\qquad \text{rate} = k_1\ [z][y]$$

$$w^* \rightarrow w+h \qquad\qquad\quad = k_2\ [w^*]$$

$$w^*+M \rightarrow w+M \qquad\quad = k_3[M][w^*]$$

in which y is the nozzle reagent, z the atmosphere reagent (present at constant concentration), and M is any 'third body'. Following the development used for the temperature pattern method (3), treating the nozzle as a point source, the steady-state diffusion equations are

[7] $$-D_y\Delta^2[y] = -k_1[z][y]$$

[8] $$-D_w\Delta^2[w^*] = -(k_2+k_3[M])[w^*]+k_1[z][y]$$

with the boundary conditions

$$y \rightarrow 0 \quad \text{as} \quad r \rightarrow \infty, \qquad b = \int_0^\infty k_1[z][y]\, dV$$

$$w^* \rightarrow 0 \quad \text{as} \quad r \rightarrow \infty, \qquad b = \int_0^\infty (k_2 + k_3[M])[w^*]\, dV$$

where D is a diffusion coefficient, b is the molar flow rate of the nozzle reagent, V is the volume, and r the radial distance from the nozzle. Spherical symmetry is assumed and equations [7] and [8] are solved in sequence by standard techniques. The solutions that satisfy the boundary conditions are

[9] $$[y] = b e^{-cr}/4\pi D_y r, \text{ where } c^2 = k_1[z]/D_y$$

[10] $$[w^*] = \frac{b}{4\pi D_w} \cdot \frac{c^2}{(a^2 - c^2)} \cdot \frac{e^{-cr} - e^{-ar}}{r}$$

where $$a^2 = (k_2 + k_3[M])/D_w.$$

If w^* were stable and the nozzle reagent concentration were studied, as in the sodium diffusion flames, equation [9] would be used for the analysis. Where w^* is the emitter and the emission pattern is studied, two simple cases can be distinguished. If $a \gg c$, that is instantaneous emission or destruction,

[11] $$[w^*] = \frac{b}{4\pi D_w} \cdot \frac{c^2 e^{-cr}}{a^2 r}$$

and then if $k_3[M] \ll k_2$

[12] $$k_2[w^*] = \frac{bc^2 e^{-cr}}{4\pi r}.$$

If $a = c$, i.e., the rates of formation and destruction of w^* are equivalent, the general expression for w^* goes to a limit of

[13] $$[w^*] = \frac{bc e^{-cr}}{8\pi D_w}$$

and then, if $k_3[M] \ll k_2$

[14] $$k_2[w^*] = \frac{bc^3 e^{-cr}}{8\pi}.$$

A scheme that is applicable to the case of $N + NO$ is

$$y + z \rightarrow p + I$$
$$p + z \rightarrow w^* \qquad\qquad \text{rate} = k_4[z][p]$$
$$w^* \rightarrow w + h$$
$$w^* + M \rightarrow w + M$$
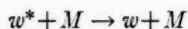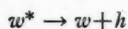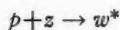
where I is an inert product, the other symbols have the meanings previously assigned,

and the same rate notation is associated with the same reagents. The diffusion equations for this case are [7] and

[15] $$-D_p \Delta^2[p] \;=\; -k_4[z][p]+k_1[z][y]$$

[16] $$-D_w \Delta^2[w^*] \;=\; -(k_2+k_3[M])+k_4[z][p]$$

with the additional boundary condition

$$p \to 0 \quad \text{as} \quad r \to \infty, \qquad b = \int_0^\infty k_4[z][p]\, dV.$$

The solution of [7] remains the same, the solution of [15] is of the same form as [8], except that p replaces w^* and a new parameter $f^2 = k_4[z]/D_p$ replaces a. (The last retains its same significance here, see eq. [10].) The solution for w^* is

[17] $$[w^*] = \frac{bc^2f^2[(f^2-c^2)e^{-ar}+(a^2-f^2)e^{-cr}-(a^2-c^2)e^{-fr}]}{4\pi D_w r (f^2-c^2)(a^2-c^2)(a^2-f^2)}.$$

We record here both the simplification that corresponds to rapid formation of p, $c \gg f$, and a

[18] $$[w^*] = \frac{bf^2[e^{-fr}-e^{-ar}]}{4\pi D_w (a^2-f^2)r},$$

which is of the same form as the general solution in the first case considered [10], and the simplification that specifies rapid destruction of w^* under the conditions leading to [18] $a \gg f$

[19] $$[w^*] = bf^2 e^{-fr}/4\pi D_w a^2 r$$

and if, as before $k_3[M] \ll k_2$

[20] $$k_2[w^*] = bf^2 e^{-fr}/4\pi r,$$

which is identical in form with [12].

This completes the development of the concentration and emission density expressions needed here. Other less limited cases differ only in the terms preceding the exponentials.

We now turn to the question of the form of the pattern recorded on a photograph of such an emission zone, or, indeed, of the resonance zone produced in sodium diffusion flames. Ideally, such a photograph is a plane representation of the three dimensional zone, at each point of which there is an emission density $k_2[w^*]$. Each point on the film represents a summation of the emission from a sequence of points in the flame. We shall assume that these points lie on a chord of the sphere that runs perpendicular to the plane of the film, and that all such points contribute radiation in proportion to their values of $k_2[w^*]$. Since the flame is 'focused' onto the film, these assumptions should be moderately good. If v represents a distance from the center of the reaction zone in the plane parallel to the film, and u a distance perpendicular to this plane, the integration of the emitter density along u yields the emission recorded by the film (or a number proportional to it).

$$F(cv, av) = 2\int_0^\infty k_2[w^*]\, du = \frac{bk_2c^2}{2\pi D_w(a^2-c^2)} \int_0^\infty \frac{e^{-cr}-e^{-ar}}{r}\, du$$

which becomes upon substitution of $u = v$ sinh and integration (for w^* given by [10] or [18] with f replacing c)

[21] $$F(cv,av) = \frac{bk_2c^2}{2\pi D_w(a^2-c^2)} [K_0(cv)-K_0(av)]$$

where $K_0(x)$ is a modified Bessel function of the second kind, for which tabulated values are available (18). For the case of instantaneous emission, equations [11] and [19], a particularly simple result is obtained

[22] $$F(cv) = bc^2K_0(cv)/2\pi.$$

When $a = c$ and equation [14] is employed

[23] $$F(cv) = bc^3vK_1(cv)/4\pi.$$

The general equation [21] can be simplified when emitter densities at large values of cv are considered. Then, the function $K_0(cv)$ is closely approximated by c^2e^{-cv}/v.

While the treatment given above completes the presentation needed here, its relationship to the classical sodium diffusion flame deserves mention (2). In such studies the 'edge' of the flame, that point at which the sodium resonance emission is just visible, is determined. This is compared to that concentration of sodium that is just visible in static experiments under similar conditions. Thus, instead of using the integral criterion

$$\int_0^\infty [y]\, du = A \int_0^\infty (e^{-cr}/r)\, du$$

the expression

$$[y]_R = A'\, e^{-cR}$$

is used. Since the factor c^2 present in [22] does not enter here (it must be considered in any analysis based on an absolute value of [y] or [w*]), the approximation is probably no worse than the neglect of spherical symmetry.

The important difference between the sodium flame and the product emitter flame is that in the latter a decrease in c or a reduces the apparent size of the reaction zone, while in the former a reduction in c may produce an apparent enlargement. In this respect, the product emitter flame behaves in a manner opposite to that of the sodium flame.

REACTION RATES: APPLICATION TO NITRIC OXIDE SYSTEMS

Studies of the $O+NO$ and the $N+NO$ systems were made in a conventional low-pressure flow system. In both cases the atom-bearing stream was the nozzle reagent and either pure NO or NO diluted with nitrogen formed the atmosphere. The NO (Matheson) was fractionally distilled before use. Tank oxygen was dried but not purified further. Nitrogen was passed over heated copper and dried before use. All gases were fed through critical orificii into the low pressure system from reservoirs, the pressures of which were adjusted to provide the desired flow rates. The reactor was a 4-in. diameter cylinder with plate glass ends through which the flame was photographed. The nozzles through which reagent y was introduced were pyrex tubes drawn down to an i.d. of 1 to 2.2 mm. The reactor pressure could be controlled by a valve near the mechanical oil pump that maintained the flow. Pressures within the reactor ranged from 0.5 to 2 mm Hg and were adjusted to provide flames 2 to 5 cm in diameter. In all cases higher pressures were needed to restrict the flames in the $NO-N_2$ mixtures than in pure NO.

The $O+NO$ flames were photographed with a Leica IIe 35 mm camera, and the $N+NO$ flames were recorded |with a Zeiss $2\frac{1}{4} \times 3\frac{1}{4}$ film pack camera. In both cases the ranges were adjusted so that the flame filled most of the film. In both cases Eastman Kodak XXX panchromatic film was used. For each set of flame pictures there was prepared a film calibration made by exposing a strip of film through a calibrated step wedge. The calibrations were processed at the same time as the corresponding flame pictures.

The flame negatives were densitometered using a Leeds and Northrup microdensitometer, traverses being taken across several regions of each flame so density maps could be prepared. These maps showed a slight elongation of the flame along the nozzle axis, this being noticeable only at small distances from the nozzle tip. After the plate densities were converted to exposures, plots of exposure versus distance from the center of the flame pattern were prepared. For this purpose only exposure values were used that were taken from points near a line perpendicular to the nozzle axis and passing through the center of the pattern.

These exposure–distance plots were analyzed in terms of the models presented in the last section. Examination of either equation [21] or [22] reveals that the *shape* of the function is determined by the behavior of the modified Bessel function. Thus, if a parameter c or two parameters, c and a, can be chosen so that the shape of the experimental curve can be reproduced, the rate constants may be obtained without knowledge of the molar flow rate of atoms through the nozzle. In this case, and in others involving unstable species, this is advantageous.

In all the cases studied here it was feasible to reproduce the experimental exposure–distance curves by means of a formula such as [22] containing only one rate parameter. For this reason, the general relation [21] has not been applied. The results of the experiments are given in Table II. The 'shape parameter' column may be interpreted as

TABLE II

Product emitter flame measurements of rates of the reaction of nitric oxide with oxygen atoms

Mole fractions		Nozzle flow	Pressure	Shape parameter	$k/D' \times 10^{-7}$
NO	N_2	Total flow	(mm Hg)	(cm^{-1})	(cm/mole at 1 mm Hg)
(a) With oxygen atoms and molecules as nozzle reagent					
0.882	0	0.135	0.65	0.7	2.4
0.886	0	0.129	0.64	1.1	6.0
0.518	0.349	0.15	1.57	1.35	2.6
0.565	0.286	0.176	1.34	1.23	2.7
0.557	0.281	0.192	1.43	2.02	6.6
(b) With active nitrogen (N and N_2) as nozzle reagent					
0.414	0.568	0.262	1.95	2.86	8.7
0.427	0.573	0.359	1.50	1.84	6.4
0.220	0.780	0.225	1.40	0.81	2.8
0.220	0.780	0.225	1.40	0.75	2.4
0.762	0.238	0.238	1.25	1.66	4.1
0.762	0.238	0.238	1.25	1.54	3.7

NOTE: Mole fractions based on the sum of atmosphere flow and nozzle flow. All experiments at room temperature, 293° K.

c, a, or f. The final column represents $k/D = c^2/[z]$, see equation [9] where z is the NO concentration and the diffusion coefficient would have its value for a pressure of 1 mm Hg (that is, the reciprocal pressure dependence of the diffusion coefficient has been factored out). The average of k/D' for set a is $(4.1 \pm 2.4) \times 10^7$, and for set b is $(4.7 \pm 2.0) \times 10^7$ (arithmetic errors).

DISCUSSION OF RATE MEASUREMENTS

The equality of the average values of k/D' for the experiments using O and N atoms indicate that the same process is controlling in both systems. The spread of values in set a, Table II, must be attributed to experimental error. The spatial resolution on the 35-mm films used here was considerably less than for set b, where the larger films were used. In the latter the reproducibility in equivalent is much better. Here there is a slight suggestion that k/D' varies with the NO pressure, but this is far from certain.

For set a, the shape parameter may be identified as c as defined by equation [9] and for set b as f defined immediately before [17]. These then apply to equation [1], or its equivalent

$$O + NO + M \rightarrow NO_2 + M. \tag{24}$$

In either case a value for the diffusion coefficient, D', must be supplied if the rate constant is to be extracted. This number is uncertain, due to our poor knowledge of the diameter of the oxygen atom. Here we assume a value of $250 = D'$. Then for equation [1], $k_1 = 1 \times 10^{10}$ cc/mole-sec. This value is tenable for the type of reaction considered but is 1000 times larger than other estimates (8,10). If [24] is assumed to dominate, $k_{24} = 1.4 \times 10^{17}$ (cc/mole)^2 sec^{-1} based on set b. This value is fivefold greater than that reported by Kaufman (8) and by Harteck, Reeves, and Mannella (10).

(An alternative interpretation of the shape parameter may be made because of the symmetry of the equations. If it is considered to be a, equation [10], either a value of $k_2 = 4 \times 10^2$ sec^{-1} or $k_3 = 7 \times 10^9$ (cc/mole)^2 sec^{-1}. The former is improbable for the decay of an excited NO_2, the latter is very low for a three-body recombination coefficient. Neither is tenable here.)

The interpretation of these flames in terms of [24] and the comparison with previous work provides an adequate justification for the model developed here for the product emitter flame. It is apparent that, as presently used as a photographic method, the precision is not high. A photometric application should markedly improve the technique. The fact that the rate, k_{24}, reported here is larger than has been determined earlier deserves some comment. The product emitter flame is a limiting case of a few oxygen atoms reacting with a large excess of NO. The more accurate work on this system has employed the reverse condition, a small amount of NO for many oxygen atoms. If there should be systematic errors in that work (and we have not found them), particularly reactions in the cycle that destroys and regenerates NO whose rates have not been considered but are only moderately fast, they would tend to reduce the apparent value of the rate. Some of the discrepancy may lie here, but most or all of it should be attributed to as yet unevaluated factors in this diffusion flame method.

REFERENCES

1. H. VON HARTEL and M. POLANYI. Z. physik. Chem. B, **11**, 97 (1931).
2. J. F. REED and B. S. RABINOVITCH. J. Phys. Chem. **61**, 598 (1957).
3. D. GARVIN and G. B. KISTIAKOWSKY. J. Chem. Phys. **20**, 105 (1952).
4. F. T. SMITH and G. B. KISTIAKOWSKY. J. Chem. Phys. **31**, 621 (1959).
5. F. T. SMITH. J. Chem. Phys. **22**, 1605 (1954). R. J. CVETANOVIĆ and D. J. LE ROY. Can. J. Chem. **29**, 597 (1951).
6. M. L. SPEALMAN and W. H. RODEBUSH. J. Am. Chem. Soc. **57**, 1475 (1935).
7. A. G. GAYDON. Proc. Roy. Soc. (London), A, **183**, 111 (1944).
8. F. KAUFMAN. J. Chem. Phys. **28**, 352, 992 (1958).
9. H. W. FORD and N. ENDOW. J. Chem. Phys. **27**, 1156 (1957).
10. P. HARTECK, R. R. REEVES, and G. MANNELLA. J. Chem. Phys. **29**, 1333 (1958).

11. F. J. LIPSCOMB, R. G. W. NORRISH, and B. A. THRUSH. Proc. Roy. Soc. (London), A, **223**, 455 (1956).
12. K. DRESSLER. J. Chem. Phys. **30**, 1621 (1959).
13. G. B. KISTIAKOWSKY and G. G. VOLPI. J. Chem. Phys. **27**, 1141 (1957); **28**, 665 (1958).
14. F. KAUFMAN and J. R. KELSO. J. Chem. Phys. **27**, 1209 (1957).
15. A. M. BASS and K. G. KESSLER. J. Opt. Soc. Am. **49**, 1223 (1959).
16. D. GARVIN and J. D. McKINLEY, JR. J. Chem. Phys. **24**, 1256 (1956).
17. D. RAPP and H. S. JOHNSTON. Final Report on Contract Nonr 222(56), Project NR 051-246, Department of Chemistry, University of California, Berkeley, California. March 10, 1960.
18. BRITISH ASSOCIATION for the Advancement of Science. Mathematical Tables. Vol. VI. Bessel Functions, Part I. Cambridge Univ. Press. 1937. pp. 266–268.

SOME OBSERVATIONS ON THE RADIATIVE COMBINATION OF ATOMIC HYDROGEN WITH ATOMIC HALOGENS IN BURNER FLAMES[1]

L. F. PHILLIPS AND T. M. SUGDEN

ABSTRACT

When small quantities of gaseous molecular halogens chlorine, bromine, and iodine are introduced into the supply to premixed hydrogen–oxygen–nitrogen flames one of the most important spectroscopic features appearing is an apparently continuous emission in the visible, sometimes extending into the near ultraviolet. The intensity of this continuous emission has been studied as a function of amount of halogen, and of temperature, composition, and position with respect to the reaction zone in a wide variety of flames. In oxygen-rich flames it has been attributed to an over-all process,

$$X + X \rightarrow X_2 + h\nu,$$

where X denotes an atom of halogen; one of the atoms may be in an excited state. Most of the work concerns hydrogen-rich flames, where a very strong correlation between the intensity and the product [H][X] is obtained. The over-all process may be written as

$$H + X \rightarrow HX + h\nu.$$
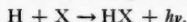
The efficiency of this over-all process is measured as 1 quantum emitted for about 10^{10} ordinary kinetic collisions of the atoms. The mechanism is discussed from the aspects of direct radiative recombination and of stabilization by collision of an intermediate excited HX* before radiation.

INTRODUCTION

A rather convenient method for studying some gaseous reactions at high temperatures has been shown to be the addition of the reactant or reactants in small amount to premixed flames of hydrogen, oxygen, and nitrogen at atmospheric pressure (1, 2). Variation of the amounts of hydrogen and nitrogen relative to oxygen enables a range of burnt gas temperatures from 1500° to 2500° K to be covered. The composition of the flame gas may also be varied isothermally. Little or no disturbance is produced in such gases by small amounts of additives, and the main flame gases can be regarded as a medium or 'solvent' in which the reactions of the additive take place.

Hydrogen–oxygen–nitrogen flames have two advantages over most other flames for this kind of work. Firstly, a great deal is known about the burnt gases and the reactions proceeding in them in the absence of additives, and secondly, the radiation from such flames is either very weak or confined to rather narrow regions of the spectrum in the visible and contiguous near ultraviolet and infrared.

The premixed flame has a narrow reaction zone close to the burner, followed by a zone of hot burnt gas extending several centimeters downstream. The use of sintered metal or Mèker-type burners allows this reaction zone to be made almost flat, and parallel with the burner surface, and it is then possible to use the downstream direction as a variable for following reactions with time. The scale is such that 1 cm corresponds with times of about 1 millisecond. The effects of entrained air from the surroundings can be reduced by shielding the flame containing the trace additive with a second flame of similar composition but without additive. In this way the inner flame is protected over a distance of several centimeters.

The major part of the burning takes place in the reaction zone in a distance of a fraction of a millimeter. The relevant properties of the burnt gases are as follows. In general, the

amounts of the free radicals H and OH emerging from the reaction zone are very much in excess (up to 1000 times for cooler flames) of the equilibrium ones for the measured temperatures (3, 4). This occurs because of the branched chain nature of the main process of combustion. These radicals recombine relatively slowly, as they proceed downstream, by reactions

$$H + H + M \rightarrow H_2 + M$$
$$H + OH + M \rightarrow H_2O + M$$
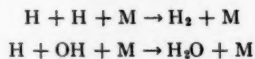
where M is a third body. This third body is usually a molecule of a major constituent of the burnt gases and, in the case of fuel-rich flames, as normally used in this work, will be H_2O, N_2, or H_2. Certain rapid, reversible, bimolecular reactions can occur, however, at such speeds that definite relations hold between the concentrations of the burnt gas molecules. The most important of these is (1, 5)

$$H + H_2O \rightleftharpoons OH + H_2; \qquad K_0 = ([OH][H_2])/([H][H_2O]).$$
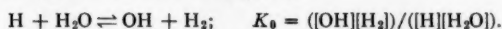
This reaction proceeds so rapidly that the concentrations of H and OH are related to each other at all points in the burnt gases by the equilibrium law for K_0, in terms of $[H_2]$ and $[H_2O]$, both of which are large, and known with reasonable accuracy for fuel-rich flames.

Flame photometric methods for measuring [H] and [OH], based on the addition of very small amounts (1 part in 10^6 or less) of various metallic compounds to the flame gases, have been devised, and shown to be consistent and reliable (3, 6, 7, 8). The temperature of the flame gases (about 2000° K) can be measured to within 10° C. It can thus be seen that the flame gases can be used as a fairly controlled source of atomic hydrogen and hydroxyl radicals.

The other great advantage of these flames is that their normal radiation is limited to strong emission from OH in the near ultraviolet, H_2O vibration–rotation bands in the far red and near infrared, and a very weak, apparently continuous, spectrum extending across most of the visible region (9). This last has been shown by Padley to arise from (10)

$$H + OH \rightarrow H_2O + h\nu$$

although whether this is a true radiative combination, or whether an excited H_2O^* is formed and stabilized by collision, is not fully established. Spectra arising from additives often stand out strongly and allow of photometric investigations.

The emission resulting from addition of amounts up to 2% of the halogens chlorine, bromine, and iodine to hydrogen–nitrogen–oxygen flames, mainly fuel-rich, is discussed in this paper. Figure 1 shows typical exposures for the reaction zone of a flame of this kind with small additions of these halogens. The addition of iodine produces the well-known IO band system (11) in the visible quite strongly, and the addition of bromine produces the BrO bands (12), weakly. No ClO bands were detected in this work, although such a system has been found in other circumstances (13, 14). These halogen oxide bands became much weaker downstream from the reaction zone, presumably because of the decrease of atomic oxygen with distance.

The most important feature from the present aspect is, however, an apparently continuous spectrum extending from the red into the ultraviolet. In the case of chlorine it is clearly visible at shorter wavelengths than the (0,0) bandhead of OH at 3064 Å, but no very sharp short wavelength cutoff can be ascribed to it. These continua persist, with some reduction in intensity, into the burnt gas. This general type of continuous spectrum appears to be quite a common feature of flames. In particular, they occur when

nitric oxide (15, 16), carbon monoxide (17, 18, 19), and alkali metals (8) are added in small quantities, and in these cases have been ascribed to

$$NO + O \rightarrow NO_2 + h\nu$$
$$CO + O \rightarrow CO_2 + h\nu$$
$$Na + OH \rightarrow NaOH + h\nu$$
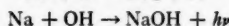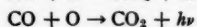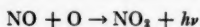
respectively. The atomic hydrogen–hydroxyl continuum has been mentioned above (10). It is not known in most cases whether an excited intermediate molecule is stabilized. Better resolution of the spectra might show discrete structure, which would be evidence in favor of this stabilization.

These apparently continuous spectra given by the halogens have been studied in a wide variety of flames, their intensities being measured as functions of wavelength, flame gas composition, temperature, and position in the flame gases.

EXPERIMENTAL

The burner consisted of a bundle of fine silica tubes, each of about 0.5 mm internal and 1.0 mm external diameter. The whole bundle was 1.2 cm in diameter. It was supplied with premixed hydrogen, nitrogen, and air, which were individually metered by calibrated capillary-type flowmeters. The gases were mixed before passing to the burner. A diagram of the burner and its supply lines is shown in Fig. 2. Silica tubes were used in preference to metal ones on account of possible corrosion by the halogens, which were also supplied to the gas mixture before it entered the burner. The bundle of tubes was held together by Araldite cement. This 'experimental' flame was surrounded by a shield flame supplied by a similar gas mixture, except for the halogen, to reduce the effects of entrained air on the inner flame. The tubing for the shield flame was stainless steel hypodermic tube, again cemented with Araldite. The arrangement gave a stable, laminar flame with primary reaction cones about 0.5 mm high, i.e. the reaction zone was almost flat. The burner was water-cooled. The total flow to the burner was of the order of 1 cubic foot/minute and was adjusted to give a stable flame for each composition.

The temperature of the burnt gas was measured by the sodium D-line reversal method (20), which has been established to be reliable for these flames provided the measurements are made more than 1 cm downstream from the reaction zone, so as to avoid effects due to chemiluminescent excitation of the sodium (2). Sodium was added as a fine spray of concentrated aqueous sodium chloride solution from an atomizer operated by part of the air supply. Measurements of the reversal were made visually, using a tungsten strip filament lamp which was calibrated with a Cambridge optical pyrometer. A Hilger, glass prism, constant deviation spectroscope was used. The temperatures ranged from 1500° K to 2300° K, depending on the composition of the mixture; most of the flames were fuel-rich. Reproducibility was to within 10° C. The potassium resonance doublet at 7665 and 7699 Å is considerably less liable to chemiluminescence, as compared with thermal excitation (5), and was used photometrically to extend temperature measurements closer to the reaction zone than 1 cm.

Measurements of the concentration of atomic hydrogen in the burnt gas were made by the Na–Li method of James and Sugden (3, 21). This involves flame photometry of

FIG. 1. Emission spectra for addition of halogen to an H_2–O_2–N_2 flame. Hilger Medium Quartz Spectrometer with Ilford H.P.3 Plates. Exposures 1 hour. Observations made on the reaction zone. Flame $H_2/O_2/N_2 = 3/1/4$, $T \sim 2300°$ K. The extension of continua into the ultraviolet below 3064 Å is only visible on the original plate. The minimum in the green corresponds with a region of low plate sensitivity.

PLATE I

λ 100 Å

Cl₂

Br₂

I₂

Blank

BrO

IO

OH

Na H₂O

FIG. 1.

SILICA BURNER

FLOW LINE
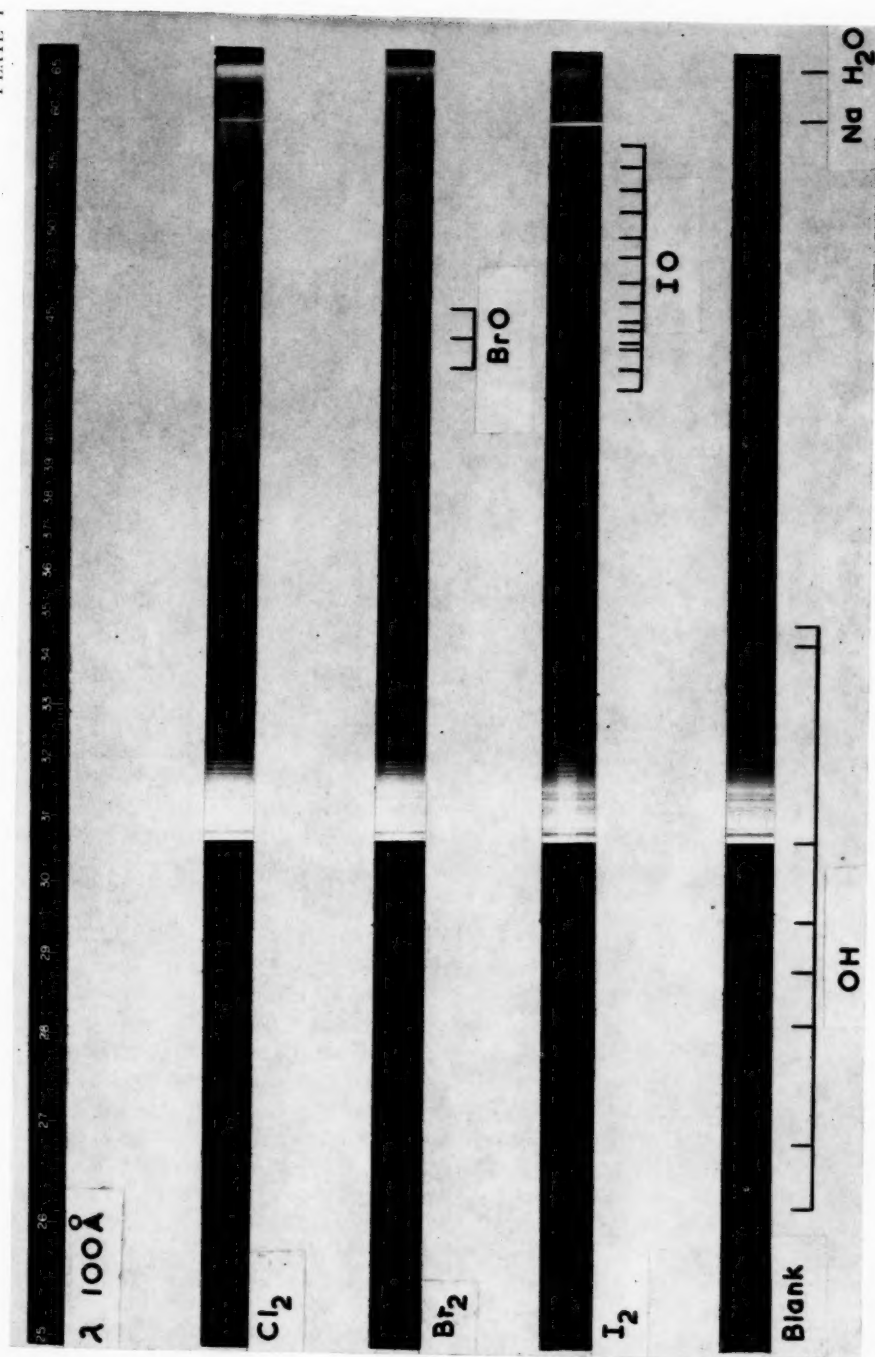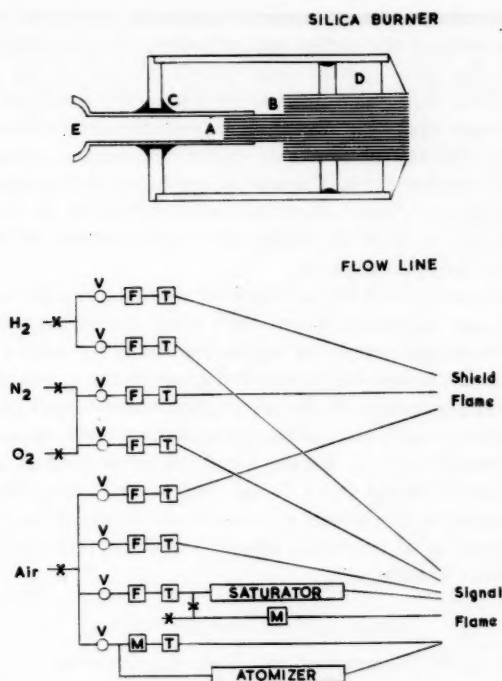
FIG. 2. Burner and supply lines. A is the 'experimental' flame with silica tubes, supplied from E. B indicates the stainless steel tubes for the shield flame (supply tubes not shown). C is a wax seal to eliminate strain. D is the water-cooling jacket, X tap, V needle valve, F flowmeter, M mercury manometer, T trap.

the emission from the resonance lines when equal amounts of sodium and lithium are introduced as salt sprays into the flame supply, the concentrations being sufficiently low to make self-reversal negligible. A significant amount of the lithium is removed as the very stable gaseous compound LiOH by the balanced reversible reaction

$$Li + H_2O \rightleftharpoons LiOH + H.$$
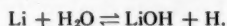
The NaOH molecule is much less stable, and the amounts of it formed can be neglected. The method leads to absolute values of [H] correct to within ±20%, and to relative values for a series of flames to within ±5%. The equilibrium constant of the reaction was calculated from a formula given by Smith and Sugden (22), with thermochemical data from Gaydon and Wolfhard (20), modified to correspond with a heat of dissociation of OH of 102.5 kcal/mole, as recommended by Gray (23). The method yields values of [H] in accordance with equilibrium ones in circumstances where equilibrium is known to obtain, i.e. at temperatures above 2400° K and at 3 cm from the reaction zone. It is valid provided that the emission of the resonance lines is thermal, a condition which holds reasonably well 1 cm or more downstream from the reaction zone.

To obtain [H] nearer to the reaction zone, the CuH photometric method of Bulewicz and Sugden (6) was adopted, as recommended by Padley and Sugden (2). This method is not absolute, but can be calibrated against the Li–Na method. It is apparently not subject to difficulties arising from chemiluminescence.

All photometric measurements were made by chopping the light from the flame with a sector disk at a frequency of 600 cycles/second before it fell on the entrance slit of the Hilger constant deviation glass spectrometer fitted with an IP 21 photomultiplier as detector. The output from this was amplified by a homodyne system, a reference signal being taken from the same chopping disk, and was finally presented as a meter reading. The wavelength sensitivity was obtained by calibration with a tungsten strip filament lamp running at known temperatures. The spatial resolution of the optical system allowed a section of the 'experimental' flame about 0.5 mm in height to be studied. The burner was mounted horizontally so that the image of a cross section of the flame filled the vertical entrance slit of the spectrometer.

Elementary halogens were added by the following means. For chlorine, cylinder supplies were transferred to a gas aspirator, where they were stored over brine. The gas was passed into the main flame gas supply by displacing the brine with a metered stream of air. Liquid bromine was contained over a sintered glass disk in a thermostatted saturator. A very small, measured proportion of the air supply was diverted through the sintered disk, and became saturated with Br_2 vapor. Independent tests showed saturation to be efficient. Iodine was contained in a similar saturator immersed in glycerol at 130° C, whereby it could be kept in liquid form. It was necessary to heat the connecting tubes to within a short distance of the burner to reduce condensation on the walls. Even so, some difficulty was experienced from this source. Vapor pressure data were taken from the International Critical Tables.

RESULTS AND CONCLUSIONS

1. The Effect of Halogens on Temperature and Flame Composition

The first point to be established is whether the addition of the halogen has any marked effect on the parameters of the main flame gases. Two of these have been examined, as being the most important—the temperature and the concentration of atomic hydrogen. Addition of 2% of chlorine causes an increase of temperature of 20–30° C. Since most of the measurements were made with amounts below 1%, the effects of change of temperature can be neglected, in first approximation. The addition of bromine and iodine had much smaller effects on the temperature than did that of chlorine. The effect of the addition of halogen on the concentration of atomic hydrogen has been estimated indirectly, since it is not possible to use the Li–Na method or the CuH method in the presence of halogen, on account of the formation of alkali halides in the one case, and of emission from gaseous cuprous halides in the other.

Addition of chlorine in amounts of the order of 0.1–1% of the gases causes a reduction of the intensity of the sodium D-line provided by adding a very small (1 part in 10^8) portion of sodium salt because of the formation of gaseous sodium chloride. By far the most stable compound of chlorine in hydrogen-rich flame gases is hydrogen chloride, and the added chlorine will be expected (see below) to be almost entirely in this form. The reaction by which sodium chloride is made will be the rapid reversible one of Na with HCl

$$Na + HCl \rightleftharpoons NaCl + H; \quad \text{eq. const. } K_1.$$

This balance will be set up in the flame gases within a few microseconds. If [H] remains unchanged on addition of chlorine, then a plot of (I_0/I) against $[Cl]_0$ should be a straight line, where I_0 and I are the intensities of the sodium D-lines in emission without and with total added chlorine $[Cl]_0$ respectively, since $[Cl]_0 \sim [HCl]$, and thus

$$[Na]_0/[Na] = 1+(K_1[Cl]_0)/[H].$$

I is proportional to [Na] for sufficiently low concentrations of sodium to make self-reversal negligible. If [H] is dependent on [Cl]$_0$, curved plots should be obtained.
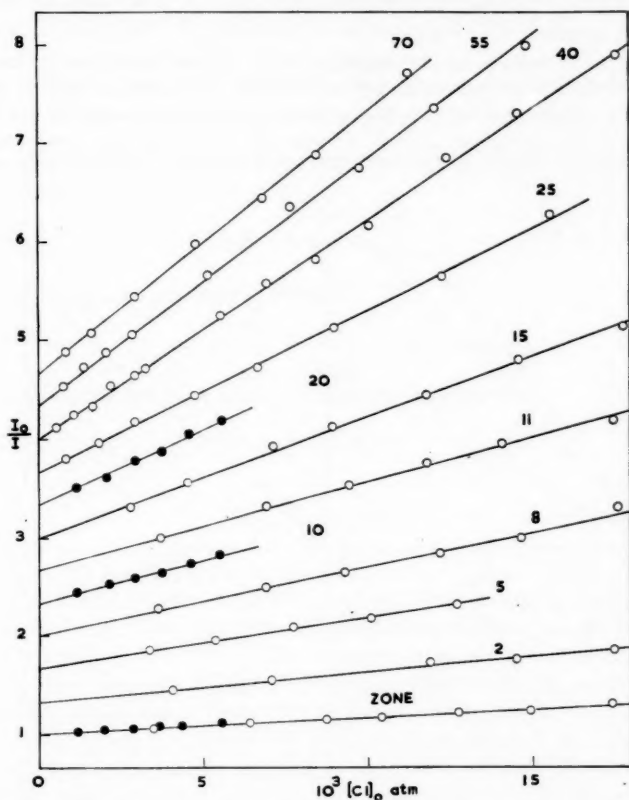
FIG. 3. (I_0/I) sodium D-lines against total added chlorine [Cl]$_0$ for a flame with $H_2/O_2/N_2 = 3/1/4$. The open circles are for addition of chlorine gas, and the full circles for addition of chlorine as chloroform. The numbers on the plots give distance in millimeters from the reaction zone. The lines (apart from that for the reaction zone) have been displaced vertically for clarity: without such displacement they have a common intercept. $M/1000$ NaCl solution sprayed from the atomizer.

Figure 3 shows typical plots of (I_0/I) against [Cl]$_0$. They are good straight lines. In the case illustrated they give evidence of decrease of [H] with increasing distance from the burner. There is thus good evidence that [H] is not significantly altered by the amounts of chlorine used. Earlier work (3) showed a slight initial curvature of plots of this kind, but this has been shown to arise from faults in the method of adding the halogens. Results with the same implication, that [H] is unaffected, hold for addition of bromine and iodine up to 0.5%. This greatly simplifies the analysis of the results to be described, insofar as they are connected with the concentration of atomic hydrogen. Some observations have also been made on the effect of chlorine on the intensity in emission of the (0,0) band of OH at 3064 Å. Two per cent of chlorine produced no significant effect. This is in agree-

ment with the absence of change in [H], since the two radicals are related to each other and the major constituents by

$$H_2O + H \rightleftharpoons H_2 + OH,$$
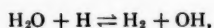
which is balanced.

2. The Halogen 'Continua'

Figure 4 shows some results on the emission from various hydrogen–oxygen–nitrogen flames to which amounts of less than 1% of chlorine, bromine, or iodine were added. They were taken at wavelengths, and in positions in the flame gases, where interference
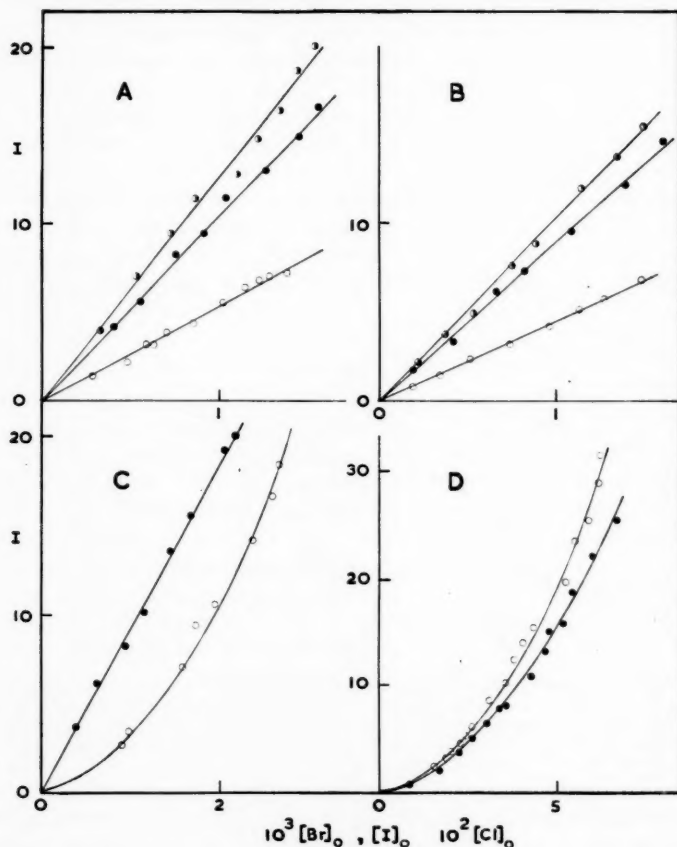
FIG. 4.   Plots of intensity of halogen continua in H_2–O_2–N_2 flames as functions of total added halogen $[X]_0$. Waveband observed about 50 Å wide.

(A) Addition of chlorine. ○, flame $H_2/O_2/N_2 = 3/1/4$ at 10 mm from the reaction zone; ●, flame $H_2/O_2/N_2 = 3.5/1/5$ at 4 mm; ◑, flame $H_2/O_2/N_2 = 4.5/1/6$ at 2 mm. All at 4900 Å.

(B) Addition of bromine, all at 2 mm from reaction zone. Flame $H_2/O_2/N_2 = 3.5/1/5$: ○, for 6400 Å; ●, for 5500 Å; ◑, for 4900 Å.

(C) Addition of iodine. ○, flame $H_2/O_2/N_2 = 1/1/4$ at 8 mm; ●, flame $H_2/O_2/N_2 = 3/1/4$ at 2 mm. Both plots for 6400 Å.

(D) Flame $H_2/O_2/N_2 = 1/1/4$ at 8 mm and 4900 Å. ○, for addition of chlorine; ●, for addition of bromine.

from known discrete spectra (such as that of IO) was negligible. The intensity of emission without added halogen was subtracted directly from the total reading. Wide slits were used, so that a section of about 50 Å was observed.

An important relation to the general flame composition is at once apparent. When a fuel-rich flame is used there is a direct proportionality between the observed intensity I and the total halogen $[X]_0$, whereas for a very oxygen-rich flame, I is proportional to $[X]_0^2$.

The heats of dissociation of X_2 halogen molecules are such that at flame gas temperatures, and with the amounts of halogen used, the proportion which would be expected, on thermodynamic grounds, to be present as X_2 are negligible. Molecules of this type entering the reaction zone would immediately be decomposed by reaction with atomic hydrogen, of which a great deal is present,

$$X_2 + H \rightarrow HX + X.$$
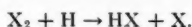
A subsequent very rapid, reversible, reaction

$$HX + H \rightleftharpoons H_2 + X; \qquad \text{eq. const. } K_2$$
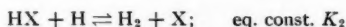
then sets up a balance between atomic X and the hydride HX

$$[HX]/[X] = [H_2]/K_2[H]$$

and

$$[X]_0 = [HX] + [X].$$

The ratio $[HX]/[X]$ may thus be obtained from the known values of the equilibrium constant K_2, and the concentrations $[H_2]$ and $[H]$. The former of these concentrations is readily calculable for a fuel-rich flame with sufficient accuracy, and the latter has been measured. The result is that $[HX]/[X] \gg 1$ for chlorine in fuel-rich flames, $\ll 1$ for iodine, and is not far from unity for bromine. In oxygen-rich flames the value of this ratio will be very severely reduced since molecular hydrogen now becomes a very minor constituent and in this case hardly any hydride HX is expected, and for all the halogens $[X] \sim [X]_0$. Consideration of the dissociation energies of the XO molecules (24) shows that they will not take up an appreciable part of the total halogen in any of the present flames.

It is therefore suggested that the observed dependence of I on $[X]_0^2$ in a very oxygen-rich flame arises from the radiation being associated with an over-all process

$$X + X \rightarrow X_2 + h\nu.$$

Whether X_2^* is stabilized by collision with other molecules before emission ensues (i.e. whether X_2^* is associated with a potential curve with a minimum) cannot be decided from the observations. since at the flame temperatures the discrete structure expected in this event would be so rich as not to be resolvable by the spectrometer. It is interesting to note that Kondratiev and Leipunski (25) observed an apparently continuous spectrum from heated halogens in this region (blue-green). This they attributed to recombination of excited and normal halogen atoms. Similar continua were observed by Ludlam, Reid, and Soutar (26) in H_2-Cl_2 diffusion flames, and by Urey and Bates (27) in H_2-Cl_2 and $H_2-O_2-X_2$ flames, and were associated with the same origin.

The main interest of this paper, however, centers on the emission from hydrogen-rich

flames, where the results of Fig. 4 exclude the possibility of radiative recombination of two halogen atoms. The direct dependence of I on $[X]_0$ implies that the radiation emerges from a molecule or process in which only one atom of halogen is concerned. On an a priori basis the over-all effect

$$H + X \rightarrow HX + h\nu$$
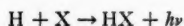
deserves consideration, since Padley (10) has shown that in these flames a very similar spectrum arises from

$$H + OH \rightarrow H_2O + h\nu.$$
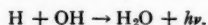
Neither the results of Ludlam *et al.* nor those of Urey and Bates exclude the possibility that such an effect gave rise to some of the emission which they observed.

3. Dependence of Intensities on [H]

The total halogen is effectively distributed between [X] and [HX] in fuel-rich flames,

$$[X]_0 = [X] + [HX] = [X]\{1 + ([H_2]/K_2[H])\}.$$

Then, if the intensity $I = k[H][X]$

$$I = (k[H][X]_0)/\{1 + ([H_2]/K_2[H])\}.$$

In the case of chlorine $[HX]/[X] = [H_2]/K_2[H] \gg 1$, so that

$$I = (kK_2[H]^2[Cl]_0)/[H_2]$$

whereas for iodine $[H_2]/K_2[H] \gg 1$, and

$$I = k[H][I]_0.$$

One way of testing these expressions is to observe I as a function of distance downstream from the reaction zone. The decrease in [H] as this distance increases, due to recombination of the excess radicals, may be followed by flame photometric methods. The most convenient one is the CuH method of Bulewicz and Sugden (6), referred to in the experimental section. The intensity of the CuH band at 4280 Å when a very small amount of copper salt is added to the flame is directly proportional to [H]. Thus, the lowest plot of Fig. 5 is effectively one of 1/[H] against distance from the reaction zone for a particular flame. It is a straight line with slope characteristic of the velocity constants of the ternary recombination processes such as

$$H + H + M \rightarrow H_2 + M$$

The first plot of Fig. 5 is of $(1/I)^{\frac{1}{2}}$ for the chlorine continuum: it is linear, and has the same (slope/intercept) as the 1/[H] plot at the bottom. The third plot is of $(1/I)$ for the iodine continuum, and is again of the same form as the 1/[H] plot. Thus the predictions based on the law $I = k[H][X]$ are borne out. Both $(1/I)$ and $(1/I)^{\frac{1}{2}}$ are plotted for bromine. The former is a little too steep, and the latter not nearly steep enough. This is in good agreement with the calculated values of [HX]/[X] in this flame at 6 mm of 22.5, 0.55, and 2×10^{-4} for X = Cl, Br, and I respectively.
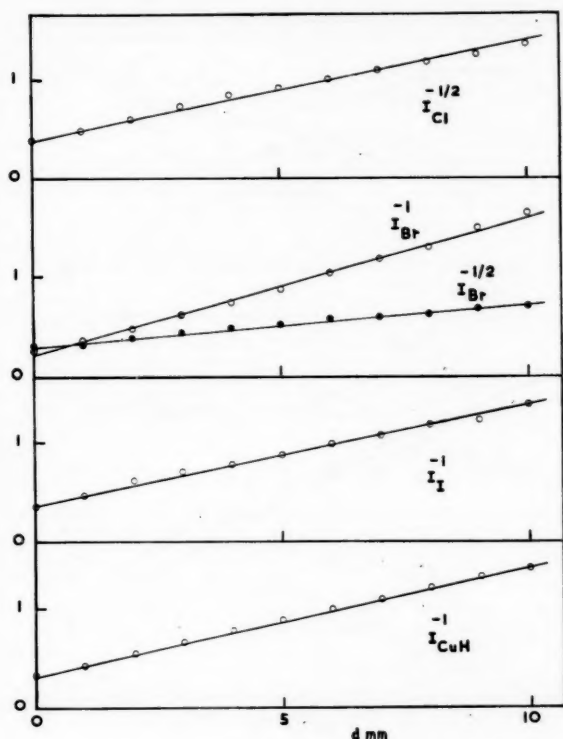
FIG. 5.   Decay of intensity of I halogen continua with distance from the reaction zone for flame $H_2/O_2/N_2$ = 3.5/1/5, $T \sim 2000°$ K. Observed at 4900 Å for Cl_2 and Br_2 addition and at 6400 Å for iodine. $[Cl]_0 = 2 \times 10^{-2}$ atm, $[Br]_0 = [I]_0 = 2 \times 10^{-3}$ atm. Compared with decay of [H] as given by the intensity of the CuH band at 4280 Å.

A more complete test of the correlation of I with [H] (for iodine) or with $[H]^2$ (for chlorine) is obtained by plotting the values of all these quantities for the reaction zone (defined here as the point of maximum [H]) for a wide series of flames. One of the most convincing ways of doing this is to use the method of 'families', first introduced by James and Sugden (8). A 'family' is a set of flames for which $[N_2]/[O_2]$ in the unburnt gas is constant, usually integral: the flames within it have various $[H_2]/[O_2]$ values, ranging in this work from 2.5 (hot end of family) to 4.5 (cold end). Their properties are plotted conveniently against $1/T$, a line connecting members of a particular family. Thus figure 6 shows such plots for the functions $[H]_0$ and $[H]_0^2/[H_2]$, $[H]_0$ denoting the value of [H] in the reaction zone. It will be seen that one function gives clearly separated families, while the other produces characteristic overlapping. Figure 7 shows the intensity of the continua for chlorine, bromine, and iodine at constant total halogen concentration, plotted in the same way. The correlation of the iodine pattern with $[H]_0$, and that of the chlorine pattern with $[H]_0^2/[H_2]$ is very striking. Bromine is again intermediate in behavior. The case that the observed emission is given by $k[H][X]$ is thus a very strong one.
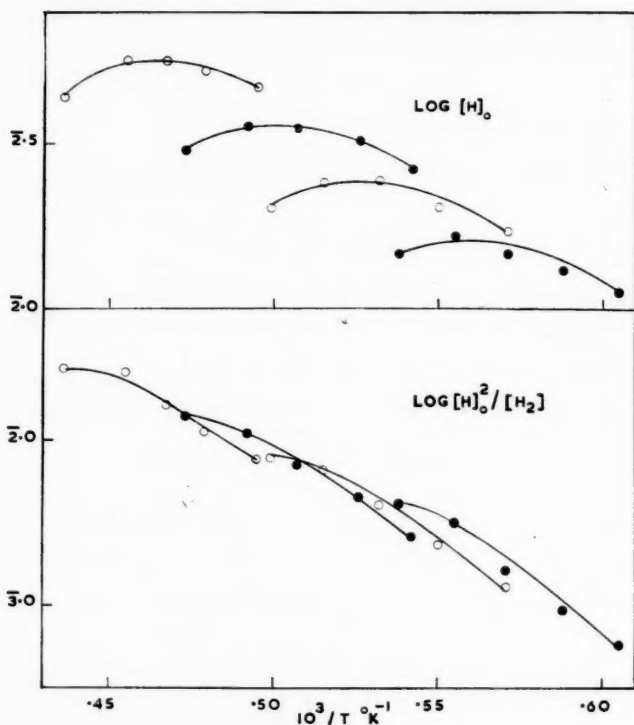
FIG. 6. Variation of $[H]_0$ and $[H]_0^2/[H_2]$ with flame composition. $[H]_0$ is the partial pressure (in atmospheres) of hydrogen atoms in the reaction zone. Flame families (N_2/O_2 in unburnt gas) 4, 5, 6, and 7. Points in each family are for unburnt H_2/O_2 ratios 2.5, 3, 3.5, 4, and 4.5. The temperature indicated is the steady value reached in the burnt gases after a time of $\sim$1 millisecond.

4. The Efficiency of Emission in the Continuum

A figure for the number of quanta emitted per cubic centimeter/second, can be obtained by suitable integration over the whole of the continuum, and comparing the result with the known thermal emission from the sodium D-lines under conditions of known sodium concentration and no self-reversal. The result of this measurement is to establish that 1 quantum in the continuum for HCl is emitted for every 4×10^{10} normal kinetic collisions of H and Cl atoms in a flame at ca. 2300° K. This figure is subject to a number of limitations. Firstly, the intensity was only observed from about 3000 Å, where it becomes very weak, to 6500 Å, where it is still quite strong; any infrared contribution is ignored. Secondly, a mean collision diameter of 3 Å for H and Cl has been assumed in calculating the frequency of 'normal' collisions. Nevertheless, the above result for the "efficiency" of emission should be correct to an order of magnitude.

Figure 8 shows plots of relative k (where $I = k[H][X]$) obtained by computing $(I/[H][X])$, and indicates the way in which k varies with temperature. The plots show that it decreases markedly with increasing temperature for chlorine, at a rate corresponding to an exponential term with an energy of about 15 kcal/mole. The corresponding
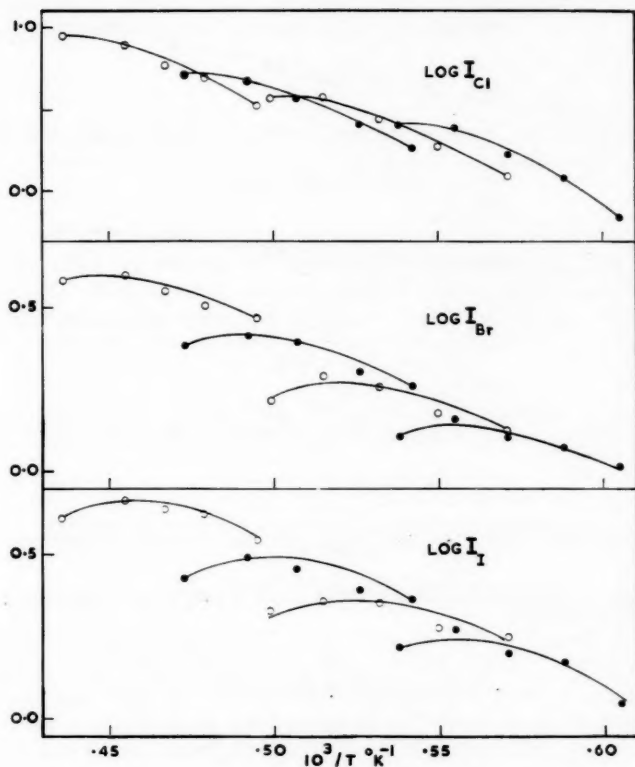
FIG. 7.   Variation of intensities of halogen continua in reaction zone with flame composition. Families as in Fig. 6. $[Cl]_0 = 2 \times 10^{-2}$ atm, $[Br]_0 = [I]_0 = 2 \times 10^{-3}$ atm.

decrease for bromine is much smaller, and no decrease is observed for iodine, although in this case there is quite a high scatter on the points. These results do not refer to complete wavelength scans, but only to the emission at 4900 Å for chlorine and bromine, and 6400 Å for iodine. They must be interpreted with caution since the dependence of intensity distribution on temperature has not yet been fully explored.

DISCUSSION

Given that the intensity of the emission is proportional to [H][X], two types of mechanism appear possible.

(i) Direct radiative recombination from an upper electronic state which is arrived at by collision of atoms (ground state H and $^2P_{3/2}$ or $^2P_{1/2}$ atoms of halogen), without the intervention of any third body.

(ii) Stabilization of an intermediate HX* formed by collision of the atoms in the presence of a third body M. A typical scheme may be written
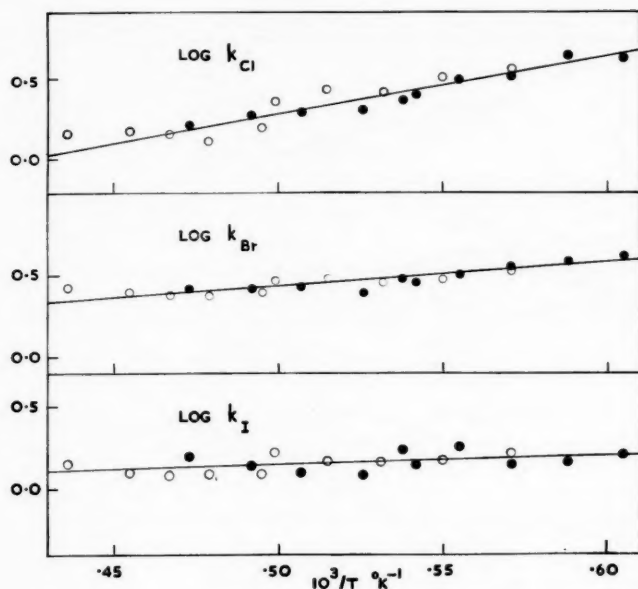
FIG. 8. Dependence of relative k, defined by I (continuum) $= k[H][X]$ on temperature for the halogen continua in hydrogen-rich flames.

$$H + X + M \overset{k_1}{\rightarrow} HX^* + M,$$

$$HX^* + M \overset{k_{-1}}{\rightarrow} H + X + M,$$

$$HX^* + M \overset{k_2}{\rightarrow} HX + M,$$

$$HX^* \overset{k_3}{\rightarrow} HX + h\nu.$$
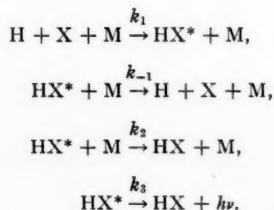
If the mean kinetic energy of approach of H and X, given by kT, is small compared with the vibrational spacing in the ground electronic state, then some fluctuations in intensity of emission corresponding with this spacing might be expected in case (i). It is interesting that Weizel, Wolff, and Binkele (28) observed multiple maxima in apparently continuous emission between the green and 2500 Å with hydrogen bromide in a weak uncondensed discharge. At flame temperatures kT is about one half of the vibrational spacing and such maxima might be obscured, giving an apparently smooth continuum. Case (ii) might be expected to give a somewhat more discrete spectrum, but if HX* has only a shallow minimum a large number of its vibrational states would be occupied, which, together with the number of rotational levels involved at flame temperatures could well make the result indistinguishable, with our resolution, from case (i).

The previously observed absorption spectra are of little use here, since only continua have been observed. Goodeve and Taylor (29, 30) obtain absorption continua for HBr and HI, which they consider are connected with dissociation to $H(^2S_{1/2})$, $Br(^2P_{3/2})$, and $I(^2P_{3/2})$. Unfortunately the long wavelength limits lie above the dissociation energy, and

it is then impossible to say whether the HX^* is in a completely repulsive state or not. These observations, as well as others by Trivedi (31), are discussed by Finkelnburg (32).

From the general kinetic point of view, case (i) leads to

$$I = k[H][X]$$

where k is the velocity constant of a single process, whereas case (ii) leads to

$$I = (k_3 k_1 [H][X][M])/(k_{-1}[M] + k_2[M])$$

provided that radiation is only a minor source of removal of HX^* molecules. M may be different for the reactions leading to dissociation and deactivation of HX^*, and so does not cancel directly. If dissociation predominates, $k_{-1}[M] \gg k_2[M]$ and [M] then cancels. Writing K_1, the equilibrium constant of $H + X \rightleftharpoons HX^*$, for k_1/k_{-1}, we have

$$I = k_3 K_1 [H][X] \quad \text{and} \quad k = k_3 K_1.$$

If the heat of dissociation of HX^* into $H(^2S_{1/2}) + X(^2P_{3/2})$ is ΔE^*, a positive quantity, then K_1 may be written

$$K_1 = Q_1 \exp (\Delta E^*/RT)$$

and a rough calculation, with reasonable rotational and vibrational parameters, leads to

$$K_1 = 10^{-23} \exp (\Delta E^*/RT) \text{ cm}^{-3}.$$

The experimental values of k are of the order of 10^{-21} cm^3 sec^{-1}, so that if $\Delta E^* = 10$ kcal/mole, at $2000°$ the value of k_3 will be of order 10 sec^{-1}. This implies a highly forbidden transition; reference to the states indicating that $^3\Pi \rightarrow {}^1\Sigma$ would be the only one to fulfil such a requirement. Increments of ΔE^* by units of 10 kcal/mole have the effect of decreasing k_3 approximately by orders of magnitude, but the absence of discrete spectra implies that HX^* cannot be very stable.

If deactivation predominates over dissociation, i.e. $k_2[M] \gg k_{-1}[M]$, k_3 is correspondingly increased, and the radiative lifetime shortened. It is improbable that this inequality would amount to a sufficient factor to make the radiative lifetime short enough for a fully allowed transition (order of 10^{-8} sec).

A very crude analysis of case (i) can be made as follows. The period of a molecular vibration is of the order of 10^{-13} sec, and this can be taken as the duration of a collision for a repulsive state. A normal radiative lifetime for electronic transition (10^{-8} sec) would then give an efficiency of order 10^{-5}, corresponding with k of order 10^{-15} cm^3 sec^{-1}. Again, therefore, the transition must be a highly forbidden one.

It is considered that the different variations with temperature found for the various halogens probably favor case (ii) insofar as ΔE^* could readily show a range of 15 kcal/mole among the halogens. No great temperature dependence of k_3 would be expected, nor of k for case (i), but the evidence presented here is not sufficient to allow of a final decision. It is of interest that the NO–O 'continuum' in flames has recently been shown (33) to derive, at least to some extent, from a mechanism of the general type (ii).

REFERENCES

1. T. M. SUGDEN. Trans. Faraday Soc. **52**, 1465 (1956).
2. P. J. PADLEY and T. M. SUGDEN. Proc. Roy. Soc. A, **248**, 248 (1958).
3. E. M. BULEWICZ, C. G. JAMES, and T. M. SUGDEN. Proc. Roy. Soc. A, **235**, 89 (1956).
4. E. M. BULEWICZ and T. M. SUGDEN. Trans. Faraday Soc. **54**, 1855 (1958).
5. P. J. PADLEY and T. M. SUGDEN. Symposium on Combustion. 7th Symposium. Butterworth Scientific Publications, London. 1959. p. 235.
6. E. M. BULEWICZ and T. M. SUGDEN. Trans. Faraday Soc. **52**, 1475 (1956).
7. E. M. BULEWICZ and T. M. SUGDEN. Trans. Faraday Soc. **52**, 1481 (1956).
8. C. G. JAMES and T. M. SUGDEN. Proc. Roy. Soc. A, **248**, 238 (1958).
9. A. G. GAYDON. The spectroscopy of flames. Chapman & Hall, London. 1957.
10. P. J. PADLEY. Trans. Faraday Soc. **56**, 449 (1960).
11. E. H. COLEMAN, A. G. GAYDON, and W. M. VAIDYA. Nature (London), **162**, 108 (1948).
12. E. H. COLEMAN and A. G. GAYDON. Discussions Faraday Soc. **2**, 166, 176 (1947).
13. G. PANNETIER and A. G. GAYDON. Nature (London), **161**, 242 (1948).
14. G. PORTER. Discussions Faraday Soc. **9**, 60 (1950).
15. A. G. GAYDON. Proc. Roy. Soc. A, **183**, 111 (1944).
16. A. G. GAYDON. Trans. Faraday Soc. **42**, 292 (1946).
17. H. P. BROIDA and A. G. GAYDON. Trans. Faraday Soc. **49**, 1190 (1953).
18. H. P. BROIDA and A. G. GAYDON. Proc. Roy. Soc. A, **222**, 181 (1954).
19. W. E. KASKAN. Combustion and Flame, **3**, 39 (1959).
20. A. G. GAYDON and H. G. WOLFHARD. Flames. Chapman & Hall, London. 1960.
21. C. G. JAMES and T. M. SUGDEN. Proc. Roy. Soc. A, **227**, 312 (1955).
22. H. SMITH and T. M. SUGDEN. Proc. Roy. Soc. A, **219**, 204 (1953).
23. P. GRAY. Trans. Faraday Soc. **55**, 408 (1959).
24. A. G. GAYDON. Dissociation energies. 2nd ed. Chapman & Hall, London. 1953.
25. V. KONDRATIEV and A. LEIPUNSKI. Z. Physik, **50**, 366 (1928).
26. E. B. LUDLAM, H. G. REID, and G. S. SOUTAR. Proc. Roy. Soc. Edinburgh, **49**, 156 (1929).
27. H. C. UREY and J. R. BATES. Phys. Rev. **34**, 1541 (1929).
28. W. WEIZEL, H. W. WOLFF, and H. E. BINKELE. Z. physik. Chem. B, **10**, 459 (1930).
29. C. F. GOODEVE and A. W. C. TAYLOR. Proc. Roy. Soc. A, **152**, 221 (1935).
30. C. F. GOODEVE and A. W. C. TAYLOR. Proc. Roy. Soc. A, **154**, 181 (1936).
31. H. TRIVEDI. Proc. Natl. Acad. Sci. India, **6**, 18 (1936).
32. W. FINKELNBURG. Kontinuierliche Spektren. Julius Springer, Berlin. 1938. p. 155.
33. H. P. BROIDA, H. I. SCHIFF, and T. M. SUGDEN. To be published.

NITRATION OF BICYCLIC GUANIDINES[1]

A. F. McKay and M.-E. Kreling

ABSTRACT

The course of the nitration of a bicyclic guanidine system has been shown to depend on substitution at an adjacent carbon atom. The pyrimidine ring in 5-keto-2,3,6,7-tetrahydro-5(H)-thiazolo(3,2-a)pyrimidine is opened more rapidly by benzylamine and ethanolic hydrogen chloride than the pyrimidine ring in 5-keto-2,3,6,7-tetrahydro-1(H),5(H)-imidazo(1,2-a) pyrimidine. These effects are interpreted in terms of the resonance ion structure at the ring junctions.

The bicyclic guanidine, 2,3,6,7-tetrahydro-1(H),5(H)-imidazo(1,2-a)pyrimidine,[2] has been converted into 1-nitro-2,3,6,7-tetrahydro-1(H),5(H)-imidazo(1,2-a)pyrimidinium nitrate by nitration in absolute nitric acid – acetic anhydride medium (1). Nitration of the 2,3,6,7-tetrahydro-1(H),5(H)-imidazo(1,2-a)pyrimidinium ion is consistent with the presence of the guanidinium ion in its structure. The model of this bicyclic guanidinium ion may be represented diagrammatically by structure I. Atoms 1, 2, 3, 4, 5, 8, and 9 are

(I)
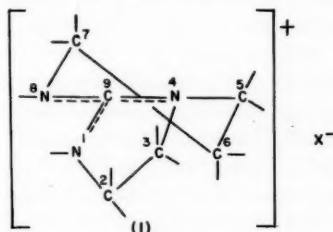
in the same plane, since the five-membered ring can be considered to be planar. A slight deviation of C atoms 2 or 3 from the plane of the ring would not contribute much to a relief of strain within this structure. A continuation of nitration studies on the 2,3,6,7-tetrahydro-1(H),5(H)-imidazo(1,2-a)pyrimidine system has shown that an electronegative substituent such as oxygen or nitrogen on C_5 affects the nitration of the guanidine structure.

Nitration of 5-imino-2,3,6,7-tetrahydro-1(H),5(H)-imidazo(1,2-a)pyrimidinium chloride (II) in absolute nitric acid – acetic anhydride medium gave 5-nitrimino-2,3,6,7-tetrahydro-1(H),5(H)-imidazo(1,2-a)pyrimidinium nitrate (III). The failure of the guanidine structure to nitrate is explained by the electron displacements within structure II. There are two opposing electron attractive forces working on N_4; one involves its participation in the guanidinium ion and the other in the electron displacement indicated by the curved unbroken arrows in structure II. These opposing forces give the resonance ion structure more of an amidinium ion character than a guanidinium ion character and the amidinium ion does not nitrate. Thus nitration occurs only on the 5-imino nitrogen. The same explanation is given for the failure of 5-keto-2,3,6,7-tetrahydro-1(H),5(H)-imidazo(1,2-a)pyrimidine to nitrate.

5-Nitrimino-2,3,6,7-tetrahydro-1(H),5(H)-imidazo(1,2-a)pyrimidinium nitrate (III) is converted into 5-keto-2,3,6,7-tetrahydro-1(H),5(H)-imidazo(1,2-a pyrimidinium nitrate (IV) on crystallization from ethanol. Because of this easy replacement of the nitrimino group, extreme care was required in the preparation of a pure sample of compound III.
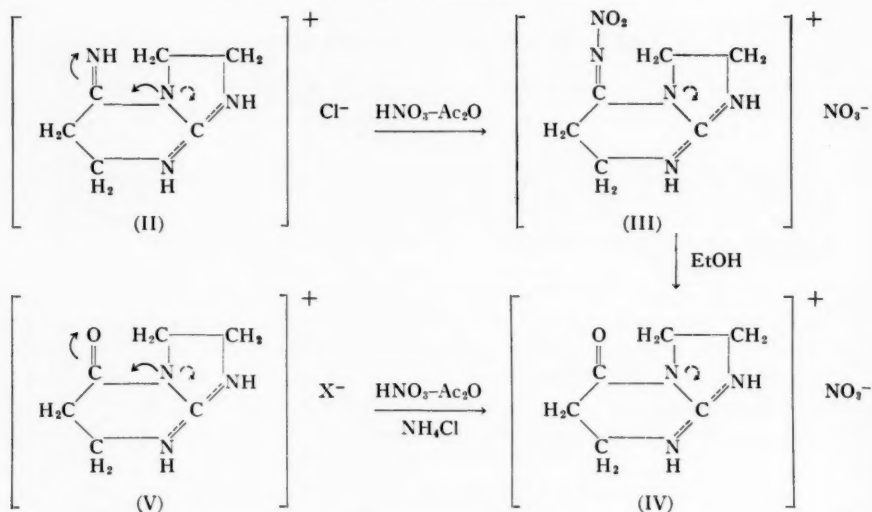
When 5-keto-2,3,6,7-tetrahydro-5(H)-thiazolo(3,2-a)pyrimidine (VI) was treated with an ethanolic solution of hydrogen chloride, a quantitative yield of 2-(β-carbethoxyethyl-amino)-2-thiazoline was obtained. Similarly benzylamine opened the pyrimidine ring of VI to give 2-(β-(N-benzylcarbamyl)-ethylamino)-2-thiazoline (2). Both ethanolic hydrogen chloride and benzylamine failed to open the pyrimidine ring of 5-keto-2,3,6,7-tetrahydro-1(H),5(H)-imidazo(1,2-a)pyrimidine (V) under similar conditions. The greater resistance of the pyrimidine ring to opening in V than in VI is due to the relative ease of electron displacements towards the carbonyl oxygen atom in these two systems. In V the opposing electron attractive force to the electron displacement indicated by the solid arrows[3] is greater than the opposing electron attractive force in VI. This is probably the main factor contributing to relative ease of opening the pyrimidine ring in these compounds although the slight difference in the conformations of the two ring systems also may make some contribution.
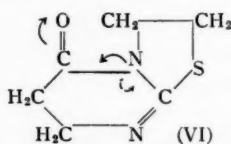
EXPERIMENTAL[4]

5-Keto-2,3,6,7-tetrahydro-1(H),5(H)-imidazo(1,2-a)pyrimidine

2-(β-Carboxyethylamino)-Δ²-1,3-diazacyclopentene (m.p. 209–211° C with decomp.) was prepared in 73.2% yield and the acid was esterified with ethanolic hydrogen chloride as previously described (3). On evaporation of the ethanolic solution 2-(β-carbethoxy-ethylamino)-Δ²-1,3-diazacyclopentene hydrochloride was obtained as a viscous oil.

[3]*The solid and broken arrows in the graphic formulas are used only for differentiation in discussion and they have no quantitative significance. Actually the degree of electron displacement in the* $\diagup$N—C═N$^+\diagdown$ *system is greater than in* $\diagup$N—C═O. *The effects of electronic displacements and resonance on the chemical reactivity of the bicyclic guanidines are under investigation.*

[4]*All melting points are uncorrected. Analyses were performed by Micro-Tech Laboratories, Skokie, Illinois.*

The above ester hydrochloride (10.3 g, 0.0465 mole) in absolute methanol (200 ml) was passed through a column of IRA-400 resin in the hydroxyl form. The resin column had been previously washed with absolute methanol. After the resin had been washed with absolute methanol (150 ml), the eluate and washings were evaporated to dryness *in vacuo*. The white crystalline residue weighed 6 g (92.8% yield). It melted at 141° C, resolidified, and melted at 148–149° C. This melting point was not changed by crystallization from absolute ethanol – ether (1:2) solution. Anal. Calc. for $C_6H_9N_3O$: C, 51.78; H, 6.52; N, 30.20%. Found: C, 51.53; H, 6.31; N, 30.34%.

The picrate (m.p. 248–249° C) of 5-keto-2,3,6,7-tetrahydro-1(H),5(H)-imidazo(1,2-*a*) pyrimidine was prepared in 95% yield from ethanol solution. Anal. Calc. for $C_{12}H_{12}N_6O_8$: C, 39.14; H, 3.29; N, 22.82%. Found: C, 38.93; H, 3.41; N, 22.75%.

5-Keto-2,3,6,7-tetrahydro-1(H),5(H)-imidazo(1,2-a)pyrimidinium Nitrate

5-Keto-2,3,6,7-tetrahydro-1(H),5(H)-imidazo(1,2-a)pyrimidine (0.695 g, 0.005 mole) was added to a nitration medium consisting of 98% nitric acid (2.33 ml, 0.05 mole), acetic anhydride (4.72 ml, 0.05 mole) and ammonium chloride (0.6 g, 0.011 mole). After the reaction mixture was stirred at 32° C for 2 hours, it was poured into cold absolute ether (75 ml). The ether was decanted from the oil, which was washed twice with fresh portions of absolute ether. After the oil was triturated with absolute ethanol, crystals (m.p. 129.5–131° C) separated from the oil, yield 0.57 g (56.4%). One crystallization from absolute ethanol raised the melting point to 132–133° C. Anal. Calc. for $C_6H_{10}N_4O_4$: C, 35.65; H, 4.99; N, 27.71%. Found: C, 35.56; H, 4.88; N, 27.38%.

The picrate (m.p. 247–249° C), which was prepared from absolute ethanol solution in 91.8% yield, did not depress the melting point of a known sample of 5-keto-2,3,6,7-tetrahydro-1(H),5(H)-imidazo(1,2-a)pyrimidine picrate (m.p. 248–249° C).

5-Imino-2,3,6,7-tetrahydro-1(H),5(H)-imidazo(1,2-a)pyrimidine

2-Methylmercapto-2-imidazolinium iodide (14.64 g, 0.06 mole) and β-aminopropionitrile (4.2 g, 0.06 mole) in absolute ethanol (15 ml) were refluxed for 7 hours. Crystals (m.p. 192–198° C) separated from the solution on cooling, yield 7.43 g (46.5%). Several crystallizations from absolute ethanol raised the melting point to 201–203° C. Anal. Calc. for $C_6H_{11}IN_4$: C, 27.08; H, 4.17; N, 21.06; I, 47.69%. Found: C, 27.26; H, 4.08; N, 20.86; I, 47.43%.

Decreasing the reflux period in the above reaction in individual runs to 2 and 5.5 hours lowered the yields of 5-imino-2,3,6,7-tetrahydro-1(H),5(H)-imidazo(1,2-a)pyrimidinium iodide to 37.6 and 41% respectively.

The picrate (m.p. 228–231° C) was formed from aqueous solution. Recrystallization from water–ethanol (1:1) solution raised the melting point to 248–249° C. This picrate was shown by analysis and a mixed melting point determination to be identical with the picrate (m.p. 248–249° C) from 5-keto-2,3,6,7-tetrahydro-1(H),5(H)-imidazo(1,2-a) pyrimidine. Thus the imino group of the original compound was hydrolyzed to a keto group during the formation of the picrate in aqueous solution.

A sample of 5-imino-2,3,6,7-tetrahydro-1(H),5(H)-imidazo-(1,2-a)pyrimidinium iodide (9.1 g, 0.034 mole) in absolute methanol (180 ml) was passed through a column of IRA-400 resin (Cl⁻ form) which had been washed thoroughly with absolute methanol. The column was washed with absolute methanol (150 ml) and the eluate was taken to dryness *in vacuo* under nitrogen. The hydrochloride salt was obtained in 98.9% (5.90 g) yield. One crystallization from absolute methanol – ether (1:1) gave crystals melting at 193–194° C. Anal. Calc. for $C_6H_{11}ClN_4$: C, 41.27; H, 6.35; Cl, 20.30; N, 32.09%. Found: C, 41.42; H, 6.36; Cl, 20.44; N, 31.89%.

An ethanolic solution of a sample of 5-imino-2,3,6,7-tetrahydro-1(H),5(H)-imidazo(1,2-a)pyrimidinium chloride on treatment with ethanolic picric acid gave a dipicrate (m.p. 218–220° C) in 77% yield. Anal. Calc. for $C_{18}H_{16}N_{10}O_{14}$: C, 36.25; H, 2.74; N, 23.49%. Found: C, 36.50; H, 2.96; N, 23.38%.

5-Nitrimino-2,3,6,7-tetrahydro-1(H),5(H)-imidazo(1,2-a)pyrimidinium Nitrate

5-Imino-2,3,6,7-tetrahydro-1(H),5(H)-imidazo(1,2-a)pyrimidinium chloride (0.75 g, 0.0043 mole) was added to a nitration medium of 98% nitric acid (2.0 ml, 0.043 mole), acetic anhydride (4.06 ml, 0.043 mole), and ammonium chloride (0.3 g, 0.0056 mole) at 0° C. The temperature was raised to 32° C and the stirred solution was maintained at this temperature for 2.5 hours. When the solution was poured into cold absolute ether (75 ml) a sticky crystalline mass separated. The ether solution was decanted from the solid, which was washed with absolute ether (3×50 cc) by decantation. The solid was triturated with absolute ethanol (50 cc) and the crystals were recovered by filtration. After this process was repeated, the crystals were dried in vacuo at room temperature. The crystals melted at 152.5–153° C with decomposition, yield 0.45 g (42.6%). Anal. Calc. for $C_6H_{10}N_6O_5$: C, 29.27; H, 4.10; N, 34.13%. Found: C, 29.27; H, 4.32; N, 34.47%.

After a sample of the 5-nitrimino-2,3,6,7-tetrahydro-1(H),5(H)-imidazo(1,2-a)pyrimidinium nitrate was refluxed in ethanol for 1.5 hours, the crystals obtained on cooling the solution melted at 131–133° C. These crystals did not depress the melting point of a known sample of 5-keto-2,3,6,7-tetrahydro-1(H),5(H)-imidazo(1,2-a)pyrimidine nitrate (m.p. 132–133° C). The infrared spectra of these two samples were also identical.

Attempts to Open the Pyrimidine Ring of 5-Keto-2,3,6,7-tetrahydro-1(H),5(H)-imidazo-(1,2-a)pyrimidine

(A) With Benzylamine

5-Keto-2,3,6,7-tetrahydro-1(H),5(H)-imidazo(1,2-a)pyrimidine (0.556 g, 0.004 mole) and benzylamine (0.43 g, 0.004 mole) in absolute ethanol (7 ml) were allowed to stand at room temperature for 17 hours. The solution was concentrated to 3 ml in vacuo and ether was added. The crystals (m.p. 141° C and 148–149° C) on admixture with the starting material gave no depression in melting point, yield 0.506 g (91%).

A similar experiment in which the reactants in ethanolic solution were refluxed for 3.5 hours gave an 81% recovery of starting material.

(B) With Ethanolic Hydrogen Chloride

A solution of 5-keto-2,3,6,7-tetrahydro-1(H),5(H)-imidazo(1,2-a)pyrimidine (0.278 g, 0.002 mole) in ethanolic hydrogen chloride (10 ml of absolute ethanol containing 79 mg, 0.0022 mole of hydrogen chloride) was refluxed for 2.5 hours. The cooled solution was divided into two equal parts. One part on treatment with ethanolic picric acid solution gave 5-keto-2,3,6,7-tetrahydro-1(H),5(H)-imidazo(1,2-a)pyrimidine picrate (m.p. 248–249° C) in 98% (0.36 g) yield. This picrate did not depress the melting point of a known sample of 5-keto-2,3,6,7-tetrahydro-1(H),5(H)-imidazo(1,2-a)pyrimidine picrate (m.p. 248–249° C).

The second portion on standing in the cold gave crystals melting at 251.5–252.5° C, yield 120 mg (68.4%). The melting point of this sample of 5-keto-2,3,6,7-tetrahydro-1(H), 5(H)-imidazo(1,2-a)pyrimidinium chloride was not changed by crystallization from ethanol–ether solution. Anal. Calc. for $C_6H_{10}ClN_3O$: C, 41.04; H, 5.74; Cl, 20.19; N, 23.93%. Found: C, 41.18; H, 5.91; Cl, 20.00; N, 23.34%.

REFERENCES

1. A. F. McKay and M.-E. Kreling. Can. J. Chem. 35, 1438 (1957).
2. A. F. McKay, D. J. Whittingham, and M.-E. Kreling. J. Am. Chem. Soc. 80, 3339 (1958).
3. A. F. McKay and W. G. Hatton. J. Am. Chem. Soc. 78, 1618 (1956).

THE STRUCTURE OF LYCODINE[1]

W. A. Ayer and G. G. Iverach

ABSTRACT

The molecular formula of the *Lycopodium* alkaloid lycodine has been revised to $C_{16}H_{22}N_2$. Transformation of β-obscurine (I) into N-methyl lycodine has shown that lycodine is the pyridine analogue of des-N-methyl-β-obscurine and is represented by structure II (R = H). The transformation of β-obscurine into α-obscurine is also described.

The alkaloid lycodine was first isolated from *Lycopodium annotinum* L. in 1958 by Anet and Eves (1), who assigned to it a molecular formula $C_{17}H_{24}N_2$. Lycodine was shown to be a tetracyclic diacidic base containing a secondary nitrogen atom, a 5,6,7,8-tetrahydroquinoline system unsubstituted in the heterocyclic ring, and a C-methyl group.

When structure I was advanced for β-obscurine (2) it was suggested that lycodine is formed by a similar biogenetic path,[2] with the exception that N-methylation has not occurred, and is represented by structure II (R = H). The correctness of this structure has now been confirmed by a series of experiments which are described in this communication.

The isolation of lycodine from *L. annotinum* L. involves a rather extended separation procedure (1). We have found that lycodine also occurs in *L. obscurum* L. and is readily separable by chromatography of the crude bases over alumina. Some lycodine was obtained directly by crystallization of the eluates. The remainder was separated from contaminating bases (mainly lycopodine and annotinine) by lithium aluminum hydride reduction, which transformed the contaminants into hydroxylic materials but did not affect the lycodine, followed by chromatography. The total yield of lycodine from dried plant material was approximately 0.003%.

I   II
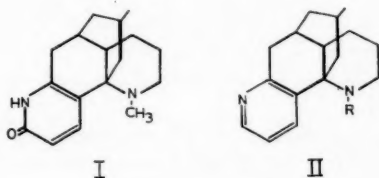
Structure II (R = H) requires that the formula of lycodine be revised to $C_{16}H_{22}N_2$. The analytical results quoted by Anet and Eves (1), especially those for the dipicrate of lycodine and the picrate of N-acetyl lycodine, do not clearly differentiate between the two possibilities. Our analytical results with lycodine and N-methyl lycodine, together with the preparation of N-methyl lycodine from β-obscurine ($C_{17}H_{24}ON_2$) described below, confirm the 16 carbon formulation. The proposed structure differs in two other respects from the partial structure advanced by Anet and Eves (1). Firstly, the more strongly basic nitrogen is attached to a carbon α to the pyridine ring. This attachment

[1]*Manuscript received June 13, 1960.*

Contribution from the Department of Chemistry, University of Alberta, Edmonton, Alberta. This work forms a portion of a thesis to be submitted by G. G. Iverach in partial fulfillment of the requirements for the degree of Master of Science.

[2]*Recently, Professor H. Conroy (3) has outlined a biogenetic scheme which accounts for the formation, from acetate units and ammonia, of all the Lycopodium alkaloids of known structure.*

Can. J. Chem. Vol. 38 (1960)

1823

was regarded as improbable by the previous workers on the basis of a comparison of the pK_a's of the pyridine nitrogen atoms in lycodine and nicotine. We believe that the greater basicity (pK_a 3.97) of the pyridine nitrogen in lycodine as compared with that in nicotine (pK_a 3.35) is explained by the presence in lycodine of an electropositive substituent in the 2-position of the pyridine ring (4). Secondly, the C-methyl group of lycodine is not attached to a quaternary carbon atom. The assignment of the C-methyl group to such a grouping was made on the basis of the fact that the C-methyl peak in the nuclear magnetic resonance spectrum of lycodine is unsplit (1). The failure of the $>$CHCH$_3$ peak to split is possibly attributable to the proximity of the aromatic ring, since in β-obscurine (I) the C-methyl peak is also unsplit, whereas in α-obscurine (III) the usual splitting occurs (2). In this connection, it is interesting to note that reduction of β-obscurine (I) with lithium and ammonia, a reagent which has been shown (5) to selectively reduce α-pyridones to the corresponding 3,4-dihydro-α-pyridones, yields α-obscurine (III).

It seemed at this point that structure II could be confirmed by direct transformation of β-obscurine (I) into lycodine (II, R = H) or, since some difficulty was anticipated in the removal of the N-methyl group of β-obscurine, into N-methyl lycodine (II, R = CH$_3$).
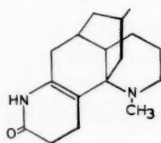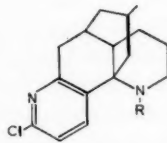
III   IV

Treatment of lycodine with formaldehyde and formic acid gave, in good yield, N-methyl lycodine (II, R = CH$_3$). The new base had no NH stretching band in the infrared and the ultraviolet spectrum was almost identical with that of lycodine. The nuclear magnetic resonance spectrum was similar to that of lycodine (1), with the addition of a strong (3-proton) signal at $\tau = 7.38$ due to the N-methyl group (6). The C-methyl peak (at $\tau = 9.21$) was again unsplit.

The transformation of an α-pyridone into the corresponding 2-chloropyridine is usually accomplished by the treatment with phosphorus oxychloride, phosphorus pentachloride, or a mixture of these two reagents (7). β-Obscurine was recovered unchanged after prolonged refluxing with phosphorus oxychloride and phosphorus oxychloride – phosphorus pentachloride. However, treatment with phosphorus pentachloride at 200° or, preferably, with phenylphosphonic dichloride (8) yielded an oily product whose spectral properties (ultraviolet maximum at 275 mμ, peak in the infrared at 1565 cm^{-1}) were consistent with those expected for the desired chloropyridine IV. The crude chloro compound was hydrogenated over platinum in acetic acid. Chromatography of the products gave N-methyl lycodine (41% yield from β-obscurine) and, unexpectedly, lycodine (23% yield). Presumably, loss of the N-methyl group occurred during the treatment with phenylphosphonic dichloride and the oily product was a mixture of the chloropyridines IV (R = CH$_3$) and IV (R = H). The appearance of a weak NH band at 3330 cm^{-1} in the infrared spectrum of the crude product is consistent with this view.

This transformation establishes that lycodine is the pyridine analogue of des-N-methyl-β-obscurine and, on the basis of the proposed (2) structure for β-obscurine, is represented by structure II (R = H).

EXPERIMENTAL

Ultraviolet spectra were measured in ethanol and, unless otherwise stated, infrared spectra in chloroform. Microanalyses are by Pascher Mikroanalytisches Laboratorium, Bonn, West Germany, and Micro-Tech Laboratory, Skokie, Illinois.

Isolation of Lycodine

Finely ground *L. obscurum* L. (10 kg) was extracted by the procedure of Manske and Marion (9). The crude alkaloids (9.3 g) yielded some lycopodine (2.0 g) on crystallization from ether. The mother liquors were dissolved in chloroform and placed on a column of basic alumina (150 g). Thorough elution with chloroform gave 3.75 g of basic material which was rechromatographed over alumina (100 g). Fraction A (2.1 g), eluted with benzene (900 ml), was mainly lycopodine. Fraction B (0.63 g), eluted with ether (850 ml), was a mixture of lycopodine and lycodine (as shown by infrared and ultraviolet measurements). Fraction C (0.17 g), eluted with 1:1 ether – methylene chloride (500 ml), contained annotinine, lycodine, and unidentified carbonyl-containing compounds. Crystallization of fraction B from pentane gave lycodine (172 mg). The residues from the crystallization were combined with fraction C, dissolved in ether, and reduced with lithium aluminum hydride in the usual manner. The product was chromatographed over alumina. Elution with benzene–ether gave crystalline lycodine (130 mg). The combined lycodine was recrystallized several times from pentane to give colorless blocks, m.p. 118–119°. Calc. for $C_{16}H_{22}N_2$: C, 79.29; H, 9.15; N, 11.56%. Found: C, 79.49, 79.33; H, 9.13, 9.09; N, 11.61, 11.47%; no N-methyl.

N-*Methyl Lycodine*

Lycodine (52 mg) was dissolved in 98% formic acid (0.25 ml) and formalin (0.25 ml) added. The solution was refluxed for 2 hours, then maintained at 50° for 12 hours. The reaction mixture was diluted with water (50 ml), basified with concentrated ammonium hydroxide, and extracted several times with chloroform. Evaporation of the dried chloroform extracts gave a pale yellow oil (0.05 g) which solidified on standing. Three recrystallizations from acetone gave N-methyl lycodine as colorless blocks (23 mg), m.p. 91–92°. Calc. for $C_{17}H_{24}N_2$: C, 79.63; H, 9.44; N, 10.93; one N—CH_3, 5.86%. Found: C, 79.61, 79.59; H, 9.36, 9.27; N, 11.25, 10.75; N—CH_3, 5.19%. Ultraviolet spectrum: λ_{max} 268 mμ (log ϵ = 3.61), shoulder at 275 mμ (log ϵ = 3.49). Infrared spectrum (Nujol): γ_{max} 3040, 1574, 1472, 812, 737 cm^{-1} (pyridine ring).

N-*Methyl Lycodine and Lycodine from* β-*Obscurine*

A solution of β-obscurine (168 mg, isolated from *L. annotinum* L. by established procedures (10, 11)) in phenylphosphonic dichloride (50 ml) was maintained at 200–210° for 45 minutes. The reaction solution was decomposed with ice and water and made basic by the addition of concentrated ammonium hydroxide. Chloroform extraction yielded the crude chloro compounds IV (R = CH_3) and IV (R = H) as a pale yellow oil (0.16 g), ultraviolet maximum 275 mμ, infrared peaks at 3330 cm^{-1} (NH) and 1565 cm^{-1} (pyridine ring). The oil was dissolved in glacial acetic acid and shaken with hydrogen (50 p.s.i.) in the presence of Adam's catalyst (100 mg) for 3 hours. The catalyst was filtered off and the filtrate concentrated, diluted with water, made basic with ammonium hydroxide, and extracted thoroughly with chloroform. Removal of the chloroform left a viscous yellow oil (0.12 g) which was chromatographed over basic alumina (3 g). Elution with benzene and crystallization from acetone gave N-methyl lycodine (65 mg), m.p. 91–92°. This did not depress the melting point of the N-methyl compound prepared from lycodine and their infrared spectra were identical.

Elution of the column with ether yielded a fraction (35 mg) which crystallized from acetone as colorless blocks, m.p. 115–116°. The infrared spectrum was identical with that of lycodine and a mixture melting point was undepressed.

α-Obscurine from β-Obscurine

A solution of β-obscurine (31 mg) in dry tetrahydrofuran (100 ml) was added during 1/2 hour to a vigorously stirred solution of lithium (0.1 g) in ammonia (40 ml). The solution was stirred for a further $2\frac{1}{2}$ hours, then the reaction mixture was evaporated to dryness. The residue was dissolved in aqueous HCl, washed with chloroform, basified, and extracted with chloroform. Evaporation of the chloroform left a solid residue which was chromatographed over alumina (1 g). Elution with chloroform and crystallization from methanol gave α-obscurine (20 mg), m.p. 285–287° (uncorrected). The mixture melting point with authentic α-obscurine was undepressed, and the infrared spectra of the two were identical.

Further elution of the column with chloroform–methanol (4:1) gave a fraction (7 mg) whose spectral properties were identical with those of β-obscurine.

ACKNOWLEDGMENTS

REFERENCES

1. F. A. L. ANET and C. R. EVES. Can. J. Chem. 36, 902 (1958).
2. W. A. AYER and G. G. IVERACH. Tetrahedron Letters. In press.
3. H. CONROY. Tetrahedron Letters. In press.
4. E. A. BRAUDE and F. C. NACHOD. Determination of organic structures by physical methods. Academic Press, New York. 1955. p. 597.
5. J. A. BERSON and J. S. WALIA. J. Org. Chem. 24, 756 (1959).
6. L. M. JACKMAN. Applications of nuclear magnetic resonance spectroscopy in organic chemistry. Pergamon Press, New York. 1959. p. 56.
7. R. C. ELDERFIELD. Heterocyclic compounds. Vol. 1. John Wiley and Sons, New York. 1950. p. 513.
8. Z. VALENTA, H. YOSHIMURA, E. F. ROGERS, M. TERNBAH, and K. WIESNER. Tetrahedron Letters. In press.
9. R. H. F. MANSKE and L. MARION. Can. J. Research, B, 20, 87 (1942).
10. R. H. F. MANSKE and L. MARION. Can. J. Research, B, 21, 92 (1943).
11. B. P. MOORE and L. MARION. Can. J. Chem. 31, 952 (1953).

SOME EQUILIBRIUM CONSTANTS OF TRANSITION METAL HALIDES[1]

M. W. LISTER AND P. ROSENBLUM

ABSTRACT

Measurements are reported on the formation of complex ions in solutions containing cupric and chloride or bromide ions, and solutions of nickel or cobalt with chloride. In each case the halide was present in very low amount. With copper a spectrophotometric method was used, and a cell voltage method with nickel and cobalt. The ionic strength was kept constant, but the temperature was varied. The data show difficulties of interpretation if it is assumed that only MX^+ ions (M is the metal, X is the halogen) are formed, the difficulties arising from the anomalous variation of the equilibrium constant with temperature, and from the general drift of the calculated constants from the e.m.f. measurements. Various explanations are considered and it is shown that postulation of M_2X^{+3} ions is at least a possible explanation.

A considerable number of measurements have been made on the dissociation constants of complex ions in aqueous solution, particularly those containing transition metals. In many cases, however, no very precise values have been obtained, or the effect of varying conditions, and especially the effect of temperature, has not been examined. The object of the present paper is to report results on the ions $CoCl^+$, $NiCl^+$, $CuCl^+$, and $CuBr^+$. The previous work on these ions will be briefly reviewed as each one is considered. The present work shows that the apparent equilibrium constants for $CuBr^+$, and to a lesser extent for $CuCl^+$, change with temperature in an anomalous manner. The possible cause of this is considered in some detail, since it is relevant to the use of spectrophotometric measurements generally for determining equilibrium constants.

The copper chloride and bromide systems were examined by means of a spectrophotometer, and the cobalt chloride and nickel chloride by means of cell voltages. The results on copper chloride and bromide will be given first, and then their explanation will be considered.

COPPER CHLORIDE MEASUREMENTS

This system has been the subject of many investigations of which the earlier ones are largely qualitative. Of recent investigations the most notable are those of Näsänen (1), who found a value of $K_1 = [CuCl^+]/[Cu^{++}].[Cl^-] = 0.90$ at 25° C; and of McConnell and Davidson (2), who found K_1 to be 1.30 at 25.2° C and 1.39 at 46.9° C, both at an ionic strength of 1.0. The discrepancy between these determinations was attributed by Kruh (3) to neglect of molecules of $CuCl_2$ (or other higher complexes) in Näsänen's calculations.

The present work largely confirms McConnell and Davidson's values. The experimental details are as follows. The optical densities of the solutions were measured by means of a Beckmann DU spectrophotometer, modified to allow water at constant temperature to circulate round the absorption cells. The temperature of the solutions being measured was thereby controlled to ±0.05° C or better.

The materials used were copper perchlorate and sodium perchlorate, supplied by the G. Frederick Smith Co.; sodium chloride (British Drug House's "analar" grade), twice recrystallized; and perchloric acid (Baker "analyzed" reagent). A stock solution of copper perchlorate (about 0.4 M), containing 0.1 M perchloric acid, was prepared, and analyzed iodometrically; other solutions were prepared by diluting the stock solution.

The results are given below in the form of tables of optical density at various copper concentrations. These original data are included because, as will be seen later, there are some difficulties in their interpretation, and their explanation is not entirely certain. Hence the original data are given so that any other possible explanations can be checked against them. All results were at an ionic strength of 2.00 (adjusted by sodium perchlorate), with a perchloric acid concentration of 0.300 M, and a sodium chloride concentration of 0.00748 M. The light path was 1.000 cm. Table I gives the optical densities. The comparison cell contained the same solution without the sodium chloride. Each measurement was repeated, and the setting at zero optical density for the comparison cell was checked after each measurement.

TABLE I

Optical densities of copper chloride at various wave lengths

Temp., °C	Total Cu, M	300 mμ	295	290	285	280	275	270	265	260	255
12.0	.07877	.025	.035	.048	.068	.099	.145	.215	.310	.413	.498
	.09452	.031	.042	.057	.081	.117	.172	.255	.366	.488	.588
	.1103	.035	.048	.065	.093	.135	.199	.294	.422	.561	.675
	.1260	.039	.055	.074	.104	.152	.225	.332	.424	.631	.754
	.1339	.041	.057	.077	.109	.159	.235	.349	.498	.662	.791
	.1417	.045	.061	.083	.116	.168	.248	.367	.522	.698	.826
	.1575	.050	.066	.090	.126	.184	.272	.402	.576	.759	.899
	.1732	.054	.072	.098	.138	.201	.298	.437	.625	.825	.976
	.1891	.057	.178	.105	.148	.216	.319	.469	.670	.876	1.044
25.0	.07877	.038	.054	.072	.102	.148	.216	.315	.439	.570	.670
	.09452	.045	.062	.085	.119	.172	.251	.363	.510	.660	.777
	.1103	.052	.070	.098	.136	.198	.290	.420	.588	.760	.839
	.1260	.059	.081	.111	.154	.225	.329	.477	.662	.860	1.000
	.1339	.061	.084	.115	.162	.236	.344	.499	.697	.900	1.044
	.1417	.066	.090	.122	.171	.249	.363	.526	.732	.946	1.092
	.1575	.073	.099	.133	.187	.271	.396	.571	.797	1.033	1.180
	.1732	.078	.107	.144	.204	.296	.432	.623	.869	1.121	1.274
	.1891	.085	.114	.154	.217	.316	.460	.663	.923	1.188	1.334
40.0	.07877	.059	.081	.111	.156	.226	.325	.462	.629	.795	.911
	.09452	.071	.097	.131	.185	.267	.384	.545	.741	.934	1.064
	.1103	.081	.110	.150	.211	.304	.438	.625	.849	1.072	1.207
	.1260	.092	.123	.168	.238	.342	.492	.698	.952	1.191	1.318
	.1339	.098	.130	.177	.251	.360	.519	.737	1.002	1.261	1.402
	.1417	.103	.137	.187	.263	.376	.542	.769	1.049	1.305	1.424
	.1575	.111	.150	.204	.288	.415	.598	.843	1.147	1.417	1.492
	.1732	.121	.162	.220	.311	.444	.645	.907	1.237	1.518	1.556
	.1891	.129	.174	.237	.333	.479	.689	.981	1.321	1.599	—

COPPER BROMIDE MEASUREMENTS

As with copper chloride, earlier measurements were largely qualitative. Riley and Smith (4) used a cell, $Cu/CuSO_4/KNO_3/CuSO_4 + NaBr/Cu$, to obtain successive equilibrium constants; their value for K_1 was 2.1×10^6. Job (5) used spectrophotometric measurements to get 0.063 for K_1 (the first equilibrium constant). Näsänen (6), using a spectrophotometer, found K_1 to be 0.94 at 25° C. Farrington (7), in 1952, obtained 2.1 ± 0.25 for K_1, at 22 ± 2° C and at unit ionic strength.

In the present work the reagents and method were the same as for copper chloride, except that recrystallized sodium bromide was used in place of sodium chloride. The results in Table II are for an ionic strength of 2.00, with perchloric acid at 0.300 M, and sodium bromide at 0.00839 M. As before, the light path was 1.000 cm, and the comparison cell contained the same solution without the sodium bromide.

TABLE II

Optical densities of copper bromide at various wave lengths

Temp., °C	Total Cu, M	305 mμ	300	295	290	285	280	275	270	265
12.0	.1260	.154	.191	.230	.263	.287	.291	.273	.237	.191
	.1496	.182	.224	.270	.308	.336	.340	.319	.278	.224
	.1732	.208	.256	.309	.353	.383	.389	.364	.317	.257
	.1969	.253	.287	.344	.395	.429	.435	.405	.351	.285
	.2205	.257	.317	.382	.437	.475	.481	.450	.390	.316
	.2441	.280	.343	.415	.475	.518	.525	.491	.427	.345
	.2677	.303	.373	.450	.515	.562	.570	.532	.462	.373
	.2914	.324	.399	.479	.550	.597	.605	.566	.492	.401
	.3149	.346	.427	.512	.590	.639	.648	.604	.523	.422
25.0	.1260	.213	.261	.311	.350	.376	.376	.348	.300	.239
	.1496	.249	.304	.361	.408	.436	.437	.404	.350	.280
	.1732	.287	.349	.414	.469	.500	.501	.463	.398	.320
	.1969	.317	.386	.460	.519	.556	.556	.512	.440	.350
	.2205	.348	.426	.505	.572	.610	.610	.565	.486	.388
	.2441	.379	.464	.552	.623	.668	.668	.618	.530	.426
	.2677	.408	.498	.590	.667	.714	.714	.659	.567	.456
	.2914	.435	.530	.627	.712	.763	.764	.705	.607	.488
	.3149	.462	.564	.668	.757	.810	.811	.751	.642	.515
40.0	.1260	.308	.370	.435	.483	.509	.501	.458	.386	.306
	.1496	.358	.429	.505	.562	.593	.583	.534	.452	.358
	.1732	.409	.490	.573	.639	.674	.662	.604	.511	.406
	.1969	.455	.545	.637	.710	.748	.735	.670	.469	.455
	.2205	.498	.602	.702	.784	.827	.815	.744	.630	.502
	.2441	.545	.656	.768	.858	.903	.890	.807	.685	.544
	.2677	.587	.710	.827	.925	.981	.965	.877	.742	.593
	.2914	.629	.756	.888	.998	1.050	1.033	.939	.795	.637
	.3149	.665	.801	.940	1.055	1.112	1.093	.997	.841	.674
12.0	.1255	.155	.191	.231	.263	.286	.291	.272	.237	.191
20.0		.194	.237	.285	.321	.346	.347	.321	.276	.219
25.0		.214	.262	.311	.351	.376	.376	.349	.300	.240
30.0		.242	.296	.348	.392	.419	.416	.381	.325	.256
35.0		.270	.328	.385	.432	.457	.451	.415	.352	.279
40.0		.307	.469	.433	.481	.505	.500	.454	.385	.304
12.0	.1961	.232	.286	.344	.394	.428	.434	.405	.353	.285
20.0		.288	.351	.423	.475	.513	.514	.476	.409	.325
25.0		.316	.385	.459	.518	.554	.554	.514	.440	.352
30.0		.355	.436	.513	.578	.616	.612	.562	.480	.379
35.0		.400	.485	.570	.640	.677	.668	.612	.519	.413
40.0		.455	.548	.642	.715	.751	.740	.673	.570	.452

DISCUSSION OF RESULTS

If we assume that, because of the high copper and low halide concentration, the only complex ion present is CuX^+ ($X = Cl$ or Br), then the law of mass action gives

$$\frac{D/\epsilon_1}{(a - D/\epsilon_1)(b - D/\epsilon_1)} = K_1$$

where a is the total copper concentration,

        b is the total halide concentration,

        D is the optical density,

        ϵ_1 is the extinction coefficient,

        K_1 is the equilibrium constant for $Cu^{++} + X^- \rightleftharpoons CuX^+$.

If $a \gg b$, this can be rearranged (as was first done by Rabinowitch and Stockmayer for an analogous system (8)) to give

$$\frac{a}{D} = \frac{1}{K_1 b \epsilon_1} + \frac{a}{b \epsilon_1} \cdot$$

Hence a plot of a/D for any wave length against a should give a straight line, from the slope and intercept of which K_1 and ϵ_1 can be found. The present data give at least nearly straight lines for this plot. If the best straight lines are drawn through the data by the method of least squares the calculated values of K_1 and ϵ_1 are as given in Table III.

TABLE III

Values of K_1

Compound	Temp., °C	295	290	285	280	275	270	265	260	Mean
Copper chloride	12	—	—	1.01	0.98	0.88	0.99	1.07	1.28	1.03
	25	—	1.29	1.13	1.11	1.14	1.24	1.30	1.32	1.22
	40	1.28	1.25	1.24	1.36	1.29	1.38	1.35	—	1.31

		305	300	295	290	285	280	275	270	265	Mean
Copper bromide	12	.689	.708	.732	.682	.709	.709	.740	.764	.743	0.72
	25	.923	.939	.984	.921	.943	.943	.946	.997	.952	0.95
	40	.913	.870	.884	.807	.804	.805	.844	.846	—	0.85

Two comments can be made on these results. At any one temperature, the K_1 values usually drift in a characteristic way with wave length, being higher at the high and low wave lengths and lower in the middle. This drift is not large, but it seems to be definite. Secondly, the average K_1 values give a rather unexpected change with temperature, in that the usual log K against $1/T$ plot is not linear. This is particularly marked with copper bromide, where K_1 at first rises with temperature and then falls. This is confirmed from the results in Table II, where the optical densities were followed in a more detailed way over a range of temperature. The mean values of K_1 calculated from Table II are

temp.:   12.0   20.0   25.0   30.0   35.0   40.0,
K_1:   0.72   0.85   0.98   0.96   0.89   0.83.

The corresponding values of the extinction coefficient for CuX$^+$ ions are given in Table IV.

TABLE IV

Extinction coefficients of CuX$^+$ ions

Ion	Temp.,°C	305 mμ	300	295	290	285	280	275	270	265	260	255
CuCl$^+$	12.0	—	—	—	—	121	176	256	383	555	753	923
	25.0	—	—	—	111	153	222	326	477	669	866	1055
	40.0	—	—	116	158	223	324	464	664	902	1161	—
CuBr$^+$	12.0	222	274	332	376	411	417	392	342	276	—	—
	20.0	240	292	353	396	428	429	397	341	271	—	—
	25.0	238	292	349	390	419	420	388	337	268	—	—
	30.0	267	328	326	435	463	460	423	361	285	—	—
	35.0	321	389	457	513	543	536	491	416	331	—	—
	40.0	388	467	547	609	640	630	573	486	385	—	—

With CuCl$^+$ the absorption band advances steadily towards the red as the temperature is raised; this is what is to be expected if the band is widened at higher temperatures. However, with CuBr$^+$ the absorption maximum rises slowly at first and then rapidly at higher temperatures.

These results, particularly the effect of temperature on K_1, need further explanation. Various possibilities will now be considered.

1. Rapidly Changing Heat of Reaction

The equation $d \ln K/dt = \Delta H/RT^2$ will, of course, only give a linear relation between $\ln K$ and $1/T$, if it is assumed that ΔH is independent of temperature. If C is the specific heats of the products minus those of the reagents, ΔH will be of the form $\Delta H = B + CT$, where B is a constant. If C is assumed to be independent of temperature, then integration gives $\ln K = A - B/RT + (C/R) \ln T$, where A is an integration constant. Hence measurements of K at three (or more) temperatures will allow A, B, and C to be evaluated. If this is done for the K_1 values quoted above, for temperatures 12.0, 25.0, and 40.0° C, the results are

$$\Delta H = 30040 - 95.5T \qquad \text{for } Cu^{++} + Cl^- \rightleftharpoons CuCl^+$$
$$\Delta H = 134200 - 446.5T \qquad \text{for } Cu^{++} + Br^- \rightleftharpoons CuBr^+$$

or if T is in °C: CuCl$^+$: $\Delta H = 3960 - 95.5T$ (°C); CuBr$^+$: $\Delta H = 12260 - 446.5T$ (°C).

These values of C seem impossibly high, since C is the difference in specific heats of relatively simple ions in solution. It is true that the sign of C makes the specific heat of the two simple ions larger than that of the complex ion, as might be expected, but the difference seems impossibly large. If these effects are genuine, it might be expected that they would also show up in the specific heats of copper chloride solutions, on which some data are available. Marignag (9) gives the specific heat of copper chloride solutions as

molar ratio, water/copper chloride:	25	50	100,
specific heat/g solution:	.779	.864	.920 cal/°C.

It is very uncertain how these figures should be interpreted, but if the concentrations of Cu^{++}, $CuCl^+$, and Cl^- ions are calculated in each solution, and if it is assumed that each ion has a certain specific heat/gram molecule, and that these are strictly additive (the specific heat of the water present being taken as that in pure water), then the above results require the specific heats/gram molecule of each ion to be $Cu^{++} - 171$, $CuCl^+ - 21$, $Cl^- + 49$ cal/°C. Hence the difference in specific heats between CuCl$^+$ and $Cu^{++} + Cl^-$ is +101 cal/°C. Although this is large, it is of the wrong sign to explain the equilibrium constant results. Thus quite apart from the question of the justification of treating specific heat results in this simplified way, the specific heats do not support the view that the heat of reaction changes rapidly with temperature.

2. Deviations from the Beer–Lambert Law

It is necessary to assume the accuracy of the Beer–Lambert law in colorimetric investigations of complex ions, since otherwise no evaluation of equilibrium constants would be possible. Evidence for the Beer–Lambert law is obtained from the internal consistency of results, but it is usual to avoid having any very high concentration of the colored species present, since deviations are generally small at low concentrations. In the present work, the CuCl$^+$ concentration varied from about 7 to 15×10^{-4} M, and the CuBr$^+$ concentration

from 8 to 18×10^{-4} M. It can be calculated that if the equilibrium constant for $CuBr^+$ was really unchanged with temperature, and its apparent rise and fall were entirely due to variations in the extinction coefficient, then the extinction coefficient of $CuBr^+$ would have to change by about 10% over the range of concentration given above (at any one temperature). This seems to be too rapid a change for such small concentrations.

3. Occurrence of Other Complex Ions

Another, and perhaps more plausible, possibility is that some other complex ion occurs in those solutions. Since the copper concentration is high and halide low, the only reasonable suggestion is that the ion Cu_2X^{+3} (where X is a halogen) is present. Ions of this type have not been often postulated, but they are not really inherently improbable, since halogen atoms are known to hold two metal atoms together in various compounds, for instance Al_2Cl_6. One other consideration shows that this is a possible ionic type: suppose that CuX^+ is purely an ion pair association, with r the distance between ionic centers, then the electrostatic energy of formation of CuX^+ is $2e^2/r$, where e is the electron charge. Similarly for Cu_2X^{+3} the energy is $2e^2/r$, but for Cu_3X^{+5}, assumed to be flat, it would be $-0.93e^2/r$. Hence CuX^+ and Cu_2X^{+3} might be stable, but probably not Cu_3X^{+5}. This, of course, is an oversimplified picture, since covalent binding is ignored, but it gives a qualitative indication of what to expect.

If we postulate the existence of Cu_2X^{+3}, then this introduces a new equilibrium constant $K_2 = [Cu_2X^{+3}]/[Cu^{++}]^2[X^-]$ and the extinction coefficient for Cu_2X^{+3}. Using the same nomenclature as earlier, this modifies the equation for a/D to

$$\frac{a}{D} = \frac{1 + K_1 a + K_2 a^2}{b(K_1 \epsilon_1 + K_2 \epsilon_2 a)}$$

and if K_2 and a are not too large this gives approximately

$$\frac{a}{D} = \frac{1}{bK_1\epsilon_1}\left\{1 + \left(K_1 - \frac{K_2\epsilon_2}{K_1\epsilon_1}\right)a + \left[K_2 - \frac{K_2\epsilon_2}{\epsilon_1} + \left(\frac{K_2\epsilon_2}{K_1\epsilon_1}\right)^2\right]a^2\right\}.$$

In theory any four measurements should suffice to evaluate K_1, K_2, ϵ_1, and ϵ_2, but it is better to combine all the data at one wave length to get the best values of these quantities. The plots of a/D against a are nearly straight lines, but many of them show a slight curvature. Accordingly the best equation of the type $a/D = A + Ba + Ca^2$ was fitted by the method of least squares to the experimental data, thus giving numerical values of A, B, and C. A comparison of the two expressions for a/D shows that

$$K_2 - K_1\left(\frac{B}{A}\right) = \frac{C}{A} - \left(\frac{B}{A}\right)^2.$$

A, B, and C, of course, vary with wave length. Hence a graph of B/A against $C/A - (B/A)^2$ should give a straight line, using data at one temperature but various wave lengths, since K_1 and K_2 are constants. As will be seen, these graphs were in fact moderately good straight lines, although the points were somewhat scattered. The small curvature of the original a/D graph makes the accuracy rather low. The best straight line was drawn through the values of B/A plotted against $C/A - (B/A)^2$; this gives K_1 and K_2, and the extinction coefficients can be found as $\epsilon_1 = 1/K_1 Ab$, and $\epsilon_2 = (K_1 - B/A)/K_2 Ab$.
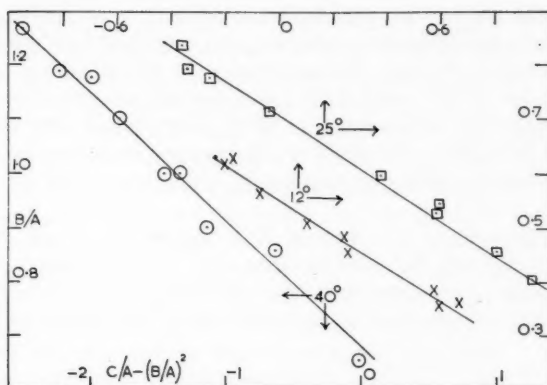
FIG. 1. Copper bromide.

The results of this treatment were as follows. Figure 1 gives the graph of B/A plotted against $C/A - (B/A)^2$ for copper bromide at various temperatures. The points are at least approximately linear. The constants calculated from these lines are as follows:

Copper bromide			Copper chloride		
Temp.	K_1	K_2	Temp.	K_1	K_2
12° C	3.08	1.73	12° C	3.92	3.40
25° C	3.56	2.31	25° C	5.47	5.21
40° C	4.15	2.77	40° C	7.35	7.79

For copper bromide, log K_1 plotted against $1/T$ gives a reasonably good straight line corresponding to $\Delta H = 1.9$ kcal; log K_2 gives only a moderately straight line corresponding to ΔH of about 3.0 kcal. For copper chloride, these give reasonably linear log K against $1/T$ plots: ΔH from K_1 is 4.0 kcal, and 5.2 kcal from K_2.

The calculated extinction coefficients are as follows:

Copper bromide	305 mμ	300	295	290	285	280	275	270	265
ϵ_1 12° C	50	68	75	86	94	95	91	78	62
25° C	66	82	98	109	118	120	110	97	77
40° C	78	91	113	125	131	127	120	99	77
ϵ_2 12° C	244	278	359	396	438	440	395	349	301
25° C	267	315	374	431	444	431	384	330	268
40° C	384	479	502	555	600	601	517	467	377

Copper chloride	295 mμ	290	285	280	275	270	265	260
ϵ_1 12° C	16	22	31	46	66	98	144	187
25° C	17	23	35	50	71	106	152	192
40° C	—	28	39	57	82	116	158	194
ϵ_2 12° C	68	87	113	158	259	375	496	758
25° C	93	123	142	196	342	494	620	887
40° C	—	163	239	328	477	682	948	1293

Although the behavior of the equilibrium constants is as might be expected, the extinction coefficients are sufficiently surprising to cast doubt on the interpretation of the experimental results through the postulation of Cu_2X^{+3} ions. In particular the absorption maxima for $CuBr^+$ and Cu_2Br^{+3} increase with temperature, and for Cu_2Br^{+3} the increase is disproportionately large at 40° C. The copper chloride results are less unusual, since the absorption only shifts to longer wave lengths at higher temperatures. However, in both cases ϵ_2/ϵ_1 seems unduly large, particularly at the absorption maximum for copper bromide.

To sum up, the linearity of the plots of B/A against $C/A - (B/A)^2$, and the more regular behavior of K_1 and K_2 with temperature favor an explanation in terms of Cu_2X^{+3}; against it is the anomalous behavior of the extinction coefficients. Thus, although there is some support for a suggestion of Cu_2X^{+3} ions, the matter cannot be definitely decided.

Cobalt and Nickel Chloride

Because of the striking color change when cobaltous ions form complexes with chloride, this system has been the subject of considerable investigation, starting with the early work on ion migration by Donnan and Bassett (10). Job (11), using a spectrophotometer, obtained evidence for $CoCl^+$ and $CoCl_3^-$, with K_1 for $CoCl^+$ equal to 4.5×10^{-3}. In 1949, Bobtelsky and Spiegler (12) investigated cobalt chloride in ethanol water mixtures, and similar measurements were made by Katzin and Gebert (13), and by Barvinok (14): these workers all found evidence of $CoCl_2$ and $CoCl_4^{--}$. Moore and Kraus (15) used anion exchange resins to investigate cobalt (II) in hydrochloric acid solutions, and obtained evidence for $CoCl_3^-$ and $CoCl_4^{--}$. However, Moore, Gootman, and Yates found evidence only for $CoCl_2$ from vapor pressure measurements (16).

The situation with respect to nickel chloride is similar, though there is less early work. Kiss and Csokan in 1941 (17) investigated nickel chloride in hydrochloric acid, obtaining evidence for $NiCl_4^{--}$ in concentrated solution. Moore and Kraus (15) examined its ion exchange behavior, obtaining evidence that anionic species were formed only to a very small extent. Beaver, Trevorrow, Estill, Yates, and Moore (18) examined nickel chloride in 2-octanol obtaining evidence for $NiCl_2$ and $(NiCl_2)_n$, and for complex ions. Herber and Irvine in 1956 (19) found evidence for $NiCl_3^-$ and $NiCl_4^{--}$ by ion exchange, but optical measurements indicated only $NiCl^+$ up to high hydrochloric acid concentrations.

The present work was undertaken initially to investigate the extent of formation of the first complex, $CoCl^+$ or $NiCl^+$, and the variation of this with temperature. However, as will be seen below, the results also provide evidence of the existence of ions of the type M_2Cl^{+3}, where M is the metal.

In the first instance, spectrophotometric measurements were made. However, even up to 0.12 M chloride, the effect of chloride was so slight over the range 240–900 mμ, that this method seemed to offer no prospects of success. In fact, one must conclude either that $NiCl^+$ is not formed, or that its absorption spectrum is very like that of Ni^{++}. The situation with cobalt was found to be very similar. Accordingly measurements were made by another method, by the use of the e.m.f. of cells, to decide between these two alternatives. Here evidence for MCl^+ was obtained, and it seems to be necessary to conclude that for both nickel and cobalt the spectrum of MCl^+ is very like that of M^{++}.

Apparatus and Method

The measurements made were on the e.m.f. of the cell: Ag, AgCl/NaCl + M(ClO$_4$)$_2$ + NaClO$_4$/NaCl + NaClO$_4$/AgCl, Ag, where M is cobalt or nickel. The two electrolytes

were adjusted to the same ionic strength and acidity by means of sodium perchlorate and perchloric acid. The sodium chloride concentrations in the two solutions were the same; so the only difference was the presence in one side of cobalt or nickel perchlorate, with an adjustment of the sodium perchlorate concentration to keep the ionic strengths equal. The sodium perchlorate was much more concentrated than the chloride (0.008 M).

The silver/silver chloride electrodes were prepared as recommended by Janz and Taniguchi (20). The electrodes so prepared gave voltages of 0.02 mv or less when placed in the same solution, this difference being found and allowed for in the subsequent calculations. The two sodium chloride solutions were separated by a salt bridge, sodium perchlorate being used for this. The voltage was measured on a Leeds and Northrup K-2 potentiometer. The cell, of course, was at constant temperature during use. Nickel and cobalt perchlorate from the G. Frederick Smith Co. were used in making up the solutions: the concentrations of the solutions were determined by E.D.T.A. titration for cobalt with murexide indicator (21), and by dimethylglyoxime for nickel.

RESULTS

The observed e.m.f. are given in Table V. In interpreting these results it has to be assumed that the liquid junction potentials cancel as a result of the similar concentrations and ionic strengths of the solutions on each side of the salt bridge. This assumption is

TABLE V
Cell voltages in millivolts

Compound	T, °C	0.0999 M	0.1497	0.1748	0.1997	0.2247	0.2496	0.2746	0.2995	0.3245
Cobalt chloride	12	1.53	2.28	2.69	3.04	3.46	3.86	4.24	4.62	5.02
	25	1.72	2.58	3.06	3.44	3.90	4.35	4.78	5.21	5.61
	40	1.91	2.94	3.44	3.90	4.39	4.85	5.35	5.82	6.34
		0.1208 M	0.1451	0.1932	0.2175	0.2416	0.2659	0.2900	0.3139	
Nickel chloride	12	1.56	1.97	2.63	3.01	3.41	3.78	4.09	4.51	
	25	1.83	2.25	3.05	3.44	3.84	4.29	4.61	5.05	
	40	2.10	2.55	3.43	3.87	4.31	4.77	5.22	5.73	

NOTE: Ionic strength = 2.0; [HClO₄] = 0.300 M.

supported by the consistency of the equilibrium constants calculated from the results. The voltages were very steady with time, which supports this assumption. In the calculations below it was assumed that the great excess of sodium perchlorate made it the effective conductor of the current. Since all runs were made with very low chloride concentration and relatively high metal, it is reasonable to assume (as for copper) that the complex ions are MCl^+ (formation constant K_1) and M_2Cl^{+3} (formation constant K_2). If, as before, a is the total metal concentration, and b the total chloride, and if $a \gg b$, and if u is the concentration of free chloride in the solution containing cobalt or nickel, then it is easily shown that $b/u = 1 + K_1 a + K_2 a^2$. But b/u is the ratio of the chloride in the two solutions, and, assuming that the activity coefficients are equal at the same ionic strengths, then

$$E = \frac{RT}{nF} \ln(b/u)$$

where E is the cell voltage. Hence b/u can be found. The first equation can be rewritten: $(b/u-1)/a = K_1 + K_2 a$. If only MCl^+ is formed $(b/u-1)/a$ will be constant; otherwise

it should increase linearly with a. Table VI gives the calculated values of $(b/u-1)/a$.

These values of $(b/u-1)/a$ are approximately linear when plotted against a, although there is evidently some random error. If the best straight line is drawn through them by the method of least squares, the following constants are obtained.

Compound	Temp.	K_1	K_2
CoCl$_2$	12° C	.611	.263
	25° C	.666	.274
	40° C	.711	.327
NiCl$_2$	12° C	.508	.426
	25° C	.569	.407
	40° C	.620	.409

The K_1 values give ΔH as 1.0 kcal for $Co^{++} + Cl^- \rightarrow CoCl^+$, and 1.25 kcal for $Ni^{++} + Cl^- \rightarrow NiCl^+$. It is impossible to calculate heats of reaction for the formation of M_2Cl^{+3}, except to say that here ΔH must be very small. Thus, if this interpretation of the results is correct, the complexes M_2Cl^{+3} are formed nearly as easily as MCl^+. While this interpretation is certainly possible, it cannot be considered as proved.

TABLE VI

Values of $(b/u-1)/a$

Compound	T, °C		.0999 M	.1497	.1748	.1997	.2247	.2496	.2746	.2995	.3245
Cobalt chloride	12	$(b/u-1)/a$	.643	.645	.661	.659	.672	.681	.685	.690	.698
	25		.693	.705	.723	.717	.729	.739	.744	.750	.751
	40		.734	.768	.777	.778	.785	.788	.798	.803	.815

	T, °C	.1208 M	.1451	.1932	.2175	.2416	.2659	.2900	.3139
Nickel chloride	12	.542	.575	.584	.599	.616	.625	.624	.641
	25	.611	.631	.652	.658	.667	.683	.677	.691
	40	.669	.682	.701	.708	.716	.726	.734	.753

REFERENCES

1. R. Näsänen. Acta Chem. Scand. 4, 140 (1950).
2. H. McConnell and N. Davidson. J. Am. Chem. Soc. 72, 3164, 3168 (1950).
3. R. Kruh. J. Am. Chem. Soc. 76, 4865 (1954).
4. H. L. Riley and H. C. Smith. J. Chem. Soc. 1448 (1934).
5. P. Job. Compt. rend. 198, 827 (1934).
6. R. Näsänen. Acta Chem. Scand. 4, 816 (1950).
7. P. S. Farrington. J. Am. Chem. Soc. 74, 966 (1952).
8. E. Rabinowitch and W. H. Stockmayer. J. Am. Chem. Soc. 64, 335 (1942).
9. C. Marignac. Ann. chim. et phys. Ser. 5, 8, 410 (1876).
10. F. G. Donnan and H. Bassett. J. Chem. Soc. 81, 939 (1902).
11. P. Job. Compt. rend. 196, 181 (1933).
12. M. Bobtelsky and R. S. Spiegler. J. Chem. Soc. 143 (1949).
13. L. I. Katzin and E. Gebert. J. Am. Chem. Soc. 72, 5464 (1950).
14. M. S. Barvinok. Zhur Obshchei Khim. 20, 1947 (1950).
15. G. E. Moore and K. A. Kraus. J. Am. Chem. Soc. 74, 843 (1952).
16. T. E. Moore, E. A. Gootman, and P. C. Yates. J. Am. Chem. Soc. 77, 298 (1955).
17. A. V. Kiss and P. Csokan. Z. anorg. u. allgem. Chem. 245, 355 (1941).
18. W. D. Beaver, L. E. Trevorrow, W. E. Estill, P. C. Yates, and T. E. Moore. J. Am. Chem. Soc. 75, 4556 (1953).
19. R. H. Herber and J. W. Irvine. J. Am. Chem. Soc. 78, 905 (1956).
20. G. J. Janz and H. Taniguchi. Chem. Revs. 53, 397 (1953).
21. G. Schwarzenbach. Complexometric titrations. Methuen and Co. Ltd., London. 1957. p. 78.

THE STUDY OF HYDROGEN BONDING AND RELATED PHENOMENA BY ULTRAVIOLET LIGHT ABSORPTION

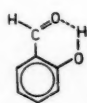## PART V. INTRAMOLECULAR HYDROGEN BONDING IN ANILINES AND PHENOLS[1]

J. C. DEARDEN[2] AND W. F. FORBES[3]

ABSTRACT

Information concerning intramolecular hydrogen bonding in phenols and anilines can be obtained from ultraviolet spectra by a variety of methods. One method is to note the spectral changes observed between the corresponding o-substituted phenols and anisoles. A second method is to compare the spectral changes between o-substituted phenols or anilines and the corresponding meta isomers. A third method is to note the absence of an appreciable spectral change, on altering the solvent conditions, which may also indicate the formation of an intramolecular hydrogen bond. The conclusions deduced from the three methods confirm previously stated generalizations concerning the nature of the hydrogen bond. One notable exception is that the spectral changes ascribed to the intramolecular hydrogen bond in o-nitrophenol can be explained in terms of an electrostatic model of the hydrogen bond.

INTRODUCTION

Intramolecular hydrogen bonds are known to cause bathochromic wavelength displacements in some of the absorption bands of the ultraviolet spectra. In order to obtain a quantitative measure of this effect for intramolecularly bonded phenols or anilines such as salicylaldehyde (IA), a reference compound must be available against which the wavelength displacement can be measured. This reference compound may be provided either by the corresponding m-isomer, for example m-hydroxybenzaldehyde (IB), or by the otherwise similar O-methyl- or N-methyl-substituted compound, for example o-methoxybenzaldehyde (IC). In the absence of interfering interactions both methods
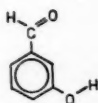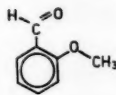
IA   IB   IC

should afford similar results. Moreover, some of the absorption bands of systems containing an intramolecular hydrogen bond should be less affected by competitive intermolecular hydrogen bonding between solute and solvent molecules than otherwise similar, but non-intramolecularly bonded, molecules.

However, the following considerations may affect the reliability of the observed spectral changes: (i) The absorption band under consideration may be determined by that part of the chromophoric system which does not contain the intramolecular hydrogen bond and consequently this absorption band will not be appreciably affected by intramolecular hydrogen bonding. For example, the similarity of the benzoic acid B-bands for o-methoxybenzoic acid and benzoic acid is explained by assuming that the intramolecular hydrogen bond in o-methoxybenzoic acid does not appreciably affect the
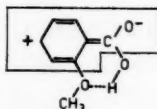
II

resonance form of type II, which can be assumed to determine predominantly the observed absorption band (see ref. 1). (ii) Steric interactions and other proximity effects, which almost always operate in *o*-disubstituted benzene derivatives, may be appreciably different in the intramolecularly hydrogen-bonded compound and in the reference compound. For example, in cyclohexane solution the nitrobenzene *B*-band of *o*-nitroanisole shows a hypsochromic wavelength displacement of ca. 11.5 mμ from this same band in *m*-nitroanisole (2a). This hypsochromic displacement is associated with steric and other short-range interactions between the methoxy and the nitro groups. It follows that *o*-nitroanisole cannot be assumed to provide a satisfactory reference compound for estimating intramolecular hydrogen bonding in *o*-nitrophenol. (iii) The absence of spectral changes with change of solvent may be caused by a strong intermolecular hydrogen bond, but it may *also* be caused by steric hindrance preventing solvent–solute interaction. For example, *o*-substituted phenols such as 2,6-di-*tert*.butyl phenol in which the ortho substituents are large, do not show the usual wavelength displacements if the spectra are determined in cyclohexane and ethanol solution, presumably because the large *o*-substituents prevent solvent–solute interactions (cf. ref. 2b and references cited there).

The purpose of the present paper is to summarize the spectral changes which can be ascribed with some degree of confidence to intramolecular hydrogen bonding, and to deduce from the data certain generalizations concerning the intramolecular hydrogen bond in phenols and anilines.

THE INTRAMOLECULAR HYDROGEN BOND IN SOME ORTHOSUBSTITUTED PHENOLS AND ANILINES

Salicylaldehyde

The relevant ultraviolet and infrared spectra of salicylaldehyde (IA) and *m*-hydroxybenzaldehyde (IB) are listed in Table I. The intense infrared carbonyl band at 1666 cm^{-1} for salicylaldehyde occurs at lower frequency than for *m*-hydroxybenzaldehyde (1700 cm^{-1}) or for benzaldehyde (1709 cm^{-1}) (see Table I) and this then indicates an intramolecular hydrogen bond in salicylaldehyde (cf. also refs. 3, 4, 5, 6).* It may also be noted that the O—H stretching frequencies of phenol and salicylaldehyde occur near 3600 and 3200 cm^{-1} respectively (7). Salicylaldehyde may therefore be taken as an example of an intramolecularly hydrogen-bonded compound where, moreover, steric interactions are likely to be small. In *n*-hexane solution, the benzaldehyde ultraviolet *B*-band of salicylaldehyde shows a slight bathochromic wavelength displacement compared with the same *B*-band in *m*-hydroxybenzaldehyde and this displacement is accompanied by an increase in the maximal extinction coefficient (ϵ_{max}) from 9500 to 11,700 (see Table I). In the corresponding methoxybenzaldehydes no significant wavelength displacement is

*The other infrared bands listed in Table I are presumably to be associated with aromatic C—H vibrations which usually occur in this region; it is worth noting that for benzaldehyde and salicylaldehyde at least three fairly intense bands occur in this region. It is therefore possible, though considered unlikely, that the band at 1644 cm^{-1} in salicylaldehyde also represents a carbonyl band.

TABLE I

Main ultraviolet maxima and infrared bands in the 1700–1560 cm^{-1} region for salicylaldehyde and reference compounds*†

Compound	Solvent	Phenol or anisole B-band		Benzaldehyde B-band		C-band		Carbonyl band	Other bands in the 1700–1560 cm^{-1} region
		$\lambda_{max}(m\mu)$	ϵ_{max}	$\lambda_{max}(m\mu)$	ϵ_{max}	$\lambda_{max}(m\mu)$	ϵ_{max}	$\nu_{max}(cm^{-1})$	$\nu_{max}(cm^{-1})$
Salicylaldehyde	Hexane	215§	17,000	{ 251	11,000	327	3,600	1,666(s)	{ 1,644(s)
				258	11,700				1,618(m)
									1,576(m)
m-Hydroxybenzaldehyde	Hexane	213	19,000	{ 245	9,500	{ 305	2,900	1,700(m)	1,683(m)
				251	9,500	ca. 311	2,850		
Benzaldehyde	Hexane	—	—	{ 242	14,000	{ 279–280	1,200	1,709(s)	{ 1,649(m)
				248	12,000	289	1,000		1,581(m)
									1,569(m)
o-Methoxybenzaldehyde	Hexane (2a)	211	20,000	{ 247	10,500	{ 309	4,600	—	—
				ca. 254	8,500	ca. 317	4,200		
Salicylaldehyde	Ether	218	15,000	{ ca. 251	10,500	325	3,500	—	—
				255–256	10,700				
m-Hydroxybenzaldehyde	Ether			{ 249	9,700	{ 308	3,250	—	—
				253–254	9,200	311	3,200		
						316	3,050		

*See also ref. 2b. †Band nomenclature in this and subsequent tables is as generally used in ref. 2. ‡Values in italics represent inflections in this and subsequent tables. §In 0.1 N ethanolic NaOH this band occurs at ca. 232 mμ. It is therefore believed to be a phenolic B-band (see ref. 2b).

observed between the o- and m-isomers and the increase in ϵ_{max} on passing from the m- to the o-isomer is from 9200 to 10,500, that is, somewhat less than for the hydroxy-benzaldehydes (see ref. 2a). Since, therefore, steric interactions in o-methoxybenzaldehyde do not give rise to appreciable wavelength displacements, the small wavelength displacement in the B-bands between salicylaldehyde and m-hydroxybenzaldehyde may be taken as an indication of intramolecular hydrogen bonding in salicylaldehyde as shown in IA.

The phenolic B-band also shows a slight bathochromic displacement (2 mμ) relative to the same band in m-hydroxybenzaldehyde and this displacement may also be related to hydrogen-bond formation. Three possible factors may account for this latter spectral change: (i) the displacement may occur because the hydrogen atom tends to become detached from the phenolic hydroxy group in the course of hydrogen-bond formation and hence the absorption maximum may tend towards that of the phenolate ion, (ii) the displacement may occur because of steric or other reasons since the hydrogen bond may cause the hydroxy group to rotate from its normal position in phenol (cf. ref. 2b), and (iii) the hydrogen bond may affect the vibrational levels of the hydroxy group in such a way as to cause the observed spectral change. C-Band data of salicylaldehyde and the other compounds studied are listed in Table I and subsequent tables. Their significance will be discussed in the Concluding Remarks.

The spectrum of salicylaldehyde compared with that of o-methoxybenzaldehyde is altered in a similar way. That is, compared with o-methoxybenzaldehyde both B-bands are again shifted to longer wavelength and these wavelength displacements are of the same order as between salicylaldehyde and m-hydroxybenzaldehyde (see Table I).

Next, it may be noted that the ultraviolet spectra of salicylaldehyde in cyclohexane and ether solution are more similar than, for example, the spectra of m-hydroxybenzalde-
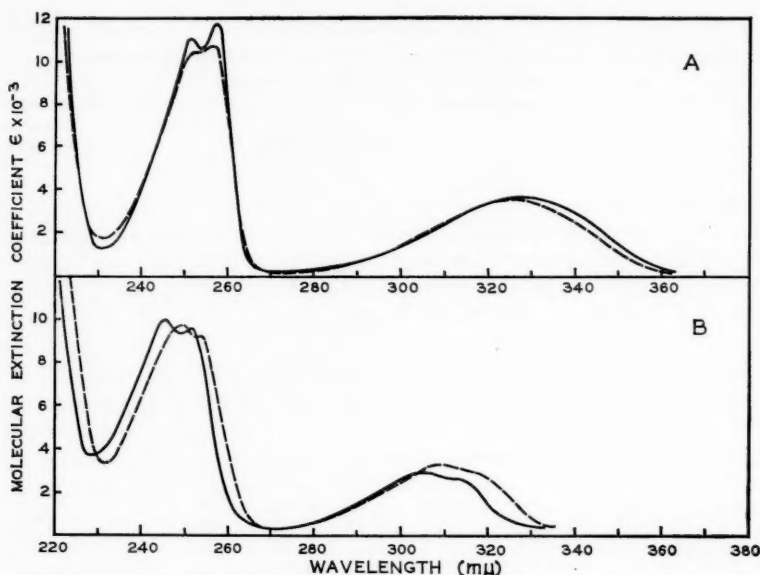
FIG. 1. The spectra of (A) salicylaldehyde and (B) *m*-hydroxybenzaldehyde in *n*-hexane (———) and ether (– – –) solutions.

hyde in these two solvents (see Fig. 1). The lack of any appreciable spectral change, particularly in the *C*-band, accompanying the solvent change for the spectrum of salicylaldehyde may again be ascribed to the presence of a strong intramolecular hydrogen bond.

All the above-mentioned spectral changes for salicylaldehyde can therefore be rationalized in terms of an intramolecular hydrogen bond, which can be schematically represented as shown in structure III.

III   IV
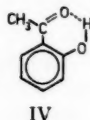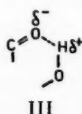
TABLE II

Main ultraviolet maxima for *o*-hydroxyacetophenone and reference compounds

Compound	Solvent	Phenol or anisole *B*-band		Acetophenone *B*-band		*C*-band	
		$\lambda_{max}(m\mu)$	ϵ_{max}	$\lambda_{max}(m\mu)$	ϵ_{max}	$\lambda_{max}(m\mu)$	ϵ_{max}
o-Hydroxyacetophenone	Cyclohexane	213	22,200	249.5	9,000	324	3,750
				256	8,700	331	3,550
m-Hydroxyacetophenone	Cyclohexane	211	20,500	243	8,650	300.5	2,550
				249	7,150	ca. 309	2,100
Acetophenone	Cyclohexane	—	—	238	12,500	279	900
o-Methoxyacetophenone	Cyclohexane	211	20,300	ca. 238	8,100	298	3,550
				242.5	8,350	ca. 308	2,500
o-Hydroxyacetophenone	Ether	214	16,000	250	9,000	324	3,700
				ca. 254	8,550	ca. 330	3,500
m-Hydroxyacetophenone	Ether			246	8,900	304	2,900
				ca. 252	7,000	ca. 310	2,600

o-Hydroxyacetophenone

The relevant ultraviolet spectral data are listed in Table II. The infrared spectrum of o-hydroxyacetophenone again shows the presence of an intramolecular hydrogen bond (cf. refs. 8, 9, and references cited there). It may also be noted that whereas the carbonyl band of o-hydroxyacetophenone does not show a doublet, the infrared carbonyl bands of compounds like m-hydroxyacetophenone (ν_{max} 1688 and 1678 cm^{-1}), o-chloro- and o-bromo-acetophenone (10) do show doublets in carbon tetrachloride solution. If structure IV indeed represents the predominant form of o-hydroxyacetophenone one would antici- pate a number of similarities between the ultraviolet spectra of salicylaldehyde and o-hydroxyacetophenone and these are in fact observed (see Table II and cf. Table I).*

o-Nitrophenol

The infrared hydroxyl band of o-nitrophenol shows one intense band at 3209 cm^{-1} with only low-intensity absorption at higher frequency (see Fig. 2). The position of this band (see ref. 9, p. 84, Table VI and refs. 11 and 12) as also the absence of any observed concentration dependence of the band (see Experimental) indicates that the band corresponds to an intramolecularly hydrogen-bonded form. The NO$_2$-valence
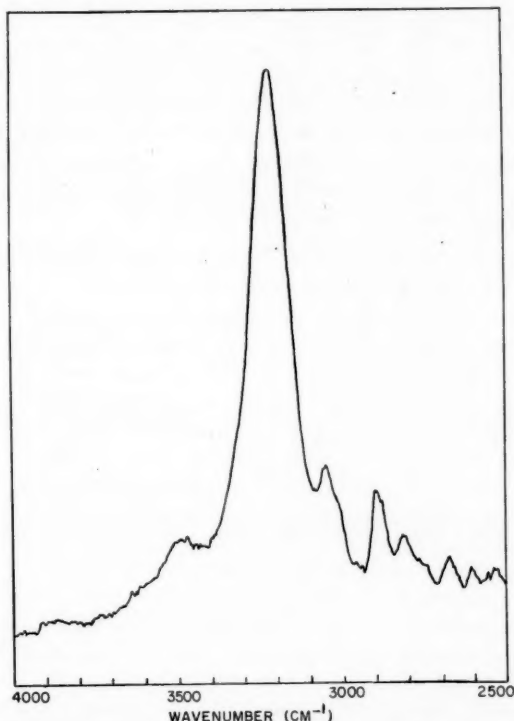
FIG. 2. The —OH stretching absorption band (3209 cm^{-1}) of o-nitrophenol, due to intramolecular hydrogen bonding (0.20 molar solution in carbon tetrachloride).

*The slightly greater displacement in o-hydroxyacetophenone compared with the o-methoxy compound is probably caused by steric interactions in the latter compound. This suggestion also receives support since for o- and m-methoxyacetophenones the acetophenone B-bands are no longer similar as they are for the corresponding benzaldehydes, but the o-isomer now absorbs at shorter wavelength indicative of steric interactions (see ref. 2a).

vibration, for reasons which will be discussed later, is not particularly influenced by intramolecular hydrogen bonding (cf. ref. 12).

TABLE III

Main ultraviolet maxima for o-nitrophenol and reference compounds

Compound	Solvent	Phenol or anisole B-band		Nitrobenzene B-band		C-band	
		$\lambda_{max}(m\mu)$	ϵ_{max}	$\lambda_{max}(m\mu)$	ϵ_{max}	$\lambda_{max}(m\mu)$	ϵ_{max}
o-Nitrophenol	Cyclohexane	ca. 231	4,000	271	7,350	346	3,700
m-Nitrophenol	Cyclohexane	222	10,200	258.5	6,100	312	2,170
Nitrobenzene (2c)	Cyclohexane	—	—	252	9,000	ca. 285	1,500
o-Nitroanisole	Cyclohexane			250	3,400	307	2,500
m-Nitroanisole	Cyclohexane	223	13,000	261.5	6,100	316	2,400
o-Nitrophenol	Ether	ca. 234	3,000	271	6,900	346	3,550
o-Nitrophenol	Ethanol	ca. 231	3,550	272.5	6,050	347	3,250
o-Nitroanisole	Ether	ca. 229	5,500	252–253	3,050	312	2,300
o-Nitroanisole	Ethanol	ca. 231	5,000	257	3,200	319	2,350

The relevant ultraviolet data are listed in Table III and again confirm the presence of an intramolecular hydrogen bond in o-nitrophenol. The nitrobenzene B-band of o-nitrophenol compared with that of m-nitrophenol is more appreciably displaced (by 12.5 mμ) and intensified (see Table III). Compared with o-nitroanisole even larger wavelength displacements are observed but steric interactions preclude the use of o-nitroanisole as a suitable reference compound (see Introduction). The phenolic B-band data (see Table III) also show the anticipated wavelength displacements (see previous sections) but show a surprisingly large decrease in the ϵ_{max} value for the o-isomer. Next, the absence of appreciable wavelength changes for o-nitrophenol on changing the solvent from cyclohexane to ether and ethanol may also again be taken as evidence for a strong intramolecular hydrogen bond (see Table III and Fig. 3).
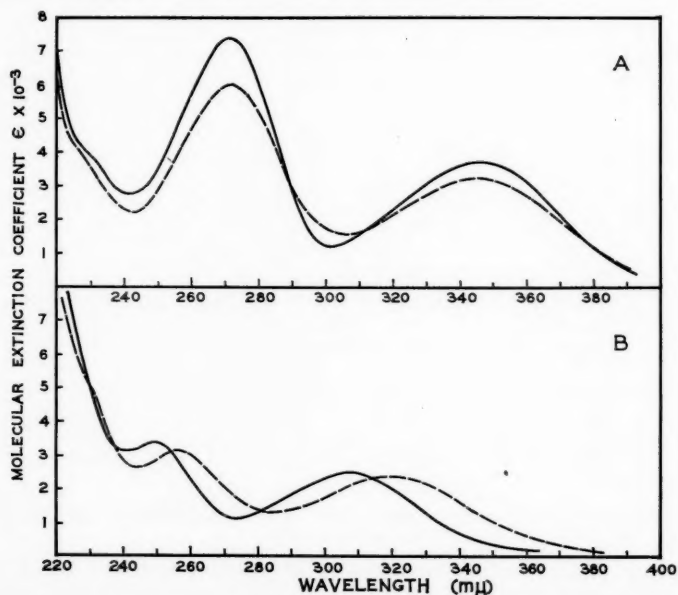

FIG. 3. The spectra of (A) o-nitrophenol and (B) o-nitroanisole in cyclohexane (———) and ethanol (– – –) solutions.

As previously shown, the wavelength displacement between *o*-nitrophenol and *o*-nitro-anisole cannot be used directly as a measure of the intramolecular hydrogen bonding because of steric interactions in *o*-nitroanisole. However, additional substituents in the benzene ring, not vicinal to the nitro or methoxy substituents, are unlikely to affect these steric interactions; hence the above-mentioned wavelength displacements may be used as a measure of the strength of the intramolecular hydrogen bond in compounds of the type as listed in Table IV, where comparison with a *m*-isomer is not possible. The spectra of the compounds listed in Table IV were collected in order to investigate whether a substituent in the absence of additional steric interactions affects the strength of an intramolecular hydrogen bond.

The infrared frequency displacements listed in Table IV indicate that the intramolecular hydrogen bond is progressively strengthened by a chloro and a methoxy substituent, if these substituents are *para* with respect to the nitro group (cf. ref. 9, p. 84, Table VI). This strengthening of the intramolecular hydrogen bond, for a *p*-methoxy substituent, would also have been anticipated from benzoic acid data since a *p*-methoxy substituent apparently strengthens the dimeric hydrogen bond in benzoic acid (1). Moreover, using resonance symbols, both *p*-chloro- and *p*-methoxy substituents would be anticipated to give rise to increased contributions of resonance forms of type V which might be expected to favor the formation of an intramolecular hydrogen bond.

The ultraviolet spectral changes (if expressed in wave numbers) show approximately parallel effects. That is, 5-chloro or 5-methoxy substituents give rise to slightly larger

V
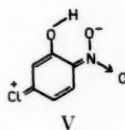
frequency displacements between the nitrobenzene *B*-bands of the phenol and the anisole (indicative of a stronger intramolecular hydrogen bond) whereas the opposite effect is observed for 4-methyl, 4-methoxy, or 4-chloro substituents (see Table IV). The data in Table IV also show that the spectra of intramolecularly hydrogen-bonded compounds are again generally only slightly affected on being determined in ethanol solution.

A simple explanation to rationalize the spectral changes is as follows: The negative charge on the NO_2 oxygen atom is increased by a *p*-methoxy or a *p*-chloro substituent and this enhanced charge formation occurs for *both* nitrophenol and nitroanisole; it accounts for the bathochromic displacement in the ultraviolet nitrobenzene *B*-band for 5-methoxy- and 5-chloro-nitrophenol and for the corresponding anisoles relative to these bands in nitrophenol or nitroanisole. This increased negative charge on the NO_2 oxygen atom, only for the *o*-nitrophenol, now also attracts the hydrogen atom of the hydroxyl group and this accounts for the lower frequency of the O—H vibration in both 5-methoxy- and 5-chloro-2-nitrophenol relative to *o*-nitrophenol. The closer proximity of the hydrogen atom, however, does not apparently affect appreciably the negative charge on the NO_2 group in the ground state (see below), and this phenomenon can be explained by assuming an electrostatic model for *this* hydrogen bond.* This model for *o*-nitrophenol also accounts for the infrared NO_2 vibrational frequencies which are remarkably constant (1530 ± 2 cm^{-1}) for the following compounds: *o*-nitrophenol, *o*-nitroanisole (cf. also ref. 12 for the

---

*Since a "covalent" contribution would be anticipated to affect the negative charge on the nitro group it should be noted that this model does of course not necessarily hold for other intramolecularly bonded systems (cf., for example, the carbonyl bands described in the previous section which are appreciably affected by a vicinal hydroxy group).

TABLE IV

Wavelength displacements between o-nitrophenols and o-nitroanisoles and infrared hydroxyl frequencies of o-nitrophenols

Compound	Solvent	Phenol or anisole B-band		Nitrobenzene B-band			C-band			Infrared hydroxyl band (in carbon tetrachloride)	
		$\lambda_{max}(m\mu)$	ε_{max}	$\lambda_{max}(m\mu)$	ε_{max}	Wavelength displacement relative to anisole	$\lambda_{max}(m\mu)$	ε_{max}	Wavelength displacement relative to anisole	$\nu_{max}(cm^{-1})$	Frequency displacement relative to o-nitrophenol (cm^{-1})
o-Nitrophenol	Cyclohexane	ca. 231	4,000	271	7,350	21 mμ (3100 cm^{-1})	346	3,700	39 mμ (3670 cm^{-1})	3.209	—
o-Nitroanisole	Cyclohexane			250	3,400	—	307	2,500	—	—	—
4-Methyl-2-nitrophenol	Cyclohexane	ca. 234	8,660	274–275	7,250	21 mμ (3020 cm^{-1})	359–360	3,600	41 mμ (3580 cm^{-1})	3.218	+9
4-Methyl-2-nitrophenol	Ethanol	ca. 234	4,000	276	6,200	—	359–360	3,150	—	—	—
4-Methyl-2-nitroanisole	Cyclohexane			253.5	3,000	—	318–319	2,450	—	—	—
4-Methoxy-2-nitrophenol	Cyclohexane	244	5,900	277	6,500	21 mμ (2960 cm^{-1})	388–389	4,000	50 mμ (3810 cm^{-1})	3.216	+7
4-Methoxy-2-nitrophenol	Ethanol	244	5,850	278–279	5,000	—	388	3,400	—	—	—
4-Methoxy-2-nitroanisole	Cyclohexane	ca. 257	6,300	ca. 266	2,100	—	338.5	2,650	—	—	—
4-Methoxy-2-nitroanisole	Ethanol	ca. 258	6,000	ca. 264	2,900	—	353	2,550	—	—	—
4-Chloro-2-nitrophenol	Cyclohexane			267	6,700	19 mμ (2870 cm^{-1})	359	3,500	39 mμ (3390 cm^{-1})	3.216	+7
4-Chloro-2-nitrophenol	Ethanol			265	5,100	—	353	3,000	—	—	—
4-Chloro-2-nitroanisole	Cyclohexane			ca. 248	3,100	—	320	2,350	—	—	—
4-Chloro-2-nitroanisole	Ethanol			ca. 256	2,750	—	342	2,350	—	—	—
5-Methoxy-2-nitrophenol	Cyclohexane	{ 233, 237 }	{ 5,300, 5,100 }	{ 307, 330–340 }	{ 8,500, 9,050 }	34.5 mμ (4120 cm^{-1})	—	—	—	3.144	−65
5-Methyl-2-nitrophenol	Ethanol	{ 232, ca. 237 }	{ 4,750, 4,560 }	{ ca. 314, 341 }	{ 8,160, 9,350 }	—	—	—	—	—	—
5-Methoxy-2-nitroanisole	Cyclohexane	231	8,700	{ 272.5, 308 }	{ 6,000, 5,450 }	—	—	—	—	—	—
5-Chloro-2-nitrophenol	Cyclohexane			281	9,700	23.5 mμ (3240 cm^{-1})	340	5,200	33 mμ (3100 cm^{-1})	3.182	−27
5-Chloro-2-nitroanisole	Cyclohexane			257.5	5,400	—	307	3,500	—	—	—

reported, but unexplained similarity of the NO_2 vibrational frequency for these two compounds), 5-methoxy-2-nitrophenol, 4-methoxy-2-nitrophenol, 4-methyl- and 5-methyl-2-nitrophenol, and 4-chloro-2-nitrophenol* (see also Concluding Remarks) and ref. 13 for a discussion of the infrared N—O stretching frequencies).

Salicylic Acid

The relevant ultraviolet and infrared spectra are listed in Table V. The monomeric infrared carbonyl band for salicylic acid occurs at lower frequency than for benzoic acid or for o-methoxybenzoic acid (see Table V) and this then again indicates an intramolecular hydrogen bond involving the carbonyl oxygen atom (see also refs. 6, 14).

TABLE V

Ultraviolet B-bands and infrared carbonyl bands of salicylic acid and reference compounds

| Compound | Solvent | Ultraviolet maximum* | | Infrared carbonyl band† (in carbon tetrachloride), ν_{max} (cm^{-1}) |
		λ_{max}(mμ)	ϵ_{max}	
Salicylic acid	Cyclohexane	239	8,000	1,691
m-Hydroxybenzoic acid	Cyclohexane containing ca. 1% ether	233–234	6,800	Insufficiently soluble
Benzoic acid	Cyclohexane	230	12,500	1,744
o-Methoxybenzoic acid	Cyclohexane	230	8,300	1,749

*Spectra are determined at concentrations at which the monomeric species are believed to predominate (see ref. 1).
†Monomeric bands from ref. 1.

Supporting evidence for this hydrogen bonding is also obtained from the ultraviolet data listed in Table V, which show that the benzoic acid B-band in salicylic acid is bathochromically displaced compared with the same band in m-hydroxybenzoic acid; for the o- and m-isomers of methoxybenzoic acid on the other hand, the m-isomer absorbs at slightly longer wavelength (2a). Moreover, salicylic acid in ether is reported to absorb maximally at 237 mμ, ϵ = 7800 (15) which is close to the absorption of the monomeric species in cyclohexane solution (see Table V).†

TABLE VI

Main ultraviolet maxima for o-aminobenzaldehyde and reference compounds

| Compound | Solvent | Aniline B-band | | Benzaldehyde B-band | | C-band | |
		λ_{max}(mμ)	ϵ_{max}	λ_{max}(mμ)	ϵ_{max}	λ_{max}(mμ)	ϵ_{max}
o-Aminobenzaldehyde	Cyclohexane			256 / ca. 263	5,600 / 3,400	356	4,700
m-Aminobenzaldehyde*	Cyclohexane containing ca. 0.2% ether	228	17,500	ca. 244 / ca. 257	9,000 / 7,500	331.5	2,000
Benzaldehyde	Hexane	—	—	242 / 248	14,000 / 12,000	279–280 / 289	1,200 / 1,000
Aniline*	Cyclohexane	234	9,000	—	—	289	1,900

*Data from ref. 2e.

*The same band in 5-chloro-2-nitrophenol occurs only at slightly lower frequency (ν_{max} 1521 cm^{-1}). It might also be noted that the infrared O—H vibrational frequencies listed in Table IV for various substituted nitrophenols are not proportional to the relevant σ values.

†Dannenberg (15) assumes that the intramolecular hydrogen bond causes a wavelength displacement of 16 mμ but this value is probably too large since it is obtained by comparing the maximal absorptions of salicylic and o-methoxybenzoic acids; that is steric interactions, as mentioned in the Introduction may operate in the latter compound and these will tend to increase the apparent wavelength displacement ascribed to the intramolecular hydrogen bond.

o-Aminobenzaldehyde

The relevant ultraviolet data are listed in Table VI, and these data show that the wavelength displacements between the o- and m-isomers may again be taken as evidence of intramolecular hydrogen bonding. An interesting difference between the spectra of amino and hydroxy compounds is that only for the amino compounds are the ϵ_{max} values of the benzaldehyde B-band substantially decreased in the o-isomer compared with the ϵ_{max} values of the m-isomer (see Table VI, and compare also later tables). A possible explanation is that the intramolecular hydrogen bond prevents the alignment of the carbonyl group in the same plane as the benzene ring since steric interactions are well known to give rise to intensity decreases. A coplanar alignment would be expected to lead to a large ϵ_{max} value, and hydrogen bonding of type VI would have been expected to facilitate this same alignment. However, if the above explanation (i.e. the hydrogen bond preventing coplanar alignment) concerning the ϵ decrease is correct, it is necessary to postulate that the six-membered ring system, involving the intramolecular hydrogen bond as shown in structure VI, is not entirely coplanar. Another more general interpretation is that the coplanar hydrogen-bonded confirmation causes some of the "normal" transitions to be "forbidden." A third explanation may be provided by supposing that

VI   VII
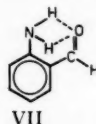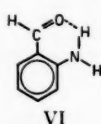
there is a tendency for *both* N-hydrogen atoms to form intramolecular hydrogen bonds as shown in structure VII, and that in this process both the NH_2 and CHO groups are twisted out of the plane of the benzene ring. A similar explanation—that is, *two* hydrogen bonds being formed at the expense of coplanarity—may also hold for the intensity decrease observed for the B-band of o-aminobenzoic acid (see Table IX) and for the ϵ decrease as observed for the phenolic B-band in o-nitrophenol (see Table III and also Concluding Remarks).

o-Aminoacetophenone

Infrared data have previously indicated (10, 16) the presence of an intramolecular hydrogen bond for this compound and the present ultraviolet spectra support this hypothesis (see Table VII); that is, the acetophenone B-band relative to the same band

TABLE VII

Main ultraviolet B-bands and infrared carbonyl bands of o-aminoacetophenone and reference compounds

Compound	Solvent	Ultraviolet maxima						Infrared carbonyl bands* (in carbon tetrachloride)	
		Aniline B-band		Acetophenone B-band		C-band			
		$\lambda_{max}(m\mu)$	ϵ_{max}	$\lambda_{max}(m\mu)$	ϵ_{max}	$\lambda_{max}(m\mu)$	ϵ_{max}	$\nu_{max}(cm^{-1})$	$\epsilon_{max}^{(a)}$ (mean)
o-Aminoacetophenone	Cyclohexane	224	23,500	253	5,500	351	4,350	1,653	549
m-Aminoacetophenone	Cyclohexane	226	26,500	247	9,000	323	2,500	1,689	540
Acetophenone	Cyclohexane	—	—	238	12,500	279	900	1,691	650
o-Aminoacetophenone	Ethanol	226	21,000	255	5,600	363	4,350	—	—
m-Aminoacetophenone	Ethanol	231	23,000	ca. 256	7,000	341	1,900	—	—

*Data from ref. 10.

in the *m*-isomer is bathochromically displaced. The intensity of the *B*-band in *o*-amino-acetophenone is again decreased (cf. Table VI). Although the ultraviolet spectrum of *o*-aminoacetophenone is not completely unaffected on altering the solvent from cyclohexane to ethanol, the observed spectral changes are less than for the corresponding *m*-isomer and particularly the ϵ values remain strikingly similar.

The ultraviolet data for this compound have also been determined by Lutskii and Dorofeev (17), who obtain spectral data similar to those obtained by us for *o*- and *m*-aminoacetophenone. Lutskii and Dorofeev also show that for the corresponding N,N-dimethyl derivatives a *hypsochromic* wavelength displacement is obtained in the acetophenone *B*-band if the spectrum of the *o*-isomer is compared with that of the *m*-isomer. This is not unexpected and suggests the presence of steric interactions in the *o*-isomer of N,N-dimethylaminoacetophenone. It follows that the latter compound is unsuitable as a reference compound for measuring the strength of the intramolecular hydrogen bond in *o*-aminoacetophenone.

o-Nitroaniline

Infrared data for *o*-nitroaniline, as judged primarily from the N—H stretching frequencies, have been assumed to show the *absence* of an intramolecular hydrogen bond in this compound (18, 19). The NO_2 vibrational frequencies are again only slightly, or not at all, lowered in the *o*-isomer compared with these same frequencies in the *m*-isomer of nitroaniline (12, 18, 19). However, this evidence cannot perhaps be regarded as entirely conclusive since some interaction would be expected to occur between the two *o*-substituents in *o*-nitroaniline, and since also there is some evidence for this interaction from other infrared data (see refs. 20, 21). The question whether a hydrogen bond exists in the ground state of *o*-nitroaniline must therefore remain undecided although, as pointed out by Dyall and Hambly (18), there is at present no unambiguous evidence of such a hydrogen bond in *o*-nitroaniline.

TABLE VIII

Main ultraviolet maxima for *o*-nitroaniline and reference compounds

Compound	Solvent	Aniline *B*-band		Nitrobenzene *B*-band		*C*-band	
		$\lambda_{max}(m\mu)$	ϵ_{max}	$\lambda_{max}(m\mu)$	ϵ_{max}	$\lambda_{max}(m\mu)$	ϵ_{max}
o-Nitroaniline	Cyclohexane	228	18,000	271	5,000	375	5,000
m-Nitroaniline	Cyclohexane	234	15,300	ca. 266	4,000	345	1,950
Nitrobenzene	Cyclohexane	—	—	252	9,000	ca. 280	1,500
o-Nitroaniline	Ethanol	232	17,000	279	5,000	408	5,500
m-Nitroaniline	Ethanol	234	18,000			380	1,600
m-Nitroaniline	Ether	235	19,000	ca. 277	4,000	373	1,800

This uncertainty is also reflected in the ultraviolet spectra (see Table VIII). On the one hand, a bathochromic wavelength displacement (of ca. 5 mμ) between the *o*- and *m*-isomers is observed in the nitrobenzene *B*-band; on the other hand, this *B*-band spectral change is less for *o*-nitroaniline than for *o*-aminoacetophenone, and on changing the solvent from cyclohexane to ethanol both *B*- and *C*-bands are appreciably more displaced for *o*-nitroaniline than for *o*-nitrophenol or *o*-aminoacetophenone.

A possible explanation is that the electronic perturbations, loosely ascribed to intramolecular hydrogen bonding, are of only minor importance *in the ground state* (cf. ref. 18 and also the dipole moment data for 2,4-dinitroaniline of Smith and Walshaw (22)), but

that these perturbations become more important in the electronic excited state and in this way give rise to the observed ultraviolet spectral changes. Even on this interpretation, however, it seems probable that intramolecular "hydrogen bonding" in o-nitroaniline is weaker than in most of the other o-amino or o-hydroxy compounds discussed in this paper.

o-Aminobenzoic Acid

The wavelength displacements between o- and m-isomers of aminobenzoic acid in ether and ethanol solution are ca. 8 and 6.5 mμ, respectively, for the ultraviolet benzoic acid B-band. The C-band ϵ_{max} values are appreciably larger in the o-isomer (see Table IX). These observations can in a general way be related to the existence of intramolecular hydrogen bonding or related interactions in o-aminobenzoic acid.

TABLE IX

Main ultraviolet maxima for o-aminobenzoic acid and reference compounds*

Compound	Solvent	Benzoic acid B-band		C-band	
		$\lambda_{max}(m\mu)$	ϵ_{max}	$\lambda_{max}(m\mu)$	ϵ_{max}
o-Aminobenzoic acid	Ether	252	7,400	333	5,200
m-Aminobenzoic acid	Ether	244	7,800	320	2,800
o-Aminobenzoic acid	Ethanol	248.5	6,700	336	4,500
m-Aminobenzoic acid	Ethanol	ca. 242	7,000	323	2,100

*Data from ref. 2e.

CONCLUDING REMARKS

In all the above o-substituted anilines or phenols, which may contain an intramolecular hydrogen bond, a bathochromic wavelength displacement of between 5 and 12.5 mμ (690 and 1780 cm^{-1}) is observed in the B-band compared with the B-band absorption in the corresponding m-isomer. (See Tables I–IX; the B-band referred to is the B-band associated with transitions involving predominantly that mono-substituted benzene derivative in which the substituent is electron-withdrawing.) Since for most of these compounds an intramolecular hydrogen bond is generally believed to be present, this suggests that intramolecular hydrogen bonding or related interactions contribute to this wavelength displacement. If this interpretation is correct this also indicates that intramolecular hydrogen bonding or related interaction give rise to approximately the *same* amount of electronic perturbation for most of the compounds discussed ($\Delta\nu = 1175 \pm 215$ cm^{-1}), except that for o-nitroaniline the observed wavelength displacement is smaller (690 cm^{-1}) and larger for o-nitrophenol (1780 cm^{-1}).

Evidence which can be interpreted in terms of an intramolecular hydrogen bond affecting *all* the above-mentioned compounds in a similar manner can also be deduced from the corresponding C-band spectral changes (see Tables I to IX). Apart from bathochromic wavelength displacements, the intensity of the C-band is also consistently increased in the o-isomer but this increase is not exclusively caused by intramolecular hydrogen bonding since it is very pronounced for o-nitroaniline compared with m-nitroaniline, although o-nitroaniline is not believed to contain a strong intramolecular hydrogen bond. Moreover, this intensity increase in the C-band is also observed for compounds like o-methoxyacetophenone compared with m-methoxyacetophenone (2a) although *no* intramolecular hydrogen bond is possible in the former compound. This suggests that C-band spectral changes are less reliable than B-band spectral changes in estimating the strength of an intramolecular hydrogen bond (cf. also ref. 2d).

The absence of an appreciable spectral change on determining the ultraviolet spectrum of a molecule in cyclohexane and ether or ethanol solution also provides support for the supposed presence of a strong intramolecular hydrogen bond. This argument is particularly convincing if the *m*-isomer or other reference compound shows an appreciable spectral change on altering the solvent in an identical manner (see Figs. 1 and 3 and Tables I, II, III, IV, and VII); only for *o*-nitroaniline the observed wavelength displacements point *against* the presence of an intramolecular hydrogen bond (the intensity values, however, again remain similar for the spectrum of *o*-nitroaniline in cyclohexane and ethanol). As anticipated, the concept of competitive hydrogen bonding is also indicated by some of the infrared data. For example, on determining the O—H vibrational band for a number of phenols under various solvent conditions, phenol affords frequency displacements of up to 300 cm^{-1}, *p*-nitrophenol affords frequency displacements of over 400 cm^{-1}, whereas the frequency displacements in *o*-nitrophenol for the same solvent range are never greater than 66 cm^{-1} (11). For salicylaldehyde both carbonyl band frequencies as also band intensities remain similar in carbon tetrachloride, chloroform, *n*-butanol, and even in acetonitrile (23).

There is also other evidence that the above eight compounds do not contain a similar intramolecular hydrogen bond. For example for phenols the ϵ_{max} value of the *B*-band not associated with the phenol or aniline system is usually increased substantially in the *o*-isomer compared with the same band in the *m*-isomer (see Tables I to V), but this same ϵ_{max} value is generally *reduced* for *o*-substituted anilines. Next, the other *B*-band, associated with the phenol or aniline chromophore, is only slightly affected if the spectrum of the *o*-isomer is compared with that of the *m*-isomer; however, a small *bathochromic* wavelength displacement is usually observed for the *o*-substituted phenol (see Tables I–III), whereas a small *hypsochromic* displacement is observed for *o*-aminoacetophenone (see Table VII). *o*-Nitroaniline may be exceptional since a slight bathochromic displacement is observed relative to the *m*-isomer and also since for *o*-nitroaniline the ϵ_{max} value of this band is increased (cf. Table VIII and other tables). Moreover, infrared spectral changes are also dissimilar. For example, the data in reference 6 show that the estimated frequency displacements of the O—H stretching bands are different for *o*-nitrophenol, salicylaldehyde, and salicylic acid. The reason for these differences remains obscure. A possible partial explanation is that the formation of N—H- - -O bonds tends to twist the carbonyl group out of the plane of the benzene ring, possibly to form hydrogen bonds or related interactions with *both* of the hydrogen atoms of the NH$_2$ group as shown in structure VII. This could account for some of the spectral differences observed between *o*-substituted anilines and phenols, but does not account for the anomalous spectral changes in *o*-nitroaniline. There is incidentally no evidence that an intramolecular O—H- - -O bond is stronger than an intramolecular N—H- - -O bond although precisely this relationship is indicated for the corresponding *inter*molecular hydrogen bonds (24).

Perhaps the most important deduction is that the data provide no evidence for other than an electrostatic linkage in the compounds discussed in this paper. That is, covalent-type hydrogen-bonded structures tend to be excluded for *o*-nitrophenols because the N—O stretching vibrations remain practically unaffected by the intramolecular hydrogen bond or related interactions for a number of substituted *o*-nitrophenols and for *m*-nitrophenol. (A covalent-type linkage would be expected to affect the N—O bond order and consequently the infrared stretching bands.) For some of the other compounds studied in this paper, for example *o*-hydroxy- and *o*-amino-acetophenone, the carbonyl

stretching vibration *is* altered, presumably by the formation of the intramolecular hydrogen bond or related interaction, but this does not necessarily provide evidence for a covalent linkage since an electrostatic linkage might also affect the negative charge on the carbonyl oxygen atom and hence the bond order of the carbonyl group.* In fact it must be supposed that the N—O bond order remaining unaffected in *o*-nitrophenol represents a somewhat exceptional behavior which *cannot* be explained readily in terms of a covalent linkage; it *can*, however, be explained in terms of an electrostatic linkage if it is assumed that the relatively large negative charge on the NO_2 oxygen atom is only slightly affected by the comparatively smaller positive charge on the neighboring hydrogen atom of the OH or NH_2 groups. For other compounds a variety of evidence has been obtained; some indicates a covalent type of linkage or at least that covalent forces play a considerable part (cf. for example, refs. 1, 6, 26), while other evidence, like the present data, may be assumed to indicate a predominantly electrostatic type of linkage (25).

Assuming that the change in the O—H stretching vibration provides the most sensitive method of determining the strength of an intramolecular "hydrogen bond" we may now attempt to summarize our observations. We can thus suppose that the interactions loosely referred to as intramolecular hydrogen bonding tend to attract the hydrogen atom(s) of the OH or NH_2 groups towards the adjoining negative center; this gives rise to the changes in bond order of the O—H or N—H bonds and consequently to the changes in the corresponding infrared vibrational bands. The bond order of the group containing the negative charge is not necessarily affected in the ground state but appears to be affected in the electronic excited state. Such a mechanism accounts for the ultraviolet spectral changes and also seems reasonable since the presence of a vicinal positive charge on the hydrogen atom might be expected to affect the bond order of the N—O bond to a greater extent in the electronic excited state than in the ground state.

EXPERIMENTAL

The ultraviolet absorption spectra were determined as described in previous parts of this series of papers (1, 24).

The infrared spectra were determined on a Unicam SP100 double-beam spectrophotometer using a NaCl prism and diffraction grating at the following solute concentrations: The spectrum of *o*-nitrophenol was determined at solute concentrations of 0.2 *M* and 1.0 *M*, and the spectra of the other *o*-nitrophenols were determined at concentrations of 0.2 *M*. The spectrum of salicylaldehyde was determined at solute concentrations of 0.05 and 0.25 *M*, the spectrum of benzaldehyde at 0.05 *M* and the spectra of *m*-hydroxybenzaldehyde and *m*-hydroxyacetophenone were determined in saturated solutions.

The phenols and anilines were either commercially available materials or prepared by standard methods as described in the literature. The compounds were purified by distillation or recrystallization until their melting points or boiling points and refractive indices showed them to be sufficiently pure. The solvents used were spectroanalyzed cyclohexane (Fisher), spectroanalyzed carbon tetrachloride, or commercially available absolute ethanol suitable for spectroscopy.

However, intramolecularly hydrogen-bonded systems containing a carbonyl group have been reported in which no effect of the hydrogen bonding on the carbonyl stretching frequency was observed (25).

ACKNOWLEDGMENTS

REFERENCES

1. W. F. FORBES, A. R. KNIGHT, and D. L. COFFEN.   Can. J. Chem. **38**, 728 (1960).
2. (a) J. C. DEARDEN and W. F. FORBES.   Can. J. Chem. **37**, 1305 (1959).
   (b) J. C. DEARDEN and W. F. FORBES.   Can. J. Chem. **37**, 1294 (1959).
   (c) W. F. FORBES.   Can. J. Chem. **36**, 1350 (1958).
   (d) W. F. FORBES, W. A. MUELLER, A. S. RALPH, and J. F. TEMPLETON.   Can. J. Chem. **35**, 1049 (1957).
   (e) W. F. FORBES and I. R. LECKIE.   Can. J. Chem. **36**, 1371 (1958).
3. P. M. G. BAVIN and W. J. CANADY.   Can. J. Chem. **35**, 1555 (1957).
4. H. TSUBOMURA.   J. Chem. Phys. **24**, 927 (1956).
5. S. PINCHAS.   Anal. Chem. **29**, 334 (1957).
6. K. NAKAMOTO, M. MARGOSHES, and R. E. RUNDLE.   J. Am. Chem. Soc. **77**, 6480 (1955).
7. P. J. KRUEGER and H. W. THOMPSON.   Proc. Roy. Soc. A, **250**, 22 (1959).
8. M. ST. C. FLETT.   Spectrochim. Acta, **10**, 21 (1957).
9. L. J. BELLAMY.   The infrared spectra of complex molecules. Methuen & Co. Ltd., London. 1954.
10. R. N. JONES, W. F. FORBES, and W. A. MUELLER.   Can. J. Chem. **35**, 504 (1957).
11. L. J. BELLAMY and H. E. HALLAM.   Trans. Faraday Soc. **55**, 220 (1959).
12. B. FRANCK, H. HÖRMANN, and S. SCHEIBE.   Ber. **90**, 330 (1957).
13. T. URBANSKI.   Roczniki Chem. **31**, 37 (1957); **32**, 241 (1958).
14. M. NEUILLY.   Compt. rend. **238**, 781 (1954).
15. H. DANNENBERG.   Z. Naturforsch. **4b**, 327 (1949).
16. A. N. HAMBLY and J. BONNYMAN.   Australian J. Chem. **11**, 529 (1958).
17. A. E. LUTSKII and V. V. DOROFEEV.   Zhur. Obshchei Khim. **27**, 1059 (1957); Cf. Chem. Abstr. **52**, 881 (1958).
18. L. K. DYALL and A. N. HAMBLY.   Australian J. Chem. **11**, 513 (1958).
19. T. URBANSKI and U. DABROWSKA.   Chem. & Ind. (London), 1206 (1958).
20. R. D. KROSS, V. A. FASSEL, and M. MARGOSHES.   J. Am. Chem. Soc. **78**, 1332 (1956).
21. R. J. FRANCEL.   J. Am. Chem. Soc. **74**, 1265 (1952).
22. J. W. SMITH and S. M. WALSHAW.   J. Chem. Soc. 4527 (1957).
23. H. YAMADA.   Bull. Chem. Soc. Japan, **32**, 1051 (1959).
24. J. C. DEARDEN and W. F. FORBES.   Can. J. Chem. **38**, 896 (1960).
25. N. MORI, Y. TSUZUKI, and H. TSUBOMURA.   Nippon Kagaku Zasshi, **77**, 459 (1956); Cf. Chem. Abstr. **52**, 7858 (1958).
26. E. W. GILL and E. D. MORGAN.   Nature, **183**, 248 (1959).

THE STUDY OF HYDROGEN BONDING AND RELATED PHENOMENA BY ULTRAVIOLET LIGHT ABSORPTION

PART VI. THE EFFECT OF STERIC INTERACTIONS ON THE INTRAMOLECULAR HYDROGEN BOND IN o-NITROPHENOL[1]

J. C. DEARDEN[2] AND W. F. FORBES[3]

ABSTRACT

Intramolecular hydrogen bonding occurring in o-nitrophenol is discussed with special reference to the effects of the steric interactions on the absorption bands and on the bonding. An alkyl substituent vicinal to the OH group, or a methyl group vicinal to the NO_2 group appears to strengthen the intramolecular hydrogen bond in o-nitrophenol. The O—H vibrational stretching frequency in o-nitrophenol appears to be more susceptible to steric than to mesomeric interactions, and a methyl substituent vicinal to the nitro group in o-nitrophenols is found to give rise to a characteristic O—H stretching vibration band. For 6-t-butyl-2-nitrophenol, a special, "protected" hydrogen bond is postulated. In some of the o-nitrophenols, intermolecular hydrogen bonding gives rise to appreciable ultraviolet intensity decreases presumably because of increased steric interactions.

INTRODUCTION

In the previous paper (1), it was shown that spectral data confirm the generally held opinion that o-nitrophenol possesses an intramolecular hydrogen bond; it was also shown that the spectral effects ascribed to this hydrogen bonding could be adequately explained in terms of an electrostatic model. That is, it may be assumed that the NO_2-group because of its negative charge merely attracts the hydrogen atom of the OH-group and that there is no need to postulate the presence of a covalent contribution since the infrared NO_2 stretching bands remain practically unaffected for a number of substituted o-nitrophenols, for o-nitroanisole, and for m-nitrophenol.

The purpose of the present paper is to investigate how steric interactions affect the spectral changes ascribed to intramolecular hydrogen bonding in various sterically hindered nitrophenols.

THE SPECTRA OF o-NITROPHENOL AND o-NITROANISOLE

The greatly reduced maximal extinction coefficient in the nitrobenzene B-band (for band nomenclature used, see ref. 2 and other papers in that series of papers, and ref. 3) of o-nitroanisole (λ_{max} 250 mμ, $\epsilon = 3400$) compared with that of o-nitrophenol (λ_{max} 271 mμ, $\epsilon = 7350$), m-nitrophenol (λ_{max} 258.5 mμ, $\epsilon = 6100$), and m-nitroanisole (λ_{max} 262 mμ, $\epsilon = 6100$) (all in cyclohexane solution) suggests the operation of steric interactions in o-nitroanisole. If intramolecular hydrogen bonding were wholly responsible for the relative intensity increase in o-nitrophenol compared with the intensity in o-nitroanisole, a similar intensity increase should be observed for o-nitrophenol compared with m-nitrophenol but this is not found to be so. Since, further, a hypsochromic wavelength displacement of 21 mμ occurs for this same band in o-nitroanisole compared with o-nitrophenol (12 mμ compared with m-nitroanisole), whereas the infrared NO_2 stretching vibrations remain approximately constant (1530 ± 2 cm^{-1}) this suggests that the energy levels of the nitrobenzene groups in the two compounds are as shown in Fig. 1.
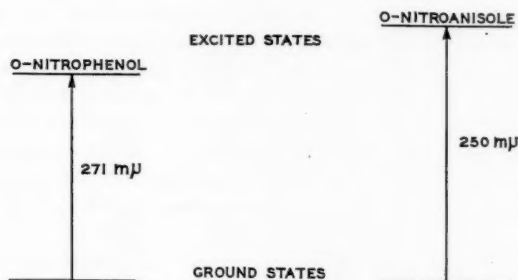
FIG. 1. Schematic representation of ground and excited states for nitrophenol and nitroanisole.

Figure 1 illustrates that the ultraviolet hypsochromic wavelength displacement is to be ascribed to the potential energy being raised predominantly in the electronic excited state of o-nitroanisole, and a contributing factor to this may be a slight twist in the interplanar angle between the NO_2-group and the benzene ring. Moreover, this slight change in interplanar angle may cause some of the transitions in o-nitroanisole to become "forbidden" and this may contribute to the observed loss of absorption intensity in this compound (4, 5, 6). It remains to explain the well-known appreciable frequency displacement in carbon tetrachloride solution for the infrared O—H band in o-nitrophenol (ν_{max} 3209 cm^{-1}) compared with that of m-nitrophenol (ν_{max} ca. 3500 cm^{-1}) on the basis of this model, but this has previously been done (1) by assuming that the negative charge on the NO_2-group attracts the hydrogen atom and thus weakens the O—H bond and consequently causes absorption at lower frequency.

THE SPECTRA OF o-NITROPHENOL, 6-METHYL-2-NITROPHENOL, AND 6-t-BUTYL-2-NITROPHENOL

The spectra of o-nitrophenol, 6-methyl-2-nitrophenol, and 6-t-butyl-2-nitrophenol are listed in Table I.

Table I shows that, as judged by the infrared O—H stretching bands, an alkyl substituent ortho to the OH group in o-nitrophenol apparently strengthens the intramolecular hydrogen bond. Moreover, this effect, associated with strengthening of the intramolecular hydrogen bond, is more pronounced for a t-butyl than for a methyl substituent. The effect of the alkyl substituents on the infrared O—H band is also paralleled by the effect on the ultraviolet maximal wavelengths, which are progressively displaced to longer wavelength (i.e. to lower frequency) with increased size of the alkyl substituent (see Table I). The above spectral changes therefore suggest that the introduction of alkyl substituents vicinal to the OH group in o-nitrophenol may be assumed to provide an example of steric facilitation of hydrogen bonding (for other examples of steric facilitation of hydrogen bonding see ref. 7 and cf. also refs. 8, 9, and footnote 14 of ref. 10).

However, there are some significant differences between the spectra of 6-methyl-2-nitrophenol and 6-t-butyl-2-nitrophenol (see Table I). First, doublet formation occurs in both infrared stretching bands for the 6-methyl compound but not for 6-t-butyl-2-nitrophenol or o-nitrophenol. The most obvious cause of this observed band splitting is conformational heterogeneity, but it is difficult to conceive of two different conformational isomers in 6-methyl-2-nitrophenol. Next, the ultraviolet data show that for o-nitrophenol and 6-t-butyl-2-nitrophenol the maximal wavelengths are altered only

TABLE I

Absorption spectra of o-nitrophenol, 6-methyl-2-nitrophenol, and 6-t-butyl-2-nitrophenol

Infrared spectra

Bands	o-Nitrophenol, ν_{max}	6-Methyl-2-nitrophenol, ν_{max}	6-t-Butyl-2-nitrophenol, ν_{max}
Spectrum in carbon tetrachloride			
O—H bands (in cm^{-1})	3,209(s)	{3,078(w)* 3,154(m)}	3,067(m)
NO$_2$ bands (in cm^{-1})	{1,532(s) 1,316(s)}	[{1,534(m) 1,552(m) 1,309(m) 1,327(m)}]	{1,536(s) 1,333(m)}

Ultraviolet spectra

Bands	o-Nitrophenol λ_{max} (mμ)	o-Nitrophenol ϵ_{max}	6-Methyl-2-nitrophenol λ_{max} (mμ)	6-Methyl-2-nitrophenol ϵ_{max}	6-t-Butyl-2-nitrophenol λ_{max} (mμ)	6-t-Butyl-2-nitrophenol ϵ_{max}
Spectrum in cyclohexane						
Nitrobenzene B-band	271	7,350	281	7,850	283	6,900
C-band	346	3,700	354	3,400	357	3,550
Spectrum in ethanol						
Nitrobenzene B-band	272.5	6,050	274	6,850	285	6,500
C-band	347	3,250	341	2,750	358	3,350

*Band assignment doubtful; this band may be a —C—H stretching band, or may correspond to associated molecules.

slightly on changing the solvent from cyclohexane to ethanol. However, for 6-methyl-2-nitrophenol an appreciable wavelength change is observed with change of solvent (see Table I), and incidentally the ϵ_{max} values are greatest for the B-band and smallest for the C-band of 6-methyl-2-nitrophenol. These changes can partly be explained by assuming that competitive intermolecular hydrogen bonding occurs for 6-methyl-2-nitrophenol (which gives rise to the observed wavelength displacement on determining the spectrum in cyclohexane and ethanol), but that such competitive intermolecular hydrogen bonding does not occur for 6-t-butyl-2-nitrophenol presumably because of the bulk effect of the t-butyl group. If this interpretation is correct it must also be assumed that for o-nitrophenol competitive intermolecular hydrogen bonding is of less importance. The reason for this may be that only for 6-methyl-2-nitrophenol (in which steric facilitation of hydrogen bonding occurs), but not for o-nitrophenol, steric interactions are increased by this competitive intermolecular hydrogen bonding. It may be noted that 6-t-butyl-2-nitrophenol therefore occupies a somewhat unique position among o-nitrophenols possessing adjacent alkyl groups (see also following sections), since only for this compound is there observed no wavelength displacement on determining the ultraviolet spectrum in cyclohexane and ethanol. This, in turn, suggests a stronger, "protected" hydrogen bond and this hypothesis also receives support from the greater frequency displacement (142 cm^{-1}) observed for the O—H stretching band and from examination of scale models of 6-t-butyl-2-nitrophenol.

THE SPECTRA OF o-NITROPHENOL, 3-METHYL-2-NITROPHENOL, AND 3,4-DIMETHYL-2-NITROPHENOL

The relevant spectral data are listed in Table II.

It may first be noted that the infrared O—H stretching vibration bands of all o-nitrophenols containing a methyl group vicinal to the nitro-group are different from these bands in other o-nitrophenols. This is illustrated in Fig. 2.

Figure 2 shows that 3-methyl-substituted 2-nitrophenols afford a broad O—H absorption band in the 3350–2900 cm^{-1} region as opposed to the more intense, sharp bands observed for the other o-nitrophenols. This broadness of the bands suggests that 3-methyl-substituted o-nitrophenols give rise to strong intramolecular bonds (cf. ref. 11), presumably again because of steric facilitation of the hydrogen bond. Apart from these diffuse O—H stretching bands, 3-methyl-substituted 2-nitrophenols also afford a sharp band which occurs at lower frequency, and which is ascribed to —C—H stretching bands. The displacement of the infrared O—H stretching band for 3-methyl-2-nitrophenol ($\Delta\nu = +41$ cm^{-1}) again indicates steric facilitation of hydrogen bonding but the displacement for the O—H band of 3,4-dimethyl-2-nitrophenol ($\Delta\nu = -136$ cm^{-1}) is in the opposite direction. This suggests that buttressing interactions also affect the intramolecular hydrogen bond in some way (see below). The infrared NO$_2$ symmetrical stretching band of 3-methyl- and 3,4-dimethyl-2-nitrophenol again shows some signs of band splitting. Moreover, there is some indication that in sterically hindered o-nitrophenols the intensity of the symmetrical NO$_2$ stretching band decreases slightly relative to the same band in o-nitrophenol, presumably because of steric interactions (cf. ref. 13).

The ultraviolet spectra in cyclohexane solution first indicate that a 3-methyl group causes a slight twist of the nitro-group away from the plane of the benzene ring as judged by the reduced ϵ_{max} value of the nitrobenzene B-band (see Table II). The ϵ_{max} value of 3-methyl-2-nitrophenol is slightly *greater* than that of o-methylnitrobenzene in isooctane

TABLE II

Absorption spectra of o-nitrophenol, 3-methyl-2-nitrophenol, and 3,4-dimethyl-2-nitrophenol

Infrared spectra

Bands	o-Nitrophenol, ν_{max}	3-Methyl-2-nitrophenol, ν_{max}	3,4-Dimethyl-2-nitrophenol, ν_{max}
Spectrum in carbon tetrachloride			
O—H bands (in cm^{-1})	3,209(s)	{ ca. 3,168 (m; diffuse), 3,042(sh)*	{ ca. 3,345 (m; diffuse), ca. 3,150(sh)*
NO₂ bands (in cm^{-1})	{ 1,532(s), 1,316(s)	{ 1,534(m), 1,325(m), 1,335(w; sh)	{ 1,524(s), 1,325(m), 1,310(vw)

Ultraviolet spectra

Bands	o-Nitrophenol λ_{max} (mμ)	o-Nitrophenol ϵ_{max}	3-Methyl-2-nitrophenol λ_{max} (mμ)	3-Methyl-2-nitrophenol ϵ_{max}	3,4-Dimethyl-2-nitrophenol λ_{max} (mμ)	3,4-Dimethyl-2-nitrophenol ϵ_{max}
Spectrum in cyclohexane						
Nitrobenzene B-band	271	7,350	278	6,500	280	5,000
Second B-band	ca. *231*	*4,000†*	ca. *234*	*3,400†*	243	3,200
C-band	346	3,700	351	2,900	361	2,600
Spectrum in ethanol						
Nitrobenzene B-band	272.5	6,050	270	1,750	275	1,650
Second B-band	ca. *231*	*3,550†*	ca. *241*	*1,750†*	251	1,425†
C-band	347	3,250	ca. *340*	*725†*	{ ca. *345*, ca. *359*	{ *550†*, *500*
Spectrum in ether						
Nitrobenzene B-band	271	6,900	278.5	3,300		
Second B-band	ca. *234*	*3,000†*	ca. *236*	*2,600†*		
C-band	*346*	*3,550*	348	1,400		

*Band assignment doubtful; this band may be a —C—H stretching band, or may correspond to associated molecules.
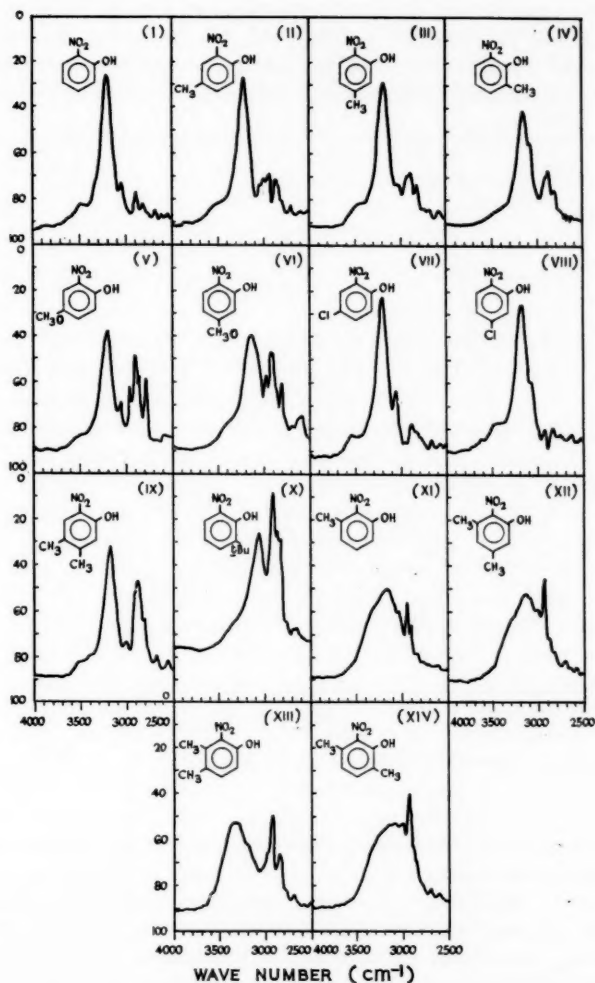†Values in italics represent inflections in this and subsequent tables.

FIG. 2. The infrared O—H stretching vibration bands at concentrations of 0.2 molar in carbon tetrachloride solution of (i) o-nitrophenol, (ii) 4-methyl-2-nitrophenol, (iii) 5-methyl-2-nitrophenol, (iv) 6-methyl-2-nitrophenol, (v) 4-methoxy-2-nitrophenol, (vi) 5-methoxy-2-nitrophenol, (vii) 4-chloro-2-nitrophenol, (viii) 5-chloro-2-nitrophenol, (ix) 4,5-dimethyl-2-nitrophenol, (x) 6-t-butyl-2-nitrophenol, and (xi) 3-methyl-2-nitrophenol, (xii) 3,5-dimethyl-2-nitrophenol, (xiii) 3,4-dimethyl-2-nitrophenol, (xiv) 3,6-dimethyl-2-nitrophenol. (Fine structure observed in these O—H bands may be caused by intermolecular hydrogen bonding.)

solution whereas in cyclohexane solution the ϵ_{max} value of o-nitrophenol is less than that of nitrobenzene (cf. Table II and ref. 2), and this may imply that the intramolecular hydrogen bonding tends to keep the NO₂-group in a position coplanar with that of the benzene ring. In 3,4-dimethyl-2-nitrophenol the ϵ_{max} value of the nitrobenzene B-band is yet further decreased, indicative of a buttressing effect of the 4-methyl on the 3-methyl

group (see Table II and cf. ref. 12). In ethanol solution, the ϵ_{max} values of all three bands in both 3-methyl- and 3,4-dimethyl-2-nitrophenol are drastically reduced, and a similar but less pronounced effect is observed for 3-methyl-2-nitrophenol in ether solution (see Table II and Fig. 3). Both 3-methyl- and 3,4-dimethyl-2-nitrophenol again give rise to
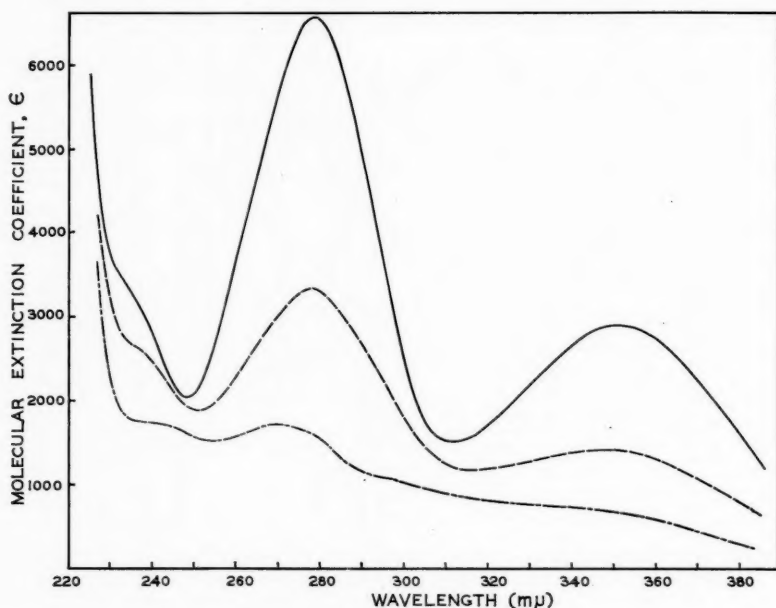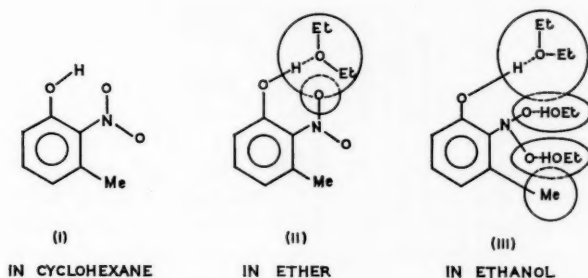

FIG. 3. The spectrum of 3-methyl-2-nitrophenol in cyclohexane (————), ether (- - -), and ethanol (- · - ·).

appreciable wavelength displacements when the solvent is altered, which indicates competing solvent–solute interactions.

The hypothesis of a coplanar conformation facilitating hydrogen bonding also receives support since this coplanarity is disturbed in ethanol *or* ether solution, as judged by the greatly reduced ϵ_{max} values of the 3-methyl-substituted compounds (see Table II), although ether presumably interacts predominantly with the OH-group only. It may thus be assumed that ether interacts competitively with the OH-group and in this way weakens the intramolecular hydrogen bonding, and that as a result of this weakening, there occurs the above-mentioned non-planarity between the nitro-group and the benzene ring. This is further illustrated by structures I, II, and III, which schematically indicate the effect of competing intermolecular hydrogen bonding on the intramolecular hydrogen bond and on the steric interactions present in 3-methyl-2-nitrophenol (cf. also the *B*-band intensities of *o*-nitrophenol in different solvents and later discussion). The steric facilitation of hydrogen bonding relative to *o*-nitrophenol, which is again observed for 3-methyl-2-nitro-phenol as judged from the infrared O—H bands, may be ascribed to the NO_2-group – OH-group distance being decreased probably through the NO_2-group being *bent* towards the OH-group.

(I)   (II)   (III)

IN CYCLOHEXANE   IN ETHER   IN ETHANOL

THE SPECTRA OF 3-METHYL-2-NITROPHENOL, 3,5-DIMETHYL-2-NITROPHENOL, 4,5-DIMETHYL-2-NITROPHENOL, AND 3,6-DIMETHYL-2-NITROPHENOL

The relevant spectral data are listed in Table III.

The infrared O—H vibrational stretching frequencies of the compounds listed in Table III again afford the expected changes in as much as only 4,5-dimethyl-2-nitrophenol, which does not possess a 3-methyl substituent, shows a sharp absorption band (see Fig. 2). It may be noted that the effect of steric interactions on this O—H band is larger than the effect of mesomeric interactions on the same band. Thus, the data in Tables II and III show that only in 4,5-dimethyl-2-nitrophenol is the O—H stretching band (ν_{max} 3191 cm^{-1}) reasonably close to that in o-nitrophenol (ν_{max} 3209 cm^{-1}) and in the previous paper of this series it was shown that the O—H bands in 4-chloro-2-nitrophenol (ν_{max} 3216 cm^{-1}), 4-methoxy-2-nitrophenol (ν_{max} 3216 cm^{-1}), 4-methyl-2-nitrophenol (ν_{max} 3218 cm^{-1}), and 5-chloro-2-nitrophenol (ν_{max} 3182 cm^{-1}), 5-methoxy-2-nitrophenol (ν_{max} 3144 cm^{-1}), 5-methyl-2-nitrophenol (ν_{max} 3185 cm^{-1}) all occur fairly close to the O—H band in o-nitrophenol (see ref. 1), whereas steric interactions give rise to larger frequency displacements (cf. Tables I, II, and III). It is also worth noting that in dimethyl-substituted o-nitrophenols frequency displacements in the infrared O—H stretching band are approximately additive, except as for the previously mentioned 3,4-dimethyl compound. Thus, relative to the O—H band in o-nitrophenol, the O—H band in 3-methyl-2-nitrophenol is displaced by 41 cm^{-1} and the relevant band in 5-methyl-2-nitrophenol by 24 cm^{-1}. Adding these displacements affords a calculated value of 65 cm^{-1} for the frequency displacement in 3,5-dimethyl-2-nitrophenol, which is identical with the observed frequency displacement of the infrared O—H band in 3,5-dimethyl-2-nitrophenol relative to the same band in o-nitrophenol. Similarly, for 3,6-dimethyl-2-nitrophenol the "calculated" frequency displacement is 96 cm^{-1} while the observed frequency displacement is 109 cm^{-1}, and the "calculated" frequency displacement for 4,5-dimethyl-2-nitrophenol is 15 cm^{-1} while the observed displacement is 18 cm^{-1}. These displacements incidentally are not quantitatively related to the wavelength displacements observed in the ultraviolet B-bands; at best, a rough semiquantitative relation holds for compounds where there is no steric effect, that is, for o-nitrophenols which have substituents only in the 4- or 5-positions.

Next, a substituent in the 4-position causes absorption at slightly higher frequency, whereas a substituent in the 5-position causes absorption at slightly lower frequency than for 2-nitrophenol (cf. ref. 1). This latter observation may in general terms be related to the ability of an electron-donating substituent in the 5-position to enhance the negative

TABLE III

Absorption spectra of 3-methyl-2-nitrophenol, 3,5-dimethyl-2-nitrophenol, 3,6-dimethyl-2-nitrophenol, and 4,5-dimethyl-2-nitrophenol

Infrared spectra

Bands	3-Methyl-2-nitrophenol, ν_{max}	3,5-Dimethyl-2 nitrophenol, ν_{max}	4,5-Dimethyl-2-nitrophenol, ν_{max}	3,6-Dimethyl-2-nitrophenol, ν_{max}
Spectrum in carbon tetrachloride				
O—H bands (in cm⁻¹)	ca. 3,108(m; diffuse) / 3,042(sh)*	ca. 3,144(m; diffuse) / 3,006(w)*	3,191(s)	ca. 3,100(m; diffuse) / 3,007(w)*
NO₂ bands (in cm⁻¹)	1,534(m) / 1,325(m) / 1,335(w;sh)	1,533(m) / 1,331(m) / 1,315(w;sh)	1,525(s) / 1,300(s)	1,539(s) / 1,327(m)†

Ultraviolet spectra

Bands	3-Methyl-2-nitrophenol λ_{max}(mμ)	ϵ_{max}	3,5-Dimethyl-2-nitrophenol λ_{max}(mμ)	ϵ_{max}	4,5-Dimethyl-2-nitrophenol λ_{max}(mμ)	ϵ_{max}	3,6-Dimethyl-2-nitrophenol λ_{max}(mμ)	ϵ_{max}
Spectrum in cyclohexane								
Nitrobenzene B-band	278	6,500	289	8,250	284	8,700	286	6,700
Second B-band	ca. 284	3,400	ca. 238	3,000	ca. 235	3,600	ca. 241	3,500
C-band	351	2,900	351	3,500	357	4,250	358	2,650
Spectrum in ethanol								
Nitrobenzene B-band	270	1,750	279	2,350‡			280	2,750‡
Second B-band	ca. 241	1,760	245	2,100			ca. 245	1,650
C-band	ca. 340	726	341	1,200			347	1,200

*Band assignment doubtful; this band may be a C—H stretching band or may correspond to associated molecules.
†Band is slightly unsymmetrical.
‡Some fine structure occurs on the longer wavelength side.

(IV)

charge on the NO_2-group by means of mesomeric interaction as shown in structure IV, which, as discussed in ref. 1, tends to facilitate the intramolecular hydrogen bond.

Related, though less pronounced effects are observed for the NO_2 stretching vibrations as follows. The asymmetrical NO_2 stretching vibrational frequency remains approximately constant, although it may be noted that for 4,5-dimethyl-2-nitrophenol the band occurs at slightly lower frequency (1525 cm^{-1}; see Table III) than for o-nitrophenol (ν_{max} 1532 cm^{-1}). This may be a general effect for o-nitrophenols possessing a substituent in the 4- or 5- positions since 3,4-dimethyl-2-nitrophenol (ν_{max} 1524 cm^{-1}), 4-methoxy-2-nitrophenol (ν_{max} 1528 cm^{-1}), and 4-chloro-2-nitrophenol (ν_{max} 1530 cm^{-1}) also absorb at slightly lower frequency than o-nitrophenol. 4-Methyl-2-nitrophenol absorbs at ν_{max} 1532 cm^{-1} like o-nitrophenol, and o-nitrophenols possessing *only* a substituent in the 5-position also tend to absorb at lower frequency than o-nitrophenol, for example 5-chloro-2-nitrophenol (ν_{max} 1521 cm^{-1}), 5-methyl-2-nitrophenol (ν_{max} 1529 cm^{-1}), and 5-methoxy-2-nitrophenol (ν_{max} 1529 cm^{-1}), but all other o-nitrophenols discussed show the asymmetric NO_2 stretching band at higher frequency.

Similar effects are observed for the symmetrical NO_2 stretching vibration near 1315 cm^{-1} except that comparisons are sometimes more difficult because of band splitting and also because 5-methoxy-2-nitrophenol absorbs at slightly higher frequency (1317 cm^{-1}) than o-nitrophenol, although it might have been expected to absorb at lower frequency. Thus it seems that the effect of both electronic and steric interactions on the NO_2 vibrational stretching bands are small but that there is a tendency for electron-donating substituents in the 4- or 5-positions to cause absorption at lower frequency and for steric interactions, brought about by substituents in the 3- or 6-positions, to cause absorption at higher frequency.

The ultraviolet spectra listed in Table III give rise to the expected wavelength displacements when it is remembered that the ultraviolet B-bands are particularly susceptible to mesomeric interactions. This presumably accounts for the nitrobenzene B-band absorption at longer wavelength for 3,5-dimethyl-2-nitrophenol in cyclohexane solution. In ethanol solution the previously discussed decrease in the ϵ values of the 3-methyl-substituted 2-nitrophenols is again observed (see Table III). The spectral changes with change of solvent for a number of o-nitrophenols and o-nitroanisoles are also listed in Table IV.

Table IV shows that changing the solvent from cyclohexane to ethanol causes a bathochromic wavelength displacement of ca. 6 mμ (ca. 900 cm^{-1}) in nitrobenzene accompanied by a slight intensity decrease (2). In sterically hindered nitrobenzenes, such as 2,4- or 2,5-dimethoxynitrobenzene, this bathochromic wavelength displacement of the nitrobenzene B-band appears to be increased to ca. 8–10 mμ (ca. 1200–1300 cm^{-1}). In cyclohexane solution, an intensity decrease occurs for this band in 2,4-dimethoxynitrobenzene relative to the same band in nitrobenzene and this decrease is considerably more pronounced in the 2,6-dimethoxynitrobenzene. An intermediate intensity value is observed in the 2,5-isomer, probably because of a buttressing effect (cf. ref. 12) and because in 2,4-dimethoxy-, but not in 2,5-dimethoxy-benzene, can the mesomeric effect of the

TABLE IV

Ultraviolet absorption maxima of nitrobenzenes in cyclohexane and ethanol

Compound	Absorption band	Cyclohexane		Ethanol	
		λ_{max} (mμ)	ϵ_{max}	λ_{max} (mμ)	ϵ_{max}
Nitrobenzene	B-band	252	9,000	258	8,000
2,4-Dimethoxy- nitrobenzene	B-band	272	6,000	282	5,200
	2nd B-band	308	5,500	321	6,100
2,5-Dimethoxy- nitrobenzene	B-band	ca. 256	2,100	ca. 264	2,200
	C-band	339	2,650	353	2,550
2,6-Dimethoxy- nitrobenzene	B-band	279	1,650		
	C-band	ca. 343	200		
o-Nitrophenol	B-band	271	7,350	272.5	6,050
	C-band	346	3,700	347	3,250
5-Methyl-2- nitrophenol	B-band	281	9,000	284	7,600
	C-band	ca. 336	4,200	345	4,200
		347	4,500		
6-Methyl-2- nitrophenol	B-band	281	7,850	274	6,850
	C-band	354	3,400	341	2,750
3-Methyl-2- nitrophenol	B-band	278	6,500	270	1,750
	C-band	351	2,900	ca. 340	725
2-Nitroresorcinol	B-band	314.5	10,800	308	4,000
	C-band	406	1,600		

p-methoxy substituent be expected to cause increased double-bond character in the C—N bond, which in turn may lead to increased coplanarity and increased absorption intensity. The low intensity value of the 2,6-isomer shows that two substituents, one on either side of the nitro-group, produce a much larger steric effect than one such substituent, which in turn implies that the interactions on the nitro-group do not only involve a twisting effect on a symmetrical nitro-group. (If these interactions merely caused a symmetrical nitro-group to twist out of the plane of the benzene ring, two like substituents would be expected to cause changes in the conformation of the nitro-group similar to those caused by a single substituent.) Changing the solvent incidentally does not appreciably affect the absorption intensity for 2,4-dimethoxy- or 2,5-dimethoxy- nitrobenzene. Next, for intramolecularly hydrogen-bonded molecules, such as o-nitrophenol and 5-methyl-2-nitrophenol, only small wavelength changes and small intensity decreases are observed on changing the solvent from cyclohexane to ethanol. For 6-methyl-2-nitrophenol a hypsochromic wavelength displacement is observed on changing the solvent from cyclohexane to ethanol and this suggests, as previously noted, that the intramolecular hydrogen bond has been affected by the 6-methyl substituent. It may be noted that the wavelength displacements are in a different direction from those observed for ordinary nitrobenzenes, and this could be because the intramolecular hydrogen bond in 6-methyl-2-nitrophenol is partially inhibited by changing the solvent. Direct steric interactions, it may be noted, are unlikely to be entirely responsible for this hypsochromic wavelength displacement since changing the solvent affects the absorption intensity only slightly.

In 3-methyl-2-nitrophenol, however, changing the solvent from cyclohexane to ethanol produces a very large intensity decrease comparable to the intensity decrease observed for 2,6-dimethoxynitrobenzene in cyclohexane solution, and this may be related to the observation that in both compounds the nitro-group has two large neighboring groups.

In this case, however, it must further be assumed that the ethanol molecule attaches itself to the OH-group, and in this way increases the effective size of the OH-group. These general hypotheses are supported by the B-bands of 2-nitroresorcinol in cyclohexane and ethanol solution since in the latter there occurs a hypsochromic wavelength displacement accompanied by a considerable intensity decrease; steric interactions and the inhibition of part of the intramolecular hydrogen bonding would be expected to give rise to precisely these spectral changes.

Summarizing, the above-mentioned and previous data all suggest that in most 3-methyl-substituted 2-nitrophenols the NO_2-group is partly twisted out of the plane of the benzene ring, and also that solvent–solute interactions become important for 3-methyl- or 6-methyl-substituted 2-nitrophenols. These latter interactions tend to weaken the intramolecular hydrogen bond and may also increase the effective size of the NO_2- and OH-groups.

EXPERIMENTAL

The ultraviolet absorption spectra were determined by standard methods using a Unicam SP500 spectrophotometer as described in previous parts of this series of papers (1, and references cited there). For each compound at least two independent sets of observations were made. The accuracy of λ_{max} values is estimated to be ± 1 mμ, and the precision of ϵ_{max} values $\pm 5\%$ or better. Values were reproducible in most cases to $\pm 2\%$.

The infrared spectra were determined on a Unicam SP100 double beam spectrophotometer using a NaCl prism and diffraction grating. The day-to-day reproducibility was better than ± 2 cm^{-1} for sharp bands. The spectra were determined in carbon tetrachloride at solute concentrations of about 0.2 M in cells of path lengths of 0.1 and 0.5 cm.

Most of the compounds were synthesized according to directions obtained from the literature. All the compounds, except 6-t-butyl-2-nitrophenol, have previously been described in the literature. 6-t-Butyl-2-nitrophenol, prepared by a modification of the method of Gibson (14) distilled under vacuum as a bright golden oil, b.p. 122° at 7 mm, $n_D^{22.5}$ 1.5562. Found: C, 61.7; H, 6.9; N, 7.5%. $C_{10}H_{13}O_3N$ requires C, 61.5; H, 6.7; N, 7.2%.

The solvents used were spectroanalyzed cyclohexane (Fisher), spectroanalyzed carbon tetrachloride, and commercially available absolute ethanol suitable for spectroscopy.

ACKNOWLEDGMENTS

REFERENCES

1. J. C. DEARDEN and W. F. FORBES.   Can. J. Chem. **38**, 1837 (1960).
2. W. F. FORBES.   Can. J. Chem. **36**, 1350 (1958).
3. W. F. FORBES and R. SHILTON.   ASTM Bull. (1960).
4. E. A. BRAUDE, F. SONDHEIMER, and W. F. FORBES.   Nature, **173**, 117 (1954).
5. E. A. BRAUDE and F. SONDHEIMER.   J. Chem. Soc. 3754 (1955).
6. W. F. FORBES and R. SHILTON.   J. Am. Chem. Soc. **81**, 786 (1959).
7. I. M. HUNSBERGER, H. S. GUTOWSKY, W. POWELL, L. MORIN, and V. BANDURCO.   J. Am. Chem. Soc. **80**, 3294 (1958).
8. L. P. KUHN.   J. Am. Chem. Soc. **80**, 5950 (1958).
9. S. MARCINKIEWICZ and J. GREEN.   J. Chem. Soc. 849 (1959).
10. A. W. BAKER and A. T. SHULGIN.   J. Am. Chem. Soc. **80**, 5358 (1958).
11. L. J. BELLAMY.   The infra-red spectra of complex molecules. Methuen & Co. Ltd., London 1954. p. 84.
12. W. F. FORBES and W. A. MUELLER.   J. Am. Chem. Soc. **79**, 6495 (1957).
13. R. N. JONES and C. SANDORFY.   *In* Chemical applications of spectroscopy. *Edited by* W. West. Interscience Publishers, Inc., New York. 1956. pp. 540–541.
14. G. P. GIBSON.   J. Chem. Soc. **127**, 42 (1925).

RADICAL TERMINATION MECHANISMS IN BULK POLYMERIZATION[1]

B. L. FUNT AND W. PASIKA[2]

ABSTRACT

The termination mechanism in the bulk polymerization of styrene and vinyl acetate initiated by α,α'-azobisisobutyronitrile has been investigated. C^{14}-Labelled initiators were employed and activities of samples were determined by internal liquid scintillation counting. Measurements of fractionated and unfractionated polystyrene showed an average of 1.94 and 2.04 tagged fragments per molecule, respectively, and indicated termination by combination at 60° C. For polyvinyl acetate 1.06 fragments were found per molecule, indicating termination by disproportionation at 60° C.

One of the features of vinyl addition reactions, which is still subject to considerable uncertainty, is the mode of termination of growing chains. It is universally accepted that termination reactions must occur as the result of the interaction of two radicals, but the mechanism of this termination, whether by direct combination or by disproportionation, has only been investigated for a few systems, and has not been proved unequivocally even for these.

Nevertheless the mode of termination is of primary importance in kinetic analysis of data, in the assignment of termination constants and the prediction of molecular weights. Unless the mode of termination is understood, these quantities are subject to an uncertainty of a factor of two.

Two sensitive methods exist for the solution of this problem. Bamford and Jenkins (1) have described a technique of coupling preformed polymer possessing suitably reactive end groups. Alternatively with the use of radioactive initiators, it is possible to determine the number of initiator fragments present per polymer molecule (2, 3, 4). Since each initiator fragment found generated a chain, then in the final polymer the presence of two initiator fragments per polymer molecule would indicate the exclusive occurrence of combination, and of one initiator fragment of disproportionation.

Previous studies have not yielded completely conclusive results. For methyl methacrylate, the monomer subjected to the most intensive study, early work by Arnett and Peterson (5) using tagged initiators, indicated combination, whereas Bevington et al. (3) found a predominance of disproportionation. Ayrey and Moore (6) also found disproportionation and combination, but their results were not in exact agreement with those of Bevington.

It is reasonable to assume that for most monomers, termination reactions by combination and disproportionation can be considered as competitive reactions, each with a definite rate constant and activation energy. It is our intention to investigate this problem in detail, and the present report represents our first work in this direction.

The systems styrene and vinyl acetate, initiated with α,α'-azobisisobutyronitrile (AIBN), were chosen for this preliminary study.

EXPERIMENTAL

Materials

α,α'-Azobisisobutyronitrile (AIBN) dicyano C^{14} was obtained from the Commissariat à L'Énergie Atomique, Saclay, France, and possessed a specific activity of 200 $\mu c/g$. It

was suitably diluted with inactive AIBN, dissolved in benzene to an activity of 1 μc/ml, and the mixture purified by the method of Ikamura and Motoyama (7).

Styrene, obtained through the courtesy of the Dow Chemical Company, was washed three times with 5% NaOH solution, three times with distilled water, dried over $CaSO_4$, slightly prepolymerized, and then distilled under reduced pressure (8).

Vinyl acetate, obtained from Carbide and Carbon Chemicals, was twice distilled at atmospheric pressure under an argon atmosphere. Prior to the second distillation it was refluxed for 1 hour under argon to destroy peroxides.

Scintillation grade p-terphenyl and 1,4-di-2-(5 phenyl oxazolyl)benzene (POPOP) were obtained from Nuclear Enterprises Ltd., Winnipeg, and were employed without further purification.

Methods

Polymerization

The monomers, with appropriate amounts of initiator added, were placed in Pyrex tubes and degassed by a series of freezing–thawing cycles under vacuum. The tubes were evacuated and sealed, and the 20-ml charges placed into a thermostatted water bath at 60.0° C. Samples were polymerized to approximately 10% conversion and blank experiments (without initiator) were performed for all samples to determine whether thermal uninitiated polymerization was also occurring.

In order to determine that the polymerizations were following established mechanisms, samples were isolated and weighed at different degrees of conversion, and it was found that the kinetics accurately obeyed the expected linear dependence of rate of polymerization on the square root of the AIBN concentration.

Isolation and Purification of Polymers

After polymerization the polystyrene was dissolved in methyl ethyl ketone and precipitated in methanol. Polyvinyl acetate was precipitated in a 25/75 methanol–water mixture (5), redissolved in acetone, and precipitated in n-hexane. The polymer was finally isolated by the freeze-drying method (9).

Molecular Weights

Molecular weights were primarily determined by viscometry, employing an Ubbelohde viscometer, with benzene and acetone as solvents for polystyrene and polyvinyl acetate respectively.

Values of K and α employed in the Staudinger equation were 1.03×10^{-4} and 0.74, respectively, for fractionated polystyrene (10), 2.62×10^{-4} and .68 for unfractionated polystyrene (11), and 1.76×10^{-4} and .68 for fractionated polyvinyl acetate (12). At a later stage a bank of five Stabin–Immergut osmometers was in operation in our laboratory (13), and where the amount of sample available was sufficient, number average molecular weights were also obtained by osmometry.

Radioassay Technique

One of the objectives of this work was to test the suitability of internal liquid scintillation counting techniques for tracer studies of this type. The scintillation counting method provides a greater inherent sensitivity, will accommodate larger samples and hence of lower specific activity, and allows energy discrimination and the concomitant reduction in background counting rate. A further important advantage in the present work is that it eliminates the necessity of sample combustion, and purification of CO_2 gas required for Geiger techniques.

The active samples of polymer were dissolved directly in 20 ml of a liquid scintillator containing 2.0% p-terphenyl and 0.04% POPOP in xylene and counted.

The counting assembly consisted of a DuMont 6292 photomultiplier, a cathode follower, linear non-overloading amplifier, a pulse height analyzer, a scaler, and a stabilized high-voltage supply, and was similar to units employed in previous work (14). The liquid scintillator cell was $1\frac{1}{2}$ inches in diameter and 2 inches high. It was surrounded by a magnesium oxide powder reflector and was fitted with a bubbling device for the removal of dissolved oxygen (15, 16) to improve its luminescent output.

RESULTS

It was first necessary to determine whether the quenching effects of added polymer would seriously affect the counting rates and thus lead to spurious results. Figure 1 shows
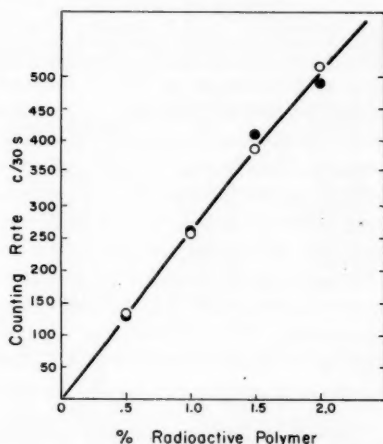

FIG. 1. Proportionality between counting rate and concentration of radioactive polymer. Solid and open circles denote duplicate experiments.

the data obtained for a tagged polystyrene sample and it can be seen that the counting rate is proportional to the amount of active polymer up to 2% concentration. It was therefore considered convenient and satisfactory to work with solutions of 1% polymer in the liquid scintillator.

The efficiency of separation of polymer from occluded initiator was tested by adding 0.2 μc of active AIBN to 0.5 g of inactive polystyrene and repeatedly precipitating the polymer from methyl ethyl ketone with methanol. For no separation one would expect 13,200 c.p.m. per 0.1500 g polymer. The counts obtained were 76 c.p.m. after one precipitation and 20 c.p.m. after two precipitations. This indicated that a double precipitation was adequate.

For the polymer samples a pulse height analyzer lower gate of 15 kev was employed and checks were made with an internal standard of C^{14} (17, 18) to detect any possible variations in counting efficiencies due to electronic drift or quenching action.

The results for unfractionated polystyrene are presented in Table I.

In order to determine whether the number of AIBN fragments incorporated in the final polymer was influenced by molecular weight, a sample of polystyrene prepared with

TABLE I

Determination of number of initiator fragments per polymer molecule in unfractionated polystyrene at 60° C

Sample No.	AIBN concentration (g/l.)	Intrinsic viscosity	Molecular weight	Weight of sample counted (g)	Counts/g min	No. of initiator fragments per polymer molecule
16	6.30	0.446	56,200	0.1718	3,749	2.02
18	4.50	0.480	64,500	0.1718	3,166	1.95
19	3.40	0.536	74,100	0.1718	2,771	1.96
20	2.70	0.585	85,100	0.1718	2,514	2.04
21	1.80	0.677	104,700	0.1718	2,165	2.14
22	0.90	0.835	141,000	0.1718	1,582	2.13
Initiator	—	—	—	—	1,274,000	—
					Average	2.04

TABLE II

Determination of number of initiator fragments per polymer molecule in fractionated polystyrene at 60° C

Sample No.	Intrinsic viscosity	Molecular weight	Weight of sample counted (g)	Counts/g min	No. of initiator fragments per polymer molecule
0	0.485	64,000	0.1720	4,884	1.97
1	0.550	109,500	0.1719	3,133	2.16
2	0.253	38,800	0.1719	7,199	1.76
1A	0.780	174,000	0.1290	2,052	2.24
1B	0.684	144,000	0.1719	2,240	2.04
1C	0.591	100,000	0.1718	2,789	1.76
1D	0.405	70,800	0.1719	3,754	1.64
Initiator	—	—	0.00045	1,953,000	—
				Average	1.94

TABLE III

Determination of number of initiator fragments per polymer molecule in fractionated vinyl acetate at 60° C

Sample No.	Intrinsic viscosity	Molecular weight	Weight of sample counted (g)	Counts/g min	No. of initiator fragments per polymer molecule
9-1	1.235	456,000	0.1639	425	1.26
10-1	1.510	602,000	0.1627	286	1.14
11-1	1.290	490,000	0.1683	350	1.14
12-1	1.370	525,000	0.1648	275	0.96
9-1-2	0.867	263,000	0.1648	575	1.00
10-1-2	1.177	426,000	0.1682	401	1.12
11-1-2	1.050	354,000	0.1645	463	1.08
12-1-2	1.046	355,000	0.0930	410	0.96
Initiator	—	—	0.00045	2,050,000	—
9-1-2-3	0.570	145,000	0.1189	1,113	0.96
10-1-2-3	0.750	214,000	0.1095	891	—
11-1-2-3	0.690	195,000	0.1241	790	1.14
Initiator	—	—	0.00045	1,850,000	0.94
				Average	1.06

active AIBN was separated into four fractions, by incremental precipitation from methyl ethyl ketone. The results are summarized in Table II, and it is evident that the results are essentially unchanged from those obtained with unfractionated material. The original sample, designated as 0, was separated into two fractions labelled 1 and 2 representing the

high and low molecular weight material, respectively, and sample 1 was fractionated into four parts labelled 1A to 1D.

The data for polyvinyl acetate polymerized at 60.0° C are presented in Table III.

DISCUSSION

The data in Tables I and II indicate that in the thermal reactions polystyrene radicals terminate by mutual combination and that the method of termination is independent of molecular weight over the range investigated. These findings are in agreement with Bevington's studies of the photopolymerized system (3), and with Bamford and Jenkins conclusions based on coupling of preformed polymer (1). Although early work (19, 20, 21) had assumed termination by combination, this cannot be construed to be the current picture, and the present results are therefore considered to extend and confirm the current views of the mechanism of termination in styrene.

In many respects the data presented here for styrene appear to be in surprisingly close agreement with the simple picture presented. It is recognized that the presence of thermal reaction, or of chain transfer to polymer or initiator, could tend to vitiate the results. After this investigation had been essentially completed it was possible to check the molecular weights of a few samples by osmometry, although the amounts of samples available were not sufficiently large for optimum conditions of osmotic measurement. Sample 16, for example, yielded a molecular weight of 61,700 by osmometry vs. 56,200 from viscosity data. The agreement is within 10% and is well within the limits necessary to discard a disproportionation mechanism in favor of one by combinaion.

The results for vinyl acetate, in Table III, indicate one initiator fragment per polymer molecule and hence the occurrence of disproportionation. Previous investigation of this system by Burnett, George, and Melville (22) indicated an unusual variation in the number of fragments from 1.6 to 6.0 per molecule at temperatures from $+27$ to $-38°$ C.

Chain transfer to polyvinyl acetate is known to occur and might be expected to affect the results. However, it should be noted that if a growing radical $IR \cdot$ were to abstract an H atom from a dead polymer molecule then $IR \cdot_m + IR_n \rightarrow IR_{(n+r)} + IR_m$ one initiator fragment per molecule would still remain and the results would be indistinguishable from those in the absence of branching if disproportionation is predominant.

A few preliminary experiments with vinyl acetate performed at 30° C showed spurious results and indicated an increase in the number of tagged fragments above a value of 3. Time did not permit an investigation of this effect in further detail as part of this work, and the few results obtained were considered tentative and were not included in the tabular presentation. A more detailed study of the variation of termination mechanism with temperature and of the determination of competitive rate constants for termination by combination and disproportionation for some systems has now begun in our laboratories.

ACKNOWLEDGMENTS

REFERENCES

1. C. H. BAMFORD and A. D. JENKINS. Nature, 176, 78 (1955).
2. I. M. KOLTHOFF, P. R. O'CONNOR, and J. L. HANSEN. J. Polymer Sci. 15, 459 (1955).
3. J. C. BEVINGTON, H. W. MELVILLE, and R. P. TAYLOR. J. Polymer Sci. 12, 449 (1954).
4. J. C. BEVINGTON, H. W. MELVILLE, and R. P. TAYLOR. J. Polymer Sci. 14, 463 (1954).

5. L. M. ARNETT and J. H. PETERSON. J. Am. Chem. Soc. **74**, 2031 (1952).
6. G. AYREY and G. G. MOORE. J. Polymer Sci. **36**, 41 (1959).
7. S. IKAMURA and T. MOTOYAMA. J. Polymer Sci. **17**, 428 (1955).
8. B. L. FUNT and E. COLLINS. J. Polymer Sci. **28**, 97 (1958).
9. F. R. MAYO and F. M. LEWIS. Ind. Eng. Chem. Anal. Ed. **17**, 134 (1945).
10. C. E. H. BAWN, R. F. J. FREEMAN, and A. R. KAMALIDDIN. Trans. Faraday Soc. **46**, 1107 (1950).
11. J. C. BEVINGTON, G. M. GUZMAN, and H. W. MELVILLE. Proc. Roy. Soc. A, **221**, 453 (1954).
12. R. N. WAGNER. J. Polymer Sci. **2**, 21 (1947).
13. B. L. FUNT and F. D. WILLIAMS. J. Polymer Sci. In press.
14. B. L. FUNT and A. HETHERINGTON. Internat. J. Appl. Radiation and Isotopes, **4**, 189 (1959).
15. R. W. PRINGLE, D. BLACK, B. L. FUNT, and S. SOBERING. Phys. Rev. **92**, 1582 (1953).
16. B. L. FUNT and E. NEPARKO. J. Phys. Chem. **60**, 267 (1956).
17. F. N. HAYES. Internat. J. Appl. Radiation and Isotopes, **1**, 46 (1956).
18. J. D. DAVIDSON and P. FEIGELSON. Internat. J. Appl. Radiation and Isotopes, **2**, 1 (1957).
19. C. H. BAMFORD and M. J. S. DEWAR. Proc. Roy. Soc. A, **192**, 308 (1948).
20. H. W. MELVILLE and L. VALENTINE. Trans. Faraday Soc. **46**, 210 (1950).
21. G. M. BURNETT. Trans. Faraday Soc. **46**, 772 (1950).
22. G. M. BURNETT, M. M. GEORGE, and H. W. MELVILLE. J. Polymer Sci. **16**, 31 (1955).

THE SEPARATION OF SOME INORGANIC IONS BY HIGH-VOLTAGE ELECTROMIGRATION IN PAPER[1]

R. A. Bailey[2,3] and L. Yaffe

ABSTRACT

A number of inorganic ions have been separated by high-voltage electromigration in paper. The systems considered include some of particular radiochemical interest, such as Sr–Y, Ba–La, Mo–Tc, Pb–Bi–Po, as well as the alkali metals, some elements of the first long period, and other metals. Background electrolytes were usually solutions of complex-forming organic acids.

INTRODUCTION

Numerous references to the separation of inorganic ions by electromigration in paper (paper electrophoresis) have appeared over the last 10 years. The present work deals with a number of separations which were performed while making a general study of the method with a view to applying it to routine radiochemical separations. As such, it deals with a fairly large number of systems, and is a preliminary survey. It does not consider in detail the effects of varying such factors as the concentration and pH of the background electrolyte solution, which would be necessary if the optimum conditions for any separation were to be determined. Nevertheless, some striking results were obtained even with this rather arbitrary choice of conditions, illustrating the power of the method. The technique of electromigration has some specialized advantages. However, as a general method of separating small amounts of inorganic material, it can compete with other means, such as ion exchange, only on the basis of speed. Therefore a very high voltage technique was adopted, and solutions of low conductivity were used. This has permitted a number of separations to be made in 10 minutes or less.

Many of the ions studied are of adjacent atomic number, since these are often of chief interest radiochemically.

EXPERIMENTAL

The technique used was basically the same as that employed for quantitative measurements of zone mobility (1). An apparatus capable of withstanding much higher voltages was used, however, and for these qualitative results much less attention was paid to details which are important for zone mobility determinations.

A closed strip technique was used wherein the paper was placed between two cooling plates. These were of aluminum, $40 \times 10 \times 1/4$ in. in size. Copper tubing was bolted to the backs of both plates to allow the circulation of cooling water. Electrical insulation was provided by a strip of mica 4 in. wide running the length of each plate. This was extended to the edges of the plates at the high-voltage end to prevent arcing from the paper. Mica combines a higher electrical breakdown potential with a greater heat conductivity than most other practical materials. The strip was built up as a lamination of thin sheets 4×4 in. in size glued together; the thickness was 0.016 in. at the high-voltage end but somewhat less over most of its length. This insulation proved to be quite suitable. It could withstand a potential of 10,000 volts, and it had the additional advantage that, if the paper did char, the mica was not damaged. The mica was protected by a thin sheet of polyethylene or polyvinylchloride which could be replaced readily.

In order to obtain the good contact between the paper and the cooling surface, which is necessary at high voltages, about 140 lb of lead weights was placed on the upper plate.

No electrolyte reservoirs were employed. The electrodes were of platinum foil and were in direct contact with the ends of the paper strip. They could be placed at any distance from the ends of the plates to give any desired migration distance up to the full length of the plates. Electrical connections were made to them by means of aluminum or copper ribbons. Products of electrolysis were trapped by means of suitable buffer solutions.

A d-c. power supply giving a continuously variable, well-filtered output of up to 10 kv was used as a source of voltage.

A number of the ions studied were radioactive; such substances are easily detected and identified. They were located after separation by means of a Geiger counter for β-radiation, or a scintillation counter for γ-rays. The strip was either cut into sections, 1 cm broad, or measured intact with a scanning device. The latter is much less tedious, but it is not as sensitive toward very low levels of radioactivity such as may be found if a zone 'trails'. Alpha particles were detected by a 2π-proportional counter operated at its α-plateau voltage. In all cases the identity of the various zones was confirmed by means of the γ-ray spectra of the migrants, or by their relative rates of decay.

Many experiments were carried out with inactive migrants when radioactive nuclides were not available and when simple chemical tests could be used. Such tests may fail to show low-concentration regions, but they are satisfactory in most cases, and are fast and simple. The reagents used were rubeanic acid – NH_3 for Co(II) and Ni(II); NH_4SCN for Fe(III); alizarin–NH_3 for Al(III), Ga(III), and In(III); and dithizone for the remainder of the inactive ions.

The concentration of the inactive solutions was 0.01 M or less, while the radioactive solutions were much more dilute. Most ions were in solution as the nitrate, sometimes with a slight excess of nitric acid, but with other substances capable of forming stable complexes absent. Ten microliters of each migrant solution was normally used.

A number of temperatures were employed in this work. The comparatively low temperatures, which many workers have used to achieve adequate cooling, were found to be unnecessary with our apparatus; the best operation was obtained at 35–40° C. Since higher temperatures lead to higher zone mobilities, they may result in more rapid separations.

RESULTS AND DISCUSSIONS

The separations made with inactive materials are shown as reproductions of a tracing of the strip; those with radioactive substances are shown as histograms. The heavy vertical line in the former indicates the starting position. The relative heights of the peaks on the histograms are not significant since the detection efficiency varies for the different nuclides. The conditions of each separation are indicated in the figure captions. Except where indicated otherwise, Whatman No. 3MM chromatography paper was used, and the absorbance used was about 1.1 ml/g.

The first series of separations are of the following groups of cations in several organic acid background electrolytes:

(a)   Fe(III), Co(II), Ni(II), Cu(II), Zn(II), Ga(III);

(b)   Ag(I), Cd(II), In(III);

(c)   Hg(II), Tl(I), Pb(II), Bi(III);

(d)   Zn(II), Cd(II), Hg(II);

(e)   Al(III), Ga(III), In(III).

Oxalic acid gave the best results in most cases, but citric, tartaric, and lactic acids were investigated as well. The latter two gave superior separations of aluminum, gallium, and indium. Complex formation occurs in most of these systems, although often it is not strong enough to cause the migrant to behave as an anion. Table I gives the migration sequences in the systems used. Figures 1 to 3 illustrate some of the separations achieved.
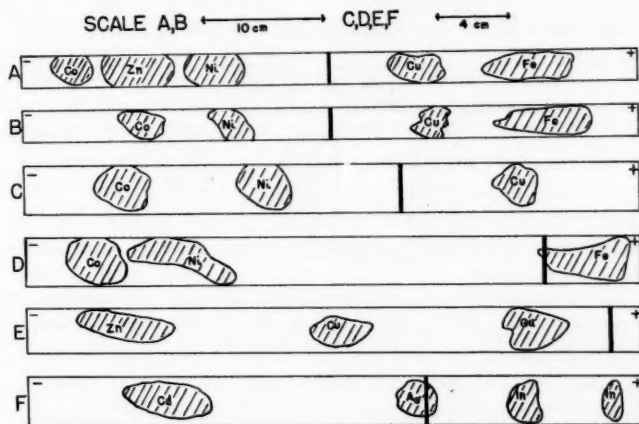

Fig. 1. (A) Separation of Fe(III), Co(II), Ni(II), Cu(II), and Zn(II) in 0.01 M oxalic acid; 60 v/cm, 55 minutes, 39° C.

(B) Separation of Fe(III), Co(II), Ni(II), and Cu(II) in 0.01 M oxalic acid; 150 v/cm, 15 minutes, 35° C.

(C) Separation of Co(II), Ni(II), and Cu(II) in 0.01 M oxalic acid; 160 v/cm, 10 minutes, 35° C.

(D) Separation of Co(II), Ni(II), and Fe(III) in 0.015 M citric acid; 160 v/cm, 10 minutes, 39° C.

(E) Separation of Zn(II), Cu(II), and Ga(III) in 0.1 M tartaric acid; 80 v/cm, 28 minutes, 25° C.

(F) Separation of Ag(I), Cd(II), and In(III) in 0.01 M oxalic acid; 120 v/cm, 9 minutes, 39° C.
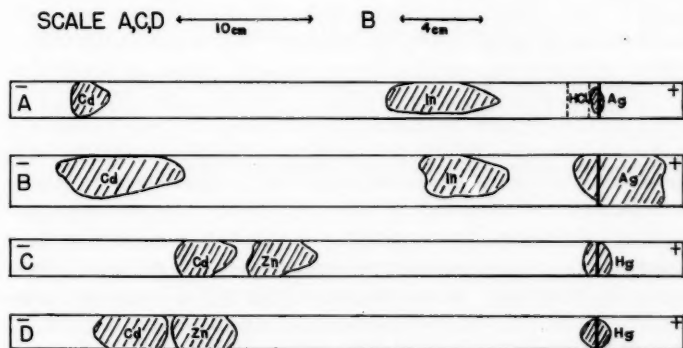

Fig. 2. (A) Separation of Ag(I), Cd(II), and In(III), utilizing a zone of HCl to prevent streaking of silver; 0.1 M lactic acid, 80 v/cm, 31 minutes, 35° C.

(B) Separation of Ag(I), Cd(II), and In(III) with KCN added to the migrant solution before application; 0.1 M tartaric acid, 80 v/cm, 24 minutes, 35° C.

(C) Separation of Zn(II), Cd(II), and Hg(II) in 0.1 M tartaric acid; 80 v/cm, 29 minutes, 25° C.

(D) Separation of Zn(II), Cd(II), and Hg(II) in 0.1 M lactic acid; 80 v/cm, 29 minutes, 25° C.
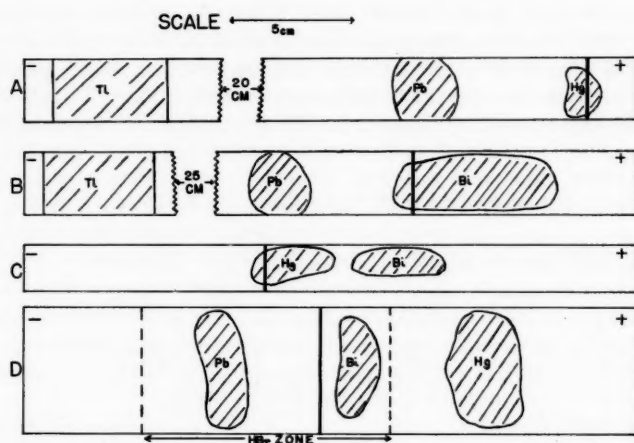
SCALE ⟵ 5cm ⟶

FIG. 3. (A) Separation of Hg(II), Tl(I), and Pb(II) in 0.01 M oxalic acid; 200 v/cm, 7 minutes, 41° C.
(B) Separation of Tl(I), Pb(II), and Bi(III) in 0.01 M oxalic acid; 200 v/cm, 6 minutes, 41° C.
(C) Separation of Hg(II) and Bi(III) in Reeve Angel 934 AH glass fiber paper with 0.1 M tartaric acid; 24 v/cm, 43 minutes, 25° C.
(D) Separation of Hg(II), Pb(II), and Bi(III) using a zone of 0.1 M HBr in a strip moistened with 0.01 M oxalic acid; nominal voltage gradient 80 v/cm, 30 minutes, 39° C. Tl(I) was separated in the same experiment, but is not shown; it has moved far toward the negative electrode.

TABLE I

Migration sequences of a number of ions in several electrolyte solutions

Acetic acid of concentration 1–2 M
 Tl(I), Co(II), Ni(II), Zn(II), Ga(III), Cd(II), Pb(II), Cu(II), In(III), Fe(III):

0.01 M oxalic acid
 Tl(I), Cd(II), Co(II), Zn(II), Ni(II), Pb(II): In(III), Cu(II), Al(III), [Ga(III)+Fe(III)], In(III)

0.015 M citric acid
 Tl(I), Cd(II), Co(II), [Ni(II)+Zn(II)] [Pb(II)+Cu(II)]: Fe(III), [Al(III)+In(III)], Ga(III)

0.1 M tartaric acid
 Tl(I), Cd(II), [Co(II)+Zn(II)], Ni(II), Pb(II), Cu(II), Al(III), In(III), Ga(III): Fe(III)

0.1 M lactic acid
 Tl(I), Cd(II), [Co(II)+Zn(II)], Ni(II), Pb(II), Cu(II), Al(III), [Fe(III)+Ga(III)]:

 In addition, Ag(I), Hg(II), and Bi(III) are adsorbed by the paper and are found near the starting position in these electrolytes.

NOTE: Ions in parentheses have similar mobilities; the relative rates were not determined.
The starting point is indicated by the symbol :. Ions to the left of this move as cations, those to the right as anions.

No difficulty was encountered in separating most of these ions in at least one of the electrolytes used. Ternary mixtures could be resolved very rapidly. Only systems involving silver, or mercury and bismuth, gave difficulty. These ions are strongly adsorbed by the paper and either will not move from the starting position, or trail back to it. In the case of silver, this may be the result of a reduction of small amounts of the silver by certain groups in the paper. In 0.01 M oxalic acid, indium formed two anionic zones, indicating that two complex species are formed which are not in rapid exchange with one another. This does not interfere with separations. The results can also indicate the relative tendency

of complex formation of some of the ions. Thus, zinc seems to form stronger complexes than cadmium, and gallium stronger complexes than aluminum or indium, in the solutions used here.

Silver, when present in small enough amounts, remains at the starting position except when complexed strongly, as with ammonia. As the amount of silver present is increased, it tends to move toward the cathode, but leaves a low-concentration trail back to the starting point. The latter was detectable when radioactive Ag^{110} was used. Although in the separation of silver, cadmium, and indium no difficulty is encountered if a very small amount of silver is present (Fig. 1F), the extended zone formed with a larger quantity may overlap the zones of the other ions, since the mobility of the moving silver is high. In order to achieve a satisfactory separation in the latter case, some means of retaining all of the silver near the starting position is required.

By adding hydrochloric acid to a narrow zone on the cathode side of the starting position, all of the silver is precipitated or adsorbed between this zone and the initial position. If the hydrochloric acid is sufficiently dilute that complex formation with the other ions is slight, these ions pass through this zone with little interference (although the indium zone does tend to become elongated). A second procedure consists of adding a little potassium cyanide to the migrant solution before application to the paper. The $Ag(CN)^-$ ion is sufficiently stable to prevent any cationic motion of the silver. Separations utilizing these techniques are illustrated in Figs. 2A and 2B respectively.

Since both Hg(II) and Bi(III) remain near the starting position, they cannot be separated from one another in the electrolytes used here with ordinary filter paper. That the failure to move is due to interaction with the cellulose is shown by the results in 0.1 M tartaric acid in glass fiber filter paper (Fig. 3C). Both ions are anionic here, and they are separated. In the same electrolyte with cellulose paper, bismuth forms a streak toward the anode but does not leave the starting point entirely, while the mercuric ion moves scarcely at all. Glass paper may also yield a separation of lead from mercury and bismuth, but the fourth member of this group, thallium, is adsorbed and trails, hence overlapping the lead zone. Separation of all four ions in cellulose paper can be brought about by utilizing the bromide complexes, which were studied for mercury, lead, and bismuth by Pucar (2). A small zone of 0.1 M hydrogen bromide serves to separate these ions (Fig. 3D). The part of the strip moistened with another electrolyte (oxalic acid in this case) serves for the migration of any ion which leaves the hydrogen bromide zone without involving the high conductance of a strip completely moistened with hydrogen bromide. Tl(I) is a much faster cation than the rest and is readily separated from them.

A number of ions considered above were also studied in lactic acid by Sato et al. (3).

The behavior of Cr(III), Mn(II), Fe(III), and Co(II) in the strong chelating agents ethylenediaminetetraacetic acid (EDTA), nitrilotriacetic acid (NTA), hydroxyethylethylenediaminetriacetic acid (HEDTA), and 1,2-diaminocyclohexanetetraacetic acid (DCTA) was investigated and a number of separations accomplished. Examples are shown in Fig. 4. Further data on the electromigration in these systems are given in Table II. The anionic complexes formed are slow and hence do not lend themselves to rapid separations. Diffuse and multiple zones were also encountered.

Separation of the alkali metals was also attempted. Potassium, rubidium, and cesium have very similar mobilities, and could not be completely separated under the conditions employed. Sodium was readily separated from the rest. Other workers have obtained similar results (4, 5, 6). Only Gross (7) has reported a separation of potassium, rubidium,
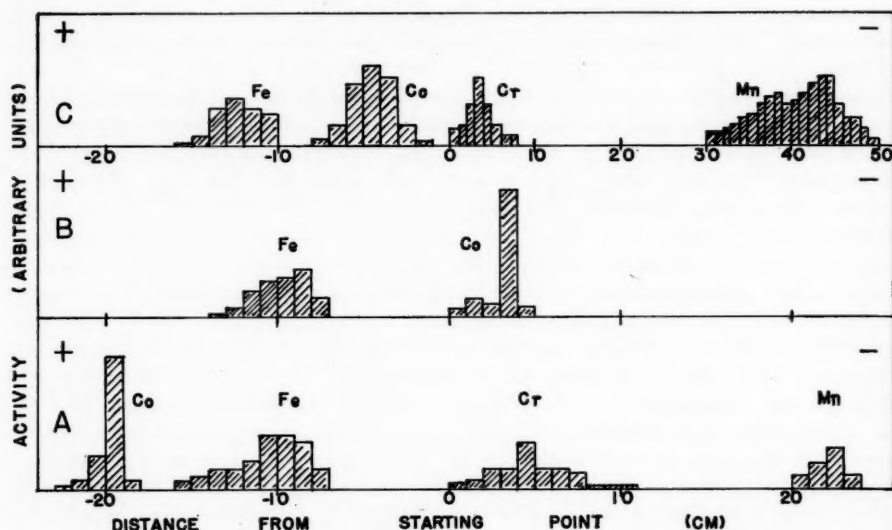
FIG. 4. (A) Separation of Cr(III), Mn(II), Fe(III), and Co(II) in 0.01 M HEDTA – 0.06 M NH$_4$OH; 80 v/cm, 114 minutes, 25° C.

(B) Separation of Fe(III) and Co(II) in a saturated solution of NTA in water; 70 v/cm, 140 minutes, 25° C.

(C) Separation of Cr(III), Mn(II), Fe(III), and Co(II) in 0.01 M NTA – 0.06 M NH$_4$OH; 75 v/cm, 116 minutes, 25° C.

TABLE II

Migration sequences of Cr(III), Mn(II), Fe(III), and Co(II) in some complexone electrolyte solutions

Complexone solution	Migration sequence	Remarks
Saturated EDTA in H$_2$O	Mn : (Cr+Co), Fe	Co, Cr have same mobility
Saturated NTA in H$_2$O	Mn, Cr, Co : Fe	Mn, Cr not complexed; Co near start
0.01 M HEDTA in H$_2$O	Mn, Cr : Fe, Co	Mn, Cr not complexed; Fe zone diffuse about start
0.01 M EDTA in 0.06 M NH$_4$OH	Cr : Mn, (Fe+Co)	
0.01 M NTA in 0.06 M NH$_4$OH	Mn, Cr : Co, Fe	
0.01 M HEDTA in 0.06 M NH$_4$OH	Mn, Cr : Fe, Co	Cr zone diffuse
0.01 M DCTA in 0.06 M NH$_4$OH	: Mn, (Cr+Fe+Co)	Cr zone diffuse; Fe, Co of same mobility
0.01 M EDTA in 1.2 M NH$_4$OH	: Cr, (Mn+Fe), Co	
0.01 M NTA in 1.2 M NH$_4$OH	: Cr, (Co+Mn+Fe)	
0.01 M HEDTA in 1.2 M NH$_4$OH	Cr : Co, Cr, (Mn+Fe)	Cr forms two zones; Mn zone diffuse
0.01 M DCTA in 1.2 M NH$_4$OH	: (Cr+Fe), Co, Cr, Mn	Cr forms two zones; one remains at start and overlaps Fe
0.03 M EDTA in 0.1 M NH$_4$OH	: Mn, Cr, Fe, Co	Cr zone diffuse, tends to overlap Mn
0.03 M NTA in 0.1 M NH$_4$OH	Mn : (Cr+Co), Fe	Cr, Co zones diffuse; Cr tends to spread on both sides of start
0.04 M EDTA in 0.1 M NH$_4$OH	: Mn, (Cr+Fe), Co	Cr tends to be diffuse

NOTE: Parentheses indicate the enclosed ions have very similar mobilities.
The starting point is represented by the symbol : . Ions to the left of this move as cations, those to the right as anions.

and cesium. Figure 5 shows typical results obtained. Alkali metal ions are readily separated from others in strong complexing agents. Figure 6 shows some separations of alkali metals and other univalent cations in NH$_4$OH–EDTA solutions. Silver forms multiple zones in this electrolyte, probably because of competition between the EDTA and the ammonia in forming complexes.
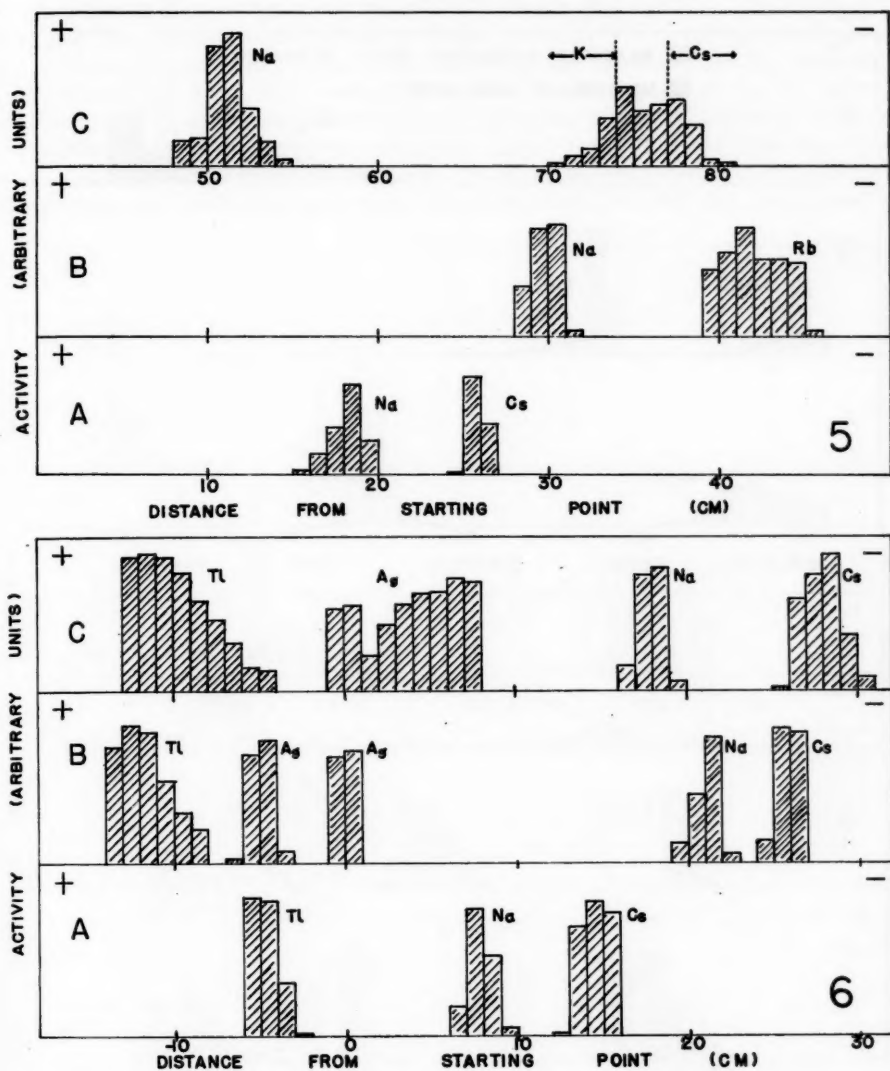
Fig. 5. (A) Separation of Na$^+$ and Cs$^+$ in 2.36 M acetic acid; 35 v/cm, 50 minutes, 25° C.

(B) Separation of Na$^+$ and Rb$^+$ in 1.18 M acetic acid; 80 v/cm, 28 minutes, 25° C.

(C) Separation of Na$^+$, K$^+$, and Cs$^+$ in 0.15% ammonium acetate solution; 60 v/cm, 63 minutes, 25° C.

Fig. 6. Separation of some univalent cations.

(A) Na$^+$, Cs$^+$, and Tl$^+$ in 0.01 M EDTA – 6.1 M NH$_4$OH; 20 v/cm, 27 minutes, 25° C. Whatman No. 52 paper.

(B) Na$^+$, Cs$^+$, Tl$^+$, and Ag$^+$ in 0.1 M EDTA – 1.2 M NH$_4$OH; 50 v/cm, 24 minutes, 25° C. Whatman No. 52 paper.

(C) Na$^+$, Cs$^+$, Tl$^+$, and Ag$^+$ in 0.01 M EDTA – 6.1 M NH$_4$OH; 50 v/cm, 38 minutes, 25° C. Whatman No. 52 paper.
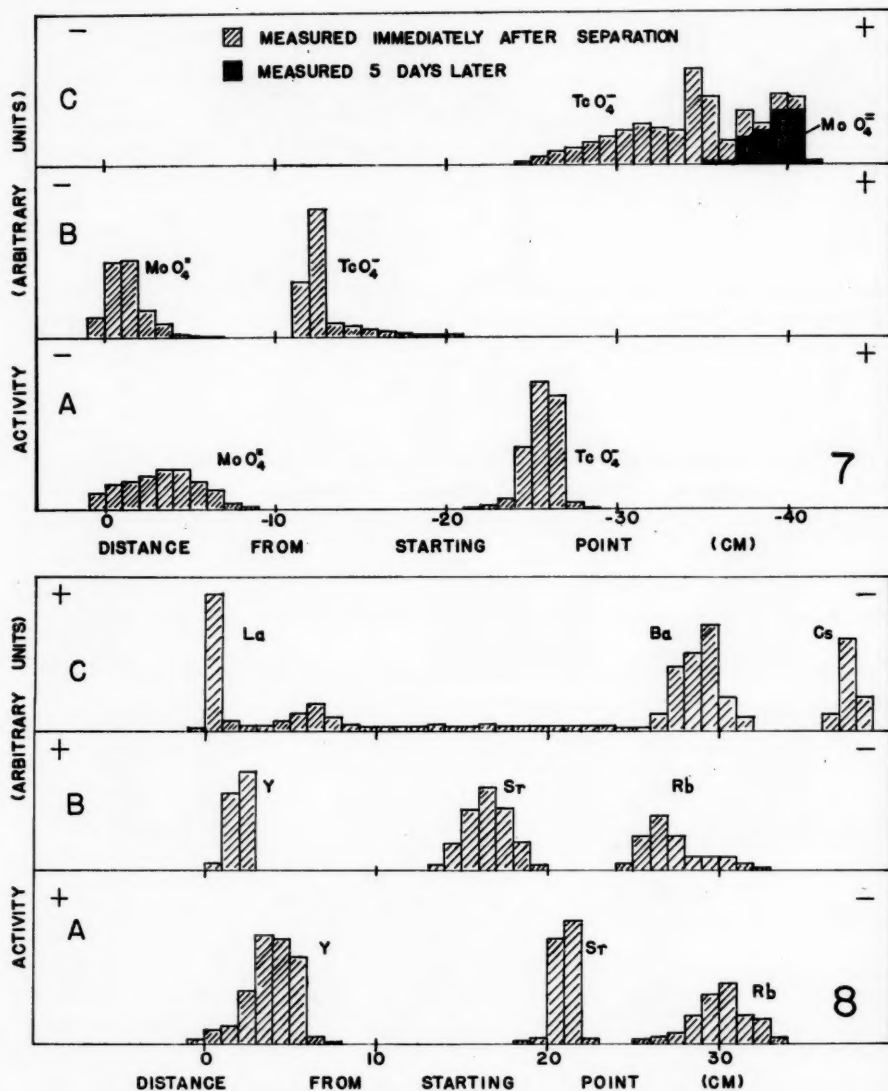
Fig. 7. Separation of molybdenum and technetium as the molybdate and pertechnate ions.
    (A) In 0.15% ammonium acetate solution; 60 v/cm, 55 minutes, 30° C.
    (B) In 1.18 M acetic acid; 100 v/cm, 25 minutes, 30° C.
    (C) In 1.2 M NH₄OH; 80 v/cm, 45 minutes, 30° C.

Fig. 8. (A) Separation of Rb, Sr, and Y in 1.18 M acetic acid; 120 v/cm, 8 minutes, 35° C.
       (B) Separation of Rb, Sr, and Y in 0.015 M citric acid; 180 v/cm, 5 minutes, 35° C.
       (C) Separation of Cs, Ba, and La in 1% citric acid; 160 v/cm, 8 minutes, 33° C.

Separation of the molybdate and pertechnate ions are shown in Fig. 7. The former, as Mo^{99}, was obtained as a product of nuclear fission, while Tc^{99m} is its radioactive daughter, and is present in 'carrier-free' form. In non-basic solution, the MoO_4^- ion may be precipitated as molybdic acid, which probably accounts for its occurrence near the starting position in ammonium acetate and acetic acid solutions. Figure 7C shows its migration in NH_4OH, where no precipitation takes place. MoO_4^- is slightly faster than TcO_4^- but, even after a movement of 40 cm, they are not completely separated. The cross-hatched region, measured immediately after separation, includes both molybdenum and technetium

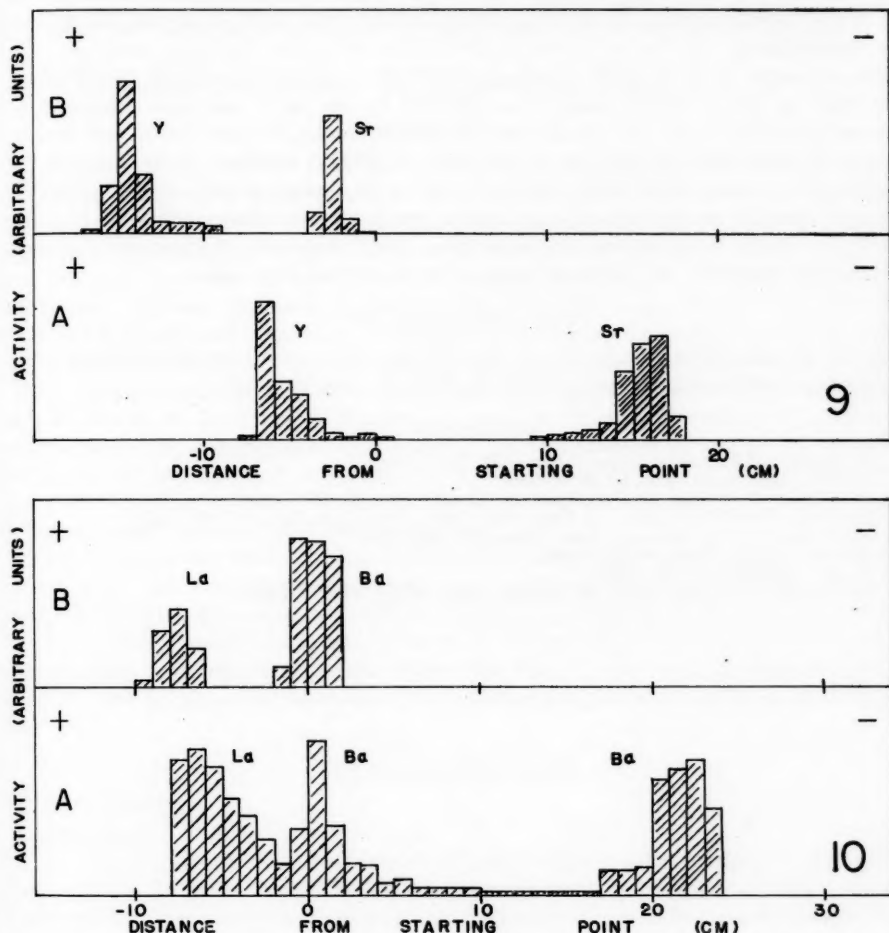FIG. 9. Separation of Sr and Y in EDTA background electrolytes.
  (A) A saturated solution of EDTA in water; 120 v/cm, 8.5 minutes, 30° C.
  (B) 0.01 EDTA – 1.2 M NH₄OH; 75 v/cm, 35 minutes, 30° C.

FIG. 10. Separation of Ba and La in EDTA background electrolytes.
  (A) A saturated solution of EDTA in water; 180 v/cm, 9 minutes, 33° C.
  (B) 0.01 M EDTA – 1.2 M NH₄OH; 80 v/cm, 37 minutes, 33° C.

activities, while the blackened region, measured 5 days later, includes none of the technetium present initially, since the half-life of Tc^{99m} is only 6 hours. Tc^{99} was not detected.

Separations of rubidium, strontium, and yttrium in acetic and citric acids are shown in Figs. 8A and 8B. Similar separations of cesium, barium, lanthanum were attempted, but barium invariably exhibited a trail back to the starting point when it moved as a cation (Fig. 8C). The cause of this is not known, but it may be due to precipitation of small amounts of barium by traces of sulphate in the paper. Further separations of strontium and yttrium, and of barium and lanthanum, in EDTA solutions, are shown in Figs. 9 and 10 respectively. In all of these experiments, the yttrium and the lanthanum were 'carrier-free'.

The separation of RaD, RaE, and RaF (Pb^{210}, Bi^{210}, and Po^{210}) was also investigated. Both bismuth and polonium tend to be adsorbed by the paper and trail. RaD can be separated from the other two in oxalic, citric, tartaric, lactic, or acetic acids, and separation of RaF from the rest may be accomplished in EDTA solution. In this, and in the other chelating agents used, RaD and RaE move with similar mobilities, so that it was not found possible to separate all three ions in one run under these conditions.

Sato *et al.* (3, 8) have reported the separation of lead, bismuth, and polonium in lactic acid, but the bismuth and polonium zones seem to overlap here also.

ACKNOWLEDGMENT

REFERENCES

1. R. A. BAILEY and L. YAFFE. Can. J. Chem. **37**, 1527 (1959).
2. Z. PUCAR. Anal. Chim. Acta, **18**, 290 (1958).
3. T. R. SATO, W. P. NORRIS, and H. H. STRAIN. Anal. Chem. **26**, 267 (1954).
4. S. HARASAWA and T. SAKAMOTO. J. Chem. Soc. Japan, Pure Chem. Sect. **74**, 862 (1953).
5. G. H. EVANS and H. H. STRAIN. Anal. Chem. **28**, 1560 (1956).
6. O. SCHIER. Angew. Chem. **68**, 63 (1956).
7. D. GROSS. Nature, **180**, 596 (1957).
8. T. R. SATO, W. P. NORRIS, and H. H. STRAIN. Anal. Chem. **27**, 521 (1955).

RELAXATION OF SURFACE PRESSURE AND COLLAPSE OF UNIMOLECULAR FILMS OF STEARIC ACID[1]

W. Rabinovitch, R. F. Robertson, and S. G. Mason

ABSTRACT

A study has been made of the time variations of $\pi-A$ isotherms of stearic acid films at air/water interfaces using an automatic recording surface balance of the vertical pull type. The existence of coherent films below molecular areas of 22 sq. Å/molecule has been found to be dependent on the temperature, rate of compression, and the history of compression of a given film. The behavior at or near collapse, the decrease in π with time after sudden compression (relaxation), and the increase in π with time after sudden expansion (recovery) have been studied.

The results have been interpreted on the basis of structural changes in the monolayer.

INTRODUCTION

Although extensive studies have been made on the pressure–area $(\pi-A)$ isotherms of simple long-chain fatty acids spread as unimolecular films at the air/water interface, little attention has been given to the possible time-dependency of these mechanical properties. By analogy with three-dimensional viscoelastic systems, it is not surprising that the $\pi-A$ isotherms of two-dimensional systems should be time-dependent. This dependency has been observed experimentally under conditions of slow manual compression for stearic and other fatty acid films (1, 2, 3) and with automatic compression and surface pressure recording techniques for films of palmitic (4) and stearic (5, 6) acids.

The collapse of stearic acid films may occur with compression to 19 sq. Å/molecule surface area (5, 6, 7) or before this area is attained (1). In more definitive studies of collapse Muller (8) has suggested that a stearic acid film collapses by a stepwise wrinkling leading to the formation of numerous strata. Kimball and Ries (9) have reported the appearance of long wrinkles two molecules deep (100 Å) in electron micrographs of collapsed hexatricontanoic acid monolayers.

In the present study the $\pi-A$ – time relations of stearic acid films have been investigated up to and beyond the collapse region in an attempt to elucidate the molecular processes associated with the formation and collapse of unimolecular films. Studies have been made of: (a) the effect of compression rate on the $\pi-A$ isotherm, (b) the variation of π with time after repeated compressions and expansions of the film at molecular areas between 19 and 24 sq. Å, and (c) the effect of repeated compressions on the $\pi-A$ isotherm of the same film.

EXPERIMENTAL PART

The Film Balance

Description

The surface pressure measurements were made with an automatically recording film balance of the Wilhelmy type. The balance incorporated a null-balance feature activated by the electronic servo-mechanism of Mauer (10) applied to a chainomatic balance. This surface balance was found to be capable of rapid and precise response to increasing or decreasing surface pressure.

A Wilhelmy dipping plate is suspended by a nichrome wire from the bottom of the left-hand pan of a chainomatic balance. A galvanometer mirror attached at the fulcrum of the balance beam reflects a light beam from a source onto the separate twin cathodes of a phototube in a bridge circuit. The phototube senses the magnitude and direction of minute displacements of the balance arm from a given equilibrium position and translates the displacements into a proportional electrical voltage of corresponding polarity. By applying this voltage to the input of a direct-coupled amplifier an output current of corresponding magnitude and phase is obtained. This current is led through a solenoid whose field exerts a force on a magnet concentric with the solenoid and suspended from the right-hand pan connection of the chainomatic balance. The magnet is so oriented in the solenoid that the polarity opposes the displacement of the balance beam from equilibrium. When a vertical force is applied to the balance pan the system can be maintained continuously in equilibrium by this instantaneous self-balancing action. The balancing current was passed through a decade resistance and the resulting voltage was recorded by a multiple-span strip chart recorder (Minneapolis-Honeywell-Brown, Extended Range, Type 153).

Calibration

A clean dipping plate suspended from the nichrome wire was allowed to dip into a clean substrate surface and the initial zero reading of the balance was obtained after taring. A calibrating weight was placed on the balance pan and the positive deflection of the recorder was adjusted to full scale by the decade resistance. Normally the calibrating weight was chosen to give $\pi = 25$ or 50 dynes/cm for the full 10 in. chart width; however, the multiple-span feature of the recorder made it possible to extend the range to 50 inches when desired.

Characteristics of the Surface Balance

The surface balance response was highly stable over long periods of time (10 hours) and was linear within 0.1% for loads from 0 to 300 mg. Beyond 300 mg the instrument was not self-balancing with the size of magnet ($1/4 \times 3$ in.) employed. The response time of the balance to rapidly changing surface pressure was limited by the response time (4.5 seconds) of the recorder pen for full-scale deflection.

With the conventional Wilhelmy surface balance in which the depth of immersion is changed by manipulation, measurement of decreasing values of π becomes uncertain since the downward movement of the dipping plate into the substrate may cause the contact angle to deviate from zero (11, 12). Since, however, vertical movement is negligible ($< 10^{-2}$ cm) in this balance it was possible to measure both increasing and decreasing π to within ± 0.1 dynes/cm.

The Trough Assembly

A description of the air thermostat and barriers employed can be found in earlier publications (13, 14). The film area could be varied by stepwise manual compression or by a motor-driven barrier-moving device which provided either a fixed trough traverse time of 10 seconds or a variable traverse time of from 10 minutes to several hours.

Materials

The stearic acid (m.p. 69° C) used in these experiments was obtained from the Defence Research Chemical Laboratories, Ottawa, Canada. A stock solution of 0.00418 M stearic acid was prepared in benzene and used in all experiments. At the standard initial area of 880.9 sq. cm, 0.1 ml of this solution formed a film at 35 sq. Å/molecule initial area. All substrates were 0.01 N HCl aqueous solution.

Experimental Techniques

The dipping plate and teflon-coated trough and barriers were cleaned with chromic acid and rinsed with copious quantities of distilled water. After the trough and barriers were placed in the thermostat, the substrate solution was added, the dipping plate installed, and the balance brought to its equilibrium zero position. The surface was then checked for contamination by advancing the barrier from its initial position to one corresponding to an area 1/4 to 1/8th of the initial area. An increase in pressure of less than 0.25 dyne/cm during this compression was taken as the criterion of a clean surface. The system was left for several hours for temperature equilibration with the barrier at its initial position and then checked for surface contamination again before a film was spread.

RESULTS

Effect of Compression Rate on the π–A Isotherms

The pressure–area (π–A) isotherms were obtained on 0.01 N HCl substrates at 25° C over a range of compression rates from 0.04 to 2.43 sq. Å/molecule per minute. The results for three freshly spread monolayers are given in Fig. 1. Curve 1 of this figure is the
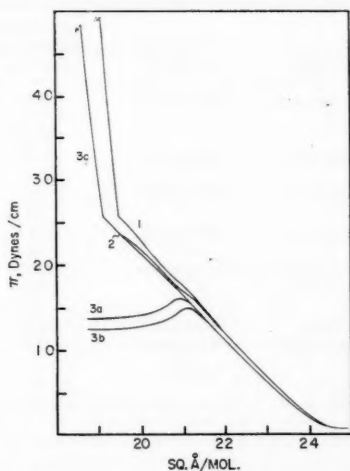

Fig. 1. Isotherms (25° C) of stearic acid monolayers determined at the following continuous compression rates in sq. Å per molecule/minute: 2.43 (curve 1), 0.213 (curve 2), 2.43 after a 7-hour rest period (curve 3). Curves 3a and 3b were obtained by slow manual stepwise compression as explained in the text, and 3c by recompression at 2.43 sq. Å/molecule per minute after expansion and resting for 7 hours at 35 sq. Å/molecule.

isotherm obtained from a film initially at a molecular area of 35 sq. Å under continuous compression at a rate of 2.43 sq. Å/molecule per minute and curve 2 is the isotherm of a similar film compressed at the rate of 0.213 sq. Å/molecule per minute. The isotherms represented by curves 3a and 3b were obtained by 30 stepwise compressions, each of 0.2 sq. Å/molecule, in the range 25 to 19 sq. Å/molecule of the surface area. The film initially at 35 sq. Å/molecule was compressed rapidly to 25 sq. Å/molecule and then by steps with 5 minutes between each compression. The surface pressure was noted immediately after each compression and immediately before the next. Curves 3a and 3b are the isotherms obtained on plotting these two values of the surface pressure. After the slow stepwise

compression the film was rapidly expanded to 35 sq. Å/molecule, left for 7 hours, and then recompressed continuously at a rate of 2.43 sq. Å/molecule per minute to obtain curve 3c. The significance of these observations is discussed later.

Surface Pressure Relaxation and Recovery

A study was made of the variation with time of the surface pressure at constant area after sudden compression and expansion. Adopting the customary nomenclature, the decrease in π with time after rapid compression is called pressure relaxation, and the increase in π with time after rapid expansion is called recovery.

All experiments were made at 25° C with the film at an initial area of 35 sq. Å/molecule. This monolayer was rapidly compressed or expanded between molecular areas of 24 and 21 sq. Å, and the pressure recorded as a function of time t at each intermediate area. The details of the experimental operations for one typical film are given in Table I and the results are given as plots of π vs. t in Figs. 2 (A, B, C, D), 3, and 4.

TABLE I

Stepwise compression and expansion of stearic acid film

| | Sq. Å/molecule | | | | Duration of | | |
Step	Initial	Final	Operation	Process studied	observation (minutes)	Figure	Curve
1	35	24	Compression	Relaxation	15	2A	1
2	24	23	"	"	12	2B	2
3	23	22	"	"	11	2C	3
4	22	23	Expansion	Recovery	11	2B	4
5	23	24	"	"	10	2A	5
6	24	23	Compression	Relaxation	10	2B	6
7	23	22	"	"	10	2C	7
8	22	23	Expansion	Recovery	11	2B	8
9	23	24	"	"	10	2A	9
10	24	23	Compression	Relaxation	10	2B	10
11	23	22	"	"	10	2C	11
12	22	21	"	"	13	2D	12(a)
13	21	21	None	Relaxation	120	3	12(b)
14	21	22	Expansion	Recovery	53	4	13
15	22	23	"	"	19	4	14
16	23	24	"	"	10	2A	15
					Total time = 335		

NOTE: Initial area = 35 sq. Å/molecule. Initial π = 0.17 dynes/cm. Temperature = 25° C.

At areas of 24, 23, and 22 sq. Å/molecule the pressure relaxation is shown in Figs. 2 and 3 to be 0.13 dyne/cm in 10 minutes. At 21 sq. Å/molecule, however, the relaxation is 1.7 dynes/cm in 10 minutes (a 10-fold increase) and after 2 hours the pressure has decayed by about 5 dynes/cm. On subsequent expansion the pressure recovery is of the same order as the relaxation (Fig. 4). The curves obtained for both the relaxation and recovery seem to indicate that these two phenomena reflect properties of the monolayer and are not the result of slow solution and diffusion of film molecules into the substrate.

Surface Pressure Relaxation at 19 sq. Å/molecule

At a compression rate of 2.43 sq. Å/molecule per minute the monolayer attained a surface pressure before collapse in excess of 45 dynes/cm at a molecular area of about 19.5 sq. Å (Fig. 1, curve 1). Other workers (5–7) have reported maximum surface pressures from 55 to 62 dynes/cm at molecular areas near 18.5 sq. Å for stearic acid films compressed
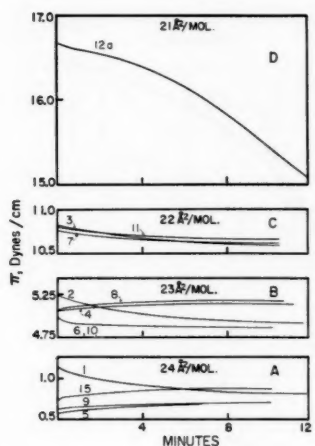
FIG. 2. Relaxation and recovery curve over 10 to 12 minutes. See Table I for details of curves.
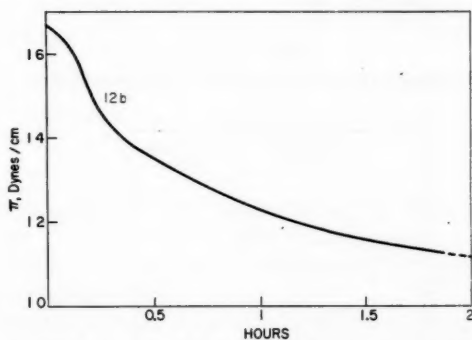

FIG. 3. Relaxation curve over a 2-hour period at 21 sq. Å/molecule (see Table I).

at rates in excess of 3 sq. Å/molecule per minute. To examine pressure relaxation at the pressure maximum obtained on rapid compression, a film initially at an area of 35 sq. Å/molecule was compressed at a rate of 2.43 sq. Å/molecule per minute until the pressure maximum was attained and the surface pressure recorded with time at constant area. Figure 5 shows the $\pi-A$ isotherm (part A) and the relaxation plot (part B), respectively, for a film at an initial pressure maximum of 45 dynes/cm and a molecular area of 19.2 sq. Å.

It is apparent from Fig. 5 that on decreasing the molecular area from 19.5 to 19.2 sq. Å during compression, 7.5 seconds were required for the film pressure to increase from 25 to 45 dynes/cm, but on stopping the barrier 12 seconds were required for the pressure to decay from 45 to 25 dynes/cm at 19 sq. Å/molecule. The rate of pressure decay changed markedly (20-fold) at 25 dynes/cm reflecting the similar discontinuity in the isotherm at 25 dynes/cm pressure. This behavior was demonstrated a number of times with different films.
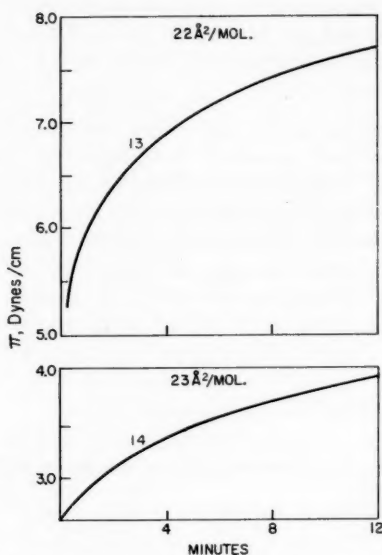
FIG. 4. Surface pressure recovery curves. See Table I for details of curves.
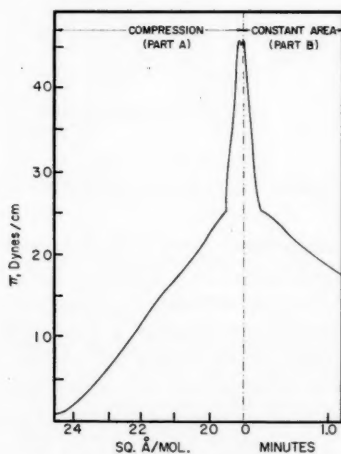
FIG. 5. Part A: π–A isotherm at a compression rate of 2.43 sq. Å per molecule/minute until an area of 19.2 sq. Å/molecule was reached.
      Part B: Relaxation of π at constant area of 19.2 sq. Å/molecule.

Isotherms on Repeated Compressions and Expansions

The π–A isotherms were obtained for films subjected to repeated compressions and expansions. After spreading a film to an initial area of 35 sq. Å/molecule the monolayer was compressed at a rate of 2.43 sq. Å/molecule per minute to the maximum pressure and immediately re-expanded to 35 sq. Å/molecule and left at this molecular area for

FIG. 6. Isotherms of a repeatedly compressed and expanded film at 15° C. Curve numbers represent the sequence of compressions.

FIG. 7. Isotherms of repeatedly compressed and expanded film at 25° C. Curve numbers represent the sequence of compressions.

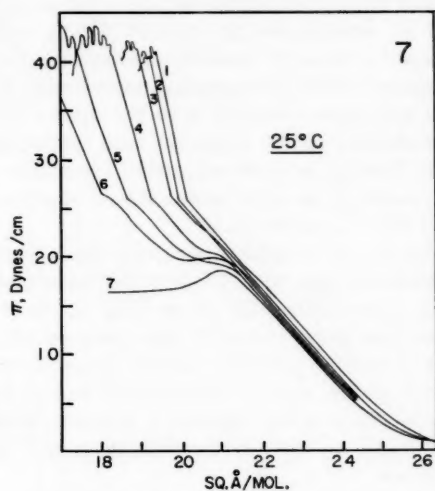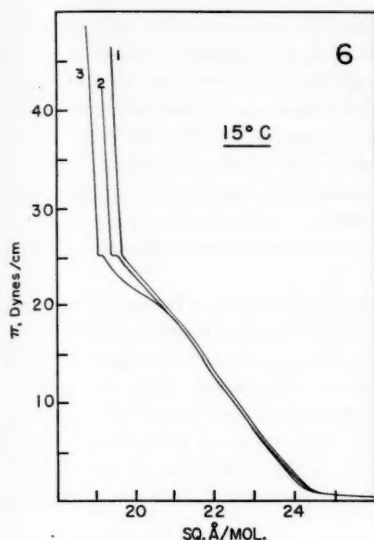1 hour to permit respreading. After this time interval the film was recompressed as before. Figures 6 and 7 are the isotherms obtained from such a series of compressions and subsequent expansions at 15° C and 25° C respectively. The curves are numbered according to the sequence of compressions.

The isotherms obtained with successive compressions are very similar to those obtained by varying the rate of compression (Fig. 1). The highly incompressible solid phase persists on the 15° C isotherm after three compressions but is shifted to smaller molecular areas with each compression (Fig. 6). The shift in area results from a change in the slope of the isotherm just before the appearance of the solid phase of constant compressibility similar to that apparent in Fig. 1. At 25° C the shift of the solid phase to progressively smaller areas with succeeding compressions becomes strikingly evident (Fig. 7). Not only does a marked change occur in the shape of the isotherm before the appearance of the solid phase, as found in varying the compression rate (Fig. 1), but the slope of the isotherm and hence the compressibility of the solid phase change with each compression and finally the phase disappears (Fig. 7, curve 7). There is some indication of a change in slope in the solid phase isotherm itself (Fig. 7, curve 5).

DISCUSSION

Heller (4) has reported that the shape of the $\pi-A$ isotherm of palmitic acid monolayers depends on the rate of compression of the film. A similar dependence with stearic acid monolayers is indicated in Fig. 1, in which substantially the same film compressibility from molecular areas of 24.5 to 21 sq. Å is shown; below 21 sq. Å/molecule, however, a

marked divergence is apparent in the shape and slope of the curves. At the highest compression rate (2.43 sq. Å/molecule per minute) the highly incompressible solid phase of stearic acid monolayer is evident (Fig. 1, curve 1). When the compression rate was reduced to 0.213 sq. Å/molecule per minute (Fig. 1, curve 2) the isotherm was identical with curve 1 until a 21 sq. Å/molecule area was reached and a more compressible intermediate film appeared. With slow manual compression (Fig. 1, curves 3a, 3b) the slope of the isotherm was again identical with the others until reaching 21 sq. Å/molecule, but on further reduction of the molecular area neither the solid film nor the intermediate film appeared. Further, pressure relaxation, essentially absent at molecular areas greater than 21 sq. Å/molecule, became measurable at smaller molecular areas when slow compression was used (Fig. 1, curves 3a, 3b).

The absence of the solid phase in curves 2, 3a, 3b of Fig. 1 seems to be associated with the compression rate, since 7 hours after slow compression the film readily exhibited the highly incompressible solid phase (Fig. 1, curve 3c). The maximum pressure attained before collapse seems similarly dependent on the rate of compression (Fig. 1); collapse occurred at surface pressures varying from 15 to 49 dynes/cm and from 21 to 19.4 sq. Å/molecule as the rate of compression was increased. The work of Dervichian (6) on stearic acid films, which reports a pressure maximum of 61 dynes/cm at 18.6 sq. Å/molecule under an estimated compression rate of 18 sq. Å/molecule/min, corroborates these findings.

The point of collapse near 21 sq. Å/molecule for slowly compressed monolayers appeared as an inflection on the isotherm obtained under rapid compression (Fig. 1). Inflections of this type have been reported for stearic acid (15) and behenic acid (16) and have been related to the appearance of a second-order phase transition in the film. The nature of this transition point is obscure, Adam (17) suggesting that the head group packing beneath the film is responsible for the effect.

According to Vold (18) a molecular cross-sectional area of 25.2 sq. Å can be calculated from the volume swept out during the rotation of vertically oriented fatty acid molecules of the stearic type with the head groups close-packed and planar in the water surface (Fig. 8(a)). The discontinuity found at 25 sq. Å/molecule in the π–A isotherms of stearic acid monolayers is assumed to reflect the appearance of such a surface configuration with free rotation permitted. When the film molecules are identically oriented on the surface but no longer free to rotate, the molecular cross-sectional area, now ovoid, is calculated to be 20.5 sq. Å for the most efficient packing (Fig. 8(b)). The π–A isotherm of stearic acid on compression from 25 to 21 sq. Å/molecule can be assumed to reflect the progressive inhibition of free rotation until at the lower area rotation is completely restricted. At this point the compressibility of the film would depend on the compressibility of the head groups only and should decrease markedly. The discontinuity in the π–A isotherm at 21 sq. Å/molecule does in fact reflect this change to a lower compressibility. As the lateral compression continues and the film approaches collapse, the planar configuration of the head groups (Fig. 8(c)) should give way to a multiplanar one as head groups are forced to a position either above or below the original plane (Fig. 8(d)). Finally some of the stearic acid molecules may invert under lateral compression to form a second molecular layer (Fig. 8(e, f)) with ensuing collapse.

If the inversion process requires time, the appearance of the solid film on rapid compression may be the consequence of insufficient time for inversion between the moment at which 21 sq. Å/molecule area was reached and the moment of general collapse of the film.
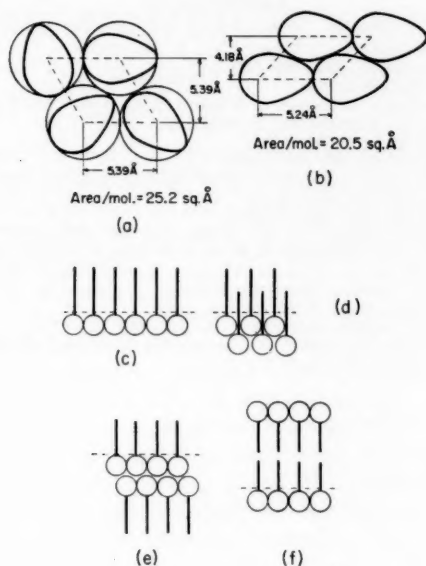
FIG. 8. Possible configuration of stearic acid monolayers.

    (a) At 25 sq. Å/molecule, free rotation (18). (b) At 21 sq. Å/molecule, no rotation (18).
    (c) Planar configuration at 21 sq. Å/molecule. (d) Below 21 sq. Å before inversion.
    (e, f) Possible modes of inversion below 21 sq. Å/molecule.

As the compression rate is decreased the time per unit change in area after attaining 21 sq. Å/molecule increases and the time available for inversion increases. Consequently the inversion process can occur to an extent dependent on the particular compression rate employed. With intermediate compression rates a competition can occur between the processes of solid film formation and inversion resulting in the $\pi-A$ isotherm of variable compressibility found by experiment. At very low rates of compression the time available for inversion is so great that the film molecules can invert at a rate at least equal to the compression rate and no solid or intermediate film is formed.

The variation in slope and hence compressibility illustrated in Figs. 6 and 7, obtained by successive compressions and expansions, can also be explained by a process of inversion. With rapid compression to areas below 21 sq. Å/molecule a small fraction of the molecules may invert but not in sufficient numbers to alter the apparent compressibility of the solid phase. With subsequent expansion the inversion process may be reversed but the molecules involved retain a configuration on the surface favorable to rapid inversion on subsequent compression. On immediate recompression these molecules rapidly invert and others follow, thus increasing the fraction of film molecules conditioned for rapid inversion in the next expansion–compression cycle. The over-all effect of this mechanism would be an apparent increase in the inversion rate with each successive compression until the rate of the inversion process approaches the rate of compression and no solid film appears (Fig. 7).

REFERENCES

1. W. D. Harkins and G. C. Nutting. J. Am. Chem. Soc. **61**, 1180 (1939).
2. W. D. Harkins and R. J. Myers. J. Chem. Phys. **4**, 716 (1936).
3. N. K. Adam. Proc. Roy. Soc. A, **101**, 452 (1922).
4. S. Heller. Kolloid-Z. **136**, 120 (1954).
5. E. Stenhagen. The Svedberg. (Almquist & Wiksells Boktryckeri Ab) Uppsala, Sweden. 1944. p. 31.
6. D. G. Dervichian. J. phys. Radium, Ser. 7, Vol. 6. 221 (1935).
7. D. G. Dervichian. Ann. phys. **8**, 361 (1937).
8. F. H. Muller. Z. Elektrochem. **59**, 316 (1955).
9. W. A. Kimball and H. E. Ries, Jr. Intern. Congr. Surface Activity. 2nd Congr. Vol. 1. Butterworth Scientific Publications, London. 1957. p. 75.
10. F. A. Mauer. Rev. Sci. Instr. **25**, 598 (1954).
11. W. D. Harkins and T. F. Anderson. J. Am. Chem. Soc. **59**, 2189 (1937).
12. E. Stenhagen. The Svedberg. (Almquist & Wiksells Boktryckeri Ab) Uppsala, Sweden. 1944. p. 29.
13. R. F. Robertson, C. A. Winkler, and S. G. Mason. Can. J. Chem. **34**, 718 (1956).
14. W. Rabinovitch, R. F. Robertson, and S. G. Mason. J. Colloid Sci. **13**, 600 (1958).
15. D. G. Dervichian. J. Chem. Phys. **7**, 931 (1939).
16. E. Stenhagen and S. Stallberg-Stenhagen. Nature, **159**, 814 (1947).
17. N. K. Adam. The physics and chemistry of surfaces, 3rd ed. Oxford Univ. Press. 1941.
18. M. J. Vold. J. Colloid Sci. **7**, 196 (1952).

ANIONIC POLYMERIZATION OF STYRENE[1]

D. J. WORSFOLD AND S. BYWATER

ABSTRACT

A study of the kinetics of the initiation and propagation reactions in the polymerization of styrene by butyllithium in benzene solution has been made. The initiation has been shown to be first order in styrene and 0.155 order in butyllithium, the propagation to be first order in styrene and half order with respect to active chain ends. The apparent activation energies of the two reactions have been shown to be 18,000 calories and 14,300 calories respectively. The ultraviolet absorption spectra of colored species produced has been measured and compared with others found in similar systems.

The polymerization of styrene by butyllithium in benzene solution is an anionic chain reaction comprising initiation and propagation steps. Chain termination is negligible if the starting materials are rigorously purified and the reaction is carried out in a high vacuum system. Previous kinetic studies on this system have followed only the rate of monomer consumption (1, 2). Since, however, the reaction is complicated by the fact that initiation and propagation rates are of comparable magnitude under many experimental conditions, it seemed desirable to study the initiation and propagation steps separately. The method employed to follow the reaction was photometric using the known absorption bands of styrene and the absorption band of the polystyryl anion measured as described later. Because of the high extinction coefficient of both compounds, the concentration ranges studied were lower than previously used or overlapped their lower concentration range.

EXPERIMENTAL

The butyllithium was supplied by Foote Mineral Company as a 16% solution in a heptane/pentane solvent mixture.

The purification of the styrene has been described before (3).

Reagent grade benzene was stirred for a week with concentrated sulphuric acid, washed with water, with dilute sodium hydroxide solution, and again with water. It was distilled from phosphorus pentoxide onto calcium hydride, degassed, and stored under vacuum. The benzene was distilled in the vacuum system as needed to a smaller reservoir containing butyllithium from which the solvent had been removed by pumping. From here it was transferred to the reaction vessel by distillation.

The techniques used in the handling of the reactants under high vacuum have been described before (3) and entailed using small fragile glass bulbs of the reactants, and glass-covered magnetic bars for breaking them. All reaction vessels were washed with a solution of butyllithium in benzene and rinsed by refluxing as before, after all the reactant bulbs had been sealed inside and the vessels evacuated.

It was necessary to dilute the stock butyllithium solution by a factor of 50 or more before it could be used. A milliliter of the stock solution was transferred by hypodermic syringe in a dry nitrogen box to a fragile glass bulb, connected to a stopcock, that previously had been evacuated and reopened in the dry box. The bulb was then pumped and sealed off. This butyllithium was diluted 50 times and sealed into a large number of similar bulbs in a vacuum apparatus by the methods referred to above. It had been

determined previously that handling 1 milliliter of the stock solution by syringe in this manner destroyed less than 2% of the butyllithium.

Lithium analyses were performed spectrophotometrically using a solution of "Thorin" on aliquots of the lithium polystyryl solution after the benzene had been evaporated on a hot plate, and the polymer burned off at a temperature of less than 500°. Higher temperatures seemed to cause loss of lithium. The analysis is reputed to have an accuracy of 3%.

The optical cells used were made of 1-cm sq. clear quartz tubing, and could be converted to 1-mm cells with appropriate square quartz blocks. The cells were calibrated with potassium chromate solution. The spectra were measured on a Beckman DU spectrophotometer.

To show that the absorption band of the polystyryl salt obeyed Beer's law, the optical cell was connected to a graduated tube, with benzene in a reservoir joined to the cell and tube. The optical density of a solution of the polystyryl lithium salt at 335 mμ was measured over a 10-fold range of dilution, and the dependence was shown to be linear. Styrene was estimated at 291 mμ after a correction for the tail of the polystyryl ion band was applied.

The vessels used for the kinetic experiments, and for the determination of the spectra of the lithium polystyryl salt, are shown in Fig. 1, which is thought to be self-explanatory. The volume of reaction mixture was about 50 milliliters. Only one bulb of catalyst was used, but successive additions of styrene were achieved by breaking in turn up to three bulbs of styrene. This enabled the propagation step to be followed separately after
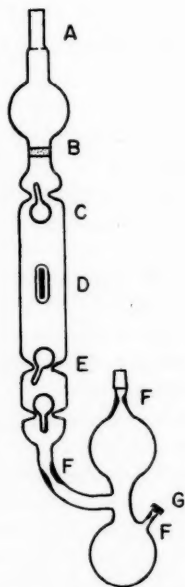
FIG. 1. Reaction vessel.

A. Optical cell.   E. Styrene.
B. Filter   F. Constrictions for sealing off.
C. Diluted catalyst solution.   G. Serum cap to introduce butyllithium
D. Breaker.   solution to wash apparatus.

measurements of the optical density at 335 mμ had indicated that chain initiation was complete. The breaking of successive bulbs of styrene after this point could sometimes decrease the optical density by 1 to 2% due to the presence of residual impurities. Otherwise once it had attained a steady value, it remained constant during the course of a kinetic run (about 4 hours) and only decreased slowly over a period of weeks. This indicates that chain termination is negligible in this system under the experimental conditions used.

The reactions were carried out at 30.3°, except those for the temperature dependence, which were carried out over the range 10.0°–30.3°.

RESULTS

The spectrum of the colored species produced by the action of butyllithium on styrene in benzene solution was found to consist of a single absorption band centered at 334 mμ, with a long wavelength wing extending into the visible region which gives the solution its yellow color. The short wavelength wing was lost in the accompanying polystyrene bands below 280 mμ. Assuming that the structure of this species is [————CH$_2$CHPhCH$_2$$\overset{-}{C}$HPh.$\overset{+}{L}$i], the extinction coefficient of the polystyryl ion was determined by analysis of the solution for lithium. The results are shown in Table I.

TABLE I

Extinction coefficient of lithium polystyryl salt

[Li], moles/liter $\times 10^4$	ϵ, $\times 10^{-4}$
2.61	1.32
6.07	1.28
7.14	1.33
8.53	1.27

To confirm that each butyllithium molecule initiated one polymer molecule, the molecular weights of three of the polymers from the kinetic experiments were determined viscometrically using a viscosity – molecular weight relationship determined using monodisperse polystyrenes (4). The conditions of preparation were such that the initiation reaction was completed rapidly compared with the propagation reaction, and the three polymers could be expected to have a low $\bar{M}_w/\bar{M}_n$ ratio. The molecular weights calculated from the butyllithium and total styrene concentrations, assuming no chain transfer, are compared with the experimental values in Table II. The first two polymers were terminated by methanol, the third by exposure to air. The last entailed two separate additions of styrene.

TABLE II

Molecular weights of polystyrenes

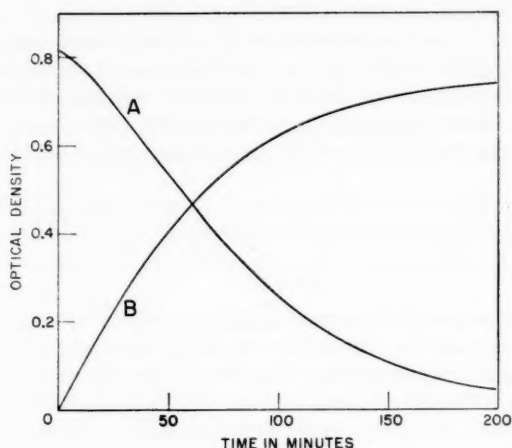| [Lithium butyl], moles/liter $\times 10^4$	[Styrene], moles/liter $\times 10^2$	Molecular weight	
		Calculated	Experimental
3.11	13.9	46,700	48,000
1.07	3.48	33,900	35,000
0.45	3.57	82,700	84,000

FIG. 2. Typical reaction curves of initiation reaction.
A. Disappearance of styrene measured at 291 mμ.
B. Appearance of polystyryl ion at 335 mμ.

Initially, [styrene] = 1.39×10^{-2} moles/liter; [butyllithium] = 1.10×10^{-3} moles/liter.

The reagent consumption curves of a typical initiation reaction are shown in Fig. 2.

The initial rates of formation of the colored species were determined from the plots of optical density versus time. The plots are usually not strongly curved and the initial tangent could probably be drawn with an accuracy of 5% or better. The results are shown in Table III.

Consideration of the first section suggests that the rate of formation of polystyryl

TABLE III

Initiation of styrene by butyllithium

[BuLi], moles/liter $\times 10^4$	[Styrene], moles/liter $\times 10^3$	Initial rate, moles/liter min^{-1} $\times 10^6$	$\dfrac{\text{Initial rate}}{\text{[Styrene]}}$ $\times 10^4$	k_i, liters$^{1/6}$ mole$^{-1/6}$ min^{-1} $\times 10^3$
6.07	27.6	11.4	4.14	1.42
6.65	7.67	3.14	4.09	1.38
7.14	6.73	2.86	4.25	1.42
8.09	3.50	1.57	4.50	1.47
6.68	2.83	1.23	4.35	1.46
6.65	7.67	3.14	4.09	1.38
60.0	9.23	5.30	5.74	1.35
388.	8.75	6.76	7.73	1.32
22.2	4.96	2.41	4.87	1.35
11.8	27.4	12.6	4.60	1.42
11.0	13.9	6.63	4.78	1.49
2.61	19.4	6.93	4.60	1.42
0.93	1.85	.581	3.14	1.48
0.675	2.73	.725	2.66	1.32
0.166	1.88	.324	1.73	1.08
0.155	2.28	.292	1.28	0.81

anions is first order in styrene, the second section shows the rate to increase very slowly with butyllithium concentration. A plot of $\log_{10}$ (initial rate/[styrene]) against $\log_{10}$ [butyllithium] is relatively insensitive at such low orders, but appears to give $0.155 \pm 10\%$ for the order with respect to the butyllithium for concentrations between 5×10^{-5} M and 4×10^{-2} M (Fig. 3). This is close to an order of 1/7 or 1/6, and for convenience, and with
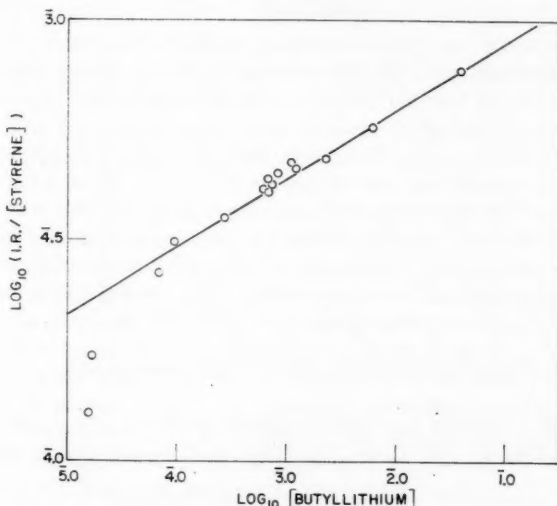

FIG. 3. Dependence of initiation rate on butyllithium concentration.

some theoretical justification the latter figure has been used subsequently. The two runs at concentration below 2×10^{-5} M showed deviation from this behavior, their rates being too low.

Plotting initial rate/[lithium butyl]$^{1/6}$ against [styrene] for the seven runs with butyllithium concentration between 6×10^{-4} M and 1.2×10^{-3} M gives a good straight line over the range of styrene concentration 3×10^{-3} M to 3×10^{-2} M (Fig. 4). Thus the over-all expression for the initial rate of formation of polymer chains, or consumption of butyllithium is given by

$$d \, [\text{butyllithium}]/dt = -k_1 \, [\text{butyllithium}]^{1/6} \, [\text{styrene}]$$

and the values of k_1 calculated for individual kinetic experiments are given in Table III.

If sufficient monomer were present, the optical density at 335 mμ would increase to a maximum and then remain constant, at which point it was assumed that all the butyllithium had reacted to form active chains. The propagation reaction, once all the chains had been initiated, was followed by the consumption of the residual monomer, or by the consumption of further bulbs of styrene broken into the reaction mixture. Here, of course, the method of initial rates could not be used. The rate of consumption of monomer, however, followed a first-order course over a matter of at least four half-life times, at which point the precision of the analysis was the limiting factor. A logarithmic plot of this first-order rate against the initial butyllithium concentration (equal to the number

FIG. 4. Dependence of intiation rate on styrene concentration.

of polystyryl ions present) showed a good half-order dependence of the rate on the butyl-lithium concentration (Fig. 5). The kinetic equation for the propagation reaction is then

$$d\,[\text{styrene}]/dt = -k_2\,[\text{styrene}]\,[\text{butyllithium}]^{1/2}.$$

The temperature dependence of the initiation reaction was found to correspond to an apparent activation energy of 18,000 calories, that of the propagation reaction to 14,300

FIG. 5. Dependence of propagation rate on butyllithium concentration.

calories, for the temperature range 10.0°–30.3°. The appropriate mean rate constants calculated assuming the same kinetics apply at the lower temperatures are shown in Table IV. The half-order dependence on the butyllithium concentration of the first-order disappearance of monomer in the pure propagation reaction was confirmed at all four lower temperatures, but not the orders of the initiation step.

DISCUSSION

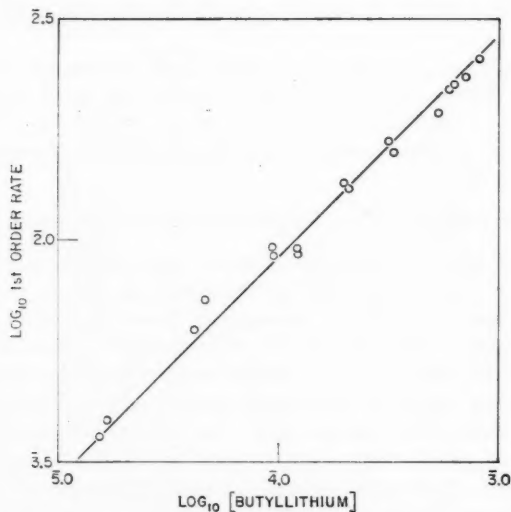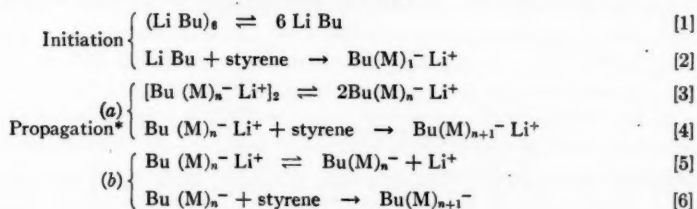The absorption band of the lithium polystyryl compound in benzene with a maximum at 334 mμ is very similar to the absorption band of the similarly prepared compound in tetrahydrofuran, which has a maximum at 340 mμ and extends rather more into the visible region. The absorption bands of the lithium compounds cut off much more sharply than do the absorption bands of the sodium and potassium polystyryl salts in tetrahydrofuran which have a maximum at 343 mμ and extend so far into the visible region to give their solution a red color, whereas the lithium salts are yellow. All the bands are sufficiently similar to suppose that they are due to the same species, the polystyryl anion, somewhat modified by the environment composed of the solvent and gegenion. The integrated area under the band of the lithium polystyrene salt in benzene, extrapolated where it is lost in the bands of polystyrene, has about 85% of the corresponding area of the sodium compound in tetrahydrofuran. If the arguments of Evans *et al.* (5) concerning similar bands of carbonium ions are valid, this would suggest that the ionic nature of the C—metal bond is very little reduced in changing to the less favorable conditions of dielectric constant and alkali metal ion. There was no change in the optical density of solutions at 335 mμ in the temperature range 10° to 30°, suggesting that there is no temperature-dependent equilibrium between ionic and nonionic forms in this range.

The most straightforward schemes that can be suggested to explain the kinetics found for the reaction of butyllithium with styrene are as follows:

$$\text{Initiation} \begin{cases} (\text{Li Bu})_6 \; \rightleftharpoons \; 6 \text{ Li Bu} & [1] \\ \text{Li Bu} + \text{styrene} \; \rightarrow \; \text{Bu(M)}_1^- \text{Li}^+ & [2] \end{cases}$$

$$\text{Propagation}^* \begin{cases} (a) \begin{cases} [\text{Bu (M)}_n^- \text{Li}^+]_2 \; \rightleftharpoons \; 2\text{Bu(M)}_n^- \text{Li}^+ & [3] \\ \text{Bu (M)}_n^- \text{Li}^+ + \text{styrene} \; \rightarrow \; \text{Bu(M)}_{n+1}^- \text{Li}^+ & [4] \end{cases} \\ (b) \begin{cases} \text{Bu (M)}_n^- \text{Li}^+ \; \rightleftharpoons \; \text{Bu(M)}_n^- + \text{Li}^+ & [5] \\ \text{Bu (M)}_n^- + \text{styrene} \; \rightarrow \; \text{Bu(M)}_{n+1}^- & [6] \end{cases} \end{cases}$$

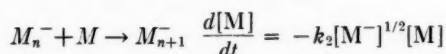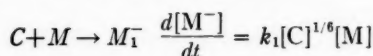The subscript 6 applied to the butyllithium aggregate is probably an average.

A strong argument in favor of the first propagation scheme can be made on the basis of the behavior in the sodium naphthenide catalyzed polymerization of α-methylstyrene in tetrahydrofuran. Here the propagation step is close to first order in initiator (6). Conductivity measurements on the sodium polystyryl salt (3) indicate that it exists largely in the form of ion pairs in this solvent. Both facts suggest that the ion pair is the reactive species in this solvent. Molecular weight determinations in boiling ether (7) suggest that lithium benzyl and lithium phenyl exist in the form of dimers so presumably lithium polystyryl would be expected also to be dimerized in solvents of low dielectric constant. The heat of dissociation of the dimer $(\text{Bu(M)}_n^- \text{Li}^+)_2$ would have to be in this

*In the first scheme (a) it is assumed that the reaction is due solely to ion pairs in equilibrium with ion pair dimers, and in the second scheme (b) it is due solely to the extremely low concentration of free ions which are in equilibrium with the ion pairs. The equilibria 1, 3, and 5 are normally predominantly on the left-hand side of the equations.

case somewhat over 10 kilocalories as the apparent activation energy of the propagation step (14,300 calories) would be composed of its heat of dissociation and the actual activation energy of the propagation step. The latter is presumably low as was the case in tetrahydrofuran solution. A heat of dissociation of this magnitude is not incompatible with the apparent high stability of alkyl and aryl lithium complexes in solutions of low dielectric constant. On the other hand, similar arguments applied to the second propagation step infer a similar heat of dissociation of the ion pair into kinetically free ions. This appears to be much too low for this process in benzene solution.

The activation energy of the initiation step of 18,000 calories would consist of an activation energy and a dissociation energy of the same type. The activation energy of attack of the comparatively covalent butyllithium on styrene would be expected to be higher than that of the propagation step, thus allowing a similar heat of dissociation of butyllithium. One difficulty which applies to the initiation scheme is the great dilutions at which the butyllithium aggregates must remain in the form of hexamers. The experimental results suggest no significant breakdown above a concentration of 5×10^{-5} M. Several studies of the degree of association of ethyllithium and butyllithium in ether and benzene by measurement of freezing point depression or boiling point elevation (8, 9, 7) have indicated a value of about six in the concentration range down to 1/10th molar. One other study under identical conditions (10) indicated a degree of association of two. A study of the infrared spectra of ethyllithium and butyllithium (11) was interpreted to show that in benzene or hexane on dilution, the hexamer fairly rapidly dissociated to dimer and monomer in the same concentration range. Further work on this topic is obviously desirable before adequate comment can be made on the low order of the initiation step with respect to butyllithium.

An attempt can be made at analysis of the system for the over-all disappearance of monomer during the period which both consecutive reactions are occurring. Whatever the detailed mechanism, the kinetic scheme may be written

$$C + M \rightarrow M_1^- \quad \frac{d[M^-]}{dt} = k_1[C]^{1/6}[M]$$

$$M_n^- + M \rightarrow M_{n+1}^- \quad \frac{d[M]}{dt} = -k_2[M^-]^{1/2}[M]$$

where $[M^-] = \Sigma[M_n^-]$, using the rate constants shown in Table IV.

TABLE IV

Summary of rate constants

Temp., °C	$k_1 \times 10^4$, liters$^{1/6}$ mole$^{-1/6}$ min^{-1}	k_2, liters$^{1/2}$ mole$^{-1/2}$ min^{-1}
30.3	14.0	0.929
25.0		0.563
20.0	4.68	0.387
15.0		0.265
10.0	1.45	0.155

The complete solution of the differential equations of consecutive, competing reactions is only available for the simplest of cases, and not for this particular case. It is possible to obtain a partial solution by eliminating the variable time, leaving C and M as the variables, and also with the simplification of ignoring monomer consumption in the

initiation stage. Then by treating the resultant equation as two separate binomial series it is possible to obtain

$$[M_0 - M] = \frac{k_2}{k_1} C_0^{4/3} \left(\frac{2}{3} \left[\frac{M^-}{C_0} \right]^{3/2} + \frac{1}{15} \left[\frac{M^-}{C_0} \right]^{5/2} + \frac{1}{36} \left[\frac{M^-}{C_0} \right]^{7/2} + \frac{91}{5832} \left[\frac{M^-}{C_0} \right]^{9/2} \ldots \right)$$

$$\text{for } 0 \leqslant M^- < C_0$$

and

$$[M_0 - M] = \frac{k_2}{k_1} C_0^{4/3} \left(\frac{6}{5} \left[\frac{C_0 - M^-}{C_0} \right]^{5/6} - \frac{6}{22} \left[\frac{C_0 - M^-}{C_0} \right]^{11/6} - \frac{6}{136} \left[\frac{C_0 - M^-}{C_0} \right]^{17/6} \right.$$

$$\left. - \frac{6}{368} \left[\frac{C_0 - M^-}{C_0} \right]^{23/6} \ldots \right)$$

$$\text{for } 0 < M^- \leqslant C_0.$$

The latter expression converges more rapidly than the first, but taking the first part for $0 \leqslant M^- \leqslant C_0/2$ and the second for $C_0 \geqslant M^- \geqslant C_0/2$, only four terms or less are necessary to evaluate either.

From these equations it should be possible to plot $[M_0 - M]$ against the computed values of the right-hand side for values $[M^-/C_0]$ in the initiation reaction, and thus evaluate k_2/k_1 from the resultant straight lines. This was done whenever possible and the value of k_2/k_1 at 30.3° for eight of the runs was 522, compared with 665 obtained from the k_1 of the initial rates, and the k_2 of the pure propagation reaction. Again at the lowest butyllithium concentration the ratio was abnormal being twice the mean, and not included in the the mean.

The discrepancy between the two values of k_2/k_1 is probably no more than the experimental error, but it could be due to the excess butyllithium complexing with the propagating species and depressing the rate, as was suggested by Tobolsky (1). This would lower the k_2/k_1 ratio obtained under conditions where both reactions were occurring simultaneously. But for the reaction with the highest concentration of lithium butyl $(3.88 \times 10^{-2}$ moles/liter), where it is in large excess (only 2% reacted whilst most of the monomer was consumed), the value of k_2/k_1 is only 30% lower than the mean, although it had the largest deviation by a factor of two. This is taken to indicate that the propagation reaction is very largely independent of the excess butyllithium, because if the kinetics were changed appreciably the equations above would not hold as well as they do.

From the form of these equations it is seen that, as is expected of a reaction with an order of less than one, the initiation reaction goes to completion at a finite monomer consumption. For any given starting butyllithium concentration, it is possible to calculate the required initial monomer concentration to ensure all the butyllithium has reacted, with the qualification that when the unreacted butyllithium concentration approaches $10^{-5} M$, the kinetic scheme is no longer valid. For an initial catalyst concentration C_0 to react completely, the monomer concentration must equal $0.84 C_0^{4/3} k_2/k_1$. Taking a mean value at 30° of 600 for k_2/k_1 and a value of $C_0 = 0.01 M$, the initial monomer concentration must be 1.08 M for complete reaction; for 50% of the butyllithium to react the monomer concentration must be 0.326 M. At points before all the butyllithium has reacted, it is possible to compute that the ratio $\bar{M}_w/\bar{M}_n \sim 1.28$; further consumption of monomer will decrease this ratio.

This implies that at initiator concentrations greater than 0.01 molar and using a molar solution of monomer the reaction will exhibit the combined characteristics of the initiation

and propagation reaction. It will not be possible to study the propagation reaction separately even at later stages in the reaction. Due to the low order in butyllithium the rate of styrene consumption will appear to be largely independent of initiator concentration. A semiquantitative study of the complex kinetic equations shows that the percentage conversion will be a linear function of time over a fairly wide conversion range and that the apparent order with respect to initial monomer concentration will be between one and two. Generally speaking therefore our kinetic scheme is compatible with the results of O'Driscoll and Tobolsky (1) even though we have postulated a different propagation step and the absence of chain termination.

A comparison with the paper of Welch (2) is somewhat more difficult. Although he claims to have followed the propagation reaction only, it seems from the analysis given above that his highest concentration reactions were performed under such conditions that he could not free the propagation reaction from the initiation reaction by his experimental procedure. This is supported by the appearance of his typical first-order polymerization plot at the highest concentration, which curves in a way that would be predicted. The apparent change to zero order in butyllithium at concentrations above 0.02 M could well be due to the reasons outlined above. It should be noted, however, that our experiments do not show that a decrease in order of the propagation reaction at these concentrations does not occur, as all the kinetic runs on this reaction were conducted well below them. In fact such a decrease in order is quite possible as higher aggregates are likely to form in more concentrated solutions, although the measurements of Wittig *et al.* (7) did not show this.

The first-order dependence found by Welch for the propagation step on lower concentrations of butyllithium is at variance with the half order found in this work. The reason for this probably lies in the different methods of analysis for active chain ends. The optical method used here is simpler and more direct than that used by Welch since he calculated the butyllithium concentration from the viscosity of the polymer produced. Although the method of Welch is basically sound, it would require a far more rigorous technique to be truly effective. This Welch demonstrated when, using as he described extreme precautions in his procedure, he found agreement with the molecular weight-viscosity relationship of Szwarc *et al.* (12), who noted a discrepancy of a factor of about two between it and the true relationship. By picking individual points from the graph in the paper of Welch, it is possible to calculate the rate constants to fit the kinetic equation in this paper, and it is found that they are generally about 25% lower than the constant found at 20° here. Although his results for the lower half of his concentration range show considerable scatter, they are a reasonable extension of the half-order dependence on butyllithium.

REFERENCES

1. K. F. O'DRISCOLL and A. V. TOBOLSKY.　J. Polymer Sci. **35**, 259 (1959).
2. F. J. WELCH.　J. Am. Chem. Soc. **81**, 1345 (1959).
3. D. J. WORSFOLD and S. BYWATER.　J. Chem. Soc. In press.
4. J. M. COWIE, D. J. WORSFOLD, and S. BYWATER.　Trans. Faraday Soc. In press.
5. A. BENTLEY, A. G. EVANS, and J. HALPERN.　Trans. Faraday Soc. **47**, 711 (1951).
6. D. J. WORSFOLD and S. BYWATER.　Can. J. Chem. **36**, 1141 (1958).
7. G. VON WITTIG, F. J. MEYER, and G. LANGE.　Ann. **571**, 167 (1951).
8. F. HEIN and H. SCHRAMM.　Z. physik. Chem. **151**, 234 (1930).
9. T. L. BROWN and M. T. ROGERS.　J. Am. Chem. Soc. **79**, 1859 (1957).
10. K. B. PIOTROVSKY and M. P. RONINA.　Doklady Akad. Nauk S.S.S.R. **115**, 737 (1957).
11. A. N. RODIONOV, D. N. SHIGORIN, T. V. TALALAEVA, and K. A. KOCHESHKOV.　Izvest. Akad. Nauk S.S.S.R. **22**, 1110 (1958).
12. R. WAAK, A. REMBAUM, J. D. COOMBES, and M. SZWARC.　J. Am. Chem. Soc. **79**, 2026 (1957).

HYDROGEN BONDING IN THE AMINE HYDROHALIDES

III. NEAR-INFRARED SPECTRA OF ALIPHATIC AMINE HYDROHALIDES[1]

P. Sauvageau and C. Sandorfy

ABSTRACT

The first overtones of the $\overset{+}{N}H_n$ ($n = 3, 2,$ or 1) stretching fundamentals are very weak and difficult to locate. Binary combinations between $\overset{+}{N}H_n$ stretching and $\overset{+}{N}H_n$ bending vibrations and also $\overset{+}{N}H_n + CH_n$ stretching-bending combinations fall into the 4600–4400 cm^{-1} area for primary and secondary amine hydrohalides and are much stronger. The intensity of these combination bands is not due to the anharmonicity of the potential surface but to the electrical anharmonicity of bending vibrations.

INTRODUCTION

There is a fargoing analogy between the vibrations of $\overset{+}{N}H_3$ and $\overset{+}{N}H_2$ groups on the one hand and CH_3 and CH_2 vibrations on the other and the most characteristic bands of the near-infrared spectra of both aliphatic hydrocarbons and alkylammonium ions are combinations between CH_n and $\overset{+}{N}H_n$ stretching and CH_n and $\overset{+}{N}H_n$ bending vibrations ($n = 3, 2,$ or 1).

Let us suppose first that these vibrations are completely localized in the respective functional groups. Then, as a CH_3 group has C_{3v} symmetry, the asymmetric stretching vibrations (near 2967 cm^{-1}) will be doubly degenerate and the symmetric one (near 2872 cm^{-1}) non-degenerate. The first overtone of the former may split into two levels, belonging to irreducible representations A_1 and E because of anharmonicity. The latter will give one overtone of symmetry A_1. Transitions from the ground state to all these levels are allowed. The combination of the two stretching vibrations (E) is also allowed.

Thus we expect to find four bands in the 5800 cm^{-1} area. This argument holds for the $\overset{+}{N}H_3$ group as well. For the hydrogen bonded species the asymmetric and symmetric stretching vibrations appear to be close to each other. They are also close to the stretching vibrations of the CH_3 group (1, 2, 3).

For the CH_3 bending vibrations again the asymmetrical one (near 1460 cm^{-1}) is degenerate (E) and the symmetrical one (near 1375 cm^{-1}) is non-degenerate (A_1). Thus again there are four binary combinations. The same applies to the $\overset{+}{N}H_3$ group with its bending bands lying close to 1600 and 1500 cm^{-1}.

Combinations between one stretching and one bending vibration yield certain new features. If the two asymmetrical vibrations are combined, A_1, A_2, and E states result. Transition from the ground state to A_2 is forbidden, so two bands remain. The two symmetrical vibrations would give one allowed totally symmetrical combination. The sum of the asymmetrical stretching vibration and the symmetrical bending vibration would give one level (E); the sum of the symmetrical stretching vibration and the asymmetrical bending vibration would also give one level. Together, five bands would result.

The situation is simpler for localized CH_2 or $\overset{+}{N}H_2$ vibrations. Under C_{2v} symmetry all vibrations are non-degenerate and all binary combinations between stretching and bending bands are allowed. This would yield three bands due to combinations of the stretching vibrations, one overtone for the bending vibration and two stretching–bending combinations. (As a general reference see (4).)

Analogous combinations between one $\overset{+}{N}H_n$ and one CH_n vibration are also expected to occur and could fall into the same part of the spectrum.

Interactions between individual groups in the molecule and between molecules in the crystal may split the bands and further complicate the spectrum. All intermolecular effects are much more likely to influence $\overset{+}{N}H_n$ vibrations than CH_n vibrations, as the former are affected by hydrogen bonding.

Under the resolution of our instrument, separation of all the expected bands would be impossible and we have to restrict ourselves to interpret the most conspicuous features of the spectra.

EXPERIMENTAL

The near-infrared spectra were measured by a Beckman DK-1 spectrometer, mounted with a fused-silica prism. The hydrohalides were taken in the form of hexachlorobutadiene mulls. With some of these compounds it is quite difficult to obtain spectra which are free of scattered light. For this reason no complete series of hydrochloride, hydrobromide, and hydriodide spectra could be obtained in every case.

The fundamentals were measured previously in this laboratory, using a Perkin–Elmer model 112 instrument with LiF and CaF_2 prisms.

RESULTS

Cyclohexylamine, piperidine, and triethylamine hydrohalides were chosen as representatives of aliphatic primary, secondary, and tertiary amine hydrohalides. Figures 1, 2, and 3 give the near-infrared spectra of one of the hydrohalides measured as a hexachlorobutadiene mull together with the spectrum of the related amine in liquid phase. The spectra of some other hydrohalides and of some related hydrocarbons were measured as well and will be referred to incidentally in the text. No detailed discussion of these seems to be warranted, however.

No originality is claimed for the spectra of the amines and the hydrocarbons. As to previous literature concerning them, we deem it sufficient to refer to review papers by Kaye (5) and Wheeler (6).

Tables I, II, and III summarize the fundamentals and binary combinations relevant to the discussion. Care should be exercised in considering the exact values of the frequencies of the fundamentals. There is a considerable amount of band overlapping in these spectra, especially in the 3000–2800 cm^{-1} region. Bands due to hydrogen bonded $\overset{+}{N}H_n$ groups are usually quite broad and carry several other bands atop themselves, making assignments difficult. Furthermore, it may be said because of reasons given in the introduction that the hydrohalide spectra offer many opportunities for Fermi resonance and the apparent peaks might be modified by it. Fermi resonance is very likely to occur frequently in the near-infrared spectra too, where binary combinations often coincide with ternary and
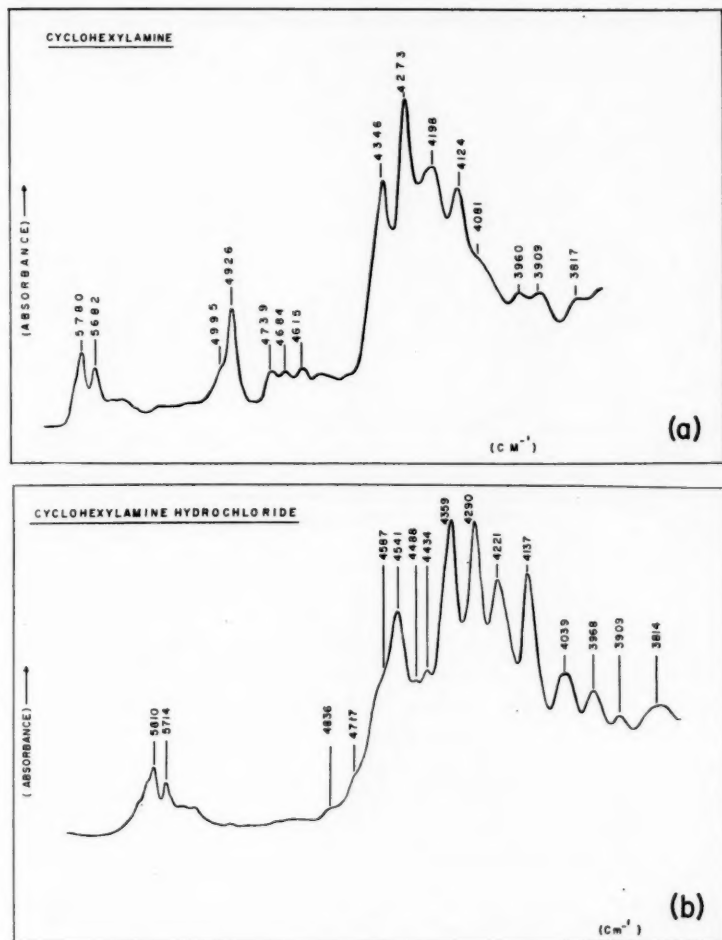
FIG. 1. Near-infrared spectra of cyclohexylamine (above) and cyclohexylamine hydrochloride (below).

other higher combinations. The tables do not contain all the observed bands, only those necessary to discuss our specific problem, the assignment of the first $\overset{+}{N}H_n$ overtones, the $\overset{+}{N}H_n$ stretching plus $\overset{+}{N}H_n$ bending combinations, and the analogous $CH_n + \overset{+}{N}H_n$ combinations. They should be regarded together with the respective figures. Intensities are given by usual symbols. Capital letters are used for the fundamental region, lower case letters for the overtone region. There is a factor of about 100 between the two scales. A "very strong" overtone would be considered as "weak" (at most) on the scale applied to the fundamentals. Indexes a and s stand for asymmetrical and symmetrical respectively.
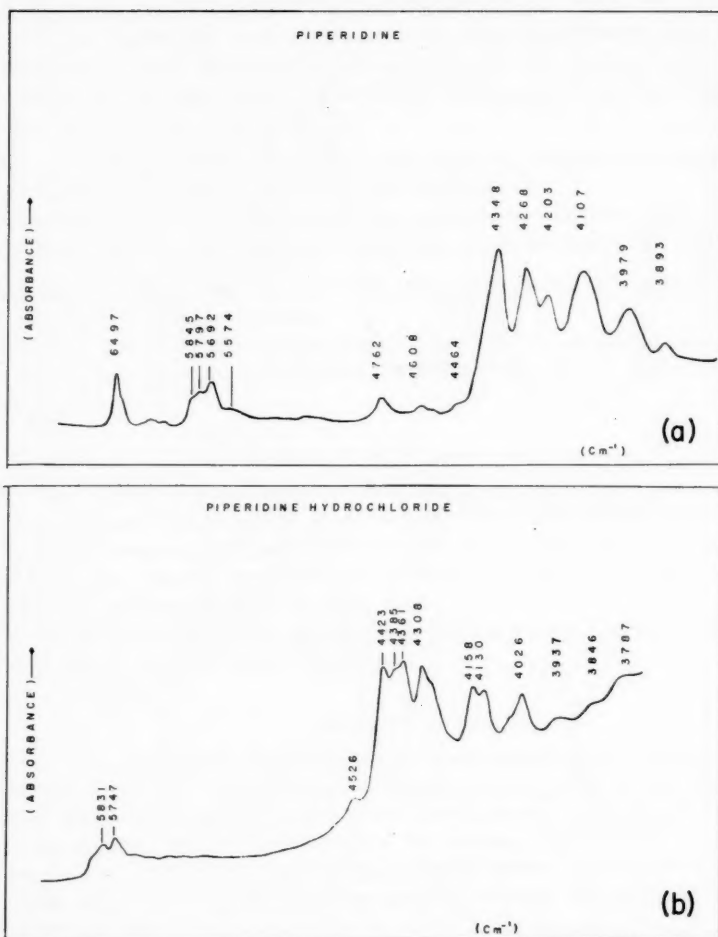
FIG. 2. Near-infrared spectra of piperidine (above) and piperidine hydrochloride (below).

DISCUSSION

G. and L. Herzberg examined the near-infrared spectrum of methyl iodide in the vapor state and established the main features pertaining to the methyl group (7). (For other methyl halides see ref. 4, p. 312.) The near-infrared spectra of liquid paraffins exhibit similar characteristics. There is a series of strong bands between 4400 and 4000 cm^{-1} due to combinations between a CH_n stretching vibration from the 2900 cm^{-1} area and a CH_n deformation vibration. These bands are much stronger than the first overtones of the stretching vibrations which are near 5800 cm^{-1}. In methyl iodide (7) the shift of the latter bands from the sum of the observed fundamentals is of the order of 40 to 50
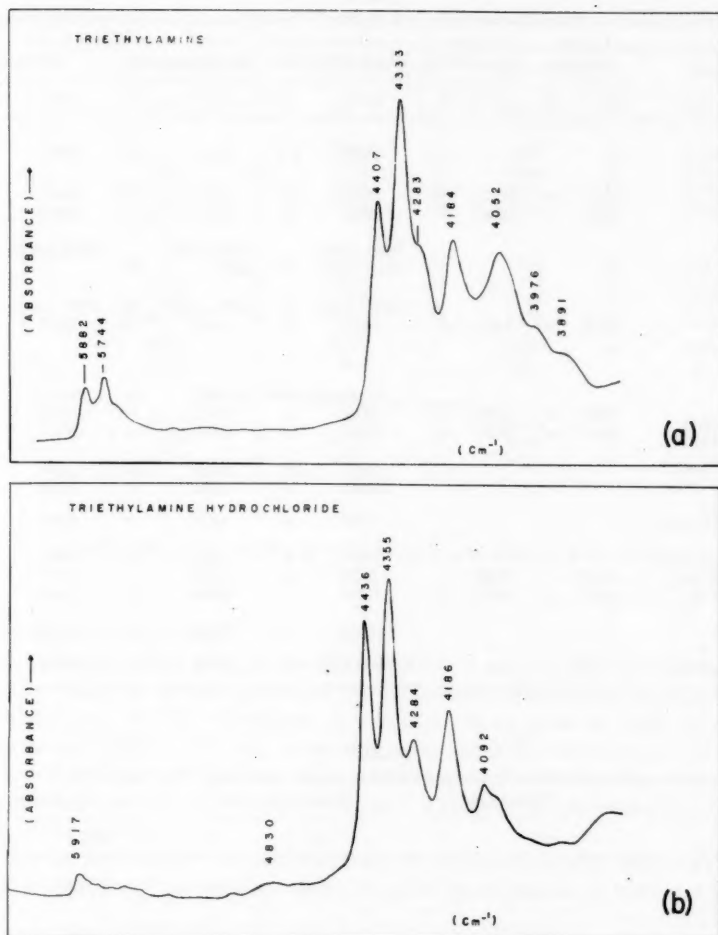
FIG. 3. Near-infrared spectra of triethylamine (above) and triethylamine hydrochloride (below).

cm^{-1}, while for the former it is only of the order of 10 to 30 cm^{-1}. This is related to the expected higher mechanical anharmonicity of the stretching vibrations but it also shows that the relatively high intensity of the combination tones in the 4400–4000 cm^{-1} area is not due to mechanical anharmonicity or, in particular, to high anharmonicity constants between stretching and bending vibrations. Therefore, electrical anharmonicity of the bending vibrations involved should explain the higher intensity of these bands.

It is important that no strong band appears above about 4400 cm^{-1} in saturated hydrocarbons. In the hydrohalides these CH_n stretching$+CH_n$ bending summation bands

TABLE I

	Cyclo-hexane		Cyclo-hexylamine		Hydrochloride		Hydrobromide		Hydriodide	
	cm⁻¹	I	cm⁻¹	I	cm⁻¹	I	cm⁻¹	I	cm⁻¹	I
$\nu_a(\overset{+}{N}H_3)$					⎧ 2980	VS	2996	VS	3011	VS
$\nu_s(\overset{+}{N}H_3)$										
$\nu_a(CH_2)$	2923	VS	2915	VS	2934	VS	2932	VS	2935	S
$\nu_s(CH_2)$	2951	S	2846	S	2859	S	2857	S	2855	M
$\delta_a(\overset{+}{N}H_3)$					1620, 1618 1615, 1610	W	1609, 1601 1591	W	1594, 1588	M
$\delta_s(\overset{+}{N}H_3)$					1505, 1498	M	1497, 1490	M	1487, 1483	M
$\delta(CH_2)$	1453	M	1451	S	1458	M	1457	M	1457	Several weak bands
$2\nu(\overset{+}{N}H_3)$					Probably 6000 to 5800			w	broad	
$2\nu_a(CH_2)$	5780	w	5780	w	5810	w	5817	w	5848	w
$\nu_a(CH_2)+\nu_s(CH_2)$	5692	w	5682	w	5714	w	5717	w	5747	w
$\nu_a(\overset{+}{N}H_3)+\delta_a(\overset{+}{N}H_3)$					4587 4541	sh s	4593 4541	s s	4591 4525	s s
$\nu_a(CH_2)+\delta_a(\overset{+}{N}H_3)$					4488	w	4476	w	4484	sh
$\nu_a(\overset{+}{N}H_3)+\delta_s(\overset{+}{N}H_3)$					4434	w	4424	sh	4464	sh
$\nu_a(CH_2)+\delta(CH_2)$	4344	s	4346	s	4359	s	4363	s	4357	s
$\nu_s(CH_2)+\delta(CH_2)$	4277	s	4273	s	4290	s	4288	s	4288	s
$2\delta_a(\overset{+}{N}H_3)$					3223	s	3203	s	3181	s
$\delta_a(\overset{+}{N}H_3)+\delta_s(\overset{+}{N}H_3)$					3112	s	3096	s	3078	s

TABLE II

	Piperidine		Hydrochloride		Hydrobromide	
	cm⁻¹	I	cm⁻¹	I	cm⁻¹	I
$\nu_a(\overset{+}{N}H_2)$ ⎫			2944	VS	2944	VS
$\nu_s(\overset{+}{N}H_2)$ ⎭						
$\nu_a(CH_2)$	2928	VS	2925	VS	2926	S
$\nu_s(CH_2)$	2851	S	2843	S	2837	S
$\delta(\overset{+}{N}H_2)$			1593	M	1590	M
$\delta(CH_2)$	1468, 1454 1444, 1437	M	1464, 1461 1455	M	1463, 1457 1449, 1437	M
$2\nu(\overset{+}{N}H_2)$			Probably 6000 to 5800			w, broad
$2\nu_a(CH_2)$	5797	w	5831	w	5845	w
$\nu_a(CH_2)+\nu_s(CH_2)$	5692	w	5747	w	5747	w
$\nu_a(\overset{+}{N}H_2)+\delta_a(\overset{+}{N}H_2)$			4526	w	4519	w
$\nu_a(\overset{+}{N}H_2)+\delta(CH_2)$			4423	s	4419	s
$\nu_s(CH_2)+\delta(\overset{+}{N}H_2)$			4385	sh	4382	sh
$\nu_a(CH_2)+\delta(CH_2)$	4348	s	4361	s	4357	s
$\nu_s(CH_2)+\delta(CH_2)$	4268	s	4308	s	4305	s

TABLE III

	Triethylamine		Hydrochloride		Hydrobromide		Hydriodide	
	cm^{-1}	I	cm^{-1}	I	cm^{-1}	I	cm^{-1}	I
$\nu(\overset{+}{N}H)$			2600	VS	2668	VS	2760	VS
$\nu_a(CH_3)$	2967	S	2972	S	2962	M	2964	S
$\nu_s(CH_3)$	2874	M	2878	M	2877	M	2873	M
$\nu_a(CH_2)$	2930	S	2935	VS	2929	S	2932	VS
$\nu_s(CH_2)$	2798	S						
$\delta(\overset{+}{N}H)$			1446	M	1435	M	1424	M
$\delta_a(CH_3)$	1464	M	1476	M	1474	M	1464	M
$\delta_s(CH_3)$	1380	S	1399	M	1398	M	1399	M
$\delta(CH_2)$	1453, 1443	M	1480	M	1476	M	1468	M
$2\nu_a(CH_3)$	5882	w	5917	w	5917	w	5920	w
$\nu_a(CH_2)+\nu_s(CH_3)$	5744	w	sh		sh		sh	
$2\nu(\overset{+}{N}H)$			4830?	w, broad				
$\nu_a(CH_3)+\delta_a(CH_3)$	4407	s	4436	s	4425	s	4425	s
$\nu_s(CH_2)+\delta(CH_2)$	4333	vs	4355	s	4348	vs	4348	s
$\nu_s(CH_3)+\delta_s(CH_3)$	4283	sh	4284	m	4264	m	4274	m

are sometimes found as high as 4430 cm^{-1}. We shall not discuss here ternary and higher combinations.

Cyclohexylamine Hydrohalides

In liquid cyclohexylamine (Fig. 1) the 4400–4000 cm^{-1} and the 5800 cm^{-1} areas are very similar to what they are in the spectra of the hydrocarbons and must be due mainly to binary combinations of CH_n vibrations. A medium strong band at 4926 cm^{-1} (with a shoulder at about 4995 cm^{-1}) represents the expected NH_2 stretching+NH_2 bending combinations. Combinations between NH_2 stretching and CH_2 bending vibrations can explain the weaker bands at 4739, 4684, 4615 cm^{-1}. The first NH_2 overtone is at 6502 cm^{-1} (not shown in the figure).

A conspicuous new feature in the spectrum of cyclohexylamine hydrochloride is a strong band at 4541 cm^{-1} with several shoulders and weaker bands at 4488 and 4434 cm^{-1} (Fig. 1).

The asymmetrical $\overset{+}{N}H_3$ stretching band near 2980 cm^{-1} and the asymmetrical $\overset{+}{N}H_3$ bending band near 1615 cm^{-1} are very probably split by removal of their degeneracy, and their frequencies are modified by Fermi resonance with other close-lying bands. Instead of the bending band we actually find a group of four bands at 1620, 1618, 1615, and 1610 cm^{-1}.

Table I contains the fundamentals and the main binary combinations down to about 4300 cm^{-1} with the proposed assignments. The main contributor to the 4600–4500 cm^{-1} absorption is very likely the asymmetrical $\overset{+}{N}H_3$ stretching+asymmetrical $\overset{+}{N}H_3$ bending combination (or combinations). The second largest contribution appears to come from the CH_2 stretching+$\overset{+}{N}H_3$ asymmetrical bending combinations. Minor contributions may come from many other combinations.

In other instances there are two well-defined peaks in this area:

Cyclohexylamine	hydrochloride	4587 sh	4541
	hydrobromide	4593	4541
	hydriodide	4630 sh	4525
		4591	
Tertiary butylamine	hydrochloride	4625 sh	4505
		4575	
	hydrobromide	4625	4484
		4566	
	hydriodide	4612	4468
		4570	
		4535	
Ethylamine	hydrochloride	4598	4525
	hydrobromide	4619	4525
	hydriodide	4617	4521

No one is a single band. This is clearly seen in the case of tertiary butylamine hydriodide where the higher frequency band is split into three well-distinguishable bands.

The value of the 4600–4500 cm^{-1} area for the identification of *primary* amine hydrohalides should be emphasized.

We have to look now for the first overtones of (and combination between) the $\overset{+}{N}H_3$ stretching vibrations. No significant band appears, however. One explanation may be that they coincide with the CH$_3$ and CH$_2$ overtones. This is how Waldron (1) interpreted the near-infrared spectrum of methylamine hydrochloride.

Assigning the 4600–4500 cm^{-1} bands to the stretching overtones (and not to the stretching–bending combinations as we did) does not seem to be reasonable. We measured the spectrum of 1.28 M ethanol in carbon tetrachloride. The associated OH stretching fundamental is at 3360 cm^{-1}, its first overtone at 6329 cm^{-1}. This amounts to a shift of about 400 cm^{-1} from the sum of the fundamentals. If the overtones for $\overset{+}{N}H_3$ are at 4600 cm^{-1}, this would correspond to a shift of almost 1400 cm^{-1}.

Thus we are led to think that the $\overset{+}{N}H_3$ stretching overtones are covered by the CH$_2$ overtones being broad an even weaker than the latter. The weakness of the overtones and their slight anharmonic shift shows that in this case hydrogen-bonding causes only a slight increase in mechanical anharmonicity. In complete analogy with the hydrocarbons the electrical anharmonicity of the bending vibrations appears again as mainly responsible for the relatively high intensity of the combination tones. This is in line with our previous conclusions relative to the infrared spectra of amine hydrohalides (3).

Reference should be made here to papers by Russell and Thompson (8) and Moccia and Thompson (9), who stressed the importance of electrical anharmonicity for the intensity of the overtones in the case of the NH and OH groups respectively.

Piperidine Hydrohalides

In the near-infrared spectrum of piperidine (Fig. 2, Table II), the first overtone of the NH stretching vibration is at 6497 cm^{-1}, the CH$_2$ stretching overtones are at their usual

places, the band at 4762 cm^{-1} may be assigned to the NH stretching+NH bending summation tone (this frequency seems to be somewhat low). The weaker bands at 4608 and 4464 cm^{-1} represent probably NH+CH$_2$ combinations. The strong CH$_2$ combination tones do not go higher than 4348 cm^{-1}.

In the spectrum of the hydrochloride a strong new band appears at 4423 cm^{-1} (with a shoulder at 4385 cm^{-1}) which must be due to the $\overset{+}{\text{N}}$H$_2$ stretching+CH$_2$ bending combinations. There is a weak band at 4526 cm^{-1} to which the $\overset{+}{\text{N}}$H$_2$ stretching+$\overset{+}{\text{N}}$H$_2$ bending and the CH$_2$ stretching+$\overset{+}{\text{N}}$H$_2$ bending combinations must contribute.

In diethyl amine hydrohalides the band between 4600 and 4500 cm^{-1} is stronger but still much weaker than in the primary amine hydrohalides. This must be linked to the lack of degenerate asymmetrical $\overset{+}{\text{N}}$H$_n$ stretching and bending vibrations.

The first overtones of the $\overset{+}{\text{N}}$H$_2$ stretching vibrations are again apparently too weak and are hidden by the CH$_2$ stretching overtones.

Triethylamine Hydrohalides

In the amine itself the strong CH$_n$ combination tone of highest frequency is at 4407 cm^{-1} and shifts to 4436 cm^{-1} in the hydrochloride. In the hydrochloride the $\overset{+}{\text{N}}$H stretching fundamental is near 2600 cm^{-1} and the $\overset{+}{\text{N}}$H deformation band of highest frequency is at 1446 cm^{-1}. Therefore, we would expect an $\overset{+}{\text{N}}$H stretching+$\overset{+}{\text{N}}$H bending summation band near 4000 cm^{-1} and the overtone of the $\overset{+}{\text{N}}$H stretching band well below 5200 cm^{-1}. No one of them can be clearly distinguished, however (Fig. 3, Table III). There are several broad but weak bands between 5600 and 4600 cm^{-1} and the one at 4830 might well be the $\overset{+}{\text{N}}$H stretching overtone. A look at the spectrum shows, however, that this cannot be asserted with any degree of certainty. Nor can we say whether there is a splitting due to a double well potential surface, which is a possibility here as the tertiary amine hydrohalides form significantly stronger hydrogen bonds than the primary and secondary ones (2, 3). The $\overset{+}{\text{N}}$H stretching+bending combination should coincide with a CH$_n$ combination band between 4100 and 4000 cm^{-1}. Actually, the shape of the latter undergoes changes due to hydrohalide formation. CH$_n$ stretching+$\overset{+}{\text{N}}$H bending combinations could explain a shoulder near 4370 cm^{-1} in the hydrobromide and hydriodide.

The weakness of the first overtones of the $\overset{+}{\text{N}}$H$_n$ fundamentals appears to be a common phenomenon for all aliphatic amine hydrohalides.

REFERENCES

1. R. D. WALDRON.   J. Chem. Phys. **21**, 734 (1953).
2. B. CHENON and C. SANDORFY.   Can. J. Chem. **36**, 1181 (1958).
3. C. BRISSETTE and C. SANDORFY.   Can. J. Chem. **38**, 34 (1960).

4. G. HERZBERG. Molecular spectra and molecular structure. Vol. II. Infrared and raman spectra of polyatomic molecules. D. Van Nostrand Co., New York. 1945. pp. 101, 126, 129, 252.
5. W. KAYE. Spectrochim. Acta, 6, 257 (1954).
6. O. H. WHEELER. Chem. Revs. 59, 629 (1959).
7. G. HERZBERG and L. HERZBERG. Can. J. Research, B, 27, 332 (1949).
8. R. A. RUSSELL and H. W. THOMPSON. Proc. Roy. Soc. A, 234, 318 (1956).
9. R. MOCCIA and H. W. THOMPSON. Proc. Roy. Soc. A, 243, 154 (1958).

SPHERICAL AGGLOMERATION OF BARIUM SULPHATE[1]

H. M. Smith[2] and I. E. Puddington

ABSTRACT

The mechanical agglomeration of barium sulphate suspended in organic media into essentially spherical masses has been studied. The presence of a small quantity of water is necessary for the phenomenon to occur. This is regarded as a bridging agent that forms liquid lenses between the particles and binds them together. An equilibrium is set up for this water between the surface of the solid and the bulk suspending medium. The methods of formation of the spherical agglomerates are discussed and their properties examined.

INTRODUCTION

Flocculation of the solid constituents, which is frequently desirable to promote more rapid settling in suspension, almost invariably results in a large increase in the final volume of the sediment obtained. An exception to this general behavior was reported by Stock (1), who observed that when dried, finely divided barium sulphate suspended in dry benzene in cylindrical containers was shaken with a reciprocating motion, discrete spheres of 0.5 to 1.0 mm in diameter were formed. These settled rapidly to a volume considerably less than that obtained from an equal amount of the suspension that had not been shaken. It was tentatively suggested that the phenomenon was owing to the tendency of the hydrophilic barium sulphate to aggregate in such a way that a minimum surface was exposed to the hydrophobic benzene. Thus the phenomenon was considered to be somewhat analogous to the formation of droplets when two immiscible liquids are shaken together.

The pronounced flocculating influence of small quantities of water on suspensions of solids having hydrophilic surfaces in organic media has been frequently reported (2, 3, 4, 5). A few preliminary experiments demonstrated that the phenomenon observed by Stock (1) did not occur if the system were thoroughly dry and the present work was undertaken to ascertain the conditions necessary for the formation of spherical agglomerates with barium sulphate suspended in benzene and, if possible, to give an indication of how the technique might be applied to other systems.

EXPERIMENTAL

Procedure

Suspensions were prepared by weighing 4-g portions of pure barium sulphate directly into sample holders which were subsequently sealed to a vacuum system equipped with facilities for B.E.T. surface area measurements. The barium sulphate was freed from water by heating the samples to 200° C and reducing the pressure to about 10^{-5} mm Hg. B.E.T. surface areas (6) were determined in the usual way. The nitrogen adsorption isotherms were all of the reversible S-type, characteristic of adsorption on a non-porous solid. A known volume of benzene, usually about 20 ml, was then condensed from a doser into the sample holder and, similarly, water was added if desired in quantities from 2 mg upwards. After being sealed off, the vessel was shaken for a period of 12 hours or more. For most of the work a mechanical horizontal shaker that had a frequency of

4 cycles per second with a displacement of 6 cm was used. Visual observation of the specimens usually showed no further change after about half an hour but the longer shaking period was convenient and it ensured that equilibrium was reached. The sedimentation volume of the barium sulphate was determined from calibrations on the sample container. Readings were taken after the suspension had been allowed to settle under gravity for a week although little change was observed after 48 hours.

A number of qualitative experiments were also carried out using flat-bottomed, stoppered cylindrical containers in which 4 g of the barium sulphate had been dried in an oven at 200° C overnight and cooled in a vacuum desiccator. The liquids were added rapidly and the tubes quickly stoppered before they were placed in the shaker. This method enabled a wider range of systems and conditions to be studied without the tedious experimentation with the vacuum system. Blank runs were always performed in order to check against accidental contamination from the atmosphere. Twenty milliliters of the suspending liquid was normally used with 0.1 ml of bridging agent.

Water in the supernatant benzene was determined by the Karl Fischer method (7). The saturation value of water in benzene at 25° C determined in the work was 0.046% w/v. This value is the same as that calculated from the nomogram given by Davis (8) based on data determined by Jones and Taylor (9) using a tritium oxide analysis method.

Preparation of Materials

Reagent grade, thiophene-free benzene was shaken and left in contact with calcium hydride for 2 weeks. After the benzene was passed through a column containing dried silica gel, alumina, and calcium hydride into a distillation flask containing more calcium hydride, it was finally distilled into a storage vessel which had been previously dried by heating under reduced pressure. Benzene was distilled from the storage vessel into the prepared system when required.

Other organic liquids were reagent grade and dried for several weeks over anhydrous calcium sulphate before use.

Deionized water was obtained from an Amberlite MB1, mixed bed ion exchange column and placed in a small water storage flask. Dissolved gases were substantially removed from the water by evacuation of the system for 1/2 hour.

Barium sulphate was prepared from reagent grade barium chloride. The chloride was first dried at 140° C and then washed with absolute ethyl alcohol to remove traces of strontium and calcium, followed by drying again at 140° C. It was dissolved in warm water and reagent grade concentrated sulphuric acid was added with stirring. After settling, the barium sulphate was washed many times with distilled water and finally with equilibrium water. Spectrographic analysis revealed fewer impurities in the specimen than the reference material (Johnson, Matthey & Co. Ltd. spectroscopically pure barium carbonate). The purified barium sulphate was crushed in an agate mortar and passed through a 200-mesh sieve before being sealed onto the vacuum system in its container. Electron micrographs showed that the particle size was mostly in the range 0.2 to 1 micron diameter. The particles were approximately spherical but had some flat faces on them extending up to 0.5 micron in length.

RESULTS

Preliminary runs showed that no agglomeration took place when the system contained no water. With small additions of water voluminous flocs were formed after agitation but it was only with further additions of water that spherical agglomerates were apparent.

Experiments were conducted with identical 4-g portions of barium sulphate using different amounts of benzene and water to determine the distribution of water between the barium sulphate and benzene. The results are given in Table I. From the analyses of the supernatant liquid, the water associated with the barium sulphate was calculated.

TABLE I

Distribution of water between barium sulphate and benzene

Benzene used, ml	Total water added, g	Water in benzene, % w/v	Water with BaSO₄, g/100 g	Water in benzene / Total water
18.35	0.0049	0.013	0.0633	0.026
18.10	0.0069	0.017	0.0953	0.025
35.25	0.0110	0.016	0.1333	0.015
16.52	0.0097	0.019	0.1633	0.020
36.91	0.0219	0.041	0.1695	0.019
34.27	0.0288	0.046	0.3258	0.016
17.61	0.0231	0.046	0.3743	0.020
17.53	0.0235	0.041	0.4083	0.017

The ratio water in benzene (g/ml)/total water added (g) was found to be approximately constant below the saturation point of the benzene, the average value being 0.020.

Further experiments established the amount of water associated with the barium sulphate over the complete range of water content where flocculation and spherical agglomeration occur. Figure 1 shows the sedimentation volume of the settled barium sulphate
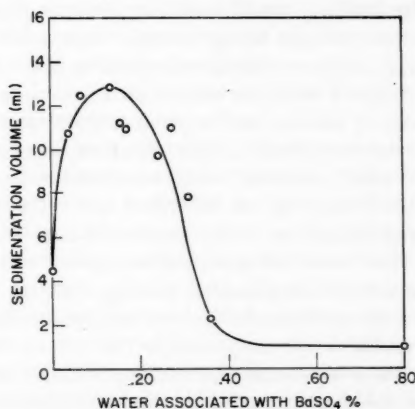

FIG. 1.   The effect of water on the sedimentation volume of barium sulphate.

as a function of its water content. It is seen that, with the first additions of water, flocculation causes the settled volume to increase. On further additions the volume decreases with some of the particles forming spherical-shaped clusters. Finally, when enough water has been added, good spherical agglomerates are formed. For the area of barium sulphate considered here, 18 sq. meter/g, the necessary amount of water to form completely spherical agglomerates is 0.3125 g/100 g. If the water is less than this amount, only partial spherical agglomeration occurs. Taking the area of the water

molecule as 10.5 sq. Å, the above water is only sufficient to give an average monolayer coverage of about 60% with the specimen considered here.

Qualitative experiments were carried out using benzene to which small amounts of nitromethane, nitrobenzene, or acetonitrile were added. These three substances would not promote the spherical agglomeration without a small quantity of added water. However, since much less water was necessary under these conditions to give agglomeration, these three substances enhanced considerably the effect of the water.

Good spheres of barium sulphate were formed on agitation when the following liquids containing the appropriate amount of water were substituted for benzene: toluene, nitrobenzene, diethyl ether, chloroform, carbon tetrachloride, n-hexane, cyclohexane. If systems were rigorously dried, however, no agglomerates were apparent.

The effect of shaking at reduced temperatures was studied using the technique of the qualitative experiments with toluene as the suspending medium. The tubes were cooled by placing them in a copper jacket which had circulating ethylene glycol in a surrounding cooling coil. A run at $-2°$ C gave the same result as the blank shaken at room temperature with good agglomerates being formed. A run held over the range $-17°$ to $-20°$ C gave no spheres and the barium sulphate remained virtually unchanged. It is to be noted that collision of the particles probably causes the temperature at the point of impact to rise and, although the outside of the tube was kept below $-17°$ C, higher temperatures may have existed at the interfaces of colliding particles. The conclusion may be drawn from the above experiments, however, that for spherical agglomeration to occur the water must be in a liquid form and free to form the linkages between the particles.

Knacke and Pohl (10) report that in the formation of granules by standard pelletization processes, added salts in the binding liquid result in stronger granules. The increased strength was attributed to salt bridges being formed. Experiments using normal and saturated (25° C) reagent grade sodium chloride solutions in place of water gave agglomerates which appeared not to differ from the blank run where only water was used.

The effect of different modes of shaking for the production of the spheres was reviewed. Although a detailed study involving different rates of motion was not made, each method was tested under conditions which appeared most favorable for the formation of agglomerates. Reciprocating horizontal shaking as described gave the best results. Rolling end-over-end gave good agglomerates but rather smaller in size. With horizontal rolling, dense agglomerates formed which were less spherical and uniform in size than those given by the other methods of agitation. Longitudinal rocking through a circular path gave few agglomerates and these were neither spherical nor uniform in size. Vibration applied to the tube gave negative results. Apparently motion that allows the initial flocs to roll with not too much impact or shear is desirable for the densification to occur. No difference in behavior was noted when the diameter of the cylindrical glass containers was varied from 15 to 45 mm, each being filled to the same height. Rendering the surfaces of the tubes lyophobic with "dri-film" eliminated the very fine coating of barium sulphate that normally occurs. It is probable that in all the experiments with untreated tubes, the glass surface adsorbs water which binds a small amount of the barium sulphate. The amounts of water and barium sulphate involved with this effect were not important in the over-all quantitative runs, however.

When the spherical agglomerates were drained of their supernatant liquid and left to dry in the air, good free-flowing particles were obtained. They could be transferred without dusting and withstood a force of the order of 10^5 dynes before being crushed. No difference was observed when the particles were maintained for 24 hours at a pressure

of 10^{-5} mm Hg, and heating at 200° C for 24 hours at this pressure produced no visible effect.

When immersed in water, some of the dried spheres rapidly shattered but most remained unaltered. There was no change after 24 hours. This shattering was probably due to a large hydrostatic pressure being set up in any small pores present. Similar results were obtained when benzene was added to the dried spheres. It is apparent that, once formed, the spherical aggregates retain their shape when allowed to air-dry, the ultimate particles being held together by fairly strong forces.

If the barium sulphate spheres were drained of their supernatant liquid and, before they had dried, a large volume of water was added, the particles lost their spherical shape leaving a creamy suspension of barium sulphate. The bridging liquid appears to bind the particles into agglomerates by virtue of surface tension forces which disappear when the interface is removed through the addition of excess bridging liquid.

X-Ray analysis showed no detectable change in crystal structure or cell size with the formation of the spheres. It appeared, however, that the spheres were of somewhat greater crystalline perfection than the original material and thus the treatment appears to have stimulated a recrystallization or its equivalent.

Increasing amounts of water beyond the minimum necessary for spherical aggregation increases the diameter of the agglomerates. The results were somewhat erratic, however, due to differences with the initial formation. If particles group in different ways initially, a direct relationship between added water and diameter of formed spheres would not be expected. With a run in which 0.50 g of water was added, the barium sulphate formed into one sphere of approximately 1.2 cm in diameter. Further additions of water resulted in the solid adhering to the walls of the tube in a sticky mass, the spherical form of the agglomerate being lost. A continued increase of water resulted in a separate aqueous phase in which the barium sulphate remains.

Apparent density measurements on two groups of six particles, having mean diameters of 0.3 and 0.8 mm, respectively, gave values of 2.7 and 2.9 g per cc. The void volume of the spheres is therefore about 30 to 35%. The two samples, examined microscopically, were remarkably good spheres and quite uniform in diameter. A possible mechanism by which the spheres grow was suggested by the examination of a third sample, where, apparently, slightly more water was present in the system than the amount required for the compact spheres that were initially formed and sufficient excess was available to flocculate a number of these spheres into groups of two, three, or four by the Kruyt and van Selms mechanism. Further agitation had compressed these into dumbells, disks, tetrahedra, etc. in which the outlines of the original spheres were clearly visible. Obviously further mechanical action could form these into new spheres with volumes approximately simple multiples of the spheres originally formed. Were the process to be carried out on a lyophilic suspension in which the particles become partially desolvated by the bridging liquid, considerable increase in the size of the spheres might be expected with continued shaking owing to the excess of bridging liquid made available by the shrinkage of the solid.

DISCUSSION

Apparently the added small quantity of water displaces organic solvent from part of the barium sulphate surface. An equilibrium is set up between the water molecules on the barium sulphate surface and in the organic solvent. When the solid particles are brought in sufficiently close proximity by the agitation, the adsorbed water links the

particles by forming a water lens or bridge between them. With the first additions of water, the particles are held together in loose clusters, voluminous flocs being formed. However, with further additions of water more linkages are possible and with the aid of mechanical agitation the particles are able to assume a more closely packed pattern and ultimately an over-all compact, spherical shape. The flat faces of the ultimate particles may have some significance in the amount of bridging liquid necessary. As still more water is added larger spheres which require more junctions per unit volume are formed with the extra bridging liquid. Where organic liquids, along with water, act as a bridging agent, it is probable that the water promotes the adsorption of both species on the solid surface. There is, as before, an equilibrium set up with the organic suspending medium.

The barium sulphate/benzene/water system is well suited for the observation of the phenomenon. The barium sulphate has a very low solubility in both benzene and water as well as being chemically inert to both liquids. The water acting as the bridging agent has a low solubility in the benzene and in this system the benzene is saturated with water before spherical agglomerates are formed. This is not regarded as being essential to the phenomenon but depends on the relative affinities of the solid and organic medium for the bridging liquid.

Other systems meeting these requirements should show the phenomenon and the success of obtaining the spherical agglomerates will depend on how readily these factors are met.

ACKNOWLEDGMENT

REFERENCES

 1. D. I. STOCK.   Nature, **170**, 423 (1952).
 2. W. D. HARKINS and D. M. GANS.   J. Phys. Chem. **36**, 86 (1932).
 3. H. R. KRUYT and F. G. VAN SELMS.   Rec. trav. chim. **62**, 415 (1943).
 4. A. E. J. EGGLETON and I. E. PUDDINGTON.   Can. J. Chem. **32**, 86 (1954).
 5. M. J. VOLD.   J. Colloid Sci. **14**, 168 (1959).
 6. S. BRUNAUER, P. H. EMMETT, and E. TELLER.   J. Am. Chem. Soc. **60**, 309 (1938).
 7. K. FISCHER.   Angew. Chem. **48**, 394 (1935).
 8. D. S. DAVIS.   Chem. Process Eng. **38**, 341 (1957).
 9. G. G. JORIS and H. S. TAYLOR.   J. Chem. Phys. **16**, 45 (1948).
10. O. KNACKE and H. POHL.   Chem. Ing. Tech. **31**, 50 (1959).

A NEW SYNTHESIS OF METHYL β-D-GULOPYRANOSIDE[1]

N. J. Antia and M. B. Perry

ABSTRACT

The oxidation of 1 mole of β-D-glycero-D-gulo-heptopyranoside with 1 mole of sodium metaperiodate, followed by reduction with sodium borohydride, gave rise to crystalline methyl β-D-gulopyranoside. The method provides a new synthetic route to the D-guloside and, thence, to D-glucose. The possibility of utilizing this reaction scheme as a general convenient method for preparing the relatively rare aldohexoses as well as for "labelling" carbon atom 1 of these compounds is discussed.

It was shown recently by Perry and Pietak (1) that the periodate oxidation of aldo-heptoses proceeds in nearly discrete stages, with the sugars being oxidized in their cyclic forms. Consumption of the first mole of oxidant per mole was correlated with the almost exclusive scission of the C_6–C_7 (exocyclic) bond of the heptose. This observation appeared to be of great potential value for the facile synthesis of hexoses not readily available. The controlled oxidation of 1 mole of the heptose with 1 mole of periodate would be expected to yield the corresponding hexodialdose, which would require a selective reduction of the —CHO group at C_6 to give the corresponding hexose. The reduction step was considered to present insuperable difficulties and, accordingly, we turned our attention to the application of the reaction sequence to the heptosides, where such selective reduction would not be required. An analogous series of reactions was used by Foster, Davies, and Crumpton (2) in their conversion of heptose units in polysaccharides to hexose units.

Methyl β-D-glycero-D-gulo-heptopyranoside had been prepared by Fisher (3) and a proof of its pyranoside structure had been offered by Haworth, Hirst, and Stacey (4). We have prepared the heptoside by the method of the latter authors, but have found difficulty in separating it from contaminating heptose. One mole of the methyl β-D-glycero-D-gulo-heptopyranoside (I) was oxidized with 1 mole of sodium metaperiodate in unbuffered medium, and the product (II) was directly reduced with an excess of sodium borohydride. After deionization with ion-exchange resins, crystalline methyl β-D-gulopyranoside (III) was isolated in 30% yield. Attempts to isolate the guloside from the borohydride reduction reaction without recourse to resin deionization, by acetylation with acetic anhydride/pyridine or by p-nitrobenzoylation, failed to yield crystalline material. The D-guloside was shown (a) to be homogeneous, by paper chromatography in three solvent systems, and (b) to be identical with a sample obtained from Dr. Isbell (5, 6). The identity was established by comparison of infrared spectra and by mixed melting point determination. The pyranoside structure of the D-guloside was confirmed by periodate oxidation studies (2 moles of periodate consumed, 1 mole of formic acid liberated). Mineral acid hydrolysis of the D-guloside gave predominantly a reducing sugar identified as gulose from paper chromatographic evidence.

The synthesis reported above suggests that other heptosides may similarly be converted to the corresponding hexosides, and the method appears to offer a convenient, general, synthetic route for the conversion of heptoses to hexoses. The particular value of this synthetic method lies in (a) the simplicity and ease of preparation, in quantity, of the relatively rare hexoses, and (b) the possibility of selectively "labelling" a hexose
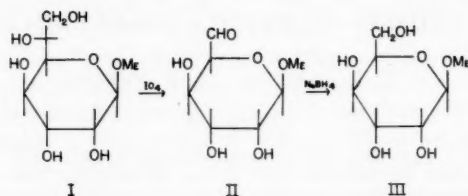
at carbon atom 1 by starting with a $1\text{-}C^{14}$-heptose. Obviously the preparative value of the method will be governed by the ease of availability of aldoheptoses. Both classical Kiliani/Fischer cyanohydrin synthetic method (7) and the more recent nitromethane/ Nef reaction scheme of synthesis (8) provide convenient preparative routes to aldoheptoses from aldohexoses. Both of these methods effect the addition of a one-carbon fragment to the carbon atom 1 of the hexose. The incoming carbon atom may be "labelled" by the use of $HC^{14}N$ or $C^{14}H_3NO_2$. In this way, a readily available hexose (e.g., D-glucose) may be converted to a $1\text{-}C^{14}$-aldoheptose (e.g., D-glycero-D-gulo-heptose) which, by the application of the synthetic scheme described above, may be further converted to the desired $1\text{-}C^{14}$-hexose (e.g., D-gulose).

EXPERIMENTAL

All melting points reported are uncorrected.

Paper chromatography was performed by the descending method on Whatman No. 1 paper, using the following solvent systems:

>   solvent I: 1-butanol/ethanol/water (3:1:1 v/v);
>   solvent II: 1-butanol/pyridine/water (10:3:3 v/v);
>   solvent III: ethyl acetate/acetic acid/water (9:2:2 v/v).

The following sprays were used to detect the sugars on the chromatograms: (A) 2% solution of p-anisidine hydrochloride in 1-butanol, (B) 1% solution of silver nitrate in acetone, followed by 2% ethanolic sodium hydroxide, and (C) saturated aqueous solution of potassium periodate followed, 6 minutes later, by benzidine reagent (9). The rate of movement of the sugars on the chromatograms is given relative to that of 2,3,4,6-tetra-O-methyl-D-glucose (R_{TMG}) or of rhamnose (R_{Rha}).

Methyl β-D-Glycero-D-gulo-heptopyranoside

The glycoside was prepared by refluxing D-glycero-D-gulo-heptose (m.p. 190–192°) with 3–5% methanolic hydrogen chloride for 24–48 hours. Yields of the crude crystalline product were of the order obtained by Haworth, Hirst, and Stacey (4). After two recrystallizations from alcohol, the glycoside had a melting point of 166–168°, $[\alpha]_D^{20} -72°\pm2°$ (c, 1.1 in water). Paper chromatography in solvents I and II showed the presence of a heptose. Treatment of the glycoside in aqueous solution with Dowex 1-X2(OH) (by agitation with the resin at room temperature for 20 hours, followed by passage of the solution down a column of the resin) effected removal of most of the contaminating heptose, but traces were still detectable. The treated glycoside crystallized from alcohol as colorless prisms with the same melting point and optical rotation as given above. The following R_{TMG} values were observed for the heptoside: solvent I, 0.33; solvent II, 0.35; solvent III, 0.41.

Methyl β-D-*Gulopyranoside*

The calculated quantity of an aqueous solution of sodium metaperiodate (49.18 ml, 0.045 M NaIO$_4$) was added slowly to a stirred solution of methyl β-D-glycero-D-gulo-heptopyranoside (0.4935 g) in water (25 ml) cooled to 0°. After addition was complete, the solution was agitated for 2 hours at room temperature and allowed to stand overnight. The solution was next cooled to 0°, and a solution of sodium borohydride (0.8 g) in water (25 ml) was added slowly, with mechanical agitation. The solution was agitated for 2 hours at room temperature and allowed to stand overnight. The pH of the solution was adjusted to 5 by the addition of 50% aqueous acetic acid with mechanical agitation and cooling. After 1 hour at room temperature, a test sample showed no reduction of Fehling's solution (absence of reducing sugar as well as of borohydride). The solution (160 ml) was divided into halves at this stage. One half was used for the attempted iso-lation of the D-guloside by (*a*) acetylation and (*b*) *p*-nitrobenzoylation. The other half was passed successively through columns of Amberlite IR-120(H) and Duolite A-4(OH) ion-exchange resins. The pH of the eluent from the latter column was ca. 3–4 and it was found necessary to deionize the solution further by passing it through Dowex 1-X2(OH) resin. This solution (pH7) was evaporated to dryness *in vacuo* and the residual boric acid was removed as methyl borate by repeated evaporation *in vacuo* with methanol. The residue was next extracted with ethanol, the ethanol-insoluble material being rejected (negative reaction to Molisch reagent). The ethanol extract (0.22 g) was taken up in boiling ethanol, allowed to cool, and ethyl acetate was added to incipient turbidity. The solution was allowed to crystallize at 0–5° for 4 days. Methyl β-D-gulopyranoside crystallized as prisms (0.065 g), m.p. 178–180°, $[\alpha]_D^{20}$ −87.9° (*c*, 1.03 in water). The mother liquors failed to yield any further crystalline product. The over-all yield of the D-guloside was ca. 30% of the theoretical. Isbell (6) has given the following constants for the D-guloside, m.p. 176°, $[\alpha]_D^{20}$ −83°. A mixed melting point determination of the D-guloside with Isbell's sample showed no depression. The infrared spectra (KBr disk) of the D-guloside samples were identical.

The attempted acetylation of the D-guloside with acetic anhydride and pyridine failed to give a crystalline product, although Isbell (5) has described a crystalline tetraacetate.

Paper chromatography of the D-guloside showed (*a*) complete absence of reducing sugars, and (*b*) a homogeneous product having the following R_{TMG} values: solvent I, 0.44; solvent II, 0.51; solvent III, 0.51.

Periodate oxidation studies: The D-guloside (19.4 mg) was oxidized at 0–4° with an aqueous solution of sodium metaperiodate (5 ml, 0.1 M NaIO$_4$), the total volume of the reaction mixture being adjusted to 100 ml with distilled water. Aliquots (5 ml) of the reaction mixture were taken at the time intervals stated in Table I, in order to determine the periodate consumed and the formic acid liberated. These determinations were carried out by standard methods.

TABLE I

Periodate oxidation of methyl β-D-gulopyranoside

Oxidation period, hours	Periodate uptake, moles per mole	Formic acid release, moles per mole
1	1.92	0.94
2	2.02	0.94
4	2.02	0.96
21	1.98	0.96

D-*Gulose*

The D-guloside (10 mg) was hydrolyzed with N HCl (10 ml) (refluxed for 2 hours), the mineral acid was neutralized with silver carbonate, and the product was worked up in the usual manner. No attempt was made to crystallize the D-gulose or to prepare a derivative.

Paper chromatography of the product showed the presence of a reducing sugar as the major component, along with traces of what may be 1,6-anhydro-D-gulose, oligosaccharides, and polymeric material formed by the acid treatment. The reducing sugar was identified as D-gulose by comparison of R_{Rha} values with those of D-mannose (see Table II). Thomas (10) has shown that these two sugars are virtually inseparable on paper chromatograms in the solvent systems used.

TABLE II

R_{Rha} values of some reducing sugars

Sugar	Solvent system		
	I	II	III
D-Gulose	0.54	0.52	0.74
D-Mannose	0.62	0.55	0.80
D-Glycero-D-gulo-heptose	0.41	0.31	0.69

ACKNOWLEDGMENTS

REFERENCES

1. M. B. PERRY and T. PIETAK. The periodate oxidation of aldoheptoses. Paper presented to the Royal Society of Canada, June Meeting, Kingston, Ontario. 1960.
2. A. B. FOSTER, D. A. L. DAVIES, and M. J. CRUMPTON. Nature, **181**, 412 (1958).
3. E. FISCHER. Ber. **28**, 1156 (1895).
4. W. N. HAWORTH, E. L. HIRST, and M. STACEY. J. Chem. Soc. 2864 (1931).
5. H. S. ISBELL. J. Research Natl. Bur. Standards, **8**, 1 (1932).
6. H. S. ISBELL. Proc. Natl. Acad. Sci. U.S. **16**, 699 (1930).
7. C. S. HUDSON. Advances in Carbohydrate Chem. **1**, 1 (1945).
8. J. C. SOWDEN. Advances in Carbohydrate Chem. **6**, 291 (1951).
9. J. A. CIFONELLI and F. SMITH. Anal. Chem. **26**, 1132 (1954).
10. G. H. S. THOMAS. Studies on Polyuronides. M.A. Thesis, Queen's University, Kingston, Ontario. 1956.

EXPERIMENTAL STUDIES OF SOLUTION PROCESSES
VI. EFFECT OF SOLVENT ON INFRARED ABSORPTION SPECTRA[1]

P. A. D. DE MAINE,[2] L. H. DALY, AND M. M. DE MAINE[2]

ABSTRACT

Here are reported infrared absorption data between 4000 cm^{-1} and 700 cm^{-1} near 19° C for methanol, n-propanol, isopropanol, cyclohexanol, benzyl alcohol, diethyl ether, anisole, 1,4-dioxane, diisopropyl ether, nitromethane, acetone, p-xylene, benzene, and hexane as pure substances and in carbon tetrachloride solution. Band frequencies accurate to within 1 cm^{-1} are reported. Except for the 3340 cm^{-1} band in dilute MeOH solutions no frequency shifts were observed even with gross changes of the electrical properties of the solutions. Molar extinction coefficients at absorption maxima are discussed briefly.

INTRODUCTION

During the last 5 years several workers have reported results of experimental and theoretical investigations of solvent effects on infrared absorption spectra. Excellent summaries of these data are found in Spectrochimica Acta (1, 2, 3, 4, 5) and in Annual Reports of the Chemical Society (6). Thompson (5), la Lau (4), and Bellamy (1) have shown that the Kirkwood–Bauer–Magat equation (7, 8) cannot be used to explain many frequency shifts observed for different solvents. Bellamy *et al.* (9, 10) have demonstrated that the frequency shifts observed for X—H and carbonyl stretching vibrations result from specific interactions between solute and solvent molecules.

De Maine (11) has reported that all the band frequencies for nitromethane dissolved in carbon tetrachloride do not shift even for gross changes in solution composition. However, Brown (2) has quoted the work of Bayliss *et al.* (12) as evidence that for non-polar solvents the frequency shifts appear to depend only on the dielectric constant of the solvent, as predicted by the Kirkwood–Bauer–Magat equation (7, 8).

La Lau (4) has shown that the Debye (13) or Onsager (14) equations for the integrated band intensities must be replaced by a more complicated expression which cannot be handled easily. Coulson (3) has attributed changes of the integrated band intensities with solvent to small changes in the term $\partial\mu/\partial Q$ (μ, dipole moment; Q, normal co-ordinate) which does not necessarily cause a frequency shift. Thompson (5) has quoted numerous workers to support his assertion that neither the Debye equation (13) nor the Onsager equation (14) gives a satisfactory explanation for changes in band intensities with solvent.

In this work we report band frequencies for five alcohols, four ethers, acetone, benzene, nitromethane, p-xylene, and hexane as pure substances and in carbon tetrachloride solution. No frequency shifts are observed even with gross changes in the composition of the solutions.

EXPERIMENTAL

Solutions were made by diluting the pure substance with carbon tetrachloride to the required volumes. Actual concentrations were calculated with density data for the pure solvents (15) as described elsewhere (16). The concentration ranges and number of samples studied are given in Table I.

TABLE I

Data of experiments with the solvents indicated

Compound	Source	Grade	Concentration range (moles/l.)	Cell length	No. of samples
Carbon tetrachloride	Fisher	Spectrograde	—	.028	—
Methanol	Fisher	Spectrograde	.019–24.75	.028, 5.00	36
n-Propanol	Fisher	Cert. reagent	.107–13.39	.028	13
Isopropanol	Fisher	Cert. reagent	.105–13.08	.028	13
Cyclohexanol	Fisher	Reagent	.095–12.10	.028	12
Benzyl alcohol	Fisher	Cert. reagent	.078–9.70	.028	12
Diethyl ether	Mallinckrodt	Anal. reagent	.077–9.63	.028	12
Diisopropyl ether	Eastman Kodak	Red Label	.057–7.10	.028	12
1,4-Dioxane	Fisher	Spectrograde	.094–11.70	.028	12
Anisole	Fisher	Reagent	.074–9.21	.028	12
Nitromethane	Eastman Kodak	Spectrograde	.278–18.51	.028	20
Actone	Fisher	Cert. reagent	.109–13.64	.028	11
p-Xylene	Eastman Kodak	White Label	.065–8.11	.028	11
Benzene	Mallinckrodt	Reagent	.090–11.25	.028	11
Hexane	Fisher	Spectrograde	.061–7.65	.028	11

All measurements were made with a Perkin–Elmer Model 21 double-beam infrared spectrophotometer with sodium chloride optics. Absorption by carbon tetrachloride was cancelled by use of a variable path-length cell filled with pure carbon tetrachloride in the reference beam. Base lines were obtained with both cells filled with carbon tetrachloride before each set of measurements. Samples were run starting with the most dilute and increasing the concentration of solute. The decreasing concentration of solvent was compensated for by a decrease in the path length of the cell in the reference beam.

Each sample was scanned from 4000 cm^{-1} to 700 cm^{-1}. The temperature was $19 \pm 2°$ C. Repeated measurements showed that band frequencies between 2000 cm^{-1} and 700 cm^{-1} could be reproduced to within 1 cm^{-1}. At higher frequencies (4000 to 2000 cm^{-1}) reproducibility was within 4 cm^{-1}. No changes in the spectra of samples were observed even after 8 hours.

RESULTS

Dielectric constants, refractive indices, and observed band frequencies for the 15 pure solvents studied are given in Table II. Except for the center of the hydrogen bond band (near 3340 cm^{-1} in pure alcohols), no measurable frequency shifts were observed for any band of any solute – carbon tetrachloride pair studied, even for large changes in the electrical properties of the solutions.

In agreement with other workers, we observed that the broad band with center near 3340 cm^{-1}, which is common to all alcohols (Table II), does not shift measurably in passing from the pure alcohol to carbon tetrachloride solutions with near 0.200 mole per liter of methanol, n-propanol, isopropanol, cyclohexanol, or benzyl alcohol. Figure 1 provides data for the methanol – carbon tetrachloride system. In carbon tetrachloride solutions with alcohol concentration less than about 0.200 M, the hydrogen bond band first changes shape and on further dilution, it disappears. Figure 2 illustrates these changes for methanol – carbon tetrachloride, together with the isolation of a weak band near 3640 cm^{-1} which is observed first in a 1.485 M methanol solution and which shows no measurable frequency shift on further dilution of the methanol solution with carbon tetrachloride.

Extinction coefficients at all absorption maxima were calculated for all solutions studied.

TABLE II

Dielectric constants (ε), refractive indices (η), and observed band frequencies for the pure liquids indicated near 20° C

CCl₄	MeOH	n-Propyl alcohol	Isopropyl alcohol	Cyclo-hexanol	Benzyl alcohol	Ethyl ether	Isopropyl ether	Dioxane	Anisole	Nitro-methane	Acetone	p-Xylene	Benzene	Hexane
975	1030	855	812	842	695	842	845	874	880	850	895	955	845	880
1002	1110	885	950	860	729	914	903	885	994	875	1085	1020	1034	900
1215	1450	901	1102	886	812	930	1010	1047	1020	917	1215	1039	1174	949
1250	2058	965	1126	924	840	1021	1106	1083	1041	1099	1359	1100	1390	980
1555	2228	1013	1158	969	906	1040	1123	1121	1075	1378	1415	1116	1480	1035
	2520	1051	1300	1025	1013	1075	1166	1254	1105	1400	1430	1180	1525	1062
	2838	1095	1340	1065	1031	1116	1186	1289	1150	1425	1710	1219	1616	1131
	2955	1232	1378	1135	1055	1150	1301	1322	1170	1565	2004	1240	1669	1170
	3340	1344	1405	1171	1076	1278	1368	1365	1180	1830	2140	1378	1746	1291
		1381	1465	1235	1205	1295	1379	1454	1245	2040	2260	1450	1810	1340
		1455	1758	1255	1300	1350	1466	1720	1286	2300	2438	1516	1967	1376
		1940	1900	1294	1330	1381	1804	1900	1301	2470	2578	1630	2210	1460
		2874	2080	1346	1380	1414	1910	1965	1335	2800	2928	1786	3040	2720
		2960	2190	1365	1455	1444	2630	2130	1390	2942	2970	1830	3080	2844
		3340	2400	1451	1495	1487	2880	2222	1440	3050	3002	1890		2960
			2657	1696	1586	1970	2936	2280	1453		3400	2100		
			2875	2660	1606	2280	2978	2572	1466		3520	2310		
			2920	2960	1704	2600	3160	2685	1496		3610	2404		
			2970	2940	1804	2858		2850	1588			2580		
			3340	3340	1874	2930		2910	1600			2724		
					1956	2970		2962	1690			2862		
					2400	3482			1765			2922		
					2865				1832			3000		
					2920				1930					
					3024				2040					
					3040				2082					
					3340				2288					
									2480					
									2540					
									2838					
									2944					
									3020					
ε 2.219[a]	31.20[a]	22.20[a]	17.95[a]	14.96[c]	13.10[c]	4.376[a]	—	2.235[a]	—	34.093[a]	21.45[a]	2.270[c]	2.2925[a]	1.904[a]
η 1.4104[c]	1.331[c]	1.385[a]	1.394[a]	1.466[c]	1.5396[b]	1.350[b]	—	1.420[a]	1.518[c]	1.5526[a]	1.3616[a]	1.4958[c]	1.5011[a]	1.3749[a]

[a]B. E. Conway. Electrochemical data. Elsevier Publ. Co., London. 1952.
[b]Handbook of chemistry and physics. 35th ed. Chemical Rubber Pub. Co., Cleveland. 1954.
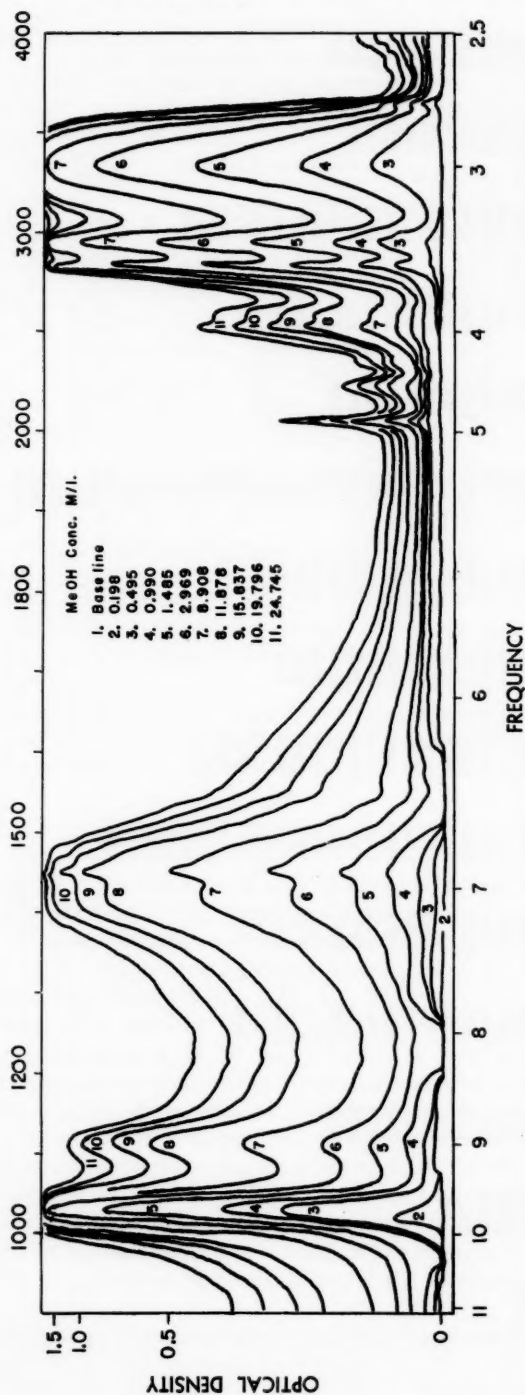[c]Langes Handbook of chemistry. 9th ed. Handb. Publ. Inc., Sandusky, Ohio. 1956.

Fig. 1. Infrared absorption spectra between 800 cm⁻¹ and 4000 cm⁻¹ for pure methanol and for methanol dissolved in carbon tetrachloride near 19° C. Absorption by carbon tetrachloride has been subtracted. The methanol concentrations (in moles/liter) are indicated. Cell length is 0.028 mm.
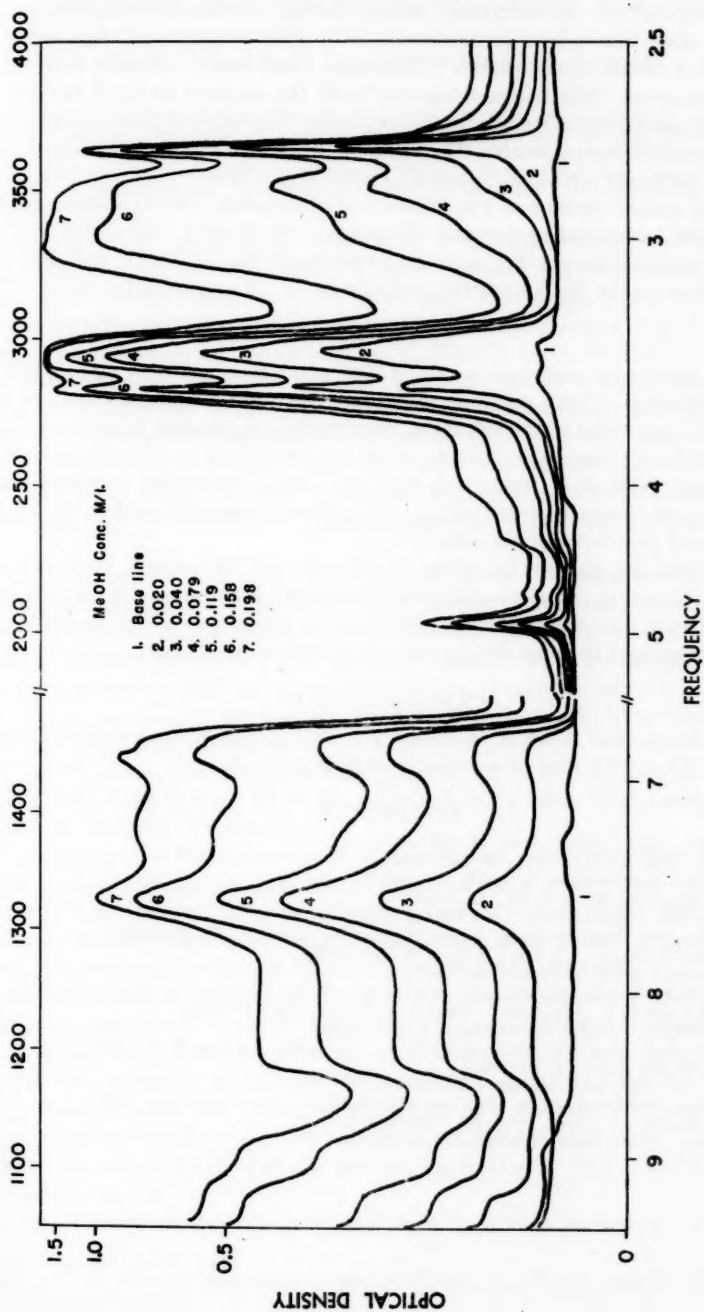
FIG. 2. Infrared absorption spectra between 1275 cm^{-1} and 4000 cm^{-1} for dilute solutions of methanol in carbon tetrachloride near 19° C. Absorption by carbon tetrachloride has been subtracted. Cell length is 5.000 mm. Methanol concentrations are indicated.

Within a 10% limit of reliability all bands between 3100 and 800 cm^{-1} for methanol, n-propanol, isopropanol, cyclohexanol, benzyl alcohol, nitromethane, acetone, hexane, and p-xylene obey Beer's law. In agreement with other workers we observed that the broad band with center near 3340 cm^{-1} (hydrogen bond band) increases with increasing alcohol concentration. This increase together with the changes in band shape reported for the dilute methanol solutions can be explained in terms of partial and reversible polymerization of alcohol molecules. The weak band with center near 3640 cm^{-1}, reported for the dilute methanol solutions, appears to obey Beer's law.

At increased concentrations of the ethers and of benzene, the extinction coefficients measured at the band centers decrease uniformly. For diethyl ether, anisole, benzene, 1,4-dioxane, and diisopropyl ether, average decreases of 50, 25, 24, 21, and 20%, respectively, were observed in the concentration range of 0.1 M to pure substance.

DISCUSSION

These data cannot be explained with the Kirkwood–Bauer–Magat equation (7, 8) or with any modification of this equation (17) since the band frequencies are independent of the electrical properties of the solutions. As a variety of alcohols have been examined, and as the 3340 cm^{-1} band common to all is not perturbed at alcohol concentrations greater than near 0.20 M, it seems that frequency shifts previously reported may arise from specific interactions between solute and solvent molecules rather than from the average electrical properties of the solution.

Inherent difficulties already described by la Lau and Thompson have prevented a thorough examination of theories which predict intensity variations with solution changes. That all the bands for alcohols (except 3340 cm^{-1}) apparently obey Beer's law, while those of the ethers and benzene do not, may be of special interest.

ACKNOWLEDGMENT

REFERENCES

1. L. J. BELLAMY. Spectrochim. Acta, **14**, 192 (1959).
2. T. L. BROWN. Spectrochim. Acta, **10**, 149 (1957).
3. C. A. COULSON. Spectrochim. Acta, **14**, 161 (1959).
4. C. LA LAU. Spectrochim. Acta, **14**, 181 (1959).
5. H. W. THOMPSON. Spectrochim. Acta, **14**, 145 (1959).
6. I. M. MILLS. Ann. Repts. on Progr. Chem. (Chem. Soc. London), **55**, 55 (1958).
7. E. BAUER and M. MAGAT. J. Phys. radium, **9**, 319 (1938).
8. J. G. KIRKWOOD. J. Chem. Phys. **5**, 14 (1937).
9. L. J. BELLAMY, H. E. HALLAM, and R. L. WILLIAMS. Trans. Faraday. Soc. **54**, 1120 (1958).
10. L. J. BELLAMY and R. L. WILLIAMS. Trans. Faraday Soc. **55**, 14 (1959).
11. P. A. D. DE MAINE. J. Mol. Spectroscopy, 4, 407 (1960).
12. N. S. BAYLISS, A. R. H. COLE, and L. H. LITTLE. Australian J. Chem. **8**, 26 (1955).
13. P. DEBYE. Handb. Radiol. **6**, 69 (1933).
14. L. ONSAGER. J. Am. Chem. Soc. **58**, 1496 (1936).
15. INTERNATIONAL CRITICAL TABLES. McGraw-Hill Book Co., Inc., New York. 1926.
16. P. A. D. DE MAINE. J. Chem. Phys. **26**, 1192 (1957).
17. D. H. WIFFEN. Quart. Revs. (London), **4**, 131 (1950).

ALKALOIDS OF LYCOPODIUM FAWCETTII. PART II[1, 2]

R. H. Burnell, B. S. Mootoo, and D. R. Taylor

β-Lofoline and fawcettiine are shown to be identical. Hydrolysis of bases from *Lycopodium fawcettii* gave rise to lycofoline and a smaller amount of an α-obscurine like base. Milder extraction procedures afford four new bases, base M, $C_{17}H_{27}NO_2$; base O, $C_{20}H_{31}NO_5$; base K, which is acetylfawcettiine, $C_{20}H_{31}NO_4$; and base N, which is diacetyllycofoline, $C_{20}H_{29}NO_4$. The isolation of fawcettiine from *Lycopodium clavatum Linn.* gathered in Jamaica is also reported.

After the initial extraction of this species (1) it was decided that a detailed study of deacetylfawcettiine was necessary and a slightly modified procedure was used to isolate this base. The stronger bases from the plant were hydrolyzed before being separated and the deacetylfawcettiine was then obtained by chromatography over alumina. These operations afforded another crystalline base, $C_{16}H_{25}NO_2$ (m.p. 140–141°), which we had not previously isolated. From the infrared spectrum and analyses it was learned that base H is an unsaturated tertiary base containing two hydroxyl groups. In a recent paper on the alkaloids of *Lycopodium annotinum* (2), Anet and Khan described an unsaturated base, lycofoline, which is identical with that described above.

Small quantities of another base which shows a great similarity to α-obscurine (3) were also obtained but insufficient material prevents a positive identification at this stage.

Using the procedures of Manske and Marion (4) for the extraction of lycopodiums affords an extremely dark crude product, a large portion of which proves to be intractable. We have found that cold percolation with dilute tartaric acid gives not only a cleaner, more readily purified extract but also affords a higher yield of tractable base. The new procedure gives rise to different proportions of the previously recorded bases (1) but base B (Marion's L.30 (5)) has not been found. Base E, $C_{17}H_{25}NO_2$, was not found in any quantity but a very similar substance base M, $C_{17}H_{27}NO_2$, was obtained. This base gives by far the least soluble perchlorate and can only be satisfactorily recrystallized from water. Like base E, base M shows a distinguishing ammonium band at 2000 cm^{-1} in the infrared (as does lycopodine).

The crude base from the tartaric acid extraction was distributed between chloroform and buffer in nine funnels and from this operation a significant quantity of a crystalline base (base J) was obtained. Analyses show a molecular formula $C_{18}H_{29}NO_3$ and melting point, mixed melting point, and infrared comparison have shown the substance to be β-lofoline, also reported by Anet and Khan (2). β-Lofoline perchlorate is indistinguishable from fawcettiine perchlorate in the infrared and shows the same melting point but fawcettiine had never been obtained crystalline and its perchlorate consistently analyzed for the monohydrate, $C_{18}H_{29}NO_3 \cdot HClO_4 \cdot H_2O$, whereas using the same conditions for drying prior to analysis, β-lofoline perchlorate analyses for $C_{18}H_{29}NO_3 \cdot HClO_4$. However, a mixed melting point determination on the two perchlorates gave no depression, showing the two to be identical. We would like to retain the name fawcettiine for this base since it represents the major alkaloid of the species. Hydrolysis of crystalline β-lofoline gives deacetylfawcettiine (1).

Oxidation of fawcettiine with chromium trioxide gave a six-membered ring ketone,

dehydrofawcettiine ($C_{18}H_{27}NO_3$) which could be readily hydrolyzed to deacetyldehydro-fawcettiine, $C_{16}H_{25}NO_2$, m.p. 145–147°. The more readily eliminated hydroxyl group in deacetylfawcettiine has been shown to be that present as the free hydroxyl in fawcettiine since the dehydration product from fawcettiine can be hydrolyzed to the previously obtained anhydrodeacetylfawcettiine, $C_{16}H_{25}NO$. These, and other transformations mentioned later, may be summarized:
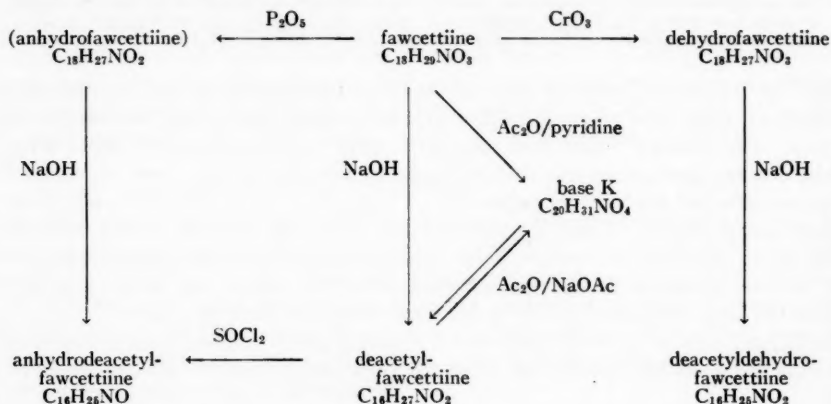
The most highly oxygenated base isolated from *L. fawcettii*, base O (m.p. 181–182°), has the molecular formula $C_{20}H_{31}NO_5$ and from spectral and analytical results contains two O-acetyl residues and a hydroxyl group.

The greatest difference between the methanol and tartaric acid extractions was found in the weaker bases. Base F was obtained only in small amounts while two diacetate bases not previously described represented the bulk of the weak base fraction. Counter-current distribution over 120 tubes did not completely separate these two bases and since neither crystallizes nor forms the usual crystalline salts, characterization was extremely difficult. Neither compound shows hydroxyl absorption in the infrared but both show bands corresponding to O-acetyl frequencies. Hydrolysis of one, base K ($C_{20}H_{31}NO_4$), affords deacetylfawcettiine and O-acetyl determinations show two such residues to be present in the base. Acetylation of fawcettiine with acetic anhydride and pyridine gave rise to base K, which can also be prepared from deacetylfawcettiine by refluxing in acetic anhydride containing sodium acetate.

The other diacetate weak base, present in much smaller quantity, gives rise to lyco-foline on hydrolysis and the absence of hydroxyl absorption in the infrared, supported by the analogy of the other acetylated bases shown to be present in the plant, suggests that this unstable compound is represented by the formula $C_{20}H_{29}NO_4$, i.e. diacetyl-lycofoline.

Tartaric acid extraction of locally collected *L. clavatum* Linn. led to the isolation of fawcettiine and smaller quantities of lycopodine. Several other bases which have been obtained from this plant will be described in a future publication.

EXPERIMENTAL

All melting points are uncorrected and the infrared spectral figures are for Nujol mulls unless otherwise stated. Paper chromatography means in all cases No. 4 Whatman

paper employing pyridine, ethyl acetate, water (2.3:7.5:1.65), the bases being spotted as the hydrochlorides.

Base H *(Lycofoline)*

The stronger bases from a methanolic extraction (see ref. 1) were hydrolyzed with 5% methanolic sodium hydroxide. The base was extracted (3.9 g) and then run over a column of ethyl acetate washed alumina in benzene. Elution with 20% chloroform in benzene gave white crystals (1.0 g), m.p. 140°, a sample of which was sublimed for analysis, m.p. 141°. Calc. for $C_{16}H_{25}NO_2$: C, 73.0; H, 9.6; N, 5.3; O, 12.2. Found: C, 73.0; H, 9.4; N, 5.2; O, 12.3.

The infrared showed both absorption in the OH stretching region (3350 cm^{-1}) and a weak band due to unsaturation (1675 cm^{-1}). The trace was identical with that published for lycofoline (2) and a mixed melting point (140–141°), kindly performed by Dr. Anet, with lycofoline (m.p. 142°) showed no depression.

Base I

Elution of the column (above) with 50% chloroform in benzene afforded another crystalline base (100 mg), m.p. 300° (decomp.). The ultraviolet spectrum showed λ_{max} 252 mμ, log ϵ (based on the molecular weight of α-obscurine) 3.77. The infrared spectrum, which was not identical with that of α-obscurine, had peaks at 3480 (OH), 3200 (NH), and 1662 (lactam C:O) cm^{-1}.

Further elution of the column with chloroform gave deacetylfawcettiine (1.1 g).

Extraction of L. fawcettii with Tartaric acid

The dried, ground plant (18 kg) was percolated with 3% tartaric acid solution and the aqueous percolate then evaporated at 40° to a manageable volume. Neutral impurities were removed by ether extraction and after basification with ammonia, the crude base (28.0 g) was obtained by ether extraction. The base was shaken between chloroform and phosphate buffer, pH 5.3, in nine 1-liter separatory funnels, and the stronger bases in funnels 1–7 (12.4 g) was distributed again between chloroform and acetate buffer, pH 5.6, in a 120-tube multiple extractor. The weight curve (Fig. 1) showed three peaks but paper chromatography showed a larger number of bases to be present.
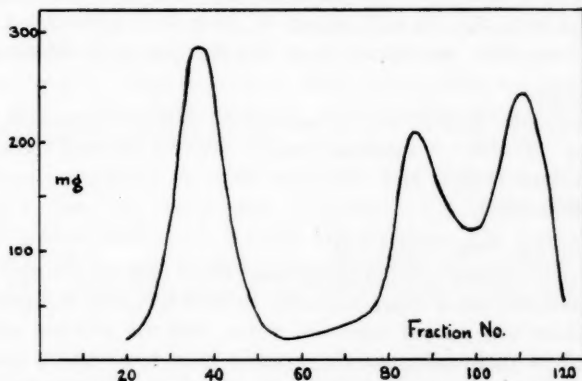
FIG. 1. Countercurrent distribution of strong bases with the system chloroform–buffer of pH 5.6.

Base A

Tubes 25–50 contained only base A (1).

The material from tubes 77–97 (3.18 g) was a mixture of three bases as shown by paper chromatography, so it was shaken between chloroform and phosphate buffer, pH 5.9, for 60 transfers. Complete separation was not obtained but from the central part of the distribution a crystalline base appeared.

Base O

The base was sublimed for analysis, m.p. 181–182°. Found: C, 65.7; H, 8.7; N, 3.9; O, 22.1; O—Ac, 23.9. $C_{20}H_{31}NO_5$ requires: C, 65.7; H, 8.6; N, 3.8; O, 21.9; (O—Ac)$_2$, 23.6. Infrared peaks at 3180 (bonded OH) and 1725 and 1235 (O—Ac) cm^{-1}.

Base M

The acetone mother liquors from base O were made slightly acidic with perchloric acid affording a sparingly soluble perchlorate, m.p. 280–282° (from water). Found: C, 54.1; H, 7.2; N, 3.8; O, 25.3; Cl, 9.3. $C_{17}H_{27}NO_2 \cdot HClO_4$ requires: C, 54.0; H, 7.4; N, 3.7; O, 25.4; Cl, 9.4. Infrared peaks at 3420 (OH), 2010 (NH), and 1692 (C:O) cm^{-1}.

The third base in this fraction is as yet uncharacterized.

The material (4.18 g) from the third peak of the first distribution (tubes 99–120, Fig. 1) was shown to contain one major and one minor component by paper chromatography, other than smaller amounts of the bases found in the second peak. Distribution between chloroform and phosphate buffer, pH 7.4, gave a central peak fraction containing the major base (2.33 g), which crystallized from an acetone solution.

β-Lofoline (Fawcettiine)

The base was sublimed for analysis, m.p. 172–173°. Calc. for $C_{18}H_{29}NO_3$: C, 70.3; H, 9.5; N, 4.6; O, 15.6; active H, 0.33. Found: C, 70.4; H, 9.6; N, 4.5; active H, 0.34. Infrared peaks at 3470 and 3100 (OH) and at 1730 and 1710 (C:O) cm^{-1}. In carbon tetrachloride solution the infrared spectrum showed only weak hydroxyl absorption and only one carbonyl band at 1733 cm^{-1}.

The methiodide was prepared in methanol, m.p. 293–296°. Calc. for $C_{19}H_{32}NO_3I$: C, 50.8; H, 7.2; N, 3.1; I, 28.2; N—Me, 3.2. Found: C, 51.1; H, 7.2; N, 3.2; I, 28.4; N—Me, 3.0.

The perchlorate was recrystallized from acetone, m.p. 272–275°. Calc. for $C_{18}H_{29}NO_3 \cdot HClO_4$: C, 53.0; H, 7.8; N, 3.4; Cl, 8.7. Found: C, 53.2; H, 7.5; N, 3.4; Cl, 8.5. Mixed melting point with fawcettiine perchlorate (m.p. 272–275°) gave no depression.

Hydrolysis of β-Lofoline

β-Lofoline (175 mg) was hydrolyzed in methanolic sodium hydroxide giving white solids (160 mg), m.p. 207–208°. A sublimed sample gave an infrared spectrum identical with that of deacetylfawcettiine, and admixture with an authentic sample caused no lowering of the melting point.

Anhydrodeacetylfawcettiine from Fawcettiine

Excess phosphorus pentoxide was added to fawcettiine (100 mg) in dry benzene and the mixture gently refluxed for 6 hours and then allowed to stand at room temperature overnight. The mixture was poured into cold water, and the solution was then made basic with solid sodium carbonate and the organic base removed by extraction with carbon tetrachloride. The pale oil obtained could not be made to crystallize nor could the perchlorate be obtained crystalline so the product was sublimed and then hydrolyzed

in ethanolic sodium hydroxide. The base, extracted with chloroform after dilution of the reaction mixture with water, gave a crystalline hydrochloride showing an infrared spectrum superimposable on that of anhydrodeacetylfawcettiine hydrochloride (1).

Dehydrofawcettiine

Fawcettiine (530 mg) in pyridine (8 ml) was added to excess chromium trioxide / pyridine complex prepared in the usual manner. After 1 hour at room temperature, the reaction mixture was poured into water, made strongly basic with ammonia, and extracted with chloroform. The chloroform solution was extracted with 10% hydrochloric acid, which was then basified with ammonia and re-extracted with chloroform giving a dark brown oil (300 mg) which showed, in addition to unchanged fawcettiine, another spot of greater R_f on paper. The crude product was chromatographed on ethyl acetate washed alumina and afforded, in the benzene eluate, a colorless oil (220 mg) which solidified on standing. The solid was sublimed, m.p. 134–137°. Found: C, 71.0; H, 9.4; N, 4.5; O, 15.5; C—Me, 9.4. $C_{18}H_{27}NO_3$ requires: C, 70.8; H, 8.9; N, 4.6; O, 15.7; (C—Me)$_2$, 9.8. Infrared peaks at 1700 (six-membered ring ketone) and 1725, 1240, and 1220 (O—Ac) cm^{-1}. No absorption in the hydroxyl region.

The methiodide was recrystallized from methanol/acetone, m.p. 267–268° (inserted at 240°).

Deacetyldehydrofawcettiine

Dehydrofawcettiine (120 mg) was dissolved in methanol (5 ml) and a solution of sodium hydroxide (1 g) in methanol (3 ml) and water (5 ml) was added. After 6 hours at room temperature, the solution was diluted with water and extracted with chloroform, yielding a white solid which after sublimation, melted over the range 145–147°. The acetate peaks were absent in the infrared spectrum but both hydroxyl (3080 cm^{-1}) and carbonyl bands (1708 cm^{-1}) were present. The substance was characterized as the methiodide prepared from the base (20 mg) in methanol (10 ml) and recrystallized from methanol/acetone, m.p. 308–309° (inserted at 240°). Found: C, 50.0; H, 7.0; N, 3.6; I, 31.8. $C_{16}H_{25}NO_2 \cdot CH_3I$ requires: C, 50.4; H, 7.0; N, 3.5; I, 31.3.

Acetylfawcettiine

Fawcettiine (100 mg) was acetylated in acetic anhydride/pyridine at room temperature for 12 hours. The product was sublimed to remove traces of pyridine and a white semisolid (m.p. ca. 110°) was obtained. In the infrared the substance showed no hydroxyl absorption but could not be crystallized from any solvent. A portion was sublimed for analysis, m.p. 116–117°. Found: O—Ac, 25.4. $C_{20}H_{31}NO_4$ requires: (O—Ac)$_2$, 24.6. Mixed melting point, paper chromatography and identical infrared spectra show acetylfawcettiine to be base K (see below).

Weak Bases

The weak base from the nine-funnel distribution (11 g) was distributed between chloroform and acetate buffer, pH 3.2, for 120 transfers. The first 27 tubes contained neutral material (1.96 g) and no significant quantities of base were encountered until tubes 52–78 (0.75 g) containing base N and 84–102 (1.91 g) mostly base K.

Base N

This substance failed to crystallize or form crystalline salts. It was not completely stable to sublimation but showed only one relatively slow-moving spot on paper. Hydrolysis (of tube 52) in methanolic sodium hydroxide for 24 hours at room temperature gave

a solid base which sublimed readily, m.p. 140°. Comparison of the infrared spectrum of the hydrolysis product with that of lycofoline showed them to be identical and a mixed melting point confirmed this. The infrared spectrum of base N shows no hydroxyl peak but a broad carbonyl band 1725–1740 cm^{-1} with complementary absorption at 1235 cm^{-1}. A shoulder at 1660 cm^{-1} is due to the carbon–carbon double bond.

Base K

The material (1.91 g) was run over alumina in benzene giving a white solid which solidified after sublimation, showed homogeneity on paper, but did not crystallize from solvents. The base was resublimed for analysis, m.p. 117°. Found: O—Ac, 24.7; N, 3.8. $C_{20}H_{31}NO_4$ requires: (O—Ac)$_2$, 24.6; N, 4.0. Infrared absorption at 1725 (C:O) and a broad peak at 1240 cm^{-1}.

Hydrolysis of base K gave an almost quantitative yield of deacetylfawcettiine as shown by the infrared spectrum, m.p. 207° and mixed melting point 207°. Base K was the major product when deacetylfawcettiine was acetylated in refluxing acetic anhydride containing sodium acetate.

Extraction of L. clavatum Linn.

Through the dried, ground plant material (4.5 kg) was percolated aqueous 3% tartaric acid solution until no alkaloid could be detected using a potassium iodide/platinic chloride spray. The crude base (7.5 g) was obtained as described earlier and then distributed between chloroform and phosphate buffer, pH 5.3 (25 transfers). Three distinct fractions were obtained, tubes 20–25 (fraction A, 2.89 g) containing one main strongly basic component. Tubes 5–19 were combined (fraction B, 1.71 g) as were tubes 1–4, but this last fraction has not been investigated further.

Fawcettiine

Fraction A (2.18 g) was distributed between chloroform and phosphate buffer, pH 7.17 (20 transfers), and from the weight curve and paper chromatography it appeared that tubes 9–15 contained a single component. The perchlorates obtained from these tubes were combined and recrystallized from acetone/ether, m.p. 271–275° (500 mg). Mixed melting point and infrared comparison showed this derivative to be fawcettiine perchlorate.

Lycopodine

Fraction B (1.71 g) after countercurrent extraction afforded a perchlorate, m.p. 281–282° (550 mg). The infrared spectrum and no depression in the melting point on admixture with an authentic sample showed this to be lycopodine perchlorate.

REFERENCES

1. R. H. Burnell. J. Chem. Soc. 3091 (1959).
2. F. A. L. Anet and N. H. Khan. Can. J. Chem. 37, 1587 (1959).
3. B. Moore and L. Marion. Can. J. Chem. 31, 952 (1953).
4. R. H. F. Manske and L. Marion. Can. J. Research, B, 24, 57 (1946).
5. G. S. Perry and D. B. MacLean. Can. J. Chem. 34, 1189 (1956).

SYNTHÈSES D'ACIDES AMINOBUTYRIQUES

1. ACIDES ALKYLAMINO-2 AMINO-4 BUTYRIQUES[1]

Réal Laliberté et Louis Berlinguet

ABSTRACT

The syntheses of eight 2-alkylamino-4-aminobutyric acids are described. The starting material is 4-butyrolactone, which is opened with potassium phthalimide to give 4-phthalimido-butyric acid. After bromination the 2-bromo-4-phthalimidobutyric acid, obtained in excellent yield, is treated with aliphatic amines in alcoholic medium to give the desired substituted 2,4-diaminobutyric acids, which were characterized as the monohydrochlorides and the di(phenylcarbamates). Three of them cyclized easily to give the corresponding hydantoins. In the course of the reaction, substituted diamides of phthalic acid were isolated and characterized.

INTRODUCTION

Les dérivés aminés de l'acide *n*-butyrique retiennent l'attention depuis quelques années. En particulier, on connaît maintenant le rôle très important de l'acide amino-4 butyrique (GABA) (1, 2) dans le système nerveux central des mammifères et sa distribution généralisée chez tous les êtres vivants: levures (3), plantes et protéines animales (4). Des études ont aussi été faites sur les propriétés physiques et le rôle biologique de l'acide amino-2 butyrique ainsi que des acides amino-2 hydroxy-4 butyrique (5) et diamino-2,4 butyrique (6). Ces substances sont des intermédiaires normaux dans le métabolisme de quelques acides aminés. L'acide diamino-2,4 butyrique est absorbé très rapidement par la cellule intacte (7).

Vu l'importance biologique de ces composés, nous avons voulu préparer une série de dérivés N-alkylés de l'acide diamino-2,4 butyrique pour les soumettre à des essais biologiques.

La synthèse de ces dérivés présente des difficultés. Si l'on désire obtenir l'acide diamino-2,4 butyrique symétriquement substitué, on peut, en théorie, utiliser un acide butyrique dihalogéné. Mais des essais récents (8, 9, 10) montrent qu'une amination directe en position 4 est difficile à cause de réactions secondaires.

Si l'on veut obtenir l'acide diamino-2,4 butyrique substitué sur l'un des azotes, il faut, lors de la synthèse, bloquer l'atome d'azote qui doit rester exempt de substituants. Ainsi Christensen (7), en partant de dérivés *p*-toluène-sulfonyles de l'acide diamino-2,4 butyrique, a préparé quelques dérivés méthylés, soit en position 2, soit en position 4.

Nous avons voulu utiliser comme produit de départ une substance facilement accessible: la butyrolactone-4. Talbot, Gaudry et Berlinguet (11), Frankel (6) ainsi que Zaoral (12) ont préparé avec de bons rendements l'acide phtalimido-4 butyrique. Nous avons bromé cet acide (Zaoral) (12) en position 2, puis nous avons remplacé l'halogène par réaction avec les amines aliphatiques voulues.

La fonction amine primaire en position 4 se trouve protégée par le radical phtalimidé, lequel peut être hydrolysé une fois la réaction terminée ou peut être scindé par aminolyse lors de la réaction pour donner le diamide de l'acide phtalique.

Théoriquement, dans cette synthèse à partir de l'acide bromo-2 phtalimido-4 butyrique (I), plusieurs réactions sont possibles. Il peut y avoir amination, hydroxylation si la réaction se fait en milieu aqueux ou encore cyclisation si le groupe phtalimide est scindé.

En plus de l'acide diamino-2,4 butyrique substitué désiré (II) on peut donc avoir, comme produit de la réaction, l'acide hydroxy-2 amino-4 butyrique (IV), l'acide bromo-2 amino-4 butyrique inchangé (III) et l'acide azétidine-carboxylique-2 (V) (9).
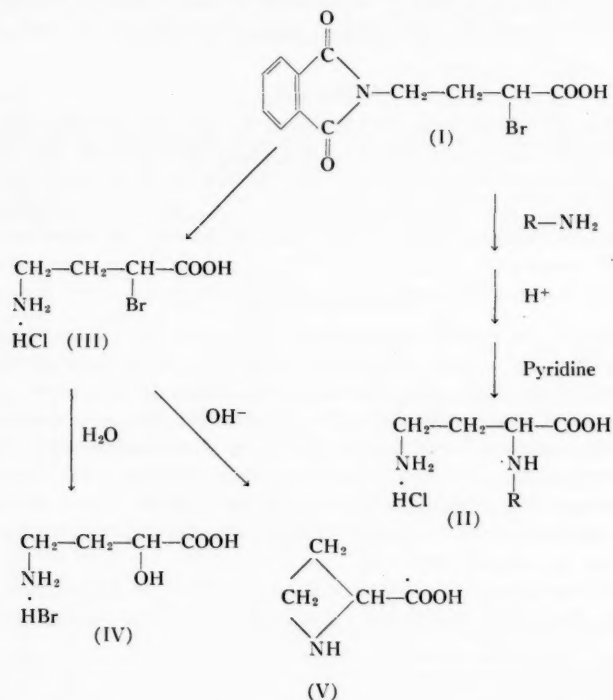
Dans les synthèses rapportées ici, la chromatographie et l'électrophorèse sur papier nous ont permis de constater la présence, après hydrolyse des produits d'amination, d'une faible quantité d'acide hydroxy-2 amino-4 butyrique en plus de l'acide diamino-2,4 butyrique voulu. La purification de ce dernier produit se fait facilement par cristallisation dans l'éthanol.

Zaoral (12) n'a pas réussi à substituer l'atome de brome de l'acide bromo-2 phtalimido-4 butyrique par de l'ammoniaque. Nous avons repris cette réaction et, à l'aide de la chromatographie sur papier, nous avons pu mettre en évidence la présence dans ces conditions d'une grande quantité d'acide hydroxy-2 amino-4 butyrique ainsi qu'un peu des acides bromo-2 amino-4 butyrique et diamino-2,4 butyrique. Il semble qu'avec l'ammoniaque il y ait hydrolyse du groupe phtalimidé et hydroxylation en position 2 plutôt que substitution comme dans le cas des amines.

Pour favoriser l'amination nous avons condensé les amines en milieu alcoolique. Sauf dans le cas de la méthylamine et de l'éthylamine, les rendements sont meilleurs en solution alcoolique qu'en solution aqueuse.

Certaines amines sont des bases assez fortes pour couper le radical phtalimidé en milieu alcoolique. Dans ces cas on recueille, après la réaction, les diamides correspondants de l'acide phtalique. Nous avons caractérisé les diamides suivants: N,N'-dibutyl phtalamide, N,N'-dicyclohexyl phtalamide et N,N'-diisopropyl phtalamide.

La température optimum pour les substitutions semble être 20° C. Les rendements sont sensiblement les mêmes, que l'on utilise l'acide halogéné ou son ester méthylique.

Nous avons caractérisé huit nouveaux acides amino-4 butyriques portant en position 2 une fonction amine secondaire ou tertiaire. Nous en avons fait les di(phénylcarbamates) et nous avons noté que trois d'entre eux se cyclisent très facilement pour donner les hydantoïnes correspondantes.

PARTIE EXPÉRIMENTALE

Acide phtalimido-4 butyrique

On peut faire la réaction dans la diméthylformamide (Talbot, Gaudry et Berlinguet) (11) ou sans solvant (Zaoral) (12). Dans ce cas, on ajoute lentement (30 minutes) à de la butyrolactone-4 (70.0 g, 0.81 mole) maintenue entre 180° et 200° de la phtalimide de potassium (150.0 g, 0.81 mole). On chauffe le mélange pendant 30 minutes, puis on dissout la masse dans 1 litre d'eau. On ajoute alors 200 ml d'éthanol et on refroidit. L'addition lente d'acide chlorhydrique concentré accompagnée d'une forte agitation précipite l'acide phtalimido-4 butyrique. Rendement brût: 160 g (85%). Il n'est pas nécessaire de recristalliser le produit pour les manipulations suivantes, p.f. 112°–115°* (lit. p.f. 117°–118°) (13). Anal. Calc. pour $C_{12}H_{11}O_4N$: N, 6.00%. Trouvé: N, 6.31%.

Acide bromo-2 phtalimido-4 butyrique

Dans un ballon muni d'un réfrigérant, on place 62 g (0.27 mole) d'acide phtalimido-4 butyrique, 1 g de tribromure de phosphore, 1 g de phosphore rouge amorphe et 250 g (1.55 moles) de brome dissous dans 200 ml de CCl_4. On chauffe à reflux pendant 18 heures. Après avoir évaporé le solvant et l'excès de brome, on lave le solide avec du benzène. Le résidu est dissous à chaud dans l'éthanol. L'addition d'eau permet la cristallisation de l'acide bromo-2 phtalimido-4 butyrique. Rendement: 80 g (96%), p.f. 150–152°. Une seconde cristallisation dans l'acétate d'éthyle donne un point de fusion de 157° (lit. 157–158°) (12). Anal. Calc. pour $C_{12}H_{10}BrO_4N$: N, 4.5; Br, 25.6%. Trouvé: N, 4.5; Br, 25.7%.

Acides alkylamino-2 amino-4 butyriques

On place dans une fiole conique 40 g (0.125 mole) d'acide bromo-2 phtalimido-4 butyrique et 200 ml d'éthanol. À la suspension refroidie, on ajoute en agitant un excès d'amine (environ 1.0 mole). La méthylamine, l'éthylamine et la diméthylamine sont en solution aqueuse de sorte que le mélange réactionnel est un mélange eau–alcool. Les autres amines réagissent en milieu alcoolique. On laisse en contact en agitant de temps à autre. Après 5 jours, les solutions sont évaporées à sec sous vide. On hydrolyse à reflux le résidu avec 500 ml d'acide chlorhydrique concentré pendant 12 heures. En refroidissant, l'acide phtalique cristallise. Après l'avoir filtré (21 g) on évapore à sec sous vide. On dissout le dichlorhydrate de l'acide diaminé dans l'éthanol chaud. On précipite le monochlorhydrate par addition de 9 ml de pyridine. Le monochlorhydrate obtenu est recristallisé deux fois par dissolution dans 75 ml d'eau chaude et addition de 400 ml d'éthanol. Le Tableau I contient la liste des acides alkylamino-2 amino-4 butyriques préparés. Dans le cas de la diméthylamine, il faut substituer la triéthylamine à la pyridine pour isoler l'acide diméthylamino-2 amino-4 butyrique libre.

Di(phénylcarbamates) des acides alkylamino-2 amino-4 butyriques

On peut caractériser les acides diaminés en les transformant en di(phénylcarbamates). Dans 5 ml de NaOH 4 N (0.02 mole), on dissout 1.68 g (0.01 mole) du monochlorhydrate

*Les points de fusion ne sont pas corrigés.

TABLEAU I

Acides alkylamino-2 amino-4 butyriques

$$CH_2—CH_2—CH—COOH$$

NH₂
·
HCl

R—N—R′
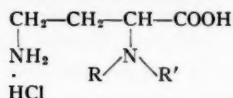
R	R′	Rendement, %	R_f‡	P.f., °C	N % Trouvé	N % Théorie	Cl % Trouvé	Cl % Théorie
—CH₃	—H	60	0.11	262–263	16.3	(16.6)	20.8	(21.0)
—C₂H₅	—H	55	0.20	277	15.2	(15.3)	19.6	(19.4)
n—C₃H₇	—H	55	0.27	280–282	14.1	(14.2)	17.9	(18.0)
iso—C₃H₇	—H	25	0.28	246–248	14.1	(14.2)	18.1	(18.0)
n—C₄H₉	—H	55	0.35	286	13.1	(13.2)	17.1	(16.8)
—C₆H₁₁	—H	80	0.36	259	11.7	(11.8)	15.0	(14.9)
—CH₃	—CH₃*	70	0.16	231–233	19.1	(19.1)	Base libre	
—C₂H₅	—C₂H₅†	30	0.28	205–206	11.3	(11.5)	28.6	(28.6)

*Le monochlorhydrate a été préparé par Christensen (6), p.f. 213–215° C.
†Le dichlorhydrate cristallise lentement dans l'alcool anhydre.
‡Dans la pyridine à 80%.

de l'acide méthylamino-2 amino-4 butyrique puis on ajoute en agitant à froid 2.39 g (0.02 mole) d'isocyanate de phényle. Après avoir agité et filtré, on précipite le di(phényl-carbamate) par un excès d'acide chlorhydrique. On recristallise le produit dans un mélange d'acétone et d'éther de pétrole. Rendement: 70%.

En procédant de façon identique, on obtient les di(phénylcarbamates) des autres acides diamino-2,4 butyriques dont les constantes sont données au Tableau II. Dans

TABLEAU II

Di(phénylcarbamates) des acides alkylamino-2 amino-4 butyriques

$$C_6H_5—NH—C—NH—CH_2—CH_2—CH—COOH$$

O

O=C—N—R
NH
C₆H₅
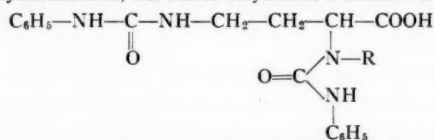
R	P.f., °C	N % Trouvé	N % Théorie
—CH₃	56–57	14.8	15.0
—C₂H₅	103	14.1	14.5
n-C₃H₇	149–150	14.0	14.0
iso-C₃H₇	102–103	13.9	14.0
n-C₄H₉	118–119	13.5	13.5
—C₆H₁₁	115	12.5	12.7

le cas des acides diamino-2,4 butyriques portant en position 2 un groupe méthyle, éthyle ou cyclohexyle, le chauffage du di(phénylcarbamate) dans l'acétone lors de la recristal-lisation provoque une cyclisation. On obtient alors les alkyl-1 phényl-3 hydantoïnes-5 correspondantes. Les constantes physiques de ces hydantoïnes sont données dans le Tableau III.

TABLEAU III
### Alkyl-1 phényl-3 (phénylcarbamate amino-2 éthyl)-5 hydantoïnes

$$C_6H_5—NH—C(O)—NH—CH_2—CH_2—CH—C=O$$
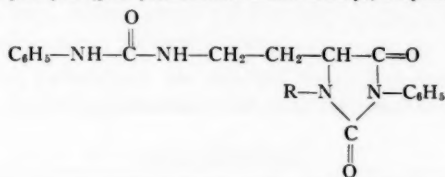
R	P. f., °C	N % Trouvé	N % Théorie
—CH₃	173–174	15.8	15.8
—C₂H₅	153–154	14.9	15.2
—C₆H₁₁	172	13.3	13.3

Le groupe phénylcarbamate en position 2 de la chaîne éthyle placée en position 5 du noyau de l'hydantoïne peut être hydrolysé par ébullition avec l'acide chlorhydrique concentré. On obtient ainsi le chlorhydrate de la méthyl-1 phényl-3 (amino-2 éthyl)-5 hydantoïne. On peut le cristalliser de l'alcool par addition d'éther, p.f. 227–228°. Anal. Calc. pour $C_{12}H_{16}N_3O_2Cl$: N, 15.6; Cl, 13.2%. Trouvé: N, 15.4; Cl, 13.3%.

Diamides de l'acide phtalique

Lors de la condensation de l'acide bromo-2 phtalimido-4 butyrique avec les amines primaires en solution alcoolique, il y a aminolyse du groupe phtalimidé et formation des diamides correspondants. On les isole en ajoutant à la solution 300 ml d'eau. On peut obtenir ainsi les 'N,N'-dibutyl phtalamide, N,N'-dicyclohexyl phtalamide et N,N'-diisopropyl phtalamide. Ces composés peuvent être recristallisés dans l'isopropanol. Leurs constantes physiques sont données dans le Tableau IV.

TABLEAU IV
Diamides de l'acide phtalique
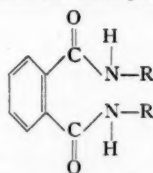
R	P. f., °C	N % Trouvé	N % Théorie	Rendement, %
iso-C₃H₇	218	11.5	11.3	45
n-C₄H₉	103–104	10.0	10.1	90
—C₆H₁₁	253	8.6	8.5	95

Chromatographie et électrophorèse

Les acides alkylamino-2 amino-4 butyriques migrent vers la cathode à l'électrophorèse

CANADIAN JOURNAL OF CHEMISTRY. VOL. 38, 1960

sur papier à pH 8.6. Ils donnent une coloration pourpre à la ninhydrine. Les distances de migration (R_f) pour un mélange pyridine et eau (80:20) sont données au Tableau I.

REMERCIEMENTS

BIBLIOGRAPHIE

1. F. Brücke (*Editeur*).   Comptes rendus des travaux du Quatrième Congrès International de Biochimie. Symposium III. Biochimie du système nerveux central. Pergamon Press, London. 1958. pp. 213–278.
2. R. A. Salvador et W. R. Albers.   J. Biol. Chem. **234**, 923 (1959).
3. L. J. Reed.   J. Biol. Chem. **183**, 451 (1950).
4. A. I. Virtanen et J. K. Miettinen.   Biochim. et Biophys. Acta, **12**, 181 (1953).
5. H. S. Mudd.   J. Biol. Chem. **234**, 1784 (1959).
6. D. H. Peterson et L. M. Reineke.   J. Biol. Chem. **181**, 95 (1949).
7. H. N. Christensen et R. Riggs.   J. Biol. Chem. **220**, 265 (1956).
8. M. Frankel, Y. Knobler et T. Sheradsky.   Bull. Research Council Israel, A, **7**, 173 (1958).
9. L. Fowden.   Biochem. J. **64**, 323 (1956).
10. L. Berlinguet et R. Laliberté.   Ann. Acfas, **25**, 84 (1959).
11. G. Talbot, R. Gaudry et L. Berlinguet.   Can. J. Chem. **36**, 593 (1958).
12. M. Zaoral.   Chem. listy, **52**, 2338 (1958).
13. S. Gabriel et J. Colman.   Ber. **41**, 513 (1908).

CONDUCTANCES OF AQUEOUS SOLUTIONS OF SODIUM HEXANOATE (SODIUM CAPROATE) AND THE LIMITING CONDUCTANCES OF THE HEXANOATE ION, AT 25° C AND 35° C[1]

A. N. CAMPBELL AND J. I. FRIESEN[2]

ABSTRACT

The equivalent conductances, densities, and viscosities of aqueous solutions of sodium hexanoate have been determined at 25° C and 35° C at concentrations ranging from 0.0003 M to saturation.

The limiting equivalent conductances of the hexanoate ion have been determined as 27.37 ± 0.04 mhos at 25° C and 34.69 ± 0.05 mhos at 35° C.

The Robinson–Stokes and the Falkenhagen–Leist equations have been applied to the data. The Robinson–Stokes equation reproduces the data within 0.7 mho up to 0.5 M at 25° C when $\mathring{a} = 13$ Å. At 35° C the data are reproduced within 0.5 mho up to 0.05 M with $\mathring{a} = 10$ Å. The Falkenhagen–Leist equation reproduces the data at 25° C within 0.4 mho up to 0.1 M with $\mathring{a} = 5.5$ Å. An $\mathring{a} = 4.0$ Å reproduces the 35° C data within 0.5 mho up to 0.05 M.

From the form of the conductance curves and from an estimation of the apparent molecular weight it was concluded that the hexanoate ion does not form ionic micelles.

This research, in which the conductances of sodium hexanoate solutions have been determined, was part of a program in which it was intended to measure the conductances of the sodium salts of the fatty acids. It was thought that, proceeding up the homologous series, the increasing size of the anions might eventually lead to a situation where the anion was essentially motionless and non-conducting. On the other hand, it was known that, after a certain number of carbon atoms in the chain is reached, micelle formation occurs and that therefore the increasing size of the anion might be to some extent counterbalanced by the increased electrical charge; hence, even the largest ions would exhibit appreciable conductance. The limiting conductances of the hexanoate ion at two temperatures were determined, from the results in very dilute solution, and the results from concentrated solutions were compared with results calculated by means of the Wishaw–Stokes (1) and the Falkenhagen–Leist (2) equations. These equations have been quoted so frequently by us that they need not be stated again here.

EXPERIMENTAL

n-Hexanoic acid was obtained from the Eastman Kodak Company and purified by redistillation. The refractive index agreed very closely with the figure given in the literature. To prepare the sodium salt the acid was neutralized with an alcoholic solution of sodium hydroxide and the solution was evaporated until the salt crystallized out. The salt was then recrystallized twice from alcohol, dried at 110° C, ground in an agate mortar, and stored in an oven at 110° C.

Attempts to determine the purity of the salt by titration with hydrochloric acid, using a Fisher titrimeter, failed. Finally, the salt was analyzed by conversion to sulphate. The method, which is crude, gave a result corresponding to 99.5% sodium hexanoate. Had the salt contained either sodium carbonate or sodium hydroxide, the result would have been high rather than low.

Solutions were prepared in two ways. For concentrations ranging from 0.02 N to saturation, at least 2.3 g was weighed to 0.2 mg and the resulting solution weighed to

0.2 mg, if it weighed less than 120 g, or to 10 mg, if it weighed more than 120 g; all weigh-
ings were reduced to vacuum. The weight concentration was therefore known to 0.01%.
Dilute solutions were prepared by successive additions of salt to a known amount of
water. At least 0.02 g of salt was weighed on a microbalance to $2\mu g$. A maximum of
six additions was made so that the weight concentrations were known to 0.01%.

For the more concentrated solutions, distilled water, having a specific conductance less
than 5×10^{-6} mhos/cm, at 25° C, was used as solvent. For the medium concentration
range, water from a Barnstead still was first passed through an Amberlite N-3 mixed
bed ion exchange resin and then "equilibrated" with the carbon dioxide of the atmosphere
by shaking for at least half an hour. The specific conductance was then about $2-3 \times 10^{-6}$
mhos/cm, at 25° C. For the very dilute region, water from the still was purified by bub-
bling purified nitrogen through it for several hours. The specific conductance was then
2 to 3×10^{-7} mhos/cm.

The electrical measurements were made on a Jones bridge and all the refinements of
good work were applied. The technique has been described frequently. Four conductance
cells, all of the type described by Jones and Bollinger (3), were used, and they had cell
constants varying from 1.4409 to 443.76.

The conductances of very dilute solutions were determined in a cell of the Shedlovsky
type (4). The constant of this cell was determined with potassium chloride, using the
equation of Fuoss (5)

$$\Lambda = 149.93 - 94.65\sqrt{C} + 58.74C \log C + 198.4C.$$

From this equation, Λ for KCl at 25° C can be calculated for any given low concentration.
But

$$\Lambda = 1000 \, A/CR$$

where R is the measured resistance of the cell and A the cell constant. In this way the
cell constant for the Shedlovsky cell was found to be 0.43246. We have pointed out, in
previous papers, that it is easy to show, by means of the Washburn equation (6) that the
effect of temperature on cell constant is, for cells of conventional geometry, exceedingly
slight. In the present case, the constant of the Shedlovsky cell changes by 0.004%, for
a 10-degree rise in temperature. It is therefore quite permissible to use, at 35° C, cell
constants determined at 25° C.

For the more concentrated solutions, thermostats of conventional type were used. All
thermometers were calibrated against a platinum-resistance thermometer. For the very
dilute solutions, where the Shedlovsky cell was used, a more complicated thermostat,
containing about six gallons of bleached petroleum oil and housed in a double-walled
insulated box, was used. Stirring was by means of a circulating pump. Temperature was
controlled by a mercury–toluene regulator and thyratron relay as described by Swinehart
(7) and it was read directly on a platinum-resistance thermometer. In all cases, the
temperature was known to about 0.005° C and it was constant within 0.002° C. When
this thermostat was operated at 35° C, the air above the bath was maintained just above
35° C to prevent distillation of solvent into the exposed section of the cell.

Viscosity measurements were made with two viscometers of the Cannon and Fenske
type (8), in which drainage and kinetic energy corrections are negligible. They were
calibrated with water at the two temperatures. The reproducibility of run times was not
better than 0.05%. Density and viscosity measurements were not made on the six
most dilute solutions, since these were made up by successive additions of salt to the
Shedlovsky-type cell.

EXPERIMENTAL RESULTS

TABLE I

Densities, viscosities, and conductances of sodium hexanoate at 25° C

Concentration (moles/liter)	Density (g/ml)	Relative viscosity	Specific conductance (mhos/cm×10⁴)	Equivalent conductance (mhos)
0.000250	—	—	0.19197	76.56
0.000632	—	—	0.48207	76.04
0.000968	—	—	0.73337	75.65
0.001579	—	—	1.1889	75.16
0.002320	—	—	1.7350	74.69
0.003249	—	—	2.4128	74.18
0.019937	0.99788	1.014	13.876	69.57
0.049792	0.99896	1.035	32.648	65.55
0.099588	1.00075	1.067	61.299	61.54
0.50023	1.01527	1.374	231.01	46.18
0.98536	1.03233	1.875	350.52	35.57
2.0019	1.05917	4.606	498.53	24.89
2.6215	1.07242	11.654	531.99	20.29
2.9987	1.08127	21.64	521.35	17.38
3.4487	1.09058	39.27	477.78	13.85

TABLE II

Data for sodium hexanoate at 35° C

Concentration (moles/liter)	Density (g/ml)	Relative viscosity	Specific conductance (mhos/cm×10⁴)	Equivalent conductance (mhos)
0.000611	—	—	0.5782	94.31
0.001164	—	—	1.0925	93.64
0.001604	—	—	1.4973	93.16
0.002241	—	—	2.0783	92.60
0.002926	—	—	2.6983	92.08
0.003014	—	—	3.5845	91.45
0.019875	0.99480	1.015	17.087	85.91
0.049637	0.99585	1.033	40.204	80.96
0.092732	0.99759	1.064	—	—
0.49838	1.01152	1.341	288.06	57.79
0.98092	1.02768	1.778	455.42	45.40
1.9909	1.05335	4.202	643.49	32.31
2.6061	1.06612	10.14	688.89	·26.43
2.9803	1.07473	17.46	682.15	22.88
3.4238	1.08270	30.26	635.93	18.57

DISCUSSION

After a careful consideration of all possible errors, we conclude that our equivalent conductances have a maximum possible error of $\pm 0.1\%$.

Limiting equivalent conductances are usually obtained either by the classical Kohlrausch method, in which equivalent conductance is plotted against the square root of the concentration, or by the Shedlovsky (4) or some other, method of extrapolation. Both the Kohlrausch and the Shedlovsky methods were used by us. In very dilute solutions hydrolysis is appreciable and correction was made for this by the method of Campbell and Bock (9). This method calculates x, the degree of hydrolysis, from the expression

$$x = -\frac{K_h}{2C} + \sqrt{\frac{K_h^2}{4C^2} + \frac{K_h}{C}},$$

where K_h is the hydrolysis constant and C is the stoichiometric concentration, and assumes that the equivalent conductance of free acid or base, as the case may be, is the limiting equivalent conductance of acid or base. It then follows that

$$\Lambda_{exp} = (1-x)\Lambda_{corr}+x\Lambda_{base}.$$

Thus Λ_{corr}, the equivalent conductance of the unhydrolyzed salt, can be calculated. The hydrolysis constants were obtained from the data of Everett, Landsman, and Pinsent (10). At 25° C, $K_h = 7.25 \times 10^{-10}$ and at 35° C, $K_h = 1.57 \times 10^{-9}$.

The Kohlrausch method gave for the limiting equivalent conductance of sodium hexanoate at 25° C a value of 77.47 ± 0.04 mhos, and at 35° C a value of 96.23 ± 0.05 mhos. The Shedlovsky extrapolation method gave the values 77.84 and 96.71 mhos, respectively. The Shedlovsky values are distinctly higher. Similar behavior was observed by Bock (9) for ammonium salts. Since the Shedlovsky method is empirical and the deviations from a straight line in the Kohlrausch plot are small (maximum deviation 0.05%, by the method of least squares), we think the Kohlrausch values are the ones that should be accepted.

The limiting conductances of the sodium ion, according to Benson and Gordon (11), are ·50.10 mhos at 25° C and 61.54 mhos at 35° C. Subtracting these values from the values obtained for sodium hexanoate, the limiting conductance of the hexanoate ion results as 27.37 ± 0.04 mhos at 25° C and 34.69 ± 0.05 mhos at 35° C.

It now appears that there is little theoretical justification for the application of Wishaw–Stokes and the Falkenhagen–Leist equations to the region of concentrated solution. Nevertheless, the manner in which these equations predict the experimental results is surprising. We note in particular the results of Campbell and Paterson on lithium chlorate (12) where the observations were pushed right up to the molten salt, without serious discrepancy. We therefore find it of interest to apply these equations to our results and we have done so in the present instance. In this case, however, both equations appear to be useless. Both conductance equations were programmed on a Bendix G-15 D computer, in such a way that the best $å$ was found for each concentration. An $å$ value was then chosen in the dilute region (usually about 0.1 N), and this $å$ value was then used to calculate a conductance value for each concentration.

TABLE III

Calculated equivalent conductances at 25° C

Concentration (moles/liter)	Equivalent conductance (mhos)	Calculated equivalent conductance			
		Robinson–Stokes (mhos)		Falkenhagen–Leist (mhos)	
		$å = 13.0$ Å	$å = 20.0$ Å	$å = 5.5$ Å	$å = 7.0$ Å
0.000250	76.56	76.31	76.34	76.52	76.52
0.000632	76.04	75.67	75.75	75.96	75.98
0.000968	75.65	75.28	75.40	75.62	75.64
0.001579	75.16	74.73	74.91	75.11	75.15
0.002301	74.69	74.23	74.48	74.63	74.69
0.003249	74.18	73.72	74.04	74.13	74.20
0.019937	69.57	69.56	70.63	69.59	69.95
0.049792	65.55	66.17	67.81	65.50	66.19
0.099588	61.54	62.58	64.65	61.14	62.18
0.50023	46.18	45.52	47.78	42.65	44.49
0.98536	35.57	32.19	33.69	29.81	31.53
2.0019	24.89	12.39	12.55	11.58	12.45
2.6215	20.29	4.739	4.622	4.503	4.867
2.9987	17.38	2.500	2.362	2.406	2.608
3.4487	13.85	1.342	1.208	1.315	1.430

TABLE IV

Calculated equivalent conductances at 35° C

Concentration (moles/liter)	Equivalent conductance (mhos)	Calculated equivalent conductances			
		Robinson–Stokes (mhos)		Falkenhagen–Leist (mhos)	
		$å = 10$ Å	$å = 17$ Å	$å = 4.0$ Å	$å = 6.0$ Å
0.000611	94.31	93.97	94.07	94.37	94.40
0.001164	93.64	93.17	93.37	93.69	93.74
0.001604	93.16	92.67	92.93	93.24	93.31
0.002241	92.60	92.14	92.45	92.71	92.81
0.002926	92.08	91.58	91.99	92.21	92.34
0.003914	91.45	90.94	91.46	91.60	91.77
0.019875	85.91	85.58	87.21	85.98	86.64
0.049637	80.96	81.04	83.54	80.48	81.78
0.49838	57.79	55.65	59.82	51.18	55.21
0.98092	45.40	40.31	43.52	35.90	39.94
1.9909	32.31	16.16	17.14	14.06	16.24
2.6061	26.43	6.514	6.755	5.661	6.638
2.9803	22.88	3.721	3.786	3.240	3.827
3.4238	18.57	2.106	1.620	1.842	2.194

The 25° C data, based on the Wishaw–Stokes equation, are given in columns 3 and 4 of Table III. Two values of $å$, viz. 13 Å and 20 Å, were used in these calculations. Even in the very dilute region, the calculated and observed conductances differ by as much as 0.3 mho. When $å = 13$ Å is used, the calculated and observed conductances agree within 0.7 mho up to a concentration of 0.5 M but for higher concentrations the calculated values differ markedly from the experimental results. For $å = 20$ Å, the deviation becomes large for a concentration of 0.02 M. Below this concentration, the agreement is similar to that observed for $å = 13$ Å. The reason for the similarity in the dilute region, despite the large difference in $å$ values, is that the equation becomes very insensitive to a change in $å$ value at lower concentrations.

The results with the Wishaw–Stokes equation at 35° C are given in columns 3 and 4 of Table IV, using $å$ values of 10 and 17 Å. Again, the agreement between observed and calculated values in the dilute region is only within 0.5 mho. For $å = 10$ Å, the conductance values are reproduced within 0.5 mho up to a concentration of 0.05 M. For $å = 17$ Å, the agreement is somewhat better in the dilute region but the region now extends only to 0.004 M. The calculated values for the higher concentrations again deviate very markedly from the experimental values.

The results of the calculations at 25° C based on the Falkenhagen–Leist equation are given in columns 5 and 6 of Table III. In the dilute region this equation reproduces the data rather well, the deviations being less than 0.1 mho up to 0.05 M and 0.4 mho at 0.1 M, when $å = 5.5$ Å. For the larger value, $å = 7.0$ Å, the deviation becomes appreciable at 0.02 M. Above 0.1 M, the equation fails rather badly.

Columns 5 and 6 of Table IV give the 35° C data obtained with the Falkenhagen–Leist equation. Behavior similar to that observed at 25° C is also observed here. The data are reproduced within 0.5 mho up to 0.05 M, with $å = 4.0$ Å, and within 0.8 mho, for $å = 6.0$ Å.

Compared with their behavior in regard to lithium chlorate, both equations perform very poorly. Moreover, the $å$ values are so large as scarcely to have any physical significance, at least with the Wishaw–Stokes equation, where the best value of $å$ is 10 Å, or greater. All conductance equations for the region of higher concentration must contain some function of the viscosity since undoubtedly a moving ion encounters a greater

resistance than it would in pure water or a very dilute solution. In the absence of a precise knowledge of the form of the viscosity function, theoretical investigators have been reduced to the necessity of dividing their calculated result by the relative viscosity of the solution and this has of course been done in all the calculations given here. If this were not done, a ludicrous result would be obtained for the very concentrated and very viscous solutions. In this connection it is perhaps significant that while the viscosity of sodium hexanoate solutions does not rise as high, at saturation, as that of lithium chlorate at saturation (an ideal salt for this kind of treatment), at comparable concentrations the viscosity of sodium hexanoate is much higher than that of lithium chlorate. This is exemplified in Fig. 1, where the viscosities of the aqueous solutions of the salts, at 25° C,
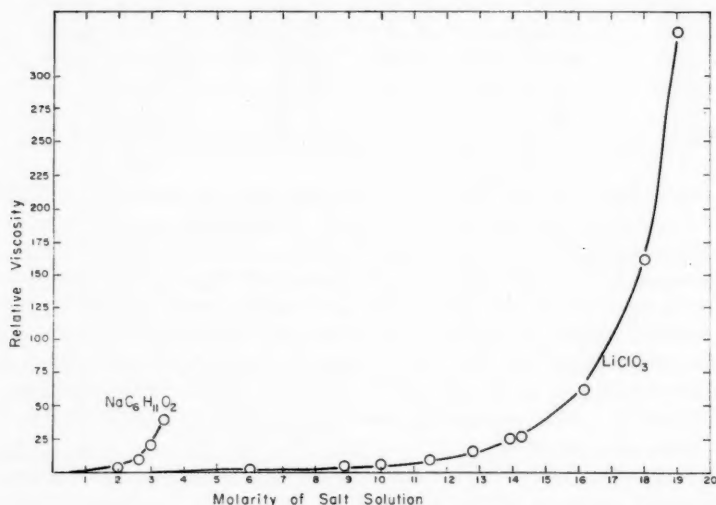
FIG. 1. Viscosity of sodium hexanoate and of lithium chlorate solution at 25° C.

are plotted against molar concentration. The graph shows that a saturated, or almost saturated, aqueous solution of sodium hexanoate, has a molarity of 3.45 but its viscosity equals that of a 15 M solution of lithium chlorate. If some power of the viscosity other than unity were used, the results might be brought into harmony, not only with one another, but with smaller d values. In the absence, however, of any theoretical indication as to what form the viscosity correction should take, there seems no point in further speculation.

An obvious explanation of the large d values would appear to exist in the assumption of micelle formation. According to McBain (13), solutions of colloidal electrolytes exhibit approximately ideal behavior until a certain concentration, characteristic of the substance, is reached. Marked deviation from ideal behavior then sets in rather suddenly. The sodium salts of the fatty acids belong to the class of compounds which exhibit this behavior. Smith and Robinson (14), employing the isopiestic vapor pressure method, conclude that the butyrate ion is the first of the fatty acid series to exhibit tendency toward micelle formation: micelle formation was observed for the hexanoate ion. On the other hand, McBain and co-workers (15) measured the conductance of the potassium

salts of the fatty acids and observed that anomalous curves were first obtained with potassium laurate (C_{12}). When our own figures for the equivalent conductance of sodium hexanoate are plotted against concentration, the curves do not show the minima characteristic of salts which form micelles. Again, if the specific conductance is plotted against concentration, there should be a "break" or sharp change of direction, at the critical micelle concentration, but no such "breaks" occur.

To clinch the question of whether or not micelle formation occurs in solutions of sodium hexanoate, we determined the apparent molecular weight of sodium hexanoate in solutions of different concentration, by the method of freezing point lowering. The liquid in equilibrium with ice at various temperatures was analyzed by evaporation to dryness. The results are given in Table V. The apparent molecular weights correspond to

TABLE V

Concentration, g salt/100 g H_2O	Apparent molecular weight
1.0517	69.2
5.1895	67.0
10.287	63.0
17.298	59.5

complete dissociation of the salt and give no evidence of micelle formation. It is strange that the apparent molecular weights decrease with increasing concentration but colligative behavior cannot be expected at these high concentrations and the activity coefficients are not known. Hence, in our opinion, micelle formation cannot be considered an explanation of the very large values of $\hat{a}$.

REFERENCES

1. B. F. WISHAW and R. H. STOKES. J. Am. Chem. Soc. **76**, 2065 (1954).
2. H. FALKENHAGEN, M. LEIST, and G. KELBG. Ann. Physik, **11** (6), 51 (1952); H. FALKENHAGEN and M. LEIST. Naturwiss. **24**, 570 (1954); Z. physik. Chem. **205**, 16 (1955).
3. G. JONES and G. M. BOLLINGER. J. Am. Chem. Soc. **53**, 411 (1931).
4. T. SHEDLOVSKY. J. Am. Chem. Soc. **54**, 1411 (1932).
5. J. E. LIND, JR., J. J. ZWOLENIK, and R. M. FUOSS. J. Am. Chem. Soc. **81**, 1557 (1959).
6. E. W. WASHBURN. J. Am. Chem. Soc. **38**, 2431 (1916).
7. D. F. SWINEHART. Anal. Chem. **21**, 1577 (1949).
8. M. J. CANNON and M. R. FENSKE. Ind. Eng. Chem., Anal. Ed. **10**, 299 (1938).
9. A. N. CAMPBELL and E. BOCK. Can. J. Chem. **36**, 330 (1958).
10. D. H. EVERETT, D. A. LANDSMAN, and B. R. W. PINSENT. Proc. Roy. Soc. A, **215**, 403 (1952).
11. G. C. BENSON and A. R. GORDON. J. Chem. Phys. **13**, 473 (1945).
12. A. N. CAMPBELL and W. G. PATERSON. Can. J. Chem. **36**, 1004 (1958).
13. M. E. L. McBAIN and E. HUTCHINSON. Solubilisation and related phenomena. Academic Press Inc., New York. 1955.
14. E. R. B. SMITH and R. A. ROBINSON. Trans. Faraday Soc. **38**, 70 (1942).
15. J. W. McBAIN, M. E. LAING, and A. F. TITLEY. J. Chem. Soc. **115**, 1279 (1919).

THE PREPARATION OF L-ARGINYL DIPEPTIDES OF ASPARAGINE, GLUTAMINE, AND SOME BASIC AMINO ACIDS[1]

Casimir Berse, Lucien Piché, and Akira Uchiyama

ABSTRACT

The synthesis of the following dipeptides is described: L-arginyl-L-asparagine acetate, L-arginyl-L-glutamine acetate, L-arginyl-L-lysine diacetate, and L-arginyl-L-ornithine diacetate. The two former were prepared by coupling a mixed anhydride of α-carbobenzoxy-ω-nitro-L-arginine directly with L-asparagine or with L-glutamine; catalytic hydrogenolysis of the resulting intermediates gave the dipeptides. The two others were obtained by combining α-carbobenzoxy-L-arginine with ω-carbobenzoxy-L-lysine methyl ester hydrochloride or with ω-carbobenzoxy-L-ornithine methyl ester hydrochloride in the presence of N,N'-dicyclohexylcarbodiimide; saponification and hydrogenation was necessary to uncover the resulting dipeptides.

Arginine is a universal constituent of proteins and is found in most of the physiologically active polypeptides. Its introduction in synthetic peptides has presented unusual difficulties caused by the strongly basic character of the guanidino group (1). The arginyl peptides, in which the carboxyl group of arginine is involved, were not prepared until three groups of workers reported initial success almost at the same time in 1953 (2, 3, 4). Although a variety of these compounds have now been synthetized by appropriate methods (5–8), the arginyl dipeptides containing basic amino acids have not hitherto been described; L-arginyl-L-arginine is the only exception (9).

Two methods were adapted to the combination of arginine with L-asparagine and L-glutamine or with L-lysine and L-ornithine respectively. In the first of these, α-carbobenzoxy-ω-nitro-L-arginine (6, 10) was converted to a mixed anhydride (11) by the action of ethyl chloroformate in the presence of an equimolar amount of tri-n-butylamine; it was then condensed directly with L-asparagine or with L-glutamine in alkaline solution. Catalytic hydrogenolysis of the resulting intermediates removed the carbobenzoxyl and nitro groups and resulted in the respective dipeptides; these were crystallized as the acetates.

The synthesis of L-arginyl-L-lysine and of L-arginyl-L-ornithine was attempted by the same procedure: the mixed anhydride of ethyl carbonate and α-carbobenzoxy-ω-nitro-L-arginine was condensed with ω-carbobenzoxy-L-lysine methyl ester hydrochloride and with ω-carbobenzoxy-L-ornithine methyl ester hydrochloride. Saponification of the resulting covered dipeptide esters was successful but the carboxylic compounds resisted hydrogenolysis in acidic, neutral, or basic media.

An alternate procedure based on the previous experience of Boissonnas *et al.* (15) was adopted. In this procedure the guanido group of α-carbobenzoxy-L-arginine is protected by a proton (2, 3) while condensation is carried out with N,N'-dicyclohexylcarbodiimide (12). Use of the proton to cover the guanido group avoided the necessity for hydrogenolysis of the nitro group and in contrast to previous experience of the authors (7) gave satisfactory yields of the protected dipeptides. The esters obtained by condensation of α-carbobenzoxy-L-arginine with ω-carbobenzoxy-L-lysine methyl ester or with ω-carbobenzoxy-L-ornithine methyl ester were saponified in the usual manner. Hydrogenation in 10% acetic acid over palladium catalyst converted the carboxylic intermediates into arginyl dipeptides; these were isolated as the diacetates.

EXPERIMENTAL

α-Carbobenzoxy-ω-nitro-L-arginyl-L-asparagine

Ethyl chloroformate (2.44 ml, 20 mmoles) was added to a solution of α-carbobenzoxy-ω-nitro-L-arginine (7.06 g, 20 mmoles) (5, 6, 10) and tri-*n*-butylamine (2.8 ml, 20 mmoles) in dry dioxane (50 ml). After 10 minutes, L-asparagine (2.64 g, 20 mmoles) in 0.4 N sodium hydroxide (50 ml) was added to the mixture at 10°. Carbon dioxide gas was given off vigorously. The mixture was shaken for 15 minutes at 10°, and then it was acidified to Congo red with N hydrochloric acid. Dioxane was evaporated *in vacuo* in the water bath, water was decanted, and the resulting oily product was triturated with cold acetonitrile until crystallization occurred. The compound was recrystallized from a mixture of N,N-dimethylformamide and acetonitrile. Yield 4.6 g (48%), m.p. 201°, $[\alpha]_D^{25}$ +6.2 (*c*, 4.17 in N,N-dimethylformamide). Anal. Calc. for $C_{18}H_{25}O_8N_7$: C, 46.25; H, 5.39; N, 20.98. Found: C, 46.27; H, 5.46; N, 20.88.

L-Arginyl-L-asparagine Acetate

α-Carbobenzoxy-ω-nitro-L-arginyl-L-asparagine (2.12 g, 4.53 mmoles) was dissolved in 0.1 N sodium hydroxide (4.65 ml). Palladium catalyst was added and the mixture was shaken with hydrogen for 5 hours. The catalyst was filtered off; pH of the solution was 8.6; it was brought to 5–6 with glacial acetic acid, then the solvent was evaporated until dryness *in vacuo* at 30–40°. The resulting product was washed with absolute ethanol and treated with N,N-dimethylformamide. On standing, the residue crystallized. The compound was recrystallized from aqueous methanol. Yield 1.2 g (75%), m.p. 260° (decomp.), $[\alpha]_D^{25}$ +11.1° (*c*, 0.83 in water). Anal. Calc. for $C_{12}H_{24}O_6N_6$: C, 41.34; H, 6.95; N, 24.13. Found: C, 41.32; H, 7.07; N, 24.16.

α-Carbobenzoxy-ω-nitro-L-arginyl-L-glutamine

This compound was prepared from α-carbobenzoxy-ω-nitro-L-arginine (3.53 g, 10 mmoles) and L-glutamine (1.46 g, 10 mmoles) in the manner described for α-carbo-benzoxy-ω-nitro-L-arginyl-L-asparagine; the product was crystallized several times from a mixture of a small amount of absolute ethanol and methylene chloride. Yield 2.8 g (45%), m.p. 168°, $[\alpha]_D^{25}$ −0.5° (*c*, 3.8 in N,N-dimethylformamide). Anal. Calc. for $C_{19}H_{27}O_8N_7$ (1/2 H_2O): C, 46.65; H, 5.72; N, 19.99. Found: C, 46.72; H, 5.91; N, 19.97.

L-Arginyl-L-glutamine Acetate

α-Carbobenzoxy-ω-nitro-L-arginyl-L-glutamine (2 g, 4.16 mmoles) was dissolved in a mixture of water (2 ml), methanol (2 ml), and glacial acetic acid (20 ml). The compound was hydrogenated for 12 hours at room temperature and at atmospheric pressure over 1 g of 10% palladium on carbon. The catalyst was filtered off and the solvent was evaporated *in vacuo* at 40–50°. The residue was crystallized from methanol–acetone. Yield 1.0 g (66%), m.p. 160°, $[\alpha]_D^{25}$ +19.2° (*c*, 3.87 in water). Anal. Calc. for $C_{13}H_{26}O_6N_6$ (1/2 H_2O): C, 42.16; H, 7.35; N, 22.65. Found: C, 42.34; H, 7.11; N, 22.67.

α-Carbobenzoxy-ω-nitro-L-arginyl-ω-carbobenzoxy-L-lysine Methyl Ester

α-Carbobenzoxy-ω-nitro-L-arginine (3.53 g, 10 mmoles) was dissolved in dry dioxane (100 ml) and tri-*n*-butylamine (2.4 ml, 10 mmoles) was added. The solution was cooled to 10° C; ethyl chloroformate (0.96 ml, 7.8 mmoles) was added with stirring and the solution was kept at 11–12° for 15 minutes. The product was then added to 150 ml of N,N-dimethylformamide containing 3.31 g (10 mmoles) of ω-carbobenzoxy-L-lysine methyl ester hydrochloride (13, 14). The mixture was shaken for 2 hours at room temperature and the solvent was evaporated at 40–50°. The residue was dissolved in ethyl acetate,

and the solution was washed successively with N hydrochloric acid, water, N sodium bicarbonate and water, dried over sodium sulphate, and evaporated to dryness *in vacuo*; it was then treated with isoamyl alcohol – methylene chloride (1:50). The resulting crystals were washed with ether and recrystallized from N,N-dimethylformamide–water. Yield 3.9 g (62%), m.p. 104°, $[\alpha]_D^{25}$ −2.5° (c, 4.64 in N,N-dimethylformamide). Anal. Calc. for $C_{29}H_{39}O_9N_7$: C, 55.35; H, 6.25; N, 15.58. Found: C, 55.28; H, 6.32; N, 15.39.

α-Carbobenzoxy-ω-nitro-L-arginyl-ω-carbobenzoxy-L-lysine

α-Carbobenzoxy-ω-nitro-L-arginyl-ω-carbobenzoxy-L-lysine methyl ester (6.35 g, 10.01 mmoles) was dissolved in methanol (20 ml) and N sodium hydroxide (20 ml, 20 mmoles) was added. The mixture was shaken for 3 hours; the alkaline solution was washed with ethyl acetate, then acidified to Congo red with N hydrochloric acid; the oily residue crystallized on standing. It was recrystallized from hot water or aqueous methanol. Yield 4.7 g (77%), m.p. 159°, $[\alpha]_D^{25}$ +3.8° (c, 1.44 in N,N-dimethylformamide). Anal. Calc. for $C_{28}H_{27}O_9N_7$: C, 54.80; H, 6.07; N, 15.93. Found: C, 54.55; H, 6.19; N, 15.74.

α-Carbobenzoxy-L-arginyl-ω-carbobenzoxy-L-lysine Methyl Ester Hydrochloride

α-Carbobenzoxy-L-arginine (3.08 g, 10 mmoles) (15, 17) and ω-carbobenzoxy-L-lysine methyl ester hydrochloride (3.65 g, 11 mmoles) were suspended in N,N-dimethylformamide (10 ml) containing diethyl phosphite (2 ml) and the mixture was stirred for 2 hours (15). To this solution was added N,N-dicyclohexylcarbodiimide (3.10 g, 15 mmoles). The mixture was stirred for 2 days at room temperature, then it was cooled to −10°; N,N-dicyclohexylurea precipitated and was filtered off. The urea was washed with a small amount of N,N-dimethylformamide which was combined with the filtrate. The solvent was removed *in vacuo*. The residue was triturated several times with anhydrous ether; it was then dissolved in methylene chloride (200 ml). The solution was washed with N ammonium hydroxide, water, N hydrochloric acid and water, and it was dried over sodium sulphate; the solvent was removed *in vacuo*. The crude product thus obtained was crystallized from methylene chloride – ether. It was recrystallized from the same solvent and again recrystallized from ethanol–ether. Yield 4.05 g (65%), m.p. 131°, $[\alpha]_D^{25}$ +9.9° (c, 5.69 in N,N-dimethylformamide). Anal. Calc. for $C_{29}H_{41}O_7N_6Cl$: C, 56.00; H, 6.66; N, 13.62. Found: C, 57.40; H, 7.01; N, 13.88.*

α-Carbobenzoxy-L-arginyl-ω-carbobenzoxy-L-lysine Hydrochloride

Sodium hydroxide (4 N, 2 ml, 8 mmoles) was added to α-carbobenzoxy-L-arginyl-ω-carbobenzoxy-L-lysine methyl ester hydrochloride (2.6 g, 4.2 mmoles) dissolved in methanol. The mixture was shaken at room temperature for 2 hours. The solution was diluted with water (2 ml), acidified with concentrated hydrochloric acid under cooling. Methanol was evaporated *in vacuo*. The product precipitated as an oil and crystallized on standing. It was recrystallized from hot water. Yield 1.53 g (60%), m.p. 205° $[\alpha]_D^{25}$ +27.8° (c, 1.82 in N,N-dimethylformamide). Anal. Calc. for $C_{28}H_{29}O_7N_6Cl$: C, 55.50; H, 6.50; N, 13.83. Found: C, 56.19; H, 7.12; N, 13.83.*

L-Arginyl-L-lysine Diacetate

(*a*) A number of attempts towards the hydrogenation of α-carbobenzoxy-ω-nitro-L-arginyl-ω-carbobenzoxy-L-lysine in methanol containing acetic acid or ammonium hydroxide or in neutral methanol, over palladium catalyst in the usual manner, were unsuccessful.

*In view of the poor agreement of the analytical data the other properties of the compound are subject to question. However, the intermediate at this stage of purity was suitable for the synthesis of L-arginyl-L-lysine diacetate.

(b) α-Carbobenzoxy-L-arginyl-ω-carbobenzoxy-L-lysine hydrochloride (1 g, 1.64 mmoles) was dissolved in methanol (20 ml) containing 10% by volume of glacial acetic acid. The compound was hydrogenated for 3 hours at room temperature and atmospheric pressure over palladium catalyst. The catalyst was removed by filtration and the filtrate was evaporated to dryness *in vacuo*. The residue was crystallized from methanol–acetone. Yield 0.41 g (58%), m.p. 167°, $[\alpha]_D^{25}$ +5.1 (c, 3.41 in water). Anal. Calc. for $C_{16}H_{33}O_7N_6$: C, 45.48; H, 8.11; N, 19.99. Found: C, 45.59; H, 8.24; N, 20.61.

α-Carbobenzoxy-ω-nitro-L-arginyl-ω-carbobenzoxy-L-ornithine Methyl Ester

This compound was prepared from α-carbobenzoxy-ω-nitro-L-arginine (3.53 g, 10 mmoles) and ω-carbobenzoxy-L-ornithine methyl ester hydrochloride (3.46 g, 10 mmoles) (16) in the manner described for α-carbobenzoxy-nitro-L-arginyl-ω-carbobenzoxy-L-lysine methyl ester hydrochloride. The product was recrystallized from methanol – methylene chloride (1:100 by volume). Yield 3.53 g (58%), m.p. 88°, $[\alpha]_D^{25}$ −16.2° (c, 1.0 in N,N-dimethylformamide). Anal. Calc. for $C_{28}H_{37}O_9N_7$: C, 54.70; H, 6.06; N, 15.91. Found: C, 54.35; H, 6.20; N, 15.85.

α-Carbobenzoxy-ω-nitro-L-arginyl-ω-carbobenzoxy-L-ornithine

α-Carbobenzoxy-ω-nitro-L-arginyl-ω-carbobenzoxy-L-ornithine methyl ester (7.00 g, 14 mmoles) was dissolved in methanol (20 ml) and N sodium hydroxide (20 ml, 20 mmoles) was added. The mixture was shaken for 3 hours. The product was isolated in the usual manner and recrystallized from hot water. Yield 4.9 g (72%), m.p. 185°, $[\alpha]_D^{25}$ −12.7° (c, 0.77 in N,N-dimethylformamide). Anal. Calc. for $C_{27}H_{35}O_9N_7$: C, 54.00; H, 5.86; N, 16.31. Found: C, 53.81; H, 5.84; N, 16.25.

α-Carbobenzoxy-L-arginyl-ω-carbobenzoxy-L-ornithine Methyl Ester Hydrochloride

This compound was prepared from α-carbobenzoxy-L-arginine (3.08 g, 10 mmoles) and ω-carbobenzoxy-L-ornithine methyl ester hydrochloride (3.80 g, 11 mmoles) in the manner described for α-carbobenzoxy-L-arginyl-ω-carbobenzoxy-L-lysine methyl ester hydrochloride. The crude product was precipitated from ethanol–ether and was recrystallized from methylene chloride – ether. Yield 3.73 g (62%), m.p. 122°, $[\alpha]_D^{25}$ +4.6 (c, 4.78 in N,N-dimethylformamide). Anal. Calc. for $C_{28}H_{39}O_7N_6Cl$: C, 55.30; H, 6.48; N, 13.85. Found: C, 55.51; H, 6.60; N, 13.88.

α-Carbobenzoxy-L-arginyl-ω-carbobenzoxy-L-ornithine Hydrochloride

α-Carbobenzoxy-L-arginyl-ω-carbobenzoxy-L-ornithine methyl ester hydrochloride (1.00 g, 1.75 mmoles) was saponified in the manner described for α-carbobenzoxy-L-arginyl-ω-carbobenzoxy-L-lysine hydrochloride. The product was recrystallized from hot water. Yield 0.61 g (58%), m.p. 103–106°, $[\alpha]_D^{25}$ +3.5° (c, 1.72 in N,N-dimethylformamide). Anal. Calc. for $C_{27}H_{37}O_7N_6Cl$: C, 54.70; H, 6.29; N, 14.17. Found: C, 54.48; H, 7.03; N, 13.80.

L-Arginyl-L-ornithine Diacetate

α-Carbobenzoxy-L-arginyl-ω-carbobenzoxy-L-ornithine hydrochloride (1.00 g, 1.68 mmoles) was dissolved in methanol (10 ml) containing 10% by volume of glacial acetic acid. The compound was hydrogenated for 3 hours at room temperature and atmospheric pressure over the palladium catalyst. The final product was obtained in the manner described for L-arginyl-L-lysine diacetate. Yield 0.53 g (77%), hygroscopic. The crude product (0.52) in 5% acetic acid (50 ml) was applied to the top of the curtain of the continuous flow paper electrophoresis cell (Spinco Model CP) and was carried downward by acetic acid solution (5%, 16 liters). Sample feed rate was 0.8 ml/hour. The acetic

acid solution was maintained at 1° C and the curtain temperature was 10° C. Power supply was 30 milliamperes and 500 volts. The curtain came to equilibrium after 2 hours. Collection of the sample solution was started 1/2 hour after the first fraction reached the drip point. Thirty-two (32) test tubes were used to collect the solution. Duration of a typical run was 65 hours. The curtain was then dried and developed with ninhydrin.

The sample solution in test tubes No. 27 to 32 was combined and the solvent was evaporated *in vacuo* at 40–50° C. The residue was precipitated from methanol–ether. Yield 0.36 g (53.9%), $[\alpha]_D^{25}$ +9.6 (c, 2.9 in water). Anal. Calc. for $C_{15}H_{22}O_7N_6$: C, 44.11; H, 7.90; N, 20.60. Found: C, 44.14; H, 8.05; N, 20.49.

ACKNOWLEDGMENTS

REFERENCES

1. J. S. FRUTON. Advances in Protein Chem. **51** (1949).
2. G. W. ANDERSON. J. Am. Chem. Soc. **75**, 6081 (1953).
3. D. T. GISH and F. H. CARPENTER. J. Am. Chem. Soc. **75**, 5872 (1953).
4. K. HOFMANN, W. D. PECKHAM, and A. RHEINER. J. Am. Chem. Soc. **75**, 6083 (1953).
5. H. O. VAN ORDEN and E. L. SMITH. J. Biol. Chem. **208**, 751 (1954).
6. K. HOFMANN, W. D. PECKHAM, and A. RHEINER. J. Am. Chem. Soc. **78**, 238 (1956).
7. C. BERSE and L. PICHÉ. J. Org. Chem. **21**, 808 (1956).
8. N. IZUMIYA and S. MAKISUMI. J. Chem. Soc. Japan, **78**, 1768 (1957).
9. L. ZERVAS, T. OTANI, M. WINITZ, and J. P. GREENSTEIN. Arch. Biochem. Biophys. **75**, 290 (1958).
10. M. BERGMANN, L. ZERVAS, and H. RINKE. Z. physiol. Chem. **224**, 40 (1934).
11. R. A. BOISSONNAS. Helv. Chim. Acta, **34**, 874 (1951).
12. J. C. SHEENAN and G. P. HESS. J. Am. Chem. Soc. **77**, 1067 (1955). J. C. SHEENAN, M. GOODMAN, and G. P. HESS. **78**, 1367 (1956).
13. A. NEUBERG and F. SANGER. Biochem. J. **37**, 515 (1943).
14. M. BERGMANN, L. ZERVAS, and F. WILLIAM. J. Biol. Chem. **111**, 249 (1935).
15. R. A. BOISSONNAS, ST. GUTTMANN, R. L. HUGUENIN, P. A. JAQUENOUD, and ED. SANDRIN. Helv. Chim. Acta, **41**, 1867 (1958).
16. R. L. M. SYNGE. Biochem. J. **42**, 100 (1948).
17. M. BERGMANN and L. ZERVAS. Ber. **65**, 1199 (1932).

PROTON MAGNETIC RESONANCE ABSORPTION IN
ANHYDROUS POTASSIUM STEARATE[1]

R. F. GRANT[2] AND B. A. DUNELL

ABSTRACT

The proton magnetic resonance absorption in anhydrous potassium stearate has been measured over the temperature range $-190°$ C to $182°$ C. Abrupt changes in line width have been found between $55°$ C and $62°$ C, and between $170°$ C and $171°$ C; these changes correspond approximately to known phase transitions. The reduction in line width and second moment with rising temperature is discussed.

INTRODUCTION

Like other alkali metal salts of long-chain fatty acids, potassium stearate passes through several transitions between solid state phases that exist in successive temperature ranges below the melting point. These transitions have been observed by various experimental methods, dilatometry (1, 2), differential calorimetry (3), and light transmission studies (4). They are, however, not so well understood in potassium stearate as in the sodium salts, for which it has been shown that the lowest temperature transitions (from a crystalline or curd phase to a waxy phase) correspond to the appearance of considerable structural disorder in the paraffin chain portion of the molecules (5, 6, 7). One infers from this appearance of disorder that the low-temperature transition may represent the onset of considerable motion in the paraffin chains. Since proton magnetic resonance has been useful in determining the nature of molecular motion in solid long-chain paraffin compounds (8, 9, 10), a magnetic resonance investigation of the lower-temperature transitions in anhydrous potassium stearate was made.

EXPERIMENTAL METHOD AND RESULTS

The potassium stearate used in this investigation was prepared from Eastman Kodak White Label grade stearic acid. This acid, which had a freezing point of $68.1°$ C, was purified by repeated crystallization at $-20°$ C from freshly distilled acetone (11) until the freezing point was raised to $69.1°$ C. The purified acid was dissolved in hot ethanol and titrated with an ethanolic solution of potassium hydroxide, using phenolphthalein as the indicator. The potassium stearate precipitate was dried at $105°$ C and then fused under vacuum to remove traces of water and alcohol. When cool, the fused soap was crushed and fused again under vacuum in 10-mm o.d. Pyrex sample tubes; dry nitrogen was admitted to the vacuum system and the sample tubes were sealed off.

The nuclear magnetic resonance spectrometer and sample thermostat have been described previously (12). The temperature of the sample was measured with a thermocouple inserted in a well in the side of the sample tube.

Figure 1 shows the variations of the proton magnetic resonance line width of potassium stearate as a function of temperature. Following the common usage, we have taken the line width as the separation, in gauss, of the points of maximum and minimum slope
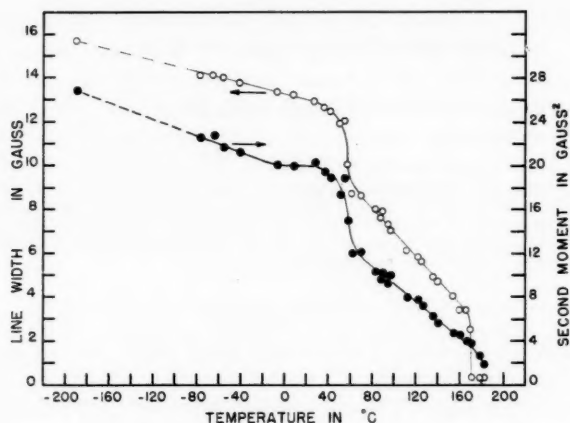
FIG. 1. Line width and second moment of potassium stearate as functions of temperature. Open circles, line width; filled circles, second moment.

on the resonance absorption line. Figure 1 also shows the corresponding variations of the second moment values with temperature. The second moments were obtained from the experimental derivative curves by the convenient method described by Powles (13) and were corrected for the effects of modulation (14).

It can be seen from Fig. 1 that there is an abrupt change in both line width and second moment between about 55° and 62° C and that there is a second discontinuity in line width between 170° and 171° C. At 171° C the line width is determined by depth of modulation and field inhomogeneity. The second moment shows no abrupt change at this temperature since the wings of the resonance line are only slightly narrowed, or decreased in intensity, as Fig. 2 shows.
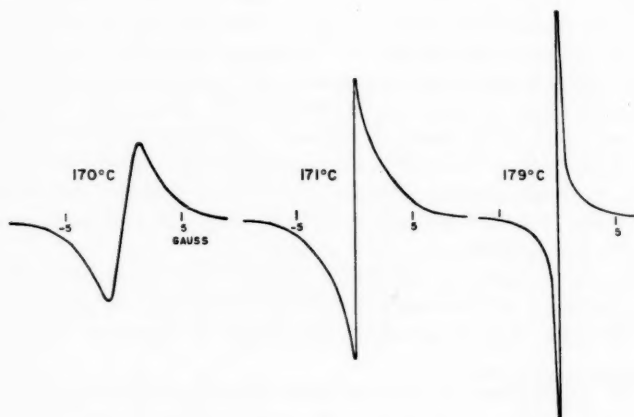
FIG. 2. Line shapes for potassium stearate near the phase transition at 170° C.

DISCUSSION

It is generally agreed that anhydrous potassium stearate passes through at least three phase transitions before melting (1–4). The lowest-temperature transition is variously located between 50° and 80° C; dilatometrically at 51° C by Vold (1) and with two changes in density at 65° and 80° C by Puddington and his co-workers (2), calorimetrically at 57° C by Ravich and Nechitaylo (3), and with X-ray studies at 78° C by Lomer (15), who has also measured the lattice parameters of the crystalline lower temperature B phase and crystalline higher temperature C phase. At least two other transitions occur before the substance melts to an isotropic liquid at 353° C (4), one in the range 160° to 170° C, and the other in the range 265° to 270° C (1–4). The positions at 160° and 170° C of the discontinuities observed in the n.m.r. line width agree with the transition temperatures observed by other techniques. Some indication of the nature of the low-temperature transition and of the solid phases may be obtained from a study of the second moment of the n.m.r. signal.

It can be shown that the rigid lattice second moment of the proton magnetic resonance for a polycrystalline sample (16, 17) is given by

$$S = \frac{716}{N} \sum_{j > k} r_{jk}^{-6}$$

where N is the number of protons whose interactions are considered and r_{jk} is the distance in angstrom units between any two protons j and k (9). In using this particular formula, it is assumed that the interactions of magnetic nuclei other than the protons in potassium stearate, such as the potassium nuclei and the nuclei of C^{13} and O^{17} in natural abundance, make a negligible contribution to the second moment.

An X-ray diffraction investigation of the A form of potassium caprate has indicated that the alternate carbon atoms in the zigzag paraffin chain are 2.60 Å apart (18), which would suggest that the bond angles differ slightly from the tetrahedral angle usually considered for long-chain paraffins. Moreover, electron diffraction studies on solid paraffin compounds have shown that the H—C—H bond angle may be about 107° and that the C—H bond length is about 1.12 Å (19, 20). A model of the paraffin chain part of potassium stearate, constructed using these bond parameters, and assuming that the C—C bond length is 1.54 Å (20), yields an intramolecular second moment of 18.0 gauss². The model in which tetrahedral bond angles and a C—H bond length of 1.094 Å are used gives an intramolecular second moment of 18.9 gauss². The intermolecular contribution will differ even less from the contribution for the non-tetrahedral model, and the total difference in second moments between the two is approximately within the error of experimental determination of second moment. If the experimental second moment of 26.8 gauss² at −190° C represents rigid lattice conditions, then the intermolecular second moment should be about 8.8 gauss².

Only the unit cell dimensions and the angle of tilt of the paraffin chains have been reported for potassium stearate (15). However, in the solid, the soap molecules are usually arranged such that the carboxylate ends form an electrically balanced ionic double layer, with the paraffin chains sticking out parallel to each other from both sides of this layer. If the paraffin chains were arranged parallel to one another with their long axes parallel to the ac planes and tilted at the angle $\tau = 53°$ (15) to the plane ab containing
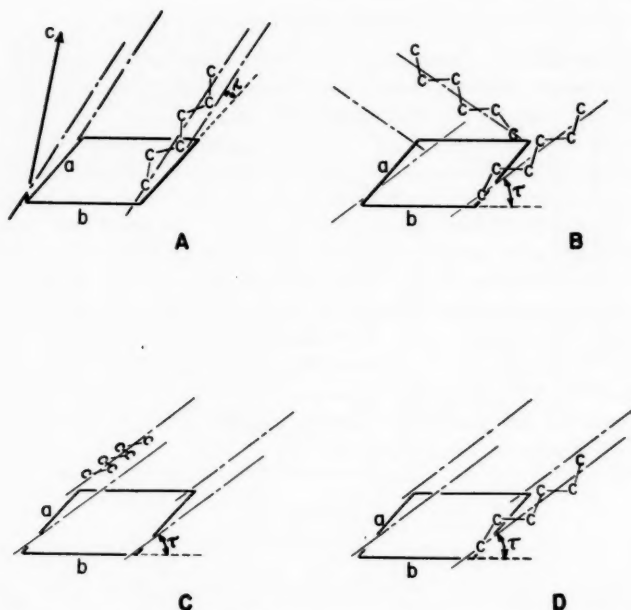
Fig. 3.   Possible orientations of the hydrocarbon chains in the potassium stearate unit cell. The dot-and-dash lines — – – – – represent the long axes of the hydrocarbon chains, and τ is the angle of tilt of 53° with respect to the plane ab.

the polar ends, as shown in Fig. 3A, some of the interhydrogen distances between chains would be reduced to values much less than the van der Waals diameter for a hydrogen atom, 2.4 Å (21). This arrangement has been dismissed as highly improbable. If the paraffin chains are inclined at 53° to the ab plane and arranged with their long axes parallel to bc planes, at least three reasonable values of the intermolecular second moment at 25° C may be obtained: 5.9 gauss² if the chains are not parallel to one another but are arranged in a crisscross fashion (Fig. 3B) as in the A phase of potassium caprate (18), 6.6 gauss² if the chains are parallel to one another and the plane of the C—C—C bonds is parallel to the a-axis (Fig. 3C), and 8.1 gauss² if the chains are parallel to one another and the plane of the C—C—C bonds is parallel to the b-axis (Fig. 3D). At −190° C the values are 6.2, 8.7, and 8.9 gauss² if one corrects the unit cell dimensions for thermal contraction using the coefficient of expansion given by Lomer (15). The first of these possibilities is considered less probable than either of the other two because of the poorer agreement between its calculated second moment of either 24.2 gauss² or 25.1 gauss² (non-tetrahedral or tetrahedral bond angles, respectively) at −190° C and the observed value of 26.8 gauss². The difference between the two remaining arrangements decreases with decreasing temperature because dimensional change in the a direction is much greater than in the b direction (15). The calculated value of the rigid lattice second moment may, then, be given as 27.2±0.5 gauss² depending mainly on whether or not tetrahedral bond angles are assumed in the hydrocarbon chain, and based on the arrangement of chains in the unit cell which gives best agreement with the experimental second moment of 26.8 gauss².

In considering the decrease of the line width and of the experimental second moment with increasing temperature, one must take note of recent modifications of the theory of Gutowsky and Pake (22), according to which theory both of these phenomena are to be expected as molecular reorientation becomes sufficiently rapid. Andrew and Newing (23) have discussed in detail the argument that the second moment must theoretically remain constant independent of the extent of molecular motion, pointing out that although the main central portion of the spectrum narrows, there is increased intensity in the wings of the spectral line because of production of side bands by modulation of the Larmor frequency by the molecular reorientation. Under some experimental conditions, however, the intensity of the side bands or the wings of the spectral line is comparable to or less than the noise level in the spectrometer. Thus the wings, which keep the second moment at its rigid lattice value, are not observable experimentally and the experimental second moment falls according to the earlier theory of Gutowsky and Pake. In the spectra of potassium stearate there were no indications of extended wings from the spectrometer with signal-to-noise ratio of 30. Further, the change of second moment with temperature effectively parallels the change in line width. Correlation frequencies can be calculated from the change of line width, which is not affected by the side bands, with temperature following the theory of Gutowsky and Pake (22). These agree substantially with correlation frequencies calculated from change of the observed second moment with temperature. One concludes, then, that the sensitivity and noise level of the spectrometer used in this work were such that side bands were not observed under any conditions, and our interpretation follows that of the original theory.

The experimental second moment at 25° C is 20 gauss², whereas the predicted rigid lattice value at this temperature is between 24.6 and 27 gauss² depending on the structure assumed. If the end methyl groups in potassium stearate reorient about their C_3 axes, a form of motion which is probably the first to take place with rising temperature in paraffins (9), the intramolecular second moment is reduced to 16.3 gauss² (17.1 gauss² for tetrahedral bond angles) (24). If the intermolecular contribution is reduced by a corresponding proportion, the total second moment should be between 22.2 and 24.4 gauss². Although zero-point vibrational motions may decrease the calculated second moment a little more (25), it will probably not be sufficient to give agreement with the experimental value of 20.0 gauss² at 25° C (12). It is suggested that the paraffin chains twist about their longitudinal axes in a torsional oscillation with amplitude somewhat in excess of the zero-point rocking vibration of the CH_2 groups. The relationship of the reduction of second moment to the amplitude of such oscillation has been calculated (8). Since each paraffin chain is clamped at one end in a strongly bonded salt layer, the amplitude of oscillation should increase along the chain with distance from this layer.

The line width and second moment change between 55° C and 62° C probably corresponds to the transition between the B and C crystalline phases (1, 2, 4). The known unit cell dimensions at 75° C (15) give an intermolecular second moment of about 6 gauss² if the paraffin chains are tilted at 53° C to ab and lie parallel to the bc plane. Thus the predicted rigid lattice second moment changes by about 2 gauss² between 25° C and 75° C, whereas the experimentally observed change is about 10 gauss². On going from the B to the C phase between 55° C and 62° C the experimental second moment is reduced by about 7 gauss², and hence greatly increased molecular motion, corresponding to more than 5 gauss² decrease in second moment, must accompany this change in structure. The complete reorientation of the potassium stearate molecules about the longitudinal axes of the paraffin chain portions would reduce the intramolecular second moment to 5.0

gauss^2 if reorientation of the end methyl groups about their C_3 axes also occurred (22, 24). The total second moment would then be 6.7 gauss^2 (8), which is the value at 130° C. There would be a further reduction of the second moment if there were reorientation about other axes in the molecule (24), which might be brought about by a bending motion of the twisting or rotating chain.

The sudden narrowing of the line width between 170° C and 171° C is probably associated with the phase transition reported to occur between 160° C and 170° C. This narrow line width must indicate comparatively great freedom of molecular motion in all directions, for most of the interaction between the proton pairs has been averaged out. However, the small change in the second moment at 171° C suggests that the molecules maintain their mean positions in the lattice (26) and that molecular motion is not yet isotropic. Infrared (6) and X-ray studies (7) on some sodium soaps suggest that a similar change in structure occurs when the temperature is raised above the "supercurd sub-waxy" transition at about 117° C. The transition between 160° C and 170° C reported in potassium stearate may therefore represent the beginning of a waxy-type phase.

ACKNOWLEDGMENTS

REFERENCES

1. R. D. VOLD, M. MACOMBER, and M. J. VOLD. J. Am. Chem. Soc. **63**, 168 (1941); R. D. VOLD and M. J. VOLD. J. Phys. Chem. **49**, 42 (1945).
2. D. P. BENTON, P. G. HOWE, R. FARNAND, and I. E. PUDDINGTON. Can. J. Chem. **33**, 1798 (1955).
3. G. B. RAVICH and N. A. NECHITAYLO. Doklady Akad. Nauk S.S.S.R. **83**, 117 (1952).
4. D. P. BENTON, P. G. HOWE, and I. E. PUDDINGTON. Can. J. Chem. **33**, 1384 (1955).
5. H. NORDSIECK, F. B. ROSEVEAR, and R. H. FERGUSON. J. Chem. Phys. **16**, 175 (1948).
6. D. CHAPMAN. J. Chem. Soc. 784 (1958).
7. A. SKOULIOS and V. LUZZATI. Nature (London), **183**, 1310 (1959).
8. E. R. ANDREW. J. Chem. Phys. **18**, 607 (1950).
9. F. A. RUSHWORTH. Proc. Roy. Soc. (London), A, **222**, 526 (1954).
10. S. KOJIMA and S. OGAWA. J. Phys. Soc. Japan, **8**, 283 (1953).
11. J. B. BROWN and D. K. KOLB. Progress in the chemistry of fats and other lipids. Vol. 3. Pergamon, London. 1955. p. 58.
12. R. F. GRANT and B. A. DUNELL. Can. J. Chem. **38**, 359 (1960).
13. J. G. POWLES. Brit. J. Appl. Phys. **9**, 299 (1958).
14. E. R. ANDREW. Phys. Rev. **91**, 425 (1953).
15. T. R. LOMER. Acta Cryst. **5**, 11 (1952).
16. J. H. VAN VLECK. Phys. Rev. **74**, 1168 (1948).
17. H. S. GUTOWSKY, G. B. KISTIAKOWSKY, G. E. PAKE, and E. M. PURCELL. J. Chem. Phys. **17**, 972 (1949).
18. V. VAND, T. R. LOMER, and A. LANG. Acta Cryst. **2**, 214 (1949).
19. B. K. VAINSHTEIN and A. N. LOBACHEV. Doklady Akad. Nauk S.S.S.R. **120**, 3 (1958).
20. B. K. VAINSHTEIN, A. N. LOBACHEV, and M. M. STASOVA. Kristallographia, **3**, 452 (1958).
21. L. PAULING. The nature of the chemical bond. Cornell University Press. 1948. p. 189.
22. H. S. GUTOWSKY and G. E. PAKE. J. Chem. Phys. **18**, 162 (1950).
23. E. R. ANDREW and R. A. NEWING. Proc. Phys. Soc. B, **72**, 959 (1958).
24. J. G. POWLES and H. S. GUTOWSKY. J. Chem. Phys. **21**, 1704 (1953).
25. J. A. IBERS and D. P. STEVENSON. J. Chem. Phys. **28**, 929 (1958).
26. E. R. ANDREW. Bristol Conference on Defects in Crystalline Solids, July 1954. The Physical Society, London. p. 60.

CONSTITUTION OF A GLUCOMANNAN FROM THE WOOD OF EASTERN WHITE PINE (PINUS STROBUS L.)[1]

M. O. GYAW AND T. E. TIMELL

ABSTRACT

Glucomannans have been isolated from the wood of eastern white pine (*Pinus strobus* L.) by two different methods, the ratios of mannose to glucose being 3.8:1 and 2.7:1, respectively. The yields, based on the mannose content of the wood, were 70 and 50%. Partial acid hydrolysis gave 4-*O*-β-D-mannopyranosyl-D-mannose, 4-*O*-β-D-mannopyranosyl-D-glucose, 4-*O*-β-D-glucopyranosyl-D-mannose, 4-*O*-β-D-glucopyranosyl-D-glucose, *O*-β-D-mannopyranosyl-(1 → 4)-*O*-β-D-mannopyranosyl-(1 → 4)-D-mannose, and *O*-β-D-mannopyranosyl-(1 → 4)-*O*-β-D-mannopyranosyl-(1 → 4)-*O*-β-D-mannopyranosyl-(1 → 4)-D-mannose. The fully methylated polysaccharide on hydrolysis gave a mixture of di-*O*-methylhexoses, 2,3,6-tri-*O*-methyl-D-mannose, 2,3,6-tri-*O*-methyl-D-glucose, and 2,3,4,6-tetra-*O*-methylhexose (mostly mannose) in a mole ratio of 4:61:21:1. The number-average degrees of polymerization of the methylated and the nitrated glucomannans were 96 and 93. On the basis of this and other evidence it is concluded that the glucomannan contains at least 90 mannose and glucose residues linked together by (1 → 4)-β-glycosidic bonds to linear macromolecules. The nature and relative composition of the oligosaccharides obtained on partial hydrolysis indicate that very few of the glucose residues are contiguous. The glucomannan is compared with similar polysaccharides from the wood of other gymnosperms.

In recent years it has become evident that the mannose residues in the wood of gymnosperms largely originate from glucomannan (1) or galactoglucomannan (2) heteropolymers. Glucomannans are the main hemicelluloses of softwoods and have lately been isolated from several species. A previous investigation (3) dealt with an arabino-4-*O*-methylglucuronoxylan from the wood of white pine (*Pinus strobus* L.). The present paper is concerned with the isolation and properties of a glucomannan from the same species.

RESULTS AND DISCUSSION

White pine wood (11.7% mannose residues) was delignified with acid chlorite (4) to give a holocellulose which still contained at least 5% lignin. Extraction with aqueous sodium hydroxide containing borate (5) gave a mixture of hemicelluloses which was not amenable to resolution by complexing with copper (6). Better results were obtained by the barium hydroxide method (7), but the precipitated glucomannan still contained 6.4% galactose residues which could not be removed by further treatments.

A glucomannan from Scots pine (*Pinus sylvestris* L.) was recently also found to retain galactose residues which could be removed only after complete elimination of residual lignin (8). The present crude glucomannan had an ultraviolet spectrum indicative of the occurrence of lignin, and the latter was accordingly eliminated by treatment with chlorine and ethanolamine (9). The hemicellulose obtained on copper complexing of the delignified material contained less than 2% galactose residues. Evidently, the lignin left in the crude hemicellulose acted as a binding agent between the main glucomannan component and other polysaccharides containing galactose residues. Whether the association was of a chemical or physical nature could not be decided on the basis of the present evidence.

The purified glucomannan, $[\alpha]_D$ $-32°$, contained glucose and mannose residues in a ratio of 1:3.8 and amounted to 10.6% by weight of the wood. Osmotic pressure measure-

ments on the nitrate derivative (10) gave a number-average degree of polymerization of 82. The polysaccharide consumed 1.0 mole of periodate per hexose residue, thus suggesting the presence of $(1 \rightarrow 4)$-glycosidic bonds.

In an alternative method of isolation of the glucomannan, wood meal was delignified with acid chlorite until the Klason lignin content was less than 1%. A hemicellulose mixture containing 5 parts of pentosan and 3 parts of hexosan was removed by extraction with aqueous potassium hydroxide. The residue, when extracted with sodium hydroxide containing borate, gave a hexosan containing only 3% xylose residues in a yield of 7% of the original wood. One precipitation with barium hydroxide lowered this yield to 6%. The glucomannan thus obtained contained 3% galactose residues and had a ratio of mannose to glucose of 2.7. Its number-average degree of polymerization was 93.

It is evident from this and other investigations (1, 11, 12) that the relative proportions of mannose and glucose residues in glucomannans are apt to vary considerably with the mode of isolation of these hemicelluloses. Of the two methods used here, the second was by far the least time-consuming and is preferable in spite of the somewhat lower yield. It is well known that prolonged treatment of wood with acid chlorite entails loss of carbohydrates (13, 14). In isolation of softwood hemicelluloses, this factor has to be weighed against the desirability of eliminating the lignin as completely as possible.

A portion of the glucomannan isolated by the first method was partially hydrolyzed with aqueous formic acid (15). The sugar mixture obtained was resolved on a column of charcoal–Celite (16) by gradient elution (17) with aqueous ethanol (18). Twelve oligosaccharides were collected, some of which were further purified by paper chromatography. Five of the oligosaccharides were crystallized and were fully identified, namely 4-O-β-D-mannopyranosyl-D-mannose (mannobiose), 4-O-β-D-glucopyranosyl-D-mannose, 4-O-β-D-glucopyranosyl-D-glucose (cellobiose), O-β-D-mannopyranosyl-$(1 \rightarrow 4)$-O-β-D-mannopyranosyl-$(1 \rightarrow 4)$-D-mannose, and O-β-D-mannopyranosyl-$(1 \rightarrow 4)$-O-β-D-mannopyranosyl-$(1 \rightarrow 4)$-O-β-D-mannopyranosyl-$(1 \rightarrow 4)$-D-mannose. Two sugars could not be crystallized but were tentatively characterized as a $(1 \rightarrow 4)$-β-linked O-mannosyl glucose and an O-glucosyl-O-mannosyl mannose. The paucity of material available prevented a characterization of the other oligosaccharides, all of which were evidently tri- or tetrasaccharides.

The mannobiose, mannosyl glucose, and glucosyl mannose have previously been isolated from many coniferous woods (12, 15, 19–24). The mannotriose has been obtained crystalline from loblolly pine (15) and white spruce wood (24) and was probably also present in glucomannan hydrolyzates from western hemlock (21), red cedar (22), and spruce sulphite pulp (23). The mannotetraose has been isolated previously only from vegetable ivory (25) and from white spruce wood (24). A mixed trisaccharide, apparently very similar to the compound obtained here, has been obtained from a spruce pulp (23).

The mannobiose was obtained in the highest yield (14.7%), followed by glucosyl mannose (5.4%), mannotriose (3.8%), mannotetraose (2.3%), mannosyl glucose (1.0%), and cellobiose (0.3%). Some of these results can undoubtedly be explained by the different stability towards acids of the glycosidic bonds, for example the five times higher yield of glucosyl mannose as compared with mannosyl glucose. This explanation cannot account, however, for the low yield of cellobiose which probably is more stable towards acids than any other of the oligosaccharides isolated. Low yields of cellobiose have been noticed on several occasions when softwood glucomannans were partially hydrolyzed (15, 23, 24, 26).

The glucomannan was methylated to completion and subsequently hydrolyzed to a mixture of sugars which was resolved on a charcoal–Celite column by gradient elution with aqueous ethanol. A mixture of di-O-methylhexoses, a tri-O-methylmannose, a tri-O-methylglucose, and a mixture of tetra-O-methylhexoses were obtained in a molar ratio of 4:61:21:1. The first fraction probably contained 2,6-di-O-methyl-D-glucose as its main component (8, 27). The following, and main, fraction was identified as 2,3,6-tri-O-methyl-D-mannose through its crystalline aniline and di-p-nitrobenzoate derivatives (28, 29). The tri-O-methylglucose crystallized and was also identified through its di-p-nitrobenzoate ester as 2,3,6-tri-O-methyl-D-glucose (29). The last fraction on demethylation gave mannose and a small quantity of glucose. Treatment with aniline, followed by repeated recrystallization, gave pure 2,3,4,6-tetra-O-methyl-N-phenyl-D-mannosylamine (30). This fraction consisted therefore predominantly of 2,3,4,6-tetra-O-methyl-D-mannose. The molar amount of this compound corresponded to one non-reducing end group per 87 hexose residues.

From the evidence adduced a simplified structure can now be assigned to the glucomannan present in the wood of white pine. The isolation of the two 2,3,6-tri-O-methyl-D-hexoses shows that the polysaccharide is composed of $(1 \rightarrow 4)$-linked D-mannopyranose and D-glucopyranose residues. The negative rotation of the original and the methylated hemicelluloses indicates that the hexose residues are present in the β-modification. The average number of hexose residues present in the methylated macromolecule was 96 while 87 such residues occurred for each non-reducing end group. An average number of 0.10 branch points per molecule was thus indicated. This number is so low, however, that the glucomannan might be regarded as essentially linear. Mannose residues apparently constituted the preponderant portion of the non-reducing end groups.

The nature of the hexose oligosaccharides isolated corroborate these conclusions. The low yield of cellobiose, in conjunction with the absence of any higher glucose oligosaccharides, show that very few of the glucose residues in the glucomannan were contiguous. The relatively high yields of mannobiose, mannotriose, and mannotetraose indicate that the glucose residues were probably interposed between blocks of contiguous mannose residues.

The mannose-to-glucose ratios of 2.7 and 3.8 found here are similar to those reported for other softwood glucomannans, such as (2.5) red cedar (22), (3) western hemlock (1, 21), (2.7) loblolly pine (15), (3.1–3.7) Scots pine (8, 31), (3.5–4) Norway spruce (27, 32), (2.5) Sitka spruce (12), and (3) white spruce (24, 33).

The evidence presently available concerning the linear or branched nature of softwood glucomannans is not conclusive. Glucomannans from red cedar (22), western hemlock (21), and Sitka spruce (12) are stated to be essentially linear, whereas similar glucomannans from Scots pine (8) and Norway spruce (27) are reported to be branched. The number-average degree of polymerization found here (93) is within the same range as the values observed for glucomannans from (130) western hemlock (21), (70–115) Scots pine (32), (68–100) Norway spruce (27), and (107) white spruce (24). All these polysaccharides were obtained after delignification of the wood with acid chlorite. In view of the now well-established depolymerizing action of this reagent on polysaccharides (9, 34), it seems almost certain that none of the above values represented the molecular magnitude of the native glucomannans. On the basis of previous results (34), an original number-average degree of polymerization of 200 for the present glucomannan does not appear unlikely.

CONCLUSIONS

The main structural features of the two preponderant hemicelluloses in the wood of white pine have now been established. One of these polysaccharides, which amounts to approximately 7% of the wood, is a $(1 \rightarrow 4)$-β-linked xylan containing numerous single side chains of either $(1 \rightarrow 2)$-α-linked 4-O-methyl-D-glucuronic acid or $(1 \rightarrow 3)$-linked L-arabinofuranose residues. The other hemicellulose, which accounts for 10–14% of the wood, is a neutral $(1 \rightarrow 4)$-linked hexosan containing about three times as many β-D-mannose as β-D-glucose residues. Both polysaccharides are linear or only slightly branched and both contain at least 100 but probably closer to 200 sugar residues in their native state.

The occurrence in the wood of gymnosperms of a predominant, neutral glucomannan together with an arabino-4-O-methylglucuronoxylan is apparently of early botanical origin. The same arrangement is found also for the wood of the now monotypical *Ginkgo biloba* (35), a phylogenetically far older gymnosperm (upper Carboniferous) than the present-day conifers. In contrast, the hemicelluloses of the botanically much younger arborescent angiosperms are characterized by the presence of a predominating 4-O-methylglucuronoxylan while the neutral glucomannan here has been relegated to a much more inconspicuous role.

EXPERIMENTAL

All specific rotations are equilibrium values and were determined at 20° C. Melting points are corrected. Evaporations were carried out *in vacuo* at 40–50° C.

Paper Chromatography

The following solvent systems (v/v) were used for separating the sugars: (A) ethyl acetate – acetic acid – water (9:2:2), (B) butan-1-ol – pyridine – water (10:3:3), (C) butan-1-ol – pyridine – water (6:4:4), and (D) butanone–water (89:11). Whatman No. 1 or, for preparative purposes, No. 3MM filter papers were used. Paper electrophoresis was carried out with Whatman No. 3MM filter paper in 0.05 M borate buffer at 750 or 2000 volts. o-Aminodiphenyl was used as a spray reagent and also for quantitative sugar analysis (36).

Isolation of a Mixture of Hemicelluloses

The preparation and properties of the wood sawdust used have been described previously (3). Extractive-free wood meal (40–60 mesh, 200 g) was suspended with stirring in water at 75–80° C. Acetic acid (20 ml) and sodium chlorite (60 g) were added and the reaction was allowed to proceed for 1 hour, when the same amounts of reagents were added. After a total time of 4 hours, the holocellulose was recovered by filtration, washed with water and then with ethanol, and dried in the air. Yield: 151 g, 75.5% of the wood. This process was repeated several times with new wood.

Chlorite holocellulose (300 g) was shaken with 17.5% (w/w) aqueous sodium hydroxide, to which 4% of boric acid had been added, in an atmosphere of nitrogen at room temperature for 3 hours. The alkaline solution was removed by filtration through fritted glass and the solid residue was washed with 17.5% sodium hydroxide (3 liters). Washing with aqueous acetic acid, water, and ethanol gave an alpha-cellulose (109 g). The alkaline solutions were poured into ice-cold ethanol (15 liters) containing glacial acetic acid (3 liters). The precipitate formed was recovered by filtration, washed in succession with

80% aqueous ethanol, ethanol, and petroleum ether (b.p. 30–60° C), and finally dried *in vacuo* to give a crude hemicellulose (118 g, 29.7% of the wood). Constituent sugars were galactose (3%), glucose (13%), mannose (41%), arabinose (8%), and xylose (35%).

Isolation of a Crude Glucomannan

The mixture of hemicelluloses (100 g) was dissolved in 5% sodium hydroxide (4 liters). The solution was centrifuged and a minor amount of insoluble material was removed. Saturated aqueous barium hydroxide (4 liters) was added dropwise with constant stirring (7). The precipitate formed was recovered on the centrifuge, washed twice with 5% sodium hydroxide, suspended in ice water, and acidified with acetic acid. The solution was poured into four times its volume of ethanol and the precipitate was recovered in the usual way. Yield: 68 g, 20.2% of the wood. Constituent sugars were galactose (6.4%), glucose (17.5%), mannose (70.3%), and xylose (5.8%). Further treatments with barium hydroxide or Fehling's solution (6) failed to alter the galactose content. The ultraviolet spectrum of the product exhibited a band at 280 mμ.

Purification of the Glucomannan

Glucomannan (35 g) was dissolved in water (3 liters). Gaseous chlorine was introduced into the solution at +6° C for 5 minutes (9). The solution was poured into ethanol (12 liters) and the recovered hemicellulose was suspended in ethanol (3 liters) containing 3% monoethanolamine for 5 minutes at 70° C. The polysaccharide was recovered by centrifuging and washed three times with ethanol after which it was added to water (3 liters). This delignification process was repeated three times. The polysaccharide was finally treated twice with Fehling's solution to yield a purified product (18 g, 10.4%). Analysis indicated the presence of galactose (2%), glucose (20%), and mannose (78%).

Isolation of a Glucomannan by an Alternative Method

Extractive-free wood meal (1385 g) was delignified with acid chlorite in the usual way (4) for 4 hours. The holocellulose (962 g, 69.6%) was extracted with 24% potassium hydroxide as described previously (3) to yield a mixture of hemicelluloses (155 g, 15.0%), containing 37% of hexosans. The solid residue (780 g) was shaken with 17.5% aqueous sodium hydroxide, to which 4% boric acid had been added, at room temperature for 5 hours. The alkaline solution was recovered by filtration and the residue was washed thoroughly with water. The filtrate and washings were poured into four times their volume of a 4:1 mixture of ethanol and acetic acid. The precipitate was recovered in the usual way to give a glucomannan (96 g, 7.0% of the wood), containing glucose and galactose (23%), mannose (68%), and xylose (3%). One precipitation with barium hydroxide (7) gave a product (83 g, 6.0%) which contained galactose (3%), glucose (26%), and mannose (71%). Specific rotation, $[\alpha]_D$ −32° (*c*, 1.0 in 10% sodium hydroxide).

Partial Hydrolysis of the Glucomannan and Resolution of the Hydrolyzate

A portion of the glucomannan obtained by the first method (10 g) was dissolved in 90% formic acid and diluted with water to 45% (100 ml). The solution, $[\alpha]_D$ −27°, was heated at 97° C for 3 hours when the specific rotation was +15° (after heating for 7 hours, $[\alpha]_D$ was +39°, equilibrium). Formic acid was removed by repeated evaporation from water after which the residue was boiled under reflux with 0.5 N sulphuric acid (320 ml) for 10 minutes for elimination of formate esters. The acid was neutralized with barium

carbonate and the solution obtained after filtration through Celite was deionized with Amberlite IR-120 (H⁺) and Dowex 1-X4 (acetate) exchange resins.

A portion of the hydrolyzate (7.5 g) was added to the top of a Darco G-60 charcoal – Celite column (9) (1:1, w/w, 6×64 cm) and the sugars were removed by gradient elution (17) with aqueous ethanol (18) in the following order: water → 2% aqueous ethanol (3 liters each), 2% ethanol → 10% ethanol (4 liters), 10% ethanol → 20% ethanol (4 liters), and 20% ethanol → 40% ethanol (2 liters). The eluate was collected in 20-ml fractions at intervals of 30 minutes.

Identification of Sugars

All sugars were chromatographically identical with authentic specimens (solvents A, B, and C).

(1) Monosaccharides

A mixture of glucose and mannose in addition to minor amounts of xylose (2890 mg) was first obtained. The sugars were characterized only by paper chromatography (solvents A and B).

(2) 4-O-β-D-Mannopyranosyl-D-mannose

Hydrolysis of this fraction (1015 mg), the first oligosaccharide to be removed from the charcoal column, indicated the presence of mannose only. The mannobiose, after recrystallization from methanol, had a melting point and a mixed melting point of 209–210° C, $[\alpha]_D$ −8° (c, 3.5 in water) (37). The X-ray diffraction pattern and infrared diagram were identical with those from an authentic specimen.

(3) 4-O-β-D-Mannopyranosyl-D-glucose

This sirupy disaccharide (73 mg) had $[\alpha]_D$ +29° (c, 2.4 in water) (38) and on hydrolysis yielded equal amounts of glucose and mannose. After reduction with sodium borohydride only mannose was obtained on hydrolysis. The mannosyl glucose could not be induced to crystallize.

(4) 4-O-β-D-Glucopyranosyl-D-glucose

This fraction (107 mg) was a mixture of a disaccharide and a tetraose. Resolution by paper chromatography (solvent C) gave pure cellobiose (23 mg), $[\alpha]_D$ +35° (c, 1.0 in water). Recrystallization from methanol gave a melting point and a mixed melting point of 234–235° C (39).

(5) O-β-D-Mannopyranosyl-(1 → 4)-O-β-D-mannopyranosyl-(1 → 4)-D-mannose

This trisaccharide (262 mg) on hydrolysis gave mannose and on partial hydrolysis mannobiose and mannose. Analysis by the method of Peat, Whelan, and Roberts (40) suggested a degree of polymerization of 2.8. The product crystallized from ethanol, m.p. and mixed m.p. 165-168° C, $[\alpha]_D$ −25° (c, 2.4 in water) (41).

(6) 4-O-β-D-Glucopyranosyl-D-mannose

Hydrolysis of this disaccharide (373 mg) gave equal amounts of glucose and mannose. The compound crystallized from ethanol, m.p. and mixed m.p. 134–137° C, $[\alpha]_D$ +10° (c, 4.0 in water) (42). The octaacetate derivative had a melting point and a mixed melting point of 201° C, $[\alpha]_D$ +34° (c, 1.0 in chloroform).

(7) O-Glucosyl-O-mannosyl Mannose

This fraction (285 mg), $[\alpha]_D$ −8° (c, 6.6 in water), on hydrolysis yielded glucose and mannose in a ratio of 1:2. Reduction with sodium borohydride followed by hydrolysis

gave equal amounts of glucose and mannose. The degree of polymerization of the compound was 2.9 (40). Partial hydrolysis with formic acid gave mannobiose, glucosyl mannose, glucose, and mannose.

(8) *O-β-D-Mannopyranosyl-(1 → 4)-O-β-D-mannopyranosyl-(1 → 4)-O-β-D-mannopyranosyl-(1 → 4)-D-mannose*

At this stage, elution of the column gave a mixture of trisaccharides which was not further examined (941 mg). Subsequent elution gave a mixture of higher oligosaccharides (1034 mg) which, on resolution by paper chromatography (solvent C), yielded a pure mannotetraose (114 mg). The compound on recrystallization from aqueous ethanol had a melting point and a mixed melting point of 232–234° C, $[\alpha]_D$ −31° (c, 1.0 in water) (25). Partial hydrolysis gave mannotriose, mannobiose, and mannose.

Methylation of the Glucomannan

Glucomannan (19 g) was dissolved in 30% (w/w) aqueous sodium hydroxide (400 ml) in an atmosphere of nitrogen, and dimethyl sulphate (200 ml) was added dropwise at 0° C over a period of 8 hours (43). This treatment was repeated twice. The reaction mixture was neutralized with sulphuric acid, concentrated to 1 liter, and dialyzed against running water for 1 week. The polysaccharide solution was concentrated to 200 ml and freeze-dried for 2 days, yielding a powder of partially methylated glucomannan (18 g, OCH_3, 26.8%). The product was dissolved in dry dimethyl formamide (44). Silver oxide (50 g) and methyl iodide (50 ml) were added and the mixture was shaken at 30° C for 20 hours. The same amounts of reagents were added and the reaction mixture was again shaken for 20 hours. The insoluble, grayish mass was washed on the centrifuge with chloroform. The solution obtained was washed with 5% aqueous potassium cyanide (3×300 ml) and then with water (3×500 ml). After drying over anhydrous sodium sulphate, the chloroform solution was concentrated to 200 ml and poured slowly with stirring into petroleum ether (2 liters) to yield a white powder (14 g).

After one more methylation as above, the product was methylated according to Purdie (45) with methyl iodide (200 ml) and silver oxide (80 g). The final product had $[\alpha]_D$ −21° (c, 1.0 in chloroform). Anal. Calc. for a fully methylated glucomannan: OCH_3, 45.3%. Found: OCH_3, 45.0%. The infrared spectrum of the polysaccharide indicated the absence of hydroxyl groups.

Hydrolysis of the Methylated Glucomannan and Resolution of the Hydrolyzate

The fully methylated polysaccharide (4.0 g) was boiled under reflux with 0.7 N methanolic hydrogen chloride for 12 hours. Most of the methanol was removed and N hydrochloric acid (120 ml) was added. The solution was refluxed for 7 hours, neutralized with silver carbonate, filtered through Celite, treated with hydrogen sulphide, and again filtered. Chromatographic examination (solvent D) of the sirupy hydrolyzate (3.6 g) revealed the presence of di-, tri-, and tetra-O-methylhexoses.

A portion of the sirup (3.4 g) was added to the top of a Darco G-60 charcoal – Celite column (5×56 cm) and subjected to gradient elution with 4 liters each of 5% aqueous ethanol → 20% ethanol and 20% ethanol → 40% ethanol.

Preliminary Characterization of Di-O-methylhexoses

Paper electrophoresis indicated the presence of three components in the fraction first eluted from the charcoal column (156 mg). The principal component gave only glucose

on demethylation with hydrobromic acid (46). It was chromatographically and electrophoretically indistinguishable from 2,6-di-O-methyl-D-glucose. The other two components were electrophoretically similar to 2,4- and 3,6-di-O-methylglucose.

Identification of 2,3,6-Tri-O-methyl-D-mannose

The second fraction (2400 mg) was further purified by paper chromatography (solvent D). The sirup had $[\alpha]_D$ −12.6° (c, 2.6 in water) (47). A portion of the compound (100 mg) was converted to the 1,4-di-p-nitrobenzoate derivative (80 mg), m.p. and mixed m.p. 187–188° C, $[\alpha]_D$ +33° (c, 1.0 in chloroform), after recrystallization from ethanol (29). Recrystallization from ethyl acetate gave needles, m.p. 187–188° C. The 2,3,6-tri-O-methyl-N-phenyl-D-mannopyranosylamine had a melting point of 125° C, $[\alpha]_D$ −152° (c, 0.6 in methanol) (28).

Identification of 2,3,6-Tri-O-methyl-D-glucose

The third fraction (814 mg) on recrystallization from ethyl ether had a melting point and a mixed melting point of 120–121° C, $[\alpha]_D$ +70° C (c, 1.0 in water) (47). The 1,4-di-p-nitrobenzoate derivative (29), on recrystallization from methanol, had a melting point and a mixed melting point of 189–190° C, $[\alpha]_D$ −34° (c, 0.7 in chloroform).

Identification of 2,3,4,6-Tetra-O-methyl-D-mannose

The fourth fraction (43.7 mg) on demethylation yielded glucose and mannose and was a mixture of the 2,3,4,6-tetra-O-methyl derivative of glucose and mannose, $[\alpha]_D$ +4.8° (c, 4.4 in water). The infrared spectrum of the sirup agreed closely with that of 2,3,4,6-tetra-O-methyl-D-mannose. Treatment with aniline gave 2,3,4,6-tetra-O-methyl-N-phenyl-D-mannosylamine, m.p. and mixed m.p. 145–146° C (30), after three recrystallizations from ethyl ether.

Periodate Oxidation of the Glucomannan

Glucomannan (150–200 mg) was oxidized for various lengths of time in the dark at 30° C with 0.05 M sodium metaperiodate (50 ml). The consumption of periodate was measured by the excess arsenite method. The molar consumption of periodate per hexose residue was 1.0.

Preparation of the Nitrate Derivative of the Glucomannan

Glucomannan (1 g) was treated with a mixture of nitric acid, phosphoric acid, and phosphorus pentoxide (64:26:10, w/w) at +17° C for 1 hour (48). The reaction mixture was poured into aqueous acetic acid (1:1) cooled to −16° C. The nitrate was recovered by filtration and washed with water until the washings were neutral. Yield, 90%; nitrogen content (49), 13.56%. A duplicate experiment gave a product with the same nitrogen content and in the same yield.

Determination of the Number-Average Molecular Weight of the Methylated and the Nitrated Glucomannans

The osmometers were of the modified (49) Zimm–Myerson (50) type. The membranes were of gel cellophane and the solvent was a mixture of chloroform and ethanol (9:1, v/v) for the methylated and n-butyl acetate for the nitrated glucomannan. The temperature was 30±0.01° C and the static method of measuring the osmotic height was used. The results obtained are summarized in Table I.

TABLE I
Osmometry data

Nitrate ester				Methyl ether	
Preparation I*		Preparation II†			
w‡	h/w§	w	h/w	w	h/w
4.429	1.176	5.004	1.026	2.511	1.444
2.218	1.163	3.151	1.018	1.952	1.363
2.198	1.139	2.225	0.991	1.399	1.343
1.121	1.108	1.330	1.006	0.823	1.334
0	1.11	0	0.98	0	1.31

*Glucomannan isolated by first method.
†Glucomannan isolated by second method.
‡Concentration in grams/kilogram of solution.
§Osmotic height in centimeters of solution/concentration.

ACKNOWLEDGMENT

REFERENCES

1. J. K. HAMILTON, H. W. KIRCHER, and N. S. THOMPSON.   J. Am. Chem. Soc. **78**, 2508 (1956).
2. J. K. HAMILTON, E. V. PARTLOW, and N. S. THOMPSON.   J. Am. Chem. Soc. **82**, 451 (1960).
3. S. K. BANERJEE and T. E. TIMELL.   Tappi. In press.
4. L. E. WISE, M. MURPHY, and A. A. D'ADDIECO.   Paper Trade J. **122**, No. 2, 35 (1946).
5. J. K. N. JONES, L. E. WISE, and J. P. JAPPE.   Tappi, **39**, 139 (1956).
6. E. SALKOWSKI.   Ber. **27**, 497 (1894).
7. H. MEIER.   Acta Chem. Scand. **12**, 144 (1958).
8. H. MEIER.   Acta Chem. Scand. **12**, 1911 (1958).
9. T. E. TIMELL and E. C. JAHN.   Svensk Papperstidn. **54**, 831 (1951).
10. C. P. J. GLAUDEMANS and T. E. TIMELL.   Svensk Papperstidn. **61**, 1 (1958).
11. G. G. S. DUTTON and K. HUNT.   J. Am. Chem. Soc. **80**, 5697 (1958).
12. G. O. ASPINALL, R. A. LAIDLAW, and R. B. RASHBROOK.   J. Chem. Soc. 4444 (1957).
13. B. L. BROWNING and L. O. BUBLITZ.   Tappi, **36**, 452 (1953).
14. H. O. BOUVENG and H. MEIER.   Acta Chem. Scand. **13**, 1884 (1959).
15. J. K. N. JONES and T. J. PAINTER.   J. Chem. Soc. 669 (1957); 573 (1959).
16. R. L. WHISTLER and D. F. DURSO.   J. Am. Chem. Soc. **72**, 677 (1950).
17. R. S. ALM.   Acta Chem. Scand. **6**, 1186 (1952).
18. B. LINDBERG and B. WICKBERG.   Acta Chem. Scand. **8**, 569 (1954).
19. J. G. LEECH.   Tappi, **35**, 249 (1952).
20. A. ANTHIS.   Tappi, **39**, 401 (1956).
21. J. K. HAMILTON and H. W. KIRCHER.   J. Am. Chem. Soc. **80**, 5703 (1958).
22. J. K. HAMILTON and E. V. PARTLOW.   J. Am. Chem. Soc. **80**, 4880 (1958).
23. E. MERLER and L. E. WISE.   Tappi, **41**, 80 (1958).
24. A. TYMINSKI and T. E. TIMELL.   J. Am. Chem. Soc. 82 (1960).
25. G. O. ASPINALL, R. B. RASHBROOK, and G. KESSLER.   J. Chem. Soc. 215 (1958).
26. J. K. HAMILTON, E. V. PARTLOW, and N. S. THOMPSON.   Tappi, **41**, 803 (1958).
27. I. CROON and B. LINDBERG.   Acta Chem. Scand. **12**, 453 (1958).
28. W. N. HAWORTH, E. L. HIRST, and H. R. L. STREIGHT.   J. Chem. Soc. 1349 (1931).
29. P. A. REBERS and F. SMITH.   J. Am. Chem. Soc. **76**, 6097 (1954).
30. W. N. HAWORTH, R. L. HEATH, and S. PEAT.   J. Chem. Soc. 833 (1941).
31. I. CROON, B. LINDBERG, and H. MEIER.   Acta Chem. Scand. **13**, 1299 (1959).
32. B. LINDBERG and H. MEIER.   Svensk Papperstidn. **60**, 785 (1957).
33. T. E. TIMELL and A. TYMINSKI.   Tappi, **40**, 519 (1957).
34. C. P. J. GLAUDEMANS and T. E. TIMELL.   Svensk Papperstidn. **60**, 869 (1957).
35. A. JABBAR MIAN and T. E. TIMELL.   Unpublished results.
36. T. E. TIMELL, C. P. J. GLAUDEMANS, and A. L. CURRIE.   Anal. Chem. **28**, 1916 (1956).
37. R. L. WHISTLER and J. Z. STEIN.   J. Am. Chem. Soc. **73**, 4169 (1951).
38. F. SMITH and H. C. SRIVASTAVA.   J. Am. Chem. Soc. **78**, 1404 (1956).
39. Z. H. SKRAUP and J. KÖNIG.   Monatsh. **22**, 1011 (1901).

40. S. Peat, W. J. Whelan, and J. G. Roberts.   J. Chem. Soc. 2258 (1956).
41. R. L. Whistler and C. G. Smith.   J. Am. Chem. Soc. 74, 3795 (1952).
42. M. Bergman and H. Schotte.   Ber. 54, 1564 (1921).
43. W. N. Haworth.   J. Chem. Soc. 107, 8 (1915).
44. R. Kuhn, H. Trischmann, and I. Löw.   Angew. Chem. 67, 32 (1955).
45. T. Purdie and J. C. Irvine.   J. Chem. Soc. 83, 1021 (1903); 85, 1049 (1904).
46. L. Hough, J. K. N. Jones, and W. H. Wadman.   J. Chem. Soc. 1702 (1950).
47. J. C. Irvine and E. L. Hirst.   J. Chem. Soc. 121, 1213 (1922).
48. W. J. Alexander and R. L. Mitchell.   Anal. Chem. 21, 1497 (1949).
49. J. V. Stabin and E. H. Immergut.   J. Polymer Sci. 14, 209 (1954).
50. B. H. Zimm and I. Myerson.   J. Am. Chem. Soc. 68, 911 (1946).

CATIONIC POLYMERIZATION OF ETHYLENE OXIDE

IV. THE PROPAGATION REACTIONS[1]

G. T. Merrall, G. A. Latrémouille, and A. M. Eastham

ABSTRACT

Studies of the boron-fluoride-catalyzed reaction of ethylene oxide with simple alcohols and low molecular weight polyglycols indicate three ways in which chain growth could occur, but only one of these is considered to be important after the initial stages of polymerization. The rate of disappearance of monomer reaches a maximum at a molecular weight of about 400. A mechanism is proposed to account for both polymerization and depolymerization and it is shown how equilibrium between these two reactions could result.

The polymerization of ethylene oxide by boron fluoride is a complex process in which the propagation reaction must compete with an apparently independent depolymerization reaction. The depolymerization process, as discussed in the previous paper (1), breaks down the polyglycol to dioxane seemingly through a chain reaction propagated by oxonium ions acting upon the ether linkages in the polymer molecule. The polymerization on the other hand appears to occur through a stepwise addition of monomer to the terminal hydroxyls of the polymer chain. A study was therefore undertaken of the reaction of ethylene oxide with alcohols in the presence of boron fluoride in an effort to obtain a mechanism for the propagation and to observe the transition from propagation to depolymerization. This paper presents the results of these studies.

EXPERIMENTAL

Ethylene chloride, ethylene oxide, and boron fluoride were prepared for use as previously described (2). Volatile alcohols were dried by distillation from their magnesium alcoholates in the usual way and ethers were dried over sodium metal or calcium hydride. Wherever the reactants were sufficiently volatile they were stored on the vacuum system and transferred by distillation. The polyglycols were either stirred under high vacuum for several hours or dissolved in dry ethylene chloride and pumped free from solvent before use.

Molecular weights were determined by viscosity measurements as before, but in a few cases were confirmed by freezing point depressions in benzene. Where hydroxyl content of the polymer was important, end group analysis by acetylation with acetyl chloride in pyridine, according to the method of Smith and Bryant (3), was used. All three methods gave satisfactory agreement.

Reactions were carried out in ethylene chloride solution at 20° C. Rates were followed either by the decrease in vapor pressure of ethylene oxide as described in the earlier work, or by a dilatometric method. The dilatometers were so constructed that they could be dried and filled under vacuum and then transferred to a constant temperature bath while exposing only the capillary tip to the atmosphere. Absolute contractions were not determined but the contraction per unit of oxide appeared to be constant over the range of the experiments. The two methods gave good agreement wherever they could be compared.

RESULTS AND DISCUSSION

Before discussing the reaction of ethylene oxide with alcohols, it is necessary to draw some conclusions as to the probable distribution of boron fluoride in a system containing both hydroxyl and ether groups. We know (4) that boron fluoride with water forms both monohydrates and dihydrates and that the second molecule of water is held, at least in the crystal, as the hydronium ion,

$$BF_3 \xrightleftharpoons[]{H_2O} BF_3:H_2O \xrightleftharpoons[]{H_2O} H_3\overset{+}{O} \ldots \overset{-}{BF_3}OH.$$
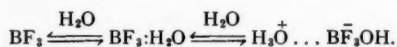
The dihydrate is much the more stable of the two complexes but in the corresponding alcoholates this difference in stability appears to be much smaller. Ethers yield 1:1 compounds with boron fluoride but in the presence of alcohols they yield ternary complexes, analogous to the dihydrates, in which the ether is held by hydrogen bonding,

$$ROH:BF_3 + R_2'O \rightleftharpoons RO:BF_3 \ldots HOR_2' \rightleftharpoons ROH + R_2'O:BF_3.$$

Obviously then, in a solution of hydroxyl and ether groups such as one has with the polyglycols, the boron fluoride will be present as an equilibrium mixture of several complexes and, since the reaction rates will depend on the concentrations and reactivities of the various species present, a rigorous interpretation of the kinetics will require an accurate knowledge of all the equilibrium constants. Information of this kind is not available nor is it likely to be for some time to come so a few simple experiments were conducted in an effort to obtain some idea of the relative importance of the various complexes.

The relative basicities of a few ethers towards boron fluoride were examined by equilibrating the ethers in ethylene dichloride solution against dimethyl ether and boron fluoride. The concentration of free dimethyl ether in solution was obtained from its vapor pressure and the position of the equilibrium was then calculated from the known initial concentrations of all reactants. Constants obtained in this way held very well over about a fivefold range of concentrations and, where comparison could be made, were in good agreement with values calculated from the data of Brown and Adams (5) for the thermal dissociation of boron fluoride etherates. A few values of the relative basicities are listed in Table I.

TABLE I

Dimethyl ether	1
Di-n-butyl ether	0.16
Dioxane (molar basis)	0.115
Tetrahydrofurane	25.

Ethylene oxide unfortunately could not be examined because of its high reactivity, but the dimethyl ether of diethylene glycol, $CH_3OCH_2CH_2OCH_2CH_2OCH_3$, is of some interest because of its similarity to the polyglycols. In our experiments this molecule was found to add only two molecules of boron fluoride and of these one seemed to be held quite loosely. At low boron fluoride concentrations, however, the triether was quite basic with a relative basicity, on a molar basis, of about 0.4. In a similar manner a little information was obtained about the ternary complexes. If one adds dimethyl ether to a solution of equimolar amounts of boron fluoride and n-butanol, then an amount of ether equal to

the boron fluoride is removed from the solution. Since addition of further alcohol regenerates some ether, an equilibrium of the type

$$\text{ROBF}_3 \ldots \text{H} \ldots \text{OR}'_2 + \text{ROH} \rightleftharpoons \text{ROBF}_3 \ldots \text{H} \ldots \text{HOR} + \text{R}'_2\text{O}$$
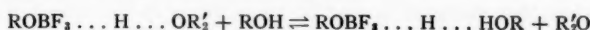
seems indicated so, on the assumption that any binary complexes present are in low concentration compared with the ternaries, an equilibrium constant can be obtained. This constant was found to hold surprisingly well over the short range of concentrations which could be examined and indicated that the dimethyl ether was about 1.5 times as basic as n-butanol towards the acid ROH:BF$_3$. From subsequent experiments it seems likely that at high ratios of ether to alcohol serious interference from the binary ether – boron fluoride complex may occur, but as much of our work has been carried out at low values of this ratio, we feel justified in assuming that the catalyst will be present largely as the ternary complex in most of our reaction mixtures. Furthermore, as alcohols and ethers seem to have rather similar basicities, we must expect that a mixture of ternary complexes will be present.

Ethylene oxide reacts with simple alcohols to give the β-alkoxyethanols which can in turn react with further monomer. Since the latter reaction is several times more rapid than the initial one, rates must be obtained either from initial slopes or from experiments at high alcohol/oxide ratios. The results obtained with n-butanol are shown in Table II

TABLE II

Reaction of n-butanol with ethylene oxide

Butanol	Oxide	BF$_3$	Initial rate, moles liter^{-1} min^{-1}	
			Observed	Calculated
Vapor pressure method				
0.26	1.10	.0093	.025	.0285
0.26	1.10	.0150	.040	.046
0.52	0.50	.0121	.0095	.0107
0.52	0.55	.0191	.017	.0202
0.52	0.52	.0191	.0175	.0192
0.52	1.10	.0066	.013	.0128
0.52	1.10	.0099	.019	.0192
0.52	1.10	.0166	.0335	.0322
0.52	1.10	.0188	.040	.0365
0.52	1.64	.0190	.062	.0502
1.0	0.52	.0220	.014	.0142
1.0	0.535	.0218	.015	.0145
1.0	1.10	.0117	.0155	.0152
1.0	1.10	.0160	.020	.0208
1.0	1.10	.0208	.030	.0270
1.0	1.56	.0069	.0115	.0123
1.0	1.56	.0118	.021	.0210
1.0	1.56	.0118	.0205	.0210
1.0	1.56	.0127	.022	.0226
1.0	1.56	.0203	.0435	.036
1.4	1.52	.0121	.018	.0172
Dilatometric method				
0.52	1.110	.0095	.00184	.00218
0.62	0.233	.0104	.0041	.00435
1.0	0.083	.0181	.00202	.00195
1.0	0.115	.0109	.00125	.00161
1.43	0.102	.0153	.00156	.00160
1.43	0.116	.0146	.00162	.00173

but essentially similar results were obtained with ethanol. The rate of the reaction decreases with increasing alcohol concentration. From our previous discussion it seems most probable that this decrease is due to an increase in the concentration of boron fluoride dialcoholate, so we may suppose that the rate is governed by the following reactions,

$$ROH + ROH \cdot BF_3 \cdot oxide \quad \overset{K_1}{\rightleftharpoons} \quad ROH \cdot BF_3 \cdot ROH + oxide$$

reaction [1] k_1 reaction [2] k_2

product
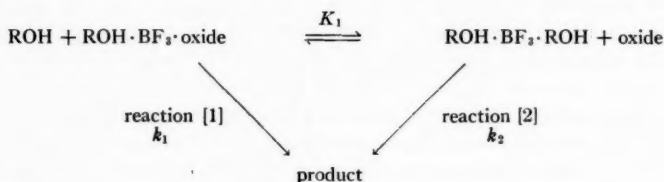
where reaction [1] is the unimolecular rearrangement of a ternary complex of all three reactants while reaction [2] is a bimolecular reaction between ethylene oxide and the boron fluoride dialcoholate. The rate expression for this system, assuming only ternary complexes, is found to be

$$-\frac{d(oxide)}{dt} = (BF_3)(oxide)\frac{k_1K_1 + k_2(ROH)}{K_1(oxide) + (ROH)}$$

which, when assigned the following values for the constants, $K_1 = 0.1$, $k_1 = 9$ min^{-1}, and $k_2 = 0.4$ liter mole^{-1} min^{-1}, gives the calculated rates shown in Table II. The agreement with the experimental values is good but since there are three constants to adjust such agreement does not mean a great deal. The real test of the mechanism would perhaps be an independent measurement of the equilibrium constant K_1, i.e. of the basicity of ethylene oxide and this, as noted above, we were unable to obtain. The above kinetic value of K_1 suggests that the oxide is about 1/10th as basic as n-butanol and hence about 15 times less basic than dimethyl ether, so is in agreement with qualitative experiments (6) which indicate that epoxides are among the least basic of the simple ethers.

The reaction of ethylene oxide with a simple alcohol is the first step in an addition polymerization in which the second and third steps can be represented by the reactions of the monoethyl ethers of glycol (Cellosolve) and diethylene glycol (Carbitol), respectively. The results of some dilatometric experiments with these alcohols are shown in Fig. 1; vapor pressure measurements were in reasonable agreement with the dilatometric measurements at the higher alcohol concentrations but diverged at the lower ones. The rate measurements show a minimum with both Cellosolve and Carbitol at low alcohol concentration. We have examined this region carefully and feel that the minimum is probably real but admittedly it could be due to a breakdown of the dilatometric method in this region or to experimental errors which tend to accumulate at low alcohol concentrations. If it is real, it would appear that the increasing rate at very low hydroxyl concentrations corresponds to an extension of the curve for n-butanol to low alcohol concentrations, i.e. to a region where reaction [1] is dominant. This view receives some support from the fact that no minimum is evident in runs with a polyglycol of molecular weight 600 (Fig. 1) where the contribution from reaction [1] would be reduced markedly by the competition of the polymer ether groups for the boron fluoride. While the presence of the minimum is disturbing, its presence should not be allowed to obscure the most important conclusion from these results, namely, that a clear change in mechanism, not
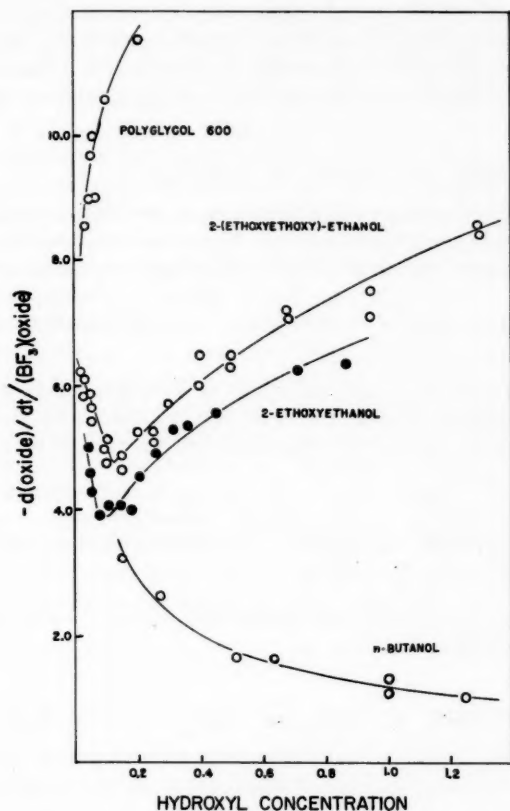
FIG. 1.

merely a change in rate, has occurred in passing from the simple alcohols to the β-ether alcohols. This change must be due to the presence of the ether groups and suggests that an oxonium ion type of reaction is important even at this early stage of the polymerization.

Meerwein and his co-workers have shown (7) that epoxides react, both rapidly and quantitatively, with anhydrous ethers and boron fluoride to form the inner oxonium salts,

$$\begin{array}{c} R \\ \diagdown \\ \diagup \\ R \end{array}\!\!O{:}BF_3 \;+\; \underset{O}{CH_2CH_2} \;\rightarrow\; \begin{array}{c} R \\ \diagdown \\ \diagup \\ R \end{array}\!\!\overset{+}{O}\underset{\cdot\cdot BF_3O^-}{\overset{\diagup CH_2}{\diagdown}}\!CH_2,$$
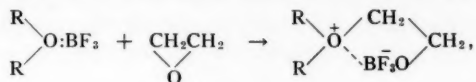
which can then react with further etherate to form the tertiary salts,

$$\begin{array}{c} R \\ \diagdown \\ \diagup \\ R \end{array}\!\!\overset{+}{O}\!\overset{\diagup CH_2CH_2}{\text{-----------------}}OB\bar{F}_3 \;+\; \begin{array}{c} R \\ \diagdown \\ \diagup \\ R \end{array}\!\!O{:}BF_3 \;\rightarrow\; R_3\overset{+}{O}B\bar{F}_4 \;+\; ROCH_2CH_2OBF_2 .$$
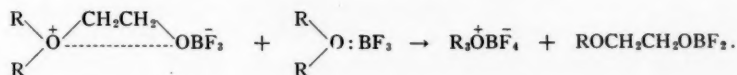
The inner salts differ from the tertiaries in being very unstable and insoluble so most probably account for the precipitation and discoloration we observe in the absence of

hydroxyl groups. It may be that the hydroxyl groups decompose the inner salts as formed, but an alternative explanation is possible and would account for other aspects of the polymerization process. Klages and Meuresch (8) showed that ether complexes of very strong acids will react with diazomethanes to form tertiary oxonium salts, both rapidly and quantitatively,

$$R_2O\text{-------}HBF_4 \; + \; R'CHN_2 \; \rightarrow \; R_2\overset{+}{O}CH_2R'\text{-------}B\bar{F}_4 \; + \; N_2.$$

The acid–ether complexes here are closely similar to the alcohol–ether – boron fluoride complexes encountered in the present work so if ethylene oxide could replace the diazomethane, tertiary oxonium ions would be formed directly according to the reaction

$$RO:BF_3\text{--------}H\text{-------}OR_2' \; + \; \underset{\diagdown O \diagup}{CH_2-CH_2} \; \overset{k_4}{\longrightarrow} \; R_2'\overset{+}{O}CH_2CH_2OH\text{-------}B\bar{F}_3OR. \qquad [4]$$
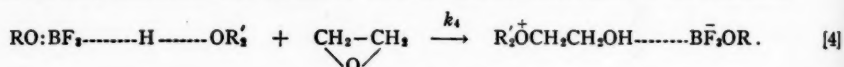
A reaction of this form seems best able to account for the rapid reaction of ethylene oxide with the lower ether alcohols and may be considered as an exact analogue of reaction [2], differing from it only in the stability of the product; in reaction [2] the catalyst is regenerated immediately

$$RO:B\bar{F}_3\text{-------}\overset{\overset{\textstyle H^+}{|}}{H\text{---}OR} \; + \; \underset{\underset{\textstyle O}{\diagdown\diagup}}{CH_2CH_2} \; \overset{k_2'}{\longrightarrow} \; R\overset{\overset{\textstyle H^+}{|}}{O}CH_2CH_2OH\text{--------}B\bar{F}_3OR \qquad [2]$$
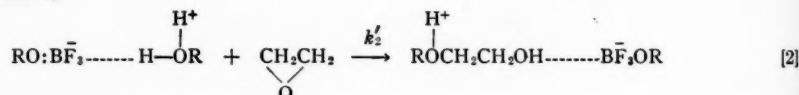
whereas in reaction [4] the oxonium ion is sufficiently stable that it must be decomposed by reaction with a hydroxyl group, i.e.

$$R_2'\overset{+}{O}CH_2CH_2OH \; + \; ROH \; \overset{k_5}{\longrightarrow} \; R_2'O \; + \; R\overset{\overset{\textstyle H^+}{|}}{O}CH_2CH_2OH. \qquad [5]$$
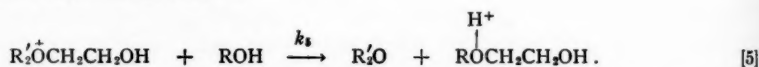
The net effect of this formation and destruction of the oxonium ion is to lengthen a chain by one oxide unit so we now have three processes which can lead to chain growth, reactions [1], [2], and [4, 5], all of which must be considered as important in the reaction of Cellosolve and Carbitol. The system is obviously too complex for complete kinetic analysis but under conditions of high alcohol/oxide ratios, as in some of the dilatometric experiments, reaction [1] should not be important and the boron fluoride will be distributed between two ternary complexes,

$$ROH\cdot BF_3\cdot alcohol/ROH\cdot BF_3\cdot ether \; = \; K_2,$$
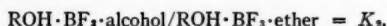
according to whether hydrogen bonding takes place at an alcohol or ether group. The value of K_2 will be governed by the ratio of ether to alcohol groups in the molecule and not by the concentration of the ether–alcohol; it will decrease as the chain grows longer. If steady-state conditions were to apply to the oxonium ion, the rate expression for the system would be

$$-\frac{d(\text{oxide})}{dt} = \frac{k_2'K_2 + k_4 k_5}{K_2 + 1 + \dfrac{k_4(\text{oxide})}{k_5(\text{ROH})}} (BF_3)(\text{oxide}),$$

or if reaction [5] were very rapid compared with [4]

$$-\frac{d(\text{oxide})}{dt} = \frac{k_2'K_2 + k_4}{K_2 + 1} (BF_3)(\text{oxide}).$$

These very similar expressions are in agreement with the observed first-order dependence on boron fluoride and ethylene oxide but require that the rate be independent of hydroxyl concentration. It is evident in Fig. 1 that at the higher alcohol concentrations where reaction [1] can be disregarded, the rates do in fact tend towards such independence without actually achieving it. This failure of the rate expressions is probably due to the high rate of reaction [4], which invalidates the assumptions used in deriving them.

Extension of these results to low molecular weight polymers is not simple. Rate expressions of the type just considered suggest that as the molecular weight increases and K_2 becomes very small, the reaction should reduce to a simple second-order process. In fact, however, at high molecular weights (3000–4000) the rate of oxide disappearance becomes very slow and independent of monomer concentration. For reasons detailed in the previous paper (1), we believe that this slow zero-order rate is due to the formation of stable oxonium ions which do not react directly with ethylene oxide with the result that reaction [5] becomes rate controlling. (In solutions of high molecular weight polymer the hydroxyl concentration is, of necessity, low.) Between the two extremes of the very low and the high molecular weight polyglycols the rate of reaction of oxide with the glycols, at constant hydroxyl concentration, passes through a maximum at a molecular weight of about 400. The order in oxide at moleculer weights below the maximum is always one or nearly so, but at higher molecular weights it drops off steadily. If, as we believe, the order is determined by the relative rates of reactions [4] and [5], then it is legitimate to compare initial rates of oxide disappearance and this is done in Fig. 2 for initial concentrations of boron fluoride and ethylene oxide of 0.012 M and 0.55 M, respectively.
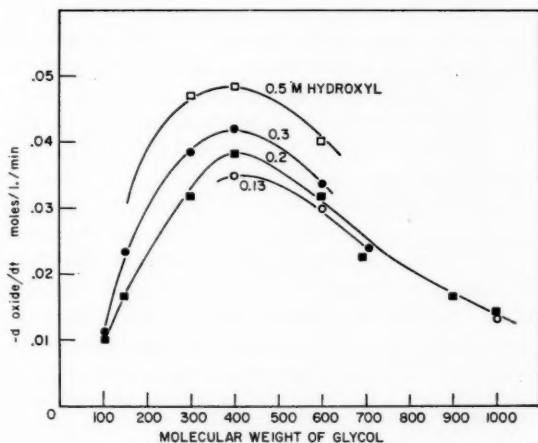
FIG. 2.

It was stated earlier that the increase in rate in passing from the simple alcohols to the ether alcohols is most probably due to a contribution from a reaction proceeding via oxonium ions. On the other hand, the decrease in both rate and order at higher molecular weights is almost certainly due to the presence of stable oxonium ions, so the problem is to resolve this apparent conflict in a way which will account for the rate maximum at molecular weight 400. Dilatometric experiments with low molecular weight polymer and very small amounts of monomer suggest strongly that reaction [4], oxonium ion formation,

is very fast even at molecular weights well above 400 (Fig. 1), so the over-all rate must be governed largely by reaction [5]. It follows that reaction [5] must be especially rapid in the molecular weight range 200–400 and since there seems no reason why reaction between an oxonium ion and *any* terminal hydroxyl group should be molecular weight dependent, this conclusion suggests that internal reaction, i.e. reaction of the oxonium ion with the hydroxyls of its own chain, is important at low molecular weights. Once reached, this conclusion seems quite reasonable for we know that an oxonium ion readily attacks the oxygen atoms of its own chain (dioxane formation), so with low molecular weight polymer there is a high probability that the oxygen attacked will be that of a hydroxyl group. With triethylene glycol, for example ($HOCH_2CH_2OCH_2CH_2OCH_2CH_2OH$, mol. wt. 150), no other reaction is possible, but with higher polymers one or more dioxane units may have to be eliminated before the attack at hydroxyl is possible. The reaction could take place in two ways, one leading to polymerization and the other to depolymerization,

$$
\begin{array}{c}
\text{ROCH}_2\text{CH}_2 \\
\text{HOCH}_2\text{CH}_2
\end{array}
\!\!\!\stackrel{+}{\text{O}}\!\!\!
\begin{array}{c}
\text{CH}_2\text{CH}_2 \\
\text{HO} \quad \text{CH}_2\text{CH}_2
\end{array}\!\!\!\text{O}
\longrightarrow
$$

$$
\begin{array}{c}
\text{ROCH}_2\text{CH}_2 \\
\text{HOCH}_2\text{CH}_2
\end{array}\!\!\!\text{OH}^+ \;+\; \text{O}\!\!\!
\begin{array}{c}
\text{CH}_2\text{CH}_2 \\
\text{CH}_2\text{CH}_2
\end{array}\!\!\!\text{O} \quad \text{depolymerization}
$$

$$
\text{H}^+
$$
$$
\text{ROCH}_2\text{CH}_2\text{OCH}_2\text{CH}_2\text{OCH}_2\text{CH}_2\text{OCH}_2\text{CH}_2\text{OH} \quad \text{polymerization}
$$
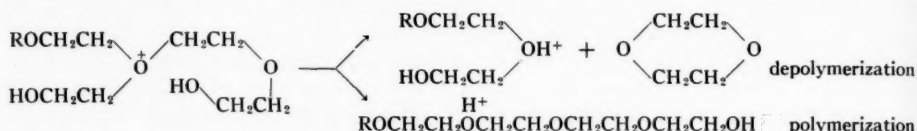
but from the point of view of rate it does not matter which occurs since both lead to destruction of the oxonium ion. Our evidence suggests, however, that polymerization is favored for we could detect no dioxane in the product of the reaction between the mono-ethylether of triethylene glycol and an equimolar amount of triethyloxonium fluoroborate.

According to the reaction scheme here proposed, the increasing rate at low molecular weights is due primarily to a transition from reaction [2] to reaction [4]. With continued chain growth, however, reaction [5], which is composed of two parts corresponding to internal and external termination, becomes steadily slower as internal termination becomes less and less probable. Since the probability of internal termination should be inversely related to the molecular weight, it is not surprising that the maximum rate occurs at a definite molecular weight at all hydroxyl concentrations. More surprising perhaps is the relatively small contribution of the external to the total termination.

With a reaction mechanism for guidance, the conditions governing molecular weight equilibrium can be considered. If equilibrium were to occur at molecular weights above about 1500, the situation would be relatively simple because it could be assumed that all termination occurred by the external route and the order in oxide could be taken as zero, with all the catalyst in the form of oxonium ion. The rates of dioxane formation and monomer disappearance would be given approximately by

$$d(\text{dioxane})/dt = k_6(\text{oxonium ion}),$$

$$-d(\text{oxide})/dt = k_7(\text{oxonium ion})(\text{ROH}),$$

and would be related at equilibrium as

$$2d(\text{dioxane})/dt = -d(\text{oxide})dt.$$

It follows that equilibrium would occur at a hydroxyl concentration equal to $2k_6/k_7$ but it would be an equilibrium in the sense that if a polymer were added to the reaction so as to give a hydroxyl concentration of $2k_6/k_7$, then that polymer would neither grow nor depolymerize. At higher hydroxyl concentrations growth would occur and at lower concentrations the polymer would disappear.

In practice equilibrium occurs at molecular weights where the order in oxide is less than about 0.5 but certainly not zero, and where internal termination is still a major part of the total termination. If the oxide concentration were important in determining the equilibrium, then the molecular weight should rise to a maximum in the course of a polymerization and fall off again as the monomer concentration declines. We have found some evidence for a maximum of this kind but it is scarcely greater than the error in the weight measurements, so the concentration of oxide will be ignored in the present discussion. The contribution of internal termination to the equilibrium, on the other hand, cannot be ignored and unfortunately cannot be expressed with our present information. It obviously will become smaller as the molecular weight increases and may perhaps be roughly inversely proportional to the molecular weight, in which case the total termination rate would be given by

$$-d(\text{oxonium ion})/dt = [k_7(\text{ROH}) + k_8/(\text{mol. wt.})](\text{oxonium ion})$$

which in turn, assuming that reaction [5] is rate controlling, would be the rate of oxide disappearance. Accordingly at equilibrium

$$2k_6(\text{oxonium ion}) = [k_7(\text{ROH}) + k_8/(\text{mol. wt.})](\text{oxonium ion})$$

giving

$$(\text{mol. wt.})_{\text{equilib}} = k_8/[2k_6 - k_7(\text{ROH})].$$

This treatment is obviously exceedingly crude but is interesting in that it suggests that the equilibrium molecular weight should be somewhat dependent on the hydroxyl concentration for this in fact seems to be the case (Table III).

TABLE III

Hydroxyl concentration	Approx. final molecular wt.
0.03	525
0.06	600
0.12	750
0.20	800
0.61	1000

A reaction as complex as this one will require a great deal of work before it yields any exact solutions and we do not pretend that the reaction schemes presented in this and the preceding paper are any more than preliminary ones. They do, however, seem to account in a qualitative and fairly logical way for almost all of our observations on the boron fluoride catalyzed polymerization of ethylene oxide. Perhaps the most interesting problem which remains unexplained is the difference in behavior of the various Friedel–Crafts catalysts in this polymerization, for the reaction schemes proposed do not seem to account satisfactorily for the fact that stannic chloride, and perhaps antimony pentachloride, can produce much higher molecular weight polymer than boron fluoride.

REFERENCES

1. G. A. Latrémouille, G. T. Merrall, and A. M. Eastham.   J. Am. Chem. Soc. **82**, 120 (1960).
2. D. J. Worsfold and A. M. Eastham.   J. Am. Chem. Soc. **79**, 900 (1957).
3. D. M. Smith and W. M. D. Bryant.   J. Am. Chem. Soc. **57**, 61 (1935).
4. N. N. Greenwood and R. L. Martin.   Quart. Rev. **8**, 1 (1954).
5. H. C. Brown and R. M. Adams.   J. Am. Chem. Soc. **64**, 2557 (1942).
6. S. Searles and M. Tamres.   J. Am. Chem. Soc. **73**, 3704 (1951).
7. H. Meerwein, E. Battenburg, H. Gold, E. Pfeil, and G. Willfang.   J. prakt. Chem. **154**, 83 (1939).
8. F. Klages and H. Meuresch.   Ber. **85**, 863 (1952); **86**, 1322 (1953).

AN IMPROVED PREPARATION OF ω-HYDROXY ALIPHATIC ACIDS AND THEIR ESTERS[1]

D. G. M. DIAPER AND D. L. MITCHELL[2]

ABSTRACT

Reductive cleavage of the ozonides of aliphatic acids and their esters by sodium borohydride or by hydrogenation produces ω-hydroxy aliphatic acids and ω-hydroxy aliphatic esters, respectively, in high yields.

INTRODUCTION

ω-Difunctional aliphatic compounds have found much employment in the synthesis of higher aliphatic compounds. Among these, substances having two different terminal functions are the most favored, and probably the most important reagents for chain extension are the esters of the ω-halogeno acids. These compounds, in various chain-lengths, were required for condensation with malonic ester derivatives in the preparation of branched alkanedioic acids (1, 2, 3, 4) in this laboratory. With the exception of those members of the series of very short chain-length, only one ω-bromo acid, 11-bromo-undecanoic, is easily available and this substance is best prepared by the peroxide-catalyzed addition of hydrogen bromide to 10-undecenoic acid (5). The latter compound is unique among the terminal unsaturated acids in that it is available in quantity and this method of preparation cannot be regarded as a method of general applicability. Use of the more common unsaturated acids with non-terminal olefinic linkages as starting materials for the preparation of ω-hydroxy acids and ω-bromo acids was first explored by Adams (6, 7), who ozonized the esters and isolated ω-aldehydo esters. These compounds were then reduced to give the esters of the ω-hydroxy acids. A practical difficulty in preparations of this type is the inevitable oxidation of a portion of the aldehydo ester to the half ester of the corresponding dicarboxylic acid. Contamination of intermediates with substances in the dicarboxylic acid series is undesirable as such compounds are usually high melting and insoluble and therefore difficult to remove. It is desirable, therefore, to obviate the sensitive aldehyde intermediate by exploitation of the new metal hydride reagents (8) and by selective reductive cleavage of the ozonide-ester prepare the hydroxy ester without isolation of the aldehyde. A similar observation on the preparation of primary alcohols by the borohydride cleavage of ozonides appeared while this work was in progress (9).

We have compared the high-pressure hydrogenolysis of certain ozonides with their reductive cleavage by sodium borohydride and the results are summarized in Table I. Yields of hydroxy ester were found to be superior when the borohydride was used and the products were also of higher purity as indicated by a narrow boiling range and ease of crystallization of the phenylurethane. When the scale of the preparation was increased, the yield by borohydride cleavage remained the same but the yield by high-pressure hydrogenation diminished. Sodium borohydride is still an expensive reagent and it may therefore be more economical to use the hydrogenation method on a large scale.

TABLE I

Olefinic substrate	Product isolated	Yield	
		Method (a)*	Method (b)
10-Undecenoic acid (undecylenic acid)	10-Hydroxydecanoic acid	91	56
Ethyl 10-undecenoate	Ethyl 10-hydroxydecanoate	94	71
9,12-Octadecadienoic acid (linoleic acid)	9-Hydroxynonanoic acid	42	—
cis-9-Octadecenoic acid (oleic acid)	9-Hydroxynonanoic acid	50	—
trans-9-Octadecenoic acid (elaidic acid)	9-Hydroxynonanoic acid	74	—
Methyl 9,12-octadecadienoate	Methyl 9-hydroxynonanoate	78	78
Ethyl 9,12-octadecadienoate	Ethyl 9-hydroxynonanoate	74	66
Methyl 9-octadecenoate (methyl oleate)	Methyl 9-hydroxynonanoate	88	66
Isopropyl 9-octadecenoate	Isopropyl 9-hydroxynonanoate	70.5	—
(+)-12-Hydroxy-9-octadecenoic acid (ricinoleic acid)	(−)-Nonane-1,3-diol	72	—

*Method (a) by sodium borohydride reduction, method (b) by Raney nickel catalyzed hydrogenation.

The working solvent employed for ozonizations has customarily been chloroform, carbon tetrachloride, acetic acid, ethyl acetate, or light petroleum. We have found absolute methanol, ethanol, and isopropanol to be convenient solvents and have used sodium borohydride in the same solvent, thus performing the ozonization and reductive cleavage in one sequence. The alcohol chosen as a solvent for the ozonolysis of an ester was that corresponding to its alkyl radical for it was found that transesterification took place if a different alcohol was employed. Presumably the basic environment of the borohydride reduction step made this transesterification possible.

A limitation on the use of methanol as a solvent is the rapid decomposition of sodium borohydride in this solvent. This can be obviated by reversing the usual order of addition and employing solid borohydride in place of an alcoholic solution.

It may be seen that 9-hydroxynonanoic acid may be obtained either from oleic acid or from linoleic acid. Using the former starting material, difficulties were encountered in freeing the hydroxy acid from the concomitant nonan-1-ol either by the method of Sousa and Bluhm (8) or by the steam-distillation method here described. When linoleic acid is the starting material, the other cleavage products are of lower molecular weight and therefore more easily removed.

10-Hydroxydecanoic acid was obtained in two ways from 10-undecenoic acid. The direct ozonization–borohydride method gives good yields and a high degree of purity. In the second method, undecenoic acid was esterified and reduced by the Bouveault–Blanc process, giving 10-undecen-1-ol without saturation or migration of the olefinic linkage. The acetate of the latter was then ozonized and the aldehyde thus obtained was oxidized to the corresponding acid, 10-acetoxydecanoic acid. This was then saponified. In the first method the carboxylic acid function of the starting material is retained and in the second it becomes the primary alcohol function of the end product.

The structure of (+)-ricinoleic acid as 12-hydroxy-9-octadecenoic acid (10) and most likely possessing the D-configuration (11) has been established by degradation studies (12, 13) and by synthesis (14, 15, 16). Early ozonolysis experiments performed on ricinoleic acid produced 3-hydroxy-nonanoic and nonanedioic acids and the corresponding aldehydes, which were characterized by the formation of crystalline derivatives (17, 18). These experiments supported the Goldsobel formula. We have found that sodium borohydride reduction of the ozonide of (+)-ricinoleic acid formed a hitherto unknown laevorotatory diol with boiling point, refractive index, and infrared spectrum very similar to those of racemic (±)-nonane-1,3-diol. The latter compound was synthesized by a

Reformatsky condensation of n-heptanal and ethyl bromoacetate followed by lithium aluminum hydride reduction of the intermediate ethyl 3-hydroxynonanoate which was not isolated. Although racemic ($\pm$)-nonane-1,3-diol formed a crystalline mono-N-phenyl-carbamate and bis-N-phenylcarbamate, attempts to form these crystalline derivatives from the optically active isomer were unsuccessful.

EXPERIMENTAL

Melting points were uncorrected. Infrared spectra were determined on 5% solutions in chloroform. Hydrogenations were carried out in a high-pressure autoclave equipped with a stirrer.*

10-Hydroxydecanoic Acid by the Sodium Borohydride Reduction Method

A stream of ozonized oxygen was bubbled through a solution of 10-undecenoic acid (undecylenic acid, b.p. 176–178° C/23 mm, 39.7 g) in absolute methanol (40 ml) at 0° C until an aliquot test portion no longer decolorized a dilute solution of bromine in a glacial acetic acid. The ozonide solution was then added dropwise to an ice-cold solution of sodium hydroxide (12.5 g) and sodium borohydride (17 g) in 50% aqueous ethanol (300 ml). A gentle evolution of hydrogen resulted and stirring was continued at room temperature for at least 10 hours. The methanol and ethanol were removed by distillation under reduced pressure and at a bath temperature of 40° C or less, and the alkaline aqueous solution was then added dropwise with stirring to an excess of ice-cold dilute hydrochloric acid (1.5 liters). The precipitated 10-hydroxydecanoic acid was collected by suction filtration, washed thoroughly with portions of ice-cold water, and dried under reduced pressure to constant weight (37.0 g, 91%). The yield was not reduced when the scale of the experiment was doubled. Recrystallization twice from benzene gave a product of constant melting point, 77° C, and mixed melting point 75.5–77° C (lit. 75.5–76.5° C (19)).

10-Hydroxydecanoic Acid by the Pressure Hydrogenolysis Method

A solution of the ozonide from 10-undecenoic acid (37.4 g) in ethanol was hydrogenated at room temperature and 2000 p.s.i. for 3 hours using Raney nickel W-2 catalyst (20). The temperature was increased to 130–150° C and the hydrogenation was continued a further 5 hours. The product was isolated by solvent removal, conversion to the sodium salt, and precipitation by pouring the alkaline solution into ice-cold dilute hydrochloric acid. The slightly syrupy crude product (33.6 g) was recrystallized from benzene – light petroleum to give a product (21.4 g, 56%) with a melting point of 75° C.

Ethyl 10-Hydroxydecanoate

The ozonide from ethyl 10-undecenoate (ethyl undecylenate) (204 g) in absolute ethanol (200 ml) was prepared according to the above method. The solution was added to sodium borohydride (60 g) in absolute ethanol (300 ml) as before and allowed to stand for 24 hours in a loosely stoppered flask at 5° C. After removal of most of the ethanol under reduced pressure, the product was taken up in ether (1500 ml), washed with acid and alkali in the usual manner, and dried. The product (197 g, 94%) distilled† at 114–115° C/0.07 mm and crystallized in the refrigerator (m.p. 15° C, thermometer immersed), n_D^{24} 1.4460.

Reduction of the ozonide from methyl 10-undecenoate (24.9 g) with a cold (3%)

*Superpressure Division of American Instrument Company, Inc., Silver Springs, Maryland, U.S.A.
†A test for ozonide (i.e. starch iodide paper) and a safety shield are recommended for this distillation. In a preliminary experiment, when the borohydride reduction step was acidified after 5 minutes of reduction, the isolated crude product decomposed explosively during distillation presumably due to unreduced ozonide present.

ethanolic solution of sodium borohydride (9 g) for 30 hours produced ethyl 10-hydroxy-decanoate (22.2 g, 82%). The derived N-phenylcarbamate had a melting point and a mixed melting point of 52–54° C.

The derived N-phenylcarbamate of ethyl 10-hydroxydecanoate melted at 52–54° C after two recrystallizations from heptane. The ethyl ester of 10-hydroxydecanoic acid was prepared; it formed a N-phenylcarbamate of melting point 52–54° C and mixed melting point 52–54° C. Both specimens gave an identical infrared absorption spectrum. Anal. Calc. for $C_{19}H_{29}O_4N$: C, 68.1; H, 8.7; N, 4.2. Found: C, 67.4; H, 8.8; N, 4.3.

Ethyl 10-hydroxydecanoate was also prepared from ethyl 10-undecenoate (25.2 g) by the ozonolysis–hydrogenation method described above. The product (18.4 g, 71%) was purified by two distillations and had a boiling point of 106–108° C/0.04 mm and n_D^{22} 1.4410.

Large-scale experiments (ca. 100 g of ozonide) produced a less pure product boiling over a 10° C range in yields of 40 to 66%.

The derived N-phenylcarbamate (m.p. 52–54° C) was prepared but did not crystallize readily.

9-Hydroxynonanoic Acid

The ozonide from linoleic acid* (50 g) in absolute ethanol (100 ml) was added dropwise to an aqueous alcoholic solution (1:1, 100 ml) of sodium hydroxide (20 g) and sodium borohydride (15 g). The solution was stirred for 48 hours, and it was acidified and extracted with ether (3×200 ml). The ethereal extracts were steam distilled until most of the alcohols had been removed. The product was recovered by ether extraction, was crystallized from benzene – light petroleum (13 g, 42%) and had a melting point of 43–45° C. Recrystallization from ethyl acetate raised the melting point to 50–51° C [lit. m.p. 53–54° C (corr.) (6), and m.p. 51–51.5° C (21)].

When the above procedure was carried out with oleic and elaidic acids, crude 9-hydroxynonanoic acid was obtained in 50% and 74% yields, respectively. The product obtained from oleic acid was difficult to purify by crystallization. Poor yields and resinous products in the ozonization of oleic acid and its esters have been attributed to excessive temperatures of ozonization (22).

Methyl 9-Hydroxynonanoate

Methyl oleate (20.6 g) in methanol (200 ml) was ozonized as described above. To minimize the borohydride–methanol reaction, however, the order of addition was reversed, the borohydride (9 g) being added in 0.5-g portions during 5 hours. Distillation at 0.1 mm produced two fractions: (a) b.p. 80–100° C (7.2 g) (72%), n_D^{22} 1.4340 (lit. for nonan-1-ol, n_D^{20} 1.4338 (23)); (b) b.p. 103–109° C/0.1 mm, 11.75 g (88%), n_D^{21} 1.4433. The derived N-phenylcarbamate melted at 53–54° C and had a mixed melting point of 53.5–55.5° C [lit. methyl 9-hydroxynonanoate N-phenylcarbamate 53–54° C (6)].

Methyl 9-hydroxynonanoate was also prepared from methyl oleate by the ozonization–hydrogenation technique and from methyl linoleate by the borohydride and catalytic hydrogenation methods. The yields are listed in Table I. Examination of the forerun (b.p. 80–105° C/0.2 mm) from the latter preparation by gas-liquid chromatography indicated the presence of at least two components.

Ethyl 9-Hydroxynonanoate

The ozonide from ethyl linoleate (b.p. 148–153° C/0.4 mm, n_D^{20} 1.4573) (50.15 g) in absolute ethanol was divided equally into two parts. One part was reduced by the dropwise

*Nutritional Biochemicals Corporation, Cleveland 28, Ohio (linoleic acid, 75%).

addition to sodium borohydride in absolute ethanol and gave a product (12.1 g, 73%) with a boiling point of 110–118° C/0.2 mm and n_D^{21} 1.4441. Anal. Calc. for $C_{11}H_{22}O_3$: C, 65.3; H, 11.0. Found: C, 65.6; H, 11.0. The second portion was reduced by the two-stage hydrogenation described above and gave a product (10.8 g, 65%) with a boiling point of 110–120° C/0.1 mm and n_D^{18} 1.4415.

When both specimens were warmed with one-half by weight of phenyl isocyanate, the derived N-phenylcarbamate was obtained (m.p. 59–60° C). Recrystallization from 2,2,4-trimethylpentane – benzene raised the melting point to 60–61.5° C. Anal. Calc. for $C_{18}H_{27}O_4N$: C, 67.3; H, 8.5; N, 4.5. Found: C, 67.5; H, 8.6; N, 4.7.

Isopropyl 9-Hydroxynonanoate

The ozonide from isopropyl oleate (b.p. 225–227° C/22 mm, n_D^{22} 1.4491) (32 g) was reduced with sodium borohydride in isopropanol according to the above method. The product (15 g, 70.5%) had a boiling point of 116–120° C/0.4 mm and $n_D^{25.5}$ 1.4399. Anal. Calc. for $C_{12}H_{24}O_3$: C, 66.6; H, 11.2. Found: C, 66.8; H, 11.3.

The derived N-phenylcarbamate was recrystallized from 2,2,4-trimethylpentane and had a melting point of 66.5–68° C. Anal. Calc. for $C_{19}H_{29}O_4N$: C, 68.1; H, 8.7; N, 4.2. Found: C, 68.3; H, 8.8; N, 4.1.

10-Hydroxydecanoic Acid by the Ozonization of the Acetate of 10-Undecen-1-ol

10-Undecen-1-ol (from ethyl undecylenate by Bouveault–Blanc reduction (24)) was acetylated by the acetic anhydride method of Chuit (25) in 83–86% yield. The acetate was ozonized in 20-g portions in acetic acid (40 cc) and the ozonide was reduced by the zinc dust – ether – water method of Adams (7). 10-Acetoxydecanal was obtained as a pungent oil, b.p. 113–118° C/0.3 mm, and was not purified before oxidation. Its oxime was obtained from ethanol as colorless prisms, m.p. 67.5–68° C. Anal. Calc. for $C_{12}H_{23}O_3N$: C, 63.0; H, 10.0; N, 6.1. Found: C, 63.0; H, 9.85; N, 5.7. Its p-nitrophenyl-hydrazone was obtained as yellow needles from aqueous acetic acid, m.p. 118° C. Anal. Calc. for $C_{18}H_{27}O_4N_3$: C, 61.9; H, 7.75; N, 12.0. Found: C, 61.8; H, 7.65; N, 11.5.

Oxidation of 10-acetoxydecanal (15 g) to the corresponding acid was performed in 65–68% yield by passing air through a rapidly stirred mixture of the aldehyde with 200 cc of 20% aqueous manganous chloride solution. The product, 10-acetoxydecanoic acid, isolated with the aid of ether and potassium carbonate, melted at 34.5–36° C and a 15–30% recovery of unchanged aldehyde was effected. By saponification of 10-acetoxy-decanoic acid in aqueous–ethanolic potassium hydroxide, 10-hydroxydecanoic acid, m.p. 74–74.5°, was obtained and found to be identical with the product described above.

(−)-Nonane-1,3-diol

After ozonolysis of ricinoleic acid (26 g, $[\alpha]_D^{22}$ 16.3°, c, 14.1, ethanol) and sodium boro-hydride reduction in aqueous alkaline methanol as described above, there was obtained an aqueous solution which was extracted with ether. From the extract of non-acidic products was obtained (−)-nonane-1,3-diol (10.0 g, 72%, b.p. 98–105°/0.1 mm). Two further distillations produced a colorless liquid with a boiling point of 97–99° C/0.1 mm, $n_D^{23.5}$ 1.4506, $[\alpha]_D^{22}$ −6.0° (neat liquid), and $[\alpha]_D^{22}$ −6.3° (c, 10, ethanol).

The product had an infrared absorption spectrum identical with that of (±)-nonane-1,3-diol prepared by the method described below. The infrared spectrum was also very similar to those of octan-1-ol and octan-2-ol with the major difference being a stronger absorption at the stretching frequency due to hydroxyl (3420 cm^{-1}).

Examination of the product by gas–liquid chromatography indicated the presence of at least three impurities which constituted approximately 6% of the product. This material was fractionally distilled in a Piros–Glover microdistillation still* with seven fractions being collected with n_D^{25} 1.4483, 1.4490, 1.4495, 1.4500, 1.4500, 1.4500, 1.4500, respectively. Anal. Calc. for $C_9H_{20}O_2$: C, 67.45; H, 12.6. Found: C, 67.3; H, 12.6.

Attempts to prepare the N-phenylcarbamate from fractions 4, 5, 6, or 7 resulted in the formation of a gel. This phenomenon of gel formation was also observed on the slightly impure product.

(±)-Nonane-1,3-diol

n-Heptanal (57 g) and ethyl 1-bromoacetate (83.5 g) were condensed by a standard Reformatsky procedure. After the reaction was complete, the solution was filtered from the unreacted zinc granules and the volume of the filtrate was adjusted to 300 ml with dry ether. The ethereal solution was added dropwise to an ethereal suspension of excess lithium aluminum hydride at such a rate that a gentle reflux was maintained. After the solution had been heated under reflux for an additional 2 hours, the residual lithium aluminum hydride was decomposed by the addition of excess ethyl acetate (100 ml). After 0.5 hour, water was added and a voluminous froth developed. The froth was suspended in ether and cold dilute hydrochloric acid was added until the solution was strongly acidic. The ethereal layer was separated and washed successively with water, sodium hydrogen carbonate solution, and water. Evaporation of the ether left an oil which distilled at 97–99° C/0.04 mm (42 g, 52.5%). A second distillation gave a main fraction with a boiling point of 97–99° C/0.1 mm and n_D^{23} 1.4512. Anal. Calc. for $C_9H_{20}O_2$: C, 67.45; H, 12.6. Found: C, 67.4; H, 12.6.

Bis-N-phenylcarbamate of (±)-Nonane-1,3-diol

Equal weights of phenyl isocyanate and (±)-nonane-1,3-diol were warmed to 60° C for 8 hours. Upon cooling, the product crystallized and was recrystallized from 2,2,4-trimethylpentane, m.p. 85–85.5° C. Examination of the infrared spectrum indicated the absence of the hydroxyl band. Anal. Calc. for $C_{23}H_{30}O_4N_2$: C, 69.3; H, 7.6; N, 7.0. Found: C, 69.3; H, 7.7; N, 7.2.

N-Phenylcarbamate of (±)-Nonane-1,3-diol

(±)-Nonane-1,3-diol was mixed with one-half by weight of phenyl isocyanate and the solution was stored at room temperature for 6 hours, then gently warmed to 60° C for 0.5 hour. The crystalline product was recrystallized from 2,2,4-trimethylpentane and melted at 83–84.5° C. The melting point was depressed upon admixture with the above bis-N-phenylcarbamate. Examination of the infrared spectrum indicated the presence of bands due to OH and NH stretching frequencies in approximately equal intensity. Anal. Calc. for $C_{16}H_{25}O_3N$: C, 68.8; H, 9.0; N, 5.0. Found: C, 69.0; H, 9.1; N, 5.0.

*H. S. Martin and Co., Evanston, Illinois, U.S.A.

REFERENCES

1. A. C. COPE, H. L. HOLMES, and H. O. HOUSE. Org. Reactions, IX, 107 (1957).
2. D. G. M. DIAPER and A. KUKSIS. Chem. Revs. **59**, 89 (1959).
3. R. ADAMS and R. M. KAMM. Organic syntheses. Coll. Vol. I. John Wiley and Sons, Inc., New York. 1941. p. 250.
4. W. J. GENSLER. Chem. Revs. **57**, 191 (1957).
5. R. ASHTON and J. C. SMITH. J. Chem. Soc. 435 (1934).
6. W. H. LYCAN and R. ADAMS. J. Am. Chem. Soc. **51**, 625 (1929).
7. C. R. NOLLER and R. ADAMS. J. Am. Chem. Soc. **48**, 1074 (1926).
8. N. G. GAYLORD. Reduction with complex metal hydrides. Interscience Publishers, New York. 1956. p. 708.
9. J. A. SOUSA and A. L. BLUHM. J. Org. Chem. **25**, 108 (1960).
10. A. G. GOLDSOBEL. Ber. **27**, 3121 (1894).
11. K. SERCK-HANSSEN and E. STENHAGEN. Acta Chem. Scand. **9**, 866 (1955).
12. J. T. SCANLAN and D. SWERN. J. Am. Chem. Soc. **62**, 2309 (1940).
13. ST. E. BRADY. J. Am. Chem. Soc. **61**, 3464 (1939).
14. L. CROMBIE and A. G. JACKLIN. J. Chem. Soc. 1740 (1955).
15. A. S. BAILEY, V. G. KENDALL, P. B. LUMB, J. C. SMITH, and C. H. WALKER. J. Chem. Soc. 3027 (1957).
16. W. J. GENSLER and C. B. ABRAHAMS. Chem. & Ind. (London), 47 (1957).
17. A. HALLER and A. BROCHET. Compt. rend. **150**, 496 (1910).
18. A. C. NOORDUYN. Rec. trav. chim. **38**, 327 (1919).
19. A. GRÜN and T. WIRTH. Ber. **55**, 2211 (1922).
20. R. MOZINGO. Organic syntheses. Vol. 21. John Wiley and Sons, Inc., New York. 1941. p. 15.
21. P. CHUIT and J. HAUSSER. Helv. Chim. Acta, **12**, 463 (1929).
22. E. H. PRYDE, D. E. ANDERS, H. M. TEETER, and J. C. COWAN. J. Org. Chem. **25**, 618 (1960).
23. V. J. HARDING and C. WEIZMANN. J. Chem. Soc. 304 (1910).
24. L. BOUVEAULT and G. BLANC. Bull. soc. chim. France, **31**, 1210 (1904).
25. P. CHUIT. Helv. chim. Acta, **9**, 1074 (1926).

STEROIDS

PART IV. CONDENSATION OF CHOLESTAN-3-ONE AND CHOLESTANE-3,6-DIONE WITH FORMALDEHYDE[1,2]

TED H. WAID AND ALFRED TAURINS

ABSTRACT

Cholestan-3-one and cholestane-3,6-dione were allowed to react under the conditions of the Mannich reaction with paraformaldehyde and amine hydrochlorides. The products obtained proved to be methylene-bis-ketones, and were formulated as di(2,2'-3-oxocholestanyl)methane and di(4,4'-3,6-dioxocholestanyl)methane respectively.

DISCUSSION

In the steroid series, the Mannich reaction has been applied to compounds containing an activated methylene group in ring D, or in the aliphatic side chain attached to C_{17} (1, 2) and also to certain estrogens (3). A 21-aminomethyl, and several 16-aminomethyl and 2-dialkylaminomethyl steroid derivatives, have been prepared in this way.

The present investigation was undertaken in order to study, by means of the Mannich reaction, the reactivity of hydrogen atoms in rings A and B of certain steroidal ketones. The steroidal materials selected for study were 5-cholesten-3-one (I) (4), 4,4-dimethyl-5-cholesten-3-one (II) (5), 4-cholesten-3-one (III) (4, 6), cholestan-3-one (IV) (7, 8), and cholestane-3,6-dione (V) (9).

The procedure used for the Mannich condensations that were attempted consisted in allowing the amine and paraformaldehyde to react, then adding the keto compound gradually. Paraformaldehyde was used instead of a 40% aqueous solution of formaldehyde because of the very low solubility of oxosteroids in water. The amines and hydrochlorides used in the reactions were morpholine, piperidine, and dimethylamine.

It was thought that if the isomerization of the double bond in 5-cholesten-3-one (I) from C_5 to C_4 could be avoided, then the hydrogen at C_4 should be particularly active due to the activation by the adjacent double bond and the keto group. In all the attempts to react morpholine with the Δ^5-3-one (I) and paraformaldehyde, brown, viscous oils, which could not be crystallized, and did not contain nitrogen, were obtained. Efforts to condense piperidine under similar conditions, using absolute ethanol, n-butyl alcohol, and isoamyl alcohol as solvents, also resulted in the formation of oils. When morpholine, piperidine, or dimethylamine hydrochloride was used in place of the free amine in the foregoing reaction, a viscous oil was obtained, and the unreacted amine hydrochloride was recovered in high yield.

In view of these results, it was felt that the high degree of reactivity of the methylene group in position 4 of 5-cholesten-3-one (I) might be responsible for the rapid formation of oily substances under various conditions. It was decided, therefore, to examine the reactivity of the methylene group in 2-position in a compound in which position 4 would be rendered inactive. Under conditions similar to those employed previously, 4,4-dimethyl-5-cholesten-3-one (II) failed to react with morpholine, piperidine, their hydrochlorides, or

dimethylamine hydrochloride, and was recovered unchanged after 4 hours refluxing in isoamyl alcohol.

Unreacted starting material also was recovered in high yield from the reactions of 4-cholesten-3-one (III) with paraformaldehyde and morpholine or piperidine. Since bromination of III occurs under enolizing conditions (10), it was concluded that the ketone was not sufficiently enolized by the secondary amines to participate in the reaction. In the reactions of III with morpholine, piperidine, and dimethylamine hydrochlorides, after refluxing for 1/2 hour in isoamyl alcohol, n-butyl alcohol, or absolute ethanol, noncrystalline oils were isolated. The absence of the characteristic odor of formaldehyde in the reaction mixtures indicated that the oils were a condensation product of III with formaldehyde.

By analogy with the acid-catalyzed halogenation of ketones (11, 12), an electrophilic substitution, it was presumed that the Mannich condensation in the cases of cholestan-3-one (IV) and cholestane 3,6-dione (V) would proceed via enolization of the ketones. Since the enol forms of IV and V were not stabilized by conjugation, as was the case in the unsaturated ketones, it was expected that the acidic hydrogen atoms of the saturated ketones would exhibit less reactivity.

When cholestan-3-one (IV) was refluxed in isoamyl alcohol for 20–30 minutes with paraformaldehyde and morpholine hydrochloride, a product melting at 208–210° and containing no nitrogen was obtained in a 35% yield. An identical material was produced when piperidine hydrochloride was substituted for the morpholine hydrochloride. The product appeared to be a condensation product of IV with formaldehyde and, on the basis of the analytical results and a comparative study of infrared spectra, was formulated as a methylene-bis-ketone. In the infrared spectrum of cholestan-3-one (IV), the carbonyl band appeared at 1710 cm^{-1}. The band of medium intensity present at 1425 cm^{-1} was considered to be due to the C–H scissoring vibrations in an unsubstituted methylene group at C_2 or C_4 in a 3-oxosteroid (13, 14). In the spectrum of the reaction product, two carbonyl bands occurred at 1735 cm^{-1} and 1700 cm^{-1}. The absorption due to methylene groups adjacent to the ketone appeared at 1413 cm^{-1}, and was of weak intensity. This spectroscopic evidence was interpreted as indicating that the new compound contained two residues of cholestan-3-one joined by a methylene bridge in either 2 or 4 position. It was noted that bromination of cholestan-3-one with bromine in acidic medium takes place in 2-position (15). Since an aldol condensation in basic or acidic medium proceeds through enolization, it is reasonable to postulate that the linkage in the methylene-bis-ketone is between the carbon atoms in 2-position. Consequently the compound was designated as di(2,2'-3-oxocholestanyl)methane (VI).

When morpholine and piperidine were used in place of their hydrochlorides in the foregoing reaction, the starting material IV was recovered unchanged. Both the ketone (IV) and the amine could be considered as competing nucleophilic reactants with regard to the electrophilic reagent formaldehyde. When the amine hydrochloride was used in the reaction, the ketone was the only nucleophilic species present, and condensation with the formaldehyde occurred.

A non-nitrogenous product melting at 242–242.5° was obtained in a 21% yield (based on V) when cholestane-3,6-dione (V) was refluxed with paraformaldehyde and morpholine or piperidine hydrochloride for 45 minutes in isoamyl alcohol. The analytical results and the infrared absorption spectrum inferred a methylene-bis-ketone structure. In the infrared, the dione (V) absorbed at 1710 cm^{-1} and with low intensity at 1420 cm^{-1}. The

spectrum of the condensation product exhibited two bands in the carbonyl region at 1727 cm^{-1} and 1710 cm^{-1}. The band due to methylene groups was shifted to 1425 cm^{-1} and existed as a shoulder on the more intense band at 1465 cm^{-1}. In V, there are methylene groups at positions 2, 4, and 7 adjacent to keto functions. The reactivity of the hydrogen atoms belonging to these methylene groups was evaluated by a consideration of other substitution reactions. Bromination of the dione (V) with 3 moles of bromine in acidic medium leads to the formation of 4,7-dibromo-4-cholestene-3,6-dione (VII) (16). Apparently an initial electrophilic attack occurs at position 4 in this reaction. Therefore it was considered that the linkage in the methylene-bis-ketone was between the carbon atoms in 4-position, and the compound was formulated as di(4,4'-3,6-dioxocholestanyl) methane (VIII).
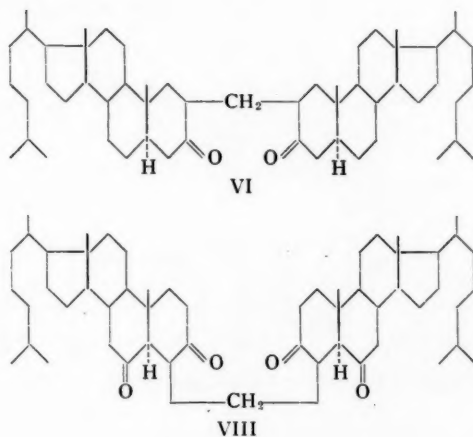
When the free amines were used in place of their hydrochloride salts, the unreacted dione (V) was recovered. The ketones IV and V also were recovered unchanged when they were allowed to react with paraformaldehyde in neutral or acidic media.

Two alternative mechanisms are offered to explain the condensation of cholestan-3-one (IV) and cholestane-3,6-dione (V) with formaldehyde. Scheme A (Fig. 1) represents an abnormal Mannich condensation in an acid–base catalyzed system. Although there is no proof of an intermediate Mannich base, several similar reactions leading to methylene-bis-molecular compounds are known to respond to alkaline and acidic catalysis in much the same manner as the Mannich reaction (17–20). According to the mechanism (Fig. 1), a carbonium ion (ix) is formed from formaldehyde and the secondary amine through the intermediate methylene-bis-amine (v) or methylolamine (vi). This cation combines then with the anion (iv) derived from the ketone as in a normal Mannich reaction. Formation of the cation (ix) is promoted by hydrochloric acid, and that of the anion (iv) by the amine present in the system. Then cleavage of the C—N bond occurs with the loss of amine and formation of the carbonium ion (xii). Such a possibility has been clearly demonstrated by Hellman (21), who reviewed and studied extensively the use of Mannich bases for alkylations. In the final step, the cation (xii) condenses with the anion (iv) to give the methylene-bis-ketone (xiii).
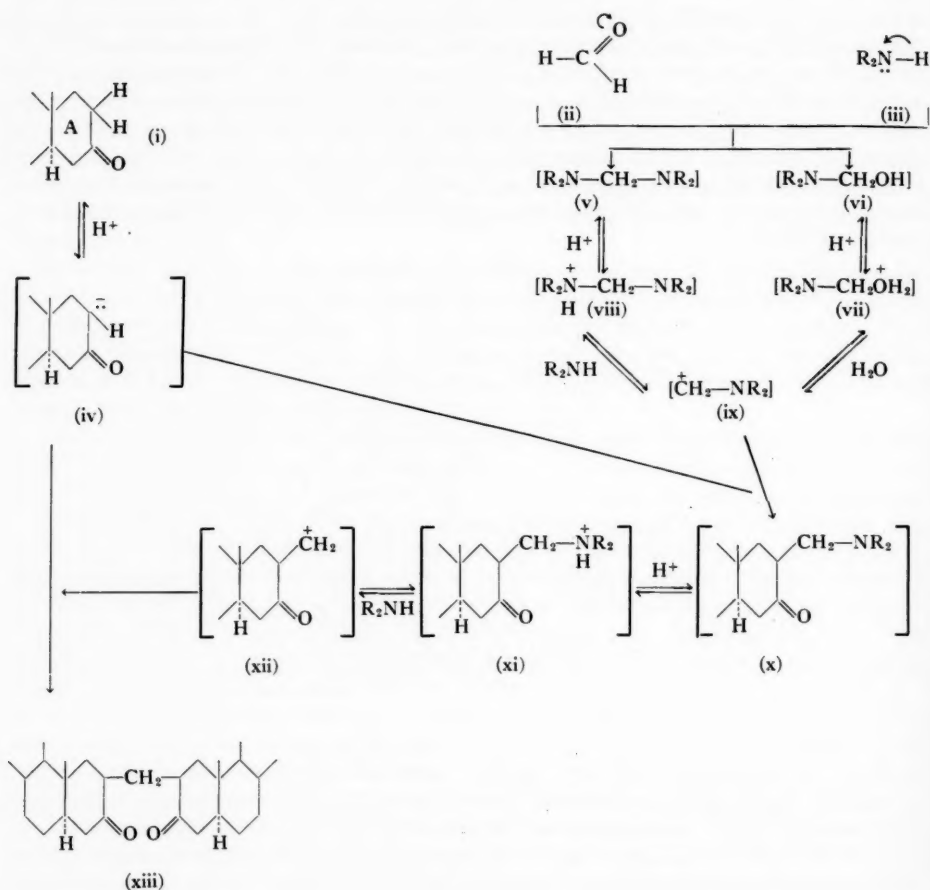
FIG. 1. Scheme A: mechanism proposed for an abnormal Mannich reaction.

The alternative mechanism is presented (Fig. 2) in view of the uncertainty about whether a secondary amine derived from its hydrochloride participates actively in the reaction or acts only as a buffer toward the hydrochloric acid. This mechanism accounts for an acid-induced aldol condensation of formaldehyde with the oxosteroid. In the first step, a transition state complex (ii) is formed which rearranges to a β-ketomethylol (iii). The latter is unstable in acidic medium, and gives, upon protonation, an oxonium ion (iv) which by loss of a molecule of water affords a carbonium ion (v). Finally the carbonium ion combines with the carbanion (vi) derived from the ketone (i) to give the methylene-bis-ketone (vii).
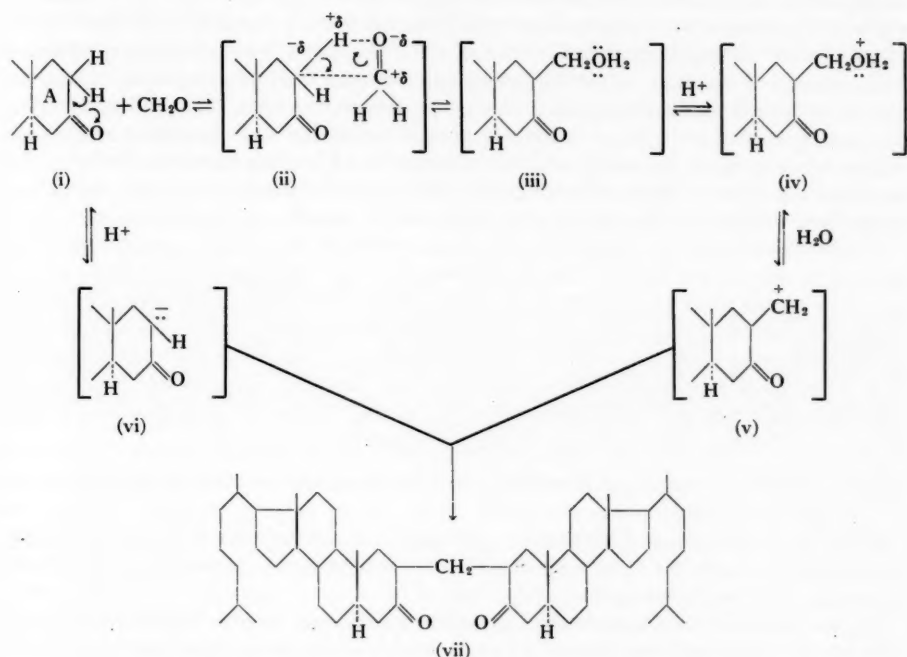
FIG. 2. Scheme B: mechanism proposed for an abnormal Mannich reaction.

EXPERIMENTAL

The melting points were determined in a Thiele-Dennis melting-point tube containing Dow Corning silicone fluid No. D.C. 550 and are uncorrected. The analyses were performed by the Schwarzkopf microanalytical laboratory, Woodside, N.Y., U.S.A. All infrared spectra were determined on a Perkin–Elmer Model 21 double-beam spectrometer equipped with a sodium chloride prism.

The secondary amines were dried by refluxing over sodium hydroxide pellets for 6 hours, distilling, and storing over solid sodium hydroxide. The hydrochloride salts of the amines were prepared by addition of a calculated amount of dilute hydrochloric acid to the amine with cooling, evaporation to dryness, and recrystallization from absolute ethanol.

Attempted Condensation of 5-Cholesten-3-one (I) with Paraformaldehyde and Secondary Amine Hydrochlorides

In a nitrogen atmosphere, morpholine hydrochloride (0.185 g), paraformaldehyde (0.04 g), and isoamyl alcohol (6 ml) were stirred for 20 minutes at room temperature. The mixture was heated to reflux, and all solids dissolved. During the next hour, 5-cholesten-3-one (I) (0.58 g) was added in portions, and refluxing was continued for an additional hour. The brown solution was allowed to cool to room temperature, and the long needles which separated were filtered off and dried. The material (0.15 g) melted at 171–172°, and the mixed melting point with an authentic sample of morpholine hydrochloride was

undepressed. The filtrate was shaken with 4% hydrochloric acid (10 ml), diluted with water, and extracted with ether. The brown ethereal extract was dried, and then allowed to stand with decolorizing carbon Nuchar-C190-N for a few hours at room temperature with occasional shaking. After filtration, the solvent was evaporated *in vacuo*, and the tarry brown residue was dried over phosphorus pentoxide. The oil contained no nitrogen, possessed a tendency to form films, and resisted all attempts of crystallization.

The aqueous layer was made alkaline with saturated sodium carbonate solution, and extracted again with ether. The ethereal extract was washed with water, dried, and evaporated to dryness. No residue remained.

Similar results were obtained when the molar ratios of the ketone, paraformaldehyde, and morpholine hydrochloride were varied from 1:1:1 to 1:2:3 and 1:5:7.5. The refluxing time was varied from 15 minutes to 2 hours in each case. The results were not affected when absolute ethanol or *n*-butanol was substituted for isoamyl alcohol under the previously described conditions. When dimethylamine and piperidine hydrochlorides were used in place of morpholine hydrochloride in the foregoing experiments, film-forming oils which could not be crystallized resulted in all cases. These oils contained no nitrogen. In each experiment, the major part of the amine salt was recovered.

Attempted Condensation of 4,4-Dimethyl-5-cholesten-3-one (II) with Paraformaldehyde and Morpholine Hydrochloride

When II, morpholine hydrochloride, and paraformaldehyde were heated in isoamyl alcohol for 4 hours under the conditions described in the previous procedure, morpholine hydrochloride was recovered in a 75% yield.

Similar results were obtained when piperidine and dimethylamine hydrochlorides were used in place of morpholine hydrochloride, and also when morpholine itself was used.

Attempted Condensation of 4-Cholesten-3-one (III) with Paraformaldehyde and Secondary Amine Hydrochlorides

The procedure outlined for the attempted condensations of 5-cholesten-3-one (I) was followed, and morpholine, piperidine, and dimethylamine hydrochlorides were used. The molar ratios of the ketone, paraformaldehyde, and amine salts were varied from 1:1:1 to 1:2:3 and 1:5:7.5. Absolute ethanol, *n*-butanol, and isoamyl alcohol were employed as solvents, and the refluxing time was varied from 1/2 hour to 2 hours in each case. Brown viscous oils, possessing film-forming tendencies were the only isolable products in all instances. The oils contained no nitrogen, and could not be crystallized.

Attempted Condensation of 4-Cholesten-3-one (III) with Paraformaldehyde and Secondary Amines

When the conditions outlined for the condensation reaction of 5-cholesten-3-one (I) were employed, using either piperidine or morpholine, an 80% recovery of the starting material III was achieved. When the refluxing time was extended to 2 hours or longer, a brown amorphous material which could not be crystallized resulted in each case. Varying the molar ratios of the reactants did not affect the course of the reaction.

Di(2,2'-3-oxocholestanyl)methane (VI)

A mixture of cholestan-3-one (IV) (0.58 g), paraformaldehyde (0.05 g), morpholine hydrochloride (0.2 g), and isoamyl alcohol (2.5 ml) was heated to reflux, with stirring, in a nitrogen atmosphere. All solids dissolved when the temperature reached 115°, after 5 minutes heating. When the solution had been refluxed for 20–30 minutes, solid material precipitated. The mixture was allowed to cool to room temperature, and was refrigerated

overnight. The product (0.33 g) was isolated. It was a white crystalline solid, melting at 205–207° to a deep brown liquid. Recrystallization from benzene provided di(2,2′-3-oxocholestanyl)methane (VI), m.p. 208–210°, ν_{max} 1725, 1700 cm^{-1} (C=O). Anal. Calc. for $C_{55}H_{92}O_2$: C, 84.18; H, 11.73. Found: C, 83.86; H, 11.64%.

A similar yield of VI was obtained in an analogous reaction in which piperidine hydrochloride was substituted for morpholine hydrochloride.

When the reaction was carried out in absolute ethanol, and refluxing was maintained for 2 hours, unreacted cholestan-3-one (IV) was recovered in 95% yield. The yield of product was unaffected by a change in the molar ratio of ketone (IV) to paraformaldehyde from 1:1 to 2:1.

Di(4,4′-3,6-dioxocholestanyl)methane (VII)

In a nitrogen atmosphere, a mixture of cholestane-3,6-dione (VI) (0.60 g), paraformaldehyde (0.05 g), morpholine hydrochloride (0.2 g), and isoamyl alcohol (3 ml) was stirred, and heated to reflux. All solids dissolved when the temperature reached 105°. After 45 minutes refluxing, the solution was dark yellow. Crystalline material separated on cooling of the solution to room temperature. The mixture was treated with water (0.5 ml), and the organic layer was separated, dried over anhydrous magnesium sulphate, and evaporated to dryness *in vacuo*. The solid residue was crystallized from acetone (250 ml) yielding soft needles (0.254 g) melting at 214–217°. Recrystallization from acetone provided di(4,4′-3,6-dioxocholestanyl)methane (VII), m.p. 242–242.5°, ν_{max}^{nujol} 1727, 1710 cm^{-1} (C=O). Anal. Calc. for $C_{55}H_{88}O_4$: C, 82.51; H, 11.83. Found: C, 82.09; H, 11.82%.

The yield of product was not affected by varying the molar ratio of ketone and paraformaldehyde from 1:1 to 2:1. In dioxane the reaction was complete after 60–70 minutes' refluxing. The yield of product was considerably lower than when isoamyl alcohol was the solvent.

ACKNOWLEDGMENT

REFERENCES

1. P. L. JULIAN, E. W. MEYER, and H. C. PRINTY. J. Am. Chem. Soc. **70**, 3872 (1948).
2. P. L. JULIAN, E. W. MEYER, and H. C. PRINTY. U.S. Patent No. 2,562,194 (1951): Chem. Abstr. **46**, P. 1598 (1952).
3. T. L. PATTON. Chem. & Ind. 923 (1959).
4. L. F. FIESER. J. Am. Chem. Soc. **75**, 5421 (1953).
5. R. V. OPPENAUER. Rec. trav. chim. **56**, 137 (1937).
6. H. H. INHOFFEN, W. LOGEMANN, W. HOHLWEG, and A. SERINI. Ber. **71**, 1032 (1938).
7. E. B. HERSHBERG, E. OLIVETO, M. RUBIN, H. STAENDLE, and L. KUHLEN. J. Am. Chem. Soc. **73**, 1144 (1951).
8. ORGANIC SYNTHESES, **17**, 43 (1937).
9. L. F. FIESER. J. Am. Chem. Soc. **75**, 4381 (1953).
10. I. HEILBRON, E. R. H. JONES, and G. F. WOODS. J. Chem. Soc. 461 (1953).
11. A. J. LAPWORTH. J. Chem. Soc. **85**, 30 (1904).
12. P. D. BARTLETT and R. H. ROSENWALD. J. Am. Chem. Soc. **56**, 1990 (1934).
13. R. N. JONES and A. R. H. COLE. J. Am. Chem. Soc. **74**, 5648 (1952).
14. R. N. JONES, A. R. H. COLE, and B. NOLIN. J. Am. Chem. Soc. **74**, 6321 (1942).
15. A. BUTENANDT and A. WOLFF. Ber. **68**, 2091 (1935).
16. A. BUTENANDT, G. SCHRAMM, and H. KUDSSUS. Ann. **531**, 176 (1937).
17. J. R. FELDMAN and E. C. WAGNER. J. Org. Chem. **7**, 31 (1942).
18. G. B. BACKMANN and M. T. ATWOOD. J. Am. Chem. Soc. **78**, 484 (1956).
19. R. D. DESAI. J. Indian Chem. Soc. **10**, 663 (1933).
20. E. C. HORNING and M. G. HORNING. J. Org. Chem. **11**, 95 (1946).
21. H. HELLMANN. Angew. Chem. **65**, 473 (1953).

CATALYTIC OXIDATION OF CARBON MONOXIDE
PRESENT IN LOW CONCENTRATIONS[1]

S. Sourirajan[2] and Mauro A. Accomazzo

ABSTRACT

The oxidation of carbon monoxide present in low concentrations has been studied in the presence of the $CuO-Al_2O_3$ (1:1) catalyst using 1,000–10,000 p.p.m. of CO in air in the temperature range 120°–322° C, and gas space velocities ranging from 8,000–16,000 hr^{-1}. It was found that for the entire concentration range studied, the percentage of oxidation of CO at a given temperature was independent of its initial concentration and at temperatures above 200° C, more than 95% of CO was removed by oxidation at all gas space velocities up to 16,000 hr^{-1}. A simple first-order rate equation was found to fit the experimental data well. The presence of water vapor in the reactant gas was found to have no effect on the efficiency of the catalyst at temperatures above 225° C. The possible practical utility of the above catalyst for the removal of carbon monoxide present in auto exhaust gases was tested using a six-cylinder Chevrolet engine run on leaded gasoline fuel. It was found that under all conditions of engine operation, more than 99% of carbon monoxide present in the exhaust gases was removed by catalytic oxidation when the initial temperature of the catalyst bed was kept at or above 220° C.

INTRODUCTION

The development of suitable catalysts for the efficient oxidation of carbon monoxide present in low concentrations in the exhaust gases emanating from various combustion sources is of particular importance as a possible method of air pollution control. An extensive literature is available on the heterogeneous oxidation of carbon monoxide (1, 2). The object of this investigation is to study the efficiency and the practical utility of the copper oxide – alumina (1:1) catalyst for the oxidation of low concentrations of carbon monoxide, in view of the proved effectiveness of the above catalyst for the total oxidation of hydrocarbons (3).

EXPERIMENTAL DETAILS

The apparatus used was similar to the one described earlier (3). The carbon monoxide gas was mixed with air before entering the catalyst bed, which was placed in a vycor glass reactor tube enclosed in a furnace. The gas flow rates were measured by appropriate flowmeters which were initially calibrated. The lower section of the vycor tube, filled with porcelain beads, served as a preheater for the reactant gases. The temperature of the catalyst bed was measured by means of a thermocouple. The gases flowing through the preheater and reactor tube could be sampled both immediately before and after passing through the catalyst bed. The carbon monoxide content of the samples was analyzed by a combustible analyzer developed by Miller (4). It consisted essentially of two cells constituting the two arms of a Wheatstone bridge arrangement; the combustion of the gas sample material took place on the surface of a hot platinum wire in one of the cells, and the resistance change resulting from the increase in temperature due to combustion measured the concentration of the combustibles in the gas mixture entering or leaving the catalyst bed. The instrument, coupled to an automatic recorder, was initially calibrated for different concentrations of carbon monoxide. The analyzer gave results reproducible within 1%.

The concentration of carbon monoxide in the reactant gas ranged from 1,000–10,000 p.p.m. in diluent air. The temperature of the catalyst bed was varied from 120°–322° C

and the gas space velocities (volume of gas per hour per volume of catalyst) ranged from 8,000 to 16,000 hr^{-1}. During the reaction, the furnace controls were set so that the temperature gradient across the different parts of the catalyst bed was less than 10° C. Under steady-state conditions, the highest temperature of the catalyst bed (taken as the reaction temperature), the gas flow rate, and the carbon monoxide concentrations in the gases entering and leaving the catalyst bed were recorded and the efficiency of the catalyst for the oxidation of carbon monoxide was evaluated.

The catalyst was prepared as follows. Copper hydroxide was precipitated on the alumina carrier from a hot dilute aqueous solution of copper nitrate by the addition of an excess of sodium hydroxide. The precipitate was then filtered and washed free of alkali. The wet solid mass was then extruded, dried, and pelleted. The composition of the catalyst was $CuO:Al_2O_3 = 1:1$. The catalyst material was heated in the reactor at 450° C for a period of 12 hours in a current of air before use in the experiments. The surface area of the catalyst, as determined by the B.E.T. method, was 128 square meters/g, and its pore volume, as determined by the helium–mercury method, was 0.56 cc/g. The mean radius of the pores in the catalyst, as calculated from its known surface area and pore volume measurements assuming cylindrical pores, was 87 Å. Twenty-five cubic centimeters of catalyst material was used in all these experiments.

EXPERIMENTAL RESULTS AND DISCUSSION

Efficiency of the Catalyst

Tables I and II give the experimental results obtained on the oxidation of carbon monoxide present in the concentration range of 1,000 to 10,000 p.p.m. in diluent air in the presence of the copper oxide – alumina catalyst described above. Figures 1 and 2 show the effect of temperature and gas space velocity, respectively, on the extent of oxidation. Most of the experiments were carried out at a gas space velocity of 10,000 hr^{-1} or more in order to simulate comparable conditions for practical utilization of the catalyst in air pollution control devices. The results showed that (i) for the entire concentration range studied, the percentage of oxidation of CO at a given temperature was independent of its initial concentration and (ii) at temperatures above 200° C, more than 95% of CO was removed by oxidation at all gas space velocities up to 16,000 hr^{-1}. Thus, the above copper oxide – alumina catalyst was found to be a very efficient one for the oxidation of CO present in low concentrations.

Rate Equation for Reactor Design

Garner, Gray, and Stone (5) investigated the nature of the interaction of carbon monoxide and oxygen on the surface of the copper oxide catalyst through surface con-ductivity and heat of adsorption measurements. They found that in the temperature range 100°–270° C, the rate-controlling step in the adsorption of oxygen on plane surfaces was first order. When a mixture of carbon monoxide and oxygen was admitted to the catalyst surface, the first process was always the saturation of the surface with carbon monoxide. They also observed that the rate of oxidation of carbon monoxide in the presence of the copper oxide catalyst was independent of carbon monoxide pressure and proportional to the oxygen pressure. They hence concluded that the CO–O$_2$ reaction occurred on the catalyst surface saturated with carbon monoxide.

The experimental data obtained in this work, however, show that the rate of catalytic oxidation of CO present in low concentrations by excess oxygen, is more nearly first order

TABLE I

Data on the oxidation of carbon monoxide present in low concentrations in the presence of the CuO–Al$_2$O$_3$ (1:1) catalyst

t, °C	X_0, p.p.m.	X_1, p.p.m.	% oxidation	Q, liters/hour	SV, hr^{-1}
120	1,000	728	27	250	10,000
140	1,000	447	55	250	10,000
160	1,000	346	66	250	10,000
180	1,000	148	85	250	10,000
200	1,000	25	98	250	10,000
268	1,000	21	98	250	10,000
120	2,000	1,760	12	250	10,000
146	2,000	1,200	38	250	10,000
160	2,000	873	57	250	10,000
170	2,000	700	65	250	10,000
186	2,000	196	90	250	10,000
200	2,000	41	98	250	10,000
304	2,000	25	99	250	10,000
124	5,000	4,420	11	250	10,000
140	5,000	3,230	35	250	10,000
168	5,000	2,060	59	250	10,000
190	5,000	780	84	250	10,000
210	5,000	154	97	250	10,000
322	5,000	72	99	250	10,000
120	10,000	8,900	11	250	10,000
140	10,000	7,500	25	250	10,000
160	10,000	3,390	65	250	10,000
190	10,000	542	94	250	10,000
242	10,000	268	97	250	10,000
200	2,000	60	97	200	8,000
200	2,000	24	99	300	12,000
200	2,000	35	98	400	16,000

TABLE II

Data on the oxidation of carbon monoxide present in low concentrations in the presence of the CuO–Al$_2$O$_3$ (1:1) catalyst

X_0, p.p.m.	t, °C	Q, liters/hour	Z	$(T/T_1)\ln[1/(1-Z)]$	$(V_R/Q)\times10^4$	$k'\times10^{-3}$
2,000	128	200	0.258	0.403	1.250	
2,000	128	250	0.230	0.350	1.000	3.33
2,000	128	300	0.210	0.318	0.833	
2,000	128	400	0.133	0.188	0.625	
2,000	146	200	0.440	0.812	1.250	
2,000	146	250	0.384	0.674	1.000	6.67
2,000	146	300	0.355	0.613	0.833	
2,000	146	400	0.256	0.412	0.625	
2,000	160	200	0.626	1.420	1.250	
2,000	160	250	0.565	1.208	1.000	
2,000	160	300	0.485	0.957	0.833	11.50
2,000	160	350	0.430	0.815	0.714	
2,000	160	400	0.385	0.706	0.625	
2,000	170	200	0.722	1.890	1.250	
2,000	170	250	0.650	1.551	1.000	14.70
2,000	170	350	0.500	1.022	0.714	
2,000	170	450	0.417	0.785	0.556	
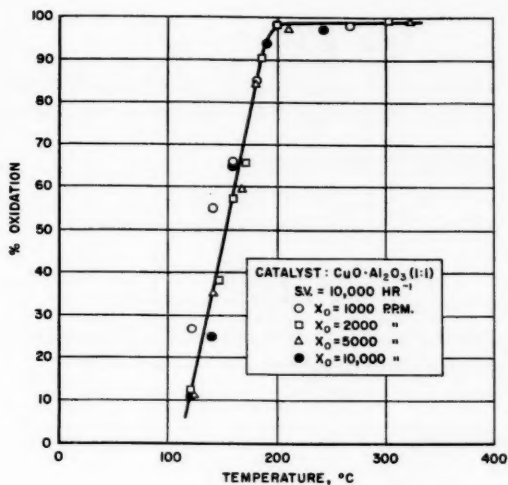
FIG. 1. Effect of CO concentration and temperature on the catalytic oxidation of carbon monoxide.
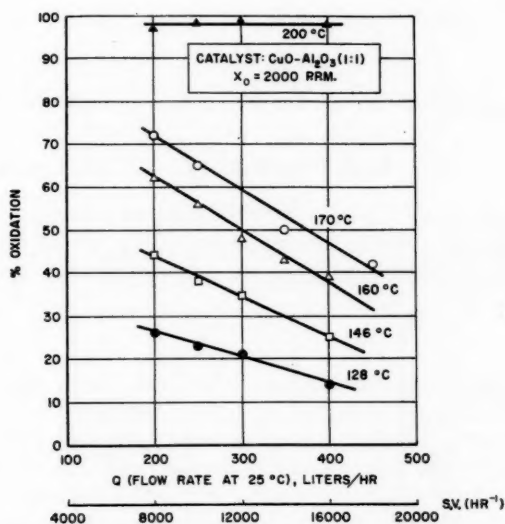
FIG. 2. Effect of gas flow rate and temperature on the catalytic oxidation of carbon monoxide.

with respect to CO concentration. For the purpose of reactor design, an empirical rate equation for the catalytic oxidation of CO by excess air can be derived as follows to fit the experimental data reported above.

For flow reactors,

[1]
$$\frac{V_R}{F} = \int_0^z \frac{dZ}{r},$$

[2]
$$r = -\frac{dC}{d\theta} = kC^n C_{O_2}^m.$$

When the oxygen concentration is much in excess,

[3]
$$kC_{O_2}^m \approx k' = f(T)$$

therefore

[4]
$$\frac{V_R}{F} = \int_0^z \frac{dZ}{k'C^n}.$$

At any point in the reactor where a conversion of fraction Z has taken place, the concentration of carbon monoxide can be written as

[5]
$$C = C_0 (1-Z).$$

Hence at constant temperature,

[6]
$$\frac{V_R}{F} = \frac{1}{k'C_0^n} \int_0^z \frac{dZ}{(1-Z)^n}$$

[7]
$$= \frac{1}{k'C_0} \ln \frac{1}{1-Z} \qquad \text{for } n = 1.$$

Since

[8]
$$F = QC_0 \frac{T}{T_1}$$

equation [7] becomes

[9]
$$k'\frac{V_R}{Q} = \frac{T}{T_1} \ln \frac{1}{(1-Z)}.$$

Hence a plot of V_R/Q vs. $(T/T_1) \ln[1/(1-Z)]$ should be a straight line (with slope $= k'$) passing through the origin. Such plots are shown in Fig. 3, and the graphs obtained are seen to be nearly straight lines justifying the essential validity of equation [9].
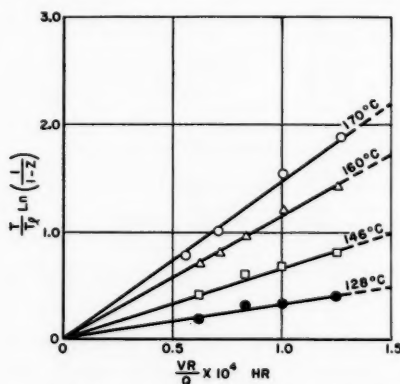
FIG. 3. Apparent first-order plot for the catalytic oxidation of carbon monoxide present in low concentrations.

Assuming

[10] $$k' = f(T) = Ae^{-E/RT}$$

the plot of ln k' vs. $1/T$ should be a straight line with slope $= -E/R$. Such a plot is shown in Fig. 4 which is also seen to be nearly a straight line giving an apparent activation
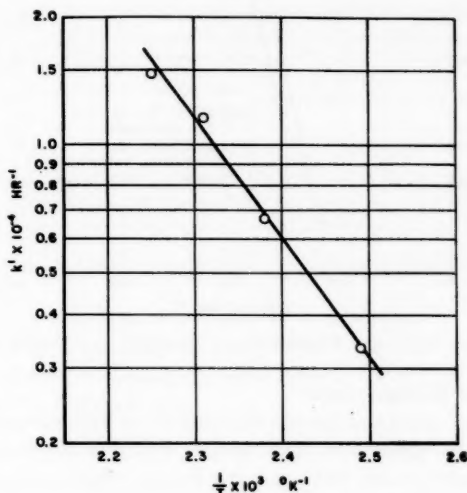
Fig. 4. Variation of reaction rate constant with temperature.

energy of 12.8 kcal/g.mole with $A = 3.1 \times 10^{10}$ hr^{-1}. Thus

[11] $$r = Ae^{-E/RT}C$$

is found to be a simple rate equation useful for reactor design applicable to the experimental data reported previously for the catalytic oxidation of carbon monoxide present in low concentrations.

Experiments with Water Vapor in Reactants

It is known that water vapor retards the catalytic oxidation of carbon monoxide (6). Since considerable amounts of water vapor may be present in gases issuing from various air-polluting sources, it is important to consider the efficiency of the above CuO–Al$_2$O$_3$ catalyst for the oxidation of CO in presence of water vapor. With 2000 p.p.m. of CO in air saturated with water vapor at the laboratory temperature (i.e., with water vapor in the feed = 3.0%) experiments were carried out on the effect of temperature on the extent of oxidation at a gas space velocity of 10,000 hr^{-1}. The results obtained are given in Fig. 5.

It was found that the presence of water vapor did retard the rate of reaction at lower temperatures, but it had no effect at temperatures higher than 225° C. Thus, at temperatures higher than 225° C, CO present in air in low concentrations, even with a large relative proportion of water vapor, was almost completely removed by oxidation in presence of the above CuO–Al$_2$O$_3$ catalyst.
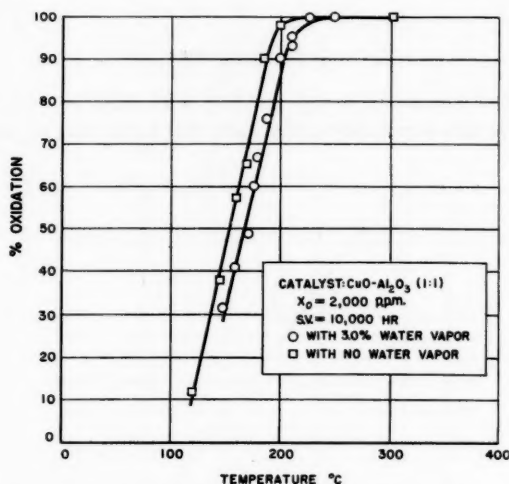
FIG. 5. Effect of water vapor and temperature on the catalytic oxidation of carbon monoxide.

Experiments with Auto Exhaust Gases

The possible practical utility of the above catalyst for the removal of carbon monoxide present in auto exhaust gases was then tested. For this purpose, a 1955 six-cylinder Chevrolet engine coupled to an eddy current dynamometer was used. The engine was run on leaded gasoline fuel. The air/fuel ratio in the engine was determined by a DuMont type 932 exhaust gas analyzer. Part of the exhaust gases from the engine was cooled to room temperature, mixed with excess air (2 to 4 times that needed for complete combustion), and then passed through the catalyst bed initially kept at 200°–220° C, at a gas space velocity of 10,000 hr^{-1} at 25° C. The amount of carbon monoxide present in the engine exhaust gases was determined by orsat analysis, and that present in the gases leaving the catalyst bed was determined by means of a Mines Safety Appliance carbon monoxide indicator (using hopcalite catalyst) capable of analyzing CO within 50 p.p.m. Under the different engine conditions tested, the concentration of CO in the exhaust gases ranged from 1.5–7%; as soon as the air-mixed exhaust gases from the engine entered the reactor, the temperature of the catalyst bed increased rapidly due to reaction and attained steady-state conditions within 10 minutes. The experimental results obtained under the varying conditions of engine operation are recorded in Table III. It was found

TABLE III

Data on the use of the CuO–Al$_2$O$_3$ (1:1) catalyst for the removal of carbon monoxide present in auto engine exhaust gases

	Engine conditions					Catalyst performance				
r.p.m.	Air/fuel ratio	Cylinder vacuum, in. of Hg	hp	% CO in exhaust	t_0, °C	t, °C	X_0, p.p.m.	X_1, p.p.m.	% oxidation	SV, hr^{-1}
580	12.0	19.8	0.00	7.0	200	600	49000	<50	>99	10000
1050	12.2	19.2	1.17	5.5	220	579	38000	<50	>99	10000
1000	12.5	19.2	2.50	4.5	210	448	31000	<50	>99	10000
1300	13.5	19.5	2.93	3.0	220	400	24000	<50	>99	10000
1600	14.0	19.2	6.00	1.5	210	400	12600	<50	>99	10000

that under all conditions of engine operation, more than 99% of carbon monoxide present in the exhaust gases was removed by catalytic oxidation. Thus, the above CuO–Al₂O₃ (1:1) catalyst was found to be practically useful for the almost complete removal of CO present in the auto exhaust gases. Coupled with the fact that the above catalyst was already shown to be effective for the removal of hydrocarbons present in low concentrations (3), the experimental results reported in this paper indicate the possibility of developing a practical antismog catalyst containing copper oxide for the simultaneous oxidation of both hydrocarbons and carbon monoxide present in low concentrations in gases issuing from various air-polluting sources.

SYMBOLS

A	constant;
C	concentration of carbon monoxide at any time θ, in moles/cc;
C_0	concentration of carbon monoxide in the gas entering the catalyst bed, in moles/cc;
C_1	concentration of carbon monoxide in the gas leaving the catalyst bed, in moles/cc;
C_{O_2}	concentration of oxygen at anytime θ, in moles/cc;
E	apparent activation energy in cal/g.mole;
F	carbon monoxide feed rate, in moles/hour;
hp	engine load in horse power;
k	constant;
k'	constant;
m	order of reaction with respect to oxygen;
n	order of reaction with respect to carbon monoxide;
p.p.m.	parts per million by volume;
Q	gas flow rate at laboratory temperature;
r	reaction rate in moles/hour cc;
R	universal gas constant in cal/g.mole °K;
r.p.m.	engine revolutions per minute;
SV	space velocity, in hr⁻¹;
t	maximum temperature of catalyst bed under steady-state reaction conditions, in °C;
t_0	initial temperature of the catalyst bed under no reaction conditions, in °C;
T	t in °K;
T_1	laboratory temperature in °K;
V_R	volume of catalyst bed;
X_0	concentration of carbon monoxide in the gas entering the catalyst bed, in p.p.m.;
X_1	concentration of carbon monoxide in the gas leaving the catalyst bed, in p.p.m.;
Z	fraction oxidation of carbon monoxide.

ACKNOWLEDGMENTS

REFERENCES

1. S. BERKMAN, J. C. MORELL, and G. EGLOFF.   Catalysis. Reinhold Publ. Corp., New York. 1940. pp. 775–780.
2. M. KATZ.   Advances in catalysis. Vol. V. Academic Press Inc., New York. 1953. pp. 177–216.
3. S. SOURIRAJAN, M. A. ACCOMAZZO, and K. NOBE.   Proc. Intern. Congr. on Catalysis. 2nd. Paris, paper 130, 1960.
4. J. MILLER.   The measurement of combustibles by a hot wire method. M. S. Thesis, Department of Engineering, University of California, Los Angeles, Calif. 1958.
5. W. E. GARNER, T. J. GRAY, and F. S. STONE.   Disc. Faraday Soc. 8, 246 (1950); Proc. Roy. Soc. A, 197, 294 (1949).
6. C. J. ENGELDER and L. E. MILLER.   J. Phys. Chem. 36, 1345 (1932).

A CHEMICAL PROCEDURE FOR DETERMINATION OF THE C14 DISTRIBUTION IN SOME LABELLED CARBOHYDRATES[1]

M. J. ABERCROMBIE AND J. K. N. JONES

ABSTRACT

A chemical procedure for the determination of the labelling in the terminal carbon atoms of some unsubstituted carbohydrates using 20 mg of material is described. The procedure has been tested on D-glucose-1-C14, D-glucose-6-C14, D-glucose-2-C14, and D-glucuronolactone-6-C14 with satisfactory results.

A procedure based on the work of Smith *et al.* for the degradation of hexoses via the methyl glucopyranosides is described and has been applied to D-glucose-1-C14 and D-glucose-6-C14 with satisfactory results. These procedures have been designed to give barium carbonate as the final product in each determination.

INTRODUCTION

There are many procedures for determining C14 distribution in carbohydrates described in the literature (1–14), but of these only two afford a complete determination of the labelling on a millimole scale (11, 13). The remainder either require large amounts of material or do not give the labelling in all of the carbon atoms. Gunsalus and Gibbs have described a fermentation procedure with *Leuconostoc mesenteroides* (11) for the degradation of glucose and Altermatt, Blackwood, and Neish (12) have extended the method to the degradation of xylose. Although this procedure yields satisfactory results it is limited to those sugars which the organism will ferment. Boothroyd, Brown, Thorn, and Neish have described chemical procedures for the determination of the C14 labelling in glucose (13) and xylose (14) (see also 10). This method is applicable to many sugars.

A limitation to the methods available for radioactive degradation procedures is the type of counting apparatus available. If counting of barium carbonate plates is the only method available then the combustion of large molecules, such as dimedone and phenylhydrazone derivatives, is not always suitable, since the labelled moiety becomes diluted with large quantities of unlabelled carbon material.

The first part of this paper describes a method by which the C14 labelling in the terminal position of any unsubstituted carbohydrate may be determined on a minimum of material (20 mg). This quantity is the amount required to give 30 mg of barium carbonate for each of the three determinations involved.

The sodium metaperiodate oxidation of sugars has (16, 17) been extensively studied in this (15) and other laboratories. It has been shown that complete oxidation of an aldohexose to 5 moles of formic acid (C 1–5) and 1 mole of formaldehyde (C-6) takes place rapidly at pH 8.0 (15) (phosphate buffer). Hough *et al.* (17) have shown that the oxidation of glucuronic acid proceeds smoothly to give 1 mole of carbon dioxide (C-6) and 5 moles of formic (C 1–5) at pH 3.6 (acetate buffer). The borohydride reduction of oligosaccharides and subsequent metaperiodate oxidation carried out *in situ* without isolation of the intermediatory glycitol derivative has been studied (18). These methods when applied to monosaccharides gave a method for determining the labelling in the terminal carbon atoms.

The specific activity of the sugar can be determined by the complete combustion of the material to carbon dioxide (C 1–6). Metaperiodate oxidation and oxidation of the formic acid liberated to carbon dioxide with mercuric acetate (7) gives the specific activity of carbon atoms 1–5. Similarly reduction with borohydride and metaperiodate oxidation

of the glycitol *in situ* gives the specific activity of carbon atoms 2–5. Thus by difference the labelling in C-1 and C-6 can be determined. Although the determination of activities by difference has been criticized by many workers it can be seen from Table II that the results obtained from the above procedure are within ±2% of those expected. The figures in Table I show that the results are reproducible within ±2% except in the determinations where the activity is very small.

TABLE I

Determination of C^{14} in terminal carbon atoms of glucose and glucuronolactone

		D-Glucose-1-C^{14},[*] counts/min mg BaCO₃	D-Glucose-1-C^{14},[†] counts/min mg BaCO₃	D-Glucose-6-C^{14},[†] counts/min mg BaCO₃	D-Glucose-2-C^{14},[†] counts/min mg BaCO₃	D-Glucurono-lactone-6-C^{14},[†] counts/min mg BaCO₃
Van Slyke	(i)	425	137.0	174.7	23.0	754.0
(C 1–6)	(ii)	413	136.6	176.8	22.7	760.0
	(iii)	420	—	—	23.3	—
Mean		419±1.5%	136.8±1%	175.7±0.6%	23.0±1.5%	757.0±0.5%
NaIO₄	(i)	515	159.0	2.6	28.4	4.0
(C 1–5)	(ii)	506	161.4	1.9	—	2.5
	(iii)	512	162.3	—	—	—
Mean		511±1.0%	160.9±1%	2.3±15%	28.4	3.25±25%
NaBH₄	(i)	5	1.3	1.10	33.9	—
NaIO₄ (C 2–5)	(ii)	4	—	—	—	—
Mean		4.5±9%	1.3	1.10	33.9	—

*Degradation by method A. †Degradation by method B.

The above method requires a minimum of material since the activity of the formic acid and not the formaldehyde is determined. The quantity of formic acid liberated is fivefold that of the formaldehyde in the metaperiodate oxidation and twice that of the formaldehyde in the borohydride/metaperiodate oxidation. Thus the same quantity of barium carbonate is obtained from a fifth and a half as much sugar respectively.

The second part of this paper describes a chemical method for the degradation of any aldohexose, using a single sample of material, for determination of the activity in each of the six positions.

The method is outlined in Fig. 1. Smith *et al.* have studied the metaperiodate oxidation of methyl glycosides (19) and have isolated the dialdehyde (II), characterized the triol (III), and isolated derivatives of glycerol and glycolic aldehyde (IV). Neish *et al.* (13) attempted to make use of these products for a degradation procedure, but found that C-2 was contaminated by C-1 due to enolization of the glycolic aldehyde.

In the present work the procedure was carried a stage further to give glycerol and ethylene glycol (V). These compounds have been characterized as glycerol tris-*p*-nitro-benzoate and ethylene glycol-bis-*p*-nitrobenzoate. The glycerol / ethylene glycol mixture is obtained in high yield (95% based on the methyl glycoside).

A considerable amount of time was spent devising methods for the separation of glycerol and ethylene glycol. The best method of separation would be to use gas-phase chromatography with a column that could separate milligram quantities. Separation on resin columns (20) has been attempted but only a partial separation has been obtained to date. The components can be separated satisfactorily on a cellulose column using butanol/ethanol/water, 6:2:1. Excellent separation is achieved by paper chromatography when the same solvent mixture was used but in the ratio 3:1:1. In the latter two

FIG. 1.
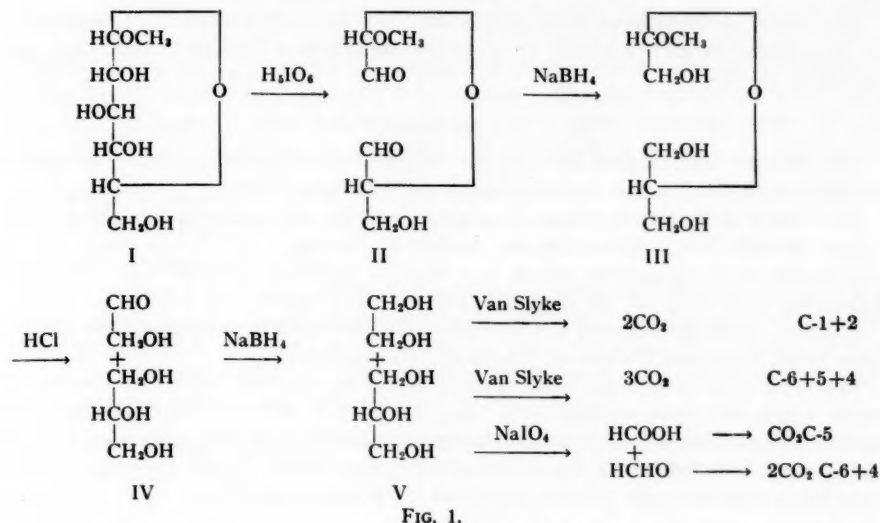
techniques 95% or better recovery of glycerol was obtained but the recovery of ethylene glycol was considerably less (50–65%).

The activity of the ethylene glycol was determined by combustion (C 1+2). The glycerol was oxidized with aqueous sodium metaperiodate to give 2 moles of formaldehyde (C 6+4) and 1 mole of formic acid (C-5). This degradation procedure gives us the labelling in C (1+2), C-3, C-5, and C (4+6). Since the labelling in C-1 and C-6 can be obtained from a small quantity of material as described at the beginning of this paper the C¹⁴ labelling in all six carbon atoms of the aldohexose can be determined. The results are collected in Table II.

TABLE II

Determination of C¹⁴ distribution in D-glucose and D-glucuronolactone

		D-Glucose-1-C¹⁴*		D-Glucose-1-C¹⁴†		D-Glucose-6-C¹⁴		D-Glucose-2-C¹⁴†		D-Glucurono-lactone-6-C¹⁴†	
		Counts/min mg glucose	% Total	Counts/min mg glucose	% Total	Counts/min mg glucose	% Total	Counts/min mg glucose	% Total	Counts/min mg glucurono-lactone	% Total
Van Slyke	C 1–6	2750	100.0	881	100.0	1152	100.0	151	100.0	768	100.0
NaIO₄	C 1–5	2780	101.0	881	100.0	12	1.1	155	102.0	3	0.4
BH₄*/IO₄*	C 2–5	21	0.7	6	0.7	5	0.4	149	98.5	—	—
Methyl-α-D-glucoside	C-3			4	0.4	5	0.4				
Glycerol											
Van Slyke	C 4–6			2	0.2	1140	99.0				
IO₄*	C-5			—	—	5	0.4				
Ethylene glycol											
Van Slyke	C 1–2			872	98.5	11	1.0				
	C-1		100.3		99.3		0.7		1.5		↑
	C-2		↑		(−0.8)		0.3		↑		
	C-3		0.7		0.4		Nil		98.5		0.4
	C-4				>0.2		(−0.3)				
	C-5		↓		>0.2		0.4		↓		↓
	C-6		(−1.0)		Nil		98.9		(−2)		99.6

*See Table I. †See Table I.

The above methods have been used in studying the biosynthesis of the sugars found in the polysaccharides produced by *Cryptococcus laurentii*. Details of this work will be published shortly.

METHODS

The chromic acid reagent used for the complete combustion of organic samples was prepared according to the directions given by Van Slyke (21).

The mercuric acetate/acetic acid reagent used for the oxidation of formic acid to carbon dioxide was prepared by the method of Bernstein (7). These oxidations were carried out in an apparatus which is a slightly modified form of that described by Johansson *et al.* (22) for the determination of uronic acid.

The radioactive sugars used in the experiments described in this paper were purchased from Isbell (National Bureau of Standards, Washington).

The separation of glycerol and ethylene glycol was carried out on Whatman 3MM paper which had been washed with acid, water, and solvent. The following solvent system was used for the chromatographic separation: butanol–ethanol–water, 3:1:1. The glycols were detected on the chromatograms by spraying them with the metaperiodate / *p*-anisidine hydrochloride reagent described by Bragg *et al.* (23).

Measurement of C^{14} in Barium Carbonate Samples

The barium carbonate plates were prepared by the method of Calvin *et al.* (24) and each sample was plated in triplicate (ca. 10 mg barium carbonate on each plate).

The activity of the barium carbonate plates was measured in a proportional methane gas flow counter comprised of the following: the detector, model CFIS2, purchased from the Atomic Energy of Canada Limited and a preamplifier, scaler, and high-voltage assembly manufactured by the Atomic Instrument Co.

The background count was determined and a standard C^{14} plate was counted before and after each counting period. The barium carbonate plates were counted until 1000–1200 counts had accumulated; each plate was counted in triplicate. A correction factor for self-absorption of the barium carbonate was applied.

EXPERIMENTAL

Degradation of Glucose-1-C^{14} (method A)

The total activity (C 1–6) of the glucose sample was determined in the usual way by use of the Van Slyke reagent.

Metaperiodate Oxidation (C 1–5)

The glucose (6–7 mg) was dissolved in phosphate buffer solution pH 8.0 ($M/20$) and 2 ml of 0.3 M aqueous sodium metaperiodate was added. The oxidation was allowed to proceed in the dark for 2 hours. An excess ($\times 10$) of sodium borohydride was added to destroy the remaining metaperiodate; after 15 minutes 2 N sulphuric acid was added until the solution was acidic (pH 2.0). The formic acid was separated from the inorganic material by steam distillation (7), the mercuric acetate/acetic acid reagent (9 ml) was added to the distillate, and after the apparatus was flushed with nitrogen for 10 minutes the reaction mixture was boiled for 20 minutes with constant stirring. The barium carbonate was collected and prepared for counting as described above.

Reduction with Sodium Borohydride and Oxidation with Sodium Metaperiodate (C 2–5)

Glucose (7–8 mg) was dissolved in water (2 ml) and sodium borohydride (9 mg) was

added; the solution was allowed to stand for 12 hours. The excess sodium borohydride was destroyed by making the solution acidic (pH 2.0) with 2 N sulphuric acid. Sodium hydroxide (2 N) solution was added until the pH of the solution was ca. 7.0, 10 ml of phosphate buffer solution and 2 ml of 0.3 M aqueous sodium metaperiodate were added, and the solution was left in the dark for 2 hours. The metaperiodate was destroyed with excess sodium borohydride and the oxidation was continued as before.

Degradation of Glucose-1-C¹⁴, -6-C¹⁴, and -2-C¹⁴ (method B)

The total activity (C 1–6) of the glucose samples was determined as above.

Metaperiodate Oxidation (C 1–5)

The metaperiodate oxidation and addition of sodium borohydride was carried out as described in method A. The excess sodium borohydride was destroyed by the addition of 2 N sulphuric acid and the mercuric acetate/acetic reagent (10 ml) was added. A bright red precipitate of mercuric salts was formed, the apparatus was flushed out with nitrogen, and the oxidation continued as described above.

Reduction with Sodium Borohydride and Oxidation with Sodium Metaperiodate (C 2–5)

The reaction was carried out in a similar manner to that described above, i.e. without distillation of the formic acid.

Degradation of Glucuronolactone-6-C¹⁴

The total activity (C 1–6) was determined as usual.

Metaperiodate Oxidation (C 1–5)

The glucuronolactone solution (7 mg in 3 ml of water) was titrated to neutrality with 0.01 N sodium hydroxide solution. The acetate buffer, pH 3.65 (10 ml), and 2 ml of 0.3 M aqueous sodium metaperiodate were added. The reaction mixture was kept in the dark for 6.5 hours, after which ethylene glycol was added to destroy the excess metaperiodate. After 10 minutes the acidic solution was gently boiled to drive off carbon dioxide (C-6) the solution was cooled and the mercuric acetate/acetic acid reagent (9 ml) was added. The oxidation was continued in the usual manner.

Preparation of Methyl-α-D-glucopyranoside

The methyl-α-D-glucopyranoside was prepared by the standard method (25). The product was recrystallized from a mixture of equal parts of ethanol and methanol until a constant melting point of 164–165° C was obtained.

Periodic Acid Oxidation of Methyl-α-D-glucopyranosides

A solution of methyl-α-D-glucopyranoside (194 mg) in water (3 ml) was treated with 0.4 M periodic acid (5.5 ml) at room temperature for 3 hours. The solution was then passed through a column of Duolite A-4 (OH) resin (1.9×6 cm). The column was washed with distilled water until the total volume of the eluate reached 110 ml. This eluate, which contained the dialdehyde (II) (Fig. 1), was concentrated to ca. 25 ml, sodium borohydride (60 mg) was added, and the reduction to the triol (III) (Fig. 1) was allowed to proceed overnight. The excess sodium borohydride was destroyed by making the solution acidic with 2 N hydrochloric acid. The triol was hydrolyzed to glycerol and glycolic aldehyde (IV) (Fig. 1) by adding 2 N hydrochloric acid (4 ml) and warming at 60° C for 20 minutes. After the solution was cooled 2 N sodium hydroxide solution was added until the pH of the solution was 6.0–6.5. Sodium borohydride (40 mg) was added to reduce the glycolic aldehyde to ethylene glycol (V) (Fig. 1); the reaction mixture

was allowed to stand for 2 hours. The excess sodium borohydride was destroyed by making the solution acid with 2 N hydrochloric acid. The solution was brought to neutrality by the addition of 2 N sodium hydroxide solution and concentrated *in vacuo* to 15 ml.

Separation of Glycerol and Ethylene Glycol from the Inorganic Material

The glycerol and ethylene glycol were separated from the inorganic material by passing the solution through a Dowex 50W (8% D.V.B.) resin column (Ba++) (20×115 cm) (20). The eluate was collected in the tubes of a fraction collector. The tubes containing the glycerol and ethylene glycol were combined and evaporated to dryness. Boric acid was still present in the fractions and was removed by codistillation with methanol (×2). A pale yellow syrup was obtained (146 mg). This syrup was passed through a short mixed resin column (Amberlite IR-120 (H) and Duolite-A-4 (OH)) and again evaporated to dryness. The colorless mobile syrup was taken up in methanol, filtered through a celite/charcoal pad, and again evaporated to dryness. A colorless, clear mobile syrup was obtained (134 mg, 100%). Chromatographic examination of an aliquot of this syrup showed spots which moved at rates corresponding to those of ethylene glycol and glycerol. A small quantity of a third material, which moved at a slower rate than glycerol, was detected. This material is probably a tetritol derived from the dimerization of glycolic aldehyde.

Separation of Glycerol (C-6, C-5, and C-4) and Ethylene Glycol (C-1 and C-2)

The syrup (134 mg) was fractionated by placing it on Whatman 3MM paper and by chromatography of the mixture with the neutral solvent. The appropriate portions of the paper containing the glycerol and ethylene glycol were eluted with water and evaporated to dryness. The syrups obtained were dissolved in water, deionized on mixed ion-exchange resin columns, and evaporated to dryness. These syrups were taken up in methanol (3 ml) filtered through small celite/charcoal pads, and evaporated to dryness. The fraction corresponding to glycerol weighed 92 mg (100%) and that corresponding to ethylene glycol 27 mg (65%). Both fractions were clear, colorless, mobile syrups. On chromatographic examination each showed a single spot which moved at a rate corresponding to either glycerol or ethylene glycol.

Identification of Glycerol and Ethylene Glycol

Each fraction was treated with a 50% molar excess of p-nitrobenzoylchloride (recrystallized) in pyridine (freshly dried and distilled) according to the method of Smith *et al.* (26). The glycerol fraction gave crystalline glycerol-tris-p-nitrobenzoate, m.p. 198–199° C; the ethylene glycol fraction gave crystalline ethylene glycol-bis-p-nitrobenzoate, m.p. 143–144° C. (Mixture melting points with authentic samples were not depressed.)

Degradation of Methyl-α-D-glycopyranoside-1-C^{14} and -6-C^{14}

Each sample (100 mg and 57 mg) was subjected to the degradation procedure described above and afforded 65 mg (95%) and 36 mg (100%) of the glycerol/ethylene glycol mixtures.

Determination of C^{14} in C-3 (13)

After removal of the dialdehyde, the resin column was washed with a further 50 ml of water and the washings were discarded. The formic acid was eluted from the column with 0.25 N barium hydroxide (20 ml) solution followed by water (30 ml). The alkaline

barium formate solution was acidified with $2 N$ sulphuric acid. The formic acid in the solution was then oxidized to carbon dioxide by refluxing it for 20 minutes with mercuric acetate. The barium carbonate was collected and assayed for C^{14} as described above.

Radiographic Examination of the Glycerol/Ethylene Glycol Mixtures

Each of the two samples was chromatographed on Whatman 3MM paper in the neutral solvent. An X-ray film was left in contact with the chromatogram for 4 weeks. On development the radiogram showed one band corresponding to the position of glycerol from the methyl-α-D-glycopyranoside-6-C^{14} and one band corresponding to the position of ethylene glycol from methyl-α-D-glucopyranoside-1-C^{14}, the latter also showed a weak band corresponding to the position of the tetritol discussed earlier. The positions of the non-radioactive samples of glycerol and ethylene glycol were determined in the usual manner. The appropriate sections of the paper were eluted and purified as described above.

The methyl-α-D-glucopyranoside-1-C^{14} yielded glycerol, 40 mg (84%), and the ethylene glycol, 10 mg (46%). The methyl-α-D-glucopyranoside-6-C^{14} yielded glycerol, 25 mg (92%), and ethylene glycol, 5 mg (40%).

Degradation of Glycerol and Ethylene Glycol

The samples of ethylene glycol (5 mg) were totally combusted in the normal manner. The total activities of the glycerol samples were determined in a similar fashion. The glycerol derived from the methyl-α-D-glucopyranoside-6-C^{14} was further degraded to determine the radioactivity in C-5. Glycerol (15 mg) was oxidized with aqueous 0.3 M metaperiodate in a similar manner to that described for the metaperiodate oxidation of glucose-1-C^{14} (method B).

REFERENCES

1. H. N. BARNET and A. N. WICK. J. Biol. Chem. **185**, 657 (1950).
2. D. A. RAPPOPART, H. A. BARKER, and W. Z. HASSID. Arch. Biochem. Biophys. **31**, 326 (1951).
3. Y. J. TOPPER and A. B. HASTINGS. J. Biol. Chem. **179**, 1255 (1949).
4. S. ABRAHAM, I. L. CHAIKOFF, and W. Z. HASSID. J. Biol. Chem. **195**, 567 (1952).
5. S. ARONOFF, H. A. BARKER, and M. CALVIN. J. Biol. Chem. **169**, 459 (1947).
6. H. G. WOOD, N. LIFSON, and V. LARBER. J. Biol. Chem. **159**, 475 (1945).
7. I. A. BERNSTEIN. J. Biol. Chem. **205**, 309 (1953).
8. H. L. FRUSH and H. S. ISBELL. J. Research Natl. Bur. Standards, **51**, 167 (1953).
9. C. T. BISHOP. Science, **117**, 715 (1953).
10. J. C. BEVINGTON, E. J. BOURNE, and C. N. TURTON. Chem. & Ind. 1390 (1953).
11. I. C. GUNSALUS and M. GIBBS. J. Biol. Chem. **194**, 871 (1952).
12. H. A. ALTERMATT, A. C. BLACKWOOD, and A. C. NEISH. Can. J. Biochem. and Physiol. **33**, 622 (1955).
13. B. BOOTHROYD, S. A. BROWN, J. A. THORN, and A. C. NEISH. Can. J. Biochem. and Physiol. **33**, 62 (1955).
14. S. A. BROWN. Can. J. Biochem. and Physiol. **33**, 368 (1955).
15. M. B. PERRY. Personal communication.
16. G. NEUMÜLLER and E. VASSEUR. Arkiv Kemi, **5**, 235 (1953).
17. L. HOUGH, J. TAYLOR, G. H. S. THOMAS, and B. M. WOODS. J. Chem. Soc. **239**, 1212 (1958).
18. L. HOUGH, B. M. WOODS, and M. B. PERRY. Chem. & Ind. 1100 (1957).
19. M. ABDEL-AKHER, J. E. CADOTTE, R. MONTGOMERY, F. SMITH, J. W. VAN CLEVE, and B. A. LEWIS. Nature, **171**, 474 (1953).
20. J. K. N. JONES, R. A. WALL, and (*in part*) A. O. PITTET. Chem. & Ind. 1196 (1959).

21. D. D. VAN SLYKE, J. PLAZIN, and J. R. WEISIGER. J. Biol. Chem. **192**, 299 (1951).
22. A. JOHANSSON, B. LINDBERG, and O. THEANDER. Svensk Papperstidn. **57**, 41 (1954).
23. P. D. BRAGG and L. HOUGH. J. Chem. Soc. 4050 (1958).
24. M. CALVIN, C. HEIDELBERGER, J. C. REID, B. TOLBERT, and P. F. YANKERVICH. Isotopic carbon. John Wiley & Sons, Inc., New York. 1949. p. 116.
25. E. FISCHER. Ber. **28**, 1145 (1895).
26. F. SMITH and J. W. VAN CLEVE. J. Am. Chem. Soc. **77**, 3091 (1955).

THE POLYSACCHARIDES OF CRYPTOCOCCUS LAURENTII (Y1401)

PART II. BIOSYNTHESIS OF THE CARBOHYDRATES FOUND IN THE ACIDIC POLYSACCHARIDE[1]

M. J. Abercrombie, J. K. N. Jones, and M. B. Perry

ABSTRACT

Cryptococcus laurentii was grown on media which contained D-glucose-1-C^{14}, D-glucose-6-C^{14}, D-mannose-1-C^{14}, D-galactose-1-C^{14}, D-xylose-1-C^{14}, and L-arabinose-1-C^{14}. The radioactive polysaccharides were isolated and hydrolyzed. The distribution of the radioactivity in D-mannose, D-xylose, and D-glucuronic acid isolated from the polysaccharides was determined.

The results show that (A) D-mannose and D-glucuronic acids are formed from the hexoses without any appreciable breakdown of the hexose skeleton; (B) D-xylose is formed from the hexoses mainly by a process involving loss of carbon-6; (C) D-xylose and L-arabinose are both converted to D-mannose, D-xylose, and D-glucuronic acid with rearrangement of the pentose skeleton that may involve the action of transaldolase and transketolase.

INTRODUCTION

In Part I of this series of papers (1) the growth, isolation, and preliminary structural investigation of the polysaccharides produced by *Cryptococcus laurentii* were reported. It was shown that two polysaccharides were present: an acidic polysaccharide containing D-mannose, D-xylose, and D-glucuronic acid and a neutral polysaccharide which consisted of D-glucose only.

In this paper the biosynthesis of the monosaccharides found in the acidic polysaccharide is discussed.

EXPERIMENTAL

Materials

D-Glucose-1-C^{14}, D-glucose-6-C^{14}, D-xylose-1-C^{14}, and L-arabinose-1-C^{14} were purchased from the National Bureau of Standards, Washington. D-Mannose-1-C^{14} and D-galactose-1-C^{14} were purchased from Merck & Co., Montreal. The uniformly labelled D-glucose-C^{14} was provided by Dr. G. Krotkov, Department of Biology, Queen's University, Kingston.

The purity of these compounds was checked by chromatographic and radioautographic examination.

Growth of Cryptococcus laurentii and Isolation of the Polysaccharide

The organism was grown on the media described in Part I (1). The aqueous solution containing the carbon-14 labelled sugar and the growth solution were steam sterilized in separate vessels. These solutions were combined in a sterile 250-ml, two-necked round-bottom flask. The final strength of the solution was $2\frac{1}{2}\%$ with respect to the sugar. A slow stream of sterilized, carbon dioxide free air was drawn through the solution; the carbon dioxide evolved was collected in a trap which contained 200 ml of 2 N sodium hydroxide solution. The media were inoculated from a freshly prepared slope on which the yeast organism was growing. The slope contained the same sugar as the growth media which were to be inoculated.

The growth of the organism was followed by sampling the carbon dioxide evolved. When the sodium carbonate content of the aqueous sodium hydroxide trap reached a constant value the growth was stopped. The conversion of carbohydrate to carbon dioxide

reached a constant value at about 55% of the theoretical assuming complete oxidation of carbohydrate to carbon dioxide (see Table I). The average growth time was 7 days.

The growth solution was diluted to 50 ml with water and the solution was shaken to wash the viscous material from the wall of the reaction vessel. The yeast cells were removed by centrifugation and the cells were washed with water (2×20 ml). The supernatant and the washings were combined and diluted to 100 ml.

A 5-ml sample of this solution was deionized by passing the solution through a small mixed bed ion-exchange resin column (Amberlite IR-120 (H)/Duolite-A-4 (OH)). The eluate was concentrated *in vacuo* to a small volume and was examined by chromatography and radioautography. In most experiments a spot moving at the same speed as the free sugar which formed part of the original substrate was the only compound detected by either method. In the other experiments no spots were observed (see Table I).

The remainder of the supernatant (95 ml) was dialyzed against distilled water (2 liters) in which was suspended mixed ion-exchange resins (as above) for 2 days. The dialyzed solution, which had become cloudy, was filtered through a small pad of "Celite" to give a clear filtrate. The pad of "Celite" was washed with a further 50 ml of water and the washings were combined with the filtrate. The solution was concentrated to about 10 ml; the polysaccharide was precipitated by addition of 75 ml of ice-cold ethanol which contained 1% of hydrochloric acid. The polysaccharide was collected by centrifugation, washed with ethanol, and dried *in vacuo*. The yields are recorded in Table I.

TABLE I

Incorporation of C^{14} into the polysaccharides produced by *Cryptococcus laurentii*

Compound fed	mg of compound	μc^* of C^{14}	Time of growth (days)	Yield				% CO_2 evolved	Radioactive yield ×100/ dry weight yield	Sugar remaining in substrate
				mg	%	μc^*	%			
D-Glucose-E-C^{14}										
I	200	67.6	10½	9.0	4.5	2.22	3.3	—	80.0	Glucose
II	200	33.8	10½	5.5	2.8	0.71	2.1	—	83.5	Glucose
III	400	106.0	7	31.5	7.8	6.2	5.9	—	83.0	Glucose
D-Glucose-1-C^{14}	400	150.0	7	57.7	14.0	11.3	7.6	53.0	45.5	Nil
D-Glucose-6-C^{14}	400	147.0	7	48.2	12.0	7.3	5.0	52.6	41.5	Nil
D-Mannose-1-C^{14}	408	150.0	7	27.8	7.0	6.2	4.1	51.5	59.0	Mannose
D-Galactose-1-C^{14}	400	103.0	7	33.5	8.5	5.3	5.2	55.0	60.0	Galactose†
D-Xylose-1-C^{14}	400	104.0	7	42.0	10.5	6.9	6.7	59.0	64.0	Xylose†
L-Arabinose-1-C^{14}	400	50.0	7	34.0	8.5	2.3	4.5	58.0	53.0	Nil

* μc=microcuries of activity.
† Showed substances other than galactose or xylose which were not identified.

Hydrolysis of the Polysaccharides

The polysaccharides isolated from media which had contained D-xylose-1-C^{14} or L-arabinose-1-C^{14} were hydrolyzed for 24 hours with ca. 7 ml of N sulphuric acid in sealed glass tubes which were suspended in a boiling-water bath. The hydrolyzates were diluted to 50 ml with water, neutralized with barium carbonate, filtered through beds of "Celite", and deionized by passage through small columns of Amberlite IR-120 (H) ion-exchange resin. These solutions were made up to a known volume (100 ml). Aliquots of each solution were then dried on aluminum disks and counted. The total activity of the hydrolyzates and the radioactive yields are recorded in Table I. Since there appeared

to be a considerable loss of material due to degradation during hydrolysis the remaining samples of polysaccharides were hydrolyzed by the following procedure.

The polysaccharides were hydrolyzed with ca. 5 ml of 2% methanolic hydrogen chloride in sealed glass tubes in a boiling-water bath for 15 hours. After the tubes had cooled they were opened and the solutions were evaporated to dryness under a stream of air. To the residues 5 ml of N hydrochloric acid was added, the tubes were sealed, and the methyl glycosides were hydrolyzed in a boiling-water bath for 5 hours. After cooling, the hydrolyzates were diluted to 50 ml with water and silver carbonate was added to neutralize the hydrochloric acid. The insoluble salts were removed by filtration and the filtrates were deionized by passage through small Amberlite IR-120 (H) ion-exchange resin columns. The solutions were diluted to known volumes and counted as before. The results are collected in Table I.

The hydrolyzates of the polysaccharides produced from the media containing uniformly labelled glucose-1-C^{14} had recoveries of ca. 80% based on the dry weight of the polysaccharides. The recoveries from the polysaccharides derived from D-glucose-1-C^{14}, D-glucose-6-C^{14}, D-mannose-1-C^{14}, and D-galactose-1-C^{14} were rather less. This is attributed to the fact that when the hydrolyzates were fractionated by chromatography considerable quantities of methyl glycosides were detected and the fractions had to be eluted from the paper and rehydrolyzed with N hydrochloric acid.

Isolation of the Radioactive Carbohydrates

The 3MM Whatman paper on which the hydrolyzate mixtures were fractionated was washed with acid, water, and solvent before use. Chromatographic fractionations were carried out using the following solvent system (v/v) n-butanol:pyridine:benzene:water, 5:3:3:1. After the chromatograms had been developed for ca. 30 hours they were dried and placed in contact with X-ray films for 9 days. The bands corresponding to the portions of mannose, xylose, glucose, and uronic acids (present on the base line) were eluted and the eluates were diluted to known volumes. Aliquots of each solution were then dried on aluminum disks and counted. The solutions were concentrated *in vacuo* at 35° C to a small volume and applied to the base line on sheets of Whatman 3MM paper (treated as above). The chromatograms were developed in ethyl acetate : acetic acid : water, 9:2:2 (v/v). The chromatograms were radioautographed and the sugars eluted and counted as before. The results are collected in Table II. The solutions of the neutral radioactive carbohydrates were passed through small columns of mixed ion-exchange resins (as

TABLE II

Total activities (μc) found in isolated monosaccharides

Compound fed	D-Mannose	D-Xylose	D-Glucose	D-Glucuronic acid		Total	D-Mannose
				A	B		D-Xylose
D-Glucose-E-C^{14}							
I	1.03	0.34	0.05	0.38	—	1.75	3.02/1.0
II	0.35	0.11	0.02	0.11	—	0.55	3.10/1.0
III	2.54	0.75	0.16	0.91	—	4.36	3.40/1.0*
D-Glucose-1-C^{14}	3.00	1.18	0.32	1.22	0.40	5.72	2.56/1.0
D-Glucose-6-C^{14}	4.10	0.09	0.25	1.01	0.29	5.45	45.0/1.0
D-Mannose-1-C^{14}	2.10	0.58	0.24	0.84	0.13	3.76	3.6/1.0
D-Galactose-1-C^{14}	1.70	0.40	0.17	0.43	0.29	2.70	4.25/1.0
D-Xylose-1-C^{14}	3.70	1.23	0.19	1.10	0.44	6.20	3.00/1.00
L-Arabinose-1-C^{14}	1.25	0.43	0.03	0.35	0.15	1.81	2.85/1.00

*Analysis of mannose/xylose ratio by colorimetric method of Smith (5) gave 3.10/1.00.

above) to remove traces of ash which were present. The radioactive monosaccharides were diluted with the quantity of cold material required for the degradation procedures.

Degradation of the Sugars

The radioactive content of the carbon atoms of D-mannose and D-glucuronic acid and of the terminal carbon atoms of D-xylose were determined by methods described previously by the authors (2). The radioactive content of the carbon atoms 3 and 4 of D-xylose were determined by methods described in the literature (3, 4). The results are collected in Table III.

TABLE III

Distribution of C^{14} in D-mannose, D-xylose, and D-glucuronic acid isolated from the polysaccharide produced by *Cryptococcus laurentii*

Compound fed	Sugar isolated	C^{14} as % total in monosaccharide					
		Carbon-1	Carbon-2	Carbon-3	Carbon-4	Carbon-5	Carbon-6
D-Glucose-1-C^{14}	D-Mannose	83.8	←————5.8————→				10.4
	D-Xylose	93.6	←———4.7———→			1.7	—
	D-Glucuronic acid	86.6	←————7.4————→				7.0
D-Glucose-6-C^{14}	D-Mannose	6.3	←————2.5————→				91.2
	D-Xylose	37.0	←———21.0———→			42.0	—
	D-Glucuronic acid	2.6	←————2.0————→				95.6
D-Mannose-1-C^{14}	D-Mannose	81.7	←————3.3————→				15.0
	D-Xylose	85.6	←———5.4———→			9.0	—
	D-Glucuronic acid	26.3	←————26.3————→				47.2
D-Galactose-1-C^{14}	D-Mannose	76.8	←————7.2————→				16.0
	D-Xylose	93.7	←———4.1———→			2.8	—
	D-Glucuronic acid	55.0	←————24.0————→				21.0
D-Xylose-1-C^{14}	D-Mannose	48.1	1.1	24.5	13.0	3.5	13.5
	D-Xylose	56.9	2.6	30.0	9.0	1.5	—
	D-Glucuronic acid	53.0	←————38.5————→				8.5
L-Arabinose-1-C^{14}	D-Mannose	50.9	0.2	27.7	9.8	2.8	7.1
	D-Xylose	56.0	0.5	32.5	7.5	4.5	—
	D-Glucuronic acid	48.5	←————45.0————→				6.5

RESULTS

The percentage yields of polysaccharides shown in the fifth column of Table I indicate that D-glucose may be a more efficient precursor for polysaccharide formation than the other sugars; however, there is little to choose between them.

In the last column of Table II the ratio of D-mannose to D-xylose in the polysaccharides from the growths on uniformly labelled D-glucose is shown to be approximately 3:1 (w/w). This is in agreement with the value obtained from the colorimetric procedure (5) which was determined on the same sample of polysaccharide. Allowing for the difficulties encountered during the hydrolysis of the radioactive polysaccharides the ratios of D-mannose to D-xylose in the other experiments are in the region of 3:1 except for the polysaccharide grown from substrate containing D-glucose-6-C^{14} where the apparent ratio is 45:1. This result shows that the main pathway for the conversion of D-glucose (or hexose) to D-xylose is via a pathway which involves the loss of carbon-6. This is in agreement with the results of previous workers (9, 14).

Columns A and B (Table II) show the total activities of the uronic acid fraction from the hydrolyzate of the polysaccharides after the first and second fractionation by paper chromatography. Column A shows the total uronic acid residue content (mono-, di-, and tri-uronic acid residues) and column B shows the amount of D-glucuronic acid obtained

from these fractions. The radioautograms showed that there was at least one aldobiouronic acid and one aldotriuronic acid plus other minor components. These figures show that in all cases the D-glucuronic acid content was 50% or less of the uronic acid containing fraction first isolated from the hydrolyzate.

Table III shows the distribution of C^{14} in D-mannose, D-xylose, and D-glucuronic acid.

The conversion of the hexoses to D-mannose is primarily a direct conversion with at least 76% retention of labelling in the original position. The bulk of the remainder of the labelling is in the other terminal carbon. This supports the conclusion of other workers (6–15, 26) that the Embden–Meyerhof glycolytic pathway is also utilized. It is interesting to note that the carbon-1 to carbon-6 rearrangement of the hexoses is greater for D-galactose and for D-mannose than for D-glucose. This is of special interest since it indicates that some of the D-mannose is not incorporated directly into the mannose-containing backbone of the polysaccharide via the mannosyl phosphate or guanosine diphosphate – mannose (16, 17) but that it is probably in equilibrium with D-fructose 1,6-diphosphate.

The distribution of C^{14} in the samples of D-xylose further supports the theory that D-xylose may arise from the hexoses via loss of carbon-6.

It has been postulated (18, 19) that uronic acids in pectin are derived from hexoses by direct oxidation of carbon-6 without significant breakdown of the carbon skeleton. The C^{14} labelling in D-glucuronic acid derived from D-glucose-1-C^{14} and D-glucose-6-C^{14} supports this theory. The D-glucuronic acid derived from D-mannose-1-C^{14} and D-galactose-1-C^{14} while retaining approximately 50% of the activity in carbon-1 also has a considerable distribution of activities in the other carbons. Thus in these cases there must be a significant amount of breakdown of the carbon skeleton to fragments followed by resynthesis.

L-Arabinose was not converted directly to D-xylose as was found by Neish (14). From the results it seems probable that L-arabinose is converted into a hexose which is the common precursor for the formation of D-mannose, D-glucuronic acid (via oxidation of carbon-6), and D-xylose via oxidation and decarboxylation of carbon-6. D-xylose follows a similar pathway to that of L-arabinose.

DISCUSSION

The topic *Biosynthesis of Monosaccharides* has been recently reviewed (20, 21, 22).

The results presented in this paper support the theory that hexoses are readily interconvertible with only a small amount of cleavage of the carbon skeleton occurring (6–15, 27). The probable intermediates for such conversions are shown in Fig. 1 (20).
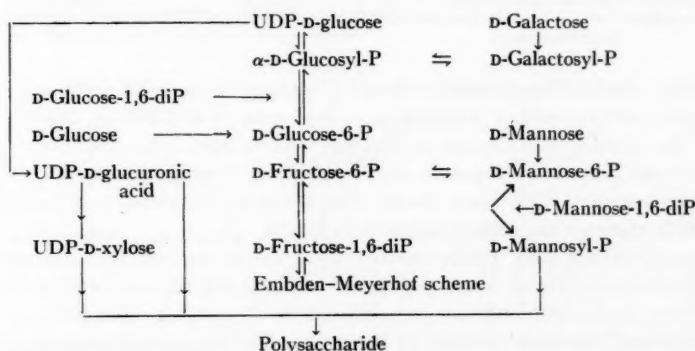
FIG. 1.   The interconversion of hexoses. P = phosphate; UDP = uridine diphosphate.

The results show that the conversion of D-galactose to the D-glucose intermediate takes place without appreciable breakdown of the carbon skeleton, probably via a "galactowaldenase" enzyme system (23). The D-glucose intermediate is epimerized to D-mannose; the over-all retention of activity in carbon-1 for the conversion of D-galactose to D-mannose is 77%. The bulk of the remainder of the activity (16%) is present in carbon-6 as would be expected if the Embden–Meyerhof pathway was operative.

The formation of D-xylose from hexoses by loss of carbon-6 is apparent, since the D-xylose derived from D-glucose-6-C^{14} contains only 6.5% of the activity that it would have contained had it been derived from D-glucose-1-C^{14}. The D-xylose derived from D-glucose-1-C^{14}, D-mannose-1-C^{14}, and D-galactose-1-C^{14} retains 85–94% of its activity in carbon-1. Similar results were obtained by other workers (12, 14, 9).

It is possible that D-xylose and D-glucuronic acid derived from D-glucose-1-C^{14} and D-glucose-6-C^{14} had the same UDP-hexuronic acid precursor since the retention of activity in carbon-1 in the former is very high. In the latter the D-glucuronic acid had 4.4% of its activity in carbons 1–5 and the D-xylose contained 6.5% of activity in carbons 1–5 as mentioned above.

The D-xylose and D-glucuronic acid derived from D-mannose-1-C^{14} and D-galactose-1-C^{14} do not come from the same UDP-hexuronic acid precursor since the retention of activity in carbon-1 of the D-xylose is high (85–93%), but the activity in the D-glucuronic acid is much more widely distributed through the molecule.

The conversion of D-xylose-1-C^{14} and L-arabinose-1-C^{14} into the polysaccharide constituents takes place with much breakdown of the pentose carbon skeleton and resynthesis to pentose, hexose, and hexuronic acid. Gibbs and Horecker (24) showed that D-ribose-5-phosphate was converted to hexose monophosphate via a pathway involving transketolase and transaldolase (Fig. 2). The results collected in Table III show that the distribution of the activity in D-mannose, D-xylose, and probably D-glucuronic acid agree with the results expected from this pathway if it is assumed that D-xylose is derived from a hexose precursor by loss of carbon-6. Neish (12, 13) and Hassid et al. (9) found with wheat seedlings that D-xylose was metabolized by such a pathway but L-arabinose was not (14). It was proposed that UDP-L-arabinose was formed as an intermediate which could be converted to UDP-D-xylose which was incorporated directly into the xylan. Neish suggested that the enzyme systems for converting free D-xylose into UDP-D-xylose were not present in wheat seedlings and that it was metabolized by the following scheme:

$$\text{D-xylose} \xrightarrow[\text{transaldolase}]{\text{transketolase}} \text{hexose} \rightarrow \text{UDP-hexuronic acid} \rightarrow \text{UDP-D-xylose} \rightarrow \text{xylan.}$$
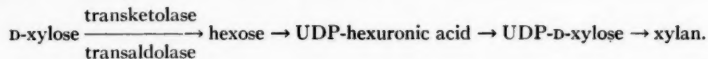
It is apparent that in the growth media of *Cryptococcus laurentii* although there is an enzyme system for converting D-galactose → D-glucose → D-mannose there is no such system for the similar L-arabinose → D-xylose conversion. The results in Table III indicate that L-arabinose and D-xylose are metabolized through the same intermediates. Recently Horecker et al. (25) have shown that D-ribose, D-xylose, and L-arabinose are interconvertible through the scheme showed in Fig. 3.

It is now recognized that D-threopentulose-5-phosphate, not D-erythropentulose-5-phosphate, is the substrate of transketolase in animals and microorganisms (22).

Since D-xylose and L-arabinose are metabolized by *Cryptococcus laurentii* via the same intermediates then it would be reasonable to propose that the enzyme systems responsible for the intermediates involved in Fig. 3 and Fig. 2 must be present.
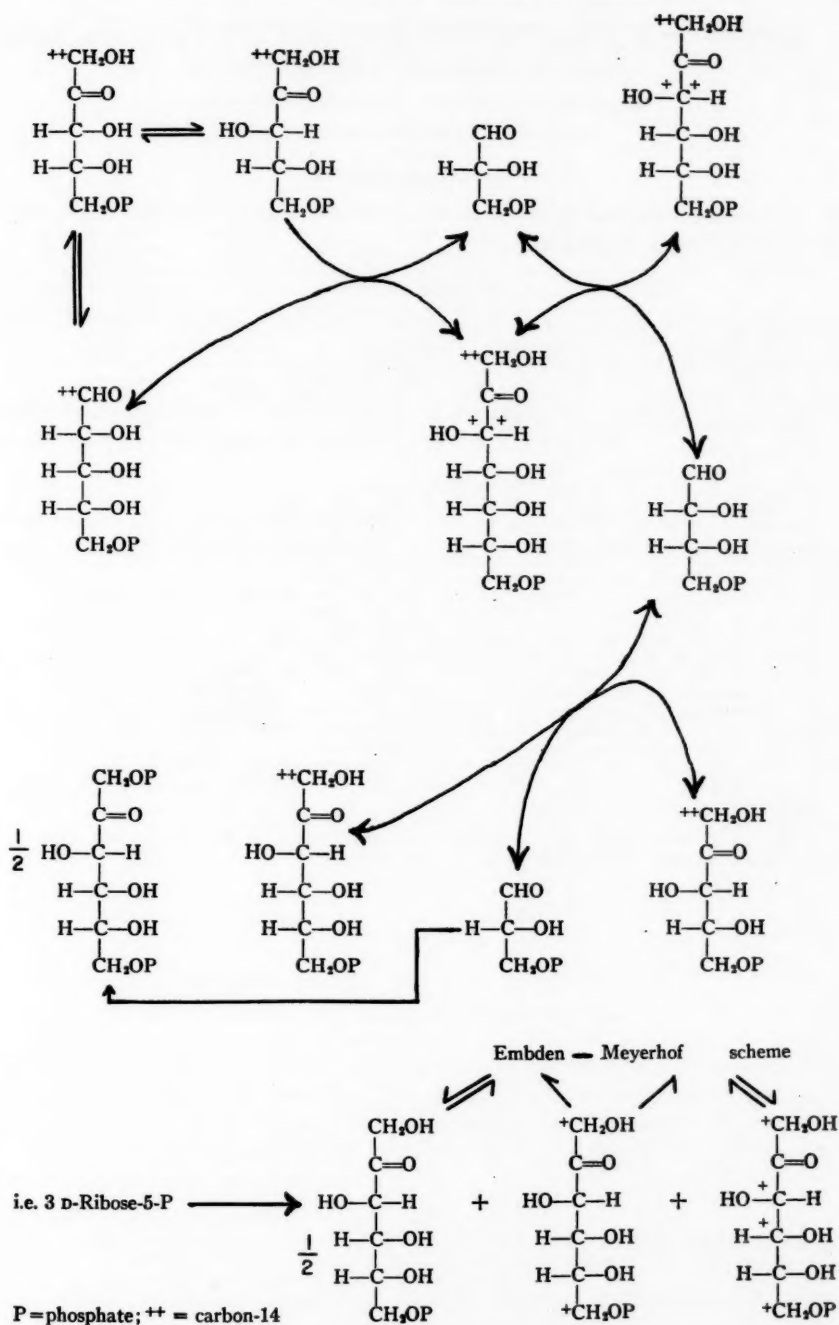
FIG. 2
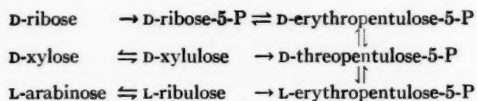
D-ribose $\rightarrow$ D-ribose-5-P $\rightleftharpoons$ D-erythropentulose-5-P

D-xylose $\leftrightharpoons$ D-xylulose $\rightarrow$ D-threopentulose-5-P

L-arabinose $\leftrightharpoons$ L-ribulose $\rightarrow$ L-erythropentulose-5-P

FIG. 3.

ACKNOWLEDGMENTS

REFERENCES

1. M. J. ABERCROMBIE, J. K. N. JONES, M. V. LOCK, M. B. PERRY, and R. J. STOODLEY. Can. J. Chem. **38**, 1617 (1960).
2. M. J. ABERCROMBIE and J. K. N. JONES. This issue.
3. S. A. BROWN. Can. J. Biochem. and Physiol. **33**, 368 (1955).
4. Y. J. TOPPER and A. B. HASTINGS. J. Biol. Chem. **179**, 1255 (1949).
5. M. DUBOIS, K. A. GILLES, J. K. HAMILTON, P. A. REBERS, and F. SMITH. Anal. Chem. **26**, 350 (1956).
6. G. A. GREATHOUSE et al. J. Am. Chem. Soc. **76**, 1658, 5052, 5157 (1954); **77**, 1244 (1955); **79**, 4505 (1957); Science, **117**, 553 (1953).
7. C. GILVARG. J. Biol. Chem. **199**, 57 (1952).
8. J. C. SOWDEN and S. FRANKEL. J. Biol. Chem. **221**, 587 (1956).
9. V. GINSBURG and W. Z. HASSID. J. Biol. Chem. **223**, 277 (1956).
10. J. ELDERMAN, V. GINSBURG, and W. Z. HASSID. J. Biol. Chem. **213**, 843 (1955).
11. S. A. BROWN and A. C. NEISH. Can. J. Biochem. and Physiol. **32**, 170 (1954).
12. A. C. NEISH. Can. J. Biochem. and Physiol. **33**, 658 (1955).
13. H. A. ALTERMATT and A. C. NEISH. Can. J. Biochem. and Physiol. **34**, 405 (1956).
14. A. C. NEISH. Can. J. Biochem. and Physiol. **36**, 187 (1958).
15. J. C. SOWDEN and S. FRANKEL. J. Biol. Chem. **221**, 587 (1956).
16. E. CABIB and L. F. LELOIR. J. Biol. Chem. **206**, 779 (1954).
17. C. W. CHUNG and W. J. NICKERSON. J. Biol. Chem. **208**, 395 (1954).
18. C. G. SEEGMILLER, B. AXELROD, and R. M. McCREADY. J. Biol. Chem. **217**, 765 (1955).
19. C. G. SEEGMILLER, R. JANG, and W. MANN. Arch. Biochem. Biophys. **61**, 422 (1956).
20. L. HOUGH and J. K. N. JONES. Advances in Carbohydrate Chem. **11**, 185 (1956).
21. S. BAYNE. Rare sugars. Ann. Rept. Chem. Soc. 1958.
22. B. L. HORECKER and A. H. MEHLER. Ann. Rev. Biochem. **24**, 207 (1955).
23. L. F. LELOIR et al. J. Biol.Chem. **179**, 497 (1949); **184**, 333 (1950); Biochem. J. (London), **51**, 426 (1952); Nature, **165**, 191 (1950).
24. M. GIBBS and B. L. HORECKER. J. Biol. Chem. **208**, 813 (1954).
25. E. C. HEATH, J. HURWITZ, B. L. HORECKER, and A. GINSBURG. J. Biol. Chem. **231**, 1009 (1958).
26. S. L. CHEN. Biochim. et Biophys. Acta, **32**, 486 (1959).

PHASE EQUILIBRIUM RELATIONSHIPS IN THE BINARY SYSTEM METHYL ETHYL KETONE – WATER[1]

IRWIN SIEGELMAN[2] AND C. H. SORUM[3]

ABSTRACT

A complete investigation of the phase equilibrium relationships in the binary system of the partially miscible liquid pair methyl ethyl ketone – water is presented. The system shows a minimum azeotrope at $73.35\pm0.05°$ C with a composition of 88.45 ± 0.15 wt.% ketone. The azeotrope falls outside of the miscibility gap for this system. The liquid–vapor curves intersect the miscibility gap at the temperature of $73.60\pm0.05°$ C at which two conjugate solutions of compositions 18.10 ± 0.10 and 87.78 ± 0.15 wt.% ketone, respectively, are in equilibrium with a vapor phase of composition 88.00 ± 0.15 wt.% ketone. The partially miscible liquid pair shows an upper consolute temperature of $139\pm0.5°$ C at a composition of 44.9 ± 0.2 wt.% ketone. The liquid–liquid curves intersect the solid–liquid curves at a temperature of $-6.0\pm0.5°$ C at which two conjugate solutions of composition 40.0 ± 0.2 and 78.0 ± 0.2 wt.% ketone, respectively, are in equilibrium with ice. A binary eutectic exists at a temperature of $-89.0\pm0.5°$ C with composition of the eutectic solid equal to 99.4 ± 0.4 wt.% ketone. The freezing point of pure, dry methyl ethyl ketone is determined to be $-83.5\pm0.5°$ C.

INTRODUCTION

Discrepancies in the literature data (1–8) on mutual solubility studies for the system methyl ethyl ketone – water, as shown in Fig. 1, and similar discrepancies in the literature
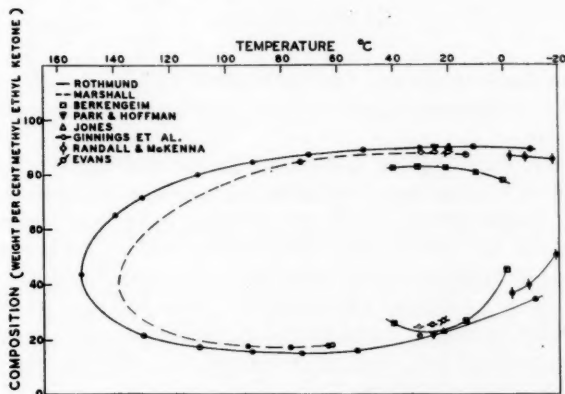
FIG· 1. Mutual solubility data as reported in the literature.

(9, 10, 11) on liquid–vapor studies of this system, as shown in Fig. 2, prompted this present work. This paper presents, then, the results of a reinvestigation of the mutual solubility and liquid–vapor relationships found in the system methyl ethyl ketone – water plus a study of the solid–liquid equilibria for a complete picture of the phase equilibrium relationships in this system.
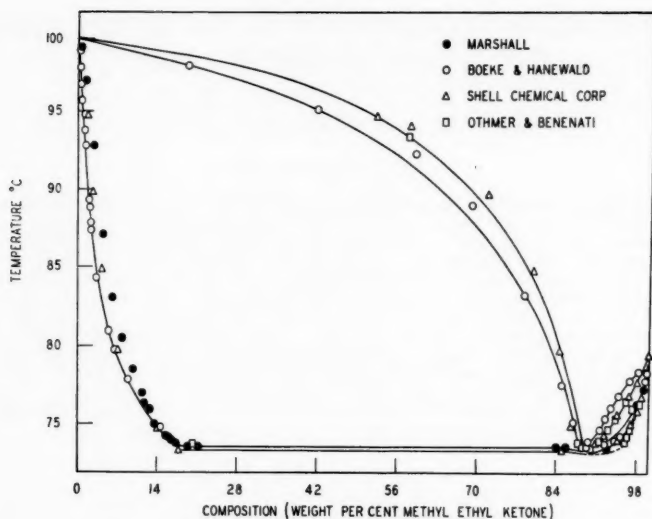
FIG. 2.   Liquid–vapor data as reported in the literature.

EXPERIMENTAL

A. Materials

The water used in these studies was distilled water from the laboratory tap which was redistilled from alkaline permanganate solution. Constancy of freezing point was used as a criterion of purity.

Commercial methyl ethyl ketone (minimum purity 99.0% by weight, b.p. 79.0–81.0° C), a straw yellow in color, was dried following the technique found in Weissberger's standard work (12). Middle fractions of doubly distilled water-clear ketone (b.p. 79.60± 0.05° C) were collected and stored over anhydrous potassium carbonate in the dark. (Methyl ethyl ketone is subject to slow photolysis.) A combination of physical techniques and visual observation used indicated a ketone purity of not less than 99.6% and probably of the order of 99.9%. As will be noted below, in the section pertaining to solid–liquid studies, the freezing point of methyl ethyl ketone as prepared for this work is further evidence of its high purity and dryness.

B. Thermometers

Throughout these studies temperatures were measured by use of conventional liquid-in-glass thermometers. The mercury-in-glass instruments (Brooklyn Thermometer Company precision grade) used between 0° C and 140° C were calibrated against a National Bureau of Standards' certified platinum resistance thermometer. The petrolate-in-glass instruments (Brooklyn Thermometer Company) used between 0° C and −90° C were calibrated and certified by the National Bureau of Standards.

C. Determination of the Liquid–Vapor Curves

The Othmer equilibrium still (13) was used to determine the liquid–vapor curves for this system. In order to present data at 1 atmosphere it was necessary to use the still in conjunction with a simple pressure line capable of maintaining the pressure in the still at 760±1 mm. Compositional analyses of boiling liquids and their condensed vapors were made by measurement of their relative refractive indices which were then compared

to working curves of relative readings of refractive index versus percentage composition of known solutions. An interesting result obtained for refractive index of ketone-rich solutions at 25° C is that a maximum occurs in the curve in the vicinity of 90% ketone (Fig. 3). Data obtained by the Shell Chemical Company (14) do not show such a maximum.
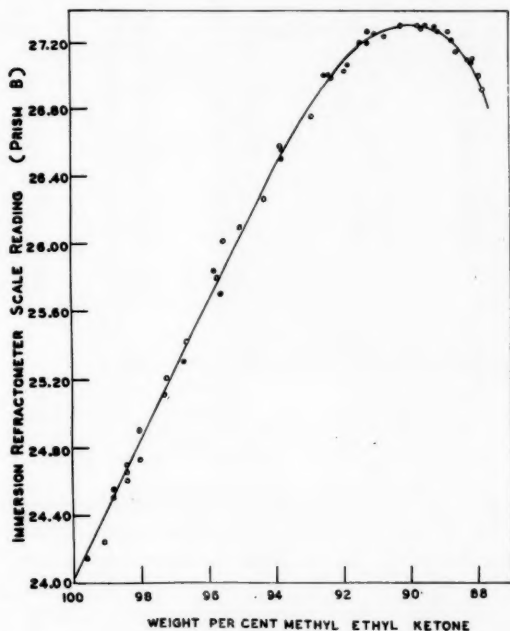
FIG. 3.   Working curve of refractive index for ketone-rich solutions.

For most solutions tapped from the Othmer still no further treatment beyond cooling them to 25° C was necessary prior to relative refractive index measurement. In some cases, however, the condensed vapors were heterogeneous and had to be mechanically agitated until equilibrium was attained. In those cases also, known weights of water were added until a homogeneous solution prevailed and then relative refractive indices were taken. A simple back calculation gave the compositional analyses for the original heterogeneous samples.

The data found for the liquid–vapor curves in the system are presented in Table I and Fig. 4. The most interesting point on this aspect of the system is that the minimum azeotrope, which occurs at 73.35±0.05° C at a composition of 88.45±0.15 wt.% methyl ethyl ketone, falls just outside of the intersection of the miscibility gap and the boiling point curve. This intersection, an invariant point of the system, occurs at 73.60±0.05° C where conjugate solutions of compositions 18.10±0.10 and 87.78±0.15 wt.% ketone, respectively, are in equilibrium with a vapor of composition 88.00±0.15 wt.% ketone.

D. Determination of the Solid–Liquid Curves

The method of thermal analysis was used throughout the study of the solid–liquid equilibria. The freezing point cell was capped with a teflon stopper through which the low-temperature thermometer and all glass stirring rod were fitted. The latter was, in

TABLE I

Vapor and liquid compositions of mixtures of methyl ethyl ketone and water

B.p.[a] (°C, 1 atm)	Wt.% methyl ethyl ketone		B.p. (°C, 1 atm)	Wt.% methyl ethyl ketone	
	Liquid	Vapor		Liquid	Vapor
100.00	0.00	0.00	73.35[d]	88.45	88.40
98.50	0.26	21.00	73.35[d]	88.45	88.65
97.30	0.54		73.60	81.10[b]	88.02
92.10	1.42			87.80[b]	
90.30	1.70	67.74[c]	73.80	93.55	91.90
85.00	2.89	78.42[c]	73.90	94.55	91.40
84.20	4.23		74.00	95.10	92.55
82.35	4.88		74.60	96.80	92.93
80.10	6.38	84.32[c]	74.80	96.55	93.25
78.20	8.58		75.30	97.10	94.20
77.00	10.34	86.24[c]	75.45	97.27	94.13
75.90	12.36	86.83[c]	77.05	98.80	96.50
73.55	18.06[b]	87.90	77.20	98.80	96.95
	87.76[b]		79.35	99.95	100.00
			79.35	99.85	100.00
			79.60	100.00	100.00

[a]To ±0.05° C.

[b]Two liquid layers and homogeneous condensed vapor.

[c]Dilution with water required to obtain homogeneity; calculated values.

[d]Minimum azeotrope.
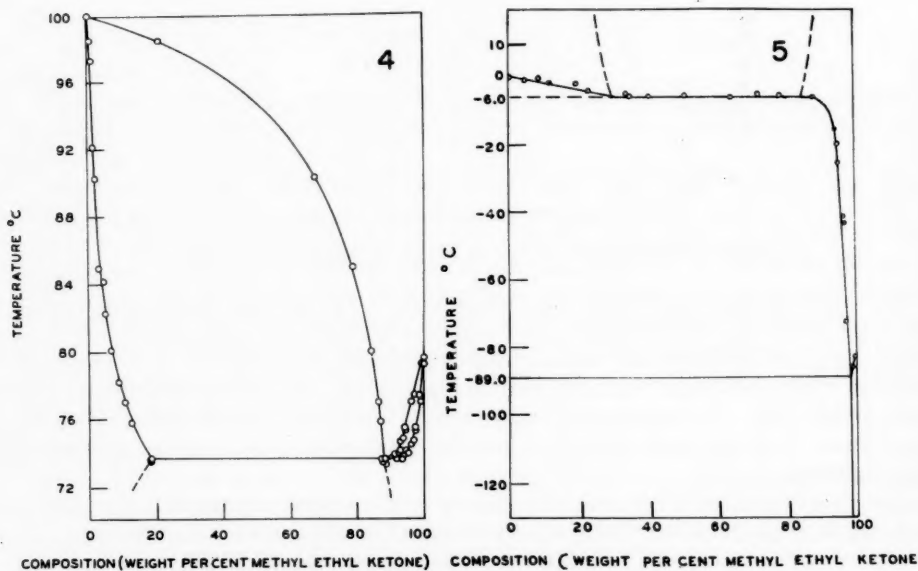
FIG. 4.   Liquid–vapor phase equilibria.
FIG. 5.   Solid–liquid phase equilibria.

turn, fitted with a semiball joint and spun in contact with the self-lubricating teflon stopper. This allowed for efficient mechanical agitation of the synthetic mixtures in the cell, particularly if they were heterogeneous, and at the same time provided a confined system, thereby preventing any loss of material through vaporization.

The temperature-controlling system employed was relatively crude. The cooling mixes

chosen were an ice slurry (for cooling to 0° C), a trichloroethylene – dry ice mix (for cooling in the range of 0° to −35° C), and liquid air (for cooling to very low temperatures). Manual raising and lowering of the cooling mix was chosen to establish a fairly well-regulated rate of cooling. Each synthetic mixture was thermally analyzed at least twice.

The data found for the solid–liquid curves in the system are presented in Table II

TABLE II

Freezing points of mixtures of methyl ethyl ketone and water

F.p.[a] (°C)	Wt.% ketone	F.p. (°C)	Wt.% ketone
0.00	0.00	−9.0	92.14
−0.05	8.63	−9.0	92.87
−2.0	11.45	−9.5	92.88
−2.5	19.19	−16.0	94.36
−4.5	22.95	−20.5	94.95
−6.0	33.72	−26.0	95.35
−5.5	34.71	−42.0	96.46
−6.0	40.34	−44.0	97.08
−6.0	51.10	−72.5	97.48
−7.0	64.20	−73.0	97.56
−6.0	71.98	−73.0	97.58
−6.0	78.30	−86.5	99.34
−6.5	87.15	−89.0[b]	99.4[b]
−8.5	91.96	−83.5	100.00

[a]All but first two to ±0.5° C.
[b]Eutectic point by extrapolation.

and Fig. 5. The first invariant point for the solid–liquid curves occurs at −6.0±0.5° C, at which a pair of conjugate solutions are in equilibrium with ice. The approximate compositions of the conjugate solutions were determined by extrapolation to be 36% and 80% by weight of methyl ethyl ketone, respectively. As a result of the liquid–liquid studies reported below, these compositions were determined with greater accuracy. The second invariant point for the solid–liquid curves occurs at −89.0±0.5° C, the eutectic point. It was impossible to determine the eutectic composition by any means other than extrapolation since this composition lies so close to that of pure ketone. Such extrapolation would indicate the eutectic composition to be 99.4±0.4% by weight methyl ethyl ketone. This piece of data would seem to account for the low freezing points of methyl ethyl ketone (−86° C to −86.9° C) as reported in standard reference tabulations (15, 16, 17). This work reports a freezing point for pure, *dry* methyl ethyl ketone of −83.5 ± 0.5° C.

E. Determination of the Liquid–Liquid Curves

The "thermostatic method" of Hill (18) was used primarily to determine the liquid–liquid curves. Two separate Hill method analyses were run. The results of those analyses are reported in Table III and Fig. 6. The Hill method allows for the calculation of the mean compositions of the conjugate liquid pair. Such calculations were made and plotted as a function of temperature. This was done in order to ascertain the general vicinity of the upper consolute temperature for the system. According to a variation of the law of Cailletet and Mathias (19) such calculations should lead to a straight line passing through the consolute point. The results of these calculations are also given in Table III and Fig. 6. From them the upper consolute temperature for this system appeared to be near 140° C at a composition of 40–45% by weight methyl ethyl ketone. In order to determine the upper consolute point more closely, several more points on the liquid–liquid curve

TABLE III

Mutual solubility of methyl ethyl ketone and water: Hill method

Temperature (°C)[a]	Calculated wt.% ketone[b,c]		Mean composition (wt.%)
	Lower layer	Upper layer	
7.50	32.9	85.4	59.7
9.50	32.3	85.1	58.7
11.00	31.1	87.1	59.1
11.00	28.7	89.0	58.8
18.00	28.6	90.1	59.4
18.50	28.3	87.6	57.9
30.50	24.0	91.4	57.7
35.00	22.4	91.2	56.8
40.00	21.1	91.0	56.0
45.00	21.0	89.6	55.3
56.00	18.8	89.3	54.0
62.00	18.6	88.7	53.7
71.00	17.6	88.4	53.0
83.00	17.5	84.0	52.8

[a] ±0.05° C.
[b] ±0.2%.
[c] First four figures are for experiment in which the two synthetic mixtures were composed of 7.1266 g ketone/8.2682 g water, and 6.9349 g ketone/9.3329 g water. All other figures are for sealed experiments in which the two synthetic mixtures were composed of 7.0760 g ketone/12.6050 g water, and 9.8135 g ketone/9.6782 g water.
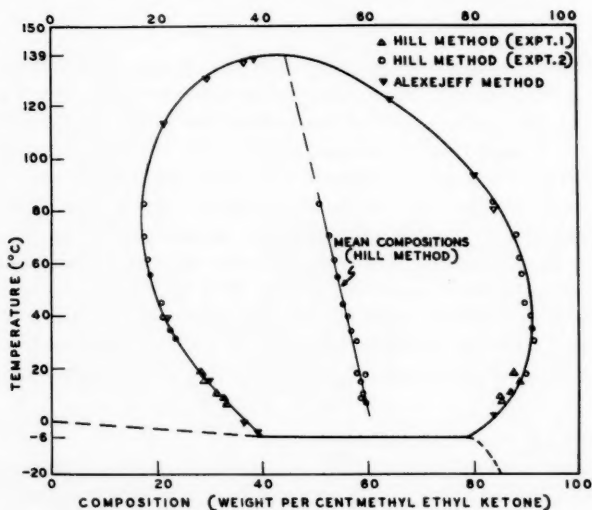
FIG. 6.   Liquid–liquid phase equilibria.

were determined using the familiar "synthetic method" (cloud-clear points) of Alexejew (20). These results are given in Table IV and also shown on Fig. 6.

With the additional points obtained from the cloud-clear point analyses, the extrapolated Cailletet–Mathias plot indicates that the upper consolute temperature for this system occurs at 139.0±0.5° C at a composition of 44.9±0.2% by weight of methyl ethyl ketone.

TABLE IV

Mutual solubility of methyl ethyl ketone and water: Alexejew method

Wt.% ketone	Cloud points[a] (°C)[b]		Clear points[a] (°C)[b]	
	Upper	Lower	Upper	Lower
21.72	113.0	39.5	115.0	39.0
29.83	132.0	15.5	131.0	16.0
36.82	137.0	−0.5	135.5	0.0
38.96	138.0	−4.0	136.5	−4.5
65.43	122.0	[c]	120.0	[c]
80.98	93.0	−2.5	91.0	−2.0
83.88	81.0	3.0	80.0	2.5

[a]Average of two experiments.
[b]±0.5° C.
[c]Ice formed at −6.0±0.5° C.

It was indicated in the solid–liquid section of this paper (Section D) that the miscibility gap intersects the freezing point curves in the vicinity of 36% and 80% by weight methyl ethyl ketone, respectively. From the liquid–liquid work a very short extrapolation to the freezing point curves indicates that these invariant points have the more accurately determined values of 40.0±0.2% and 78.0±0.2% by weight methyl ethyl ketone, respectively, at the temperature of −6.0±0.5° C.

DISCUSSION

A summary of all the equilibrium phase relationships for the binary system, methyl ethyl ketone – water, as found in this study is given by a total phase diagram shown in Fig. 7.

From the liquid–vapor studies, the results of this work (Table I and Fig. 4) compare quite well with the data reported by the Shell Chemical Corporation (10) and, earlier, by Marshall (2). The minimum azeotrope found in this study, at a temperature of 73.35±0.05° C and a composition of 88.45±0.15% by weight methyl ethyl ketone, is consistent with their reported figures of 73.4° C and 73.6° C, and 88.7% and 88.62% by weight, respectively. Othmer and Benenati (11) report a higher composition, 89.1%, while Boeke and Hanewald (9) report a lower figure, 87.8%.

From the liquid–liquid studies given here (Tables III and IV and Fig. 4) agreement with Marshall's studies (2) from 20° C to approximately 100° C is found. However, the enhanced solubility of methyl ethyl ketone in water and vice versa at temperatures below 20° C found in this work are at variance with Marshall's data for the same temperature region, but are in close agreement with the solubilities found by Ginnings et al. (6). It appears probable that the results reported in other previous investigations (1, 3, 4, 5, 7, 8) are in error. The most recent investigation on this aspect of the system is that of Campbell et al. (21), which is less extensive than the present work. Their work agrees closely with the combined data of Marshall and Shell Chemical Corporation investigators (22) with which this work is in some slight disagreement at temperatures near the upper consolute point. In particular, the initial study on the mutual solubilities to be reported for this system by Rothmund (1) is further shown to be incorrect by consideration of the upper consolute point. The data of this study, 139.0±0.5° C and 44.9±0.2% by weight methyl ethyl ketone, and that of Campbell et al. (21) and the Shell Chemical Corporation (22), 143° C and 45% by weight ketone, would indicate that Rothmund's data of 151.8° C and 44.2% by weight ketone is probably in error.
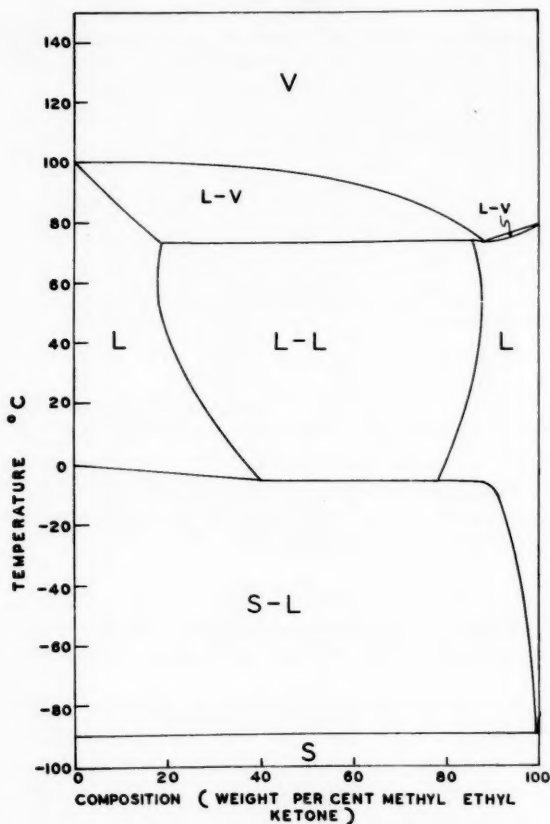
FIG. 7. Summary phase equilibria diagram.

The solid–liquid studies reported here (Table II and Fig. 5) are in good agreement with those of Randall and McKenna (7), who report the eutectic temperature to be −88.88±0.01° C at a composition of 99.91% by weight methyl ethyl ketone, while this work reports values of −89.0±0.5° C and 99.4±0.4% by weight ketone.

ACKNOWLEDGMENTS

REFERENCES

1. V. ROTHMUND. Z. physik. Chem. 26 (1898).
2. A. MARSHALL.   J. Chem. Soc. 89, 1350 (1906).
3. T. I. BERKENGEIM.   Chem. Abstr. 40, 6961 (1946).
4. J. G. PARK and H. E. HOFFMAN.   Ind. Eng. Chem. 24, 132 (1932).
5. D. C. JONES.   J. Chem. Soc. 799 (1929).
6. P. M. GINNINGS, D. PLONK, and E. CARTER.   J. Am. Chem. Soc. 62, 1923 (1940).
7. M. RANDALL and F. E. MCKENNA.   J. Am. Chem. Soc. 73, 4859 (1951).

8. T. W. EVANS.   Ind. Eng. Chem. Anal. Ed. **8**, 206 (1936).
9. J. BOEKE and K. H. HANEWALD.   Rec. trav. chim. **61**, 881 (1942).
10. SHELL CHEMICAL CORPORATION.   Methyl ethyl ketone. 2nd ed. New York. 1950. p. 68.
11. D. OTHMER and R. BENENATI.   Ind. Eng. Chem. **37**, 299 (1945).
12. A. WEISSBERGER (*Editor*). Techniques of organic chemistry. Vol. VII. Organic solvents. 2nd ed. Interscience Publishers, Inc., New York. 1955. p. 382.
13. D. F. OTHMER, *et al.*   Ind. Eng. Chem. **20**, 743 (1928); **37**, 299, 895 (1945); **40**, 168 (1948); Ind. Eng. Chem. Anal. Ed. **4**, 232 (1932).
14. Shell Chemical Corporation. Methyl ethyl ketone. 2nd ed. New York. 1950. p. 66.
15. N. LANGE (*Editor*).   Handbook of chemistry. 9th ed. Handbook Publishers, Inc., Sandusky, Ohio. 1956. p. 604.
16. THE HANDBOOK OF CHEMISTRY AND PHYSICS. 35th ed. Chemical Rubber Publishing Co., Cleveland, Ohio. 1953. p. 808.
17. THE MERCK INDEX OF CHEMICALS AND DRUGS.   6th ed. Merck and Co., Inc., Rahway, N.J. 1955. p. 382.
18. A. E. HILL.   J. Am. Chem. Soc. **45**, 1143 (1923).
19. S. GLASSTONE.   Textbook of physical chemistry. 2nd ed. D. Van Nostrand Co., Inc., New York. 1946. p. 431.
20. W. ALEXEJEW.   Bull. soc. chim. France, **38**, 145 (1882); Ann. phys. chim. **28**, 305 (1886).
21. A. N. CAMPBELL, E. M. KARTZMARK, and W. E. FALCONER.   Can. J. Chem. **36**, 1475 (1958).
22. Shell Chemical Corporation. Methyl ethyl ketone. 2nd ed. New York. 1950. p. 67.

VAPOR/LIQUID PARTITION OF TRITIUM IN TRITIATED WATER

O. Sepall and S. G. Mason

INTRODUCTION

In a study of the exchange of tritium between cellulose and tritiated water, it was necessary to extend the published data on the ratio of isotopic concentrations $[H^3]/[H^1]$ in the saturated vapor and liquid phases of tritiated water so as to cover the temperature range 0° to 90° C.

METHOD

Isotopic concentrations in tritiated water were determined by the gas counting method of Robinson (3) in which the hydrogen in the water is converted to methane by reaction with methyl grignard. Vapor samples were obtained by an equilibrium distillation technique.

The distillations were carried out in the arrangement shown in Fig. 1. The tritiated
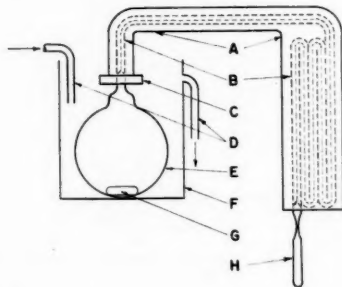
FIG. 1. Equilibrium distillation apparatus.

A. Asbestos covering with heater wire.
B. Capillary tube.
C. Rubber isolating disk between water and heater.
D. Recirculation lines for temperature regulated water.

E. 100-ml flask.
F. Copper vessel.
G. Magnetic stirrer.
H. Sample collecting tube.

water was contained in the flask E, immersed in a constant temperature bath. The vapor was distilled through the capillary tube B into a collecting tube H. The capillary served to restrict the distillation rate and to prevent diffusion back from the collecting tube to the flask. As the temperature was raised, the length of capillary was increased so as to ensure equilibrium distillation. The complete length of tubing was heated electrically by a resistance wire embedded in the asbestos covering to avoid condensation.

For a distillation, 50 ml of tritiated water (0.8 μcurie/g, $[H^3]/[H^1] = 10^{-10}$) were introduced into the flask. This quantity was large enough that concentration changes during distillation were negligible. The system was evacuated through the sampling tube until all air had been removed, and the sample tube was sealed off. The capillary heater was adjusted to give a temperature about 30° C higher than the saturation temperature for the experiment. A sample of 0.3 ml was then distilled over by immersing the collecting tube in liquid air. The length and size of the capillary had been selected so that

distillation time was at least 30 minutes. Longer times gave the same result. The sample was then isolated by sealing off the constriction in the tube.

RESULTS AND DISCUSSION

The measured ratios of isotopic concentrations in vapor and liquid are listed in Table I, and are seen to agree with the values of Brown (2). They are much higher than those of Price (1), which are concluded to be in error.

TABLE I

Isotopic ratios in tritiated water vapor and liquid

Temperature, °C	$\dfrac{[H^3]/[H^1]_{vapor}}{[H^3]/[H^1]_{liquid}}$	
	Present data	Brown (2)
0 ±0.5	0.86±0.005	
0.5		.88
14	0.90	
19.5		.91
20	0.91	
30	0.92	
50	0.94	
56.5		.945*
70	0.96	
90	0.97	

*From reference 4.

The accuracy of the data is limited by the gas-counting assay for tritium. The results of this analysis show a scatter with a standard deviation of 0.6%. The data reported here are averages of duplicate determinations and have been rounded off to the nearest 0.5%.

The procedure used in this work was found to be quite satisfactory. The results were reproducible for distillation times of 30 minutes or longer. For times as short as 5 minutes, the ratios tended to rise, indicating a non-equilibrium distillation.

This technique could readily be adapted for measurements above 100° C by making provision for the pressure developed.

1. A. H. PRICE.   Nature, **181**, 262 (1958).
2. R. M. BROWN.   Atomic Energy of Canada, Ltd. Private communication. 1960.
3. C. V. ROBINSON.   Nucleonics, **13** (11), 90 (1955).
4. E. C. BERTSCHE.   U.S. Atomic Energy Commission Rept. DP325. 1958.

THE REACTION OF THE O- AND N-METHYL DERIVATIVES OF AROMATIC KETOXIMES WITH CARBON MONOXIDE AND HYDROGEN

ALEX ROSENTHAL

It has been previously shown that benzophenone oxime cyclizes with carbon monoxide containing about 1% hydrogen to yield 3-phenylphthalimidine in high yield (1). The

present work was initiated in an attempt to devise a method for obtaining N-hydroxy-phthalimidines using similar high-pressure reactions described before (1). It was hoped that by blocking the labile hydroxyl group on the oxime with an O-methyl ether group concurrent or subsequent elimination of the former group would be prevented, without obstruction of the cyclization with carbon monoxide. Thus, reaction of O-methyl-benzophenone oxime with carbon monoxide might be expected to yield N-methoxy-3-phenylphthalimidine (I) as shown below:

$$\text{C=N-OCH}_3 \quad \xrightarrow[\text{CO}_2\text{(CO)}_8]{\substack{\text{CO}+\text{H}_2 \\ (99:1)}} \quad \left[\ \text{I}\ \right] \quad \longrightarrow \quad \text{II}$$
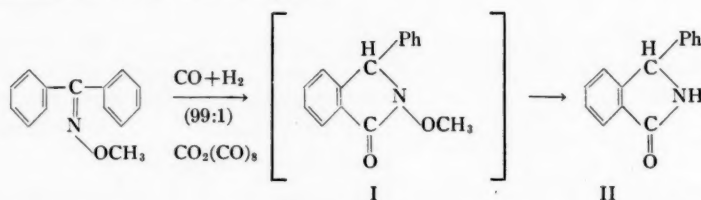
Subsequent demethylation of the latter might produce N-hydroxy-3-phenylphthalimidine since the lactam ring is stable to acid hydrolysis.

When a benzene solution of O-methylbenzophenone oxime was reacted with a mixture of carbon monoxide and hydrogen (99:1) at about 300 atmospheres and at about 220° for 70 minutes in the presence of preformed dicobalt octacarbonyl the main product was 3-phenylphthalimidine (II). Compound II was characterized by direct comparison (mixed melting point and infrared) with an authentic sample (2). No attempt was made to determine whether the cleavage of the ether took place prior or subsequent to the cyclization with carbon monoxide.

As carbon monoxide cyclized readily with nitrogen (in the trivalent state) to the aromatic ring (1), it seemed of interest to determine if the nitrogen in the N-methyl ether might undergo a similar attachment to the aromatic ring. When α-benzildioxime N,N'-dimethyl ether was reacted with carbon monoxide and hydrogen at about 225° for 2 hours the main product was tetraphenylpyrazine (III) as shown below:

$$\begin{matrix} \text{Ph-C}\!-\!-\!-\!\text{C-Ph} \\ \text{CH}_3\text{-N}\quad\text{N-CH}_3 \\ \text{O}\quad\text{O} \end{matrix} \quad \xrightarrow[\text{CO}_2\text{(CO)}_8]{\text{CO}+\text{H}_2} \quad \text{III}$$
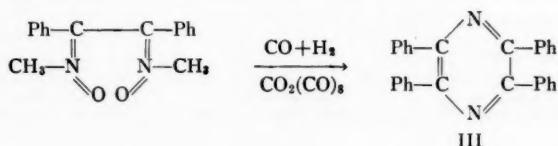
The structure of compound III was unequivocally established by direct comparison (mixed melting point and infrared) with an authentic sample (3).

Various analyses were carried out in an attempt to ascertain the mechanism of formation of the unexpected tetraphenylpyrazine. Three moles of gases per mole of substrate was consumed in the reaction. Reaction of the gases with dilute hydrochloric acid gave a trace amount of a crystalline salt melting at approximately the correct temperature for ammonium chloride. Treatment of the salt with sodium hydroxide produced a gas which turned red litmus blue. Gas chromatographic analyses of the liquid component of the reaction mixture showed only benzene to be present. The residual organic material remaining after extraction of tetraphenylpyrazine appeared to be polymeric in nature as evidenced by the fact that the residue was insoluble in organic solvents. Since none of these experiments shed any light on the mechanism, further work was abandoned.

EXPERIMENTAL

General Considerations

The equipment was described previously (1).

Reaction of O-Methylbenzophenone Oxime with Carbon Monoxide and Hydrogen

1. Preparation of O-Methylbenzophenone Oxime

Benzophenone (20 g) and O-methylhydroxylamine hydrochloride (14 g) were refluxed for 4 hours with 20 ml of pyridine and 200 ml of ethanol. The ethanol was then removed under reduced pressure. Slow addition of water with stirring caused the product to crystallize (87% yield). O-Methylbenzophenone oxime was twice recrystallized from acetone–methanol–water according to the method described by Hauser and Hoffenberg (4), m.p. 60–61°; reported m.p. 60–61° (4).

2. Carbonylation of O-Methylbenzophenone Oxime

To a solution of O-methylbenzophenone oxime (10.5 g, 0.05 mole) and dicobalt octacarbonyl (0.026 mole) in 50 ml of purified thiophene-free benzene contained in a glass liner in the bomb was added a mixture of carbon monoxide and hydrogen (99:1) at 2300 p.s.i. The bomb was rocked and heated at 220° for 70 minutes. The over-all pressure drop was 125 p.s.i. measured at 0° C (1.3 moles of gas per mole of substrate). After the dicobalt octacarbonyl was decomposed at 70–80°, the benzene was removed under reduced pressure. The solid residue was extracted with two 100-ml portions of ether. The remaining residue was extracted with hot chloroform. After the chloroform was evaporated the residue was recrystallized from ethanol to yield 3-phenylphthalimidine, m.p. 218–220°, mixed melting point with an authentic sample of 3-phenylphthalimidine (2), 218–220°.

After removal of the catalyst and solvent, a portion of the crude product (0.55 g) in 10 ml of benzene was added to the top of a glass column containing a 80×38 mm (diameter) adsorbent column of alumina. Elution of the column with 200 ml of benzene gave a trace of brown oil. An amount of 0.40 g (about 75%) of 3-phenylphthalimidine was eluted using benzene–ethanol (9:1) as developer.

When the reaction product (after removal from the bomb) was fractionated on alumina using benzene as developer, an unstable brown organo–cobalt complex was eluted which on being warmed in petroleum ether became insoluble. Attempts to characterize this material were unsuccessful.

Reaction of α-Benzildioxime N,N'-Dimethyl Ether with Carbon Monoxide and Hydrogen

In a similar way a mixture of 5.9 g of α-benzildioxime N,N'-dimethyl ether (5) in 60 ml benzene containing 2 g of dicobalt octacarbonyl as catalyst was reacted with 3800 p.s.i. of carbon monoxide and hydrogen (99:1), at 225–230° for about 2 hours. The over-all pressure drop was 130 p.s.i. measured at room temperature. The gaseous product was bubbled through dilute hydrochloric acid. Evaporation of the solvent left a few milligrams of a crystalline product which melted at 300–340°. Treatment of the salt with dilute sodium hydroxide evolved a gas which was basic to litmus paper.

An aliquot of the reaction mixture was allowed to stand at room temperature until the catalyst was decomposed. Vapor phase chromatography of the distillate showed benzene only to be present.

After the catalyst was decomposed, the crude product (0.75 g) was fractionated by chromatography on alumina (85×38 mm diameter) using benzene ethanol (99.5:0.5) as developer. Evaporation of the eluate from the main zone gave a faint yellow residue (0.28 g, about 55% yield) which after several recrystallizations from acetone yielded pure

tetraphenylpyrazine (III), m.p. 252–253°. The mixed melting point of the main fraction and an authentic sample of tetraphenylpyrazine (3) was 252–253°. The infrared spectra of both compounds were identical. Anal. Found: C, 87.86; H, 5.29; N, 7.26. Calc. for $C_{28}H_{20}N_2$: C, 87.48; H, 5.24; N, 7.29. Infrared of II (KBr): 3040(m), 1625(w), 1580(w), 1448(s), 1393(s), 1215(m), 1160(m), 1107(s).

A second minor component could not be purified.

1. A. ROSENTHAL, R. F. ASTBURY, and A. HUBSCHER. J. Org. Chem. **23**, 1037 (1958); A. ROSENTHAL and J. P. O'DONNELL. Can. J. Chem. **38**, 457 (1960).
2. R. E. ROSE. J. Am. Chem. Soc. **33**, 388 (1911).
3. D. DAVIDSON, M. WEISS, and M. JELLING. J. Org. Chem. **2**, 328 (1937).
4. C. R. HAUSER and D. S. HOFFENBERG. J. Org. Chem. **20**, 1482 (1955).
5. O. L. BRADY and H. M. PERRY. J. Chem. Soc. **127**, 2874 (1925).

STOICHIOMETRY OF THE REACTION OF CHROMYL CHLORIDE WITH CYCLOHEXENE

R. A. STAIRS

In the reactions of chromyl chloride with hydrocarbons, brown precipitates of unknown structure, that have been formulated in most cases as (HC).$2CrO_2Cl_2$, are obtained (1). However, where the hydrocarbon is an olefin, analysis of the precipitate has led to very uncertain results. Cristol and Eilar have suggested (2) that only one molecule of chromyl chloride is essential. A simple experiment has been performed that strongly supports this suggestion, consisting of a calorimetric "titration" of cylohexene with chromyl chloride in carbon tetrachloride solution. The two solutions were mixed in various proportions in a crude calorimeter, the temperature rise was measured, and the quantity of heat liberated in the reaction was calculated and plotted against the logarithm of the molar ratio in each mixture. The result, shown in the figure, indicates a pronounced maximum. This was located at $\log_{10} R = 0 \pm .02$ by linear extrapolation of the two branches, corresponding to $R = 1.00 \pm 0.05$. This may be compared with results from analysis of precipitates, which yield values of r from 1.2 to 2.3 depending on the conditions, and on whether chlorine or chromium content is the basis of calculation (2).

In the figure the solid curves represent the theoretical effect of a heat of reaction of 50 kcal/mole. (The asymmetry arises from the inequality of the concentrations of the two reagent solutions.)

It is apparent that an additional heat effect is present when chromyl chloride is in excess. Comparison with the analyses suggests that further attack by chromyl chloride on the main product occurs, leading to chlorination, as all the results reported (2) are high in chlorine. To avoid this in preparative use of this reaction, it should be carried out at as low a temperature as possible and with the olefin always in excess.
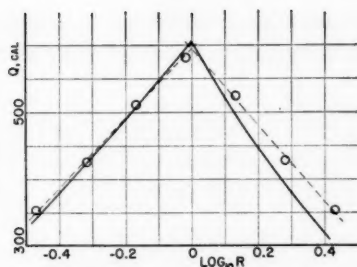
FIG. 1. Heat evolved on mixing vs. the logarithm of the molar ratio $R = (CrO_2Cl_2)/(C_6H_{10})$.

EXPERIMENTAL

Solutions were prepared as follows:

(A) Cyclohexene (Matheson, once distilled, b.p. 82.0–82.8° C, 755 mm) made up by direct weighing, 0.197 ± 0.002 mole/l., and (B) chromyl chloride (prepared from CrO_3 and dry HCl, b.p. 115.5–117° C, 755 mm) standardized iodometrically, 0.134 ± 0.001 mole/l., both in reagent CCl_4 dried over calcium sulphate.

A certain volume of solution B was measured into a Dewar flask (the calorimeter), and a volume of solution A to make the total 150 ml was measured into another Dewar vessel. In view of other inaccuracies in the method, and to avoid stopcock troubles and lessen troubles from evaporation these volumes were measured with graduated cylinders.

The temperature of each was read, A was poured into B, and the mixture was stirred. Temperature readings were taken about every half minute until successive readings agreed to 0.2° C (about 5 minutes). Temperature rises of 5 to 10 degrees were observed. No attempt was made to correct for the effects of stirring or of heat exchange with the room, since these systematic errors would not affect the conclusions respecting stoichiometry.

The approximate heat evolved, Q, was calculated by the formula

$$Q = K[t(V_A+V_B+C)-t_A V_A-t_B(V_B+C)],$$

where t_A and t_B, V_A and V_B are the initial temperatures and volumes of the solutions, C is the CCl_4 equivalent of the calorimeter (estimated to be 30 ± 15 ml, from the water equivalent found by students in teaching laboratory), and K is the volume specific heat of carbon tetrachloride, about 0.32 cal ml^{-1} deg^{-1}.

1. W. H. HARTFORD and M. DARRIN. Chem. Revs. **58**, 1 (1958).
2. S. J. CRISTOL and L. D. EILAR. J. Am. Chem. Soc. **72**, 4353 (1950).

3,5-DI-O-METHYL-D-GALACTOSE, A NEW METHYLATED SUGAR FROM A FULLY METHYLATED POLYSACCHARIDE OF GIBBERELLA FUJIKUROI (FUSARIUM MONILIFORME)*

I. R. SIDDIQUI AND G. A. ADAMS

During methylation studies of the extracellular acidic polysaccharide of *Gibberella fujikuroi* A.T.T.C. 10052 (*Fusarium moniliforme*), a di-O-methyl fraction was obtained

*Issued as N.R.C. No. 5911.

which gave, *inter alia*, a di-O-methyl sugar which has been identified as 3,5-di-O-methyl-D-galactose. This is a new sugar derivative and proof of its identification is provided by the following evidence.

The aforementioned di-O-methyl sugar showed $[\alpha]_D^{26}$ $-24.8°\pm0.5°$ in water and a methoxyl content of 28.7%; a di-O-methyl hexose requires OMe, 29.8%. On demethylation (1) it gave only galactose as the parent sugar. The di-O-methyl galactose moved as a single spot on paper electrophoresis (2) in borate buffer and on paper chromatograms in three different solvent systems.

In addition to indicating homogeneity the results of these experiments also suggested that the di-O-methyl galactose was in the furanose rather than in the pyranose ring form. None of the reported di-O-methyl-D-galactopyranoses show negative rotation (3). The di-O-methyl galactose gave a higher M_g value (0.66) on paper electrophoresis in borate (2) than is to be expected for a di-O-methyl hexopyranose (4). The R_g value (0.65) on paper chromatography in *n*-butanol: ether: water (5:1:4) was much higher than reported for the known di-O-methyl galactopyranoses (5).

Confirmation of the furanose structure was obtained by methylation and oxidation studies. Complete methylation by Purdie's method of the glycoside of the di-O-methyl galactose yielded the glycoside of 2,3,5,6-tetra-O-methyl-D-galactose as shown by gas–liquid partition chromatography (6, 7). Oxidation of the di-O-methyl galactose with bromine water afforded a crystalline lactone which showed the slow hydrolysis in water typical of γ-lactones (8). An additional piece of evidence in support of the γ-lactone structure was provided by the infrared spectrum of the compound. It showed a strong C=O stretching peak at 1786 cm^{-1}. For comparison the infrared spectra of 2,5-di-O-methyl-L-arabonolactone and gluconic acid δ-lactone were also examined. The former compound showed the C=O stretching peak at 1772 cm^{-1} while in the latter it occurred at 1720 cm^{-1}. These values are in agreement with those given by Bellamy (9) for γ- and δ-lactones respectively. Barker *et al.* have also pointed out that in the five-membered lactone rings the increase of strain results in an increase of the C=O stretching frequency from 1733 cm^{-1} in δ-hexanolactone to 1770 cm^{-1} in γ-butyrolactone (10). The γ-lactone was converted by methanolic ammonia into a crystalline amide which gave a positive Weerman test (11), thereby proving the presence of a free hydroxyl group at position 2.

Finally, reduction of the di-O-methyl-D-galactose by potassium borohydride (12) yielded a crystalline di-O-methyl hexitol having the same melting point and equal but opposite specific rotation as 2,4-di-O-methyl-D-galactitol (13). The infrared spectrum of this hexitol and authentic 2,4-di-O-methyl-D-galactitol were superimposable. These findings proved that the derived galactitol was 2,4-di-O-methyl-L-galactitol, which is the same as 3,5-di-O-methyl-D-galactitol. Hence the parent sugar was 3,5-di-O-methyl-D-galactose.

EXPERIMENTAL

The organic phases of the following solvents (v/v) were used for paper chromatographic separations: (A) *n*-butanol:ethanol:water (5:1:4); (B) benzene:ethanol:water: ammonia (200:47:14:1); (C) 2-butanone saturated with water containing 2% ammonia; (D) pyridine : ethyl acetate : water (1:2.5:2.5). Sugars were detected on chromatograms by spraying with *p*-anisidine hydrochloride spray reagent. Infrared spectra were measured using the Nujol mull technique and a microcell. Measurements were made in the frequency range 3800–600 cm^{-1}.

The di-O-methyl sugar under consideration was found as a product of hydrolysis of

the methylated polysaccharide from *Gibberella fujikuroi*. It was separated from other di-*O*-methyl hexoses by preparative paper chromatography using solvent C.

3,5-Di-O-methyl-D-galactose

The syrupy di-*O*-methyl sugar showed $[\alpha]_D^{26}$ $-24.8°\pm0.5°$ (*c*, 1.935 in water) and a methoxyl content of 28.7%; a di-*O*-methyl hexose requires OMe, 29.8%. Paper chromatographic analysis of this sugar in solvents A, B, and C gave R_g values of 0.64, 0.23, and 0.41 respectively. Paper electrophoretic (2) examination of this sugar in borate buffer, pH 10, showed a single component (M_g, 0.66). A small quantity of the syrup (1–2 mg) was dissolved in dichloromethane (0.2 ml) and was demethylated (1) with boron trichloride (0.5 ml) at $-70°$ C. Paper chromatographic analysis of the demethylated sugar in solvent D showed that only galactose was the parent sugar. The di-*O*-methyl sugar (ca. 1 mg) was heated in a sealed tube with 4% methanolic hydrogen chloride for 24 hours, neutralized with silver carbonate, filtered, evaporated, and methylated by Purdie's reagents (silver oxide ca. 20 mg + methyl iodide 2 ml). Examination of the fully methylated sugar by gas–liquid partition chromatography, using a 4-ft column of 20% Apiezon M on Celite 545 at 150° C and an argon flow rate of 150 ml/minute, showed that the relative retention time of the sample with respect to quinoline was 1.54. The authentic methyl glycoside of 2,3,5,6-tetra-*O*-methyl-D-galactose gave a retention time of 1.52 under the same conditions.

3,5-Di-O-methyl-D-galactitol

Di-*O*-methyl-D-galactose (35 mg) in water (2 ml) was mixed with a solution of potassium borohydride (12) (75 mg in 1 ml) and the solution was left overnight. Excess borohydride was destroyed with glacial acetic acid (few drops) and the solution was deionized with Amberlite resins IR-120 and IR-4B. The resulting hexitol crystallized when kept as a syrup overnight. It was recrystallized from ethyl acetate containing a little methanol. The crystals showed a melting point of 134–135° C, $[\alpha]_D^{26}$ $-23.7°\pm1°$ (*c*, 1.01 in methanol). Anal. Calc. for $C_8H_{18}O_6$: C, 45.71%; H, 8.63%. Found: C, 45.92%; H, 8.32%. Reported values for 2,4-di-*O*-methyl-D-galactitol are m.p. 134–135° C, $[\alpha]_D^{28}$ $+23.5°\pm0.5°$ (*c*, 2.04 in methanol) (13). The unknown hexitol and 2,4-di-*O*-methyl-D-galactitol showed superimposable infrared spectra.

3,5-Di-O-methyl-D-galactonic Acid Lactone

3,5-Di-*O*-methyl-D-galactose (180 mg) in water (4 ml) was oxidized with bromine (15 drops), in the presence of barium carbonate (100 mg), for 60 hours. Bromine was removed by aeration and the solution was extracted with chloroform for 3 days. The chloroform extract was dried with anhydrous sodium sulphate and concentrated to a syrup which was lactonized by distillation (bath temperature 130–160° C/0.02 mm). Crystallization of the syrup from ether : petroleum ether containing a few drops of methanol gave 3,5-di-*O*-methyl-D-galactonic acid-γ-lactone; m.p. 89.5–91° C; $[\alpha]_D^{26}$ $-72.9°\pm2° \rightarrow -49.2°\pm2°$, 18 days (incomplete) (*c*, 1.015 in water); ν_{max} 1786 cm^{-1}. Anal. Calc. for $C_8H_{14}O_6$: C, 46.60%; H, 6.84%. Found: C, 46.84%; H, 6.93%.

3,5-Di-O-methyl-D-galactonamide

3,5-Di-*O*-methyl-D-galactonic acid lactone (15 mg) was kept in methanol saturated with ammonia at 5° C for 24 hours. Removal of the solvent gave a syrup which crystallized when scratched. Recrystallization from ethanol : ether gave the amide, m.p. 131–133° C; $[\alpha]_D^{27}$ $+9.2°\pm2°$ (*c*, 0.87 in methanol). Anal. Calc. for $C_8H_{17}O_6N$: N, 6.27%. Found: N, 6.26%.

A portion of the amide (ca. 4 mg) was oxidized with sodium hypochlorite and on addition of semicarbazide hydrochloride (14) gave a white precipitate of hydrazodicarbonamide.

ACKNOWLEDGMENTS

1. S. ALLEN, T. G. BONNER, E. J. BOURNE, and N. M. SAVILLE.   Chem. & Ind. (London), 630 (1958).
2. A. B. FOSTER.   J. Chem. Soc. 982 (1953).
3. D. J. BELL.   Advances in Carbohydrate Chem. 6, 1 (1951).
4. S. A. BARKER, A. B. FOSTER, I. R. SIDDIQUI, and M. STACEY.   J. Chem. Soc. 2358 (1958).
5. E. L. HIRST and J. K. N. JONES.   Discussions Faraday Soc. 7, 268 (1949).
6. A. G. MCINNES, D. H. BALL, F. P. COOPER, and C. T. BISHOP.   J. Chromatog. 1, 556 (1958).
7. C. T. BISHOP and F. P. COOPER.   Can. J. Chem. 38, 388 (1960).
8. H. D. K. DREW, E. H. GOODYEAR, and W. N. HAWORTH.   J. Chem. Soc. 1237 (1927).
9. L. J. BELLAMY.   The infrared spectra of complex molecules. Methuen & Co. Ltd., London. 1954. p. 153.
10. S. A. BARKER, E. J. BOURNE, and D. H. WHIFFEN.   Methods of Biochem. Anal. 3, 213 (1956).
11. M. R. A. WEERMAN.   Rec. trav. chim. 37, 16 (1918).
12. M. ABDEL-AKHER, J. K. HAMILTON, and F. SMITH.   J. Am. Chem. Soc. 73, 4691 (1951).
13. C. T. BISHOP.   Can. J. Chem. 38, 1636 (1960).
14. J. I. CUNNEEN and F. SMITH.   J. Chem. Soc. 1146 (1948).

CONTENTS